Universität Hamburg
DER FORSCHUNG | DER LEHRE | DER BILDUNG

Synthesis of Modified T-1106-5´-α-Thio-Triphosphates as Exoribonuclease-Stable Inhibitors of the SARS-CoV-2 RNA-dependent RNA polymerase

Dissertation

to obtain the Scientific Doctoral Degree

by

Benedikt Ganter

presented to

the Department of Chemistry of the Faculty of Sciences at

the University of Hamburg

Hamburg 2025

This thesis was conducted at the Institute of Organic Chemistry at the University of Hamburg from March 2020 to August 2025

First Reviewer: Prof. Dr. Chris Meier

Second Reviewer: Prof. Dr. Ralph Holl

Third Reviewer: Prof. Dr. Piet Herdewijn

Disputation Date: 20.02.2026

“Alles ist gut, solange du wild bist!”

I. List of Publications

V. Nikolova, K. Linnemannstöns, M.-E. Bendel, M. Machado, B. Ganter, P. Budimir, M. Vogts, C. Fischer, M. Ganter, C. Meier, M. Dobbelstein, *ACS Infect. Dis.* **2025**, *11*, 11, 3138–3151: *Membrane-Permeable 5-Fluorodeoxyuridine Triphosphate Derivatives Inhibit the Proliferation of Plasmodium falciparum*

B. Ganter, M. Zickler, J. Huchting, M. Winkler, A. Lüttjohann, C. Meier, G. Gabriel, S. Beck, *Pharmaceutics* **2023**, *15*, 1732: *T-705-Derived Prodrugs Show High Antiviral Efficacies against a Broad Range of Influenza A Viruses with Synergistic Effects When Combined with Oseltamivir.*

X. Jia, B. Ganter, C. Meier, *Annual Reports in Medicinal Chemistry* **2021**, *57*, 1-47: *Improving properties of the nucleobase analogs T-705/T-1105 as potential antiviral;*

Conferences

09/2025	XII. Nucleinsäurechemietreffen, Hamburg, Germany
	Poster: *Synthesis of Modified T-1106-5´-α-Thio-Triphosphates as Exoribonuclease (ExoN) Stable Inhibitors of SARS-CoV-2 RdRp*
06/2025	33rd Annual GP_2A Medicinal Chemistry Conference, XIVth Paul Ehrlich MedChem Euro-PhD Network Meeting, Nantes, France
	Poster and Flash Presentation: *Synthesis of Modified T-1106-5´-α-Thio-Triphosphates as Exoribonuclease (ExoN) Stable Inhibitors of SARS-CoV-2 RdRp*
09/2023	XI. Nucleinsäurechemietreffen, Würzburg, Germany
	Poster: *Synthesis of Modified T-1106-5´-Triphosphate Prodrugs as Inhibitor of the SARS-CoV-2 RdRp*
09/2023	IX EFMC International Symposium on Advances in Synthetic and Medicinal Chemistry, Zagreb, Croatia
	Poster: *Synthesis of Modified T-1106-5´-Triphosphate Prodrugs as Inhibitor of the SARS-CoV-2 RdRp*
09/2022	XXVII EFMC International Symposium on Medicinal Chemistry, Nice, France
	Poster and Presentation: *Synthesis of Modified T-1106-5´-Triphosphates as Potential Inhibitor of the SARS-CoV-2 RdRp*

09/2021 Online Meeting of the 5th Innovative Approaches for Identification of Antiviral Agents Summer School

Presentation: *Synthesis of Modified T-1106-5´-Triphosphates as Potential Inhibitor of the SARS-CoV-2 RdRp*

II. Table of Contents

III. List of Abbreviations

A	adenosine
AB	acyloxybenzyl
Ac	acetyl
ACE2	angiotensin-converting enzyme 2
AIBN	azobis(isobutyronitril)
aq.	aqueous
ATP	adenosine triphosphate
AZT	azidothymidin
BAB	bisacyloxybenzyl
Bn	benzyl
Bz	benzoyl
C	cytosine
CC_{50}	half-maximal cytotoxic concentration
CDC	Centers for Disease Control and Prevention (U.S.)
CES1	carboxylesterase 1
conc.	concentrated
CoV	coronavirus
CTP	cytosine triphosphate
d	doublet (NMR)
DAST	diethylaminosulfur trifluoride
DBU	1,8-diazabicyclo[5.4.0]undec-7-ene
DCI	*N*,*N*'-dicyclohexylcarbodiimide
dd	doublet of doublet (NMR)
ddd	doublet of doublet of doublet (NMR)
Di*PP*ro	a nucleoside diphosphate prodrug
4-DMAP	4-dimethylaminopyridine

DMF	*N,N'*-dimethylformamide
DMSO	dimethyl sulfoxide
DNA	deoxyribonucleic acid
dt	doublet of triplets (NMR)
EBOV	zaire ebolavirus
EC_{50}	half-maximal effective concentration
ER	endoplasmic reticulum
equiv.	equivalents
ERGIC	ER-Golgi intermediate compartment
ESI	electron spray ionization
EUA	emergency use authorization
FDA	food and drug administration (U.S.)
Fm	9-Fluorenylmethyl
FRMP	Favipiravir-ribofuranosyl-5'-monophosphate
FRTP	Favipiravir-ribofuranosyl-5'-triphosphate
G	guanosine
gRNA	genomic RNA
GTP	guanosine triphosphate
HCV	hepatitis C virus
HGPRT	hypoxanthine guanine phosphoribosyltransferase
HINT1	histidine triad nucleotide-binding protein 1
HIV	human immunodeficiency virus
HMDS	bis(trimethylsilyl)amine (hexamethyldisilazane)
HPLC	high performance liquid chromatography
HRMS	high resolution mass spectrometry
IMPDH	inosine-5'-monophosphate dehydrogenase
*i*Pr	*iso*-propyl

J	coupling constant (NMR)
kb	kilo base
KLK5	kallikrein-5
LASV	lassa virus
LDA	lithium diisopropylamide
M	molar ($mol \cdot L^{-1}$)
m/z	mass-to-charge ratio
m	multiplet (NMR)
MALDI	matrix assisted laser desorption ionization
m-CPBA	meta-chloroperbenzoic acid
MMP16	matrix metalloproteinase 16
M^{pro}	main protease
mRNA	messenger RNA
MS	molecular sieve
MTP	molnupiravir-5´-triphosphate
nAbs	neutralizing antibodies
NCS	*N*-chlorosuccinimide
NDP	nucleoside diphosphate
NiRAN	*N*-terminal nidovirus RdRp-associated nucleotidyltransferase
NMI	*N*-methylimidazole
NMP	nucleoside monophosphate
NMPA	National Medical Products Administration
NMR	nuclear magnetic resonance
NOESY	nuclear Overhauser effect spectroscopy (NMR)
NSP	non-structural protein
NTD	*N*-terminal domain
NTP	nucleoside triphosphate
o/n	overnight

ORF	open reading frames
PCTF	*O*-phenyl chlorothionoformate
PG	protecting group
Ph	phenyl
PL^{pro}	papain-like protease
pp	polyproteins
pRNA	product RNA
RBD	receptor-binding domain
RBM	receptor-binding motif
RdRp	RNA-dependent RNA polymerase
RTC	Replication transcription complex
RNA	ribonucleic acid
RP	reversed phase
rt	room temperature
RTP	remdesivir triphosphate
s	singulet (NMR)
S	spike protein
sat.	saturated
SI	selectivity index
sgRNA	subgenomic RNAs
t	triplet (NMR)
TBAI	tetrabutylammonium iodide
TBDMS	*tert*-butyldimethylsilyl
TBDPS	*tert*-butyldiphenylsilyl
TBHP	*tert*-butyl hydroperoxide
TBTH	tributyltin hydride
*t*Bu	*tert*-butyl
TEA	triethylamine

TEAB	triethylammonium bicarbonate
TFA	trifluoroacetic acid
TFAA	trifluoroacetic anhydride
THF	tetrahydrofuran
TLC	thin layer chromatography
TMP	trimethyl phosphate
TMPRSS2	type 2 transmembrane serine protease
TMSCN	trimethylsilyl cyanide
Tri*PPP*ro	a nucleoside triphosphate prodrug
TRS	transcription regulatory sequences
U	uridine
USA	United States of America
USAMRIID	U.S. Army Medical Research Institute of Infectious Diseases
UMP	uridine monophosphate
UTP	uridine triphosphate
WHO	World Health Organization

Abstract

The COVID-19 pandemic, spanning from 2020 to 2022, has clearly shown the urgent need for effective antiviral therapies. Nucleoside analogues have historically been used to combat viral infections by targeting the viral RNA-dependent RNA polymerase (RdRp). Previous studies have demonstrated that the triphosphate form of the nucleoside analogue T-1106 is rapidly incorporated into the SARS-CoV-2 genome by its RdRp, inducing C-to-U and G-to-A transition mutations, and causing an antiviral effect through lethal mutagenesis.

This work aims to synthesize and evaluate modified T-1106-5'-triphosphates for their potential antiviral properties. These modifications are expected to alter the mechanism of polymerase inhibition and to improve *in vivo* efficacy compared to the parent unmodified nucleoside analogue T-1106.

In the first part of the work, a robust route for the synthesis of these modified triphosphates was developed. Through SARS-CoV-2 primer extension assays, in cooperation with the group of B. CANARD, their properties as RdRp substrates were assessed. Notably, 2'-*C*-methyl-T-1106-5'-triphosphate demonstrated efficient incorporation by RdRp, substituting GTP and causing immediate chain termination. However, it remained susceptible to excision by the ExoN proofreading complex.

To enhance stability against ExoN, in the second part of the work, an α-thio modification was introduced. This resulted in 2'-*C*-methyl-T-1106-5'-α-thio-triphosphate, which maintained efficient incorporation by RdRp and exhibited resistance to ExoN-mediated excision.

Based on these results, in the last part of this work, several prodrugs of 2'-*C*-methyl-T-1106-5'-α-thio-triphosphate were synthesized. Preliminary results indicate that prodrugs with an α-thio modification may exhibit enhanced antiviral potency.

Zusammenfassung

Die COVID-19-Pandemie, die sich von 2020 bis 2022 erstreckte, hat deutlich den dringenden Bedarf an wirksamen antiviralen Therapien aufgezeigt. Nucleosidanaloga wurden in der Vergangenheit zur Bekämpfung viraler Infektionen eingesetzt, indem sie die virale RNA-abhängige RNA-Polymerase (RdRp) inhibieren. Frühere Studien haben gezeigt, dass die Triphosphat-Form des Nucleosidanalogons T-1106 effizient in das SARS-CoV-2-Genom durch die SARS-CoV-2 RdRp eingebaut wird, was C-zu-U- und G-zu-A-Transition Mutationen verursacht und einen antiviralen Effekt durch letale Mutagenese erzielt.

Das Ziel dieser Arbeit war es, modifizierte T-1106-5'-Triphosphate zu synthetisieren und ihre potenziellen antiviralen Eigenschaften zu evaluieren. Durch die Einführung dieser Modifikationen sollte der Mechanismus der Polymeraseinhibition verändert und die *in vivo* Wirksamkeit im Vergleich zu unmodifiziertem T-1106 verbessert werden.

Im ersten Teil der Arbeit wurde eine verlässliche Synthesestrategie für diese modifizierten Triphosphate entwickelt. Durch SARS-CoV-2-Primer-Extension-Assays, in Zusammenarbeit mit der Arbeitsgruppe von B. CANARD, wurden ihre Eigenschaften als Substrate für die RdRp bestimmt. Es konnte gezeigt werden, dass 2'-*C*-methyl-T-1106-5'-Triphosphat effizient durch die RdRp in die virale RNA eingebaut wird, anstelle von GTP. Dies führt wiederum zu einem sofortigen Kettenabbruch führt. Allerdings bleibt 2'-*C*-methyl-T-1106-5'-Triphosphat anfällig für den Ausbau aus dem viralen Genom durch den ExoN-Proof Reading Komplex.

Um die Stabilität gegenüber ExoN zu verbessern, wurde im zweiten Teil der Arbeit eine α-thio-Modifikation eingeführt. Es konnte gezeigt werden, dass 2'-*C*-methyl-T-1106-5'-α-thio-Triphosphat weiterhin ein effizientes Substrat für die RdRp darstellt, jedoch stabil gegenüber dem Ausbau aus dem viralen Genom durch ExoN ist.

Basierend auf diesen Ergebnissen wurden im letzten Teil der Arbeit mehrere Prodrugs des 2'-*C*-methyl-T-1106-5'-α-thio-Triphosphats synthetisiert und auf ihre antivirale Aktivität getestet. Erste Ergebnisse deuten darauf hin, dass Prodrugs mit einer α-thio-Modifikation eine erhöhte antivirale Potenz aufweisen könnten.

1. Introduction

The oldest known evidence of a viral infection was obtained from a 150-million-years-old bone of a Jurassic dinosaur, which showed signs of osteitis deformans, which was caused by an infection with Paramyxoviridae.[1] The first known descriptions of humans infected by viruses date back 4,000 years, when Sumerians were able to link the death of humans from rabies to a bite of a rabid animal.[2] The terminology "virus", which derived from the latin word for "venom", was first used by the Roman encyclopaedist AULUS CORNELIUS CELSUS in A.D. 50 as the cause of rabies.[3] Despite the fact that LOUIS PASTEUR was able to develop the rabies vaccine, he was not able to identify the virus under an optical microscope, due to the small size of a virus compared to the size of bacteria.[4] In 1892, DIMITRI IWANOWSKI identified the pathogen causing the tobacco mosaic disease as a virus by pressing infectious plant sap through a bacteria-proof filter.[5,1] Ten years later, FRIEDRICH LOEFFLER and PAUL FROSCH described the pathogen of foot-and-mouth disease as the first animal virus.[5]

In 1900, contagious diseases caused by bacteria were the most common cause of death in the USA, whereas nowadays only a negligible number of people in developed country die from infectious diseases caused by bacteria.[6] This is mainly due to the development of broad-spectrum antibiotics and their widespread application since the 1940s.[7] In contrast to bacterial infections, the most effective way to combat viral infections is with vaccines, which, for example led to the global eradication of smallpox.[8] However, there are still many viruses, such as the human immunodeficiency viruses (HIV), for which no vaccine is available.[9]

Today, the biggest threat is not only the many viruses that exist already but also the numerous unidentified viruses that remain undetected in domestic or wild animals. These viruses can potentially infect humans and have the potential to cause a global pandemic.[10,11] Most of the major pandemics since the beginning of the 20th century have been caused by zoonotic viruses.[10] For example, the Influenza-A-Virus H1N1 virus responsible for the Spanish flu in 1918 was most likely transmitted from swine to humans.[12] The pathogens responsible for the Ebola pandemic in 2014[13] and for the severe acute respiratory syndrome coronavirus 2 (SARS-CoV-2) pandemic in 2020 were most likely also of zoonotic origin.[14]

The probability that a virus will cross the species barrier is further increased by the ongoing growth of the global population, which is expected to continue until the middle of the 21st

century.[15] To feed the growing world population, former rural and forested areas are being converted for agricultural production. This greatly increases the exposure of humans and domesticated animals to wildlife, thereby raising the likelihood of pathogens crossing the species barrier.[16] Additionally, in today's highly connected and globalized world, travellers can act as vectors, spreading pathogens across the globe in a short period of time.[17,18] Another contributing factor is that human activities have already caused global warming of around 1.0°C, and this number is projected to rise in the coming years. Rising global temperatures will allow tropical and subtropical species to expand their ranges, thereby significantly increasing the number of people exposed to certain pathogens.[16,19]

The recent SARS-CoV-2 pandemic, which resulted in millions of deaths, combined with global population growth and the ongoing climate crisis in a highly interconnected world, has shown that the question is not if a currently unknown pathogen will cause another global pandemic, but rather when the next "Disease X" will occur. This underlines the importance of developing new antiviral agents in order to be as well prepared as possible for future outbreaks of novel pathogens.

2. Theory

2.1 Severe acute respiratory syndrome coronavirus 2 (SARS-CoV-2)

Coronaviruses (CoVs) are a genetically diverse family belonging to the order *Nidovirales*. The family is further specified into the subfamily *Orthocoronavirinae*, which consists of four genera: *Alphacoronavirus*, *Betacoronavirus*, *Gammacoronavirus*, and *Deltacoronavirus*. Only alphacoronaviruses and betacoronaviruses are able to infect mammalian species. For example, HCoV-229E and the more recently identified HCoV-HKU1 primarily infect the respiratory tract and are typically associated with mild, seasonal symptoms commonly referred to as the "common cold." In contrast to these members of the coronavirus family, three highly pathogenic CoVs have emerged in the last 20 years: SARS-CoV, Middle East respiratory syndrome coronavirus (MERS-CoV), and SARS-CoV-2.[20,21]

The non-segmented, positive-stranded ribonucleic acid (RNA) genome of CoVs have a size between 26 and 32 kilobases (kb), making it one of the largest among RNA viruses.[22] Approximately two-thirds of the viral RNA, located at the 5' end, comprises the replicase gene, which encodes two open reading frames (ORF1a and ORF1b). Translation of ORF1a and ORF1b produces two polyproteins, pp1a and pp1b, respectively. In the SARS-CoV-2 genome, these polyproteins are subsequently processed into 16 distinct non-structural proteins (NSPs). At the 3´-end, the remaining third of the genome translates into ORFs that encode structural and accessory proteins. There are four vital structural proteins: Spike (S), Envelope (E), Membrane (M), and Nucleocapsid (N) proteins. A fundamental understanding of the viral replication cycle and the involved viral enzymes is crucial for identifying suitable targets for the treatment of SARS-CoV-2 infections.[23,24] A schematic overview of the viral replication cycle is shown in Figure 1.

Entry of coronaviruses into the host cell. The initial step in the viral replication cycle is the fusion of the virus particle with the host cell. The SARS-CoV-2 spike (S) glycoprotein plays a crucial role in this step of the cycle. The spike protein is divided into two parts: S1 and S2.[25] The S1 subunit is exposed on the surface and contains the receptor-binding domain (RBD), which binds to the host cell receptor angiotensin-converting enzyme 2 (ACE2).[26,27] Whereas the S2 subunit mediates the fusion of viral and cellular membranes.[28] An essential step in the fusion process is

the proteolytic cleavage of the coronavirus S protein by host cell proteases. So far, several host proteases have been identified that are used by SARS-CoV-2 to cleave the S protein, among them

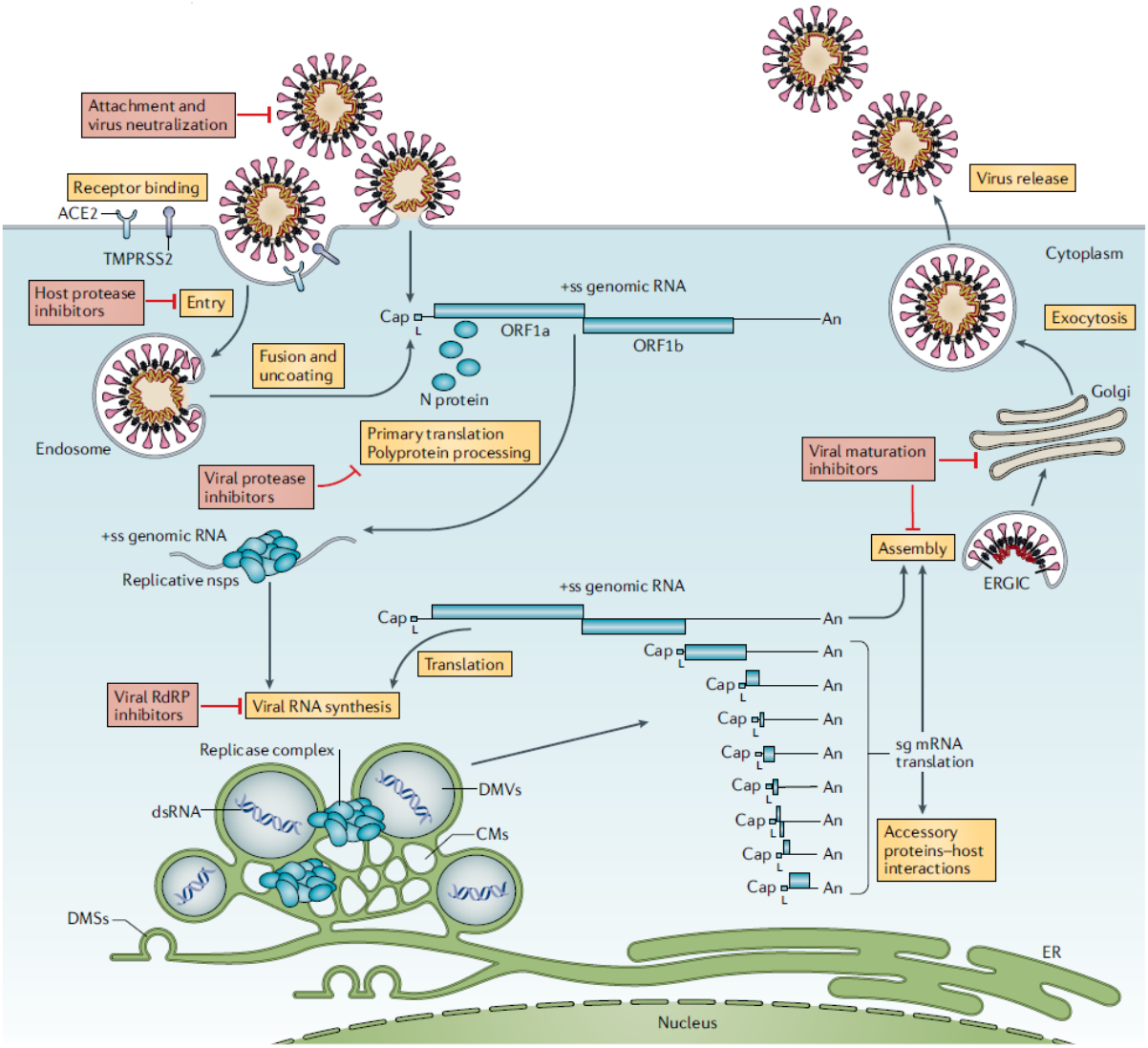

Figure 1: Overview of the SARS-CoV-2 replication cycle: The cycle begins with the binding of the viral spike glycoprotein to the angiotensin-converting enzyme 2 (ACE2) receptor on the host cell surface (step 1). Following membrane fusion, the viral genome is released into the cytoplasm, where the ORF1a and ORF1b regions are translated by host-cell ribosomes (step 2). The resulting polyproteins are processed into non-structural proteins (nsp1–16), which assemble into the RTC (step 3). The ER membranes are then reorganized into DMVs, creating specialized replication organelles (step 4). Inside these DMVs, RTCs mediate the replication of gRNA and the transcription of sgRNAs (step 5). The sgRNAs are translated into structural and accessory proteins required for viral assembly (step 6). Newly synthesized gRNA associates with nucleocapsid (N) protein to form nucleocapsids (step 7). Structural proteins are transported to the ERGIC, where they are incorporated into nucleocapsids to assemble viral particles (step 8). These virus particles are subsequently transported through the Golgi and trans-Golgi network, undergoing further maturation, and finally egress from the cell via lysosomal exocytosis (step 9).[24,29]

type 2 transmembrane serine protease (TMPRSS2),[30,31] cathepsin B,[32] matrix metalloproteinase 16 (MMP16),[33] and furin.[34] A more recent study suggests that kallikrein-5 (KLK5) also plays a crucial role.[35] Due to the important function of host proteases in viral replication, they are a valuable target for chemical inhibition to prevent infection with SARS-CoV-2.[27,36]

Expression of non-structural proteins. After the fusion of the virus particle with the host cell, the 5'-capped SARS-CoV-2 genomic RNA (gRNA) with a poly(A) 3' tail is released into the cytoplasm. After this release into the cytoplasm, the gRNA utilizes host ribosomes, which use the gRNA as messenger RNA (mRNA) for the translation of ORF1a and ORF1b. This translation produces the replicase polyproteins pp1a and pp1b.[37] After proteolytic cleavages performed by the virus-encoded papain-like protease (PL^{pro}), located in nsp3,[38] and the chymotrypsin-like or main protease (M^{pro}), located in nsp5,[39] 16 nsps are released. Following the release of nsp1 into the cytoplasm, it mediates the shutdown of host mRNA translation,[40] whereas nsp2 to nsp16 form the viral RTCs. Responsible for RNA synthesis is the nsp12 RNA-dependent RNA polymerase (RdRp) and its two cofactors, nsp7 and nsp8. In contrast to many other RNA viruses, SARS-CoV-2 possesses proofreading function mediated by the 3' to 5' exonuclease (ExoN) activity of nsp14.[41] Due to their essential role in the formation of RTCs, the viral proteases represent promising targets for antiviral therapies aiming to inhibit viral replication.[24]

Formation of replication organelles. Like all other coronaviruses, SARS-CoV-2 utilizes intracellular membranes of host cells to establish replication organelles.[42,43] These organelles function as a protected environment for RNA synthesis by concentrating necessary building blocks such as metabolites, cofactors, and viral enzymes, while simultaneously shielding viral RNA from the host immune system. These replication organelles, known as double-membrane vesicles (DMVs), are formed from reorganized membranes of the endoplasmic reticulum (ER) and remain connected to the ER via thin double-membrane connectors.[42,43] The formation of DMVs is mediated by nsp3, nsp4, and nsp6.[44]

The replication and transcription complex. The RTC, which is responsible for the synthesis of viral RNA, is assembled inside the DMVs from all NSPs except nsp1. At the centre of the complex are nsp12, a nsp7–nsp8 heterodimer, and an additional nsp8. Although the RdRp domain is contained in nsp12, nsp7 and nsp8 serve as essential cofactors that enhance RdRp activity. It is assumed that nsp8 stabilizes the newly synthesized RNA strand during synthesis and acts as a

scaffold for various viral proteins.[45–47] Nsp13 functions as a viral helicase that unwinds the viral RNA, with two nsp13 molecules positioned at the centre of the RTC during elongation.[48] During RNA synthesis, one nsp13 binds to the 5'-end of the template RNA and guides it to the RTC.[22,49] These nsp13 molecules prevent backtracking during elongation, however, upon incorporation of a mismatched nucleotide, one nsp13 relocates and forces the RdRp to move backwards along the newly synthesized RNA strand.[50] This backtracking may allow the ExoN access to the misincorporated nucleotide at the 3'-end of the nascent RNA strand, which would otherwise be blocked by the RdRp.[51] The RdRp of SARS-CoV-2 is the fastest viral RdRp known so far, which may be necessary to efficiently synthesize the large viral genome. This high replication speed results in an elevated error rate during elongation, which allows the virus to adapt more rapidly under selective pressure but also leads to lower fidelity.[52] To maintain genomic stability and replication fidelity, SARS-CoV-2, like other coronaviruses, requires a proofreading function. This proofreading activity is provided by the 3'- to 5'-exonuclease domain in nsp14, which forms a complex with nsp10 acting as a cofactor.[53,54]

Viral RNA synthesis. After the assembly of the RTC, genomic replication starts with the synthesis of full-length, negative-sense copies of the viral genome, for which the viral gRNA is used as a template. The negative-sense gRNA functions as a template for the synthesis of new positive-sense gRNA, which is used for further translation to generate more nsps and RTCs, or is enveloped into new virions.[24,29] A characteristic feature of coronaviruses is the discontinuous viral transcription process, which generates a set of nested subgenomic RNAs (sgRNAs). During the synthesis of negative-sense RNA, the RTC interrupts transcription after encountering transcription regulatory sequences (TRSs), which are located upstream of most ORFs that encode structural and accessory genes in the 3´-one-third of the viral genome. This process results in the formation of a nested set of negative-sense sgRNAs. These sgRNAs function as templates for the synthesis of positive-sense sgRNAs, which are used as templates to translate structural and accessory proteins.[55,56] The importance of the RTC for the replication of the viral genome, as well as for the transcription of sgRNAs, makes nsp12, which represents the centre of the RTC, one of the most promising targets for antiviral agents.

Virion assembly and virus release. The assembly of new virions may be initiated directly after the release of gRNA from the DMVs, by forming complexes with the N protein. At the ER-to-Golgi intermediate compartment (ERGIC), the N protein from the previously formed condensates

interacts with the cytoplasmic tail of the M protein.[57,58] The M protein plays a key role in virion assembly by interacting with the other structural proteins. It coordinates with the E protein, which directs the S protein to the sites of virion assembly and mediates their maturation[59,60]. The E protein acts as a viroporin, forming homopentameric, calcium-selective ion channels in the viral membrane.[61] Subsequently, like other betacoronaviruses, SARS-CoV-2 utilizes ADP-ribosylation factor-like protein 8B (Arl8b)-dependent lysosomal exocytosis to exit the cell into the extracellular environment.[62,63]

2.2 Treatments for SARS-CoV-2

So far, the most effective strategy to prevent infection with SARS-CoV-2 has been large-scale prophylactic vaccination. To date, four different vaccines have been approved for use in the European Union. Bimervax and Nuvaxovid are recombinant protein vaccines. Bimervax contains a recombinant RBD fusion dimer of the S protein as its active antigen. Following vaccination, this antigen induces an immune response and the production of neutralising antibodies. These antibodies target the RBD of SARS-CoV-2, blocking its interaction with the ACE2 receptor and thereby preventing membrane fusion and subsequent viral entry.[64] Nuvaxovid acts similarly, but employs the full-length recombinant spike protein, stabilised in its prefusion conformation, as its antigen.[65]

Comirnaty and Spikevax are both mRNA vaccines, marking the ground-breaking first use of this cutting-edge technology in widespread immunization. They deliver messenger RNA encoding various forms of the spike protein, including different variants. Once the mRNA is translated within host cells, the expressed spike protein is recognised as a foreign antigen, which stimulates both T-cell and B-cell responses. This leads to the generation of neutralising antibodies, contributing to robust protection against future SARS-CoV-2 infection.[66,67]

Although SARS-CoV-2 vaccines have been highly successful in mitigating the impact of the global pandemic, SARS-CoV-2 remains a significant public health concern and continues to circulate worldwide. This ongoing transmission is due to several factors, including vaccine shortages, public hesitancy towards vaccination, reduced vaccine efficacy in immunosuppressed individuals, and the ongoing emergence of new viral variants.[68] As of 2025, it is evident that, unlike MERS or SARS, SARS-CoV-2 will not be eradicated and has instead become established as a seasonal endemic virus. These persistent infections may facilitate the appearance of further mutations,

potentially leading to reduced vaccine effectiveness in the future.[69,70] For these reasons, the search for effective drugs against SARS-CoV-2 remains important despite the availability of efficient vaccines.[68]

Each of the 29 proteins encoded by the SARS-CoV genome represents a potential drug target. Among these, the spike protein, proteases, and the RNA-dependent RNA polymerase are particularly crucial for the viral replication cycle and have therefore been identified as especially promising candidates for drug development. In recent years, numerous structural studies of these viral proteins have established a strong foundation for the development of new antiviral drugs.[71,72]

2.2.1 RBD-targeting antibodies

As mentioned above, the S protein plays a key role in mediating the fusion of the viral and host cell membranes. One of the key steps in this process is the binding of the RBD within the S1 subunit to the ACE2 receptor. Binding to ACE2 stabilizes the RBD in the "up" conformation,[71] which triggers the cleavage of the S protein by human proteases (Chapter 2.1). The other subunit of S1 is the N-terminal domain (NTD) (Figure 2).

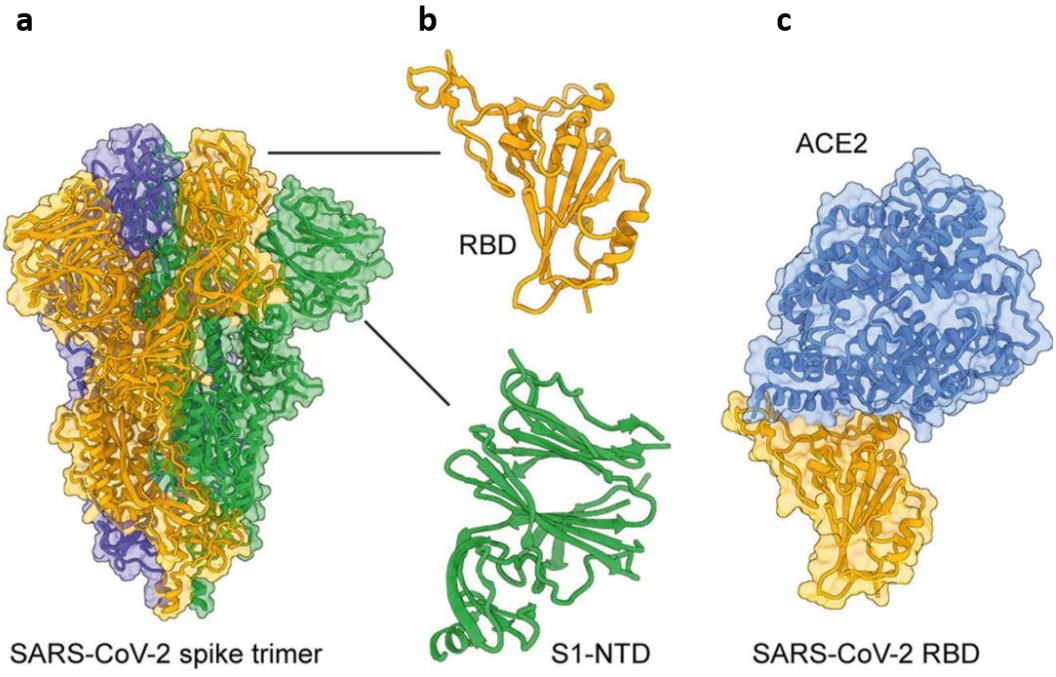

Figure 2: a| Cryo-EM structure of the SARS-CoV-2 S protein trimer. **b**| RBD and NTD. **c**| RBD in complex with human ACE2.[73]

In animal models, it has been shown that naturally occurring antibodies are capable of binding to the S protein. Most of these antibodies target the RBD, leading to neutralization of the S protein. Based on their binding sites, they are classified into four distinct classes[74]. These neutralizing antibodies (nAbs) are human monoclonal antibodies (mAbs) derived from patients who have successfully recovered from SARS-CoV-2 infection[71]. Antibodies that bind to the NTD subunit are not discussed in this work.

Class 1 nAbs bind to the RBM in the RBD only in the "up" conformation (Figure 3)[74]. These antibodies are able to neutralize the S protein by preventing its binding to the ACE2 receptor.[75,76] Members of this class of nAbs that have received emergency use authorization (EUA) from the US Food and Drug Administration (FDA) include AZD8895[77] (tixagevimab), P2C-1F11[78] (amubarvimab), LY-CoV016[79] (etesevimab), and REGN-10933[80] (casirivimab). However, most class 1 antibodies show high neutralizing activity only against wild-type SARS-CoV-2, and lose their neutralizing capability against variants such as Beta, Gamma, and Omicron, as a result of mutations in the S protein.[81]

Similar to class 1 nAbs, class 2 nAbs bind to the RBM within the RBD, blocking its interaction with ACE2 and thereby neutralizing the S protein through the same mechanism. However, unlike class 1, class 2 antibodies can bind to the RBD in both the "up" and "down" conformations of the S protein.[74] Notable members of this class include CT-P59[82] (regdanvimab), which has been approved in the European Union and South Korea. AZD1061 (cilgavimab) and LY-CoV555[83] (bamlanivimab) have received emergency use authorization for the treatment of mild infections in high-risk patients.[71] Like class 1 nAbs, class 2 nAbs lose much of their activity against later-emerging SARS-CoV-2 variants due to mutations in the S protein.[84,85]

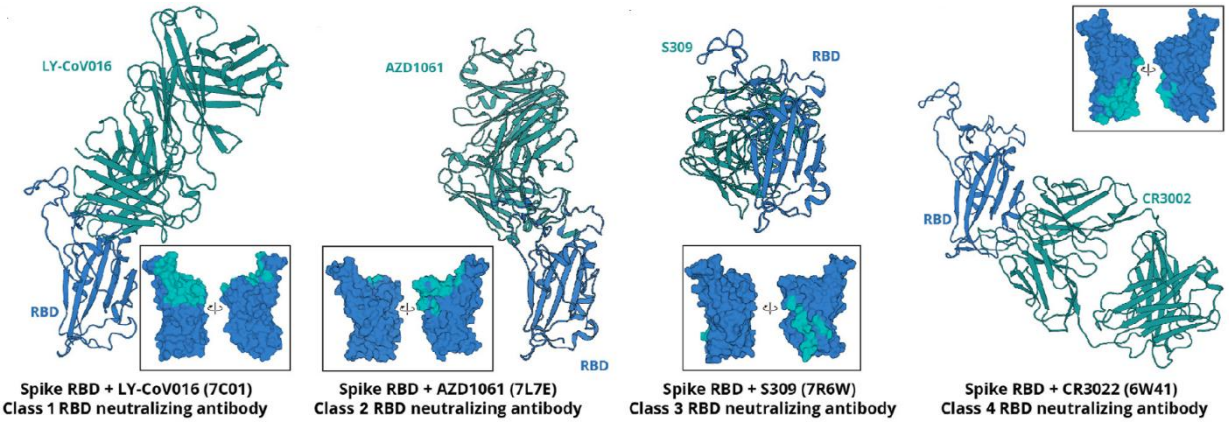

Figure 3: Structure of RBD complexes with different class 1,2,3, and 4 nAbs[71].

Class 3 nAbs bind a conserved region on the RBD outside of the ACE2 binding region in both the "up" and "down" conformations of the RBD.[74] Not all class 3 nAbs share the same neutralizing mechanism. For example, the neutralization mechanism of S309[86] (sotrovimab) does not rely on directly blocking the binding of the RBD to the ACE2 receptor, but instead on inducing steric hindrance and cross-linking of adjacent RBDs.[71,87,86] The advantage of class 3 nAbs over class 1 and 2 nAbs is their ability to bind to highly conserved epitopes outside of the rapidly evolving ACE2 binding site.[71] The epitopes recognized by S309 belong to the most highly conserved regions in the SARS-CoV and SARS-CoV-2 RBDs, which enables S309 to broadly neutralize sarbecoviruses, including all known SARS-CoV-2 variants.[86] The S309-derived antibodies VIR-7831 and VIR-7832 received EUA for the treatment of high-risk patients with mild symptoms.[71]

In contrast to S309, LY-CoV1404[88] (bebtelovimab) binds to an RBD epitope that overlaps with the ACE2 binding site, and neutralization is achieved by preventing the RBD from binding to ACE2.[88] However, although the bound epitope is structurally closer to epitopes that are bound by other class 2 nAbs, LY-CoV1404 still belongs to class 3 and not class 2.[88] The epitope LY-CoV1404 binds to a region of the S protein that is conserved in SARS-CoV-2 across its variants. Therefore, LY-CoV1404 is able to neutralize all SARS-CoV-2 variants.[88] Notably, only small changes in neutralization potency were observed against Omicron variants.[89] LY-CoV1404 was the only antibody in clinical trials that maintained neutralization potency against Omicron sub lineages.[88–90]

Class 4 nAbs recognize an epitope of the RBD that is highly conserved, which does not directly prevent the RBD from binding to the ACE2 receptor. Instead, they bind to an epitope that is only accessible when at least two RBDs are in the "up" conformation. The binding of these nAbs leads to an unstable state of the S protein, which subsequently prevents the fusion of the viral and host cell membranes. The most intensively studied antibody in this class is CR3022, which, together with its derivatives, is part of preclinical investigations for therapeutic use.

Overall, it can be said that class 1 and class 2 nAbs, which target the ACE2 receptor binding site in the RBD, will most likely lose their neutralizing abilities with the emergence of SARS-CoV-2 variants that have mutations in the RBM. In contrast, class 3 and class 4 nAbs are much more promising candidates for the development of new broad-spectrum antibodies against coronavirus family due to their ability to bind to highly conserved regions of the RBD. However,

their mechanisms of neutralization, in contrast to class 1 and 2 nAbs, are not fully understood and require further investigation.

2.2.2 Inhibitors of SARS-CoV-2 proteases

Viral proteases have been successfully targeted in the past to treat viral infections caused by the HIV and hepatitis C virus (HCV). Viral proteases also play a crucial role in the replication cycle of SARS-CoV-2. After the release of the viral gRNA into the cytoplasm of the host cell, translation of ORF1a and ORF1b produces the polyproteins pp1a and pp1b. The SARS-CoV-2 main protease, M^{pro}, is responsible for the cleavage of these polyproteins at more than 11 sites, which releases several nsps that are crucial for further viral replication (Chapter 2.1). In addition to processing viral polyproteins, M^{pro} is involved in the cleavage of several host proteins that are important for antiviral signalling pathways. For example, melanoma-associated antigen D2 (MAGED2) suppresses viral genome replication by binding to the viral nucleocapsid protein.[91] Therefore, inhibition of M^{pro} should disrupt viral replication and promote the host immune response. For these reasons, SARS-CoV-2 proteases represent promising targets for the treatment of COVID-19.[92] An additional advantage of targeting M^{pro} lies in its high degree of genetic conservation among coronaviruses, suggesting that M^{pro} inhibitors could serve as effective broad-spectrum antivirals against various coronavirus species.[93]

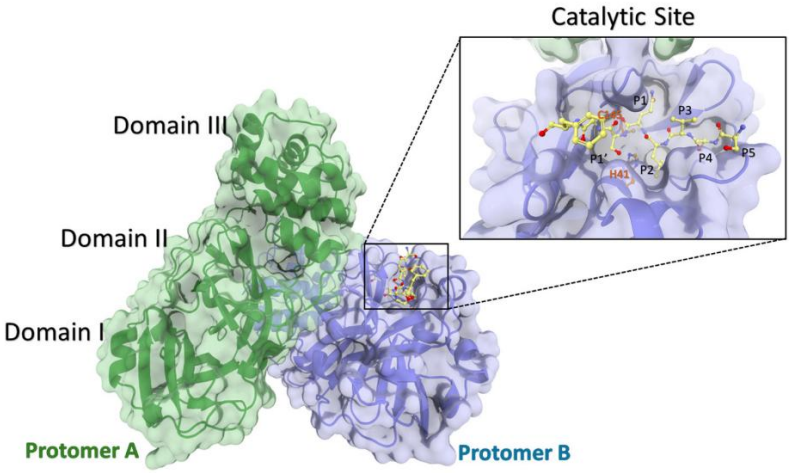

Figure 4: Structure of the M^{pro} homodimer, highlighting the catalytic domain H41 and C145.[94]

M^{pro} is a homodimer composed of two protomers A and B, which acts as a cysteine protease. Each of the protomers can be divided into three domains. The catalytic region consists of domain I (residues 8–101) and II (residues 102–184). In the cleft between these two domains the catalytic H41-C145 dyad and the substrate binding site are located. Domain III (residues 201–306)

binds to domain II and is responsible for the formation of the dimer, which is crucial for the catalytic activity (Figure 4).[95,96,94]

Inhibitors that target the active site of M^{pro} can be divided into two classes: peptidomimetics and small molecules. Peptidomimetics are synthetic compounds that mimic peptides through their molecular structure. By mimicking peptides, they provide high specificity and selectivity for targets, fewer off-target effects, and reduced toxicity. Compared to natural peptides, peptidomimetics also offer enhanced metabolic stability through chemical modifications. However, they frequently suffer from poor oral bioavailability and limited membrane permeability, compared to small molecules.[94] One of the most promising members of this class is Nirmatrelvir **1**, which received approval by the FDA in 2023. Leritrelvir **2**, another peptidomimetic M^{pro} inhibitor, has also been approved by the National Medical Products Administration (NMPA) in China.[71]

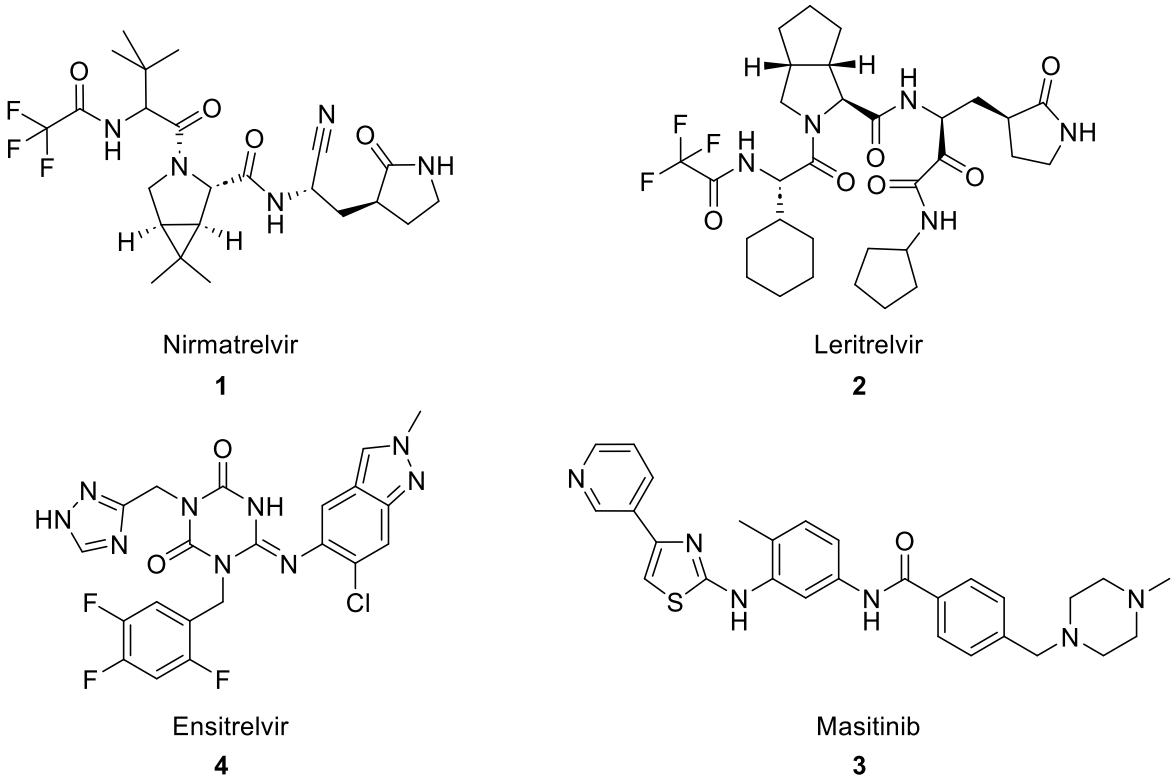

Figure 5: Structures of the different M^{pro} inhibitors.

The second class, small molecule inhibitors, generally exhibit better membrane permeability and oral bioavailability than peptidomimetics. Nevertheless, they may face challenges related to metabolic stability, which can necessitate more frequent dosing due to their shorter half-lives.

Additionally, small molecules tend to have a higher risk of off-target effects and toxicity, primarily due to lower selectivity for the target enzyme. This class of inhibitors is also more likely to contribute to the development of drug resistance.[94] One of the most prominent members of this class of M^{pro} inhibitors is Ensitrelvir **3**, which was developed through virtual screening followed by structure-based optimization. Ensitrelvir **3** has achieved approval for clinical use in Japan.[71,97] Masitinib **4** is another promising M^{pro} inhibitors that is approved for the treatment of mast cell tumours in dogs, and was discovered through the screening of 1900 clinically safe drugs against human coronavirus OC43.[71,98]

2.2.3 Inhibitors of SARS-CoV-2 RdRp

As described above, the nsp7-nsp8-nsp12 holo RdRp complex is situated at the centre of the RTC of SARS-CoV-2 (Chapter 2.1). The RdRp catalyses the incorporation of nucleoside triphosphates (NTPs) into the newly synthesized product RNA (pRNA) using a template RNA strand. Due to its essential role in the viral replication cycle, RdRp represents a particularly attractive target for antiviral drug development.[71]

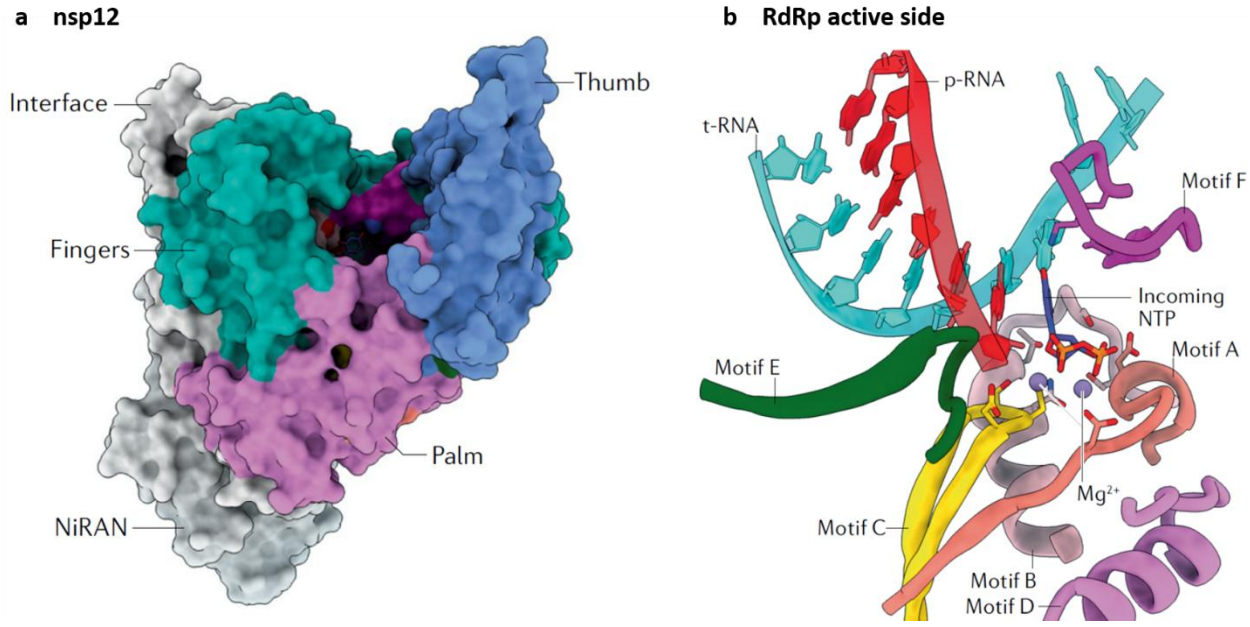

Figure 6: a| Structure of nsp12. **b**| View of the RdRp active site.

Within the RdRp complex, nsp12 serves as the catalytic subunit responsible for RNA synthesis.[99] Nsp12 consists of three major domains: a N-terminal nidovirus RdRp-associated nucleotidyltransferase (NiRAN) domain (residues 1–250), an interface domain connecting the NiRAN and RdRp regions (residues 251–398), and the core RdRp domain (residues 399–

932).[100,101] The architecture of the core RdRp domain resembles a hollow hand, which is reflected in the naming of its three subdomains: fingers, palm, and thumb. The active site of the core RdRp domain can be further subdivided into seven highly conserved functional motifs, labelled A through G, which are characteristic of positive-stranded RNA viruses (Figure 6).[68,102]

The role of these motifs in RNA synthesis has been resolved through X-ray crystallography studies of the RdRp of HCV, owing to their conserved structure among positive-stranded RNA viruses.[103,104] In the initial step, positively charged Lys and Arg residues in motifs D and F recognize the incoming NTP via charge–charge interactions. Subsequently, the NTP diffuses through the entry channel to reach the active site.[105] Through interactions with residues in motifs A, B, and F, the NTP is positioned into the binding site. Specifically, the NTP forms stabilizing hydrogen bonds with motifs A and B, while motif F helps to establish a Watson–Crick base pair with the template nucleotide.[105,106] If the incoming NTP is correctly positioned inside the active site, the two catalytic Mg^{2+} ions are stabilized through interactions with the α and β phosphates of the NTP, the 3’-hydroxy group of the pRNA, and the catalytic Asp residues in motif C. Subsequently, interactions involving motifs A and B with the base promote the closure of the active site, thereby facilitating the nucleophilic attack of the deprotonated 3’-hydroxy group on the α-phosphorus atom of the incoming NTP. This reaction results in the elongation of the pRNA by one nucleotide and the release of pyrophosphate (Figure 6).[68,107]

A wide range of different non-natural nucleoside analogues have been evaluated for their ability to inhibit the RdRp activity of the SARS-CoV-2 RTC. These nucleoside analogues exhibit different mechanisms of action with respect to the inhibition of RdRp. The most prominent nucleoside analogue used for the treatment of COVID-19 is Remdesivir **5**, which received approval from the FDA in 2020. Remdesivir **5** was originally developed in an effort to find a broad-spectrum antiviral effective against RNA viruses in general, and the EBOV specifically, in response to the EBOV outbreak in 2014. This research was conducted as a collaboration between Gilead Sciences, the U.S. Centers for Disease Control and Prevention (CDC), and the U.S. Army Medical Research Institute of Infectious Diseases (USAMRIID).[108]

Remdesivir **5** is a phosphoramidate monophosphate prodrug of the 1´-cyano-substituted adenosine C-nucleoside GS-441524. The monophosphate prodrug is able to penetrate cell membranes and subsequently releases GS-441524-5´-monophosphate inside the cell, which is

then further phosphorylated by host cell kinases to form the antiviral active triphosphate, Remdesivir nucleoside-5´-triphosphate (RTP) **6** (Chapter 2.3). RTP **6** competes with adenosine-5´-triphosphate (ATP) during RNA synthesis and can be incorporated into the pRNA by RdRp. Incorporation of RTP **6** does not lead to immediate chain termination. Instead, the 3´-OH group of RTP **6** allows the RdRp to continue RNA synthesis. However, when the incorporated RTP **6** reaches position i+3, a steric clash between the 1´-cyano group and S861 of nsp12 prevents further elongation of the RNA strand by the RdRp. This mechanism of action is called "delayed chain termination".[47,109]

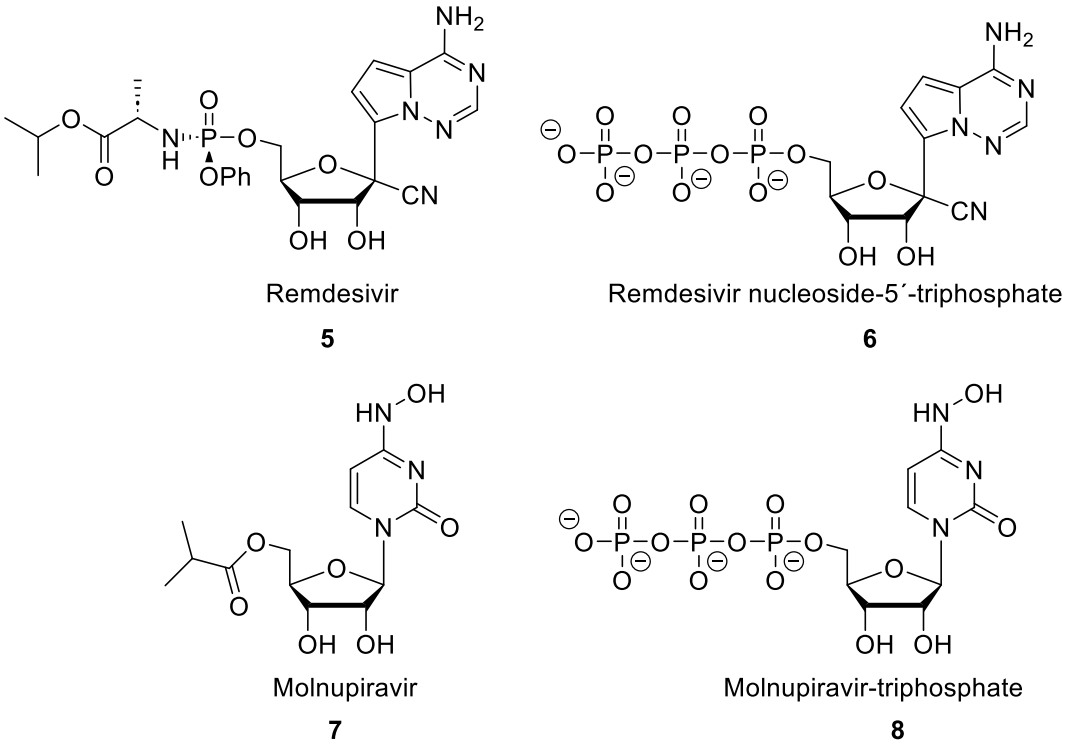

Figure 7: Structures of Remdesivir **5** and Molnupiravir **7** and the respective triphosphates **6** and **8**.

Another prominent nucleoside analogue used for the treatment of infections with SARS-CoV-2 is Molnupiravir **7**, which received EUA from the FDA in 2021.[110] Molnupiravir **7** is a prodrug that is intracellularly metabolized into its active form, β-D-N^4-hydroxycytidine-5´-triphosphate (MTP) **8**.[111] MTP **8** can be used by the SARS-CoV-2 RdRp as a substrate in place of uridine-5´-triphosphate (UTP) or cytidine-5´-triphosphate (CTP). The incorporation of MTP into the viral RNA strand does not lead to immediate or delayed chain termination. Instead, when the RdRp synthesizes -gRNA and -sgRNA using +gRNA as a template, M is frequently incorporated instead of U or C. This is possible because MTP exists in different tautomeric forms that allow base pairing

with both G and A. In the subsequent step, RNA strands containing M are used as templates for the synthesis of +gRNA and +sgRNA. The presence of M in the template strand induces such a high degree of mutation that too much genomic information is lost to produce functional RNA products, which leads to the termination of viral replication. This mechanism of action is referred to as lethal mutagenesis or error catastrophe.[111,112] The SARS-CoV-2 RdRp possesses high selectivity for Remdesivir **5** and Molnupiravir **7**, as such, their incorporation does not affect the initial round of RNA synthesis. This limits their recognition and excision by the ExoN.[71,112]

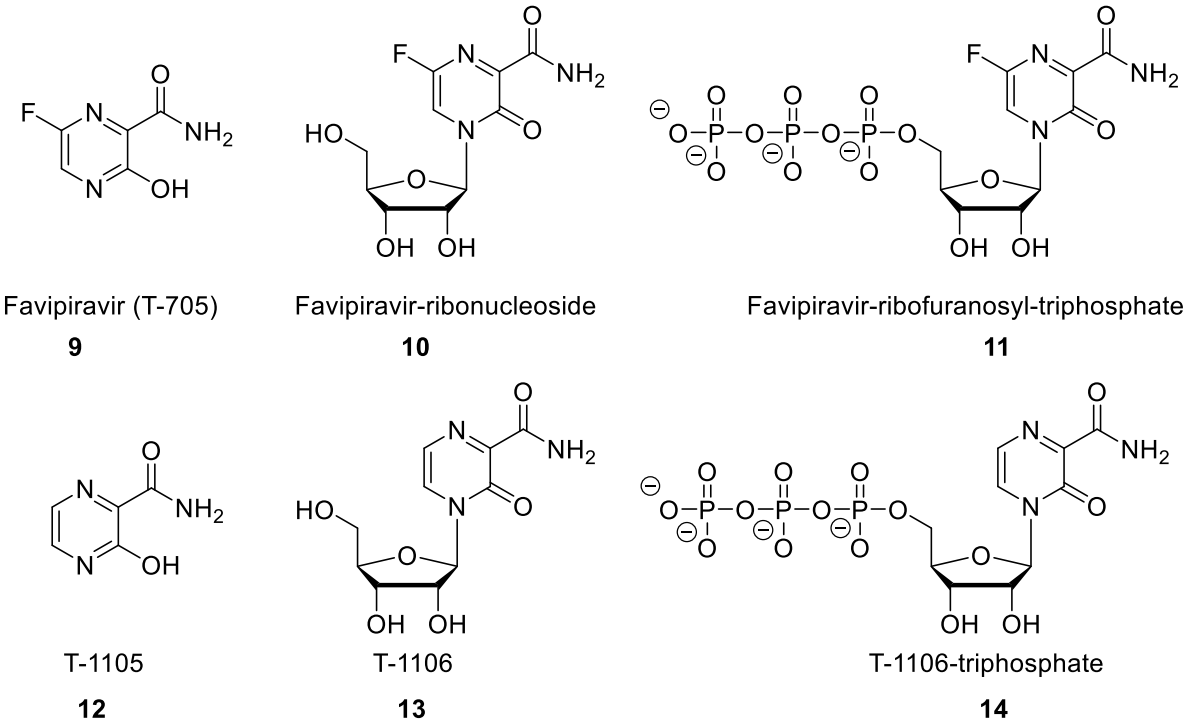

Figure 8: Structures of Favipiravir analogues, their nucleosides as well as their nucleoside triphosphates.

Favipiravir, also known as T-705 **9**, is a nucleoside analogue originally developed by Toyama Chemical Co. Ltd. for the treatment of influenza, receiving clinical approval in Japan in 2014.[113] In addition to influenza[113], Favipiravir **9** exhibits broad-spectrum activity against various RNA viruses, including Ebola virus (EBOV)[114] and Lassa virus (LASV).[115] It functions as a prodrug that is metabolized by the host enzyme hypoxanthine guanine phosphoribosyltransferase (HGPRT) to generate Favipiravir-ribofuranosyl-5'-monophosphate (FRMP) **10**, which is subsequently phosphorylated to the active triphosphate form, Favipiravir-ribofuranosyl-5'-triphosphate (FRTP) **11**.[116] Favipiravir exerts its antiviral effect through a mechanism similar to that of Molnupiravir **7**. However, unlike Molnupiravir **7**, FRMP **11** is incorporated into viral RNA by the SARS-CoV-2 RdRp as a substitute for ATP or guanosine-5´-triphosphate (GTP), owing to its ability to form

Watson–Crick base pairs with U and C (Figure 9). This misincorporation leads to lethal mutagenesis, ultimately preventing further viral replication.[117]

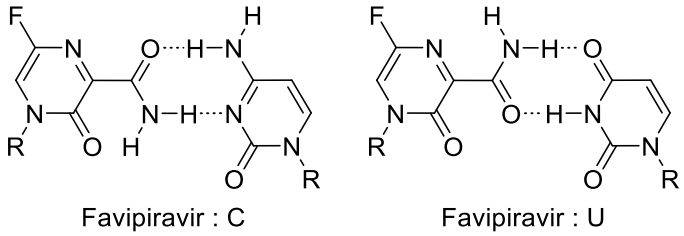

Figure 9: Base pairing of Favipiravir **9** with cytosine and uridine.

Recent studies indicate that the non-fluorinated analogue of Favipiravir, T-1105 **12**, offers several advantages. Research from the group of C. MEIER has shown that Favipiravir-ribonucleoside **10** is challenging to handle due to its chemical instability, which complicates phosphorylation and subsequent modifications.[118] In contrast, T-1106 **13** displays significantly greater stability, enabling reliable synthesis of both phosphorylated and ribose-modified T-1106 derivatives.[119] Furthermore, removal of the fluorine atom from the pyrazine ring not only enhances chemical stability but also increases antiviral potency. For example, T-1105 **12** exhibits fivefold higher activity against influenza compared to Favipiravir **9**.[120] Additionally, T-1106-5'-triphosphate (T-1106-TP) **14** has been shown to be incorporated more efficiently by the SARS-CoV-2 RdRp into viral RNA than FRTP **11**.[52]

2.3 Prodrug systems for nucleoside analogues

In Chapter 2.2, it was demonstrated that, following cellular uptake, nucleoside analogues must be phosphorylated by host cell enzymes to their corresponding triphosphate forms, which represent the pharmacologically active species. Each phosphorylation step may present a potential “bottle-neck”, as nucleoside analogues are not the natural substrates for human kinases (Figure 10). This can lead to inefficient phosphorylation and, consequently, reduced levels of the active compound. Direct administration of the active triphosphates is not feasible, however, due to their high negative charge, which prevents their passage through the lipophilic cell membrane. To overcome this limitation, several prodrug strategies have been developed.[121]

Prodrugs are pharmacologically inactive derivatives designed to release the active compound at the target site, most commonly through chemical or enzymatic cleavage. By converting nucleoside analogues into prodrugs that either lack negative charges or possess charges masked

by lipophilic groups, cellular uptake is facilitated. Once inside the cell, these prodrugs can release the phosphorylated active species, thereby significantly enhancing the bioavailability of the active compound.[121] Importantly, the cleaved masking units must not exhibit cytotoxic effects. Several approaches have been established to enable the intracellular delivery of mono-, di-, and triphosphates. Beyond improving bioavailability, prodrug systems can also enhance the physicochemical and pharmacokinetic properties of nucleoside analogues, including solubility, chemical stability, first-pass metabolism, and toxicity profiles.[122–124]

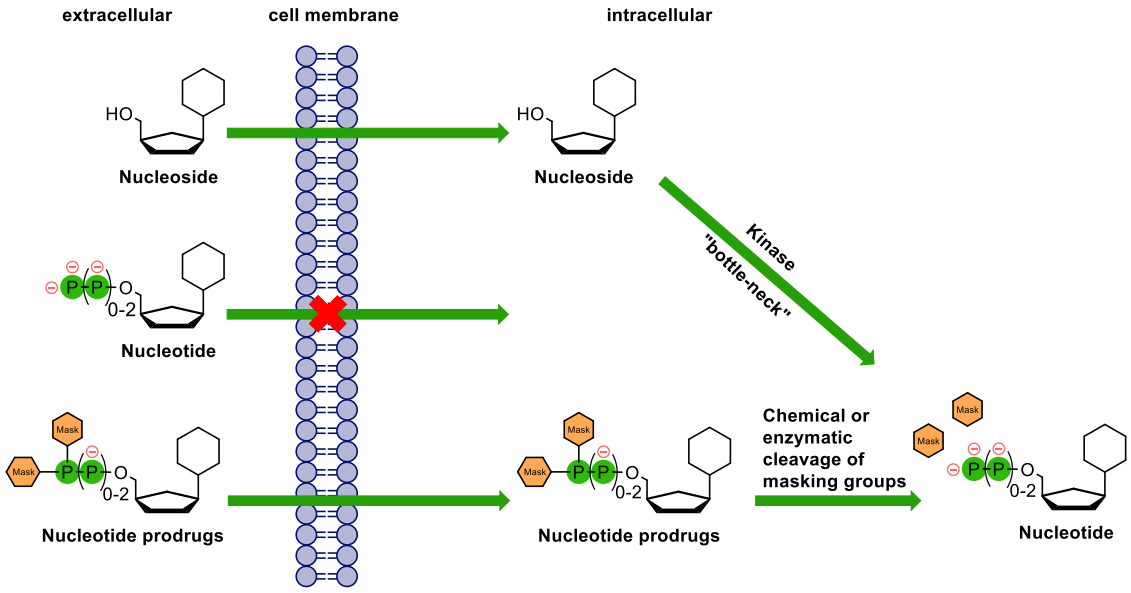

Figure 10: Cell-membrane diffusion and metabolic pathway of nucleosides and nucleotide prodrugs.

The ProTide (**Pro**drug + nucleo**tide**) strategy developed by McGuigan *et al.* in 1992 is one of the most commonly used prodrug strategies at the moment. This is due to the fact that ProTides are relatively easy to prepare, and it has been shown that they significantly increase the potency of their parent nucleotides. Another factor that has boosted the popularity of this prodrug system is the fact that numerous FDA-approved drugs rely on it. Examples include Remdesivir **5** (SARS-CoV-2), Sofosbuvir (hepatitis C), and Tenofovir alafenamide (hepatitis B, HIV).[125]

ProTides are phosphoramidates, where the hydroxyl groups of the monophosphate are masked by an aromatic group and an amino acid ester moiety. This lipophilic masking enables ProTides to permeate the cell membrane. Once inside the cell, the monophosphate is released following the metabolic cleavage of the masking units. The mechanism of the cleavage is shown in Figure 11. In the first step, the amino acid ester is cleaved by esterases. Cathepsin A and carboxylesterase 1 (CES1) have been identified as the enzymes primarily responsible for ester

cleavage.[126,127] Extensive research by MCGUIGAN has shown that the structure of the ester moiety has a significant impact on the efficiency of the cleavage, which correlates with biological activity.[128] Another factor that influences biological activity is the lipophilicity of the ester moiety, as it affects cellular uptake.[128] Additionally, beyond the influence of the ester moiety, the aryl motif also impacts the lipophilicity of the ProTide. The most commonly used aryl moieties are the phenyl and naphthalene groups. By introducing electron-withdrawing substitutions on these aryl groups, biological activity can be increased, whereas electron-donating groups tend to have a negative impact on biological activity.[129] It has also been shown that the structure of the amino acid significantly influences the efficiency of ester hydrolysis.[130] For example, cathepsin A is unable to hydrolyse ProTides with amino acids like L-valine or L-isoleucine due to their branched structures.[131]

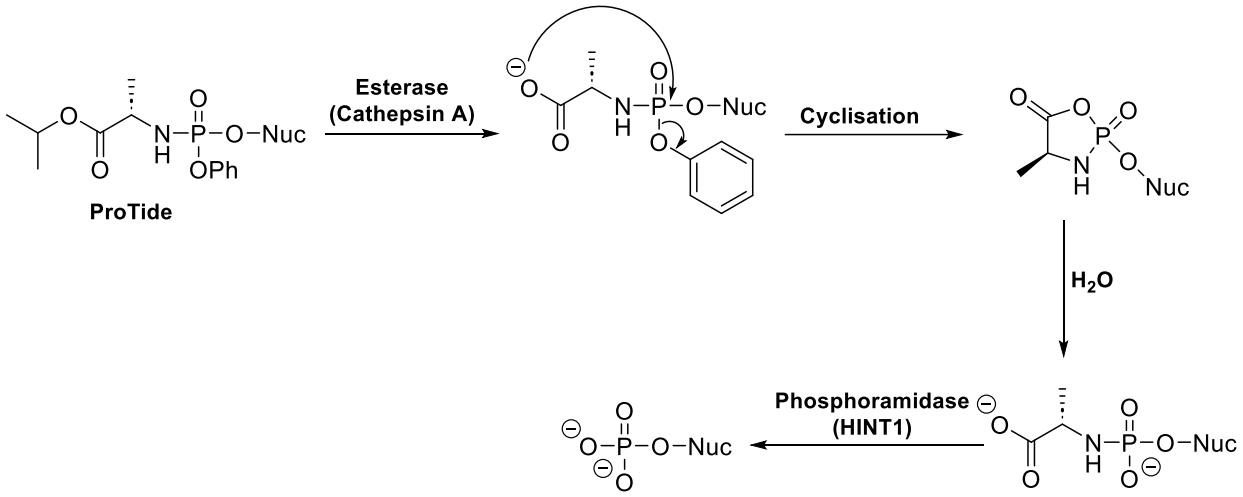

Figure 11: Mechanism of the metabolic cleavage of ProTides.[125]

Ester cleavage leads to the formation of a carboxylate, which subsequently undergoes an intramolecular nucleophilic attack on the phosphate group. After the aryl leaving group is cleaved, a five-membered anhydride ring is formed.[125] In the following step, a water molecule nucleophilically attacks either the phosphate or the carbonyl carbon, both of which lead to ring opening and the formation of a phosphoramidate intermediate. In the final step, the monophosphate is released upon cleavage of the P–N bond. The enzyme responsible for this cleavage is the histidine triad nucleotide-binding protein 1 (HINT1), which functions as a phosphoramidase (Figure 11).[125]

In 1993, THOMSON *et al.* developed the acyloxybenzyl (AB) and bis(acyloxybenzyl) (BAB) prodrug concepts by masking azidothymidine-5´-monophosphate (AZT-MP) with two acyloxybenzyl moieties.[132] Once the lipophilic masked monophosphate passes through the cell membrane, the acyl group is cleaved off by host cell esterases. The resulting electron-donating alcoholate undergoes a 1,6-elimination, leading to the cleavage of the benzyl moiety and the release of the monophosphate (Figure 11).[132]

This concept was adopted by the group of C.MEIER in 2008 for the development of masked diphosphate prodrugs. The coupling of bis(acyloxybenzyl) phosphoramidates with NMPs yielded upon oxidation the desired BAB diphosphate prodrugs (Di*PP*ro). Due to the high lipophilicity of the acyl residues, it was possible to mask the remaining negative charge of the diphosphate, enabling the Di*PP*ro compounds to cross the cell membrane and release the corresponding diphosphate inside the cell.[133]

This breakthrough paved the way for the development of BAB triphosphate prodrugs (Tri*PPP*ro).[134,135] Tri*PPP*ro compounds can be synthesized in the same way as Di*PP*ro, by coupling a BAB phosphoramidate with an NDP followed by oxidation of the γ-phosphorus. However, this strategy faces the challenge of synthesizing the corresponding NDPs, which are significantly more complex to prepare compared to NMPs. As a result, an alternative synthetic approach for Tri*PPP*ro compounds was developed. In the first step, a BAB-*H*-phosphonate is activated using *N*-chlorosuccinimide (NCS), transforming it into the corresponding masked diphosphate through reaction with tetrabutylammonium phosphate. After activating this diphosphate by reacting it with trifluoroacetic anhydride and 1-methylimidazole, subsequent coupling with NMPs yields the desired TriPPPro compounds. (Figure 12).[134,135]

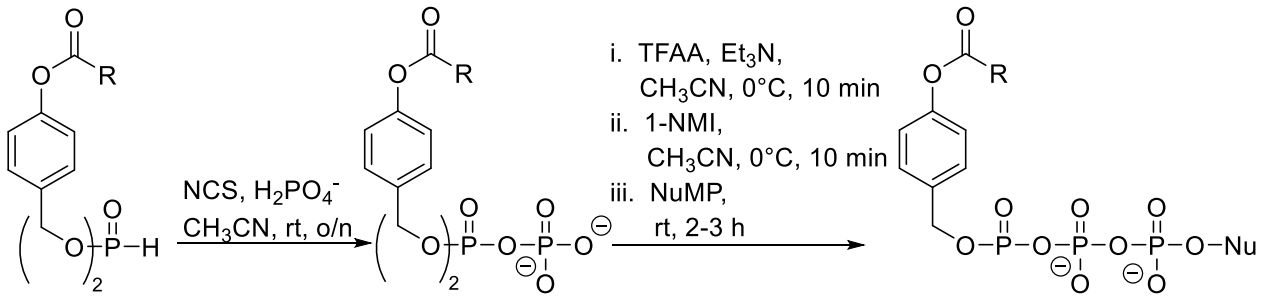

Figure 12: General synthesis of Tri*PPP*ro compounds via *H*-phosphonate route. [134,135]

3. Objectives

In a previous study conducted by our research group in collaboration with the research group of B. CANARD, it could be demonstrated that the SARS-CoV-2 RdRp readily incorporates T-1106-TP **14** into the viral RNA in place of guanosine[52]. This study indicates that T-1106-TP **14** primarily functions as a mutagen rather than a chain terminator. The ultimate goal of the current work is to develop a T-1106-derived RdRp inhibitor that acts as an immediate chain terminator, which may enhance the antiviral properties of these compounds compared to T-1106.

To achieve this objective, the first aim of this thesis was to synthesize a library of T-1106-derived 5'-triphosphates for use in primer extension assays to evaluate their efficiency in being incorporated into viral RNA by the RdRp. Only those T-1106 analogues proven to be efficient substrates for the RdRp will be considered in the development of a future prodrug strategy.

Screening 5'-triphosphates through primer extension assays offers a more time- and cost-efficient approach to identifying new potential RdRp inhibitors. In contrast, synthesizing and testing prodrugs for each potential candidate would significantly increase both the synthetic workload and the number of different compounds needing evaluation in cell-based infection assays.

The most common modification of a nucleoside that leads to chain termination is the removal or replacement of the 3’-hydroxyl group, which prevents the RdRp from incorporating the subsequent nucleoside building block during RNA synthesis. These nucleoside analogues are referred to as “obligate” chain terminators because their incorporation inevitably leads to chain termination in the viral RNA[136].

For this thesis, three distinct 3’-modifications were chosen: First, the 3’-deoxy modification, the simplest alteration, in which the hydroxyl group is removed and replaced by a hydrogen atom. Second, the 3’-hydroxyl group is substituted with a fluorine atom. The replacement of hydroxyl groups with fluorine is a well-known bioisosteric modification in medicinal chemistry, particularly during lead optimization[137]. Lastly, the 3’-hydroxyl group is replaced by an azide group, derived from the antiretroviral drug AZT, which also features a 3’-azide modification.

Besides 3'-deoxy-obligate chain-terminating NAs, there are also non-obligate chain-terminating NAs. These NAs retain their native 3'-hydroxy group but can still lead to chain termination, even though they could theoretically be incorporated without disrupting chain extension[136].

One of the most common modifications to nucleosides that result in non-obligate chain-termination, is the introduction of a 2'-*C*-methyl group. When NAs with a 2'-*C*-methyl modification are integrated into viral RNA, the 2´-*C*-methyl group hinders further extension of the RNA strand by sterically hindering the binding of the next incoming NTP[138]. This strategy has already been used successfully to treat HCV in past[138–140].

In addition to the 2´-*C*-methyl modification, the 2´-deoxy-2´-α-fluoro-2´-β-*C*-methyl modification has also proven effective in treating HCV, particularly in the FDA-approved drug Sofosbuvir[141].

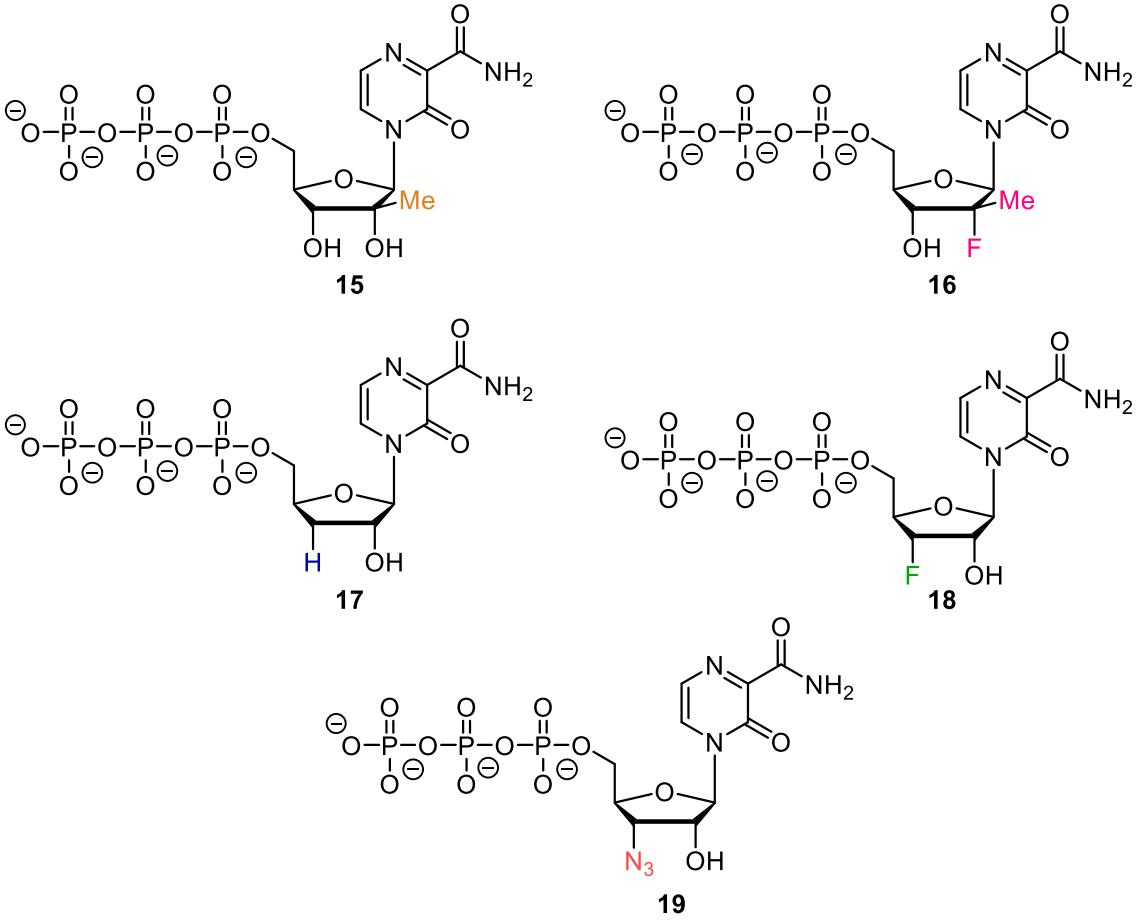

Figure 13: Selected modified T-1106-5´-triphosphates for testing in primer extension assay.

Given the substantial success of these two modifications in the past, they should also be applied to T-1106. Figure 13 illustrates all the modified T-1106-5'-triphosphates that are proposed for synthesis and subsequent testing in the primer extension assay.

After identifying a triphosphate that serves as an effective substrate for the SARS-CoV-2 RdRp, the second aim of this thesis is to develop a prodrug strategy for the corresponding nucleoside, to assess its antiviral activity in cell-based infection assays.

4. Results and Discussion

4.1 Retrosynthesis of modified T-1106-5´-triphosphates

The modified T-1106-5´-triphosphates should be synthesized in a single step from the corresponding nucleosides. These nucleosides are obtained through the coupling of methyl 3-hydroxy-2-pyrazinecarboxylate **20** with the appropriate ribose building block, followed by deprotection. The retrosynthetic Figure is illustrated in Figure 14.

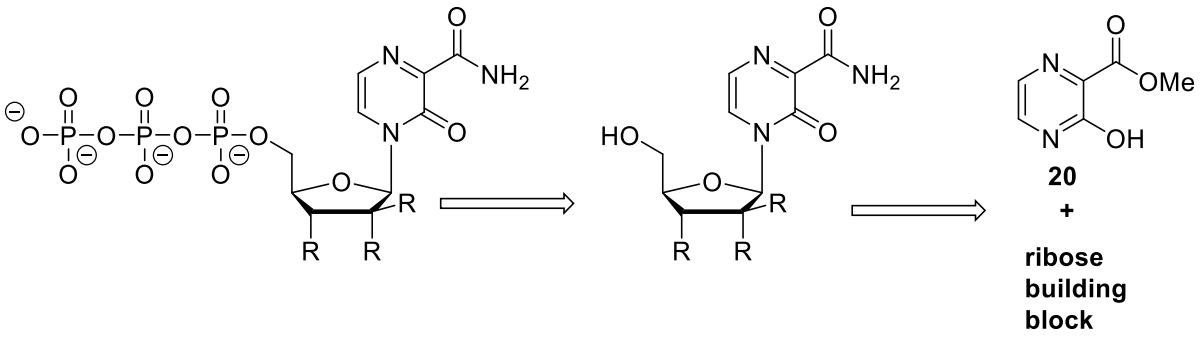

Figure 14: Retrosynthetic Figure for the synthesis of modified T-1106-5´-triphosphates.

Methyl 3-hydroxy-2-pyrazinecarboxylate **20** should be synthesized in two steps from commercially available 3-amino-2-pyrazinecarboxylic acid **21**, as shown in Figure 15.

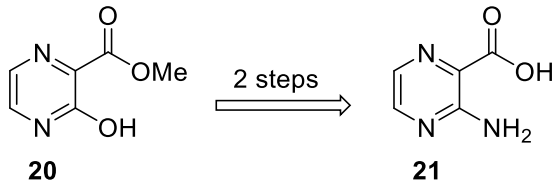

Figure 15: Retrosynthetic Figure for the synthesis of modified methyl 3-hydroxy-2-pyrazinecarboxylate **20**.

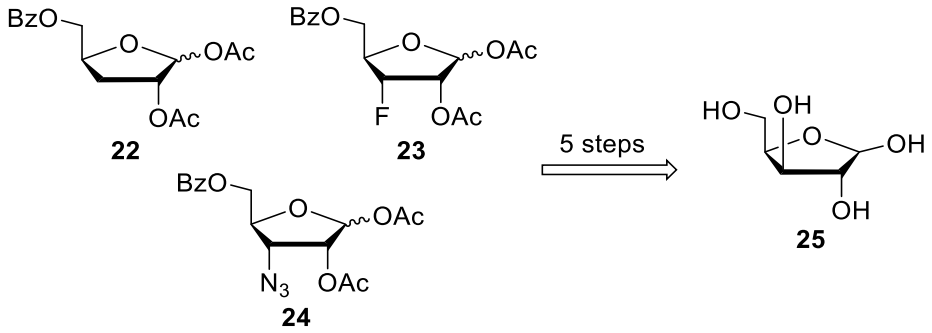

Figure 16: Retrosynthetic Figure for the synthesis of the 3-deoxy ribose building blocks.

All three ribose building blocks required for the 3´-modified triphosphates should be synthesized in five steps from D-Xylose **25** (Figure 16). The first two synthetic steps are identical for all three building blocks, which significantly reduces the overall number of synthetic steps required.

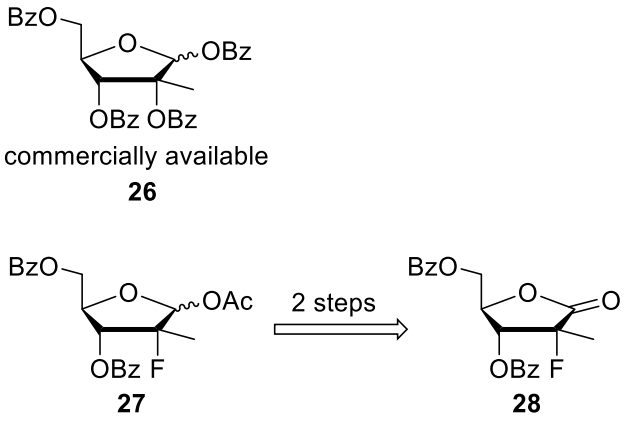

Figure 17: Retrosynthetic Figure for the synthesis of the 2-*C*-methyl ribose building blocks.

1,2,3,5-Tetra-*O*-benzoyl-2-*C*-methy-D-ribofuranose **26**, which is used as building block for the synthesis of the 2´-*C*-methyl-T-1106-5´-triphosphate **15** is commercially available and doesn't need to be synthesized. The 2-deoxy-2-fluoro-2-*C*-methyl building block **27** should be synthesized in two steps from commercially available 3,5-di-*O*-benzoyl-2-deoxy-2-α-fluoro-2-β-*C*-methyl-D-ribono-1,4-lactone **28** (Figure 17).

4.2 Synthesis of the nucleoside building blocks

4.2.1 Synthesis of pyrazine building block

Methyl 3-hydroxy-2-pyrazinecarboxylate **20** was synthesized according to established literature methods.[119,142] In the initial step, 3-amino-2-pyrazinecarboxylic acid **21** was converted to 3-hydroxypyrazine-2-carboxylic acid **29** via diazotisation using sodium nitrite and sulfuric acid, followed by aqueous workup, resulting in a yield of 77%.

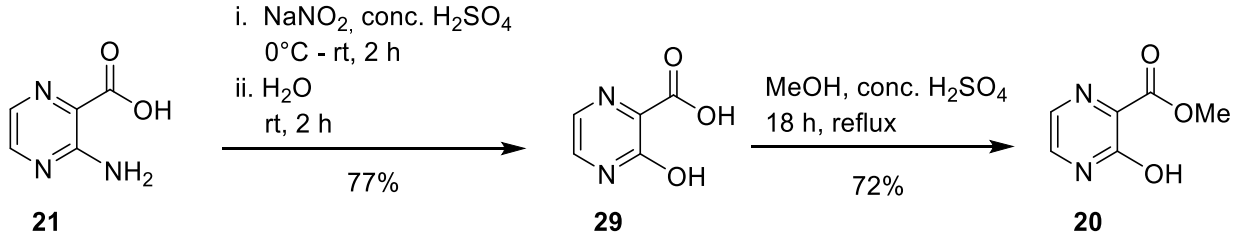

Figure 18: Synthesis of methyl-3-hydroxy-2-pyrazinecarboxylate **20**.

Subsequently, 3-hydroxypyrazine-2-carboxylic acid **29** was transformed into its corresponding methyl ester **20** in methanol in the presence of sulfuric acid, resulting in a yield of 72% (Figure 18).

4.2.2 Synthesis of the ribose building blocks

The 3-deoxy ribose building block 5-*O*-benzoyl-1,2-di-*O*-acetyl-3-deoxy-D-ribofuranose **22**, was synthesized starting from D-xylose **25** in five steps. This method was previously established in a thesis[119] and combines two distinct literature protocols.[143,144] In the initial step D-xylose **25** was protected with 1,2-isopropylidene group, which was introduced with acetone in the presence of a catalytic amount of sulfuric acid, achieving a yield of 81%. In the subsequent step, the 5-position was protected with a benzoyl group by reacting compound **30** with benzoyl chloride and triethylamine, resulting in a yield of 87%.

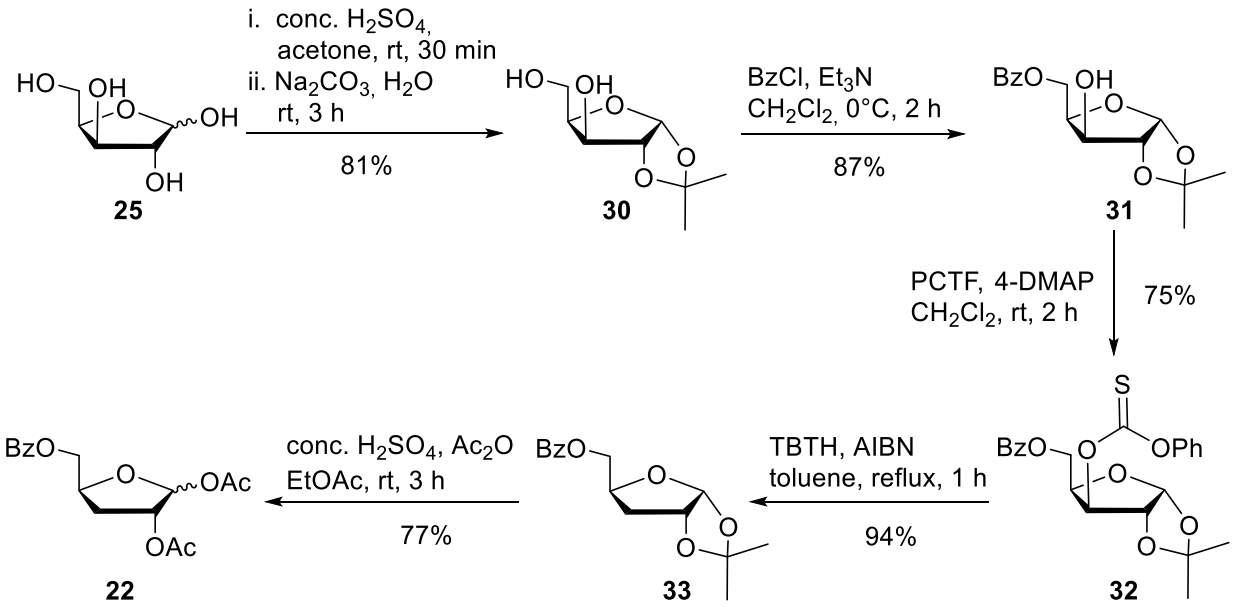

Figure 19: Synthesis of 5-*O*-benzoyl-1,2-di-*O*-acetyl-3-deoxy-D-ribofuranose **22** starting from D-Xylose **25**.

To remove the 3-hydroxy group, a BARTON-MCCOMBIE deoxygenation was performed. Compound **31** was reacted with *O*-phenyl chlorothionoformate and 4-dimethylaminophenol (4-DMAP), resulting in the corresponding thionoester **32** in a yield of 75%. The subsequent deoxygenation with tributyltin hydride and azobisisobutyronitrile (AIBN) produced the 3-deoxy ribose **33** in a yield of 94% (Figure 19). The 1,2-isopropylidene protection group was then cleaved by reacting compound **33** with sulfuric acid and acetic anhydride, resulting in replacement with 1,2-di-*O*-acetyl protecting groups. Finally, the desired 3-deoxy ribose building block, 5-*O*-benzoyl-1,2-di-

O-acetyl-3-deoxy-D-ribofuranose **22**, was obtained as an anomeric mixture in 77% yield, giving an overall yield of 38% over the five steps.

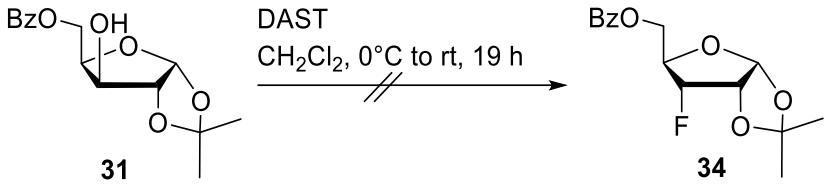

Figure 20: Attempt to fluorinate compound **31** with DAST.

The initial approach to synthesize the 3-fluoro ribose building block, 5-*O*-benzoyl-1,2-di-*O*-acetyl-3-deoxy-3-fluoro-D-ribofuranose **23**, involved reacting compound **31** with diethylaminosulfur trifluoride (DAST), followed by the exchange of the 1,2-protecting groups (Figure 20). This route was expected to yield the desired building block. However, after the fluorination step, the isolated compound exhibited a missing proton signal in the 1H-NMR spectrum, and the expected mass was not observed. Although the exact structure of the isolated compound could not be determined, it is assumed that an elimination reaction occurred during the process. Due to the failure of this initial fluorination attempt, an alternative method, previously published[145] and successfully used for the synthesis of 3'-fluoro nucleosides,[146] was adopted. In the initial step, the 1,2-isopropylidene acetal of compound **31** was cleaved, and a methoxy group was introduced at the 1-position by refluxing **31** in a 1% iodine in methanol solution, yielding **35** with 76% yield.[147] Fluorination of **35** using DAST under the established conditions resulted in a 52% yield of an anomeric mixture of compound **36**. This yield was approximately 10% lower than the published results, despite there being no evidence of difluorinated products or epoxide formation. In the final step, the 1,2-isopropylidene protecting group was removed and replaced with 1,2-di-O-acetyl groups under the same reaction conditions previously established for the 3-deoxy ribose building block. 5-*O*-Benzoyl-1,2-di-*O*-acetyl-3-deoxy-3-fluoro-D-ribofuranose **23** was obtained in a yield of 73%, with an overall yield of 20% as an anomeric mixture (Figure 21). The synthesis of the 3-azido ribose building block followed a previously published procedure, which describes the preparation of 3-azido-5-*O*-benzoyl-3-deoxy-1,2-*O*-diacetyl-D-ribofuranose **24** starting from D-xylose **25** in five steps.[148,149] The first two reaction steps were identical to those previously used for the synthesis of 3-modified ribose building blocks. Subsequently, compound **31** was treated with trifluoromethanesulfonic anhydride to convert the 3-hydroxy group into a superior leaving group. Due to the lability of the intermediate **37**, it was reacted immediately in

the next step with sodium azide and a catalytic amount of tetrabutylammonium iodide (TBAI) as a phase transfer catalyst, yielding the azide **38** in 29% over two steps. The lower yield compared to the literature may be attributed to slight differences in reaction conditions. Finally, the 1,2-isopropylidene protecting group was replaced with 1,2-di-*O*-acetyl groups under the previously described conditions, resulting in a yield of 73% and an overall yield of 15% as an anomeric mixture for 3-azido-5-*O*-benzoyl-3-deoxy-1,2-*O*-diacetyl-D-ribofuranose **24** (Figure 21).

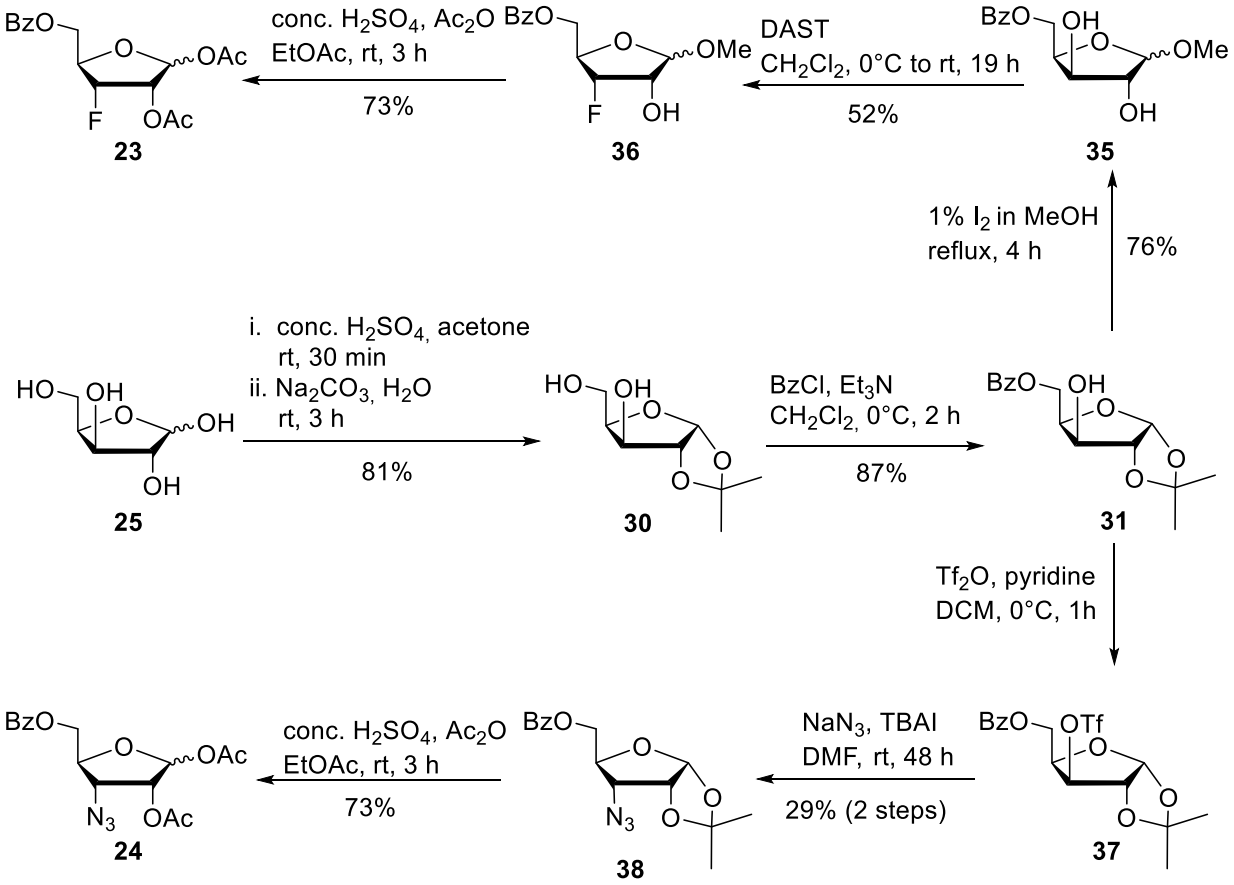

Figure 21: Synthesis of 5-*O*-benzoyl-1,2-di-*O*-acetyl-3-deoxy-3-fluoro-D-ribofuranose **23** and 3-azido-5-*O*-benzoyl-3-deoxy-1,2-*O*-diacetyl-D-ribofuranose **24** starting from D-Xylose **25**.

The 2-deoxy-2-α-fluoro-2-β-*C*-methyl ribose building block, 1-*O*-acetyl-2-deoxy-3,5-di-*O*-benzoyl-2-α-fluoro-2-β-*C*-methyl-D-ribofuranose **27**, was synthesized according to a previously published procedure starting from 3,5-di-*O*-benzoyl-2-deoxy-2-α-fluoro-2-β-*C*-methyl-D-ribono-1,4-lactone **28** in two steps.[150–152] In the initial step, the lactone **28** is reduced to the corresponding lactol **39** using the sterically hindered reducing agent lithium tri-*tert*-butoxyaluminum hydride, which prevents the reduction of the carbonyl functions of the protecting groups. In the second step the hydroxy group is acetylated by reacting the lactol **39** with acetic anhydride and 4-DMAP. This

reaction yielded 1-*O*-acetyl-2-deoxy-3,5-di-*O*-benzoyl-2-α-fluoro-2-β-*C*-methyl-D-ribofuranose **27** in a yield of 93% over two steps as an anomeric mixture (Figure 22).

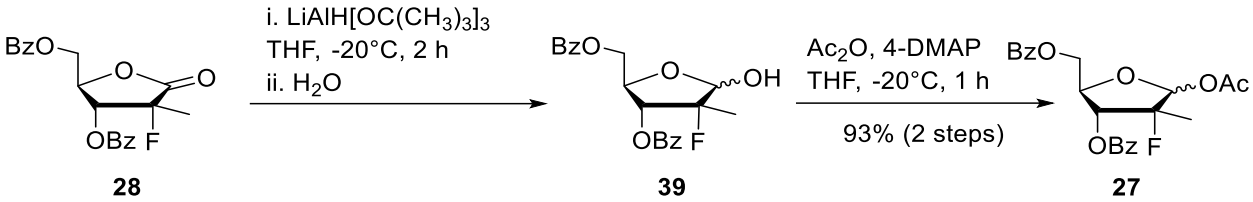

Figure 22: Synthesis of 1-*O*-acetyl-2-deoxy-3,5-di-*O*-benzoyl-2-α-fluoro-2-β-*C*-methyl-D-ribofuranose **27.**

4.3 Synthesis of the modified T-1106 nucleosides

The nucleosides **40**, **41**, and **42** were prepared following an already published procedure for the synthesis of modified T-1106 nucleosides,[118] which was slightly modified in a previous thesis.[119] The method is based on the VORBRÜGGEN glycosylation, which is an extension of the silyl-HILBERT-JOHNSON reaction.[153] In the initial step, **20** is silylated with hexamethyldisilazane (HMDS) to form compound **43**. This increases the lipophilicity of compound **43**, enhancing its solubility in organic solvents, and it also increases the electron density in the aromatic ring, making **43** a significantly better nucleophile than **20** (Figure 23).

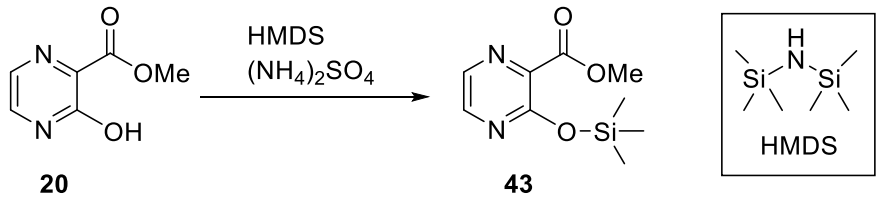

Figure 23: Silylation of methyl-3-hydroxy-2-pyrazinecarboxylate **20**.

In the second step, the acetyl group at the 2-position of the ribose building block **23** undergoes an intramolecular attack on the anomeric carbon, catalyzed by tin(IV) chloride. The mechanism is illustrated using the 3-deoxy-3-fluoro building block **23** (Figure 24), but it applies similarly to all other ribose building blocks. This process releases the 1-acetyl group, which is coordinated by a tin(IV) chloride molecule, leading to the formation of a cyclic oxonium ion, **44**. The electrophilic oxonium ion is then nucleophilically attacked by the intermediate **43**, resulting in the release of trimethylsilyl acetate and the formation of the desired nucleoside **41**. Due to the steric hindrance imposed by the oxonium ion, which prevents a nucleophilic attack from the lower face, the β-anomer of the nucleoside is formed exclusively (Figure 24).

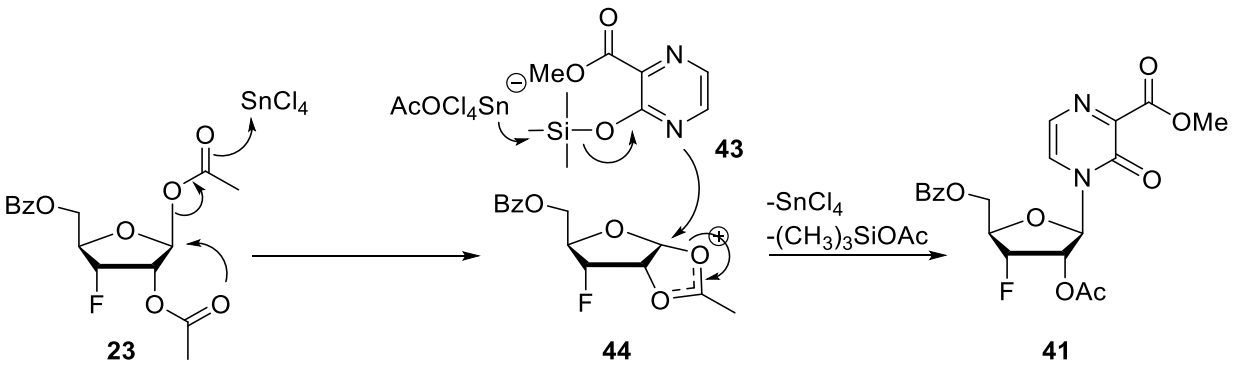

Figure 24: Mechanism of the silyl-HILBERT-JOHNSON reaction.

In the synthesis of nucleosides **40**, **41**, and **42** the first step involves refluxing **20** in HMDS for one hour. After removing the HMDS under reduced pressure, the silylated compound **43** is obtained as a solid. This solid is then redissolved in acetonitrile and dichloromethane, and the corresponding ribose building block along with tin(IV) chloride is added. The reaction mixture is stirred overnight at room temperature and then refluxed for 30 to 60 minutes to enhance conversion. Extending the reflux time can further improve ribose conversion and increase yields, but it also raises the risk of forming the undesired α-anomer. The yields for those protected nucleosides ranged from 57% to 85%, depending on the size of the modification at the 3´-position. A larger modification better protects the ribose from nucleophilic attack from the underside, allowing longer reflux times without forming the α-anomer (Figure 25).

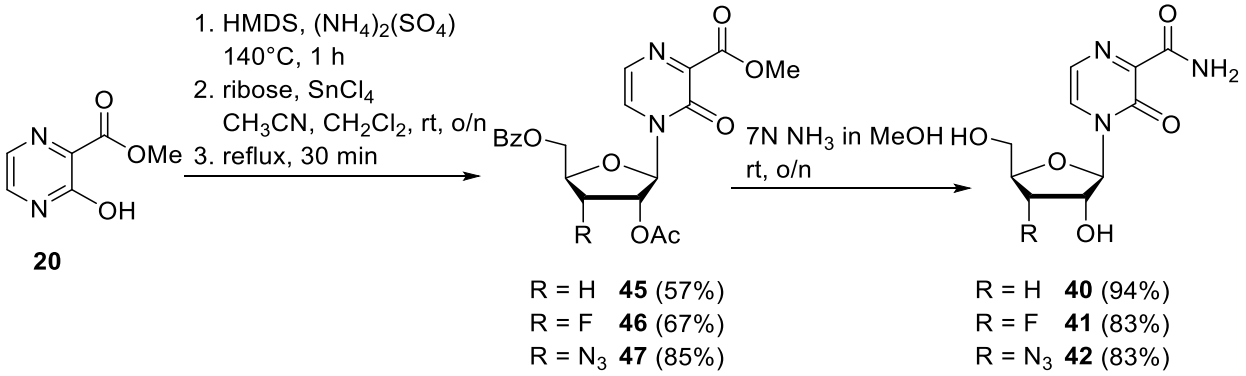

Figure 25: Synthesis of the nucleosides **40**, **41**, and **42** starting from their corresponding ribose building blocks.

In the second step, the benzoyl groups were cleaved by stirring compounds **45**, **46**, and **47** overnight in 7 N methanolic ammonia. At the same time, the methoxy group was cleaved as well, leading to the formation of the corresponding amides **40**, **41**, and **42** in good yields (Figure 25). No traces of the α-anomer could be detected by nuclear OVERHAUSER effect spectroscopy (NOESY).

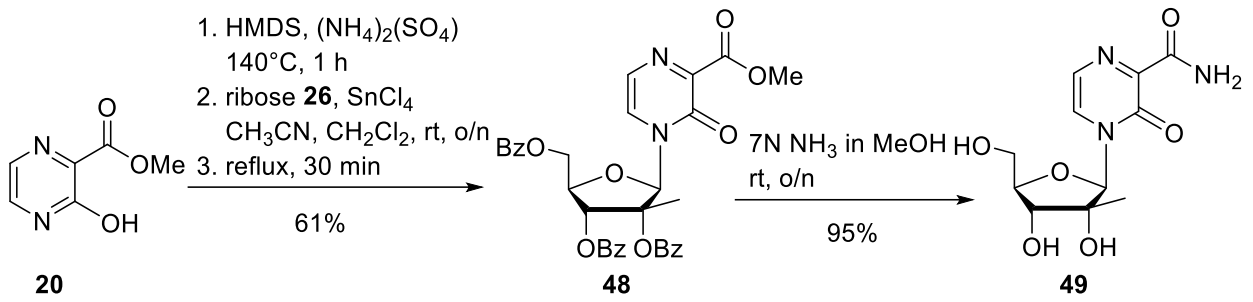

Figure 26: Synthesis of the nucleoside **49** starting from the ribose building block **26**.

2´-*C*-Methyl-T-1106 **49** was synthesized under same reaction conditions as shown in Figure 25. The coupling with 1,2,3,5-tetra-*O*-benzoyl-2-*C*-methyl-β-D-ribofuranose **26** under the established VORBRÜGGEN conditions afforded the tribenzoylated nucleoside in 61% yield and the cleavage of the protecting groups with methanolic ammonia proceeded in 91% yield, comparable to the other synthesized T-1106 nucleosides (Figure 26).

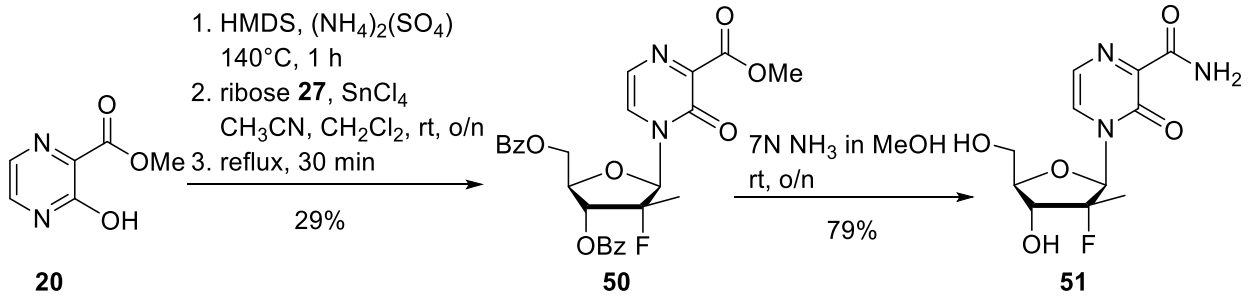

Figure 27: Synthesis of the nucleoside **51** starting from the ribose building block **27**.

For the synthesis of 2´-α-fluoro-2´-β-*C*-methyl-T-1106 **51**, the same reaction conditions were used as well. In contrast to the literature HMDS was used instead of *N*,*O*-bis(trimethylsilyl)acetamide as silylation reagent, which did not had any influence on the yield.[150] Due to the fact, that the ribose building block **27** lacks a carbonyl function at the 2-position, no oxonium ion could be formed, which led to the formation of a mixture of anomers of compound **50**, that had to be separated by column chromatography (Figure 27).

Additionally, the non-modified T-1106-5´-triphosphate **14** needed to be synthesized as a reference compound for the RdRp assay. The triphosphate **14** can be synthesized starting from T-1106 **13**. For the synthesis of T-1106 **13**, peracetylated ribofuranose **52** was coupled under standard conditions with **20**, yielding the protected nucleoside **53** with a yield of 77%. Subsequently, **53** was deprotected under standard conditions using ammonia in methanol to yield T-1106 **13** in a yield of 93%. As synthesizing T-1106-5´-triphosphate **14** directly from T-1106

13 proved unfeasible (Chapter 4.4), the corresponding methyl ester of T-1106 **54** was prepared by deprotecting **53** with sodium methoxide in methanol, leading to a yield of 92% (Figure 28).

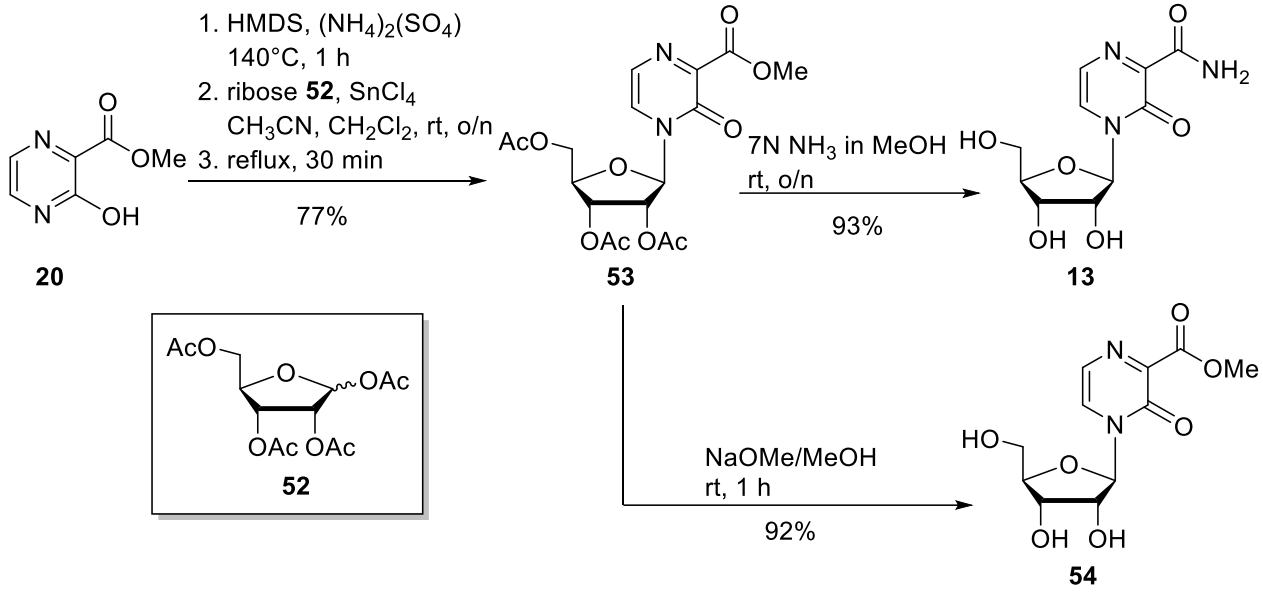

Figure 28: Synthesis of T-1106 **13** and the corresponding methyl ester **54**.

4.4 Synthesis of modified T-1106-5´-triphosphates

Several methods exist for synthesizing nucleoside 5'-triphosphates from the corresponding nucleoside 5'-monophosphates activated as phosphoramidite,[154,155] morpholidate,[156–158] or imidazolidate.[159,160] The JESSEN protocol,[161] which utilizes an iterative approach, has been successfully applied in the past to synthesize T-1106-5´-triphosphate **14**.[120] All of these different methods have in common that they require three to four synthetic steps from the corresponding nucleoside to synthesize the 5´-triphosphate. Given the large number of triphosphates that needed to be synthesized for this thesis, these procedures were considered impractical due to their considerable time requirements. The LUDWIG & ECKSTEIN protocol[162] offers a more efficient solution with its "one-pot, three-step" strategy, enabling the synthesis of 5'-triphosphates in a single step starting from the nucleoside. In Figure 29 the synthesis of 2´-α-fluoro-2´-β-*C*-methyl-T-1106-5´-triphosphate **16** is discussed in detail. However, the same approach was applied to all other nucleoside 5'-triphosphates synthesized in this thesis using the LUDWIG & ECKSTEIN protocol. Although this protocol has been optimized multiple times in the past, the exact reaction conditions still vary considerably depending on the nucleoside employed.[163–166] In particular, reaction time, the amount of phosphoryl chloride, and the choice of base vary according to the

nucleoside. For the synthesis of the various modified T-1106-5'-triphosphates described herein, consistent reaction conditions were used, with slight optimizations based on those previously established in earlier work.[119]

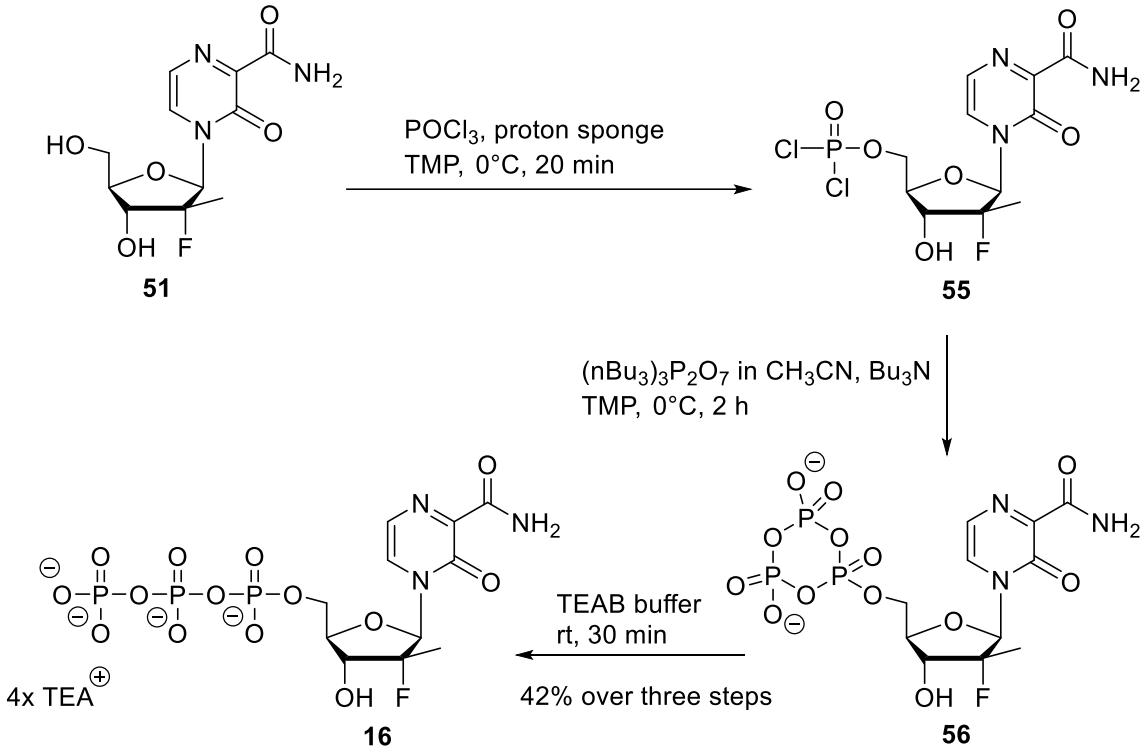

Figure 29: Synthesis of 2´-α-fluoro-2´-β-*C*-methyl-T-1106-5´-triphosphate **16** using LUDWIG & ECKSTEIN conditions.

In the initial step, nucleoside **51** reacts using YOSHIKAWA conditions[167] to form the corresponding dichlorophosphoridate **55**. This step presents the greatest challenge when applying the LUDWIG & ECKSTEIN protocol. The first phosphorylation can generate a complex mixture of different phosphorylation products due to the use of an unprotected nucleoside. If this occurs, the subsequent reaction step may result in an inseparable mixture of various products. To avoid this, it is essential to carefully select the reaction temperature and time, as well as the precise amounts of phosphoryl chloride and base in the first step (Figure 29). For the synthesis of the modified T-1106-5´-triphosphates, the use of five equivalents of phosphoryl chloride and two equivalents of proton sponge (1,8-bis(*N,N*-dimethylamino)naphthalin) proved effective. At 0°C, this high concentration of phosphoryl chloride resulted in good conversions and the minimal formation of side products, even with short reaction times. Figure 30 illustrates the HPLC chromatograms at various stages of the reaction. After 15 minutes, nearly all of the nucleoside **51** was consumed, and only the dichlorophosphoridate **55** was formed. (Note: The

dichlorophosphoridate **55** is rapidly hydrolysed during the reaction quenching before HPLC analysis. Therefore, the detected compound is the corresponding monophosphate rather than the dichlorophosphoridate **55**.) After 20 minutes tris(tetrabutylammonium) hydrogen pyrophosphate (abbreviated as PPi in Figure 30) is added together with tributylamine at 0°C. Within 40 minutes upon pyrophosphate addition, two additional peaks began to form. The first peak following the dichlorophosphoridate **55** corresponded to the intermediate cyclic triphosphate **56**. Due to the reaction being quenched prior to HPLC analysis, an additional peak appears, representing the desired 5'-triphosphate **16** formed through hydrolysis of the intermediate **56**. Twenty minutes later, the amount of dichlorophosphoridate **55** has further decreased, and two hours after the addition of the pyrophosphate, the reaction is quenched by the addition of 1 M triethylammonium bicarbonate (TEAB) buffer. The mixture was stirred for an additional 30 minutes to ensure complete hydrolysis of the remaining intermediate cyclic triphosphate **56** (Figure 29).

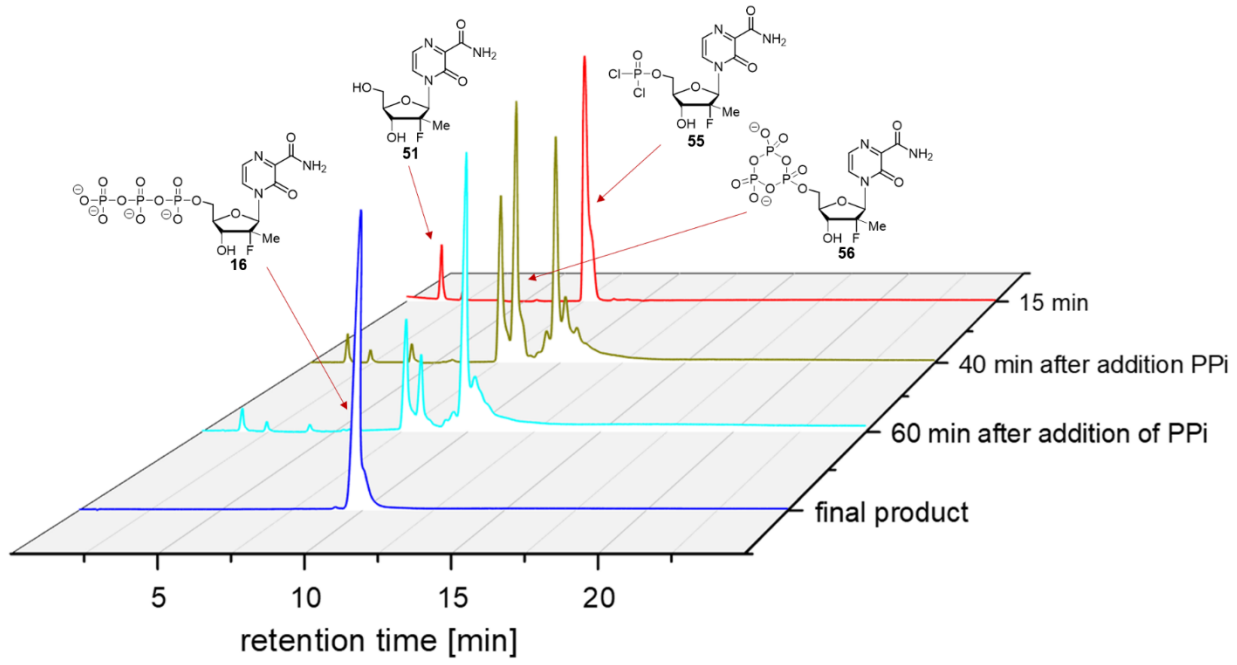

Figure 30: Stack of HPLC chromatograms of reaction controls of the synthesis of 2´-α-fluoro-2´-β-C-methyl-T-1106-5´-triphosphate **16** at different reaction times at 340 nm.

Afterwards it was very important to remove all trimethyl phosphate (TMP) by extracting the reaction mixture with dichloromethane, otherwise it can be hard to remove it later on. Subsequent chromatography of the crude product on diethylaminoethyl cellulose (DEAE) Sephadex© A25 using TEAB buffer efficiently removes all unwanted side products and unreacted

monophosphate, yielding the desired 2´-α-fluoro-2´-β-*C*-methyl-T-1106-5´-triphosphate **16** in a high yield of 42% over three steps, with excellent purity of 99% at 340 nm.

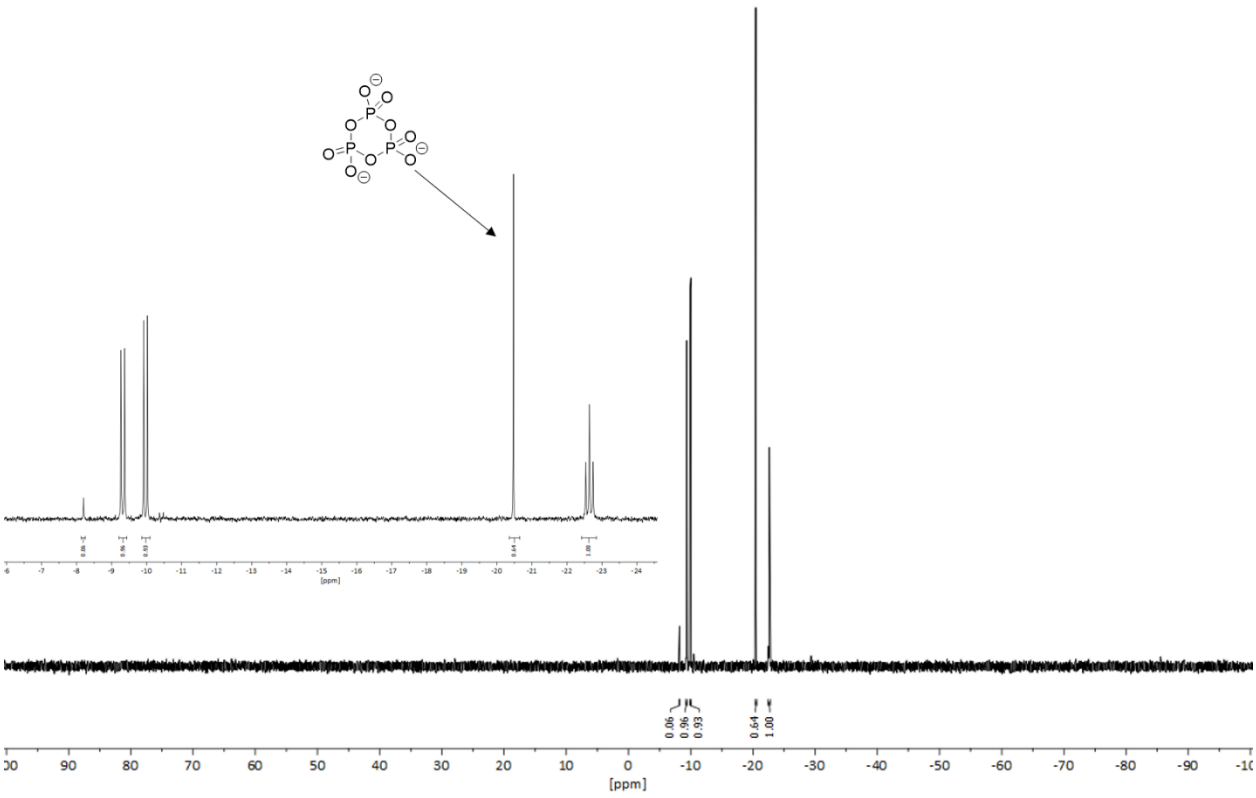

Figure 31: ^{31}P-NMR of 2´-α-fluoro-2´-β-*C*-methyl-T-1106-5´-triphosphate **16** after purification on DEAE Sephadex© A25.

After purification of the crude product on DEAE Sephadex® A25, no impurities could be detected by HPLC. However, in the ^{31}P-NMR spectrum, a large singlet can be detected at around -20.5 ppm (Figure 31). This signal is caused by the trimetaphosphate formed from the reaction of the pyrophosphate with phosphoryl chloride. Due to the use of five equivalents of phosphoryl chloride in the initial step, an excess remained in the reaction mixture and can react with pyrophosphate to produce trimetaphosphate. This highlights an area for potential optimization: reducing the amount of phosphoryl chloride used initially or removing the excess before addition of pyrophosphate would likely increase yields and decrease the amount of trimetaphosphate formed. To remove the trimetaphosphate impurity, the crude product was further purified using an RP_{18} silica column, which in most cases completely eliminates this contaminant. The ^{31}P-NMR

spectrum of pure 2´-α-fluoro-2´-β-*C*-methyl-T-1106-5´-triphosphate **16** is shown in Figure 32.

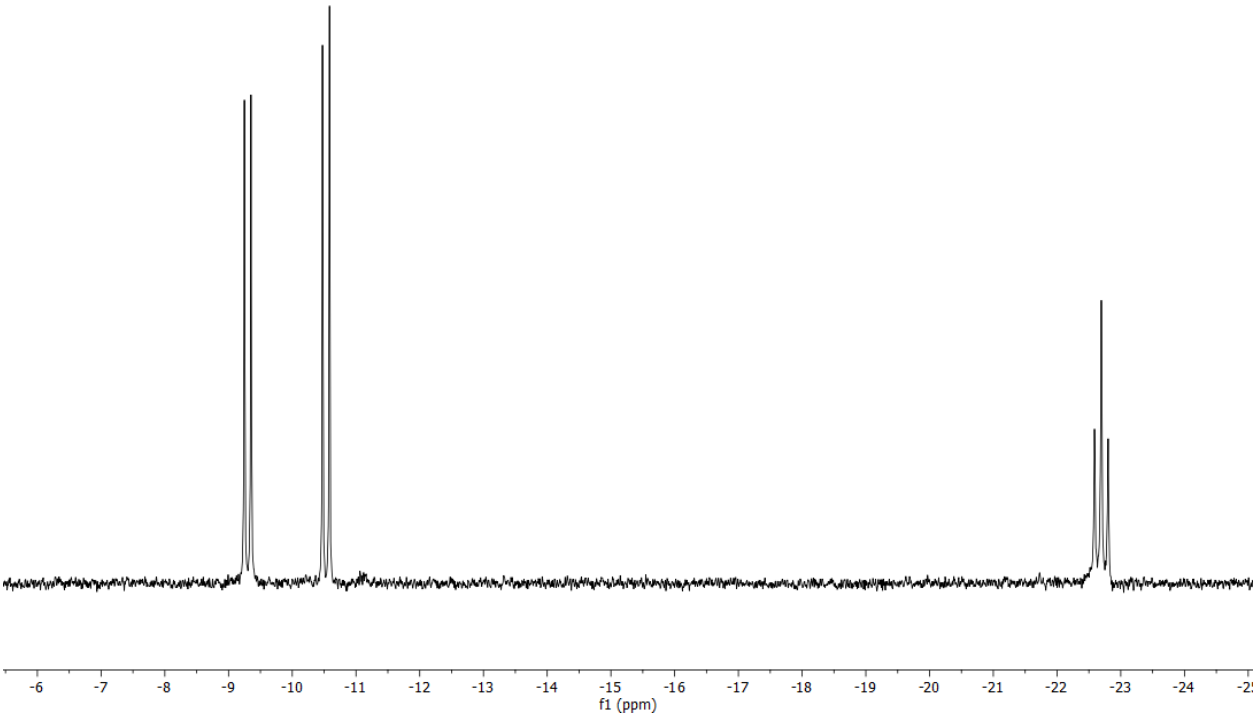

Figure 32: ^{31}P-NMR of 2´-α-fluoro-2´-β-*C*-methyl-T-1106-5´-triphosphate **16** after the second column chromatography on RP_{18} silica gel.

In comparison to a previous work,[119] in which 2'-*C*-methyl-T-1106-5´-triphosphate **15** was synthesized, the temperature of the second step was changed from -15°C to 0°C. This higher temperature had no adverse effect on the reaction outcome and made handling of the reaction easier, thereby saving a considerable amount of time. Additionally, the reaction was quenched by the addition of cooled TEAB buffer rather than ice water, as the excess phosphoryl chloride could be neutralized more gently with buffer than with water.

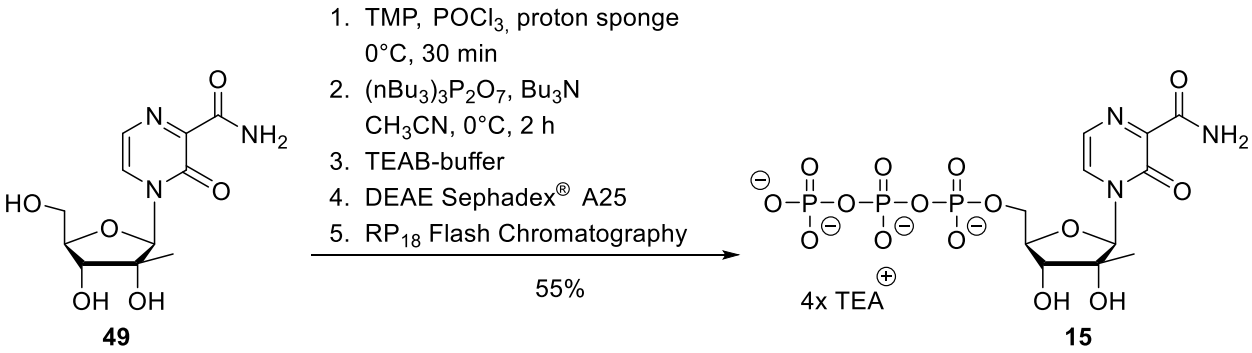

Figure 33: Synthesis of 2´-*C*-methyl-T-1106-5´-triphosphate **15**.

Overall, the changes had only a minor impact on the yield. However, they significantly simplified the handling of the reaction. As a result, 2'-*C*-methyl-T-1106-5´-triphosphate **15** was obtained as a triethylammonium salt with a yield of 55%.

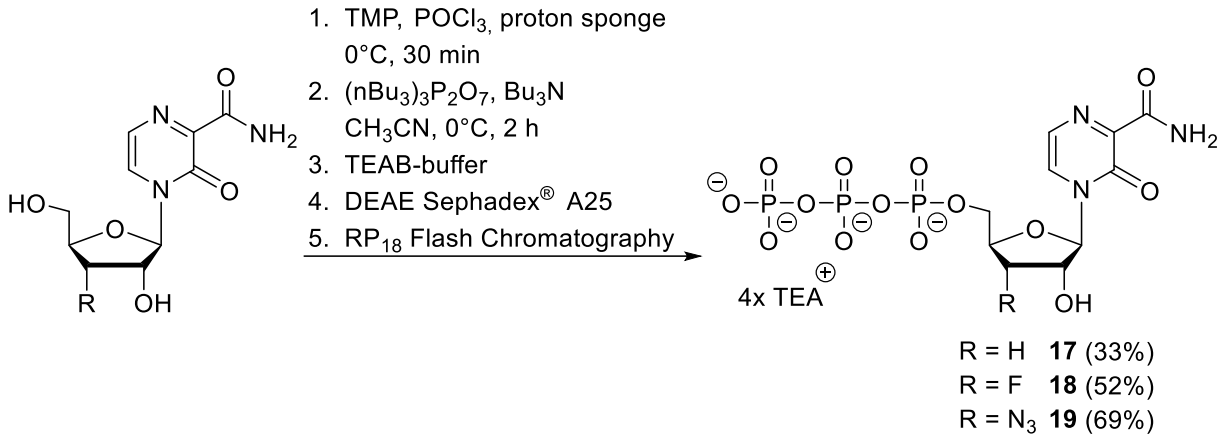

Figure 34: Synthesis of the modified T-1106-5´-triphosphates **17**, **18**, and **19**.

The 3´-modified T-1106-5´-triphosphates **17**, **18** and **19** where synthesized after the exact same procedure in good yields between 52% and 69% (Figure 34).

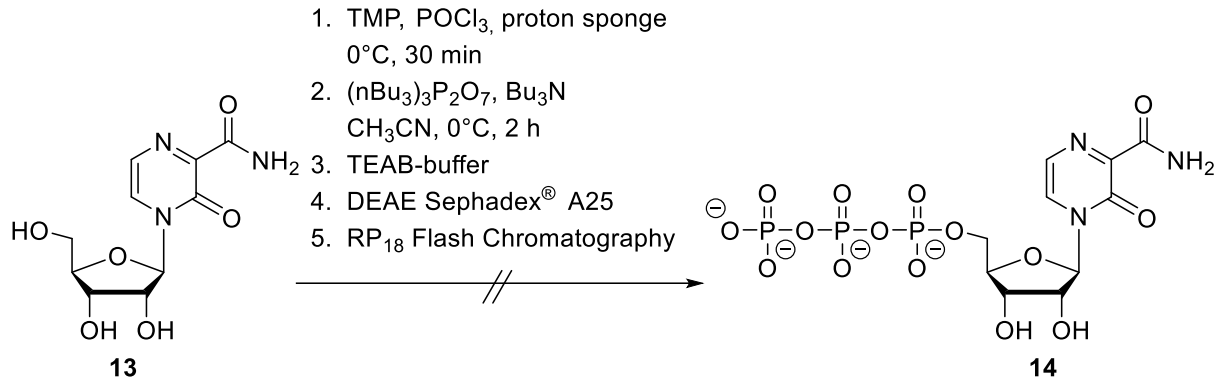

Figure 35: Attempt of the synthesis of T-1106-5´-triphosphate **14**.

Although T-1106-5´-triphosphate **14** has been extensively tested in SARS-CoV-2 polymerase assays[52], it was necessary to re-synthesize it for use as a reference compound in upcoming assays. As mentioned above, in a previous work, T-1106-5´-triphosphate **14** was synthesized from the corresponding T-1106-5´-monophosphate via a multi-step process, achieving an overall yield of 25% using phosphoramidite chemistry.[120] While this method is reliable, it is also quite time-consuming. Therefore, in this thesis the established LUDWIG & ECKSTEIN protocol was applied for the synthesis of T-1106-5´-triphosphate **14**. Unfortunately, under the established standard

reaction conditions, no conversion was observed. This can be attributed to the low solubility of T-1106 **13** in the reaction medium, likely due to its higher polarity in comparison to the modified T-1106 compounds. Increasing the amount of phosphoryl chloride to 10 or 15 equivalents led to some formation of the dichlorophosphoridate, but also resulted in a broad range of undesired phosphorylation products (Figure 35).

To address this issue, the lipophilicity of T-1106 **13** was increased by using the corresponding methyl ester **54** to improve its solubility in TMP. Application of the methyl ester **54** under the established LUDWIG & ECKSTEIN protocol resulted in no side-product formation during the initial phosphorylation step, allowing the corresponding triphosphate **57** to be isolated with a yield of 41%. For the cleavage of the methyl ester to form the corresponding amide **14**, the ester was stirred overnight in 7 N methanolic ammonia, a method already established for nucleoside synthesis (Chapter 4.3) (Figure 36). This approach was also effective for the triphosphate, although the reaction was challenging due to the low solubility of **57** in methanol. For future experiments, cleavage of the ester using aqueous ammonia is recommended. This alternative method was successfully implemented later in this thesis for the deprotection of nucleoside 5'-triphosphates (Chapter 4.7).

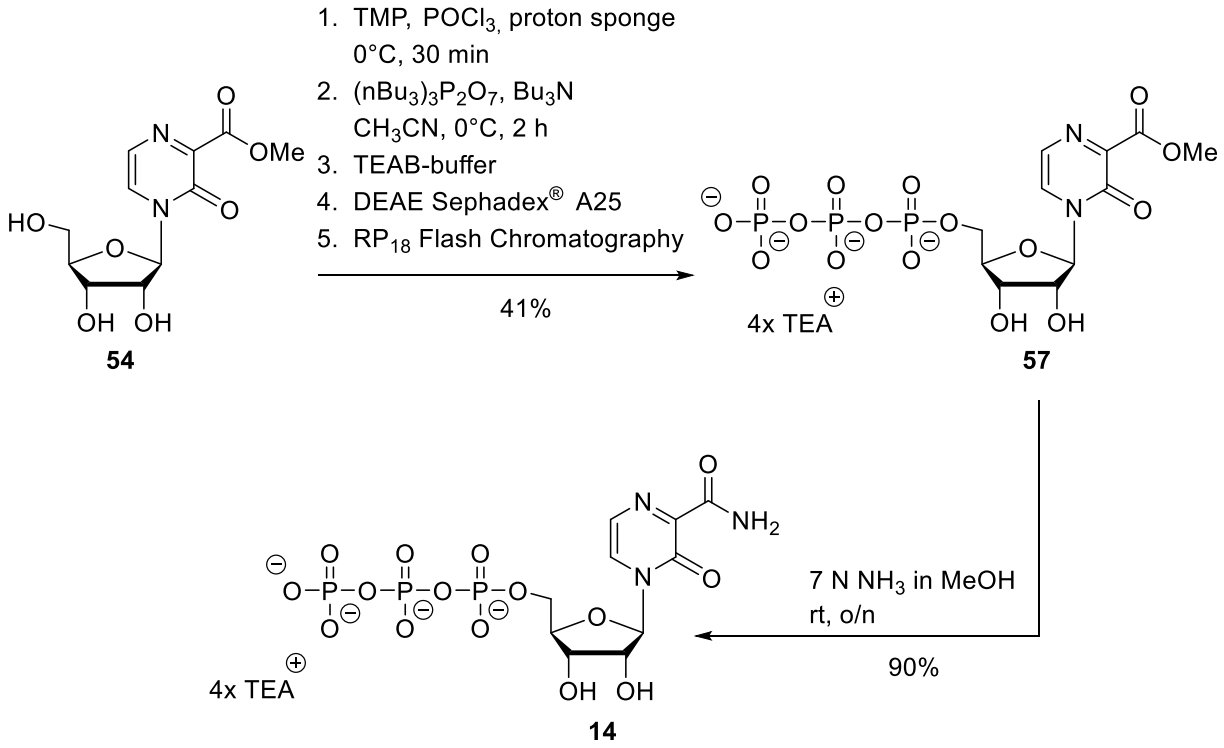

Figure 36: Synthesis of T-1106-5´-triphosphate **14** via the corresponding methyl ester **54**.

The SARS-CoV-2 RdRp is the fastest RdRp to date,[168,169] which results in a relatively high error rate of approximately one error per 10,000 nucleotides.[170] This error rate is similar to that of HIV reverse transcriptase (HIV-RT).[171] In a previous work conducted in the group of C. MEIER, it was demonstrated that not only nucleoside 5'-triphosphates but also nucleoside 5'-diphosphates are efficient substrates for HIV-RT.[172] To investigate whether the SARS-CoV-2 polymerase is also able to accept diphosphates as substrates, T-1106-5'-diphosphate **58** was synthesized and tested in polymerase assays.

In the initial step, the T-1106 methyl ester **54** was monophosphorylated under the previously established YOSHIKAWA conditions, followed by the ester cleavage using methanolic ammonia, gave T-1106-5´-monophosphate **59** in yield of 74% (Figure 37).

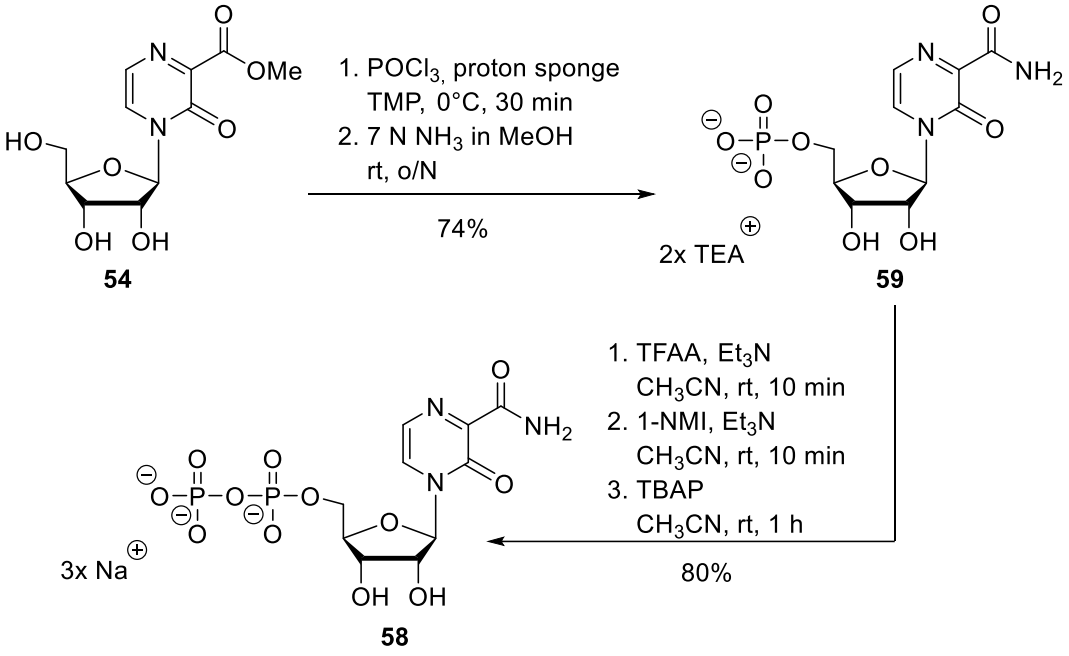

Figure 37: Synthesis of T-1106-5´-diphosphate **58**.

In the second step, the T-1106-5´-monophosphate **59** was converted to the corresponding 5´-diphosphate **58** using a method developed by S. MOHAMADY.[173] The monophosphate **59** was activated by reacting it with trifluoroacetic anhydride (TFAA). The resulting anhydride then reacted with 1-methylimidazole to produce the reactive 1-methylimidazolium salt of **59**. This salt was slowly added via a syringe pump over the course of one hour to a solution of tetrabutylammonium phosphate monobasic (TBAP) in acetonitrile. The slow addition of the activated nucleoside-5'-monophosphate prevented undesired coupling of a single phosphate

with a second nucleoside 5'-monophosphate. This method successfully yielded the desired T-1106-5'-diphosphate **58** with an 80% yield.

All of the synthesized T-1106-5'-phosphates were tested in SARS-CoV-2 polymerase assays by the group of B. CANARD at Aix-Marseille University. The results of these assays are discussed in Chapter 4.6.

4.5 Synthesis of nucleoside-5´-triphosphates

In the early days of the SARS-CoV-2 pandemic in 2020, Remdesivir **5** emerged as the most promising nucleoside analogue for treating patients with severe infections. However, its precise mechanism of action was not fully understood at the time. To gain further insight, the research group of B. CANARD aimed to test RTP **6** in the SARS-CoV-2 polymerase assay. At that time the triphosphate **6** was not commercially available. However, the nucleoside form of Remdesivir **60** could be obtained commercially, allowing for the synthesis of the triphosphate **6** according to established literature protocols[174], resulting in a yield of 22% (Figure 38). Notably, in this particular synthesis, no base was used during the initial phosphorylation step. Attempts to improve the yield by adding a proton sponge or tributylamine did not lead to better results.

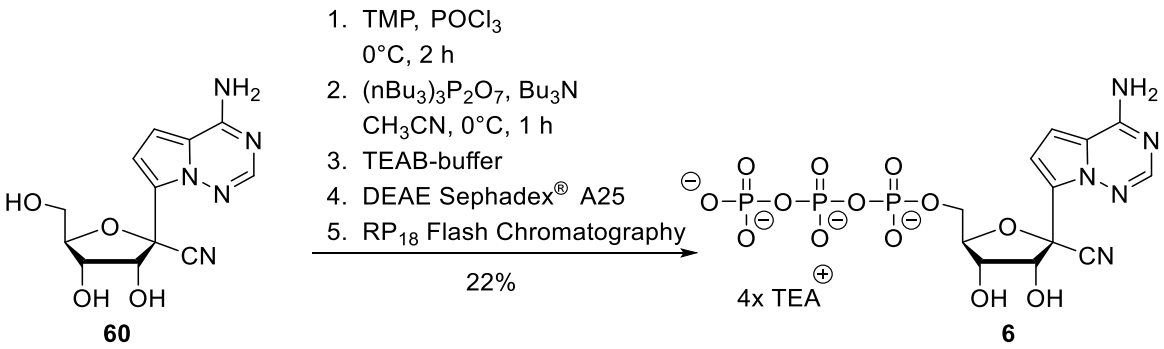

Figure 38: Synthesis of Remdesivir-nucleoside-5´-triphosphate **6**.

In this thesis, in addition to the modified T-1106-5´-triphosphates, several other promising nucleoside 5´-triphosphates were synthesized for evaluation in SARS-CoV-2 polymerase assays. One notable candidate is Tiazofurin **61**, which is recognized for its antiviral activity against a broad spectrum of RNA and DNA viruses through inhibition of inosine-5'-monophosphate dehydrogenase (IMPDH)[175–177]. However, the widely used antiviral drug Ribavirin **62**, which also targets IMPDH, is known to exhibit multiple mechanisms of action[178]. Among these, Ribavirin **62** induces antiviral effects by promoting lethal mutagenesis, a mechanism shared with T-1106 **13**

and Favipiravir **9** (Chapter 2.2.3). Given the structural similarities between Tiazofurin **61**, Ribavirin **62**, Favipiravir **9**, and T-1106 **13**, it is hypothesized that tiazofurin-5´-triphosphate could serve as an effective substrate for the SARS-CoV-2 polymerase and exert antiviral effects through lethal mutagenesis.[179]

Tiazofurin **61** was first synthesized in 1976 by SRIVASTAVA *et al.*[177] However, a more optimized synthetic route was published in 1999 by RAMASAMY *et al.*[180] In the initial step, a nitrile group is introduced at the 1-position of ribose **63** through a Lewis-acid-catalyzed reaction with trimethylsilyl cyanide, achieving a yield of 94% (Figure 39). Only the β-anomer is formed due to the generation of an oxonium ion (Chapter 4.3). In the original procedure, the nitrile **64** was reacted with hydrogen sulfide to yield the corresponding thioamide **65**. However, due to the high toxicity of hydrogen sulfide, an alternative was sought in this work. An alternative method for the preparation of thioamide from nitriles was developed by NAGL *et al.*[181]. This method involves reacting nitriles with Lawesson's reagent in the presence of an excess Lewis-acid, yielding the corresponding thioamides in good yields. Unfortunately, when nitrile **64** was subjected to these conditions, the thioamide **65** could only be isolated in a yield of 55%.

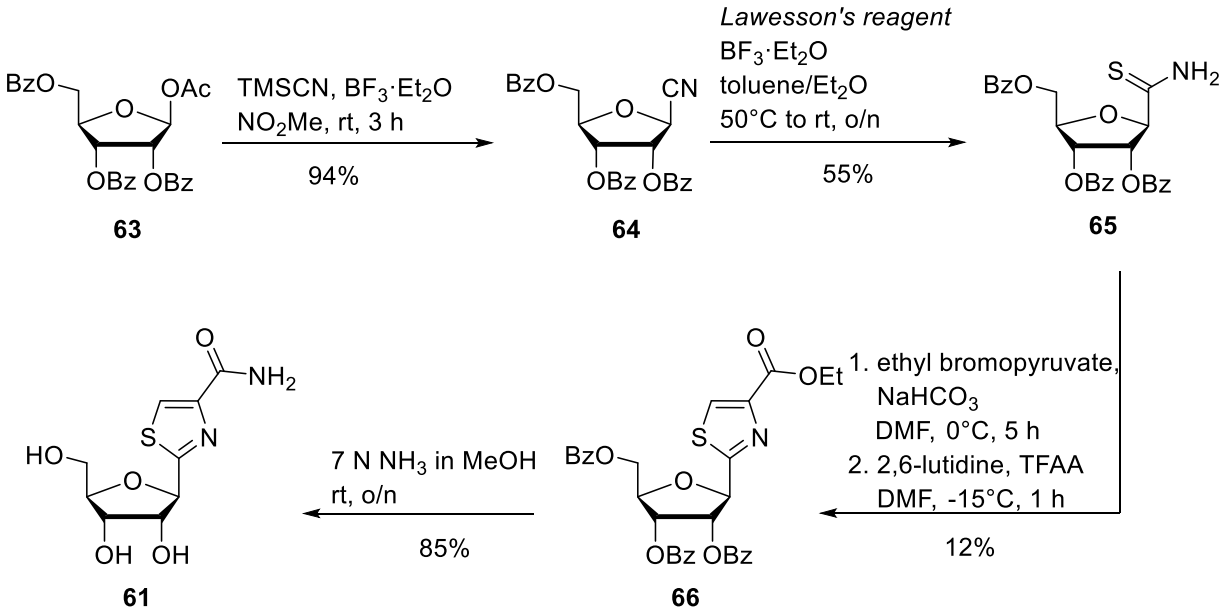

Figure 39: Synthesis of Tiazofurin **61.**

This low yield can be attributed to the undesired side reaction of the Lawesson's reagent with carbonyl groups, resulting in the formation thioesters. In the third step, the thioamide **65** can be condensed with an α-haloketone, specifically ethyl bromopyruvate, via a HANTZSCH thiazole

synthesis to form the corresponding thiazole **66**.[182] However, the product was obtained in a low yield of only 12%, and yield improvements could not be achieved despite multiple attempts. Final cleavage of the benzoyl protection groups with methanolic ammonia afforded the desired Tiazofurin **61** in a yield of 85%, although the overall yield across four steps was only 5%.

Due to these unsatisfactory results, an alternative synthetic route for the synthesis of Tiazofurin **61** was applied, as published by BROWN *et al.* in 2002.[183] This represents an optimized version of the originally published route by RAMASAMY *et al.* (Figure 40).[184]

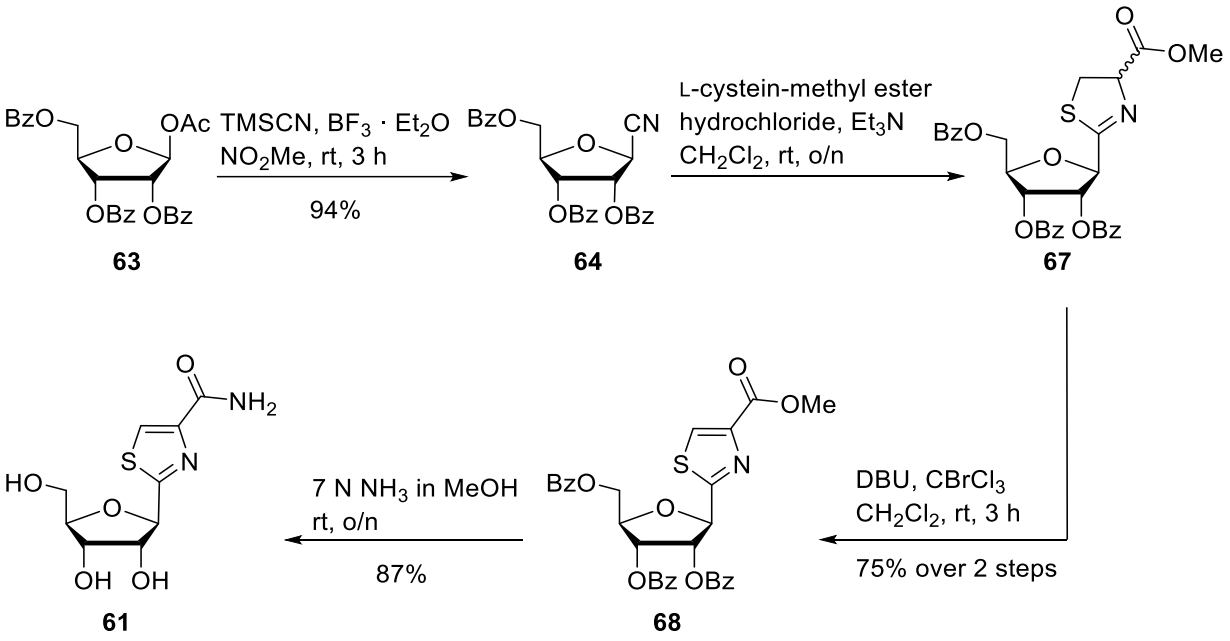

Figure 40: Synthesis of Tiazofurin **61** using the improved method.

Initially, nitrile **64** is formed under the same reaction conditions as in the previous method. In the subsequent step, nitrile **64** is reacted with L-cysteine ethyl ester hydrochloride in the presence of triethylamine, yielding the thiazoline intermediate **67**, which is used directly in the next step without further purification. The thiazoline intermediate **67** is then oxidatively dehydrogenated using bromotrichloromethane and DBU. This approach is considered a mild dehydrogenation method, offering the advantage over alternative methods that it can be performed in the presence benzoyl groups.[185] Using this approach, the protected Tiazofurin **68** was obtained in a yield of 75% over two steps. Subsequent deprotection with methanolic ammonia provided Tiazofurin **61** in a yield of 87% (Figure 40). The overall yield across four steps was 61%, marking a significant improvement over the previous method (see page 43). Moreover, the synthetic procedures used are significantly easier to handle. In the final step, Tiazofurin **61** was reacted

under the previously established LUDWIG & ECKSTEIN conditions without any problems, affording tiazofurin-5´-triphosphate **69** in a satisfactory yield of 53% (Figure 41).

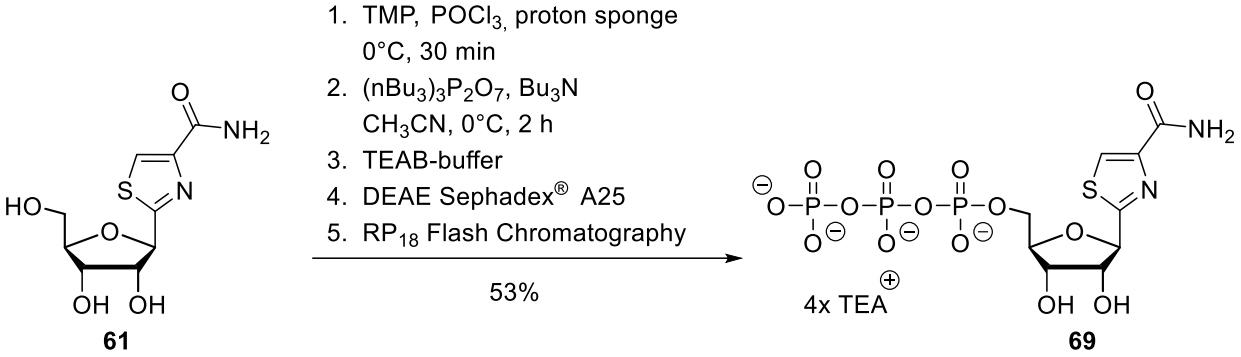

Figure 41: Synthesis of tiazofurin-5´-triphosphate **69**.

Other notable nucleoside analogues with a broad antiviral activity include 6-azauridine **70** and its prodrug azaribine, both of which have demonstrated antiviral efficacy against various RNA-viruses in the past[186–188]. Mizoribine **71** is a another nucleoside analogue with broad antiviral activity[189–191], and is of particular interest in this work due to its structural similarity to T-1106 **13**. The corresponding 5'-triphosphates **72** and **73** of both nucleosides were synthesized and tested in the SARS-CoV-2 polymerase assay.

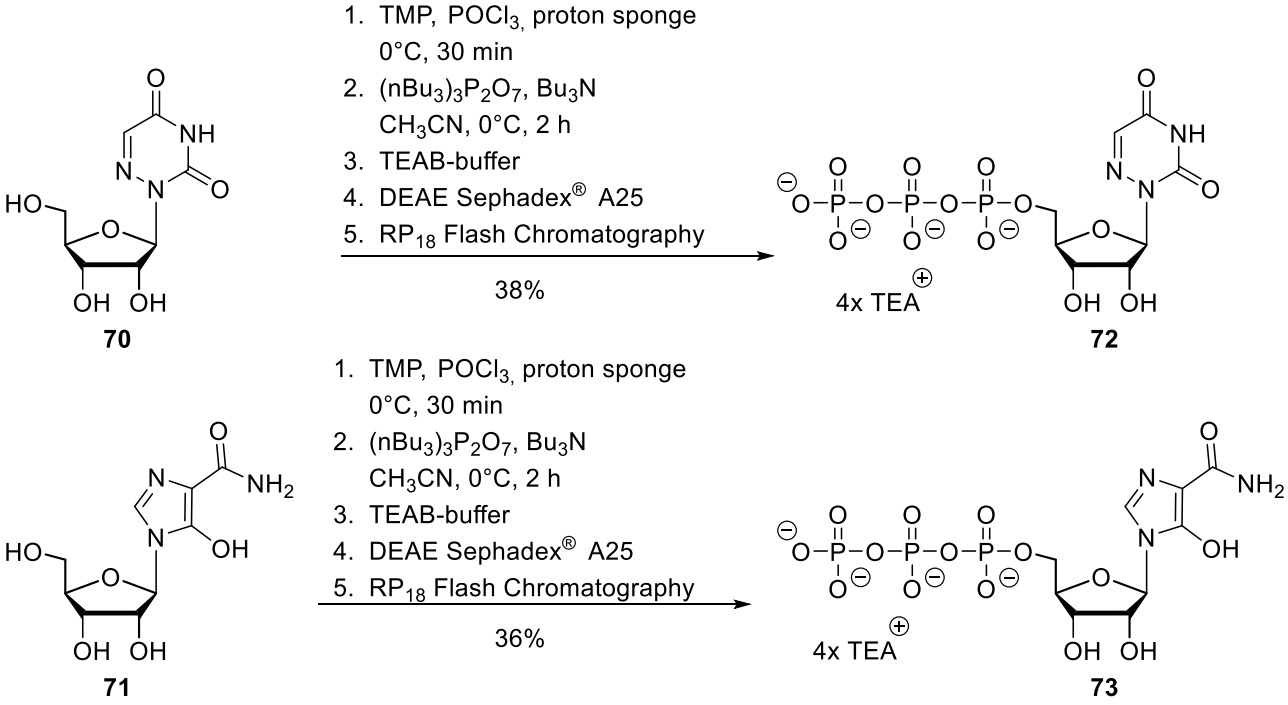

Figure 42: Synthesis of 6-azauridine-5´-triphosphate **72** and Mizoribine-5´-triphosphate **73**.

An additional advantage of these two nucleosides is that they are both commercially available, allowing the corresponding triphosphates to be synthesized in a single step using standard LUDWIG & ECKSTEIN conditions. Under these conditions, 6-azauridine-5´-triphosphate **72** was synthesized with a yield of 38% and Mizoribine-5´-triphosphate **73** with a yield of 36% (Figure 42).

The final triphosphate synthesized for the initial polymerase assay was *N*4-hydroxycytidine-5´-triphosphate **74**. As early as 2004, *N*4-hydroxycytidine **74** was shown to possess high antiviral activity against SARS-CoV[192] as well as a broad range of other RNA-viruses[193]. Therefore, its strong antiviral activity against SARS-CoV-2 was not unexpected [194,195]. This triphosphate can be synthesized easily and cost-effectively in a single step from commercially available cytidine-5'-triphosphate **75** by reacting it with an aqueous hydroxylamine solution in a yield of 31% (Figure 43).[196] As a result, it was included in the SARS-CoV-2 polymerase assays.

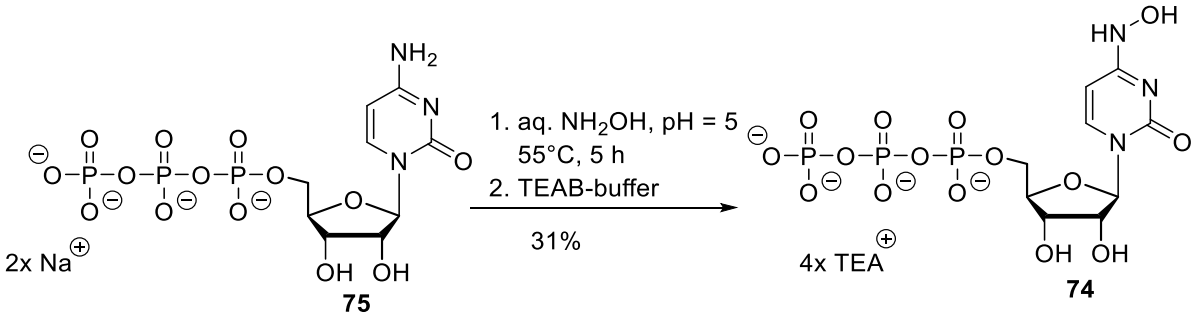

Figure 43: Synthesis of *N*4-hydroxycytidine-5´-triphosphate **74**.

4.6 SARS-CoV-2 RdRp primer extension assays

The synthesized nucleoside-5'-phosphates were comprehensively evaluated using primer extension assays specific to the SARS-CoV-2 RdRp, conducted by the research group of B. CANARD at the University of Marseilles. In these assays, a chemically synthesized template strand (5'-UAGCUUCUU(A/G/C)GGAGAAUGAC-3') is annealed to a Cy5-labeled primer (5'-Cy5-GUCAUUCUCC-3'). This primer/template duplex forms the basis for subsequent reactions.

The assays proceed by combining the prepared primer/template duplex with the SARS-CoV-2 RdRp complex, which comprises the proteins nsp12, nsp7, and nsp8 in a 1:3:6 stoichiometric ratio. As a positive control, this complex is able to completely elongate the RNA strand in the presence of all four natural NTPs.

Furthermore, to investigate the potential of non-natural NTPs as substrates, four additional assays were performed. Each of these assays omits one of the natural NTPs and incorporates a non-natural NTP being studied to determine its substrate properties. If the non-natural NTP can serve as an effective substrate for RdRp, it will substitute for the absent natural NTP and be incorporated into the growing viral RNA strand. Should the non-natural NTP acts solely as a substrate without terminating the chain elongation, a fully elongated product will form. Conversely, if it acts as a chain terminator, elongation will be arrested immediately following its incorporation, thus preventing further extension of the RNA chain.[52]

This methodological approach not only evaluates the substrate capability of each non-natural NTP for RdRp but also identifies the specific natural NTP it most closely mimics by examining the base opposite which it is incorporated in the template strand. These assays, through careful design and execution, provide critical insights into the functionality and potential therapeutic applications of non-natural nucleotides in combating SARS-CoV-2, contributing to our understanding of their role in viral replication and inhibition.

The first triphosphate evaluated in the primer extension assay was *N*4-hydroxycytidine-5´-triphosphate **74**. As expected, the primer was fully elongated in the presence of all natural NTPs. The addition of *N*4-hydroxycytidine-5´-triphosphate **74** did not inhibit primer elongation, even at a concentration of up to 250 µM (Figure 44). This indicates that the presence of **74** does not interfere with the natural elongation process at these concentrations. When assays were conducted without GTP, elongation predictably stalled after the incorporation of the first three NTPs, underscoring the critical role of GTP in subsequent RNA strand extension. If *N*4-hydroxycytidine-5'-triphosphate **74** would be able to substitute for GTP, its presence would enable continued elongation, leading to longer RNA products. However, even at a concentration of 50 µM, no advancement in elongation was noted, clearly indicating that **74** is not incorporated in place of GTP by RdRp. Similarly, in the absence of ATP, elongation did not proceed. Conversely, the exclusion of CTP from the assay resulted in rapid and full elongation within one minute. Furthermore, assays run without UTP still resulted in fully elongated products, though a noticeable band appeared at position eight on the gel. This band suggests a temporary pause before the incorporation of UTP, potentially indicating a minor kinetic preference or delay when **74** is incorporated.

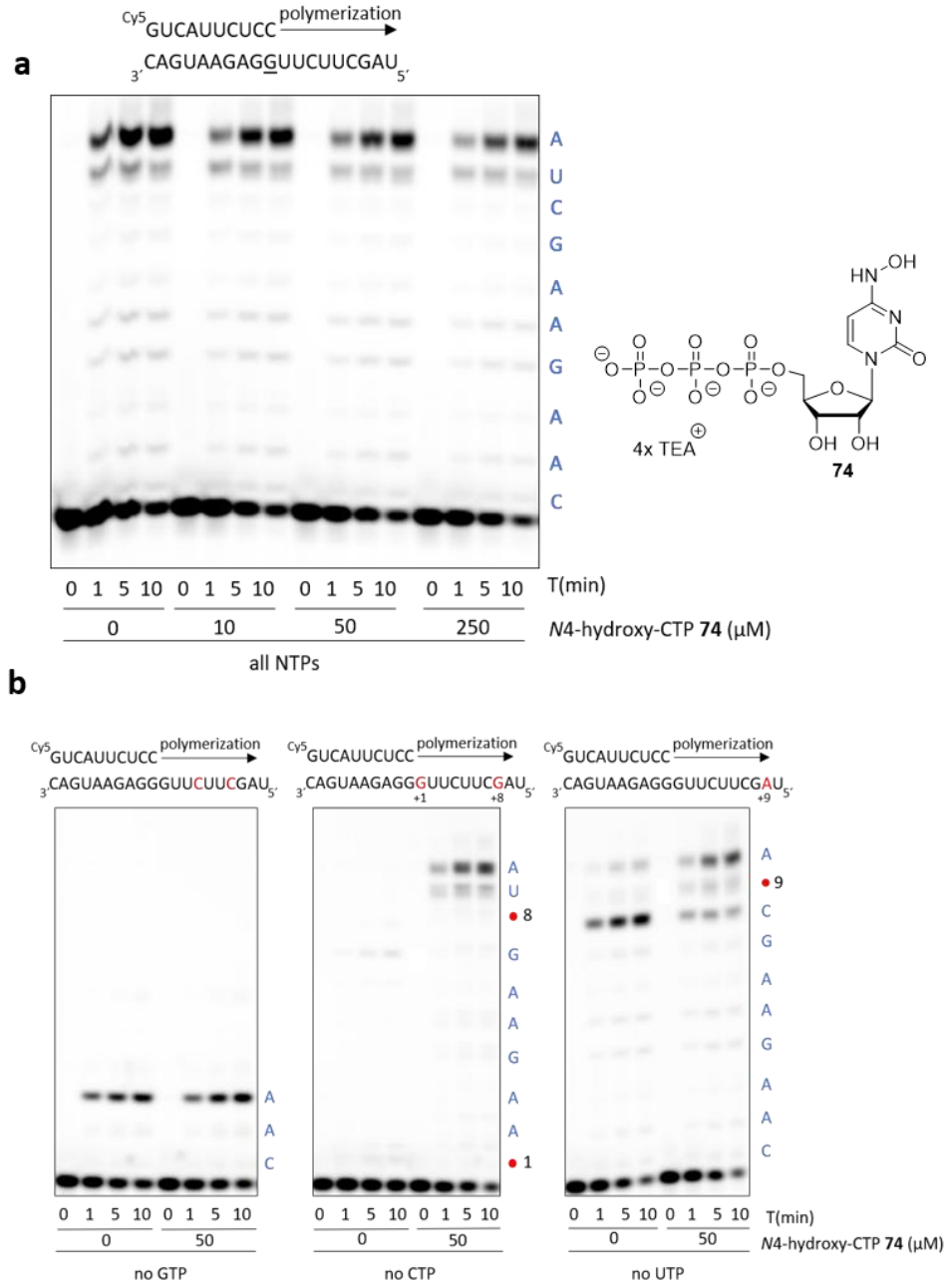

Figure 44: a| Time course of primer elongation in the presence of all natural NTPs (50 µM each) at different concentrations of *N*4-hydroxycytidine-5′-triphosphate **74** (0-250 µM). **b**| Time course of *N*4-hydroxycytidine-5′-triphosphate **74** incorporation (red dots) as a substitute of different natural NTPs (50 µM each) at different concentrations (0 or 50 µM).

These findings collectively indicate that *N*4-hydroxycytidine-5'-triphosphate **74** is efficiently incorporated into the viral RNA in place of CTP and, to a lesser extent, UTP, as illustrated in Figure 44. The ability of **74** to effectively replace these nucleotides highlights its potential utility in antiviral research.

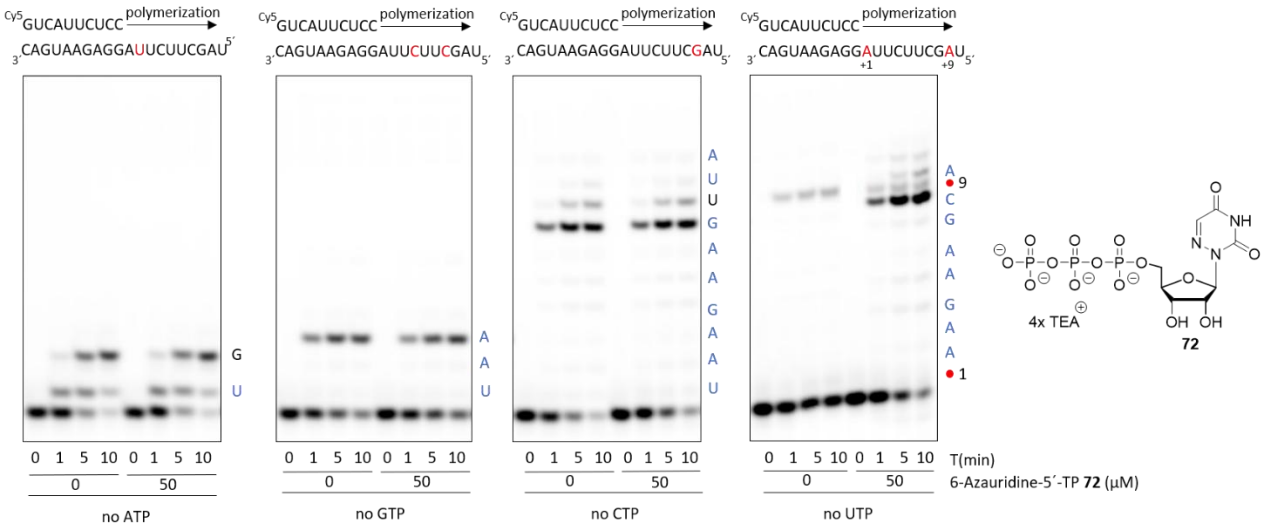

Figure 45: Time course of 6-azauridine-5´-triphosphate **72** incorporation (red dots) as a substitute of different natural NTPs (50 µM each) at different concentrations (0 or 50 µM).

When 6-azauridine-5'-triphosphate **72** was assessed under the same experimental conditions, it became clear that this compound was not incorporated in the absence of ATP, GTP, or CTP, suggesting its inability to substitute for these nucleotides (Figure 45). Notably, in scenarios where ATP and CTP were absent, the SARS-CoV-2 RdRp displayed a propensity for slow misincorporation of GTP or UTP, respectively. These misincorporations hindered further elongation of the RNA strand, indicating that the RdRp could not continue extending beyond these points of erroneous incorporation. Interestingly, in the absence of UTP, 6-azauridine-5'-triphosphate **72** was rapidly incorporated at the one position along the RNA strand. However, the synthesis of RNA nearly stalled entirely before the second incorporation event at position nine, resulting in significant delay in elongation. Despite this stalling, some fully elongated RNA products were eventually detected, albeit in reduced quantities. These observations suggest that 6-azauridine-5'-triphosphate **72** does not function as a direct substitute for ATP, GTP, or CTP, but notably acts as a UTP analogue. However, its incorporation efficiency is limited, likely due to structural factors or interactions within the RdRp active site that reduce its incorporation rate compared to natural UTP. Given these findings, 6-azauridine-5'-triphosphate **72** may not represent a molecule worthy of further investigation in this context, as its limited efficiency and specificity suggest it may not be a viable candidate for therapeutic use.

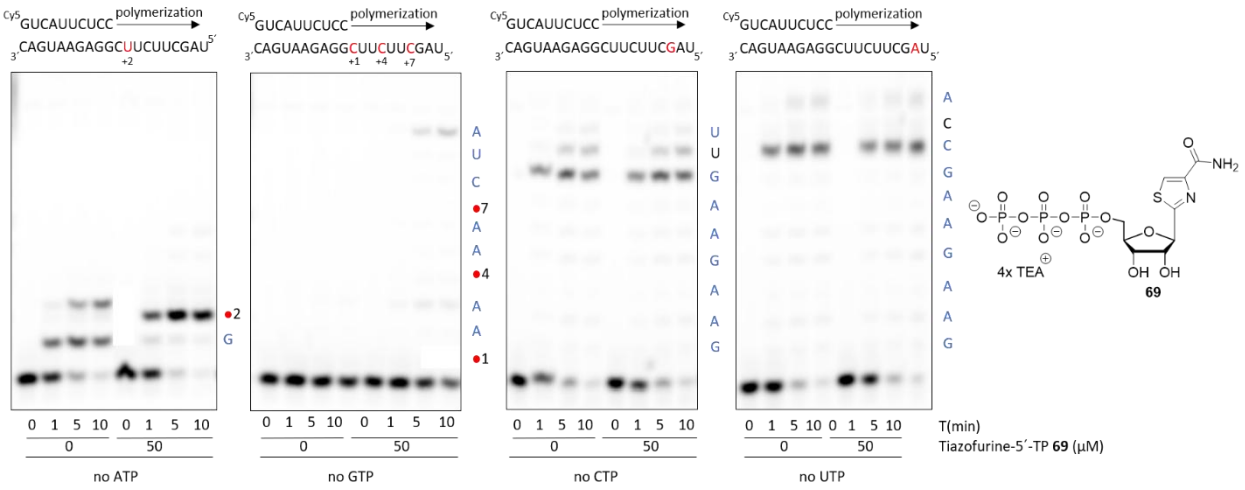

Figure 46: Time course of Tiazofurin-5´-triphosphate **69** incorporation (red dots) as a substitute of different natural NTPs (50 µM each) at different concentrations (0 or 50 µM).

In the primer extension assays conducted with Tiazofurin-5'-triphosphate **69**, no incorporation was observed when UTP and CTP were absent (Figure 46). This suggests that Tiazofurin-5'-triphosphate **69** does not serve as a viable substitute for these nucleotides under the tested conditions. In experiments where GTP was missing, a fully elongated product was detectable, albeit in small quantities even after an extended incubation of ten minutes. This observation implies that while there might be some interaction, Tiazofurin-5'-triphosphate **69** is not efficiently incorporated as a substitute for GTP. Interestingly, in the absence of ATP, tiazofurin-5'-triphosphate **69** demonstrated the ability to act as an effective substrate. For the specific experimental setup, the primer sequence design necessitated the consecutive incorporation of Tiazofurin-5'-triphosphate **69** at the second and third positions.

However, this sequential incorporation was not feasible, resulting in chain termination immediately after the first incorporation event. This suggests that while Tiazofurin-5'-triphosphate **69** can be incorporated initially, subsequent incorporations are hindered, possibly due to structural constraints or reduced affinity for the active site after initial binding. These interesting results raise several important questions that warrant further investigation. For instance, is Tiazofurin-5'-triphosphate **69** capable of effectively competing with ATP in a mixed nucleotide environment? Additionally, when Tiazofurin-5'-triphosphate **69** is present as a template base, does it lead to misincorporation, potentially causing errors in sequence reading or replication fidelity?

Evaluation of Mizoribine-5′-triphosphate **73** in primer extension assays revealed that the compound exhibited only limited interactions with the SARS-CoV-2 RdRp. Specifically, Mizoribine-5′-triphosphate **73** was not incorporated into the RNA strand in the absence of any natural NTP, highlighting its inability to act as a functional substitute for the natural nucleotides required by the viral polymerase (Figure 47). The results of this assay suggest that Mizoribine-5′-triphosphate **73** does not possess the properties needed to serve as an effective SARS-CoV-2 inhibitor. Given these findings, further research and development efforts into exploring this compound as a potential antiviral agent are deemed unnecessary.

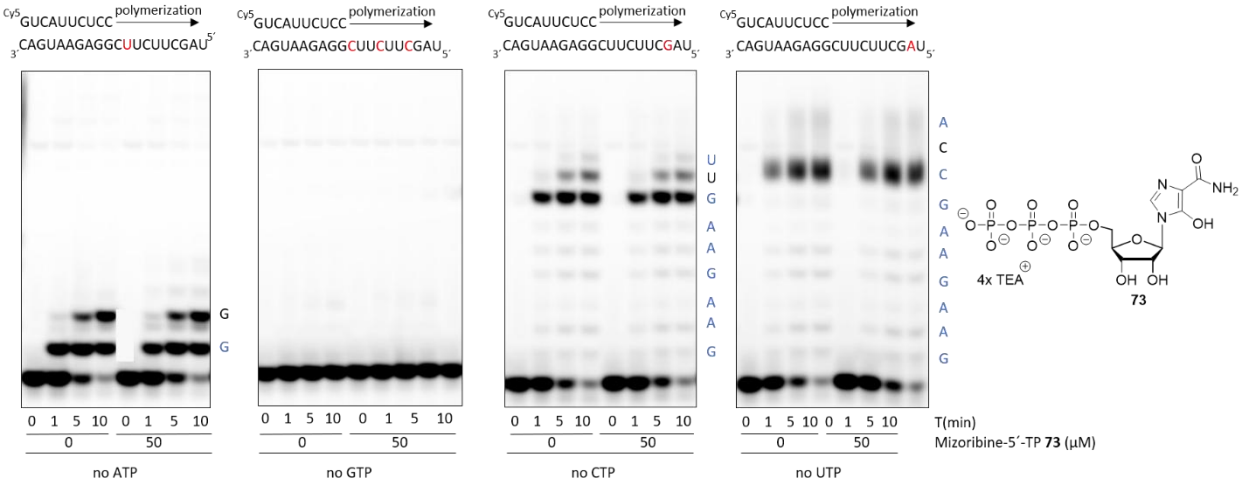

Figure 47: Time course of Mizoribine-5′-triphosphate **73** incorporation as a substitute of different natural NTPs (50 µM each) at different concentrations (0 or 50 µM).

Due to prior work that demonstrated T-1106-5′-triphosphate **14** is incorporated most efficiently in place of GTP, and with reduced efficiency compared to ATP,[52] the modified T-1106-5′-triphosphates were not evaluated for their incorporation by the SARS-CoV-2 RdRp in the absence of UTP and CTP. In Figure 48, the findings from the primer elongation assays conducted with the previously synthesized modified T-1106-5′-triphosphates while excluding ATP from the reaction are shown. The data illustrates that the control substance, T-1106-5′-triphosphate **14**, is effectively incorporated opposite U. Notably, consecutive incorporation of this triphosphate is achievable, indicating its compatibility with the RNA polymerization process. However, it must be pointed out that the second incorporation step is significantly slowed down, leading to an accumulation of the monophosphate at positions two and five of the growing RNA strand.

Furthermore, both the 3´-deoxy-T-1106-5´-triphosphate **17** and the 3´-fluoro-T-1106-5´-triphosphate **18** demonstrate the capacity to be incorporated in place of ATP. As anticipated based on their structural modifications, these compounds lead to immediate chain termination during the synthesis of the RNA strand. However, their incorporation is strikingly inefficient. In fact, the results suggest that even the incorporation of a G mismatch is achieved with greater probability than that of these modified triphosphates. The other modified T-1106-5´-triphosphates, specifically the 2´-*C*-methyl-T-1106-5´-triphosphate **15**, the 2´-α-fluoro-2´-β-*C*-methyl-T-1106-5´-triphosphate **16**, and the 3´-azido-T-1106-5´-triphosphate **19** were not incorporated at all by the SARS-CoV-2 RdRp under the tested conditions.

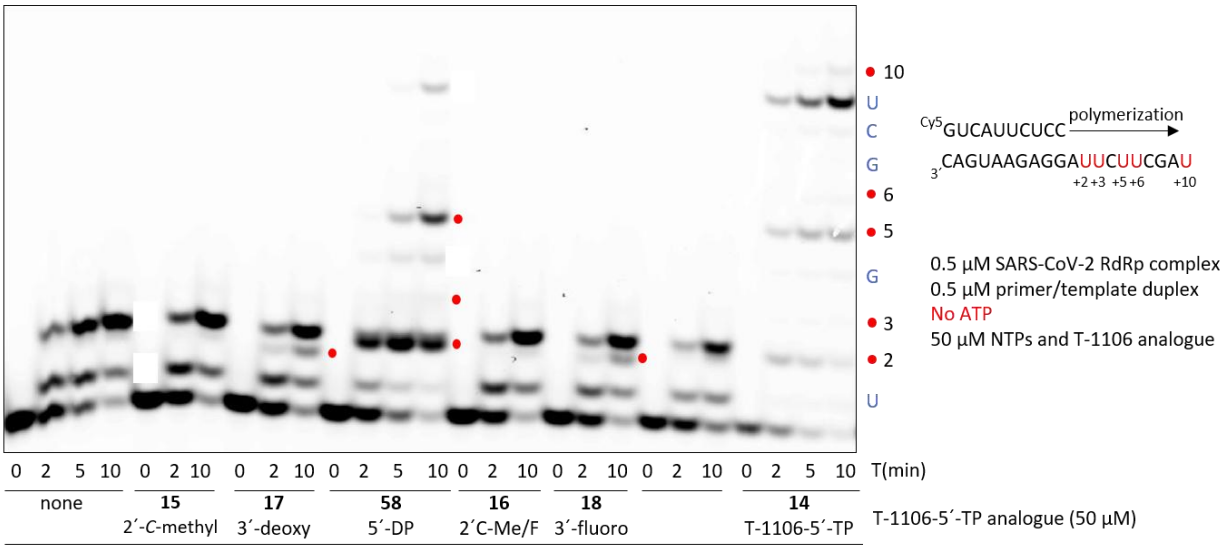

Figure 48: Time course of different modified T-1106-5´-triphosphates (50 µM)) incorporation (red dots) as a substitute of ATP in the presence of the remaining natural NTPs (50 µM each).

In Figure 49, the same experiment is conducted again with GTP omitted. In this experiment, the RdRp successfully incorporates the control T-1106-5´-triphosphate **14** as an alternative to GTP with remarkable efficiency. Within a brief span of five minutes, a majority of the RNA chains are fully elongated, indicating the high efficacy of T-1106-5´-triphosphate **14** in mimicking the function of GTP in the polymerization process. In contrast, 3´-azido-T-1106-5´-triphosphate **18** shows a complete lack of incorporation into the RNA strand. This result suggests that modifications at the 3´-position, particularly the addition of an azido group, may significantly hinder interactions with the RdRp active site. Consequently, this lack of incorporation led to the conclusion that the 3´-azido modification is not a promising candidate for developing antiviral

agents targeting SARS-CoV-2, as it cannot be effectively used by the viral polymerase to arrest viral replication.

Furthermore, both 3´-deoxy-T-1106-5´-triphosphate **17** and 3´-fluoro-T-1106-5´-triphosphate **18** are incorporated in place of GTP and they induce immediate chain termination upon incorporation. Despite being incorporated, their incorporation efficiency is considerably low, likely due to disturbances in necessary interactions at the active site of the RdRp. These results indicate that these 3´-modified triphosphates fail to compete effectively with natural NTPs and are thus deemed unsuitable candidates for further development as antiviral agents against SARS-CoV-2.

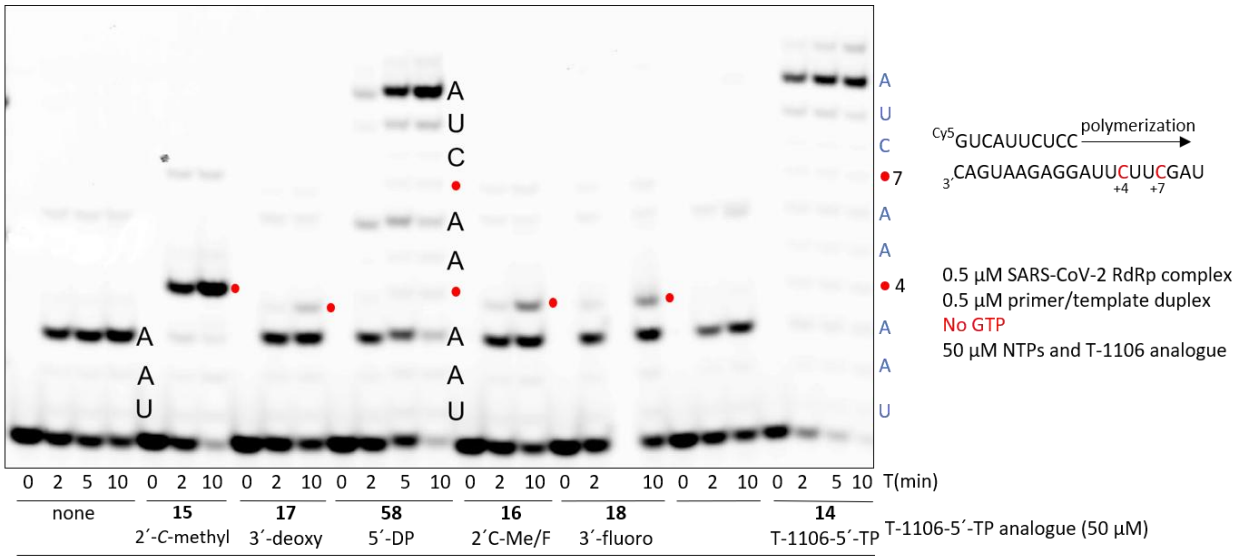

Figure 49: Time course of different modified T-1106-5´-triphosphates (50 µM)) incorporation (red dots) as a substitute of GTP in the presence of the remaining natural NTPs (50 µM each).

The examination of 2´-α-fluoro-2´-β-*C*-methyl-T-1106-5´-triphosphate **16** reveals that it is incorporated as a substitute for ATP, resulting in immediate chain termination. However, even after a ten-minute reaction period, only a faint band corresponding to position four is visible on the gel, indicating poor incorporation efficiency by the RdRp. Consequently, it is not a suitable candidate for further development.

Conversely, the 2´-*C*-methyl-T-1106-5´-triphosphate **15** demonstrates rapid and effective incorporation by the RdRp instead of GTP, immediately leading to chain termination. Impressively, within two minutes, a strong band forms at position four on the gel, and by ten minutes, almost all of the initial primer/template duplex is processed. These results showcase

the potential of the 2´-*C*-methyl modification in effectively mimicking GTP under the given conditions. This promising outcome suggests that 2´-C-methyl-T-1106-5´-triphosphate **15** could be a highly viable candidate for further antiviral development, provided it can compete effectively with natural GTP in the presence of physiological concentrations of the natural NTPs.

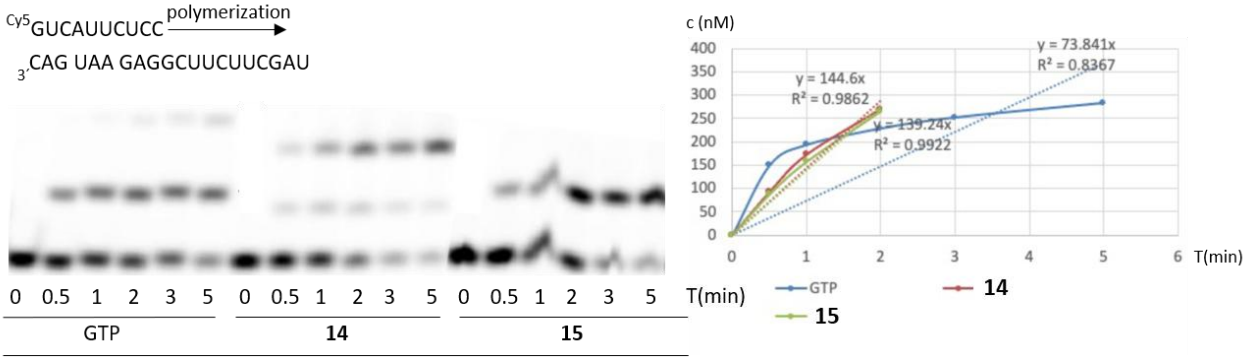

Figure 50: Single nucleotide incorporation of GTP, T-1106-5´-TP **14** and 2´-*C*-methyl-T-1106-5´-TP **15** (left). Calculated initial velocities (v_i) based of the linear regression (right) are 110.2 ± 43.4 nM/min for **14**, and 119.8 ± 51.5 nM/min for **15**.

In the subsequent step, the initial incorporation velocities (v_i) of GTP, T-1106-5´-TP **14**, and 2´-*C*-methyl-T-1106-5´-TP **15** were measured and compared in order to assess their respective kinetic properties. Attempts to determine a v_i value for GTP, however, were unsuccessful due to the non-linear nature of its incorporation rate under the assay conditions. Specifically, the data revealed the occurrence of a burst phenomenon, characterized by a rapid incorporation of GTP during the initial 45 seconds, followed by a notable decline to a slower, linear incorporation rate (Figure 50). In contrast to GTP, the incorporation rates for both T-1106-5´-TP **14** and 2´-*C*-methyl-T-1106-5´-TP **15** remained linear over the entire measurement period. These differences in kinetic behaviour may be attributed to structural or chemical differences between GTP and the analogues, potentially affecting their binding affinity, catalytic rate, or the overall mechanism of nucleotide incorporation. The consistent linearity enabled a straightforward calculation of the initial velocities for these analogues. The v_i values determined for T-1106-5´-TP **14** and 2´-C-methyl-T-1106-5´-TP **15** were 110.2 ± 43.4 nM/min and 119.8 ± 51.5 nM/min, respectively. The calculated initial incorporation velocities fall within a similar range, suggesting that the analogues are incorporated with comparable efficiency under the experimental conditions.

To evaluate whether 2´-*C*-methyl-T-1106-5´-TP **15** can effectively compete with GTP during nucleotide incorporation, further primer extension assays were conducted. These assays included all natural triphosphates together with varying concentrations of **15**. The results demonstrated the formation of chain-terminated products specifically at positions four and seven, while no termination products were observed at position one (Figure 51). This suggests that, under the conditions tested, incorporation of **15** can occur at certain template positions but may depend on sequence context or the efficiency of analogue competition with GTP at the active site.

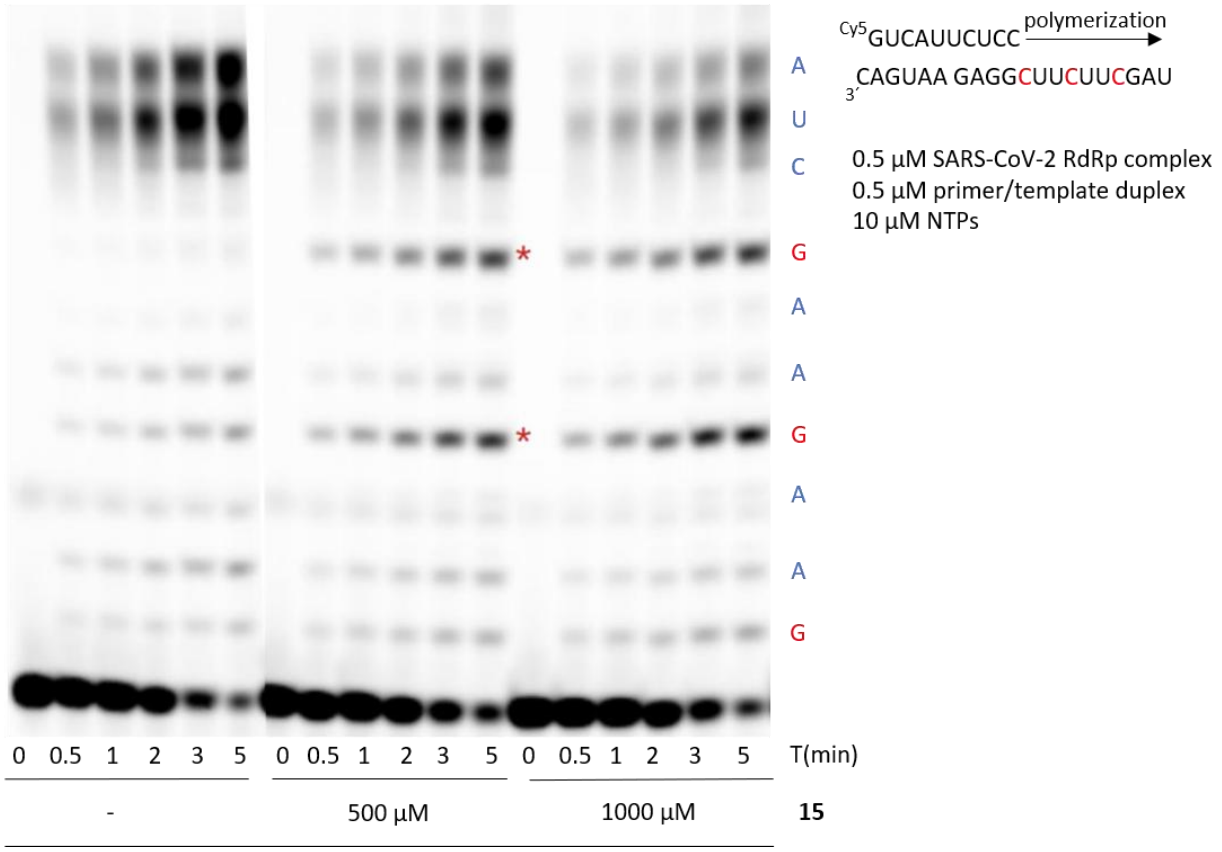

Figure 51: Competitive incorporation of 2´-*C*-methyl-T-1106-5´-TP **15** in the presence of GTP.

Quantitative analysis revealed that GTP is preferred over **15** by a factor of approximately 250 to 520, indicating that the SARS-CoV-2 polymerase exhibits a much higher selectivity for the natural nucleotide versus the analogue. Consequently, **15** functions as a significantly less efficient substrate for the viral polymerase compared to GTP.

Despite this substantial difference in substrate preference, the potential effectiveness of **15** as an antiviral agent should not be underestimated. The SARS-CoV-2 genome is approximately 30 kb

in length, 19.6% of which corresponds to guanine residues[197]. This translates to roughly 6,000 GTP incorporation events required per genome replication cycle. In contrast, even a single successful incorporation of **15** at any one of these positions could result in premature chain termination, thereby potentially halting viral replication.

Taken together, while **15** is a considerably poorer substrate for the RNA-dependent RNA polymerase of SARS-CoV-2 compared to GTP, its ability to induce chain termination following just one incorporation event highlights its potential as a promising antiviral agent, particularly when considering the large number of opportunities for incorporation throughout the viral genome.

In contrast to most other RNA viruses, CoVs present an exceptional challenge when it comes to inhibiting their replication with nucleoside analogues. This difficulty primarily arises from a unique proofreading mechanism in CoVs that is absent in many other RNA viruses. Specifically, SARS-CoV has evolved the ability to excise nucleoside analogue inhibitors from their viral RNA, even after these have been initially incorporated by the viral RdRp[198,199]. Responsible for the exonuclease activity is a complex of two non-structural proteins nsp14, which possesses 3´-to-5´ exonuclease activity, and its co-factor nsp10[200]. Together, these proteins can recognize and remove mismatched nucleotides or incorporated nucleoside analogues from the nascent RNA strand. As a result, antiviral drugs that are effective against other RNA viruses frequently display greatly reduced efficacy against coronaviruses.

Experimental evidence supports the crucial role of the nsp14-nsp10 complex in antiviral resistance. For instance, studies have shown that the antiviral activity of ribavirin increases by approximately 200-fold in strains of SARS-CoV that contain mutations disabling the ExoN activity, compared to wild-type virus which retains functional proofreading[201]. Even Remdesivir **5**, an antiviral nucleoside analogue believed to be at least partially resistant to excision by ExoN[202], demonstrates significantly improved inhibitory activity, about 4.5-fold higher, against SARS-CoV mutants lacking the nsp14-mediated exonuclease activity, compared to its effect on wild-type virus[198,203]. These observations highlight the necessity of considering the unique proofreading capabilities of coronaviruses when designing effective antiviral therapies, as well as the potential benefits of targeting or bypassing the ExoN function to boost drug efficacy.

To further assess the suitability of 2'-*C*-methyl-T-1106-5'-TP **15** as a potential antiviral agent against SARS-CoV-2, its resistance to excision by the SARS-CoV-2 ExoN was examined. For this

purpose, an incorporation-excision assay, developed in the working group of B. CANARD, was employed to compare the performance of 2'-*C*-methyl-T-1106-5'-TP **15** with that of GTP, and AT-9010 **75** (Figure 52). In this assay, a fluorescently labelled hairpin RNA substrate was extended by the RdRp. After 20 minutes of elongation, the reaction was halted and the nsp14/nsp10 complex was added to initiate the excision step. The excision reaction was then stopped at various time points to assess whether the incorporated nucleotide analogues were removed from the RNA strand.

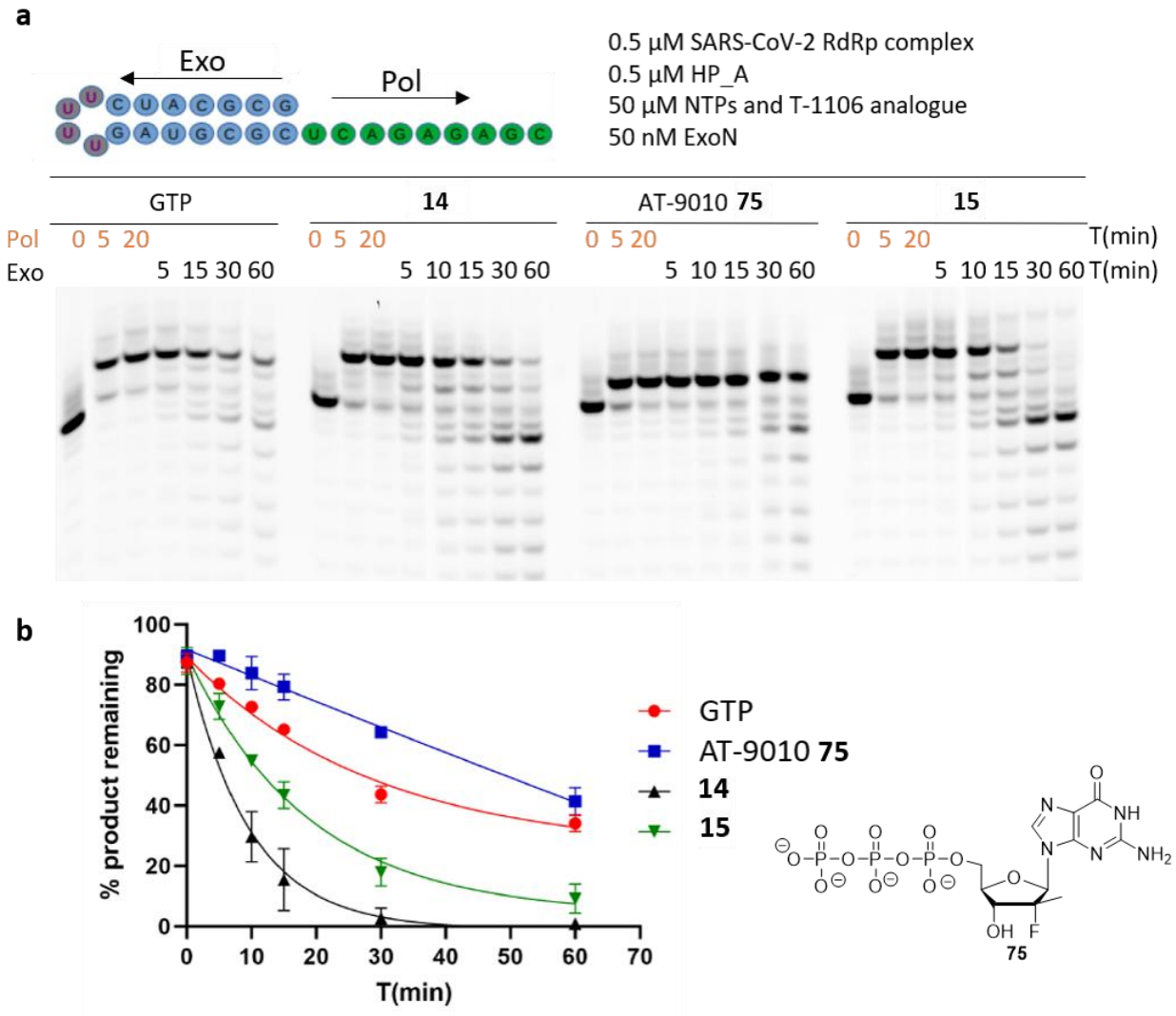

Figure 52: Incorporation and excision of 2'-*C*-methyl-T-1106-5'-TP **15**, T-1106-5'-TP **14**, AT-9010 **75**, and GTP. Time course of incorporation of 2'-*C*-methyl-T-1106-5'-TP **15**, T-1106-5'-TP **14**, AT-9010 **75**, and GTP by the SARS-CoV-2 RdRp. Polymerization (Pol) timepoints are shown in orange. After 30 minutes, the reaction was stopped and nsp14/nsp10 complex was added. Timepoints at, which the excision reaction (Exo) was stopped are shown in black.

Unfortunately, as illustrated in Figure 52, the results indicate that 2'-*C*-methyl-T-1106-5'-TP **15** is rapidly excised by the viral ExoN. After one hour of exposure to ExoN, almost the entire amount of this nucleoside analogue was removed from the RNA strand, highlighting its limited resistance to the proofreading activity of the viral polymerase machinery. Despite this rapid excision, a slight improvement in stability was observed compared to T-1106-5'-TP **14**, which was completely excised after only 30 minutes under the same experimental conditions. This relative improvement, while noteworthy, remains insufficient when considering the results obtained for the natural nucleotide GTP and the nucleoside analogue AT-9010 **75**. For both GTP and AT-9010 **75**, significant resistance to excision was observed, as only approximately half of the incorporated nucleotides were excised after one hour.

Taken together, these results underscore the importance of developing nucleoside analogues with increased resistance to excision by viral exonucleases. Improving the chemical structure of 2'-*C*-methyl-T-1106-5'-TP **15** to enhance its stability against ExoN could be a crucial next step for increasing its antiviral potential against SARS-CoV-2. Without such improvements, rapid excision by ExoN is likely to limit the compound's efficacy as an antiviral agent. In the following, the aim was to stabilize 2'-C-methyl-T-1106-5'-TP **15** against excision by ExoN.

4.7 Synthesis of α-thio-2´-*C*-methyl-T-1106-5´-triphosphate

In a previous study conducted by the research group of B. CANARD, it was demonstrated that the excision of AT-9010 **75** by the SARS-CoV-2 ExoN could be prevented by substituting the α-phosphate with an α-thiophosphate. This modification results in the formation of a chiral centre at the α-phosphorus atom, resulting in the formation of two distinct epimers (R_P and S_P) of the α-thiotriphosphate analogue of AT-9010 **75**, referred to as AT-9052 **76** (Figure 53). Further investigations revealed that the S_P isomer is preferentially incorporated as a substrate by the viral RdRp, and, importantly, once incorporated, this isomer is completely resistant to excision by ExoN.[204]

Building on these findings, the next objective of this study was to enhance the stability of 2'-*C*-methyl-T-1106-5'-TP **15** against ExoN-mediated excision by introducing an α-thiotriphosphate modification. Consequently, both the R_P and S_P isomers of α-thio-2'-C-methyl-T-1106-5'-TP **15** were synthesized and evaluated using the incorporation-excision assay. The initial approach to synthesizing α-thiotriphosphates was based on the established LUDWIG & ECKSTEIN protocol

(Chapter 4.4). In the modified protocol, phosphoryl chloride was substituted with thiophosphoryl chloride as the reagent for phosphorylation, with the intention of directly obtaining the corresponding α-thiomonophosphate **77** from the unprotected nucleoside **13**. This substitution represented the only significant alteration to the original method. However, no product formation was observed, even after reaction times of up to twelve hours at room temperature. In the literature, the reaction was performed successfully on various nucleosides without using a base and with triethyl phosphate as the solvent.[205] However, even under the exact same reaction conditions, no conversion could be observed by HPLC for the nucleoside **13**.

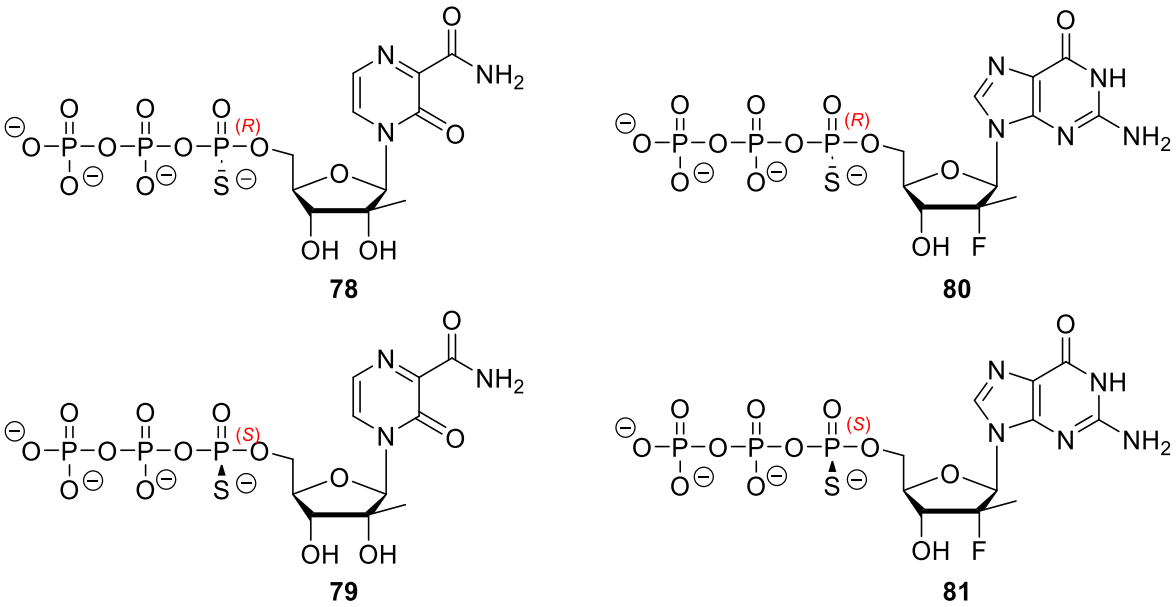

Figure 53: Both isomers of α-thio-2'-C-methyl-T-1106-5'-TP **78**, **79** and both isomers of AT-9052 **80**, **81**.

To address the lack of conversion, further modifications were made to the reaction conditions. Previous studies[206] have demonstrated that *N*-methylimidazole can serve as an effective base for thio-phosphorylation of 4'-fluoro nucleosides, which are presumed to be even less reactive than nucleoside **13**. Nevertheless, using *N*-methylimidazole as the base still did not yield any formation of the desired α-thio-monophosphate **77**, as confirmed by HPLC analysis (Figure 54).

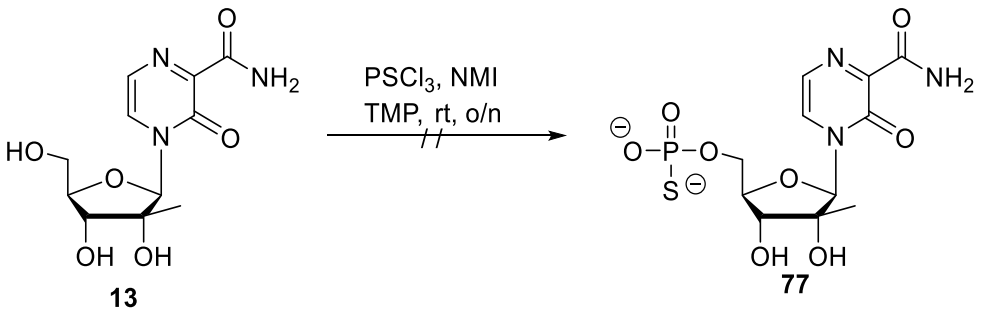

Figure 54: Initial attempt of the synthesis of α-thio-2'-C-methyl-T-1106-5'-MP **77**.

After encountering initial difficulties with the synthesis of α-thio-phosphates it was decided not to invest additional time and resources into further optimizing these types of reactions for nucleoside **13**. The main drawback of the traditional methods is that they yield a mixture of both isomers, necessitating separation by preparative RP-HPLC after synthesis. Instead, a stereoselective method for the synthesis of α-thio-triphosphates, published in 2024, was employed.[207] This method uses a new stereocontrolled approach in which a nucleoside is coupled with an in situ generated chiral triphosphate transfer reagent **81** or **82**, resulting in the selective formation of either the R_P **78** or S_P **79** isomer (Figure 55), depending on the chirality of the triphosphate transfer agent.

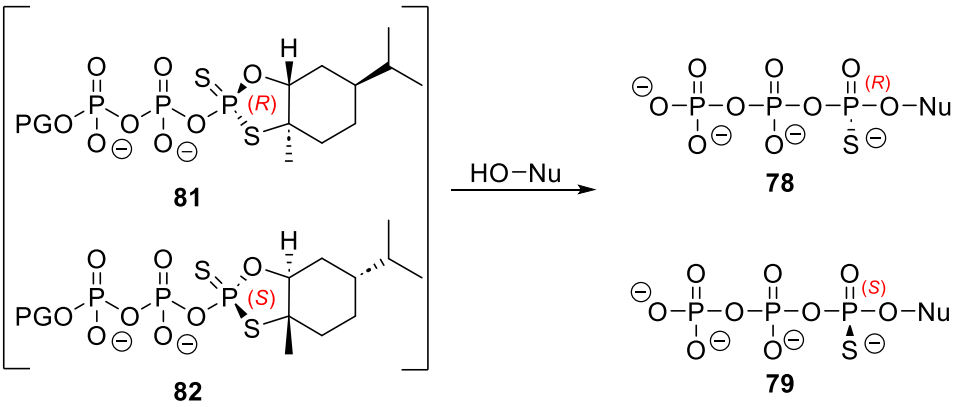

Figure 55: General reaction of the chiral triphosphate transfer reagent **81** and **82** with a nucleoside to give the respective R_P **78** or S_P **79** α-thio-triphosphates.

Since this method does not produce reliable results when applied to unprotected nucleosides, it was necessary to protect the 2'- and 3'-hydroxyl groups of the nucleoside **49** with benzoyl groups. In addition to introducing protecting groups, the methyl ester was selected in place of the corresponding amide **49**. This choice was made because the amide functionality could potentially participate in side reactions under the conditions required for the subsequent transformations,

thereby reducing the yield or purity of the desired product. The methyl ester was therefore considered more suitable for this synthetic route. Furthermore, the final coupling reaction was carried out in acetonitrile. Since the methyl ester is more lipophilic than the amide, it was expected to have a better solubility in acetonitrile, thereby facilitating the reaction and enhancing the overall efficiency of the coupling step. Importantly, choosing the methyl ester as a functional group did not introduce additional challenges for protecting group removal. Both the methyl ester and the benzoyl protecting groups could be cleaved simultaneously under standard conditions, thereby streamlining the deprotection process and eliminating the need for an extra step in the synthetic sequence.

In the initial step, the benzoyl groups of the protected nucleoside **48** were cleaved using a catalytic amount of sodium methanolate, selectively retaining the methyl ester at the pyrazine ring and affording nucleoside **83** in a yield of 94%. In the following step, the 5'-position was selectively protected with *tert*-butyldimethylsilyl chloride, resulting in a 84% yield of compound **84**. Subsequent protection of the 2'- and 3'-positions with benzoyl chloride yielded **85** in 92%. This approach was preferred over conventional silyl ether deprotection methods utilizing fluorides, as it provides milder and more convenient reaction conditions, as well as the high yields reported in the literature for cleavage of silyl ethers at the 5'-position of nucleosides.[208] However, the observed yield of 82% for compound **86** for this step was not entirely satisfactory, since yields exceeding 95% are typically expected for the cleavage of 5’-silyl ethers (Figure 56).

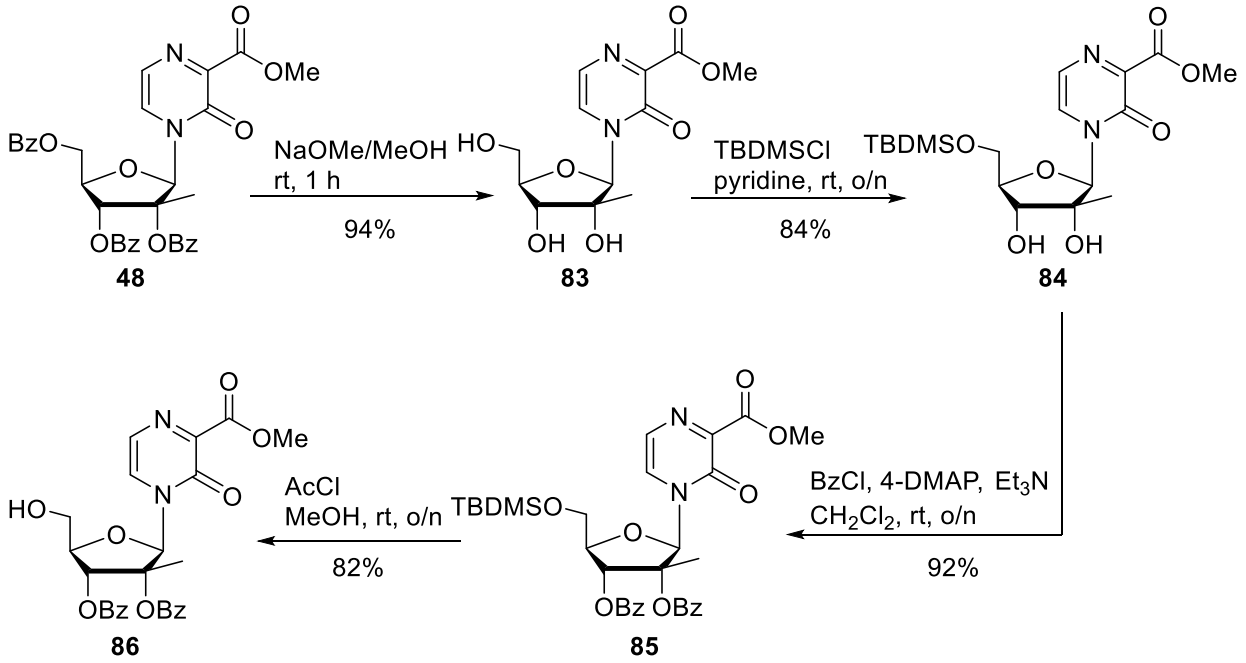

Figure 56: Synthesis of the 5´-deprotected nucleoside **86**.

After successful synthesis of the nucleoside precursor, the chiral phosphor-transfer agents **81** and **82** had to be synthesized. **81** and **82** are formed in situ from a non-chiral diphosphate building block **87** and a chiral thio-monophosphate building block **88** and **89**, respectively (Figure 57).

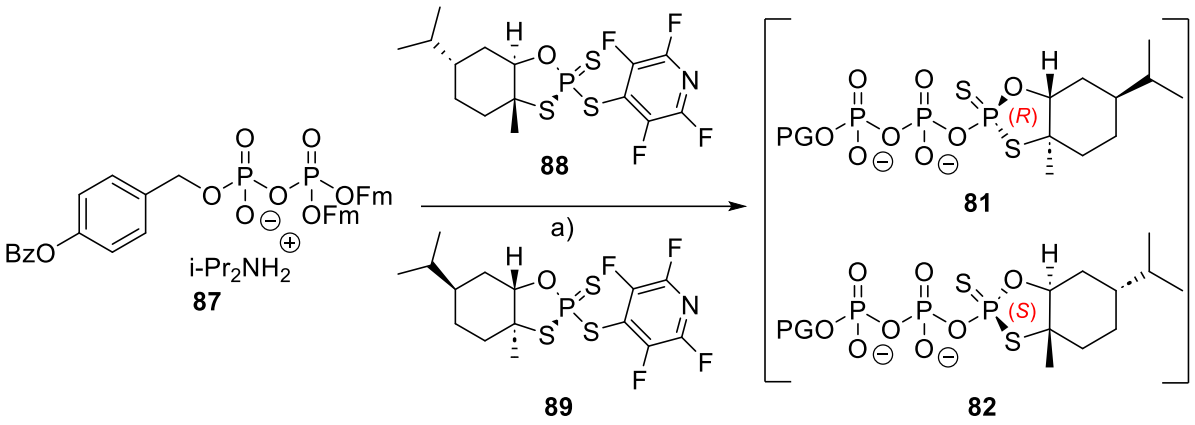

Figure 57: In situ formation of the chiral phosphor-transfer agents **81** and **82**.

In the initial step of the synthesis of the chiral building block, pentafluoropyridine **90** was reacted with sodium hydrosulfide hydrate to give tetrafluoropyridine-4-thiol **91** after an acidic workup, in a yield of 85%. In the subsequent step, **91** was reacted with phosphorus pentasulfide and *tert*-butylamine to give compound **92** in a yield of 59% (Figure 58).

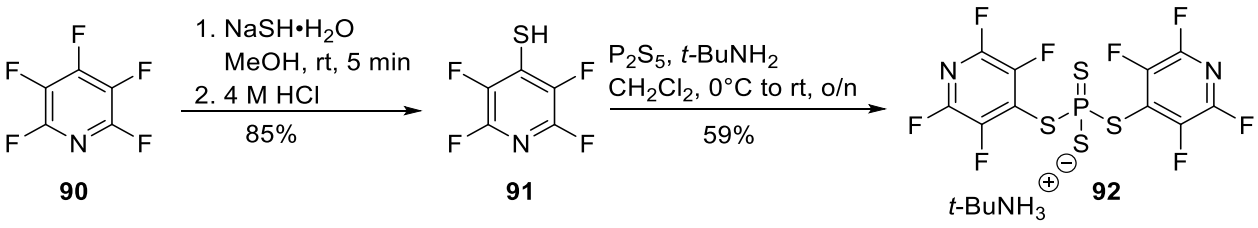

Figure 58: Synthesis of **92**.

Simultaneously, (-)-*cis*-limonene oxide **93** and (+)-*cis*-limonene oxide **94** were reduced using hydrogen in the presence of a catalytic amount of platinum dioxide. After complete consumption of the starting material was indicated by TLC, the reaction mixture was filtered, and the solvent was removed under reduced pressure to afford **95** and **96**, which were directly used in the next step (Figure 59).

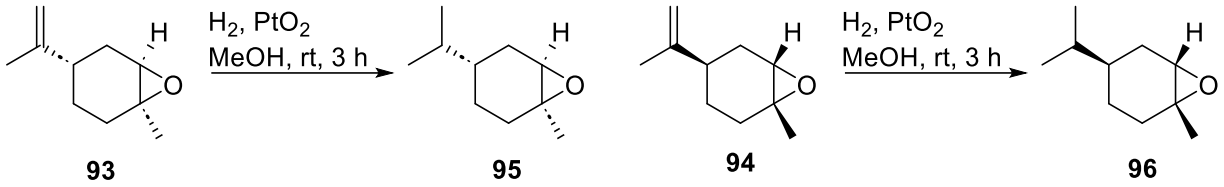

Figure 59: Reduction of (-)-*cis*-limonene oxide **93** and (+)-*cis*-limonene oxide **94**.

In the final step of the synthesis of the chiral building block, both epoxides **95** and **96** were coupled with **92** using trifluoroacidic acid to afford the chiral reagents **97** and **98** in yields of 53% and 49%, respectively (Figure 60). The diastereoselectivity of the reaction was determined by ^{31}P-NMR spectroscopy, the phosphorous signal of the mayor isomer has a shift of ~96 ppm, whereas the minor isomer has a shift of ~102 ppm. According to the literature,[207] the diastereomeric ratio of the major to minor isomer should not be less than 20:1. In this synthesis, a ratio of approximately 50:1 was achieved for both isomers.

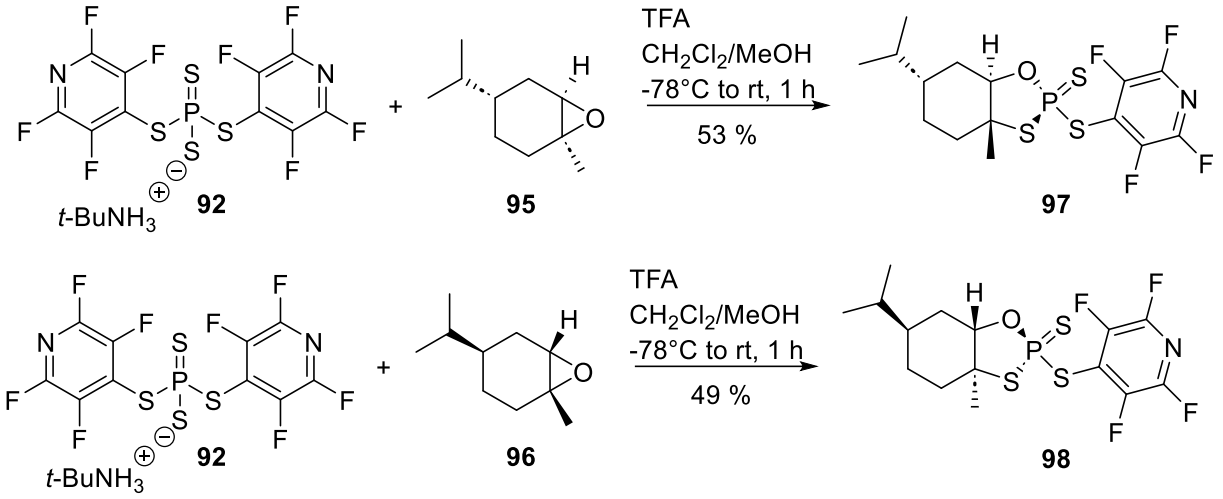

Figure 60: Synthesis of the chiral building block **97** and **98**.

The synthesis of the diphosphate building block began with the esterification of 4-hydroxybenzaldehyde **99** using benzoyl chloride and triethylamine. After aqueous work up, the resulting 4-formylphenyl benzoate **100** was used in the next step without further purification. In the subsequent step, the aldehyde function of 4-formylphenyl benzoate **100** was selectively reduced using sodium borohydride to obtain 4-(hydroxymethyl)phenyl benzoate **101**, in a yield of 98% over two steps (Figure 60).

Afterwards, 4-(hydroxymethyl)phenyl benzoate **101** was reacted with pyrophosphoryl chloride at -78°C. After four hours, the reaction was quenched by the addition of water, and the pH was

adjusted to 8 using saturate $NaHCO_3$ solution, resulting in the formation and precipitation of the sodium salt of the monophosphate. In the next step an attempt was made to redissolve the precipitate by adding concentrated HCl, with the aim of generating the dihydrogen phosphate. However, even after substantial addition of concentrated HCl, the precipitate could not be fully redissolved to obtain a clear solution. Consequently, the process was continued by extracting with ethyl acetate, but only 29% of the desired product **102** was isolated (Figure 61). Repeating the reaction several times did not improve the yield, primarily because complete conversion of the monophosphate to the dihydrogen phosphate form could not be achieved.

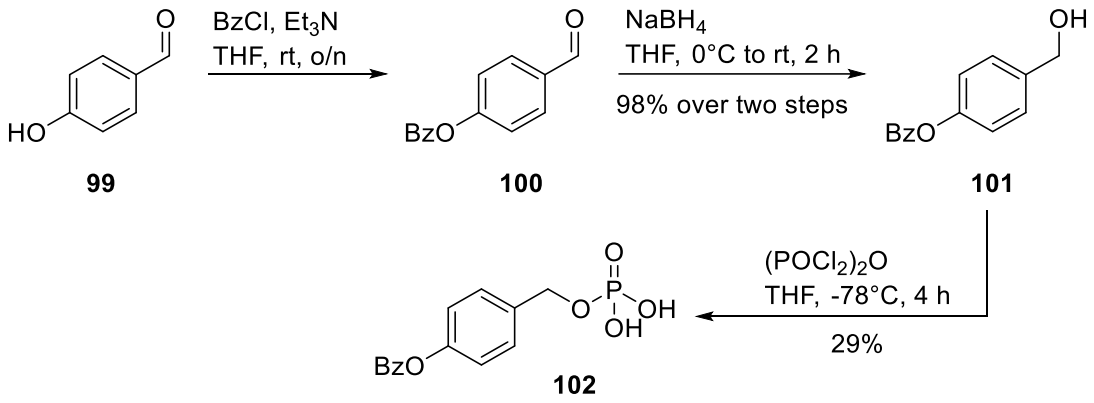

Figure 61: Synthesis of the monophosphate **102** starting from 4-hydroxybenzaldehyde **99**.

For further conversion of the monophosphate **102** to the desired diphosphate building block **87**, bis(fluorenylmethyl) phosphoramidite **103** was synthesized following a protocol established by the research group of C. MEIER[209] (Figure 62). In the first step, phosphorus trichloride **104** was reacted with diisopropylamine **105** to yield the corresponding amidite **106**. However, **106** was synthesized on a large scale and was stored for an extended period, minor decomposition could be observed, due to the sensitivity of **106** toward hydrolysis and oxidation. In the subsequent step, the amidite was reacted with 9-fluorenylmethanol **107** and triethylamine. After filtration and purification on silica gel, the desired phosphoramidite **103** was obtained in a yield of 67% (Figure 62).

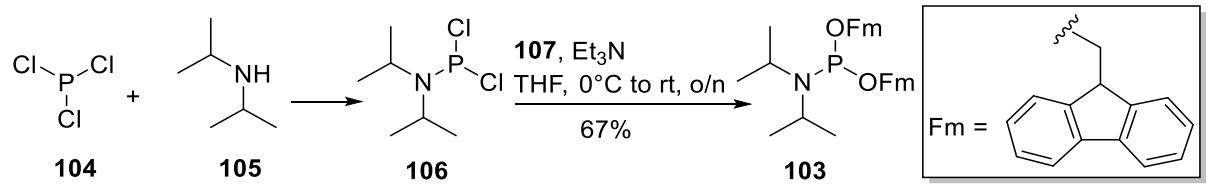

Figure 62: Synthesis of bis(fluorenylmethyl) phosphoramidite **103**.

It is noteworthy that, during silica gel purification, minimizing the product's retention time on the column is crucial, as the slightly acidic nature of silica gel can cause product decomposition. To address this, automated flash column chromatography was employed using a relatively polar eluent. Additionally, 1% triethylamine was added to the eluent to buffer the acidic conditions. Using this method, the desired amidite **103** was obtained in a yield of 67%, which is slightly lower compared to the literature, where a yield of 81% was reported.[209] This difference can be attributed to the fact that the starting material **106** was not freshly prepared and already exhibited minor decomposition.

The freshly prepared phosphoramidite **103** was subsequently reacted with the monophosphate **102** (Figure 63). 5-Phenyl-1*H*-tetrazole was used as an activator. After stirring at room temperature for one hour, the resulting phosphite was oxidized with *tert*-butyl hydroperoxide. The crude diphosphate was then purified via column chromatography on silica gel, yielding the desired product in 46% overall yield.

Despite multiple purification attempts, complete removal of the 5-phenyltetrazolate salts formed during the reaction was not achieved. Further purification attempts resulted in significant product loss. Consequently, it was decided to proceed with the impure material in the subsequent steps without further purification. To minimize decomposition caused by residual salts, the diphosphate building block **87** was stored at -80 °C.

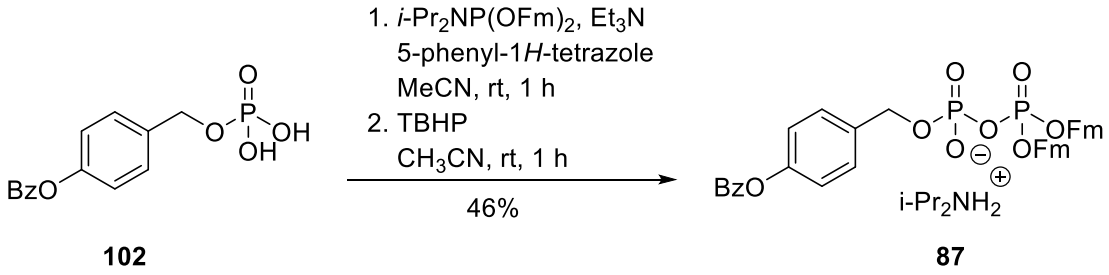

102 **87**

Figure 63: Synthesis of the diphosphate building block **87**.

With all the necessary precursors available, the synthesis of α-thio-triphosphates **78** and **79** was performed. In the first step, the diphosphate building block **87** was stirred with DBU for 10 minutes to remove the Fm protective group. Subsequently, the chiral building blocks **97** or **98** were added alongside freshly flame-dried 3 Å molecular sieves. After fifteen minutes of reaction time, the chiral phosphor-transfer agent **81** or **82** was formed. Then, the protected nucleoside **86** followed by a second portion of DBU was added.

After the reaction mixture was stirred for six hours, no remaining signals corresponding to the chiral phosphor-transfer agents **81** or **82** could be detected by ^{31}P-NMR (observed as a doublet at approximately 85 ppm). However, the formation of a significant amount of protected α-thio-triphosphate **107** was observed, a smaller amount of deprotected α-thio-triphosphate **78** was also formed during the reaction (Figure 64).

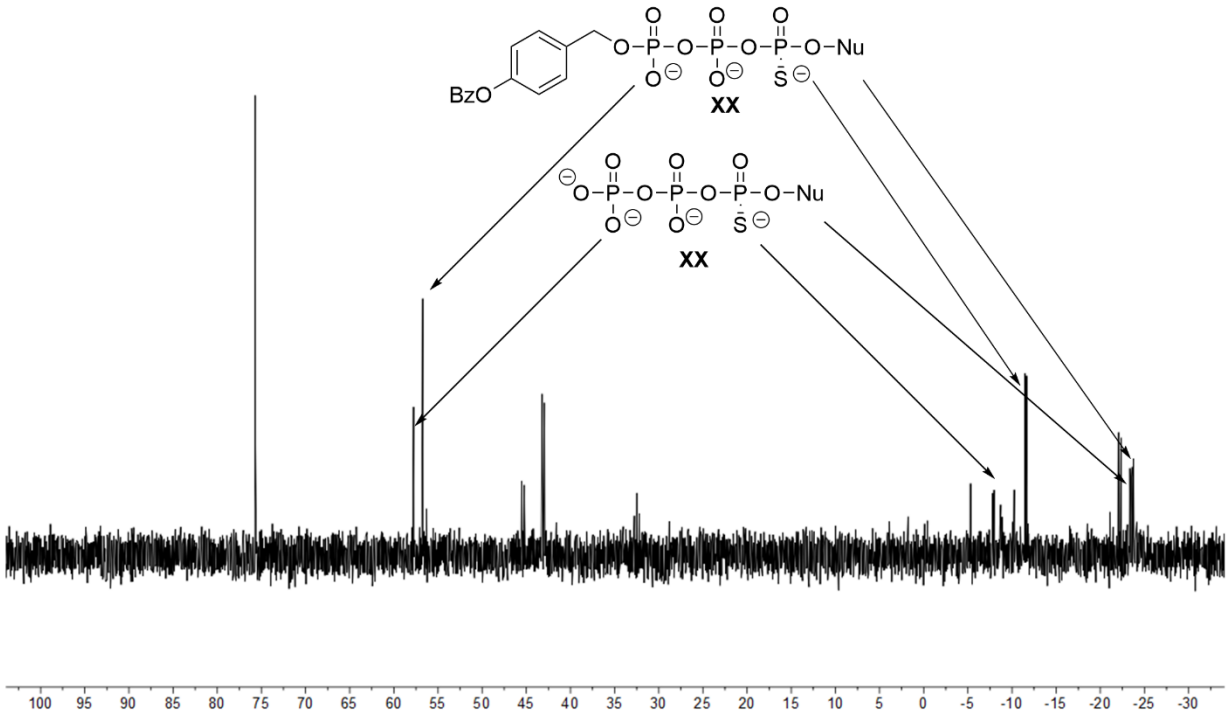

Figure 64: ^{31}P-NMR after six hours reaction time of the phosphate transfer step before deprotection. The formation of protected α-thio-triphosphate **107**, as well as the formation of already γ-deprotected α-thio-triphosphate **78** could be observed.

Subsequently, the reaction mixture was filtered and concentrated under reduced pressure. To achieve complete deprotection of the γ-phosphate and simultaneous cleavage of the ester at the pyrazine ring, concentrated ammonia was added. The crude product was then precipitated from a 0.2 M sodium perchlorate solution in acetone to remove most impurities. Final purification was performed on a DEAE Sephadex® A25 column using a gradient of 1 M NH_4HCO_3 in water, yielding the desired α-thiotriphosphates **78** and **79** as ammonia salts.

The same reaction conditions were applied to both isomers. 2´-*C*-methyl-T-1106-5´-α-thio-(R_P)-triphosphate **78** was obtained in a yield of 24%, while the 2´-*C*-methyl-T-1106-5´-α-thio-(S_P)-

triphosphate **79** in a yield of 32%. These yields are satisfactory and compare favorably with literature reports for ribonucleoside analogues, which range from 27% to 47% (Figure 65).[207]

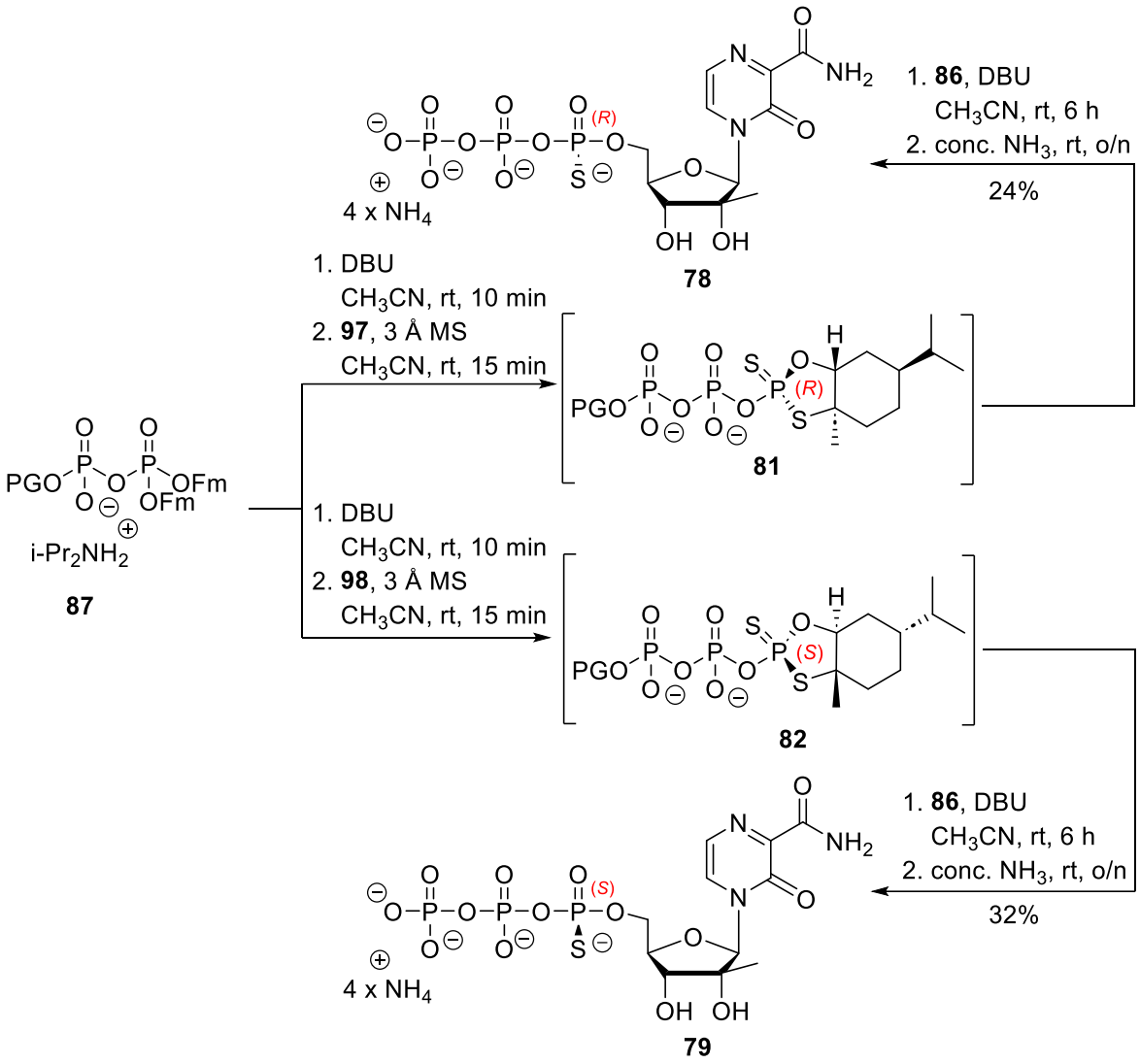

Figure 65: Synthesis 2´-*C*-methyl-T-1106-5´-α-thio-(R_P)-triphosphate **78** and 2´-*C*-methyl-T-1106-5´-α-thio-(S_P)-triphosphate **79**.

4.8 SARS-CoV-2 RdRp primer extension and excision assays

To assess whether the synthesized α-thio-triphosphates **78** and **79** can serve as substrates for SARS-CoV-2 RdRp, primer extension assays were performed in the research group of B. CANARD. Subsequently, the stability of these α-thio-triphosphates against excision from viral RNA by the SARS-CoV-2 ExoN was evaluated. Figure 66 illustrates the SARS-CoV-2 primer extension/excision assay. In this experiment, a synthetic hairpin RNA acts as the primer and is combined with the SARS-CoV-2 RdRp complex. The reaction mixture contains all natural NTPs except for GTP. GTP is

specifically excluded because previous results have shown that 2'-*C*-methyl-T-1106-TP **15** functions as a guanosine analogue (see Chapter 4.6).

The results demonstrate that 2´-*C*-methyl-T-1106-5´-α-thio-(S_P)-triphosphate **79** is rapidly incorporated by the SARS-CoV-2 RdRp into the growing viral RNA strand, leading to immediate chain termination upon incorporation, as expected. In contrast, the 2´-*C*-methyl-T-1106-5´-α-thio-(R_P)-triphosphate **78** is also recognized as a substrate by the RdRp, but is incorporated much less efficiently compared to the S_P isomer. Even after prolonged incubation times of up to 120 minutes, full elongation of the RNA strand is not achieved, indicating a reduced rate of incorporation by the R_P isomer. This difference highlights the importance of stereochemistry in the interaction between nucleotide analogues and the viral polymerase.

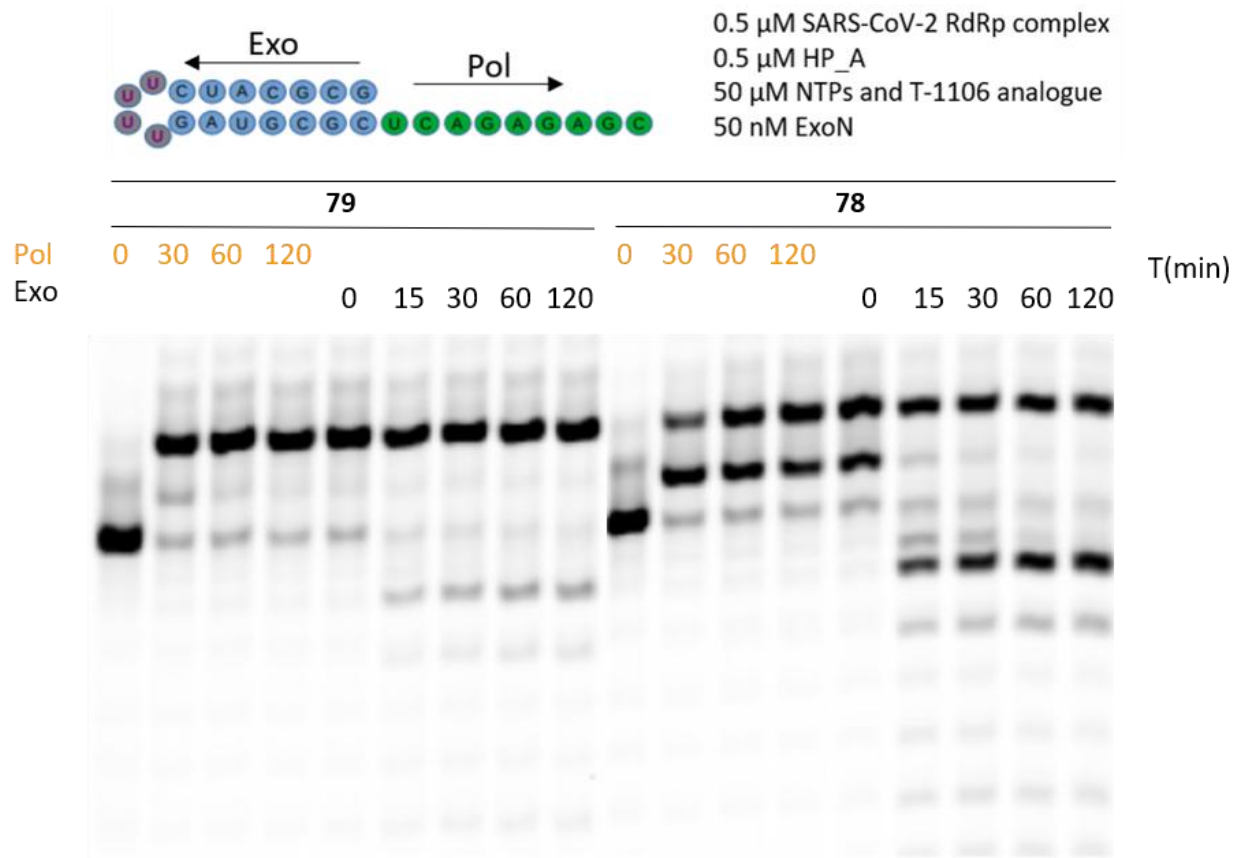

Figure 66: Incorporation and excision of 2'-*C*-methyl-T-1106-5'-α-thio-(R_P)-triphosphate **78** and 2'-*C*-methyl-T-1106-5'-α-thio-(S_P)-triphosphate **79**. Polymerization (Pol) timepoints are shown in orange. After 120 minutes, the reaction was stopped and ExoN was added. Timepoints at, which the excision reaction (Exo) was stopped are shown in black.

To further assess the stability of the incorporated analogues, the SARS-CoV-2 ExoN was added to the reaction mixture after 120 minutes. The results showed that, following the addition of ExoN, both the S_P and R_P isomers remained completely resistant to excision. No detectable removal of either isomer was observed even after an additional 120 minutes of incubation, demonstrating that both forms of the nucleotide analogue confer high stability against the viral proofreading function.

Taken together, these results suggest that 2'-*C*-methyl-T-1106-5'-α-thio-(S_P)-triphosphate **79** is a potent inhibitor of viral RNA synthesis. Its rapid incorporation by SARS-CoV-2 RdRp, coupled with its ability to induce irreversible chain termination and its high stability against excision by SARS-CoV-2 ExoN, highlight its potential as an effective antiviral agent. This suggests that 2'-*C*-methyl-T-1106-5'-α-thio-(S_P)-triphosphate **79** could serve as a promising candidate for the development of novel therapeutics against SARS-CoV-2.

4.9 Prodrug synthesis

Nucleoside triphosphates face a major challenge in drug development due to their limited ability to efficiently cross the lipophilic cell membrane. This is primarily due to their high polarity and the presence of four negative charges on the phosphate group. To overcome this obstacle, prodrug strategies can be employed to mask these negative charges and enhance lipophilicity, thereby facilitating cellular uptake. Once inside the cell, enzymatic or chemical processes trigger the release of the active compound. Specifically, these prodrugs can be designed to directly release the antiviral active triphosphate or to generate the mono- or diphosphate forms, which are then phosphorylated by host cell enzymes to produce the active triphosphate necessary for antiviral activity.

To investigate the impact of the α-thio group on antiviral activity, prodrugs of 2'-*C*-methyl-T-1106 **49** with and without this functional group were synthesized. The prodrug approach employed involved ProTide technology (Chapter 2.3).[210] Compared to other approaches such as Tri*PPP*ro, ProTide technology offers the advantage of more straightforward incorporation of the α-thio group due to a simplified synthetic route. Moreover, ProTide technology has been successfully utilized in the development of various antiviral nucleoside analogues that have received FDA approval for clinical use.[211–213] However, a limitation of the ProTide technology is that it exclusively releases the nucleoside-5'-monophosphate within the cell. Consequently, this

approach depends on host cell kinases to convert the monophosphate into the pharmacologically active triphosphate.

Phosphoramidate prodrugs can be synthesized with a wide variety of leaving groups attached to the phosphorus atom. For initial cell-based testing, two amino acid ester variants were selected: L-alanine isopropyl ester and L-alanine 2-ethylbutyl ester, each combined with a phenol residue. These particular combinations were chosen because they have been successfully employed in FDA-approved antiviral drugs. The isopropyl ester is found in Tenofovir alafenamide [213] and Sofosbuvir,[211] while the 2-ethylbutyl ester was used in the development of Remdesivir **5**.

For the synthesis of phosphoramidate prodrugs lacking an α-thio function, an established synthetic approach was employed. In this method, the unprotected nucleoside **49** is treated with *tert*-butylmagnesium chloride to form the corresponding magnesium salt, which subsequently was reacted with the phosphoramidite precursor **107**. The commercially available precursor **107** contains a pentafluorophenol leaving group, which, after overnight reaction, yields the desired phosphoramidate prodrug **108** in a satisfactory yield of 46% (Figure 67). Under identical reaction conditions, the synthesis was successfully carried out using the precursor **109** to yield the prodrug **110**.

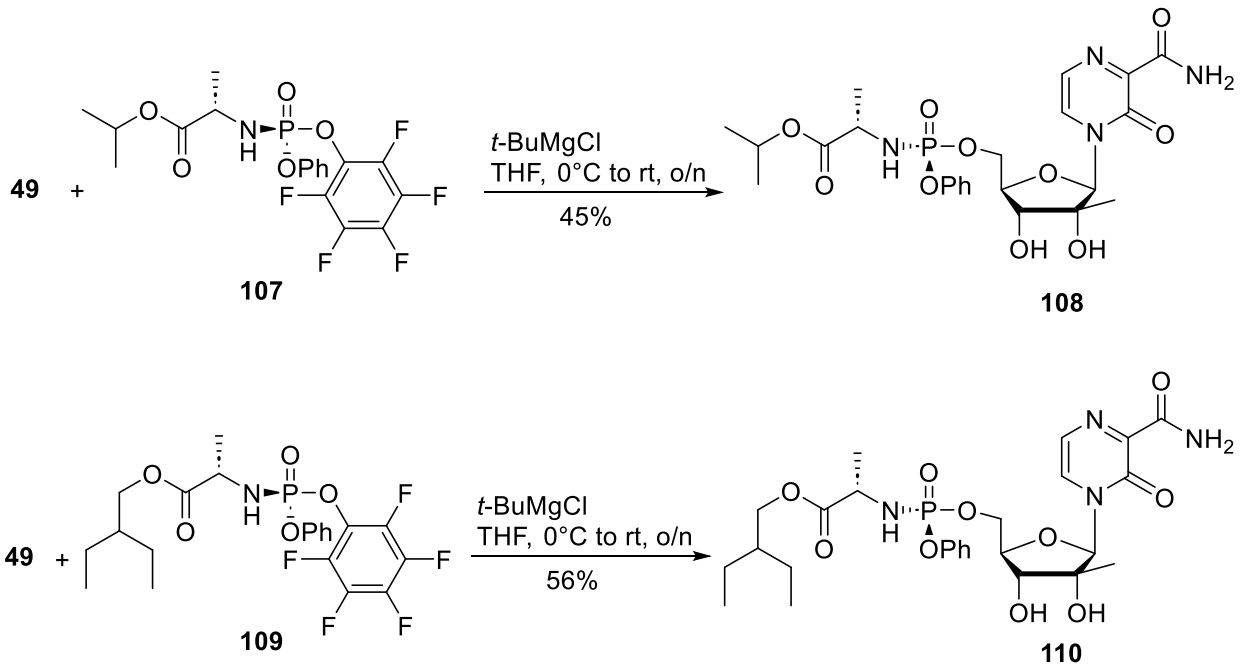

Figure 67: Synthesis of the phosphoramidate prodrugs **108** and **110**.

Previous studies have demonstrated that the S_P isomers of phosphoramidate prodrugs exhibit significantly higher antiviral activity than the corresponding R_P isomers.[211]. Consequently, only the S_P isomers of the phosphoramidate prodrugs **108** and **110** were synthesized. This approach was straightforward, as the necessary precursors **107** and **109** are commercially available in the pure S_P isomeric form.

For the synthesis of the phosphoramidate prodrugs containing an α-thio function, the same overall synthetic strategy was employed. However, in this case, the required precursors were not commercially available and therefore had to be synthesized. In the first step, phenol **111** was reacted with thiophosphoryl chloride in the presence of triethylamine to yield *O*-phenyl dichlorothiophosphate **112** in a yield of 90%. Subsequently, **112** was reacted with L-alanine isopropyl ester hydrochloride in the presence of triethylamine, to obtain compound **113** in a yield of 89%. Finally, **113** was reacted with pentafluorophenol in the presence of triethylamine, yielding the precursor **114** in 70% yield as a mixture of isomers (Figure 68).

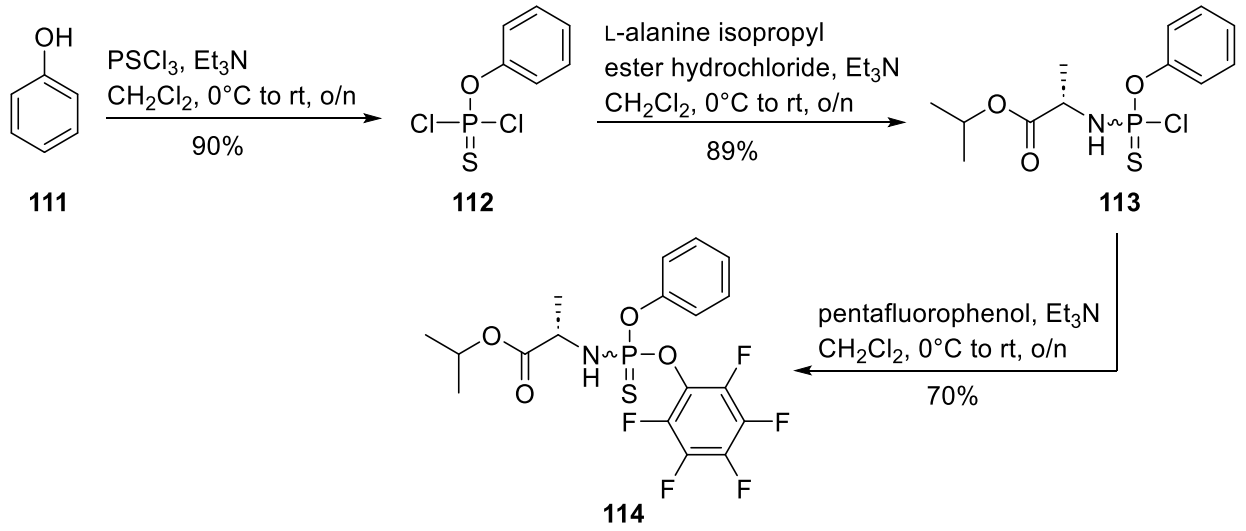

Figure 68: Synthesis of the phosphoramidate precursor **114**.

The isomers of compound **114** can be separated either by preparative HPLC using chiral columns or by recrystallization, with the latter generally being preferred due to lower costs. Another approach involves synthesizing single diastereomers of phosphoramidates using a chiral auxiliary. However, this method's applicability to thio-phosphoramidates is questionable, given the lower reactivity of the phosphorus atom.[214] Before investing significant time and effort into the separation of isomers, it was therefore decided to first assess whether the desired phosphoramidate prodrug could be synthesized from the isomeric mixture of **114**.

In the subsequent step, the synthesized precursor **114** was reacted with the nucleoside **49** under the same conditions that had previously been successful for the synthesis of **108** and **110**. However, no conversion of the starting material was observed. Even when the reaction temperature was increased to 50°C, there was still no detectable conversion. A possible explanation for the reduced reactivity of precursor **114** is the substitution of the oxygen atom bound to the phosphorus atom with a sulfur atom. This replacement decreases the polarization of the phosphorus center, thereby reducing its electrophilicity and making it less susceptible to nucleophilic attack by the deprotonated nucleoside (Figure 69).

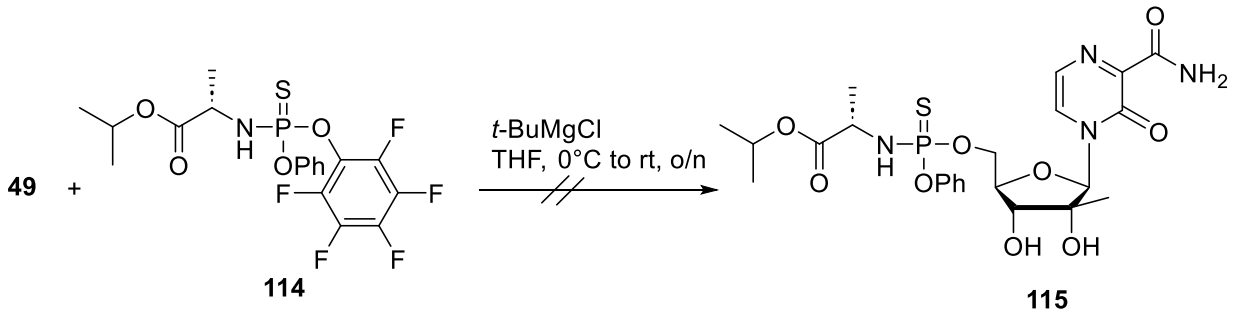

Figure 69: Attempt of the synthesis of the α-thio-phosphoramidate prodrug **115**.

Based on these results, it was decided to use chloride **113** as the precursor, as it is expected to exhibit significantly higher reactivity toward nucleophilic attack due to superior leaving group properties of the chloride anion compared to pentafluorophenol. However, since these compounds are prone to decomposition and cannot be stored for extended periods, they must be freshly synthesized immediately prior to use.

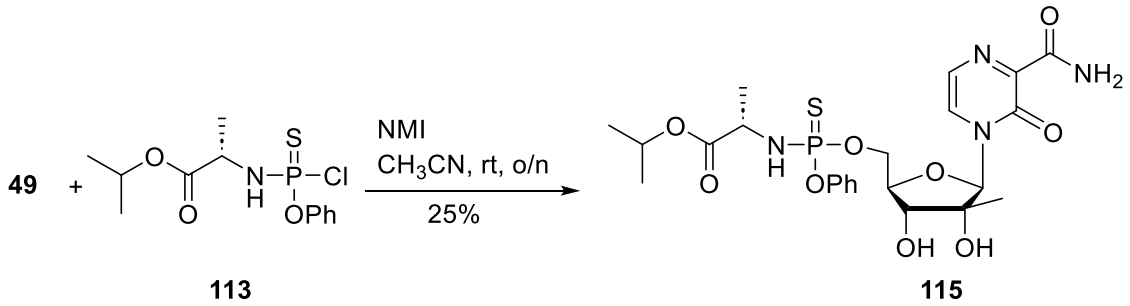

Figure 70: Synthesis of the α-thio-phosphoramidate prodrug **115**.

By reacting the nucleoside **49** with **113** in the presence of 1-methylimidazole it was possible to synthesize the desired α-thio-phosphoramidate prodrug **115** in a yield of 25% as a mixture of isomers (Figure 70).

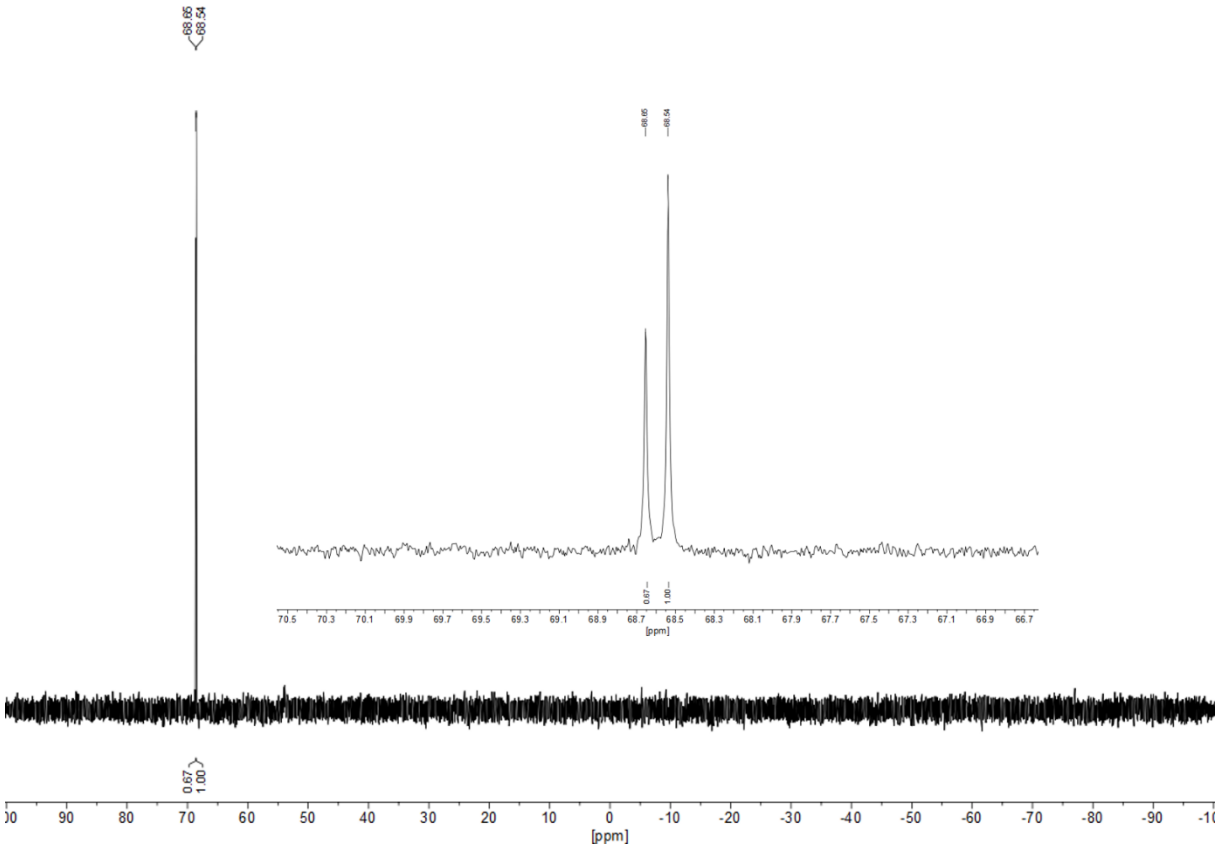

Figure 71: 31P-NMR of α-thio-phosphoramidate prodrug **115**.

The diastereomeric ratio of the resulting mixture was determined by ^{31}P-NMR spectroscopy to be approximately 1:0.67 (Figure 71). However, it was not possible to determine which isomer was present in excess. For the current objective, evaluating whether the α-thio function has a beneficial effect on the antiviral activity of 2'-*C*-methyl-T-1106-TP **15**, this uncertainty is not a critical issue.

Following the successful synthesis of the isopropyl ester α-thio-phosphoramidate **113**, the corresponding α-thio-phosphoramidate **116** bearing a 2-ethylbutyl residue was synthesized using the same strategy. Initially, *O*-phenyl dichloridothiophosphate **112** was reacted with L-alanine 2-ethylbutyl ester hydrochloride in the presence of triethylamine, resulting in precursor **116** with a yield of 62%. In the subsequent step, **116** was coupled with the nucleoside **49** in the presence of 1-methylimidazole, affording the desired α-thio-phosphoramidate **117** in 73% yield, obtained as a mixture of isomers (Figure 72). The diastereomeric ratio, as determined by ^{31}P-NMR spectroscopy, was found to be approximately 1:0.63. As in the previous cases, the specific configuration of the major isomer was not assigned.

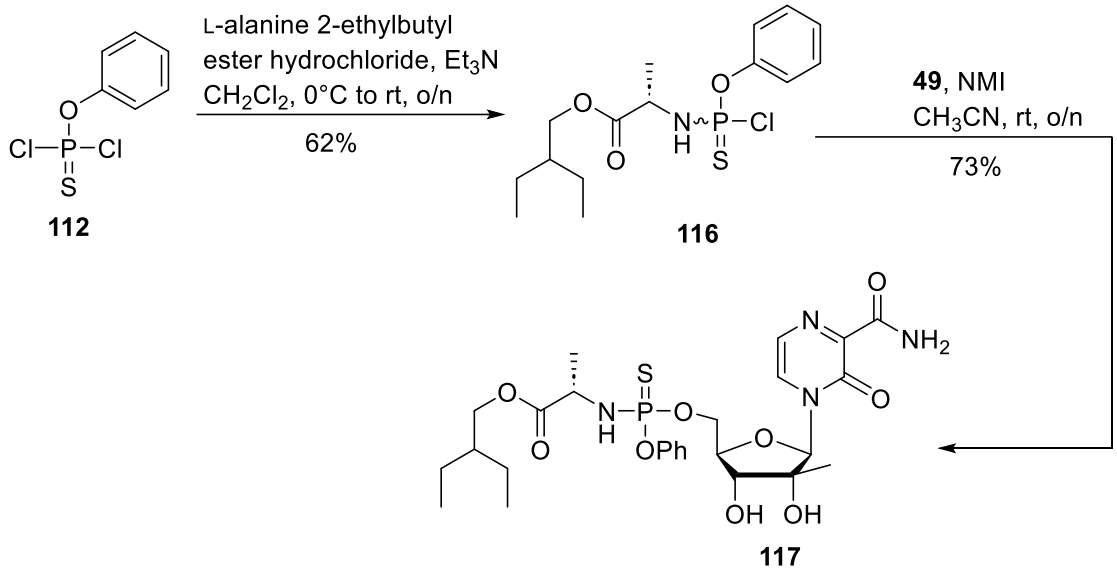

Figure 72: Synthesis of the α-thio-phosphoramidate prodrug **117**.

Following the successful synthesis of phosphoramidate prodrugs of 2'-*C*-methyl-T-1106 **49**, both with and without an α-thio function, the next objective was to prepare the corresponding prodrugs of T-1106 **13** in order to investigate the influence of the 2'-methyl group on antiviral activity. The initial approach was to use the same synthetic strategy as employed for the synthesis of **108** and **110**. However, no conversion of the starting material was observed, even after heating the reaction mixture to 50°C. This lack of reactivity was attributed to the poor solubility of T-1106 **13** in THF. Subsequent attempts to improve solubility by using a 1:1 mixture of THF and CH_3CN also failed to produce any detectable conversion (Figure 73).

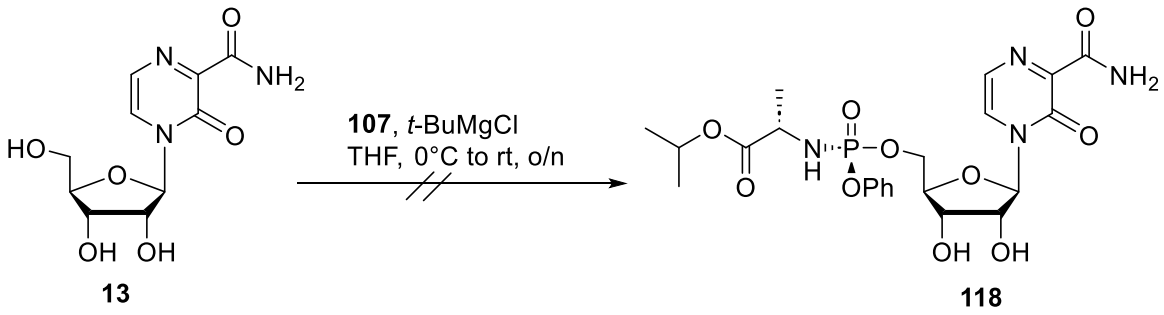

Figure 73: Attempt of the synthesis of the phosphoramidate prodrug **118**.

Due to these challenges, it was decided to adopt the same synthetic strategy previously used for the synthesis of the α-thio-phosphoramidate prodrugs **115** and **117**. This approach offers the advantage of conducting the reaction in CH_3CN, which is expected to provide better solubility for T-1106 **13**. However, as in the previous case, this method only yields a mixture of isomers.

Initially, phenyl dichlorophosphate **119** was reacted with L-alanine isopropyl ester hydrochloride and L-alanine 2-ethylbutyl ester hydrochloride, affording the two phosphoramidates **120** and **121**in yields of 92% and 86%, respectively. Both products were obtained as 1:1 mixtures of isomers (Figure 74).

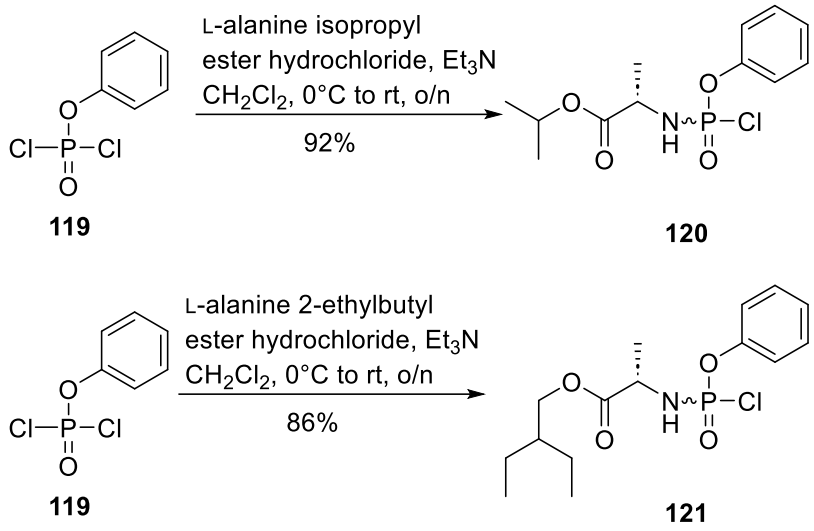

Figure 74: Synthesis of the phosphoramidate precursors **120** and **121**.

Both precursors **120** and **121** were subsequently reacted with T-1106 **13** in the presence of 1-methylimidazole to produce the target phosphoramidates. This reaction resulted in a yield of 22% for **122**, and 42% for **123**. Both phosphoramidates were obtained as a mixture of isomers (Figure 75). The relatively low overall yields are likely attributable to the limited solubility of T-1106 **13** in acetonitrile, which can hinder reaction efficiency and product formation. Enhancing the solubility of T-1106 **13** might be a key factor to enhance yields in future experiments.

For future studies, it may be beneficial to consider introducing protecting groups, such as isopropyl groups, on the 2'- and 3'-hydroxy groups of T-1106 **13**. This modification would primarily aim to increase the molecule's lipophilicity, potentially improving its solubility in organic solvents and simplifying purification procedures. While protecting hydroxyl groups can sometimes prevent unwanted side reactions, in this context, the main goal is to enhance the compound's lipophilic character rather than to suppress specific side reactions. The approach used for synthesizing T-1106-5'-triphosphate **14**, which involved utilizing the methyl ester of **13** instead of the free amine to enhance the solubility (Chapter 4.5), is not feasible here. This is because selective cleavage of the ester on the pyrazine ring cannot be achieved without also cleaving the ester on the alanine residue.

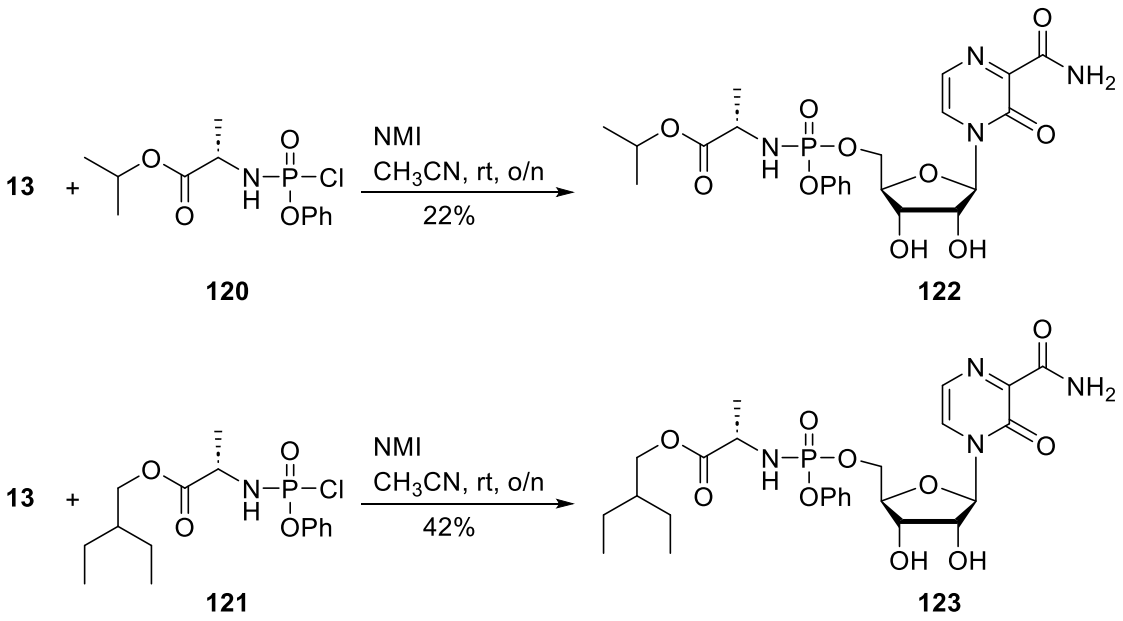

Figure 75: Synthesis of the phosphoramidate prodrugs **122** and **123**.

Following the successful synthesis of the phosphoramidates **122** and **123**, the subsequent objective was to synthesize the corresponding α-thio-phosphoramidate **124**. Using the established synthetic strategy that was previously successful for the formation of **115** and **117**, attempts to convert the starting materials did not yield any significant products, as indicated in Figure 76.

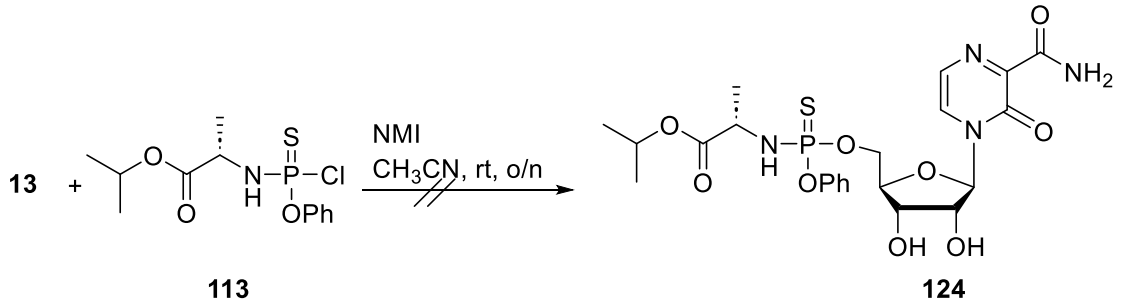

Figure 76: Attempt of the synthesis of the phosphoramidate prodrug **124**.

The low solubility of **13** in the reaction solvents posed an initial barrier, which was already a limiting factor in the prior reactions with the same precursors. Furthermore, the inherently lower reactivity of the α-thio-phosphoramidates can be attributed to the nature of the phosphorus-sulfur bond, which is less polarized compared to phosphorus-oxygen bonds. This decreased polarization diminishes the electrophilicity of the phosphorus center, leading to decreased reactivity and, consequently, no observable conversion of the starting materials despite the

application of the established synthetic protocols. Due to time constraints, the synthesis of suitable α-thio-phosphoramidate prodrugs of T-1106 **13** was not achievable within the scope of this work. As with the previous compounds, increasing the lipophilicity of **13** could potentially improve its reactivity and overall synthetic efficiency.

All the synthesized prodrugs were subsequently evaluated for their antiviral activity in cell-based assays, in collaboration with the research group of B. COUTARD. The results are discussed in chapter 4.10.

4.10 Cell base assays

To evaluate the antiviral activity of the synthesized prodrugs, cell-based assays were performed using HUH 7.5 cells infected with the SARS-CoV-2 strain G614 BavPat. EC_{50} values for the prodrugs were determined in this system. The results of these assays, summarized in Figure 77, present the activity profiles of various phosphoramidate prodrugs of 2´-*C*-methyl-T-1106 **49**.

The data indicate that the phosphoramidate prodrug **110** lacking an α-thio function and bearing a 2-ethylbutyl residue display no detectable antiviral activity. Substitution of this residue with an isopropyl group resulted in a measurable, but modest EC_{50} value of 71.8 µM for compound **108**. Notably, introduction of the α-thio function leads to a marked improvement in potency, reducing the EC_{50} value for compound **115** to 39.9 µM.

A particularly significant enhancement is observed when the α-thio function is introduced to **110**, yielding an EC_{50} of 1.8 µM for **117**, where previously no antiviral activity was detected. Alongside this promising potency, a CC_{50} value of 48.1 µM was determined, corresponding to a SI of 27.

Overall, these preliminary results suggest that incorporation of an α-thio function substantially enhances the antiviral activity of this class of prodrugs. The observed EC_{50} of 1.8 µM provides a strong foundation for further structural optimization and development.

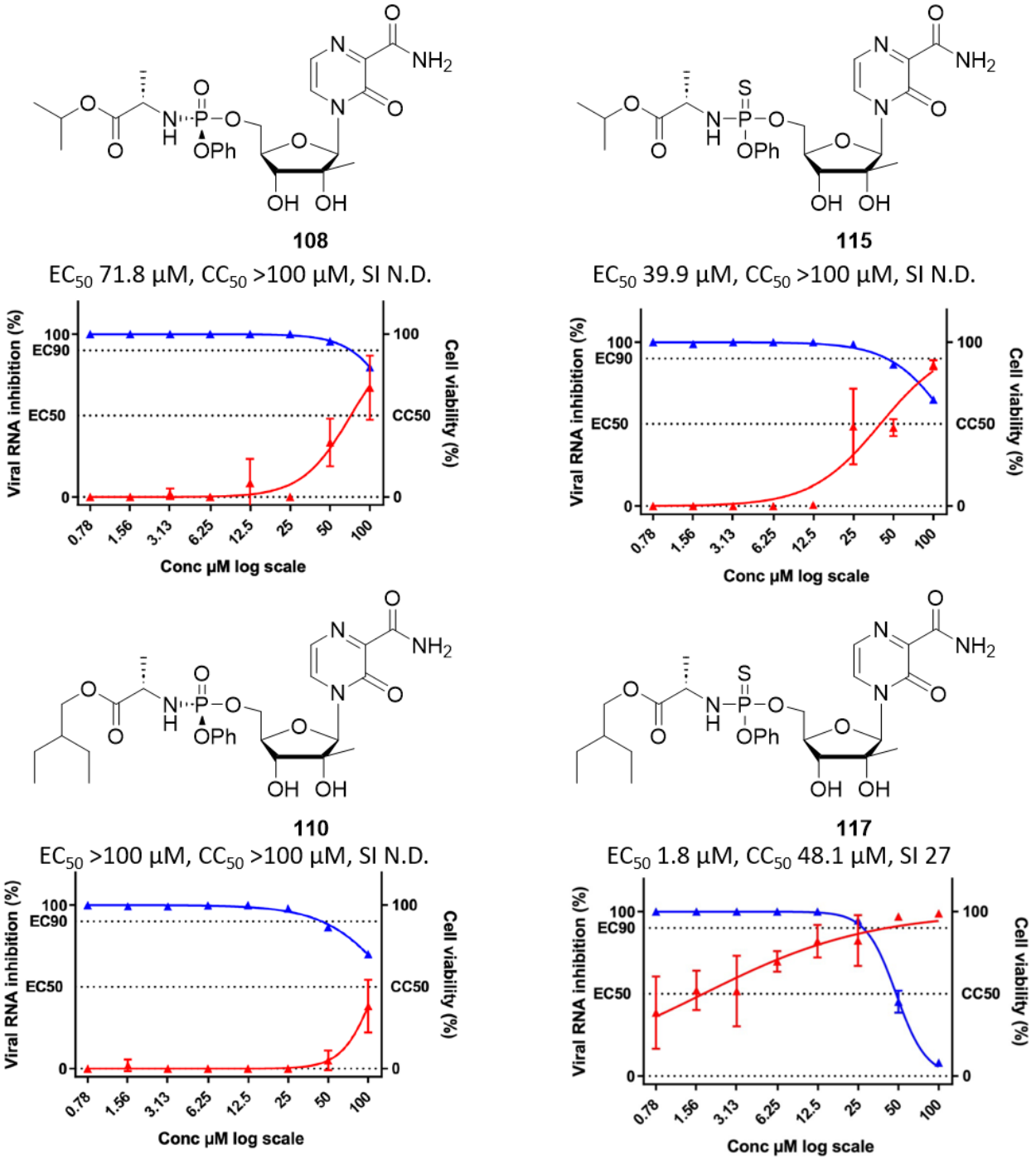

Figure 77: EC_{50} and CC_{50} values of phosphoramidates prodrugs of 2´-*C*-methyl-T-1106 **15**.

In Figure 78, the measured EC_{50} values for the phosphoramidate prodrugs of T-1106 **13** are presented. Notably, these compounds already exhibit single-digit micromolar antiviral activity even in the absence of an α-thio functional group. Compound **122** with an isopropyl residue exhibits an EC_{50} of 7.4 µM and a CC_{50} of 28.4 µM, resulting in a SI of 3.8. When the isopropyl

residue is replaced by a 2-ethylbutyl group, the EC_{50} for compound **123** improves slightly to 6.5 µM, and, importantly, no cytotoxicity was detectable in this case.

Overall, this limited data set strongly suggests that T-1106 **13** may be a superior candidate for further antiviral drug development compared to 2´-*C*-methyl-T-1106. Additionally, the data indicate that introduction of an α-thio function could further enhance antiviral activity, possibly due to increased stabilization of the RNA building blocks against excision by the SARS-CoV-2 ExoN.

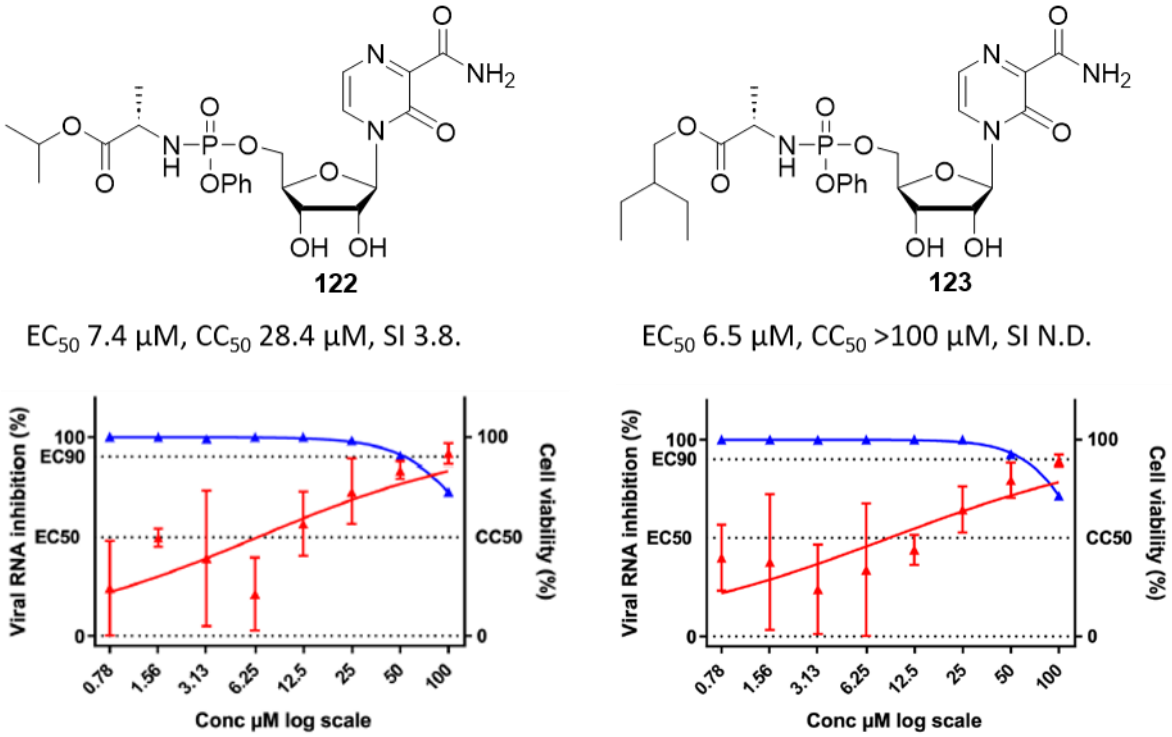

Figure 78: EC_{50} and CC_{50} values of phosphoramidates prodrugs of T-1106 **122** and **123**.

In addition to the phosphoramidate prodrugs, the C9C9-Tri*PPP*ro derivatives of both 2´-*C*-methyl-T-1106 **49** and T-1106 **13**, which were previously synthesized in an earlier work,[119] were also evaluated for their antiviral activity in cell-based assays. The results are presented in Figure 79. Notably, the C9C9-T-1106-Tri*PPP*ro compound **125** demonstrates superior antiviral activity, with an EC_{50} value of 2.3 µM, accompanied by a CC_{50} of 86 µM. This translates to a SI of 37, indicating good efficacy relative to cytotoxicity. In contrast, the C9C9-2´-*C*-methyl-T-1106-Tri*PPP*ro compound **126** exhibited considerably lower potency, with an EC_{50} of 15.6 µM, and higher toxicity, as reflected by a CC_{50} of 62.1 µM, resulting in a much lower SI of 4.

These findings are consistent with the results obtained for the phosphoramidate prodrugs, further suggesting that unmodified T-1106 **13** remains the more promising scaffold for antiviral drug development within this series. Importantly, these results also demonstrate that the Tri*PPP*ro approach is highly competitive with the phosphoramidate strategy in terms of antiviral potency, as reflected by EC_{50} values.

Looking ahead, it may be worthwhile to explore the introduction of an α-thio function into the T-1106 Tri*PPP*ro compounds. Such a modification holds the potential to further enhance antiviral activity and improve the overall performance of this prodrug strategy.

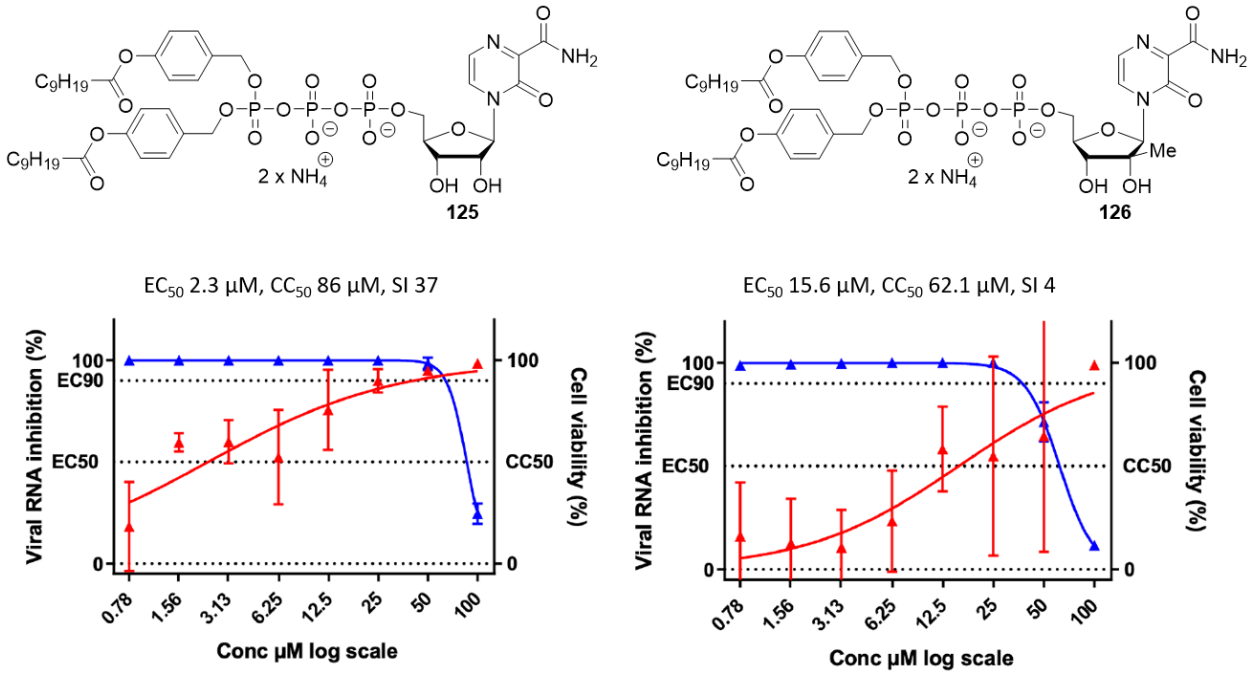

Figure 79: EC_{50} and CC_{50} values for Tri*PPP*ro compounds of 2´-*C*-methyl-T-1106 **125** and T-1106 **126**.

In summary a series of cell-based assays using HUH 7.5 cells infected with SARS-CoV-2 were performed to evaluate the antiviral activity of phosphoramidate and C9C9-Tri*PPP*ro prodrugs derived from 2´-*C*-methyl-T-1106 **49** and T-1106 **13**. Phosphoramidate prodrugs of 2´-*C*-methyl-T-1106 **49** required the presence of an α-thio function to exhibit strong antiviral activity (EC_{50} as low as 1.8 µM), while T-1106 prodrugs displayed potent single-digit micromolar activity even without this modification. C9C9-T-1106-Tri*PPP*ro **125** showed the highest potency (EC_{50} = 2.3 µM, SI = 37), outperforming the corresponding 2´-*C*-methyl derivative, which was less potent and more toxic. Overall, unmodified T-1106 derivatives appear to be the most promising candidates

for further development, and introduction of an α-thio function, especially into Tri*PPP*ro compounds, may further enhance antiviral activity.

4.11 Synthesis of pyrazine modified T-1106-5´-triphosphates

After the successful synthesis of ribose-modified T-1106 analogues, the focus shifted to the preparation of analogues with modifications at the pyrazine moiety. As an initial modification, a methyl group was introduced at the 6-position of the pyrazine ring. This modification was chosen because replacement of the fluorine atom at the 6-position in T-705 **9** with a hydrogen in T-1105 **12** has been shown to significantly enhance antiviral activity.[52]

The synthetic strategy employed was straightforward. Methyl 3-amino-6-bromopyrazine-2-carboxylate **127** was subjected to a SUZUKI coupling with methylboronic acid, using palladium with Xantphos as the ligand and tripotassium phosphate as the base. This reaction yielded methyl 3-amino-6-methylpyrazine-2-carboxylate **128** in a yield of 45%, which is somewhat lower than the literature value of 60%.[215] In the subsequent step, the amino group was converted to the corresponding hydroxy group by diazotization with sodium nitrite, resulting in a yield of 88% for the pyrazine **129** (Figure 80).

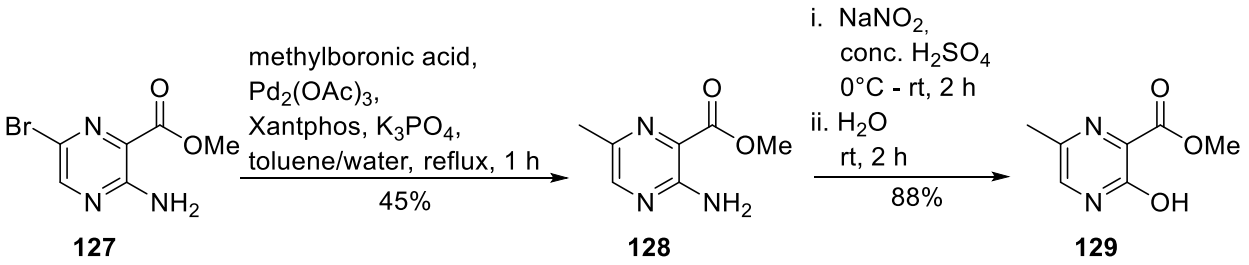

Figure 80: Synthesis of methyl 3-hydroxy-6-methylpyrazine-2-carboxylate **129** starting from methyl 3-amino-6-bromopyrazine-2-carboxylate **127**.

Following the successful synthesis of the modified pyrazine **129**, the compound was subjected to glycosylation with peracetylated ribofuranose **52** under the established VORBRÜGGEN conditions (see Chapter 4.4). This reaction yielded the protected nucleoside **130** in a yield of 65%. The resulting intermediate was then deprotected using methanolic ammonia to afford 6-methyl-T-1106 **131** in a yield of 72%. In the final step, 6-methyl-T-1106 **131** was converted to its 5'-triphosphate form following the established LUDWIG & ECKSTEIN protocol (Chapter 4.4), resulting in 6-methyl-T-1106-5'-triphosphate **132** with an overall yield of 38% (Figure 81).

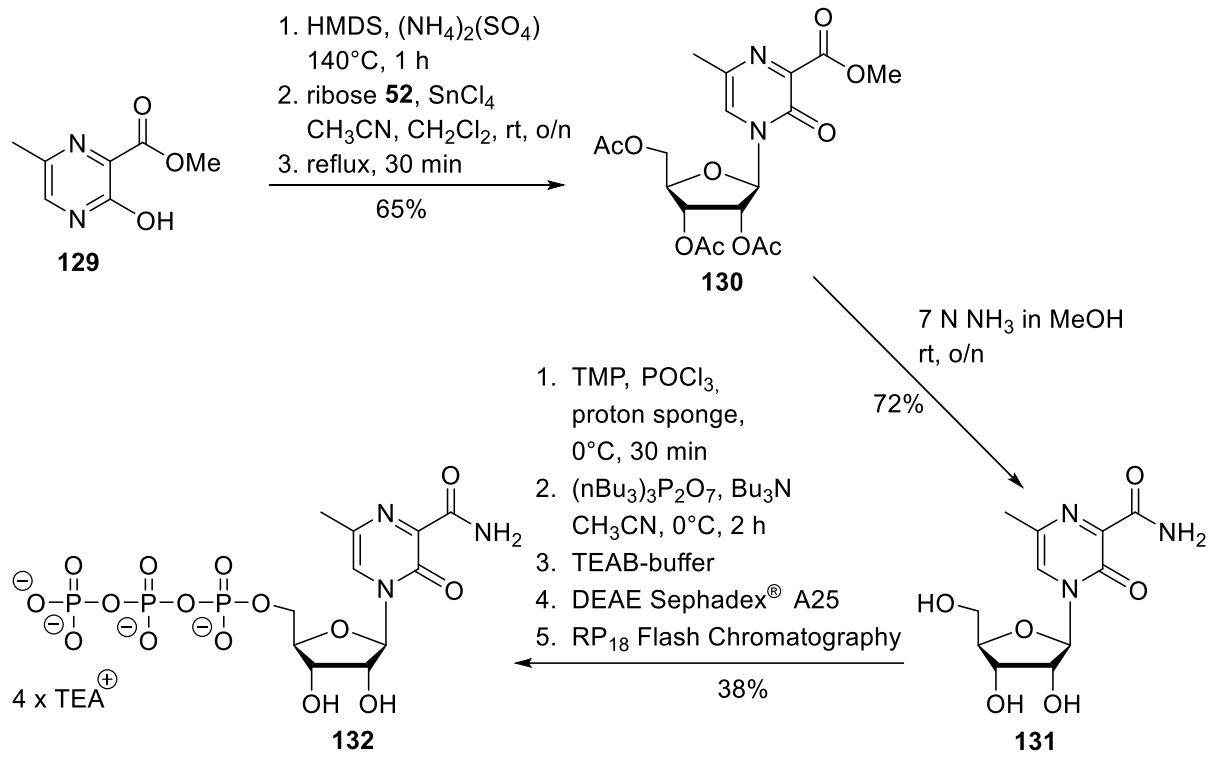

Figure 81: Synthesis of 6-methyl-T-1106-5´-triphosphate **132**.

Because the 2'-*C*-methyl group was identified as the most promising ribose modification, it was decided to combine both the pyrazine and ribose modification.

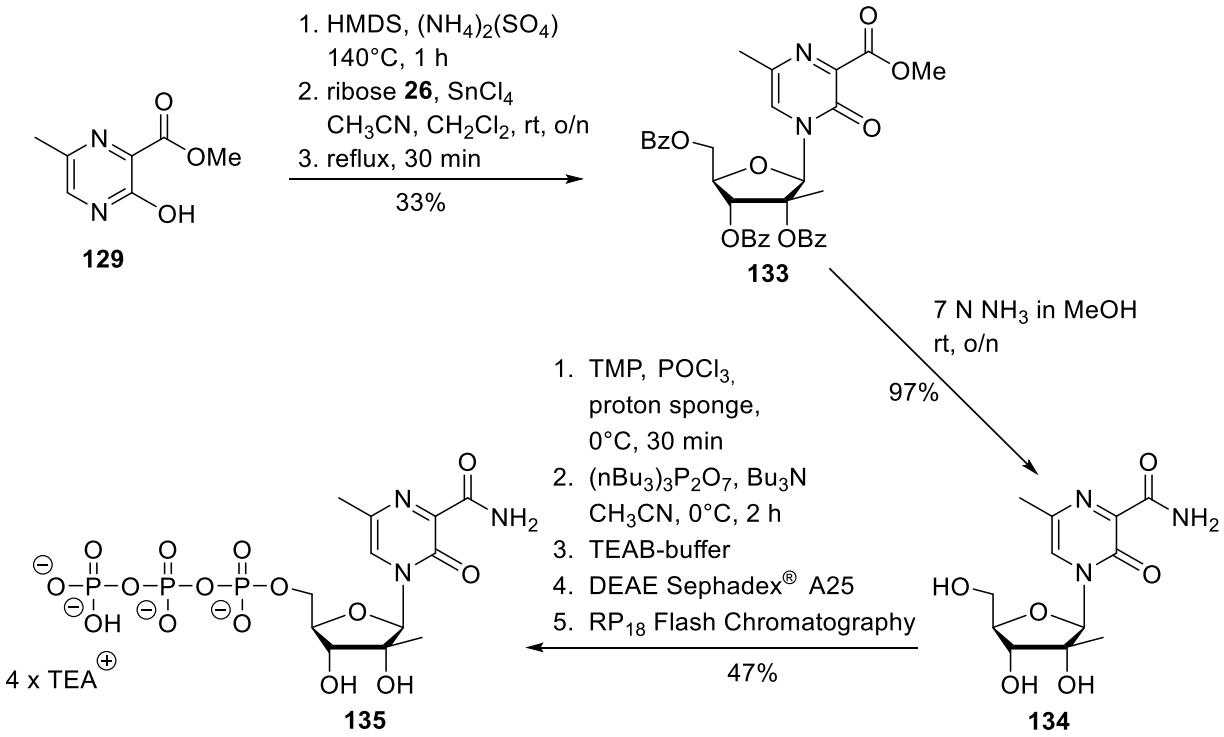

Figure 82: Synthesis of 6-methyl-2´-*C*-methyl-T-1106-5´-triphosphate **135**.

Methyl 3-hydroxy-6-methylpyrazine-2-carboxylate **129** was coupled under the established VORBRÜGGEN conditions with 1,2,3,5-tetra-*O*-benzoyl-2´-*C*-methyl-β-D-ribofuranose **26**, yielding the corresponding protected nucleoside **133** in a yield of 33%. Subsequent deprotection with methanolic ammonia gave 6-methyl-2'-*C*-methyl-T-1106 **134** in a yield of 97%. Phosphorylation according to the LUDWIG & ECKSTEIN protocol yielded the corresponding triphosphate **135** with a yield of 47% (Figure 82). Both synthesized triphosphates will be part of SARS-CoV-2 polymerase assays in the future.

4.12 Synthesis of T-1106-5´-triphosphates C-nucleosides

An additional objective of this work was the synthesis of C-nucleoside analogues structurally related to T-1106 **13**, specifically by replacing the pyrazine moiety with a pyridine moiety. The motivation for focusing on C-nucleosides arises from their distinct structural and biological advantages over conventional N-nucleosides. While traditional N-nucleosides contain a glycosidic C–N bond, which is susceptible to cleavage by human nucleoside hydrolases and other enzymes, C-nucleosides feature a direct C–C bond between the nucleobase and the sugar moiety. This substitution significantly enhances the chemical and enzymatic stability of the glycosidic linkage, resulting in molecules that are more resistant to metabolic degradation.[216–218]

The replacement of the endocyclic nitrogen atom in the nucleobase with a carbon atom is also of considerable interest from a medicinal chemistry perspective. This structural modification alters the electronic properties of the nucleoside, which can, in turn, influence its interactions with biological targets such as viral polymerases. Such changes may enhance the compound's antiviral activity, selectivity, or pharmacokinetic properties. By introducing a pyridine ring in place of the pyrazine ring, further modulation of these properties is possible, potentially leading to compounds with improved therapeutic potential.[218] C-nucleosides derived from T-1106 **13** are of particular interest due to the existence of several successfully synthesized analogues that have already demonstrated promising biological activity.[219] Notably, when the original pyrazine ring is replaced by a pyridine moiety, the resulting nucleoside **136** exhibits significant antiviral potency with an EC_{50} value of 1.3 µM against Influenza A/WSN/33. However, this compound also shows cytotoxicity, as indicated by a CC_{50} value of 2.0 µM. Interestingly, when the hydroxy group at the 3-position of the pyridine ring is substituted by a fluorine atom, a slight reduction in antiviral activity is observed (EC_{50} = 1.9 µM) for the nucleoside **137**. Nevertheless, this modification results

in a significant improvement in the compound's safety profile, as no detectable cytotoxicity is observed at the tested concentrations (Figure 83).[219]

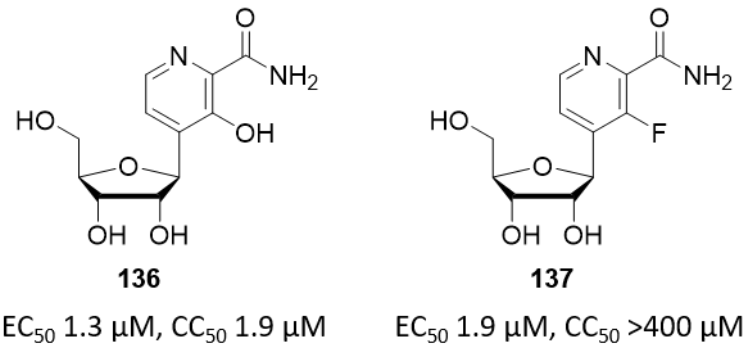

Figure 83: Antiviral activity against Influenza of previously synthesized T-1106 C-nucleoside analogues.[219]

Building on these results, the aim of the present work was to synthesize the fluorinated analogue (compound **137**) and further modify it by introducing a 2'-*C*-methyl group. This additional substitution is expected to further modulate the mechanism of action based on the previous results. Following synthesis of the nucleosides, the corresponding nucleoside triphosphates will be prepared and evaluated in SARS-CoV-2 polymerase assays to assess their potential as antiviral agents against the coronavirus. The synthesis of compound **137**, following the procedure reported by L. BEIGELMAN *et al.*[219], began with the preparation of the required ribose building block. Initially, D-ribono-1,4-lactone **138** was protected at the 2- and 3-positions with an isopropylidene group by reacting it with acetone under acidic conditions overnight, affording intermediate **139** in a yield of 73%. In the subsequent step, this intermediate was treated with *tert*-butyldiphenylsilyl chloride and imidazole, resulting in the formation of the desired ribose building block **140** with a yield of 60% (Figure 84).

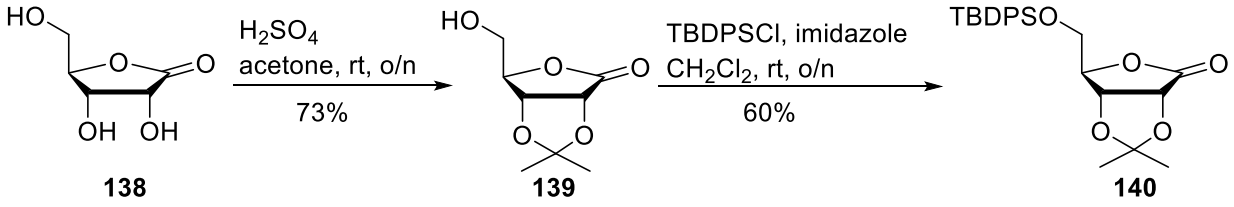

Figure 84: Synthesis of the ribose building block **140**.

In the initial attempt to synthesize compound **137**, the synthetic strategy previously reported in the literature was followed with only minor modifications. The overall sequence of reactions is illustrated in Figure 85. Synthesis commenced with the deprotonation of 2-cyano-3-

fluoropyridine **141** using LDA. After stirring for 30 minutes to ensure complete deprotonation, lactone **140** was added. The resulting nucleophilic addition of the deprotonated pyridine to the anomeric carbon of the lactone afforded lactol **142**. Since this nucleophilic attack could occur from either the top (β) or bottom (α) face of the lactone ring, the product was obtained as a mixture of anomers in a yield of 69%. At this stage, efforts to separate the isomers by column chromatography proved unsuccessful due to their similar polarity and chromatographic behaviour. The reaction sequence continued with the deprotonation of the lactol **142** intermediate using LiHMDS, followed by acetylation with acetic anhydride. This step afforded the acetylated lactol **143** in a yield of 71%, again as a mixture of the two anomers. As before, all attempts to resolve the anomeric mixture using standard chromatographic techniques failed.

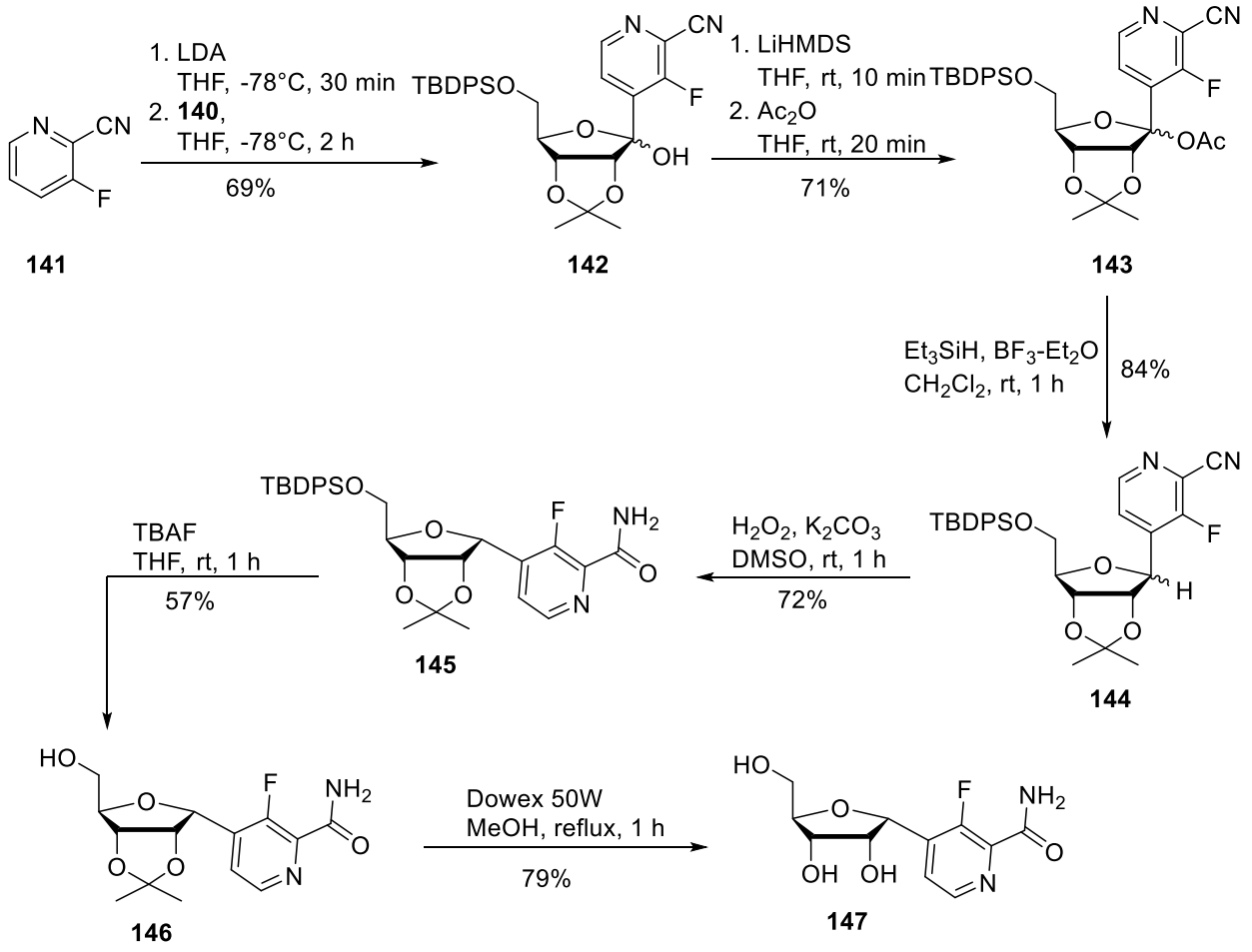

Figure 85: Synthesis of the α-anomer of the T-1106 C-nucleoside **147**.

Finally, the acetyl group at the 1'-position was removed by treating the compound **143** with triethylsilane in the presence of the Lewis acid boron trifluoride etherate, affording the desired C-nucleoside **144** in 84% yield. However, even at this stage, separation of the anomers was not

achieved. In the subsequent step, the nitrile group was hydrolysed with hydrogen peroxide in the presence of potassium carbonate, affording the corresponding carboxamide **145** in 72% yield. Notably, only a single anomer was isolated. Based on the high yield and reference to a previously published synthetic route, it was initially assumed that this product was the β-anomer. Subsequent cleavage of the 5'-silyl ether with TBAF yielded the 5'-deprotected compound **146** in 57% yield. This lower-than-expected yield was surprising, as TBAF-mediated deprotection of 5'-silyl ethers typically gives yields above 90%. In the final step, the 2',3'-isopropylidene protecting group was removed under acidic conditions using Dowex 50W, resulting in the desired C-nucleoside **147** in 79% yield (Figure 85). However, NOESY NMR analysis revealed that the isolated product was the α-anomer, not the expected β-anomer.

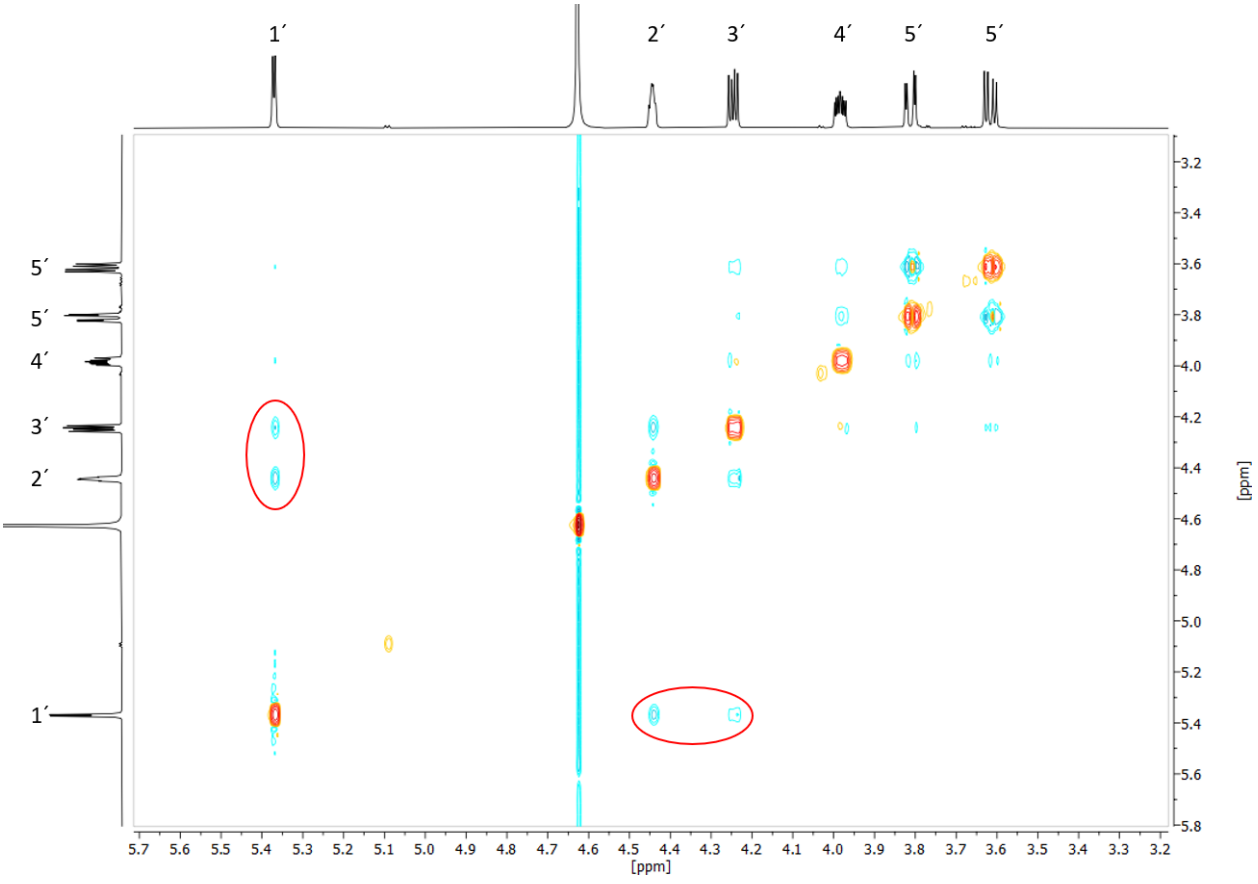

Figure 86: Excerpt from the NOESY NMR spectrum of compound **147**. The correlations between the 1´-proton and the 2´- and 3´-protons are clearly observable (red circles) (600 MHz, 25 °C, D_2O).

The NOESY spectrum clearly show that the 1'-proton couples with both the 2'- and 3'-protons, a pattern that is only possible if the α-anomer of **147** is present. In contrast, for the β-anomer, the 1'-proton would couple exclusively with the 4'-proton (Figure 86).

The predominance of the α-anomer observed in this case is unexpected and contradicts previously published reports.[219] To address this issue, the synthetic strategy was modified by employing a different ribose building block. Instead of the original precursor, commercially available 2,3,5-tri-*O*-benzyl-D-ribono-1,4-lactone **148** was used. Earlier publications reported that when benzoyl protecting groups are employed, reduction of acetylated lactols with triethylsilane results in exclusive formation of the β-anomer.[220] However, more recent studies have suggested that selectivity for the β-anomer depends not only on the steric hindrance of the larger protecting group but also on the conformation of the oxonium ion formed upon acetyl group cleavage[221,222]. Despite these insights, it remains unclear why the use of a 2',3'-isopropylidene protecting group led to a mixture of anomers. M. HOCEK *et al.* proposed that the formation of the hemiketal is reversible and that the β-hemiketal is preferentially reduced, resulting in predominant formation of the β-anomer[223]. It is also stated by M. HOCEK *et al.* that the reduction is heavily influenced by the solvent used and the reaction temperature[224]. Additionally, other studies have demonstrated that employing a HANTZSCH ester instead of triethylsilane also leads to exclusive formation of the β-anomer[225]. In summary, it can be said that to date, it is not completely clear under which exact conditions preferential formation of the β-anomer occurs.In the initial approach, 2-cyano-3-fluoropyridine **141** was deprotonated with LDA and subsequently reacted with lactone **148** (Figure 87). Although this synthetic strategy has previously been successfully applied to the preparation of 3-chloro and 3-bromo C-nucleosides,[219] all attempts in this case were unsuccessful. Repeated trials resulted in decomposition of both starting materials, for reasons that remain unclear.

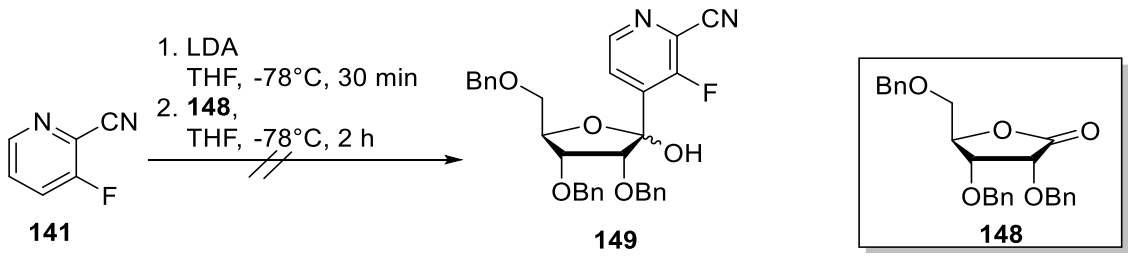

Figure 87: Approach to synthesize **149** starting from 2-cyano-3-fluoropyridine **141**.

To overcome this problem, a different pyridine building block was used. The overall sequence of reactions is illustrated in Figure 88. Using 3-fluoropyridine in place of 2-cyano-3-fluoropyridine **150** allowed isolation of the desired lactol **151** as a mixture of anomers under the same conditions, with a yield of 69%. In the next step, the hydroxy group was acetylated using LiHMDS

and acetic anhydride, affording the acetylated product **152** in 82% yield. The subsequent reduction provided the pure β-anomer **153** in 58% yield (Figure 88).

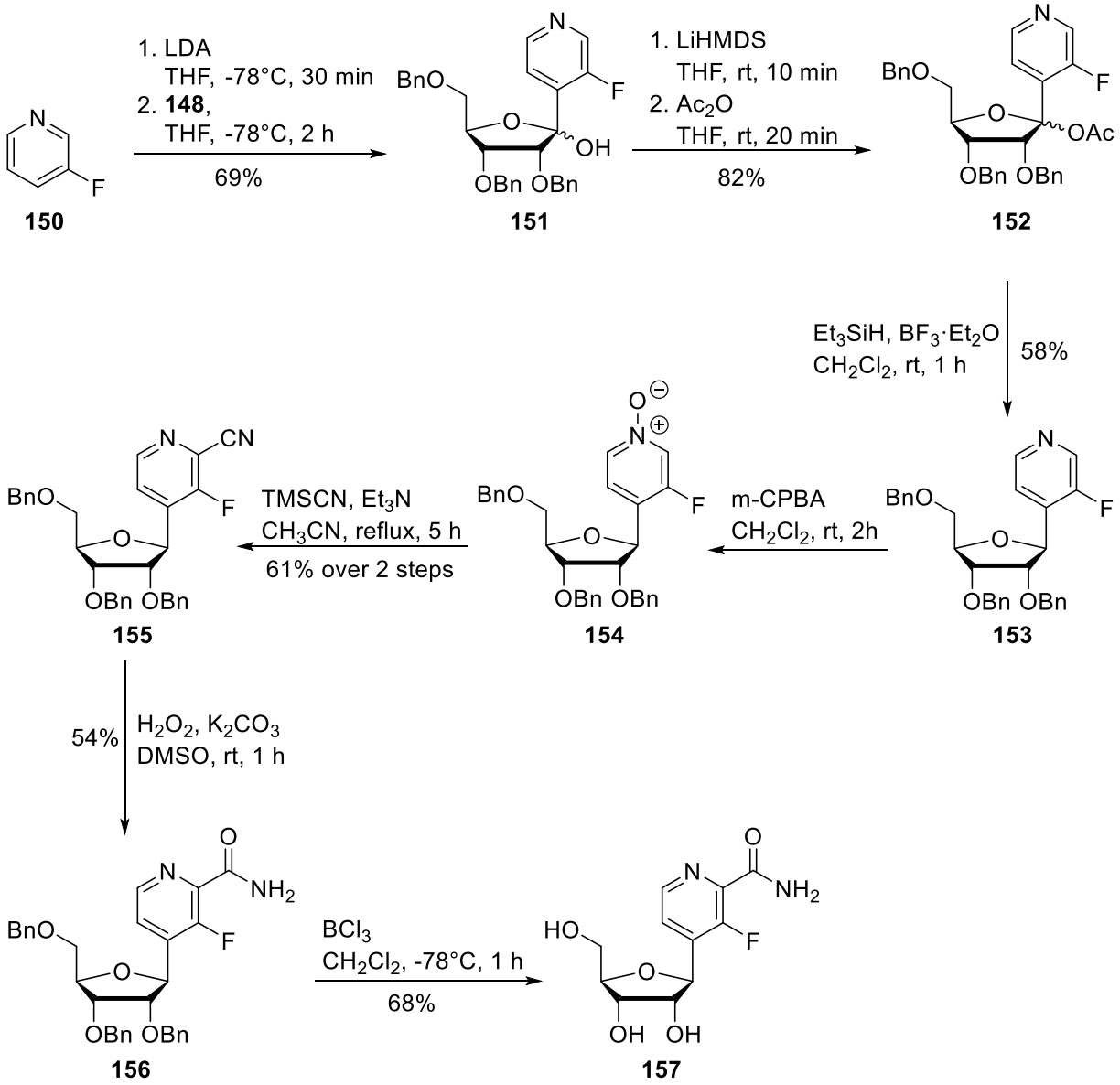

Figure 88: Synthesis of the β-anomer of the T-1106 C-nucleoside **157**.

To introduce the nitrile function at the 2-position, the *N*-oxide **154** was first formed by reacting **153** with *m*-CPBA. The nitrile group was then selectively introduced at the 2-position using trimethylsilyl cyanide in the presence of triethylamine, affording **155** a yield of 61%.[226] In the subsequent step, the nitrile group was hydrolysed with hydrogen peroxide in the presence of potassium carbonate, yielding 54% of carboxamide **156**. Finally, the benzyl protecting groups were removed by treatment with boron trichloride, providing the desired C-nucleoside **157** as the pure β-anomer in 68% yield. Subsequently, the C-nucleoside **157** was converted to the

corresponding triphosphate **158** using the established LUDWIG & ECKSTEIN conditions, affording a yield of 65% (Figure 89).

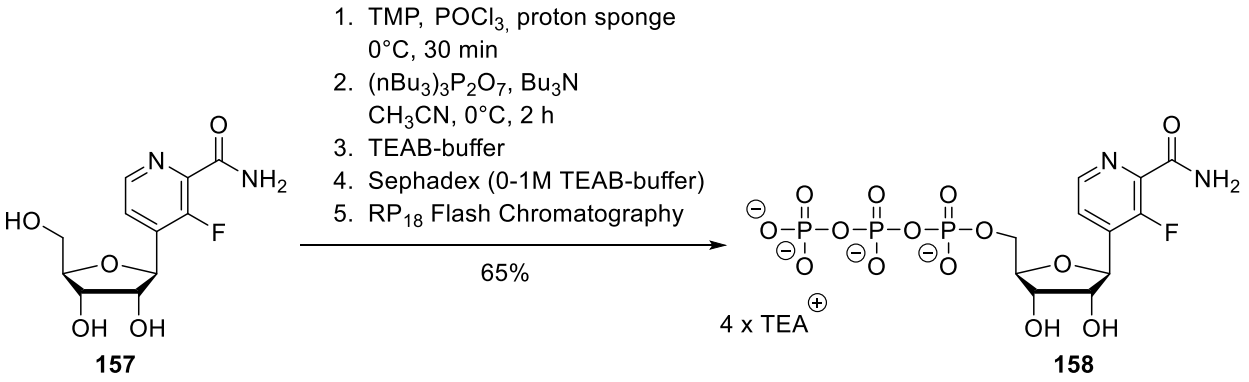

Figure 89: Synthesis of the T-1106 C-nucleoside-5´-triphosphate **158**.

For the synthesis of the 2'-*C*-methyl-C-nucleoside, the ribose building block was first prepared using the same strategy previously employed for the synthesis of ribose building block **148**. In the initial step, the hydroxy groups at the 2- and 3-positions of commercially available 2-*C*-methyl-D-ribono-1,4-lactone **159** were protected by introducing an isopropylidene group through reaction with acetone in the presence of concentrated sulfuric acid, affording **160** in quantitative yield. In the subsequent step, compound **160** was treated with *tert*-butyldiphenylsilyl chloride and imidazole, resulting in the formation of the desired ribose building block **161** in 55% yield (Figure 90).

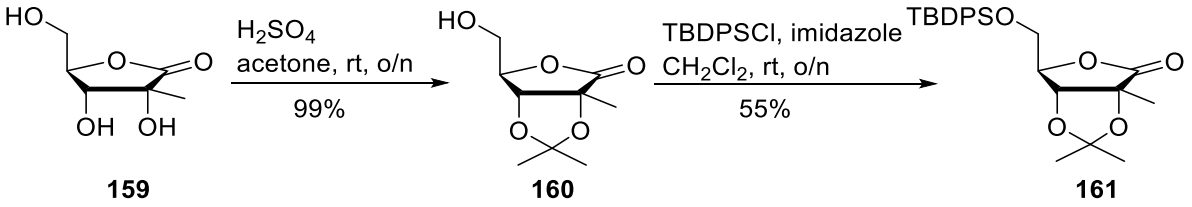

Figure 90: Synthesis of the ribose building block **161**.

For the synthesis of 2'-*C*-methyl-C-nucleoside, 2-cyano-3-fluoropyridine **141** was first deprotonated using LDA and subsequently coupled with lactone **161**, affording the corresponding lactol **162** in 65% yield as a mixture of anomers. In the following step, the 1'-hydroxy group was deprotonated with LiHMDS and acetylated with acetic anhydride to produce **163** in 79% yield. Final reduction with triethylsilane in the presence of boron trifluoride etherate yielded the α-anomer **164** with 38% and the desired β-anomer **165** with 42% (Figure 91).

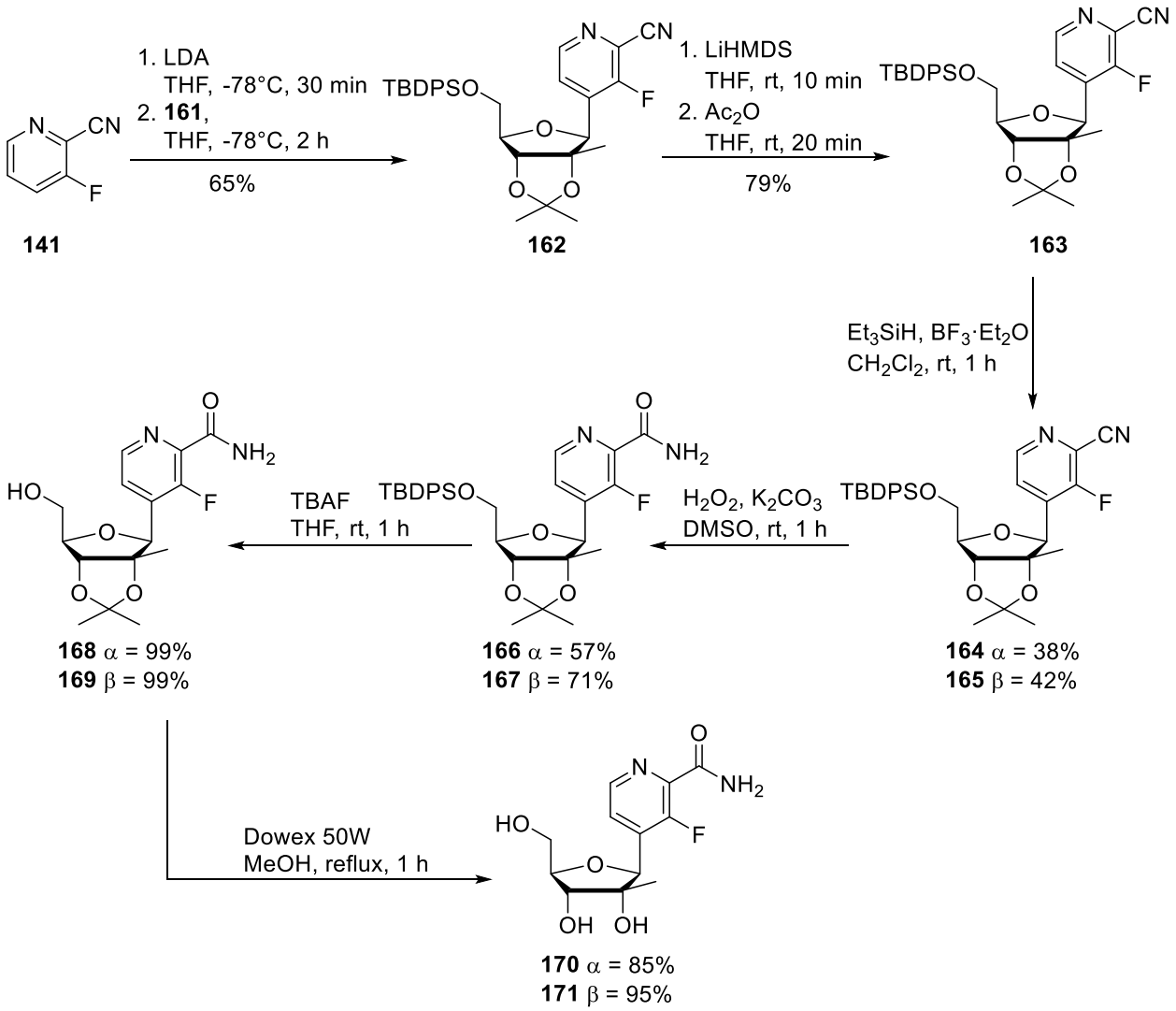

Figure 91: Synthesis of the α- and β-anomer of the 2´-*C*-methyl-T-1106 C-nucleoside **170** and **171**.

In this case, the α- and β-anomers could be separated by column chromatography due to a significant difference in their retention times. Figures 92 and 93 show the NOESY NMR spectra of compounds **164** and **165**, respectively. In the spectrum of the α-anomer, it is evident that the 1'-proton shows correlation with the protons of the methyl group at the 2'-position. This observation indicates that the pyridine ring is oriented on the lower face and the 1'-proton on the top face of the ribose ring. In contrast, the NOESY NMR spectrum of the β-anomer reveals that the 1'-proton correlates with the 4'-proton and with one of the methyl groups of the isopropylidene protecting group, which is only possible if the 1'-proton is positioned on the underside of the ribose ring.

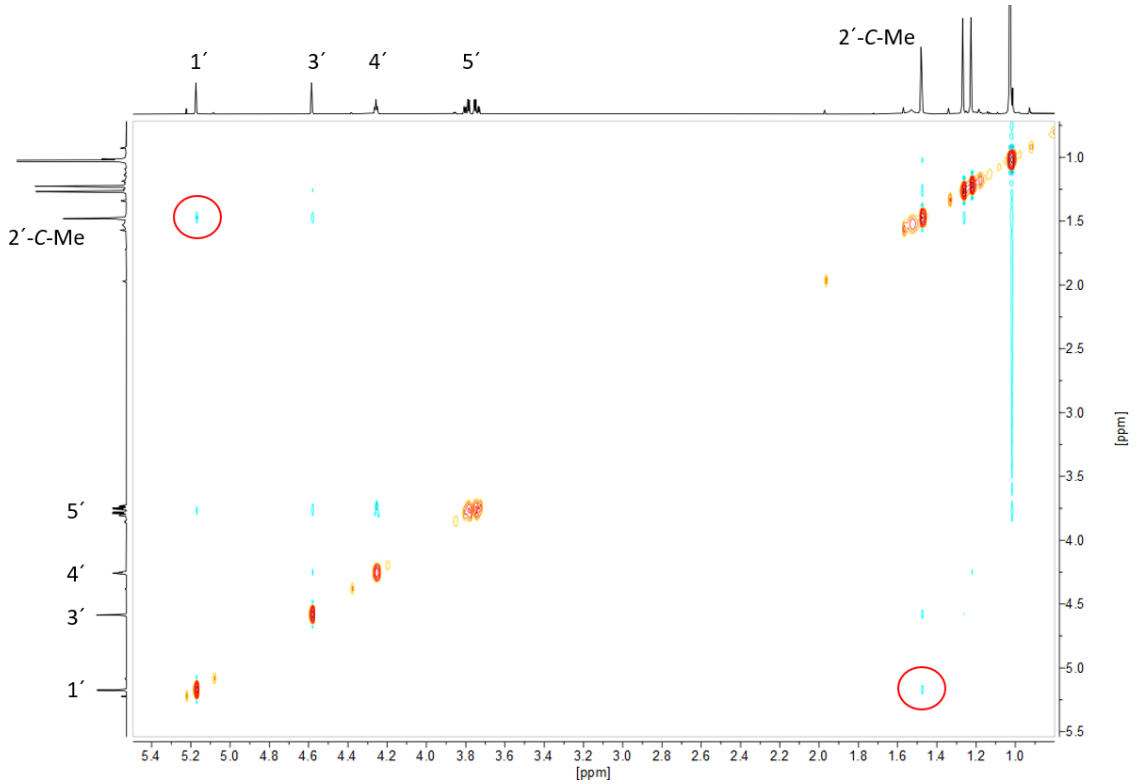

Figure 92: Excerpt from the NOESY NMR spectrum of compound **164**. The correlations between the 1´-proton and the 2´-methyl group are clearly observable (red circles) (600 MHz, 25 °C, $CDCl_3$).

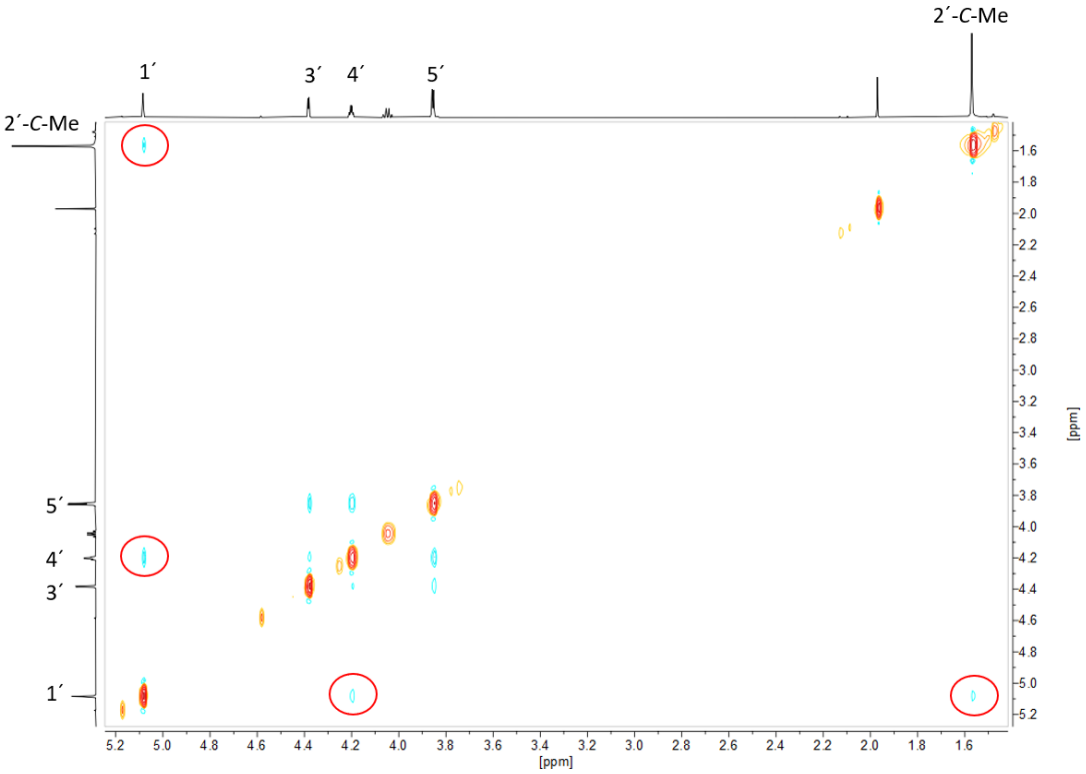

Figure 93: Excerpt from the NOESY NMR spectrum of compound **165**. The correlations between the 1´-proton, the 4´-proton and the isopropylidene group are clearly observable (red circles) (600 MHz, 25 °C, $CDCl_3$)

Hydrolysis of the nitrile group with hydrogen peroxide in the presence of potassium carbonate yielded the α-carboxamide **166** in 57% yield and the β-carboxamide **167** in 71% yield. Subsequent cleavage of the 5′-silyl ether with TBAF afforded the 5′-deprotected nucleosides quantitatively for both anomers. Finally, removal of the isopropylidene protecting group under acidic conditions provided the α-C-nucleoside **170** in 85% yield and the desired β-C-nucleoside **171** in 95% yield (Figure 91).

The synthesis of the 5′-triphosphate was carried out only for the β-C-nucleoside **171**. Under standard LUDWIG & ECKSTEIN conditions, the corresponding 5′-triphosphate **172** was obtained in 42% yield (Figure 94).

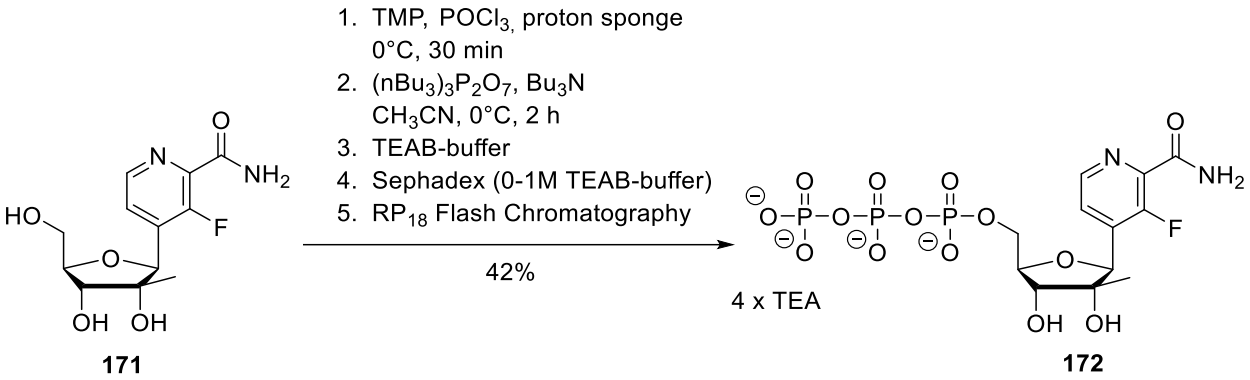

Figure 94: Synthesis of the triphosphate **172**.

After the successful synthesis of the C-nucleoside **157** and the 2′-*C*-methyl-C-nucleoside **171** the next goal was to also synthesize the corresponding 2′-*C*-methyl-2′-fluoro-C-nucleoside. The required ribose building block was synthesized in one step from 2-deoxy-2-fluoro-2-C-methyl-D-ribono-1,4-lactone **173**. Compound **173** was therefore reacted with Markiewicz reagent ($TIPDSiCl_2$) in the presence of 4-DMAP and pyridine, to give the 5- and 3-protected lactone **174** in a yield of 90% (Figure 95).[227]

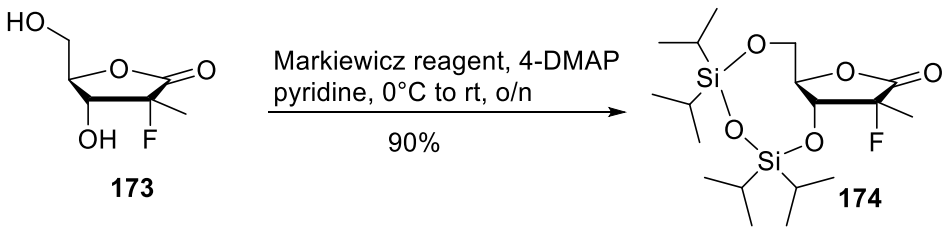

Figure 95: Synthesis of the ribose building block **174**.

In the next step, 2-cyano-3-fluoropyridine **141** was first deprotonated with LDA and then reacted with lactone **174** to afford the corresponding nucleoside **175** as a mixture of anomers. Subsequent acetylation of the 1'-hydroxy group proceeded in 68% yield (Figure 96). Unfortunately, attempts to reduce **176** to the desired nucleoside **177** were unsuccessful, as no conversion was observed under standard reaction conditions. Increasing the amount of Lewis acid, as well as extending the reaction time and raising the temperature, either resulted in no conversion or led to decomposition of the starting material. These issues could not be resolved during this work, further studies could focus on optimizing the reaction by testing alternative Lewis acids.

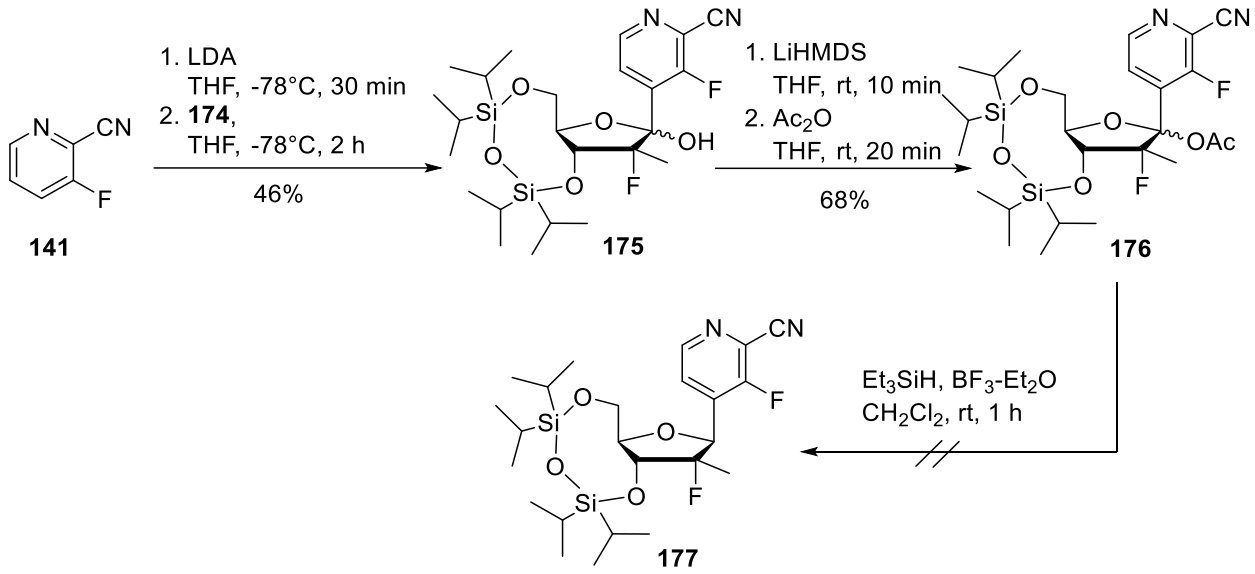

Figure 96: Attempt to synthesize nucleoside **177**.

Another objective was to introduce a nitrile group at the 1'-position, motivated by the notable success of Remdesivir **5** and the critical role of the 1'-nitrile group in both antiviral mechanism of action[228,109,47] and selectivity towards viral enzymes.[229,230] This selectivity for viral, rather than host enzymes is known to significantly reduce the cytotoxicity of nucleoside analogues.

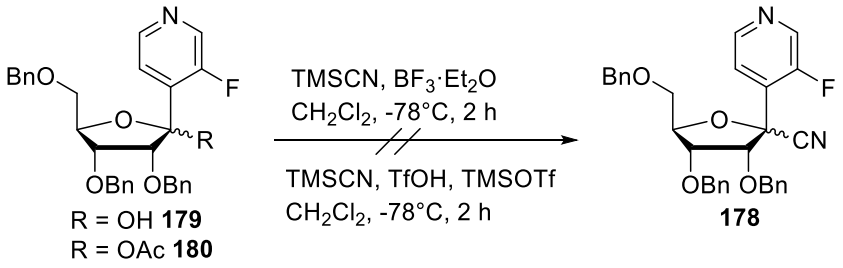

Figure 97: Attempt to synthesize nucleoside **178**.

Unfortunately, the desired 1'-nitrile nucleoside **178** could not be synthesized successfully, despite several attempts using different approaches. Both methods that had previously been employed for the synthesis of Remdesivir **5** were applied[174,212], but neither proved effective when applied to the pyridine-based C-nucleoside **179**, as no conversion of the starting material was observed in either case. This lack of reactivity is most likely attributable to the differing electronic properties of the pyridine moiety, which exerts a stronger electron-withdrawing effect compared to the moiety present in Remdesivir **5**, thereby significantly altering the chemical environment at the 1'-position and reducing its reactivity. Even when the more reactive acetylated lactol **180** was used as the substrate,[231] no formation of the desired product was detected. These results highlight a significant limitation in adopting established nitrile introduction methods for this class of C-nucleosides, and further optimization or the development of entirely new synthetic strategies may be required to achieve the target compound.

4.13 Synthesis of 2´-C-modified T-1106 analogues

After successfully synthesizing 2'-*C*-methyl-T-1106 **49**, efforts were made to synthesize further 2'-modified T-1106 analogues. In 1997, M. WOLFE *et al.* published an efficient method for the preparation of 2'-*C*-branched ribonucleosides.[232]

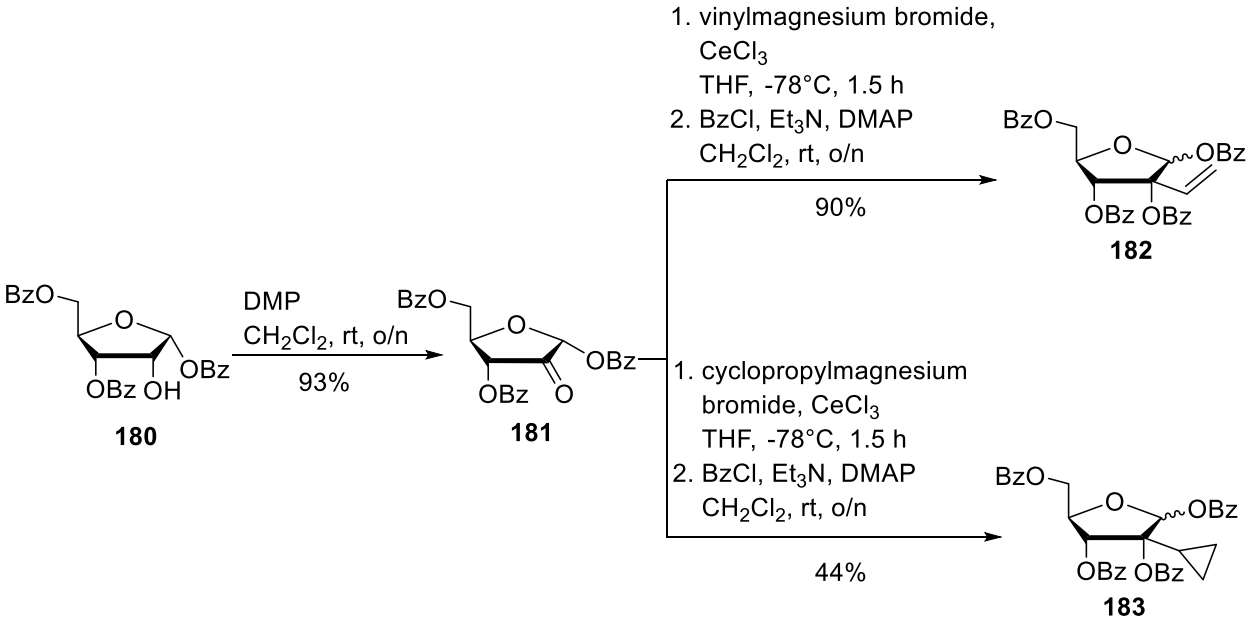

Figure 98: Synthesis of the 2-C-modifed ribose **182** and **183**.

Initially, commercially available 1,3,5-tri-*O*-benzoyl-α-D-ribofuranose **180** was oxidized to the corresponding ketone **181** using Dess–Martin periodinane, affording a yield of 93%. WOLFE *et al.*

demonstrated that selective reduction of ketones with Grignard reagents in the presence of esters is possible by converting Grignard reagents to organocerium reagents via reaction with cerium(III) chloride. In this case, the addition of the alkyl group occurs exclusively from the top face of the ribose ring, as both adjacent bulky protecting groups are oriented toward the bottom face of the ribose ring. Applying this strategy, followed by benzoylation, 2-*C*-vinyl ribose **182** was obtained in a yield of 90%, and 2-*C*-cyclopropyl ribose **183** in a yield of 44% (Figure 98). However, the synthesis of the corresponding nucleosides could not be completed as part of this study.

4.14 Supplementary Projects

4.14.1 Synthesis of T-1106 Di- and Tri*PPP*ro compounds

In collaboration with the group of G. GABRIEL from the Leibniz Institute in Hamburg, several T-1106 Di*PP*ro and Tri*PPP*ro compounds were evaluated for their antiviral activity against various influenza strains.

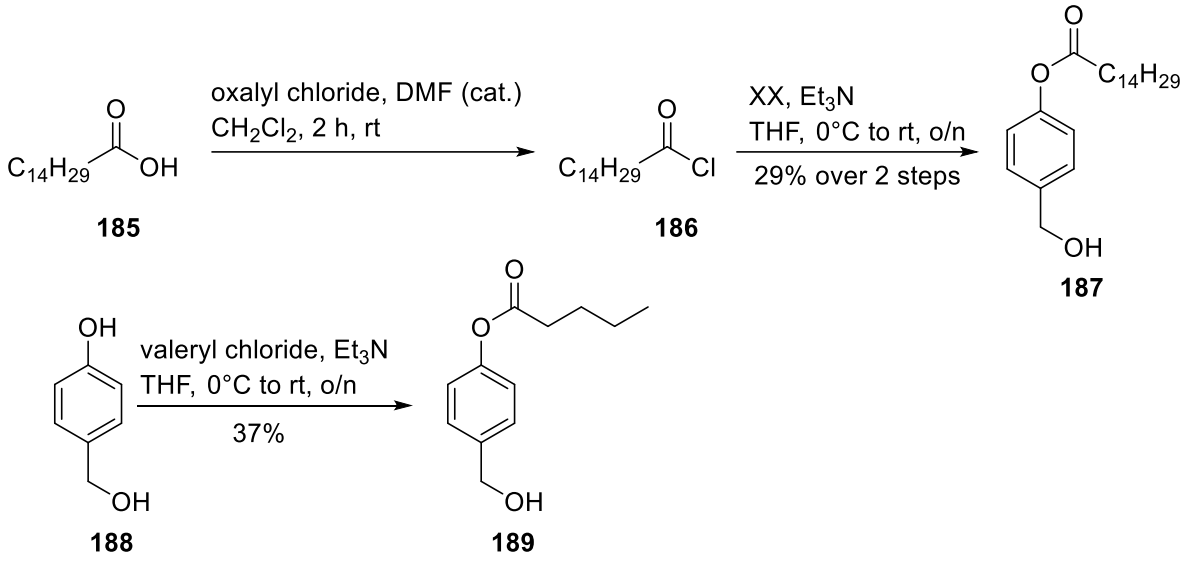

Figure 99: Synthesis of the acyloxybenzyl ester **187** and **189**.

For this purpose, the C4C14-T-1106-Di*PP*ro **184** was synthesized, as it demonstrated promising results in a previous study.[120] The synthesis involved a previously established phosphoramidite chemistry strategy.

First, the acid chloride **186** of pentadecanoic acid **185** was prepared by reacting it with oxalyl chloride in the presence of a catalytic amount of DMF. This acid chloride was then directly used in the esterification with 4-hydroxybenzyl alcohol **188**, yielding the desired C14-acyloxybenzyl

ester **187** with a 29% yield. Similarly, the C4-acyloxybenzyl ester **189** was synthesized using commercially available valeryl chloride under the same conditions, obtaining a 37% yield (see Figure 99). Subsequently, bis(diisopropylamino)chlorophosphine **190** was reacted with the C4-acyloxybenzyl ester **189** in the presence of triethylamine, resulting in compound **191** with a 91% yield. In the next step, this intermediate was reacted with the C14-acyloxybenzyl ester **187** using 4,5-dicyanoimidazole as an activator, yielding the phosphoramidite **192** with 60% (Figure 100).

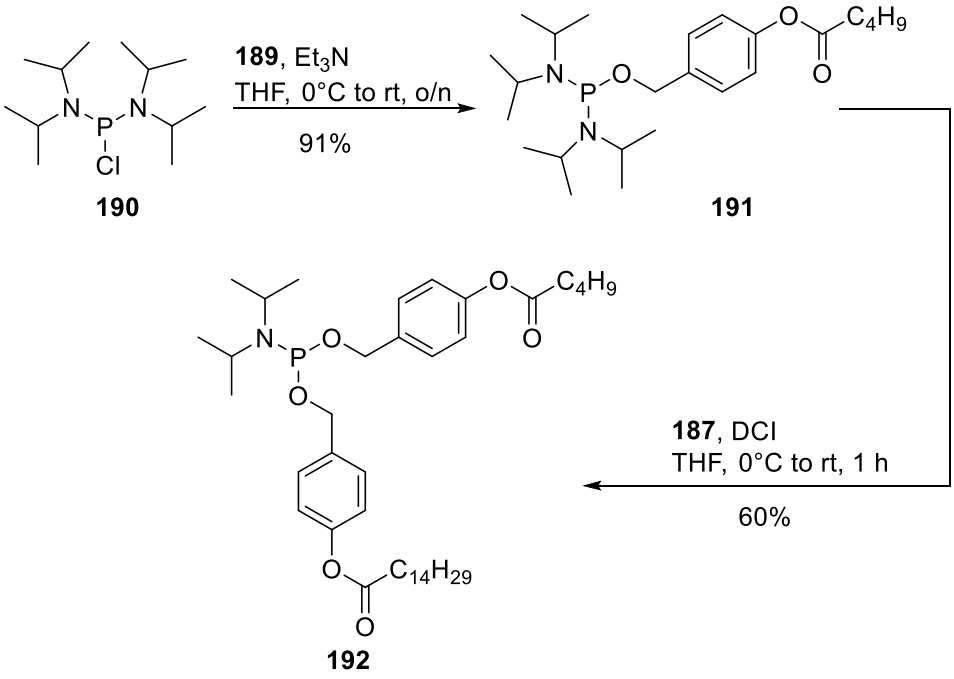

Figure 100: Synthesis of the phosphoramidite **192**.

Subsequent coupling of the phosphoramidite **192** with the T-1106-5´-monophosphate **59** using DCI as activator followed by oxidation with *tert*-butyl hydroperoxide yielded the desired C4C14-T-1106-Di*PP*ro **184** in a yield of 53% (Figure 101).

The antiviral data of C4C14-T-1106-Di*PP*ro **184** together with the other tested T-1106 prodrugs were published in 2023.[233] It was demonstrated that these prodrugs exhibit high antiviral efficacy against a broad range of Influenza A viruses. Furthermore, when combined with Oseltamivir, they show synergistic effects.

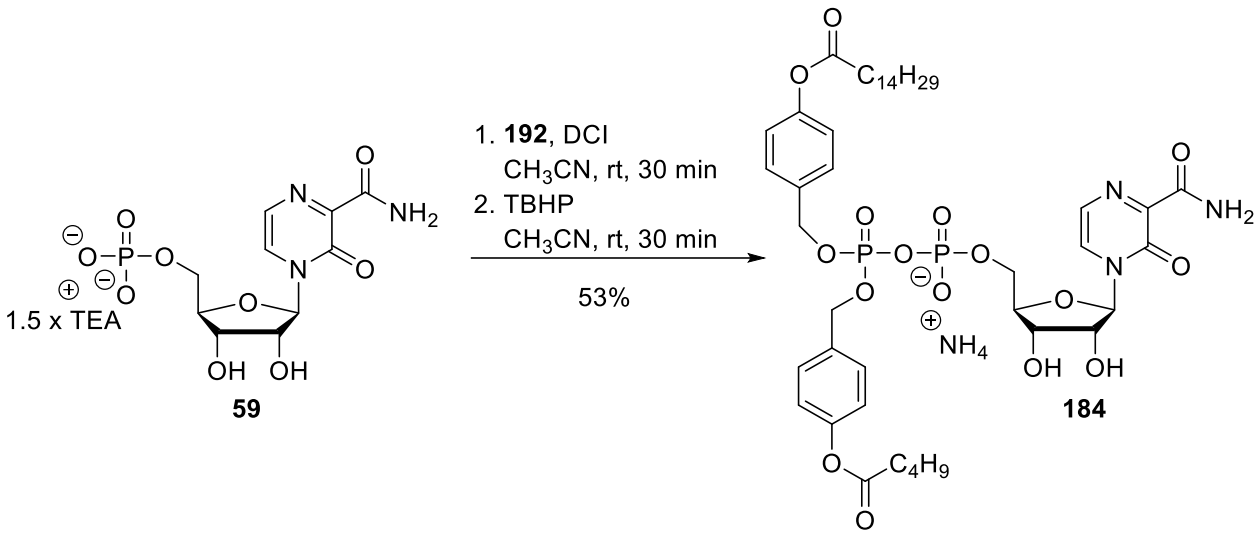

Figure 101: Synthesis of the T-1106 Di*PP*ro compound **184**.

As part of this cooperation, it was initially planned to also test Tri*PPP*ro compounds of ribose-modified T-1106. Since the C9C9-2´-*C*-Me-T-1106-Tri*PPP*ro **126** had already been synthesized in a previous project, the next target molecule was the C9C9-3´-fluoro-T-1106-Tri*PPP*ro **194**. For this synthesis, the *H*-phosphonate route was employed, which had already been successfully established by the group of C. MEIER.[134,133]

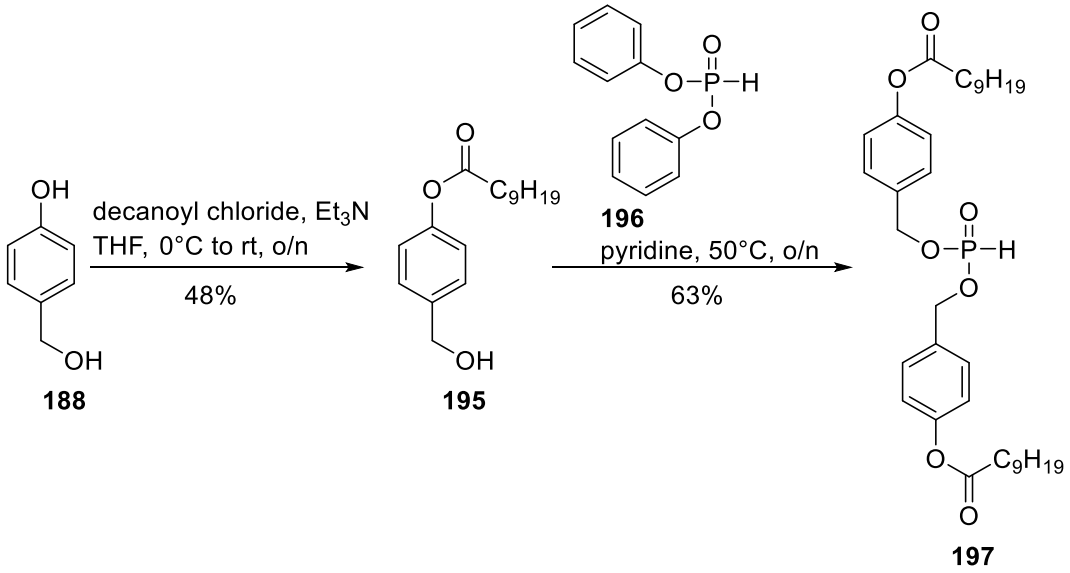

Figure 102: Synthesis of the *H*-phosphonate **197**.

The C9-acyloxybenzyl ester **195** was synthesized via the reaction of decanoyl chloride with 4-hydroxybenzyl alcohol **188**, affording a yield of 48%. Subsequently, this ester was reacted with

diphenyl phosphonate **196** to produce the corresponding *H*-phosphonate **197**, in a yield of 63% (Figure 102).

The 3'-fluoro-T-1106-5'-monophosphate **198**, necessary for Tri*PPP*ro synthesis, was prepared in a single step from the respective nucleoside **41** using established YOSHIKAWA conditions, resulting in a yield of 31% (Figure 103).

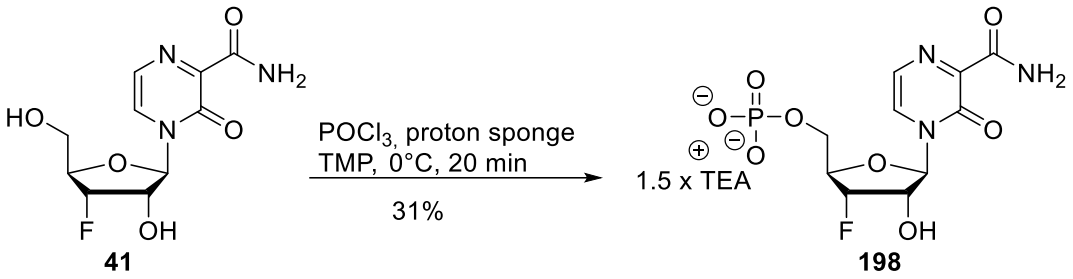

Figure 103: Synthesis of 3´-fluoro-T-1106-5´-monophosphate **198**.

The synthesis of the symmetrically masked pyrophosphate **199** was performed using an established strategy developed by GOLLNEST[134]. In the first step, the *H*-phosphonate **197** was reacted with *N*-chlorosuccinimide in an oxidative chloridation to generate the activated intermediate **200**. Subsequently, tetra-*n*-butylammonium phosphate was added, which nucleophilically attacked the intermediate **200**, resulting in the formation of the pyrophosphate **199** in an overall yield of 80% across both steps (Figure 104). Due to its high lability toward hydrolysis, pyrophosphate **199** must be freshly prepared and can be stored in the freezer for only up to two days.

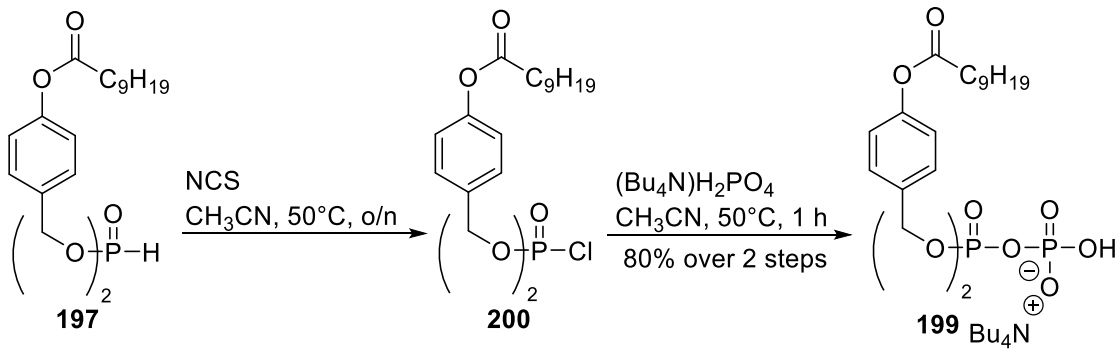

Figure 104: Synthesis of the pyrophosphate **199**.

Following the successful synthesis of the monophosphate **198** and the pyrophosphate **201**, both precursors were coupled using a protocol originally described by MOHAMADY[234] and subsequently

modified by GOLLNEST[134]. First, the pyrophosphate **199** was activated with trifluoroacetic anhydride. After removal of all volatiles under reduced pressure, the residue was redissolved in DMF and treated with 1-methylimidazole to form the imidazolidate intermediate of the pyrophosphate. The imidazolidate serves as an excellent leaving group, making it highly susceptible to nucleophilic attack. In the subsequent step, monophosphate **198** was added. Nucleophilic attack of the monophosphate on the imidazolidate intermediate led to the formation of the target Tri*PPP*ro compound **194**, which was obtained in a yield of 25% (Figure 105).

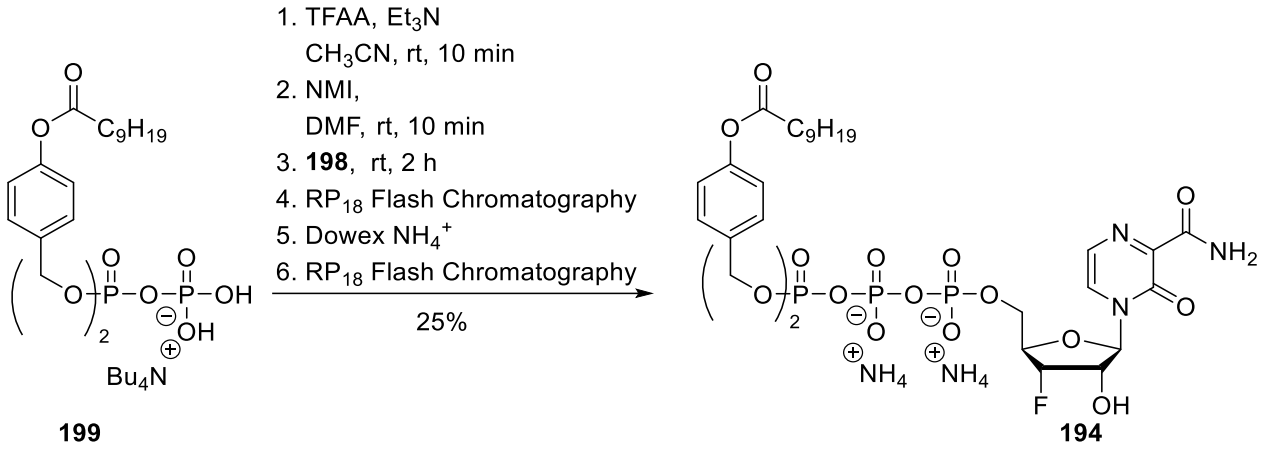

Figure 105: Synthesis of the C9C9-3´-fluoro-T-1106-Tri*PPP*ro **202**.

4.14.2 Synthesis of C9C9AB-adenosine-Tri*PPP*ro compounds

In collaboration with the research group of K. FUGGER from the University College London, the C9C9-Tri*PPP*ro derivative of 2-aminoadenosine **203** was prepared for evaluation of its anticancer activity. As a reference compound, the C9C9-Tri*PPP*ro of adenosine **204** was also synthesized. Since adenosine-5´-monophosphate **205** is commercially available, its synthesis was not necessary.

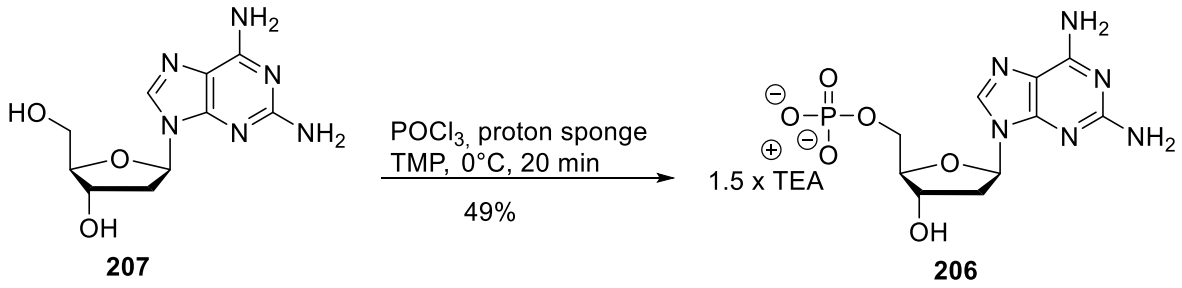

Figure 106: Synthesis of adenosine-5´-monophosphate **206**.

The 2-amino-adenosine-5´-monophosphate **206** was synthesized from 2-aminoadenosine **207** using established YOSHIKAWA conditions, resulting in a yield of 49% (Figure 106). Subsequently, the Tri*PPP*ro **208** and **209** derivatives were synthesized under previously established protocols, with yields of 35% and 22%, respectively (Figure 107).

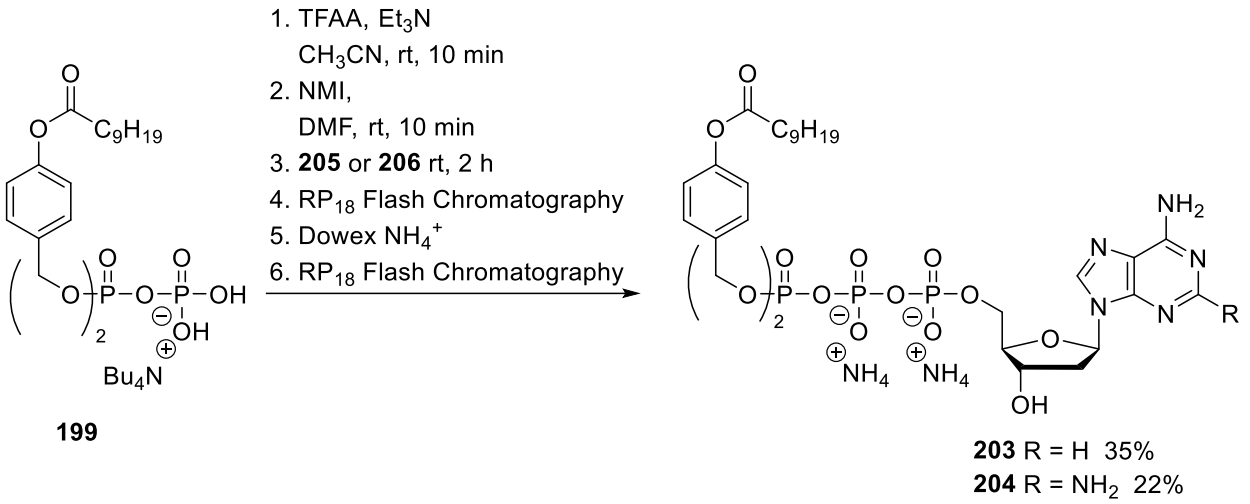

Figure 107: Synthesis of the C9C9-adenosine-Tri*PPP*ro **203** and C9C9-2-amino-adenosine-Tri*PPP*ro **204**.

4.14.3 Synthesis of C9C9-thymidine-Tri*PPP*ro 205

In collaboration with the research team of M. DOBBELSTEIN from the University of Göttingen, the C9C9-thymidine-Tri*PPP*ro **205** was synthesized using previously established protocols, achieving a yield of 34% from commercially available uridine-5´-monophosphate (UMP) **206** (Figure 108). The results of this cooperation were published in 2025.[235]

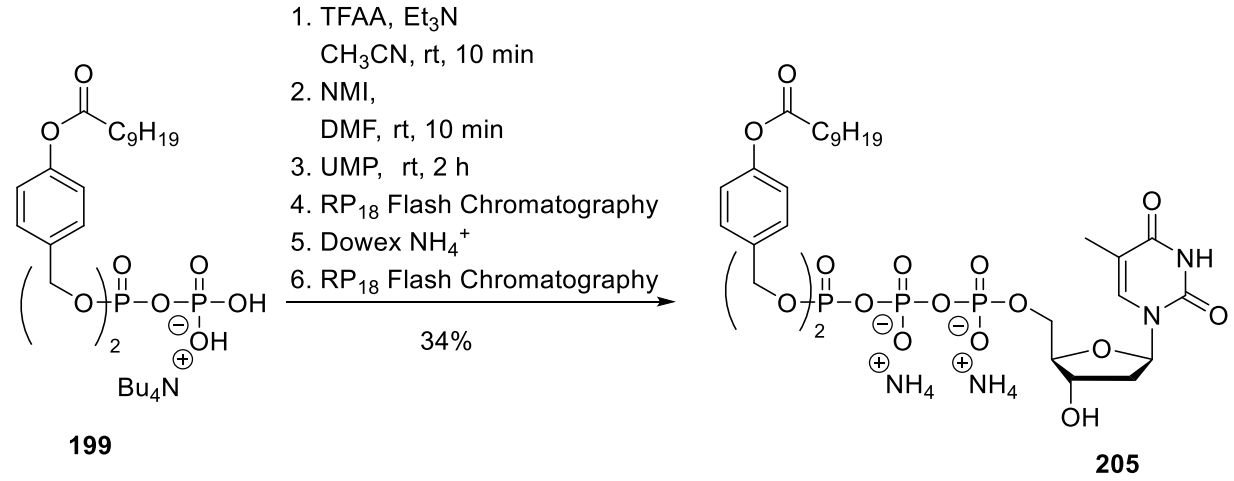

Figure 108: Synthesis of the C9C9-thymidine-Tri*PPP*ro **205**.

4.15.4 Synthesis of double γ-alkyl-masked JD-004-5´-triphosphates

In the research group of K. SELEY-RADTKE, the flex nucleoside JD-004 **207** and its corresponding monophosphate prodrug JD-006 were synthesized and evaluated for their antiviral activities. Previous studies by JIA demonstrated that the antiviral efficacy of nucleosides can be significantly enhanced by preparing their double-alkyl-masked triphosphate derivatives.[236–238] Building on this knowledge, the goal was to synthesize double γ-alkyl-masked phosphate and phosphonate prodrugs of nucleoside **207**. The synthesis of these double γ-alkyl-masked triphosphates can be achieved using the same approach as for the preparation of Tri*PPP*ro derivatives.

The JD-004-5'-monophosphate **208** was successfully synthesized under standard YOSHIKAWA conditions, affording a yield of 81% (Figure 109).

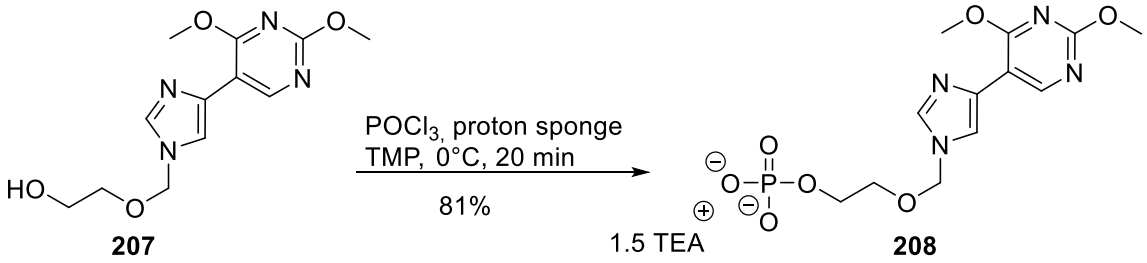

Figure 109: Synthesis of JD-004-5´-monophosphate **208**.

The pyrophosphates **209** and **210** were synthesized following the same procedure as used for the double acyloxybenzyl-masked pyrophosphate **199**, starting from the corresponding *H*-phosphonates **211** and **212**. The yields of these pyrophosphates were not determined, and they were directly used in the subsequent step (Figure 110).

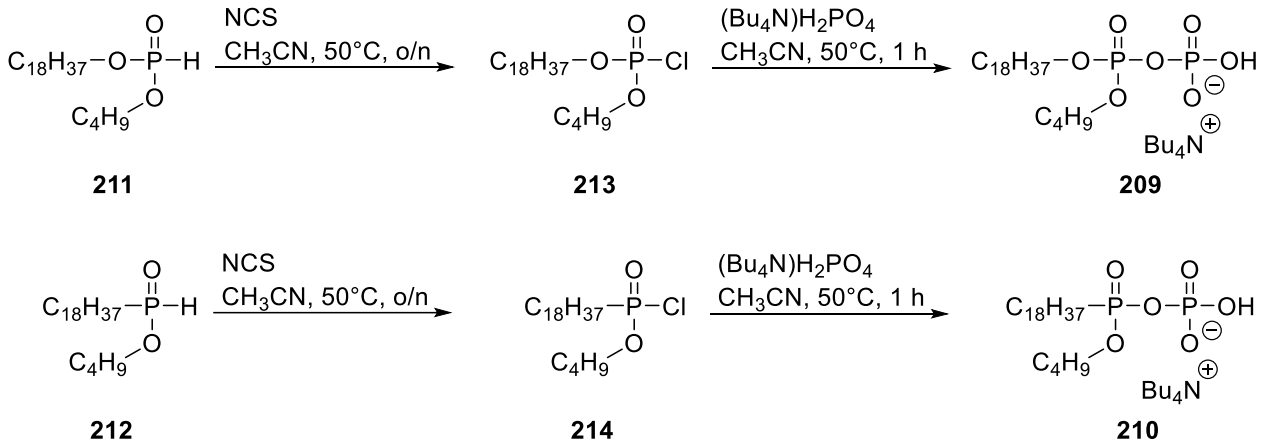

Figure 110: Synthesis of the pyrophosphate **209** and **210**.

The respective double γ-alkyl-masked triphosphates **211** and **212** were synthesized following the established protocols, with yields of 28% and 12%, respectively (Figure 111). These compounds are currently being evaluated in cell-based antiviral assays for their activity against a diverse range of RNA viruses.

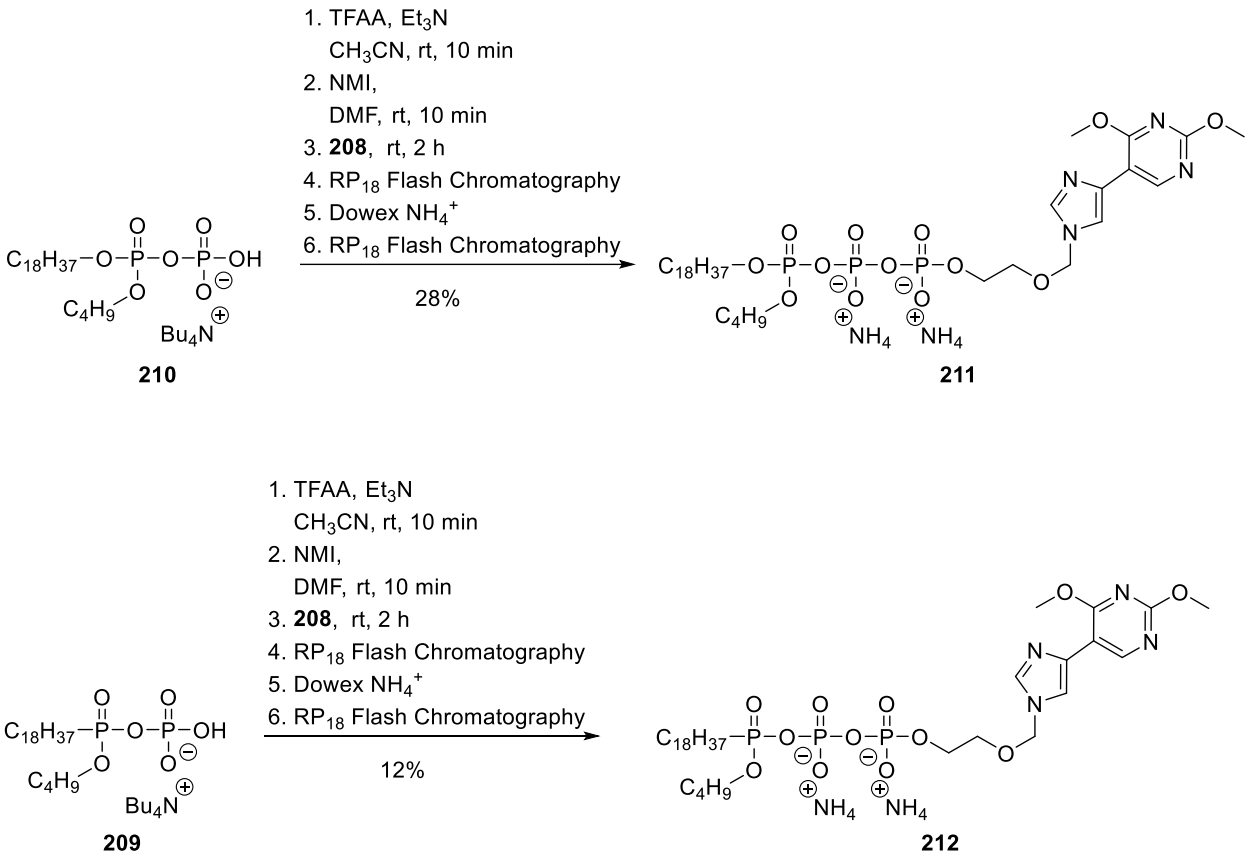

Figure 111: Double γ-alkyl masked triphosphates **211** and **212**.

4.14.5 Synthesis of 5-fluoro-uridine-5´-triphosphate 213

In previous work, prodrugs of 5-fluoro-uridine demonstrated promising activity as anti-cancer agents.[209] The aim was to introduce a 2´-*C*-methyl group to 5-fluoro-uridine in order to potentially enhance its potency as an anti-cancer or antiviral agent.

In the initial step, 5-fluoro-uracil **214** was reacted with 1,2,3,5-tetra-*O*-benzoyl-2-*C*-methyl-D-ribofuranose **49** under standard VORBRÜGGEN conditions (Chapter 4.3). It should be noted that the silylation of 5-fluoro-uracil **214** with HMDS required three hours of reflux to achieve complete conversion to the silylated compound, in contrast to the one-hour reaction time observed for T-1105 **12**. After this extended reaction time, a clear solution was obtained, indicating successful silylation. Under these conditions, the protected nucleoside **215** was isolated in 86% yield.

Subsequent deprotection with methanolic ammonia afforded the desired 2´-*C*-methyl-5-fluoro-uridine **216** in 93% yield. The resulting compound was then phosphorylated at the 5´-position using YOSHIKAWA conditions to produce the corresponding 5´-monophosphate **217**.[239] This monophosphate was further converted to the 5´-triphosphate derivative **218** under MOHAMADY conditions,[173] giving an overall yield of 80% (Figure 112). The synthesized 2´-C-methyl-5-fluoro-uridine-5´-triphosphate **218** is currently being evaluated in SARS-CoV-2 polymerase assays.

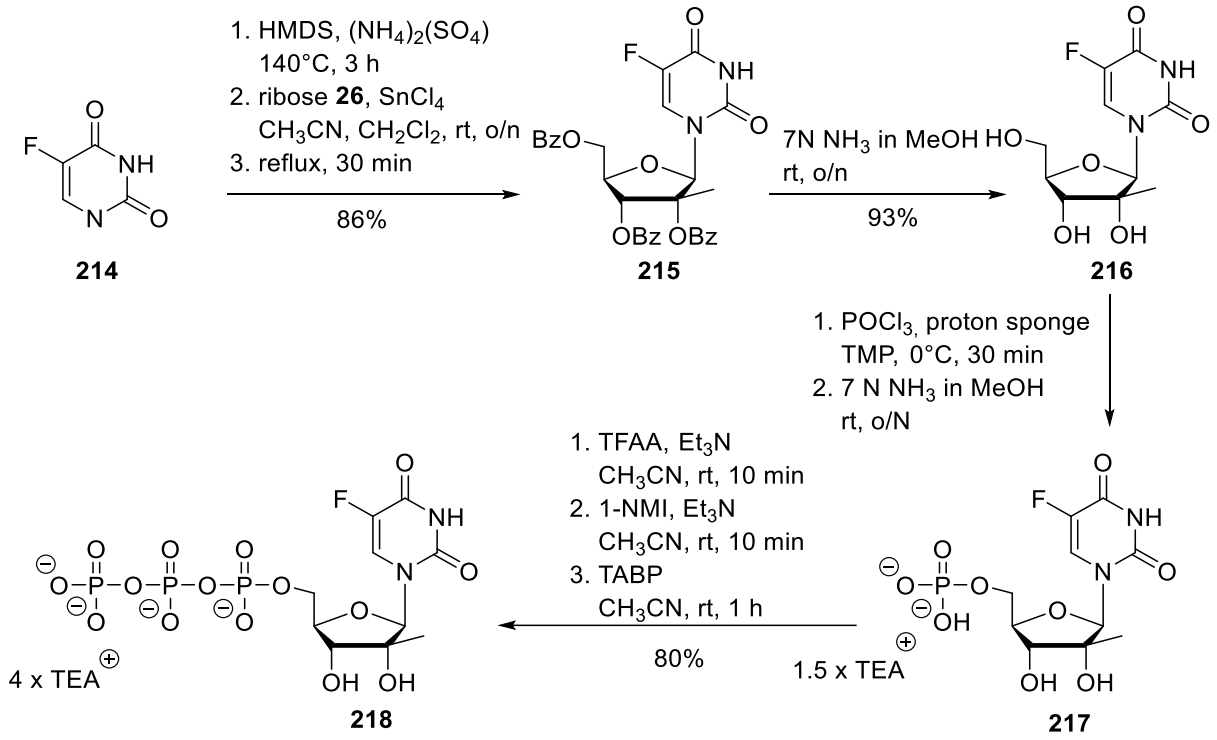

Figure 112: Synthesis of 2´-*C*-methyl-5-fluoro-uridine-5´-triphosphate **218**.

4.14.6 Synthesis of Remdesivir nucleoside-5'-diphosphate 219

In collaboration with the research group led by R. FLIEGERT at the University Medical Centre Hamburg-Eppendorf, the inhibitory effect of Remdesivir nucleoside-5'-diphosphate **219** on the de-ADP-ribosylating MacroD-like macrodomain (Mac1) of SARS-CoV-2 should be investigated.

In the initial step, GS-441524 **60** was phosphorylated at the 5'-position using established YOSHIKAWA conditions, achieving a yield of 56%. Notably, higher yields for this nucleoside were obtained when no base was added. In the subsequent step, the resulting monophosphate **220** was converted to the corresponding diphosphate **219** using established MOHAMADY conditions, resulting in a 89% yield (Figure 113).

The Remdesivir nucleoside-5'-diphosphate **219** was then successfully tested at the University Medical Centre Hamburg-Eppendorf, and the results were prepublished in 2025.[240]

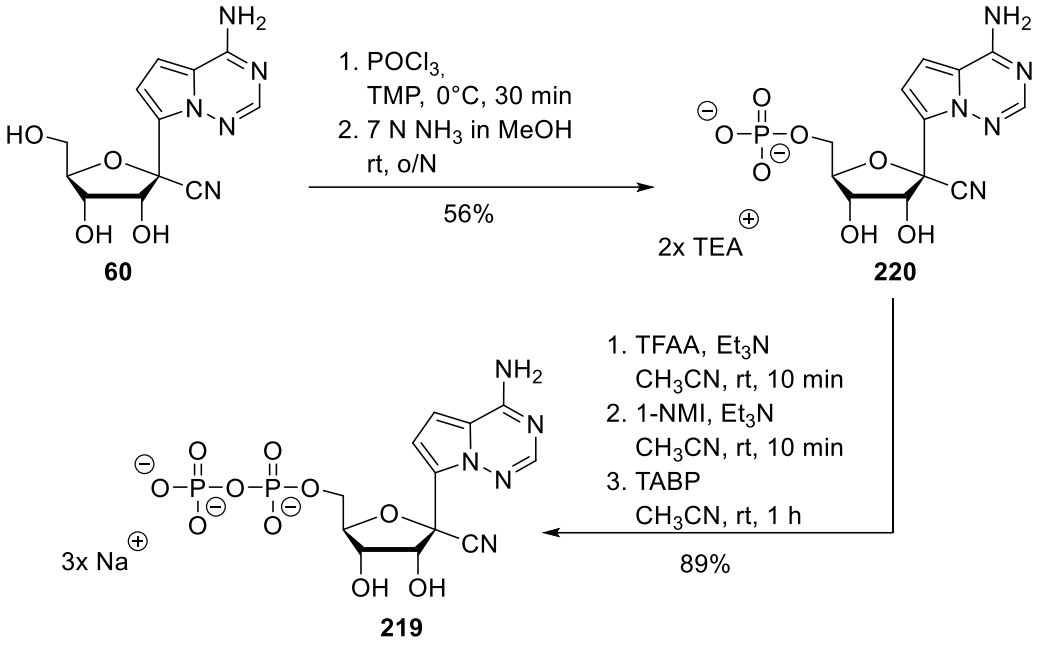

Figure 113: Synthesis of Remdesivir nucleoside-5´-diphosphate **219**.

5. Experimental Part

5.1 Solvents, chromatography and devices

Solvents

Aceton-d_6	C_3D_6O; bp.: 55.5 °C; Deutero 00105; for spectroscopic use.
Acetonitrile	C_2H_3N; bp.: 81°C; VWR chemicals, HPLC grade anhydrous: Fisher Scientific 10353732.
Chloroform-d_1	$CDCl_3$, bp.: 62°C; Euriso-Top D007H; for spectroscopic use.
Dichloromethane	CH_2Cl_2; bp.: 40°C; distilled before use; anhydrous: Fisher Scientific 10429252.
Diethyl ether	$C_4H_{10}O$; bp.: 35°C; distilled before use.
Dimethyl sulfoxide-d_6	C_2D_6OS; bp.: 190°C; Euriso-Top D010ES; for spectroscopic use.
Ethyl acetate	$C_4H_8O_2$; bp.: 77°C; distilled before use.
n-Hexane	C_6H_{14}; bp.: 69°C; VWR chemicals, HPLC grade.
Methanol	CH_4O; bp.: 65°C; distilled before use; anhydrous: Fisher Scientific 10323442.
Methanol-*d4*	CD_4OD; bp.: 65°C; Euriso-Top D0234ES; for spectroscopic use.
N,N-Dimethylformamide	C_3H_7NO; bp.: 153°C; anhydrous: Fisher Scientific 10045421.
Nitromethane	CH_3NO_2; bp.: 101°C; Sigma-Aldrich 230731.
Petroleum ether (50-70)	bp.: 50-70°C; distilled before use.
Pyridine	C_5H_5N; bp.: 116°C; anhydrous: Fisher Scientific 12834741
Tetrahydrofuran	C_4H_8O; bp.: 65°C; VWR chemicals, HPLC grade; anhydrous: Fisher Scientific 10292182
Water-d_2	D_2O; bp.: 101.4°C; Deutero 00506; for spectroscopic use.

Chromatography

Thin-layer chromatography

Thin layer chromatography was performed on precoated MACHEREY-NAGEL Alugram Xtra SIL G/UV_{254}. UV-active substances were visualized with UV light at 254 nm. Furthermore, compounds were stained with one of the following reagents.

1. Methanol (180 mL), water (20 mL), glacial acetic acid (25 mL), conc. sulfuric acid (5 mL), vanillin (1 g).
2. $Ce(SO_4)_4$ (1g), phosphomolybdic acid (2.5 g), conc. sulfuric acid (8 mL), water (100 mL).

Column chromatography

Normal phase column chromatography was performed on silica gel MN 60 (0.040-0.063 mm) from Macherey-Nagel.

Automated flash chromatography

Normal phase automated flash chromatography was performed using cartridges filled with silica gel MN 60 (0.040-0.063 mm) from Macherey-Nagel. The purification was performed on an Interchim Puriflash 430 or X520 Plus.

Reversed phase automated flash chromatography on RP_{18} silica gel was performed using MN RS 16 C_{18} ec, MN RS 40 C_{18} ec or MN RS 120 C_{18} ec columns on an Interchim Puriflash 430 or X520 Plus.

High-performance liquid chromatography

Analytical high-performance liquid chromatography was performed on an Agilent 1260 Infinity II system.

Software:	Agilent OpenLabs CDS
Pump:	1260 Quat Pump VL
Autosampler:	1260 Vialsampler
Detector:	1260, Dioden Array Detector (DAD)

Column: EC 125/3 NUCLEODUR 100-5 C18ec (length: 125 mm, ID: 3.0 mm, particle size: 5 µm) from MACHEREY NAGEL; Pre-column EC 4/3 Nucleodur 100-5 C18ec from MACHEREY-NAGEL.

Method: CH_3CN gradient in 2 mM tetrabutylammonium acetate buffer (pH 6.0); 0-20 min; 5-80%, flow 1 mL min^{-1}.

Spectroscopy

Nuclear magnetic resonance spectroscopy (NMR)

All NMR spectra were measured at the institute of organic chemistry or inorganic chemistry at the University of Hamburg. NMR spectra were recorded on a Bruker Fourier 300 (300 MHz), a Bruker AV 400 (400 MHz), a Bruker DRX 500 (500 MHz) or a Bruker AVIII 600 (600 MHz). The chemical shifts were quoted in parts per million [ppm] and were calibrated on the used solvent signals: Acetone-d_6: 2.05 (^{1}H), 29.84 (^{13}C); Chloroform-*d1*: (^{1}H), 77.16 (^{13}C); Dimethyl sulfoxide-d_6: 2.50 (^{1}H), 39.52 (^{13}C); Methanol-*d4*: 3.31(^{1}H), 49.00 (^{13}C); Water-*d2*: 4.79 (^{1}H). For further identification, two-dimensional experiments (*H,H*-COSY; HMBC; HSQC; NOESY) were performed.

Mass spectrometry

All mass spectra were measured at the institute of organic chemistry at the University of Hamburg or at the University Medical Centre Hamburg-Eppendorf (UKE). ESI mass spectrometry was performed on an Agilent 6224 ESI-TOF spectrometer in positive and negative mode.

Polarimeter

For the determination of the optical rotation an A. Krüss Optic GmbH P8000 polarimeter was used. The optical rotation values were measured in a cuvette with a length of 100 mm, at a wavelength of 589 nm.

Further Devices

Centrifuge

For centrifugation a Hereaus Biofuge R with 8000 rpm or a Eppendorf 5418 R with 14000 rpm were used.

Freeze Dryer

A Christ ALPHA 2-4 LDplus was used for freeze drying.

5.2 Preparation of buffer-solutions

Preparation of 2 mM tetrabutylammonium acetate buffer

To a solution of 10% aqueous tetrabutylammonium hydroxide (12.7 mL, 4.9 mmol) in deionized ultrapure water (2.4 L) acetic acid (~6 mL) was added until the pH value was set to 6.0.

Preparation of 1 M triethylammonium bicarbonate buffer (1 M TEAB)

Triethylamine (319 mL, 2.00 mol) was added to deionized ultrapure water (2.3 L). Gaseous carbon dioxide evolving from sublimating dry ice was bubbled through the solution until the pH of the solution reaches pH 8.0.

Preparation of 0.05 M triethylammonium bicarbonate buffer (0.05 M TEAB)

50 mL of the 1 M TEAB solution was filled up to 1 L with deionized ultrapure water.

5.3 Synthesis

5.3.1 General Procedures

General procedure I for the synthesis of 2´-*C*-modified ribose

To a solution of $CeCl_3$ (4.3 equiv.) in THF was added the appropriate Grignard reagent (4.0 equiv.) over 20 min at -78°C. After the reaction mixture was stirred for 1.5 h a solution of 1,3,5-tri-*O*-benzoyl-α-D-2-ketoribofuranose **181** (1.0 equiv.) in THF was added over 20 min. After the reaction mixture was stirred for 30 min TLC showed complete consumption of the starting material, whereupon the reaction was quenched by the addition of sat. aq. NH_4Cl. After the reaction mixture was warmed to room temperature, the mixture was filtered through a pad of Celite. The filtrate was extracted with CH_2Cl_2 three times. The combined organic layers were dried over $MgSO_4$, and all volatiles were removed under reduced pressure to provide the crude product.

The crude product was solved in CH_2Cl_2 and consecutively DMAP (2.0 equiv.), Et_3N (15 equiv.) and benzoyl chloride (3.0 equiv.) were added. After the reaction mixture was stirred overnight at room temperature the reaction was quenched by the addition of sat. aq. $NaHCO_3$. The aqueous phase was extracted with CH_2Cl_2 three times. The combined organic layers were dried over

$MgSO_4$, afterwards all volatiles were removed under reduced pressure purification of the crude product on silica gel provided the appropriate 2´-*C*-modified ribose.

General procedure II for the synthesis of nucleosides using modified VORBRÜGGEN protocol

The appropriate base (1.0 equiv.) and ammonium sulfate (0.015 equiv.) were suspended in HMDS and heated at 130°C for 1 h until a clear solution was formed. After all volatiles were removed under reduced pressure the residue was taken up in CH_3CN and CH_2Cl_2 and the appropriate ribose (0.3 to 0.7 equiv.) followed by tin tetrachloride (1 M solution in CH_2Cl_2, 0.3 to 0.7 equiv.) were added. The reaction mixture was stirred for 16 h at room temperature, if no full conversion could be observed the reaction mixture was refluxed for further 30 to 60 min. After full conversion of the ribose could be observed the reaction was quenched by the addition of saturated Na_2HCO_3 solution. CH_2Cl_2 was added and the organic layer was separated. The aqueous layer was extracted two times with CH_2Cl_2. The combined organic layers were dried over $MgSO_4$, and afterwards all volatiles were removed under reduced pressure, purification of the crude product on silica gel provided the appropriate protected nucleosides.

General procedure III for the cleavage acyl protection groups using sodium methanolate

After the appropriate amount of the protected nucleoside was solved in methanol, sodium methoxide solution (5.4 M in MeOH, 0.1 equiv.) was added and the reaction mixture was stirred for 30 to 60 min at room temperature. After TLC showed full conversion of the starting material the pH was adjusted to 6 by adding a 1 M HCL solution, afterwards all volatiles were removed under reduced pressure. The crude product was subjected to a RP_{18} silica gel using automated flash chromatography (H_2O/CH_3CN; 100:0 to 0:100) to provide the appropriate nucleoside.

General procedure IV for the cleavage acyl protection groups with simultaneously ester ammonolysis using methanolic ammonia

The appropriate protected nucleoside was solved in methanolic ammonia (7 M NH_3 in MeOH) and the resulting mixture was stirred for 16 h at room temperature. After complete consumption of the starting material all volatiles were removed under reduced pressure. The residue was taken up in H_2O and the aqueous phase was washed with CH_2Cl_2 four times and with Et_2O once, afterwards all volatiles were removed under reduced pressure. The crude product was subjected

to a RP_{18} silica gel using automated flash chromatography (H_2O/CH_3CN; 100:0 to 0:100). to provide the appropriate nucleoside.

General procedure V for synthesis of nucleoside monophosphates using YOSHIKAWA protocol

The appropriate nucleoside (1.0 equiv.) was dried *in vacuo* overnight and solved in trimethyl phosphate. Depending on the solubility of the nucleoside gentle heating is required to obtain a solution. If the nucleoside is not completely solvable under these conditions, it is also possible to proceed with a suspension. After 1,8-bis(dimethylamino)naphthalene (proton sponge) (2.0 equiv.) was added, the reaction mixture was cooled to 0°C and $POCl_3$ (4.0 equiv.) was added slowly. Afterwards the reaction mixture was stirred at 0°C while the reaction was monitored using a RP_{18} HPLC. After the starting material was consumed completely or the formation of side products could be observed the reaction was quenched by the addition of 1 M TEAB buffer. Afterwards the reaction mixture was warmed to room temperature and stirred for 30 min and subsequently washed with CH_2Cl_2 three times. Then all volatiles were removed under reduced pressure, and the residue was subjected to a RP_{18} silica gel using an automated flash chromatography (0.05 M TEAB/CH_3CN; 100:0 to 0:100). Product containing fractions were pooled and freeze dried to yield the appropriate nucleoside-5´-monophosphate as triethylammonium salt.

General procedure VI for the synthesis of nucleoside triphosphates using modified LUDWIG & ECKSTEIN protocol

The appropriate nucleoside (1.0 equiv.) was dried *in vacuo* overnight and solved in trimethyl phosphate. Depending on the solubility of the nucleoside gentle heating is required to obtain a solution. If the nucleoside is not completely solvable under these conditions, it is also possible to proceed with a suspension. After 1,8-bis(dimethylamino)naphthalene (proton sponge) (2.0 equiv.) was added, the reaction mixture was cooled to 0°C and $POCl_3$ (4.0 equiv.) was added slowly. Afterwards the reaction mixture was stirred at 0°C while the reaction was monitored using a RP_{18} HPLC. After the starting material was consumed completely or the formation of side products could be observed a precooled mixture containing tributyl ammonium pyrophosphate (2.5 equiv.) and tributylamine (6 equiv.) in CH_3CN was added. The reaction mixture was further stirred at 0°C while being monitored using a RP_{18} HPLC. After full conversion of the starting material, or when no more conversion could be observed the reaction

was quenched by the addition of 1 M TEAB buffer. Afterwards the reaction mixture was warmed to room temperature, stirred for 30 min, and subsequently washed with CH_2Cl_2 three times. After all volatiles were removed under reduced pressure the residue was subjected to a DEAD-Sephadex A-25 column using an automated flash system (0–1 M TEAB). Fractions containing the desired product were concentrated under reduced pressure and subjected to a RP_{18} silica gel using an automated flash chromatography (0.05 M TEAB/CH_3CN; 100:0 to 0:100). Product containing fractions were pooled and freeze dried to yield the appropriate nucleoside-5´-triphosphate as triethylammonium salt.

General procedure VII for the synthesis of Tri*PPP*ro-NTP-Prodrugs using the *H*-phosphonate route

The appropriate *H*-phosphonate (1.0 equiv.) was dissolved/suspended in CH_3CN and *N*-chlorosuccinimide (2.5 equiv.) was added. After the reaction mixture was stirred overnight at 50 °C tetrabutylammonium phosphate monobasic (0.4 M solution in CH_3CN, 3.0 equiv.) was added and the reaction mixture was stirred for 1 h at room temperature. Subsequently, the solvent was removed under reduced pressure, the resulting residue was taken up in CH_2Cl_2, washed with cold 1 M aq. NH_4OAc, and cold H_2O (phase separation via centrifuge). The organic layer was dried over $MgSO_4$, and all volatiles were removed under reduced pressure to yield the appropriate pyrophosphate, that was used in the next step without further purification (Note: the pyrophosphate can be stored overnight under nitrogen as inert gas at -20 °C).

To a solution of the appropriate pyrophosphate (1.0 equiv.) in CH_3CN was added a solution of TFAA (5.0 equiv.) in Et_3N (8.0 equiv.) at 0°C. After the resulting reaction mixture was stirred for 10 min at room temperature all volatiles were removed under reduced pressure. After the resulting residue was co-evaporated once with CH_3CN, it was dissolved again in CH_3CN. Then the reaction mixture was cooled to 0°C and Et_3N (5.0 equiv.) as well as 1-methylimidazol (2.5 equiv.) were added. The reaction mixture was stirred for 10 min at room temperature before the appropriate nucleoside 5´-monophosphate triethylammonium salt (0.3-0.5 equiv.) dissolved in DMF was added. The reaction mixture was stirred at room temperature until full conversion of the monophosphate was observed (RP_{18} HPLC monitoring). Afterwards all volatiles were removed under reduced pressure and the residue was subjected to a RP_{18} silica gel using an automated flash chromatography (H_2O/CH_3CN; 100:0 to 0:100), followed by ion exchange to ammonia (Dowex-NH_4^+), and a final purification on RP_{18} silica gel using automated flash chromatography

(H_2O/CH_3CN; 100:0 to 0:100). Product containing fractions were pooled and freeze dried to yield the appropriate Tri*PPP*ro-NTP-Prodrug as ammonium salt.

General procedure VIII for the synthesis of C-nucleosides

The appropriate pyridine derivative (1.0 equiv.) was dissolved in THF before LDA (1 M solution in THF, 1.0 equiv.) was added dropwise at -78°C. After the reaction mixture was stirred for 30 min at -78°C a solution of the appropriate protected ribonolactone (0.5 equiv.) in THF was added dropwise. Then the reaction mixture was stirred for an additional hour and quenched by the addition of sat. aq. NH_4Cl. CH_2Cl_2. Afterwards the organic layer was separated and the aqueous layer was extracted two times with CH_2Cl_2. The combined organic layers were dried over $MgSO_4$, and all volatiles were removed under reduced pressure. Purification of the crude product on silica gel provided the appropriate lactol.

General procedure IX for the acetylation of C-nucleosides

The appropriate lactol (1.0 equiv.) was dissolved in THF before LiHMDS (1 M solution in THF, 1.5 equiv.) was added dropwise at room temperature. After the reaction mixture was stirred for 10 min acetic anhydride (1.5 equiv.) was added and the reaction mixture was stirred for further 20 min. The reaction was quenched by the addition of aq. sat. $NaHCO_3$. CH_2Cl_2 was added and the organic layer was separated. The aqueous layer was extracted two times with CH_2Cl_2. The combined organic layers were dried over $MgSO_4$, and all volatiles were removed under reduced pressure. Purification of the crude product on silica gel provided the appropriate acetylated lactol.

5.3.2 Synthesis of pyrazine building blocks

3-Hydroxypyrazine-2-carboxylic acid 29

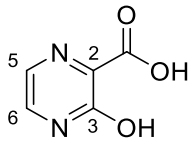

29
$C_5H_4N_2O_3$
140.0980 g/mol

3-Amino-2-pyrazinecarboxylic acid **21** (20.0 g, 144 mmol) was suspended in 100 mL conc. H_2SO_4. At 0°C, sodium nitrite (14.9 g, 216 mmol) was added portion-wise. The suspension was afterwards stirred at room temperature for two hours until a clear solution was formed. The reaction was quenched by pouring the reaction mixture on ice water (500 mL). The precipitated

solid was collected by vacuum filtration and washed with ice-cold water and redissolved in a 5% sodium carbonate solution. 3-Hydroxypyrazine-2-carboxylic acid **29** was precipitated by the addition of 1 M HCl (300 mL), collected by vacuum filtration, washed with ice-cold water, and dried under vacuum to give 16.0 g of **29** (114 mmol, 79%) as a yellow solid and was used without further purification.

The analytical data was in accordance with those described.[142]

^{1}*H*-NMR (300 MHz, DMSO-d_6): δ [ppm] = 7.80 (d, $^3J_{HH}$ = 3.7 Hz, 1H, *H*-5), 7.65 (d, $^3J_{HH}$ = 3.7 Hz, 1H, *H*-6).

Methyl 3-hydroxy-2-pyrazinecarboxylate 20

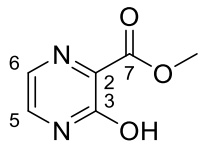

20
$C_6H_6N_2O_3$
154.1250 g/mol

3-Hydroxypyrazine-2-carboxylic acid **29** (16.0 g, 114 mmol) was dissolved in MeOH (300 mL), and conc. H_2SO_4 (2 mL) was added. After the reaction mixture was refluxed for 16 h, all volatiles were removed under reduced pressure. Purification on silica gel (CH_2Cl_2/MeOH; 30:1 v/v) provided 14.0 g of **20** (90.8 mmol, 80%) as a yellow solid.

The analytical data was in accordance with those described.[142]

^{1}*H*-NMR (300 MHz, DMSO-d_6): δ [ppm] = 7.71 (d, $^3J_{HH}$ = 3.7 Hz, 1H, *H*-5), 7.47 (d, $^3J_{HH}$ = 3.7 Hz, 1H, *H*-6), 3.81 (s, 3H, -OC*H*$_3$).

Methyl 3-amino-6-methylpyrazine-2-carboxylate 128

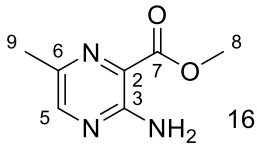

128
$C_7H_9N_3O_2$
167.1680 g/mol

Methyl 3-amino-6-bromo-2-carboxylate **127** (2.00 g, 8.62 mmol), $Pd_2(OAc)_4$ (193 mg, 0.86 mmol), Xantphos (748 mg, 1.29 mmol), methylboronic acid (773 mg, 19.9 mmol), and potassium phosphate tribasic (3.65 g, 17.2 mmol) were dissolved in toluene (30 mL) and water (1 mL). The reaction mixture was refluxed for 1 h before it was allowed to cool to room temperature, filtered through Celite, and washed with CH_2Cl_2. The filtrate was concentrated under reduced pressure

and subjected to a silica gel column using automated flash chromatography (CH_2Cl_2/ethyl acetate; 100:0 to 80:20 v/v). The desired product **128** (650 mg, 45%) was obtained as a brown solid.

The analytical data was in accordance with those described.[215]

^{1}*H*-NMR (400 MHz, $CDCl_3$): δ [ppm] = 8.10 (s, 1H, *H*-5), 6.31 (bs, 2H, -N*H*$_2$), 3.97 (s, 3H, *H*-8), 2.47 (s, 3H, *H*-9).

^{13}*C*-NMR (101 MHz, $CDCl_3$): δ [ppm] = 167.1 (*C*-7), 154.3 (*C*-3), 147.5 (*C*-5), 142.3 (*C*-6), 122.9 (*C*-2), 53.0 (*C*-8), 20.6 (*C*-9).

HRMS (ESI$^+$): *m/z* = calcd: 168.0767 $[M+H]^+$, found: 168.0768 $[M+H]^+$.

Methyl 3-hydroxy-6-methylpyrazine-2-carboxylate 129

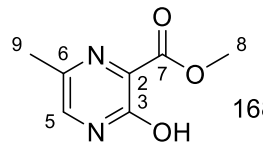

129
$C_7H_8N_2O_3$
168.1520 g/mol

Methyl 3-amino-6-methylpyrazine-2-carboxylate **128** (677 mg, 4.05 mmol) was suspended in conc. H_2SO_4 (2 mL). At 0°C, sodium nitrite (558 mg, 8.10 mmol) was added portion-wise. The suspension was then stirred at room temperature for two hours, until a solution was formed. The reaction was quenched by pouring the reaction mixture onto ice water (500 mL). The precipitated solid was collected by vacuum filtration and washed with ice-cold water. The obtained crude product was purified on silica gel with automated flash chromatography (CH_2Cl_2/MeOH; 100:1 to 15:1 v/v), which provided **129** (596 mg, 88%) as a light-brown solid.

The analytical data was in accordance with those described.[215]

^{1}*H*-NMR (400 MHz, DMSO-d_6): δ [ppm] = 7.70 (s, 1H, *H*-5), 3.81 (s, 3H, *H*-8), 2.25 (s, 3H, *H*-9).

5.3.3 Synthesis of ribose building blocks

1,2-*O*-Isopropyliden-α-D-xylofuranose 30

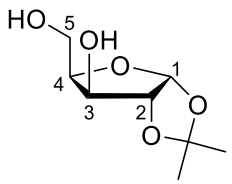

30
$C_8H_{14}O_5$
190.1950 g/mol

D-Xylose **25** (20.0 g, 0.13 mol) was dissolved in acetone (520 mL), and conc. H_2SO_4 (20 mL) was added. After the reaction mixture was stirred for 30 min, the reaction mixture was cooled to 0°C, and Na_2CO_3 (34.1 g, 0.24 mol) dissolved in 100 mL water was added carefully. Afterwards, the reaction mixture was stirred at room temperature for 3.5 h before solid Na_2CO_3 was added until a pH = 7 was reached. The precipitated solid was removed by filtration and extensively washed with acetone. After all volatiles were removed under reduced pressure, the crude product was purified on silica gel (CH_2Cl_2/MeOH; 50:1 v/v), providing **30** (20.5 g, 81%) as a light-yellow oil.

The analytical data was in accordance with those described.[144]

^1H-NMR (600 MHz, $CDCl_3$): δ [ppm] = 5.98 (d, $^3J_{HH}$ = 3.60 Hz, 1H, *H*-1), 4.52 (d, $^3J_{HH}$ = 3.80 Hz, 1H, *H*-2), 4.33 (d, $^3J_{HH}$ = 2.72 Hz, 1H, *H*-3), 4.18 – 4.16 (m, 1H, *H*-4), 4.13 (dd, $^2J_{HH}$ = 12.54 Hz, $^3J_{HH}$ = 3.76 Hz, 1H, *H*-5), 4.03 (dd, $^2J_{HH}$ = 12.59 Hz, $^3J_{HH}$ = 2.57 Hz, 1H, *H*-5), 1.48 (s, 3H, C-CH_3), 1.32 (s, 3H, C-CH_3).

^{13}C-NMR (150 MHz, $CDCl_3$): δ [ppm] = 111.9 (*C*-CH_3), 106.0 (*C*-1), 85.8 (*C*-2), 78.7 (*C*-3), 77.2 (*C*-4), 61.4 (*C*-5), 26.9 (*C*-*C*H_3), 26.3 (*C*-*C*H_3).

HRMS (ESI^+): *m/z* = calcd: 213.0733 $[M+Na]^+$, found: 213.0732 $[M+Na]^+$.

5-*O*-Benzoyl-1,2-*O*-isopropylidene-α-D-xylofuranose 31

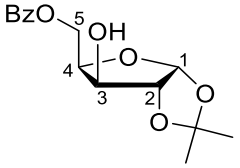

31
$C_{15}H_{18}O_6$
294.3030 g/mol

To a solution of xylose **30** (630 mg, 3.31 mmol) in CH_2Cl_2 (25 mL) was added Et_3N (689 µL, 4.96 mmol) at 0°C. Afterwards, benzoyl chloride (419 µL, 3.61 mmol) was added over 10 min. After the reaction was stirred at 0°C for 2 h, the reaction was quenched by the addition of sat. aq. $NaHCO_3$. The organic phase was washed with sat. aq. $NaHCO_3$, dried over $MgSO_4$, and all volatiles were removed under reduced pressure. The resulting residue was purified on silica gel (petroleum ether/ethyl acetate; 2:1 v/v), providing **31** (850 mg, 87%) as a white solid.

The analytical data was in accordance with those described.[144]

^1H-NMR (600 MHz, $CDCl_3$): δ [ppm] = 8.06 – 8.05 (m, 2H, *H*-Bz), 7.61 – 7.58 (m, 1H, *H*-Bz), 7.47 – 7.45 (m, 2H, *H*-Bz), 5.95 (d, $^3J_{HH}$ = 3.65 Hz, 1H, *H*-1), 4.83 – 4.79 (m, 1H, *H*-5), 4.60 (d, $^3J_{HH}$ = 3.71 Hz,

1H, *H*-2), 4.40 – 4.36 (m, 2H, *H*-3, *H*-5), 4.18 – 4.17 (m, 1H, *H*-4), 1.51 (s, 3H, C-CH_3), 1.32 (s, 3H, C-CH_3).

^{13}*C*-NMR (150 MHz, $CDCl_3$): δ [ppm] = 167.6 (*C*-Bz), 133.8 (*C*-Bz), 130.1 (2C, *C*-Bz), 129.3 (*C*-Bz), 128.7 (2C, *C*-Bz), 112.0 (*C*-CH_3), 104.9 (*C*-1), 85.2 (*C*-2), 78.7 (*C*-3), 74.5 (*C*-4), 61.3 (*C*-5), 26.9 (C-*C*H_3), 26.3 (C-*C*H_3).

HRMS (ESI$^+$): *m/z* = calcd: 317.0995 $[M+Na]^+$, found: 317.0995 $[M+Na]^+$.

5-*O*-Benzoyl-3-*O*-phenylcarbonothioate-1,2-*O*-isopropylidene-α-D-xylofuranose 32

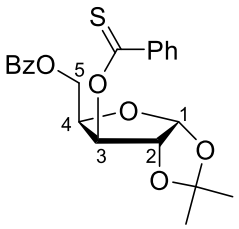

32
$C_{22}H_{22}O_6S$
414.4720 g/mol

The reaction was carried out as described in the literature with xylose **31** (318 mg, 1.08 mmol), 4-DMAP (330 mg, 2.70 mmol), and *O*-phenyl chlorothionoformate (224 mg, 1.30 mmol) in CH_2Cl_2 (10 mL). Purification on silica gel with automated flash chromatography (petroleum ether/ethyl acetate; 8:1 to 4:1 v/v) provided **32** (384 mg, 75%) as a colorless solid.

The analytical data was in accordance with those described.[119]

5-*O*-Benzoyl-3-deoxy-1,2-*O*-isopropylidene-α-D-xylofuranose 33

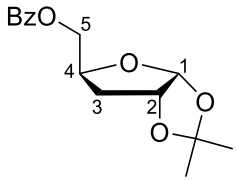

33
$C_{15}H_{18}O_5$
278.3040 g/mol

The reaction was carried out as described in the literature with xylose **32** (340 mg, 0.79 mmol), AIBN (26 mg, 0.16 mmol), and tributyltin hydride (315 mg, 1.16 mmol) in toluene (10 mL). Purification on silica gel with automated flash chromatography (petroleum ether/ethyl acetate; 7:1 to 3:1 v/v) provided **33** (208 mg, 94%) as a colorless oil.

The analytical data was in accordance with those described.[119]

5-*O*-Benzoyl-1,2-di-*O*-acetyl-3-deoxy-D-ribofuranose 22

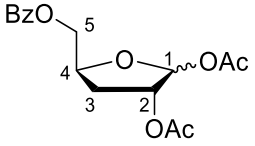

22
$C_{16}H_{18}O_7$
322.3130 g/mol

The reaction was carried out as described in the literature with ribose **33** (1.50 g, 5.38 mmol), acetic anhydride (3.24 g, 31.7 mmol), and conc. H_2SO_4 (0.75 mL) in acetic acid (30 mL). Purification on silica gel with automated flash chromatography (petroleum ether/ethyl acetate; 6:1 to 2:1 v/v) provided **22** (1.34 g, 77%) as a colorless oil.

The analytical data was in accordance with those described.[119]

^{1}*H*-NMR (600 MHz, $CDCl_3$): δ [ppm] = α-Anomer: 8.09 – 8.03 (m, 2H, *H*-Bz), 7.59 – 7.56 (m, 1H, *H*-Bz), 7.48 – 7.43 (m, 2H, *H*-Bz), 6.20 (s, 1H, *H*-1), 5.24 (d, $^3J_{HH}$ = 4.24 Hz, 1H, *H*-2), 4.74 – 4.70 (m, 1H, *H*-4), 4.54 (dd, $^2J_{HH}$ = 11.94 Hz, $^3J_{HH}$ = 3.74 Hz, 1H, *H*-5), 4.35 (dd, $^2J_{HH}$ = 11.89 Hz, $^3J_{HH}$ = 5.53 Hz, 1H, *H*-5), 2.29 – 2.19 (m, 2H, *H*-3) 2.10 (s, 3H, *H*-Ac), 1.97 (s, 3H, *H*-Ac).

^{13}*C*-NMR (150 MHz, $CDCl_3$): δ [ppm] = α-Anomer: 170.1 (*C*-Ac), 169.4 (*C*-Ac), 166.4 (*C*-Bz), 133.4 (*C*-Bz), 129.9 (2C, *C*-Bz), 129.8 (*C*-Bz), 128.5 (2C, *C*-Bz), 99.6 (*C*-1), 78.9 (*C*-4), 77.1 (*C*-3), 66.2 (*C*-5), 31.7 (*C*-3), 21.2 (*C*-Ac), 21.0 (*C*-Ac).

HRMS (ESI$^+$): *m/z* = calcd: 345.0945 $[M+Na]^+$, found: 345.0946 $[M+Na]^+$.

5-*O*-Benzoyl-1-*O*-methyl-α-D-xylofuranose 35

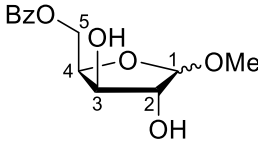

35
$C_{13}H_{16}O_6$
268.2650 g/mol

To a solution of xylose **31** (1.00 g, 3.40 mmol) in MeOH (20 mL) was added iodine (166 mg, 0.65 mmol), and the mixture was heated under reflux for 4 h. Afterwards, the reaction mixture was poured into sat. aq. $Na_2S_2O_3$ and extracted with CH_2Cl_2 three times. The combined organic layers were washed with sat. aq. NaCl, dried over $MgSO_4$, and all volatiles were removed under reduced pressure. Purification of the crude product on silica gel (petroleum ether/ethyl acetate; 2:1 v/v) provided **35** (695 mg, 76%) as a white solid, as a mixture of anomers.

The analytical data was in accordance with those described.[145]

^{1}*H*-NMR (600 MHz, $CDCl_3$): δ [ppm] = α-Anomer: 8.07 – 8.03 (m, 2H, *H*-Bz), 7.59 – 7.53 (m, 1H, *H*-Bz), 7.46 – 7.42 (m, 2H, *H*-Bz), 5.04 (d, $^3J_{HH}$ = 4.34 Hz, 1H, *H*-1), 4.71 – 4.66 (m, 1H, *H*-5), 4.44 – 4.42 (m, 1H, *H*-4), 4.39 (dd, $^2J_{HH}$ = 11.45 Hz, $^3J_{HH}$ = 5.30 Hz, 1H, *H*-5), 4.27 (t, $^3J_{HH}$ = 5.06 Hz, 1H, *H*-3), 4.18 – 4-16 (m, 1H, *H*-2), 3.50 (s, 3H, -OC*H*$_3$).

β-Anomer: 8.07 – 8.03 (m, 2H, *H*-Bz), 7.59 – 7.53 (m, 1H, *H*-Bz), 7.46 – 7.42 (m, 2H, *H*-Bz), 4.89 (s, 1H, *H*-1), 4.71 – 4.66 (m, 1H, *H*-5), 4.65 – 4.62 (m, 1H, *H*-3), 4.50 (dd, $^2J_{HH}$ = 11.48 Hz, $^3J_{HH}$ = 6.90 Hz, 1H, *H*-5), 4.24 (s, 1H, *H*-4), 4.18 – 4-16 (m, 1H, *H*-2), 3.40 (s, 3H, -OC*H*$_3$).

^{13}*C*-NMR (150 MHz, $CDCl_3$): δ [ppm] = α-Anomer: 167.8 (*C*-Bz), 133.5 (*C*-Bz), 129.9 (2C, *C*-Bz), 128.6 (*C*-Bz), 128.5 (2C, *C*-Bz), 102.1 (*C*-1), 78.0 (*C*-2), 76.9 (*C*-4), 76.6 (*C*-3) 63.0 (*C*-5), 56.2 (-O*C*H$_3$).

β-Anomer: 167.07 (*C*-Bz), 133.3(*C*-Bz), 129.9 (2C, *C*-Bz), 128.60 (*C*-Bz), 128.51 (2C, *C*-Bz), 108.8 (*C*-1), 80.9 (*C*-3), 79.7 (*C*-4), 76.1 (*C*-2), 64.5 (*C*-5), 55.4 (-O*C*H$_3$).

HRMS (ESI$^-$): *m/z* = calcd: 291.0839 $[M+Na]^+$, found: 291.0839 $[M+Na]^+$.

5-*O*-Benzoyl-3-deoxy-3-fluoro-1-*O*-methyl-D-ribofuranose 36

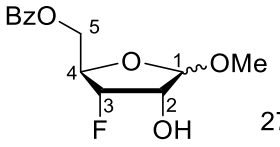

36
$C_{13}H_{15}FO_5$
270.2564 g/mol

Xylose **35** (2.12 g, 7.93 mmol) was dissolved in DCM (40 mL), and diethylaminosulfur trifluoride (5.78 g, 35.7 mmol) was added. The reaction mixture was stirred for 20 h at room temperature. After the reaction mixture was cooled in an ice bath, it was poured into cooled sat. aq. $NaHCO_3$ and extracted with CH_2Cl_2 three times. The combined organic layers were washed with saturated aqueous NaCl, dried over $MgSO_4$, and all volatiles were removed under reduced pressure. Purification of the crude product on silica gel (petroleum ether/ethyl acetate, 2:1 v/v) provided **36** (1.12 g, 52%) as a colorless oil, as a mixture of anomers.

The analytical data was in accordance with those described.[145]

^{1}*H*-NMR (600 MHz, $CDCl_3$): δ [ppm] = α-Anomer: 8.00 – 7.98 (m, 2H, *H*-Bz), 7.60 – 7.56 (m, 1H, *H*-Bz), 7.47 – 7.44 (m, 2H, *H*-Bz), 5.98 (d, $^3J_{HH}$ = 4.72 Hz, 1H, *H*-1), 4.90 (ddd, $^2J_{HF}$ = 55.88 Hz, $^3J_{HH}$ = 5.69 Hz, $^3J_{HH}$ = 1.43 Hz, 1H, *H*-3), 4.62- 4.50 (m, 2H, *H*-4, *H*-5), 4.46 – 4.42 (m, 1H, *H*-5), 4.20 (dt, $^3J_{HF}$ = 22.31 Hz, $^3J_{HH}$ = 5.21 Hz, 1H, *H*-2), 3.50 (s, 3H, -OC*H*$_3$).

β-Anomer: 8.08 – 8.06 (m, 2H, *H*-Bz), 7.60 – 7.56 (m, 1H, *H*-Bz), 7.47 – 7.44 (m, 2H, *H*-Bz), 4.89 (dt, $^{2}J_{HF}$ = 54.00 Hz, $^{3}J_{HH}$ = 4.93 Hz, 1H, *H*-3), 4.91 (t, $^{3}J_{HH}$ = 1.78 Hz, 1H, *H*-1), 4.62- 4.50 (m, 2H, *H*-4, *H*-5), 4.46 – 4.42 (m, 1H, *H*-5), 4.25 (ddd, $^{3}J_{HF}$ = 4.80 Hz, $^{3}J_{HH}$ = 4.80 Hz, $^{3}J_{HH}$ = 1.52 Hz, 1H, *H*-2), 3.35 (s, 3H, -OC*H*$_3$).

^{13}*C*-NMR (150 MHz, $CDCl_3$): δ [ppm] = α-Anomer: 166.1 (*C*-Bz), 133.6(*C*-Bz), 129.7 (2C, *C*-Bz), 129.5 (*C*-Bz), 128.7 (2C, *C*-Bz), 108.1 (d, $^{3}J_{CF}$ = 3.40 Hz, *C*-1), 90.6 (d, $^{1}J_{CF}$ = 185.56 Hz, *C*-3), 80.7 (d, $^{2}J_{CF}$ = 25.08 Hz, *C*-4), 72.5 (d, $^{2}J_{CF}$ = 16.58 Hz, *C*-2), 63.1 (d, $^{3}J_{CF}$ = 10.17 Hz, *C*-5), 55.9 (-O*C*H$_3$).

β-Anomer: 166.3 (*C*-Bz), 133.4(*C*-Bz), 129.9 (2C, *C*-Bz), 129.8 (*C*-Bz), 128.6 (2C, *C*-Bz), 102.4(*C*-1), 92.4 (d, $^{1}J_{CF}$ = 187.07 Hz, *C*-3), 78.6 (d, $^{2}J_{CF}$ = 25.48 Hz, *C*-4), 74.6 (d, $^{2}J_{CF}$ = 15.23 Hz, *C*-2), 64.3 (d, $^{3}J_{CF}$ = 4.57 Hz, *C*-5), 55.7 (-O*C*H$_3$).

^{19}*F*-NMR (564 MHz, $CDCl_3$): *δ* [ppm] = α-Anomer: -213.1, β-Anomer: -195.4.

HRMS (ESI^+): *m/z* = calcd: 293.0796 $[M+Na]^+$, found: 293.0796 $[M+Na]^+$.

5-*O*-Benzoyl-1,2-di-*O*-acetyl-3-deoxy-3-fluoro-D-ribofuranose 23

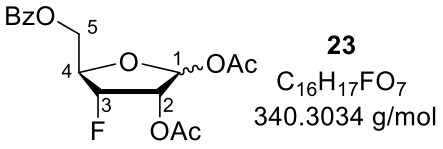

23
$C_{16}H_{17}FO_7$
340.3034 g/mol

Ribose **36** (2.30 g, 8.51 mmol) was dissolved in acetic acid (20 mL), and acetic anhydride (4.32 g, 42.3 mmol) was added. Afterwards, the reaction mixture was cooled to 0 °C before conc. H_2SO_4 (1.5 mL) was added dropwise. The reaction mixture was stirred at room temperature for 4 h before it was poured into ice water and stirred for further 30 min. The solution was extracted with CH_2Cl_2 three times, and the combined organic layers were washed with sat. aq. $NaHCO_3$, sat. aq. NaCl, dried over $MgSO_4$, and all volatiles were removed under reduced pressure. Purification of the crude product on silica gel (petroleum ether/ethyl acetate, 2:1 v/v) provided **23** (2.11 g, 73%) as a colorless oil, as a mixture of anomers.

^{1}*H*-NMR (600 MHz, $CDCl_3$): *δ* [ppm] = α-Anomer: 8.03 – 8.01 (m, 2H, *H*-Bz), 7.60 – 7.58 (m, 1H, *H*-Bz), 7.48 – 7.45 (m, 2H, *H*-Bz), 6.51 (d, $^{3}J_{HH}$ = 4.78 Hz, 1H, *H*-1), 5.23 (ddd, $^{2}J_{HF}$ = 55.24 Hz, $^{3}J_{HH}$ = 5.40 Hz, $^{3}J_{HH}$ = 1.44 Hz, 1H, *H*-3), 5.15 (dt, $^{3}J_{HF}$ = 23.64 Hz, $^{3}J_{HH}$ = 5.18 Hz, 1H, *H*-2), 4.81 – 4.75 (m,

1H, *H*-4), 4.52 (dd, $^{2}J_{HH}$ = 12.30 Hz, $^{3}J_{HH}$ = 3.79 Hz, 1H, *H*-5), 4.47 (dd, $^{2}J_{HH}$ = 12.30 Hz, $^{3}J_{HH}$ = 3.64 Hz, 1H, *H*-5), 2.17 (s, 3H, *H*-Ac), 2.15 (s, 3H, *H*-Ac).

β-Anomer: 8.08 – 8.06 (m, 2H, *H*-Bz), 7.60 – 7.58 (m, 1H, *H*-Bz), 7.48 – 7.45 (m, 2H, *H*-Bz), 6.24 (t, $^{3}J_{HH}$ = 1.93 Hz, 1H, *H*-1), 5.30 (dt, $^{2}J_{HF}$ = 52.68 Hz, $^{3}J_{HH}$ = 4.65 Hz, 1H, *H*-3), 5.35 – 5.33 (m, 1H, *H*-2), 4.67 – 4.61 (m, 2H, *H*-4, *H*-5), 4.44 – 4.41 (m, 1H, *H*-5), 2.18 (s, 3H, *H*-Ac), 1.95 (s, 3H, *H*-Ac).

^{13}*C*-NMR (150 MHz, $CDCl_3$): *δ* [ppm] = α-Anomer: 170.0 (*C*-Ac), 169.3 (*C*-Ac), 166.0 (*C*-Bz), 133.7 (*C*-Bz), 129.8 (2C, *C*-Bz), 129.3 (*C*-Bz), 128.8 (2C, *C*-Bz), 98.3 (d, $^{3}J_{CF}$ = 2.30 Hz, *C*-1), 88.5 (d, $^{1}J_{CF}$ = 191.80 Hz, *C*-3), 82.4 (d, $^{2}J_{CF}$ = 25.40 Hz, *C*-4), 71.3 (d, $^{2}J_{CF}$ = 15.37 Hz, *C*-2), 63.5 (d, $^{3}J_{CF}$ = 9.52 Hz, *C*-5), 21.0 (*C*-Ac), 20.5 (*C*-Ac).

β-Anomer: 170.0 (*C*-Ac), 169.3 (*C*-Ac), 166.3 (*C*-Bz), 133.6(*C*-Bz), 129.9 (2C, *C*-Bz), 129.6 (*C*-Bz), 128.7 (2C, *C*-Bz), 93.9 (*C*-1), 89.3 (d, $^{1}J_{CF}$ = 194.04 Hz, *C*-3), 80.8 (d, $^{2}J_{CF}$ = 24.89 Hz, *C*-4), 74.8 (d, $^{2}J_{CF}$ = 14.54 Hz, *C*-2), 63.2 (d, $^{3}J_{CF}$ = 5.51 Hz, *C*-5), 21.2 (*C*-Ac), 20.6 (*C*-Ac).

^{19}*F*-NMR (564 MHz, $CDCl_3$): *δ* [ppm] = α-Anomer: -209.1, β-Anomer: -195.2.

HRMS (ESI^+): *m/z* = calcd: 363.0850 $[M+Na]^+$, found: 363.0849 $[M+Na]^+$.

1-*O*-Acetyl-2-deoxy-3,5-di-*O*-benzoyl-2-fluoro-2-methyl-D-ribofuranose 27

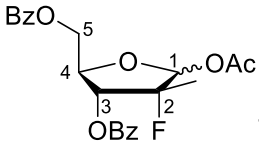

27
$C_{22}H_{21}FO_7$
416.4014 g/mol

The protected lactone **28** (4.60 g, 12.3 mmol) was dissolved in THF (50 mL) and cooled to -20 °C. Subsequently, lithium tri-*tert*-butoxyaluminium hydride (18.5 mL, 18.5 mmol, 1 M solution in THF) was added dropwise over 20 min. After the reaction mixture was stirred at -20 °C for 3 h and complete conversion of the starting material was confirmed by TLC, 4-DMAP (1.86 g, 13.6 mmol) and acetic anhydride (10.7 mL, 113 mmol) were added. The reaction mixture was stirred for a further 1.5 h at -20 °C, after which the reaction was quenched by the addition of water and ethyl acetate. The solution was extracted with CH_2Cl_2 three times, and the combined organic layers were washed with sat. aq. $NaHCO_3$, sat. aq. NaCl, dried over $MgSO_4$, and all volatiles were removed under reduced pressure. Purification of the crude product on silica gel by automated

flash chromatography (petroleum ether/ethyl acetate, 10:1 to 4:1 v/v) provided **27** (4.82 g, 93%) as a colorless oil, as a mixture of anomers.

The analytical data was in accordance with those described.[151]

^{1}*H*-NMR (600 MHz, $CDCl_3$): δ [ppm] = α-Anomer: 8.10 – 8.07 (m, 2H, *H*-Bz), 8.03 – 8.00 (m, 2H, *H*-Bz), 7.63 – 7.59 (m, 1H, *H*-Bz), 7.57 – 7.51 (m, 1H, *H*-Bz), 7.49 – 7.45 (m, 2H, *H*-Bz), 7.37 – 7.34 (m, 2H, *H*-Bz), 6.22 (d, $^{3}J_{HF}$ = 9.61 Hz, 1H, *H*-1´), 5.67 (dd, $^{3}J_{HF}$ = 24.21 Hz, $^{3}J_{HH}$ = 8.28 Hz, 1H, *H*-3´), 4.70 (dd, $^{2}J_{HH}$ = 11.92 Hz, $^{3}J_{HH}$ = 3.94 Hz, 1H, *H*-5´), 4.66 – 4.63 (m, 1H, *H*-4´), 4.43 (dd, $^{2}J_{HH}$ = 12.09 Hz, $^{3}J_{HH}$ = 4.63 Hz, 1H, *H*-5´), 1.97 (s, 3H, *H*-Ac), 1.51 (d, $^{3}J_{HF}$ = 22.74 Hz, 1H, 2´-C-C*H*$_3$).

β-Anomer: 8.10 – 8.07 (m, 2H, *H*-Bz), 8.03 – 8.00 (m, 2H, *H*-Bz), 7.63 – 7.59 (m, 1H, *H*-Bz), 7.57 – 7.51 (m, 1H, *H*-Bz), 7.49 – 7.45 (m, 2H, *H*-Bz), 7.43 – 7.39 (m, 2H, *H*-Bz), 6.18 (d, $^{3}J_{HF}$ = 2.13 Hz, 1H, *H*-1´), 5.26 (t, $^{3}J_{HF}$ = 5.97 Hz, 1H, *H*-3´), 4.66 – 4.63 (m, 1H, *H*-4´), 4.68 (dd, $^{2}J_{HH}$ = 12.83 Hz, $^{3}J_{HH}$ = 3.66 Hz, 1H, *H*-5´), 4.55 (dd, $^{2}J_{HH}$ = 12.18 Hz, $^{3}J_{HH}$ = 4.94 Hz, 1H, *H*-5´), 2.18 (s, 3H, *H*-Ac), 1.70 (d, $^{3}J_{HF}$ = 22.42 Hz, 1H, 2´-C-C*H*$_3$).

^{13}*C*-NMR (150 MHz, $CDCl_3$): δ [ppm] = α-Anomer: 168.8 (*C*-Ac), 165.9 (*C*-Bz), 165.7 (*C*-Bz), 133.9 (*C*-Bz), 133.2 (*C*-Bz), 130.1 (*C*-Bz), 129.7 (*C*-Bz), 129.6 (*C*-Bz), 128.6 (*C*-Bz), 128.5 (*C*-Bz), 128.3 (*C*-Bz), 99.5 (d, $^{1}J_{CF}$ = 183.03 Hz, *C*-2´), 98.4 (d, $^{2}J_{CF}$ = 35.47 Hz, *C*-1´), 78.7 (d, $^{3}J_{CF}$ = 1.26 Hz, *C*-4´), 73.6 (d, $^{2}J_{CF}$ = 15.28 Hz, *C*-3´), 63.6 (*C*-5´), 20.9 (*C*-Ac), 16.5 (d, $^{2}J_{CF}$ = 24.14 Hz, 2´-C-*C*H$_3$).

β-Anomer: 169.6 (*C*-Ac), 166.1 (*C*-Bz), 165.7 (*C*-Bz), 133.6 (*C*-Bz), 133.3 (*C*-Bz), 129.9 (*C*-Bz), 129.7 (*C*-Bz), 129.4 (*C*-Bz), 129.0 (*C*-Bz), 128.6 (*C*-Bz), 128.5 (*C*-Bz), 98.2 (d, $^{2}J_{CF}$ = 18.15 Hz, *C*-1´), 94.3 (d, $^{1}J_{CF}$ = 206.70 Hz, *C*-2´), 80.4 (d, $^{3}J_{CF}$ = 1.27 Hz, *C*-4´), 73.2 (d, $^{2}J_{CF}$ = 15.97 Hz, *C*-3´), 63.3 (*C*-5´), 21.9 (d, $^{2}J_{CF}$ = 25.50 Hz, 2´-C-*C*H$_3$), 21.0 (*C*-Ac).

^{19}*F*-NMR (564 MHz, $CDCl_3$): δ [ppm] = α-Anomer: -169.3, β-Anomer: -171.3.

HRMS (ESI$^+$): *m/z* = calcd: 439.1163 $[M+Na]^+$, found: 439.1162 $[M+Na]^+$.

3-Azido-5-*O*-benzoyl-3-deoxy-1,2-*O*-isopropylidene-α-D-ribofuranose 38

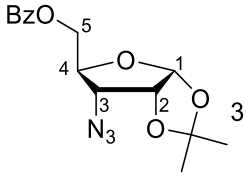

38
$C_{15}H_{17}N_3O_5$
319.3170 g/mol

The xylose **31** (2.76 g, 9.38 mmol) was dissolved in CH_2Cl_2 (25 mL), and pyridine (2.42 mL, 28.1 mmol) was added. The reaction solution was cooled to 0 °C, and trifluoromethanesulfonic anhydride (1.93 mL, 11.3 mmol) was added dropwise. The reaction mixture was then stirred at 0 °C. After 1 h, the reaction was quenched by the addition of water. Subsequently, the mixture was extracted with CH_2Cl_2 three times, and the combined organic layers were washed with sat. aq. $NaHCO_3$, sat. aq. NaCl, dried over $MgSO_4$, and all volatiles were removed under reduced pressure. The obtained solid was then dissolved in DMF (20 mL), and sodium azide (2.25 g, 34.6 mmol) as well as tetrabutylammonium iodide (109 mg, 0.256 mmol) were added. After the reaction mixture was stirred at room temperature for two days, the reaction was quenched by the addition of water. Subsequently, the mixture was extracted with ethyl acetate three times, and the combined organic layers were washed with sat. aq. $NaHCO_3$, sat. aq. NaCl, dried over $MgSO_4$, and all volatiles were removed under reduced pressure. Purification of the crude product on silica gel (petroleum ether/ethyl acetate, 5:1 v/v) provided **38** (874 mg, 29%) as a colorless oil.

The analytical data was in accordance with those described.[148]

^1H-NMR (500 MHz, $CDCl_3$): δ [ppm] = 8.08 – 8.04 (m, 2H, *H*-Bz), 7.61 – 7.55 (m, 1H, *H*-Bz), 7.48 – 7.42 (m, 2H, *H*-Bz), 5.86 (d, $^3J_{HH}$ = 3.70 Hz, 1H, *H*-1), 4.78 (t, $^3J_{HH}$ = 4.19 Hz, 1H, *H*-2), 4.68 (dd, $^2J_{HH}$ = 12.28 Hz, $^3J_{HH}$ = 3.24 Hz, 1H, *H*-5), 4.48 (dd, $^2J_{HH}$ = 12.30 Hz, $^3J_{HH}$ = 4.71 Hz, 1H, *H*-5), 4.42 – 4.37 (m, 1H, *H*-4), 3.65 (dd, $^3J_{HH}$ = 10.02 Hz, $^3J_{HH}$ = 4.71 Hz, 1H, *H*-3), 1.61 (s, 3H, C-CH_3), 1.39 (s, 3H, C-CH_3).

3-Azido-5-*O*-benzoyl-3-deoxy-1,2-*O*-diacetyl-D-ribofuranose 24

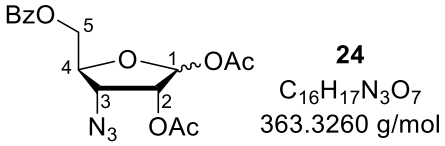

24
$C_{16}H_{17}N_3O_7$
363.3260 g/mol

The ribose **38** (819 mg, 2.56 mmol) was dissolved in acetic acid (24 mL) followed by the addition of acetic anhydride (2.94 g, 42.3 mmol). Afterwards, the reaction mixture was cooled to 0 °C before conc. H_2SO_4 (0.33 mL) was added dropwise. The reaction mixture was stirred at room temperature for 4 h before it was poured into ice water and stirred for further 30 min. The solution was extracted with CH_2Cl_2 three times and the combined organic layers were washed

with sat. aq. $NaHCO_3$, sat. aq. NaCl, dried over $MgSO_4$, and all volatiles were removed under reduced pressure. Purification of the crude product on silica gel (petroleum ether/ethyl acetate, 2:1 v/v) provided **24** (679 mg, 73%) as a colorless solid, as a mixture of anomers.

The analytical data was in accordance with those described.[148]

^1H-NMR (600 MHz, $CDCl_3$): δ [ppm] = α-Anomer: 8.09 – 8.02 (m, 2H, *H*-Bz), 7.60 – 7.57 (m, 1H, *H*-Bz), 7.48 – 7.44 (m, 2H, *H*-Bz), 5.98 (d, $^3J_{HH}$ = 4.58 Hz, 1H, *H*-1), 5.29 (dd, $^3J_{HH}$ = 7.50 Hz, $^3J_{HH}$ = 4.50 Hz, 1H, *H*-2), 4.54 (dd, $^2J_{HH}$ = 13.17 Hz, $^3J_{HH}$ = 4.85 Hz, 1H, *H*-5), 4.48 – 4.46 (m, 1H, *H*-4), 4.44 (dd, $^2J_{HH}$ = 12.24 Hz, $^3J_{HH}$ = 3.97 Hz, 1H, *H*-5), 4.19 (dd, $^3J_{HH}$ = 7.35 Hz, $^3J_{HH}$ = 3.89 Hz, 1H, *H*-3), 2.18 (s, 3H, *H*-Ac), 2.15 (s, 3H, *H*-Ac).

β-Anomer: 8.09 – 8.02 (m, 2H, *H*-Bz), 7.60 – 7.57 (m, 1H, *H*-Bz), 7.48 – 7.44 (m, 2H, *H*-Bz), 6.16 (s, 1H, *H*-1), 5.38 (d, $^3J_{HH}$ = 4.76 Hz, 1H, *H*-2), 4.67 (dd, $^2J_{HH}$ = 12.16 Hz, $^3J_{HH}$ = 3.75 Hz, 1H, *H*-5), 4.44 (dd, $^2J_{HH}$ = 12.24 Hz, $^3J_{HH}$ = 3.97 Hz, 1H, *H*-5), 4.39 – 4.36 (m, 1H, H-4), 4.22 (dd, $^3J_{HH}$ = 8.48 Hz, $^3J_{HH}$ = 4.76 Hz, 1H, *H*-3), 2.19 (s, 3H, *H*-Ac), 1.91 (s, 3H, *H*-Ac).

^{13}C-NMR (150 MHz, $CDCl_3$): δ [ppm] = α-Anomer: 169.9 (*C*-Ac), 169.8 (*C*-Ac), 166.1 (*C*-Bz), 133.6 (*C*-Bz), 129.6 (2C, *C*-Bz), 129.4 (*C*-Bz), 128.7 (2C, *C*-Bz), 94.0 (*C*-1), 81.3 (*C*-4), 72.2 (*C*-2), 63.9 (*C*-5), 59.0 (*C*-3), 21.2 (*C*-Ac), 20.4 (*C*-Ac).

β-Anomer: 169.7 (*C*-Ac), 168.9 (*C*-Ac), 166.1 (*C*-Bz), 133.6(*C*-Bz), 129.9 (2C, *C*-Bz), 129.8 (*C*-Bz), 128.6 (2C, *C*-Bz), 98.2 (*C*-1), 80.0 (*C*-4), 75.9 (*C*-2), 63.2 (*C*-5), 60.2 (*C*-3), 20.9 (*C*-Ac), 20.7 (*C*-Ac).

HRMS (ESI^+): *m/z* = calcd: 386.0958 $[M+Na]^+$, found: 386.0955 $[M+Na]^+$.

1,3,5-Tri-*O*-benzoyl-α-D-2-ketoribofuranose 181

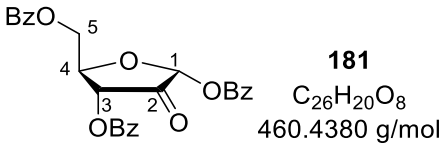

181
$C_{26}H_{20}O_8$
460.4380 g/mol

Dess–Martin periodinane (11.0 g, 25.9 mmol) was added to a solution of 1,3,5-tri-*O*-benzoyl-α-D-ribofuranose **180** (10.0 g, 21.6 mmol) in CH_2Cl_2 (100 mL) at 0 °C. After the reaction mixture was stirred overnight at room temperature, all volatiles were removed under reduced pressure. The obtained residue was treated with methyl *tert*-butyl ether (200 mL). Subsequently, the resulting suspension was filtered through a pad of Celite, and the filtrate was washed consecutively with

sat. aq. $Na_2S_2O_3$, sat. aq. $NaHCO_3$, sat. aq. NaCl and dried over $MgSO_4$. After all volatiles were removed under reduced pressure, **181** (9.21 g, 93%) was obtained as a white foam.

The analytical data was in accordance with those described.[232]

^{1}*H*-NMR (500 MHz, $CDCl_3$): δ [ppm] = 8.13 – 8.10 (m, 3H, *H*-Bz), 8.09 – 8.06 (m, 1H, *H*-Bz), 8.03 – 8.01 (m, 2H, *H*-Bz), 7.64 – 7.52 (m, 3H, *H*-Bz), 7.50 – 7.46 (m, 3H, *H*-Bz), 7.43 – 7.37 (m, 3H, *H*-Bz), 6.21 (d, $^4J_{HH}$ = 1.07 Hz, 1H, *H*-1), 5.88 (dd, $^3J_{HH}$ = 8.80 Hz, $^4J_{HH}$ = 1.19 Hz, 1H, *H*-3), 5.07 – 5.04 (m, 1H, *H*-4), 4.83 (dd, $^2J_{HH}$ = 12.37 Hz, $^3J_{HH}$ = 3.41 Hz, 1H, *H*-5), 4.65 (dd, $^2J_{HH}$ = 12.87 Hz, $^3J_{HH}$ = 4.57 Hz, 1H, *H*-5).

^{13}*C*-NMR (125 MHz, $CDCl_3$): δ [ppm] = 201.5 (*C*-2), 166.6 (*C*-Bz), 166.1 (*C*-Bz), 165.4 (*C*-Bz), 130.5 (2C, *C*-Bz), 130.4 (2C, *C*-Bz), 130.1 (*C*-Bz), 129.9 (2C, *C*-Bz), 128.72 (2C, *C*-Bz), 128.70 (2C, *C*-Bz), 128.66 (*C*-Bz), 128.59 (*C*-Bz), 128.56 (2C, *C*-Bz), 128.53 (*C*-Bz), 128.39 (*C*-Bz), 128.37 (*C*-Bz), 91.5 (*C*-1), 78.2 (*C*-4), 72.2 (*C*-3), 63.4 (*C*-5).

HRMS (ESI$^+$): *m/z* = calcd: 483.1050 $[M+Na]^+$, found: 483.1045 $[M+Na]^+$.

5-*O*-Benzoyl-1-*O*-methyl-α-D-xylofuranose 182

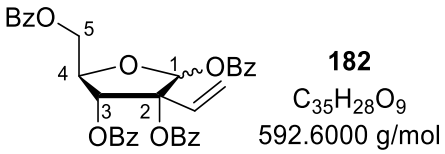

182
$C_{35}H_{28}O_9$
592.6000 g/mol

The reaction was carried out according to general procedure I with 1,3,5-tri-*O*-benzoyl-α-D-2-ketoribofuranose **181** (550 mg, 1.19 mmol), $CeCl_3$ (1.26 g, 5.13 mmol), and vinylmagnesium bromide (6.82 mL, 4.77 mmol, 0.7 M solution in THF). The benzoyl protection was performed using 4-DMAP (291 mg, 2.38 mmol), Et_3N (2.5 mL) and benzoyl chloride (412 µL, 3.58 mmol). Purification on silica gel with automated flash chromatography (petroleum ether/ethyl acetate; 10:1 to 4:1 v/v) provided **182** (641 mg, 90%) as a white syrup, obtained as a mixture of anomers.

The analytical data was in accordance with those described.[232]

^{1}*H*-NMR (600 MHz, $CDCl_3$): δ [ppm] = α-Anomer: 8.21 – 8.19 (m, 2H, *H*-Bz), 8.12 – 8.11 (m, 2H, *H*-Bz), 8.06 – 8.05 (m, 2H, *H*-Bz), 8.00 – 7.96 (m, 1H, *H*-Bz), 7.91 – 7.89 (m, 2H, *H*-Bz), 7.67 – 7.60 (m, 3H, *H*-Bz), 7.59 – 7.52 (m, 2H, *H*-Bz), 7.50 – 7.38 (m, 4H, *H*-Bz), 7.18 – 7.15 (m, 2H, *H*-Bz), 7.14 (s, 1H, *H*-1), 6.46 (dd, $^3J_{HH}$ = 17.63 Hz, $^3J_{HH}$ = 11.36 Hz, 1H, *H*-vinyl), 6.25 (d, $^3J_{HH}$ = 8.33 Hz, 1H, *H*-3),

5.43 (d, $^3J_{HH}$ = 17.58 Hz, 1H, *H*-vinyl), 5.38 (d, $^3J_{HH}$ = 11.55 Hz, 1H, *H*-vinyl), 4.82 – 4.79 (m, 1H, *H*-4), 4.73 (dd, $^2J_{HH}$ = 12.09 Hz, $^3J_{HH}$ = 3.79 Hz, 1H, *H*-5), 4.53 (dd, $^2J_{HH}$ = 12.29 Hz, $^3J_{HH}$ = 4.85 Hz, 1H, *H*-3).

β-Anomer: 8.25 – 8.24 (m, 2H, *H*-Bz), 8.12 – 8.11 (m, 2H, *H*-Bz), 8.08 – 8.06 (m, 2H, *H*-Bz), 8.03 – 8.01 (m, 1H, *H*-Bz), 7.87 – 7.85 (m, 2H, *H*-Bz), 7.76 – 7.75 (m, 2H, *H*-Bz), 7.76 – 7.75 (m, 3H, *H*-Bz), 7.59 – 7.52 (m, 2H, *H*-Bz), 7.50 – 7.38 (m, 3H, *H*-Bz), 7.18 – 7.15 (m, 2H, *H*-Bz), 7.14 (s, 1H, *H*-1), 6.37 (dd, $^3J_{HH}$ = 17.59 Hz, $^3J_{HH}$ = 11.00 Hz, 1H, *H*-1), 5.83 (d, $^3J_{HH}$ = 3.10 Hz, 1H, *H*-3), 5.76 (d, $^3J_{HH}$ = 17.56 Hz, 1H, *H*-vinyl), 5.51 (d, $^3J_{HH}$ = 11.22 Hz, 1H, *H*-vinyl), 4.86 – 4.83 (m, 1H, *H*-4), 4.74 (dd, $^2J_{HH}$ = 11.85 Hz, $^3J_{HH}$ = 4.50 Hz, 1H, *H*-5), 4.68 (dd, $^2J_{HH}$ = 11.73 Hz, $^3J_{HH}$ = 5.20 Hz, 1H, *H*-3).

^{13}C-NMR (150 MHz, $CDCl_3$): δ [ppm] = α-Anomer: 166.5 (*C*-Bz), 166.2 (*C*-Bz), 164.5 (*C*-Bz), 164.4 (*C*-Bz), 133.9 (*C*-Bz), 133.83 (*C*-Bz), 133.81 (*C*-Bz), 133.1 (*C*-Bz), 130.2 (*C*-Bz), 130.1 (4C, *C*-Bz), 130.0 (2C, *C*-Bz), 129.8 (2C, *C*-Bz), 129.6 (*C*-vinyl), 129.3 (*C*-Bz), 129.0 (*C*-Bz), 128.82 (2C, *C*-Bz), 128.80 (4C, *C*-Bz), 128.7 (*C*-Bz), 128.3 (2C, *C*-Bz), 119.5 (*C*-vinyl), 97.4 (*C*-1), 87.3 (*C*-2), 78.7 (*C*-4), 74.0 (*C*-3), 64.0 (*C*-5).

HRMS (ESI^+): *m/z* = calcd: 615.1625 $[M+Na]^+$, found: 615.1624 $[M+Na]^+$.

5-*O*-Benzoyl-1-*O*-methyl-α-D-xylofuranose 183

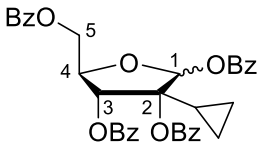

183
$C_{36}H_{30}O_9$
606.6270 g/mol

The reaction was carried out according to general procedure I with 1,3,5-tri-*O*-benzoyl-α-D-2-ketoribofuranose **181** (550 mg, 1.19 mmol), $CeCl_3$ (1.26 g, 5.13 mmol) and cyclopropylmagnesium bromide (4.77 mL, 4.77 mmol, 1 M solution in THF). The benzoyl protection was performed using 4-DMAP (291 mg, 2.38 mmol), Et_3N (2.5 mL) and benzoyl chloride (412 µL, 3.58 mmol). Purification on silica gel with automated flash chromatography (petroleum ether/ethyl acetate; 10:1 to 4:1 v/v) provided **183** (319 mg, 44%) as a white foam, obtained as a mixture of anomers.

^1H-NMR (600 MHz, $CDCl_3$): δ [ppm] = α-Anomer: 8.21 – 8.20 (m, 2H, *H*-Bz), 8.11 – 8.08 (m, 2H, *H*-Bz), 7.91 – 7.90 (m, 2H, *H*-Bz), 7.72 – 7.71 (m, 2H, *H*-Bz), 7.67 – 7-39 (m, 8H, *H*-Bz), 7.31 (s, 1H, *H*-1´), 7.29 – 7.27 (m, 2H, *H*-Bz), 7.17 – 7.14 (m, 2H, *H*-Bz), 6.03 (d, $^3J_{HH}$ = 7.79 Hz, 1H, *H*-3´), 4.86 –

4.69 (m, 2H, *H*-4´, *H*-5´), 4.50 – 4.47 (m, 1H, *H*-5´), 2.15 – 2.10 (m, 1H, -C*H*-$(CH_2)_2$), 0.97 – 0.71 (m, 2H, -CH-(CH_2)$_2$), 0.61 – 0.51 (m, 2H, -CH-(CH_2)$_2$).

β-Anomer: 8.11 – 8.08 (m, 4H, *H*-Bz), 8.03 – 8.01 (m, 2H, *H*-Bz), 7.67 – 7-39 (m, 10H, *H*-Bz), 7.29 – 7.27 (m, 2H, *H*-Bz), 7.17 – 7.14 (m, 2H, *H*-Bz), 6.66 (s, 1H, *H*-1´), 5.81 (d, $^3J_{HH}$ = 2.80 Hz, 1H, *H*-3´), 4.86 – 4.69 (m, 3H, *H*-4´, *H*-5´), 1.86 – 1.82 (m, 1H, -C*H*-$(CH_2)_2$), 0.97 – 0.71 (m, 4H, -CH-(CH_2)$_2$).

^{13}*C*-NMR (150 MHz, $CDCl_3$): *δ* [ppm] = α-Anomer: 166.2 (*C*-Bz), 165.2 (*C*-Bz), 164.9 (*C*-Bz), 164.8 (*C*-Bz), 134.1 (*C*-Bz), 133.7 (*C*-Bz), 133.6 (*C*-Bz), 133.0 (*C*-Bz), 130.6 (*C*-Bz), 130.0 (2C, *C*-Bz), 129.9 (2C, *C*-Bz), 129.8 (2C, *C*-Bz), 129.7 (2C, *C*-Bz), 129.6 (*C*-Bz), 128.9 (*C*-Bz), 128.7 (2C, *C*-Bz), 128.48 (2C, *C*-Bz), 128.45 (2C, *C*-Bz), 128.3 (2C, *C*-Bz), 128.2 (*C*-Bz), 98.3 (*C*-1), 89.4 (*C*-2), 79.3 (*C*-4), 73.3 (*C*-3), 64.1 (*C*-5), 13.4 (-*C*H-$(CH_2)_2$), 5.38 (-CH-(*C*H_2)$_2$), 1.76 (-CH-(*C*H_2)$_2$).

β-Anomer: 166.4 (*C*-Bz), 165.6 (*C*-Bz), 164.9 (*C*-Bz), 164.7 (*C*-Bz), 133.58 (*C*-Bz), 133.56 (*C*-Bz), 133.4 (*C*-Bz), 133.2 (*C*-Bz), 130.1 (2C, *C*-Bz), 130.0 (2C, *C*-Bz), 129.96 (2C, *C*-Bz), 129.95 (2C, *C*-Bz), 129.8 (2C, *C*-Bz), 129.5 (*C*-Bz), 129.4 (*C*-Bz),128.9 (2C, *C*-Bz), 128.8 (*C*-Bz), 128.5 (*C*-Bz), 128.3 (2C, *C*-Bz), 97.2 (*C*-1), 84.5 (*C*-2), 82.7 (*C*-4), 76.0 (*C*-3), 63.9 (*C*-5), 15.9 (-*C*H-$(CH_2)_2$), 4.37 (-CH-(*C*H_2)$_2$), 3.23 (-CH-(*C*H_2)$_2$).

HRMS (ESI^+): *m/z* = calcd: 629.1781 $[M+Na]^+$, found: 629.1782 $[M+Na]^+$.

5.3.4 Synthesis of nucleosides

T-1106 13

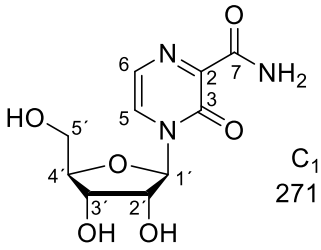

13
$C_{10}H_{13}N_3O_6$
271.2290 g/mol

Step 1: The reaction was carried out according to general procedure II with **20** (5.09 g, 33.0 mmol), ammonium sulfate (65 mg, 0.49 mmol) and HMDS (100 mL), followed by addition of tetra-*O*-acetyl-β-D-ribofuranose **52** (7.35 g, 23.1 mmol) and tin tetrachloride (33.0 mL, 33.0 mmol, 1 M solution in CH_2Cl_2) in CH_3CN (250 mL) and CH_2Cl_2 (100 mL). Purification of the crude product on silica gel (CH_2Cl_2/MeOH; 60:1 v/v) provided **53** (7.32 g, 77%) as a colorless foam.

^{1}H-NMR (300 MHz, $CDCl_3$): δ [ppm] = 7.68 (d, $^{3}J_{HH}$ = 4.50 Hz, 1H, *H*-5), 7.50 (d, $^{3}J_{HH}$ = 4.42 Hz, 1H, *H*-6), 6.13 (d, $^{3}J_{HH}$ = 3.40 Hz, 1H, *H*-1´), 5.41 (dd, $^{3}J_{HH}$ = 5.72 Hz, $^{3}J_{HH}$ = 3.30 Hz, 1H, *H*-2´), 5.30 – 5.26 (m, 1H, *H*-3´), 4.48 – 4.44 (m, 1H, *H*-4´), 4.41 – 4.40 (m, 2H, *H*-5´), 3.96 (s, 3H, -OCH_3), 2.14 (s, 3H, *H*-Ac), 2.12 (s, 3H, *H*-Ac), 2.08 (s, 3H, *H*-Ac).

Step 2: The reaction was carried out according to general procedure IV with the protected nucleoside **53** (2.80 g, 6.79 mmol) and 30 mL of 7 M NH_3 in MeOH. Purification on RP_{18} silica gel by automated flash chromatography (H_2O/CH_3CN; 100:0 to 0:100 v/v) provided **13** (1.72 g, 93%) as a light-yellow solid.

The analytical data was in accordance with those described.[120]

^{1}H-NMR (400 MHz, D_2O): *δ* [ppm] = 8.30 (d, $^{3}J_{HH}$ = 4.25 Hz, 1H, *H*-5), 7.78 (d, $^{3}J_{HH}$ = 4.25 Hz, 1H, *H*-6), 6.10 (d, $^{3}J_{HH}$ = 1.88 Hz, 1H, *H*-1´), 4.33 (dd, $^{3}J_{HH}$ = 5.02 Hz, $^{3}J_{HH}$ = 1.84 Hz, 1H, *H*-2´), 4.29 – 4.26 (m, 1H, *H*-4´), 4.19 (dd, $^{3}J_{HH}$ = 8.17 Hz, $^{3}J_{HH}$ = 4.98 Hz, 1H, *H*-3´), 4.08 (dd, $^{2}J_{HH}$ = 13.04 Hz, $^{3}J_{HH}$ = 2.49 Hz, 1H, *H*-5´), 3.92 (dd, $^{2}J_{HH}$ = 13.12 Hz, $^{3}J_{HH}$ = 4.09 Hz, 1H, *H*-5´).

^{13}C-NMR (125 MHz, D_2O): *δ* [ppm] = 165.8 (*C*-7), 155.8 (*C*-3), 142.7 (*C*-2), 129.1 (*C*-5), 124.9 (*C*-6), 91.2 (*C*-1´), 83.7 (*C*-4´), 74.6 (*C*-2´), 68.2 (*C*-3´), 59.9 (*C*-5´).

HRMS (ESI^+): *m/z* = calcd: 294.0696 $[M+Na]^+$, found: 294.0695 $[M+Na]^+$.

T-1106 methyl ester 54

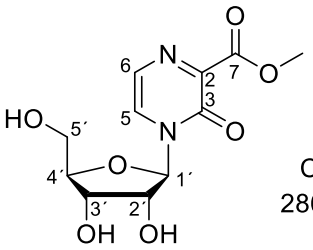

54
$C_{11}H_{14}N_2O_7$
286.2400 g/mol

The reaction was carried out according to general procedure III with the protected nucleoside **53** (2.22 g, 5.40 mmol) in MeOH (25 mL) and sodium methoxide solution (80 µL, 5.4 M in MeOH). Purification on RP_{18} silica gel by automated flash chromatography (H_2O/CH_3CN; 100:0 to 0:100 v/v) provided **54** (1.42 g, 92%) as a colorless solid.

The analytical data was in accordance with those described.[120]

^{1}H-NMR (400 MHz, D_2O): δ [ppm] = 8.26 (d, $^{3}J_{HH}$ = 4.23 Hz, 1H, *H*-5), 7.62 (d, $^{3}J_{HH}$ = 4.20 Hz, 1H, *H*-6), 6.10 (d, $^{3}J_{HH}$ = 1.67 Hz, 1H, *H*-1´), 4.33 (dd, $^{3}J_{HH}$ = 4.96 Hz, $^{3}J_{HH}$ = 1.72 Hz, 1H, *H*-2´), 4.20 – 4.16 (m, 1H, *H*-4´), 4.09 (dd, $^{3}J_{HH}$ = 8.25 Hz, $^{3}J_{HH}$ = 5.00 Hz, 1H, *H*-3´), 4.00 (dd, $^{2}J_{HH}$ = 13.09 Hz, $^{3}J_{HH}$ = 2.51 Hz, 1H, *H*-5´), 3.90 (s, 3H, -OCH_3), 3.82 (dd, $^{2}J_{HH}$ = 13.13 Hz, $^{3}J_{HH}$ = 4.14 Hz, 1H, *H*-5´).

^{13}C-NMR (125 MHz, D_2O): δ [ppm] = 164.4 (*C*-7), 154.6 (*C*-3), 141.5 (*C*-2), 129.8 (*C*-5), 125.2 (*C*-6), 91.4 (*C*-1´), 83.7 (*C*-4´), 74.7 (*C*-2´), 68.1 (*C*-3´), 59.8 (*C*-5´), 53.2 (-O*C*H_3).

HRMS (ESI^+): *m/z* = calcd: 309.0693 $[M+Na]^+$, found: 309.0692 $[M+Na]^+$.

Methyl 4-(2´,3´,5´-tri-*O*-benzoyl-2´-*C*-methyl-β-D-ribofuranosyl)-3-oxo-2-pyrazinecarboxylate 48

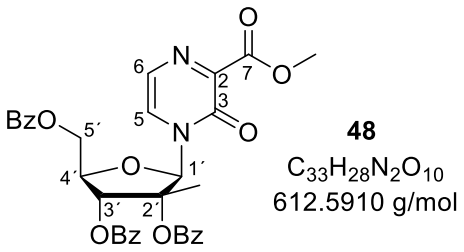

48
$C_{33}H_{28}N_2O_{10}$
612.5910 g/mol

The reaction was carried out according to general procedure II with **20** (1.10 g, 7.13 mmol), ammonium sulfate (10 mg, 0.08 mmol) and HMDS (20 mL), followed by addition of 1,2,3,5-tetra-*O*-benzoyl-2-*C*-methyl-D-ribofuranose **26** (1.38 g, 2.37 mmol) and tin tetrachloride (7.13 mL, 7.13 mmol, 1 M solution in CH_2Cl_2) in CH_3CN (60 mL) and CH_2Cl_2 (25 mL). Purification of the crude product on silica gel by automated flash chromatography (CH_2Cl_2/MeOH; 100:0 to 40:1 v/v) provided **48** (769 mg, 61%) as a colorless foam.

^{1}H-NMR (600 MHz, $CDCl_3$): δ [ppm] = 8.14 – 8.05 (m, 4H, *H*-Bz), 7.85 (d, $^{3}J_{HH}$ = 8.36 Hz, 2H, *H*-Bz), 7.67 (d, $^{3}J_{HH}$ = 4.39 Hz, 1H, *H*-5), 7.62 – 7.55 (m, 3H, *H*-Bz), 7.51 – 7.41 (m, 5H, *H*-6, *H*-Bz), 7.24 (d, $^{3}J_{HH}$ = 7.77 Hz, 2H, *H*-Bz), 6.31 (s, 1H, *H*-1´), 5.78 (bs, 1H, *H*-3´), 4.89 (dd, $^{2}J_{HH}$ = 12.40 Hz, $^{3}J_{HH}$ = 3.06 Hz, 1H, *H*-5´), 4.84 (dd, $^{2}J_{HH}$ = 12.18 Hz, $^{3}J_{HH}$ = 5.90 Hz, 1H, *H*-5´), 4.80 – 4.78 (m, 1H, *H*-4´), 3.99 (s, 3H, -OCH_3), 1.67 (s, 3H, 2´-C-CH_3).

^{13}C-NMR (150 MHz, $CDCl_3$): δ [ppm] = 166.4 (*C*-Bz), 165.6 (*C*-Bz), 165.4 (*C*-Bz), 163.6 (*C*-7), 152.8 (*C*-3), 146.9 (*C*-2), 133.9 – 133.7 (m, *H*-Bz), 130.3 (*C*-Bz), 130.2 (*C*-Bz), 130.0 (*C*-Bz), 129.9 (*C*-Bz), 129.8 (*C*-Bz), 129.6 (*C*-Bz), 128.8 – 128.6 (m, *C*-Bz), 128.5 (*C*-5), 122.6 (*C*-6), 100.2 (*C*-1´), 81.2 (*C*-4´), 76.5 (*C*-2´), 75.6 (*C*-3´), 63.3 (*C*-5´), 53.2 (-O*C*H_3), 20.6 (2´-C-*C*).

HRMS (ESI$^+$): *m/z* = calcd: 635.1636 [M+Na]$^+$, found: 635.1627 [M+Na]$^+$.

2´-*C*-Methyl-T-1106 49

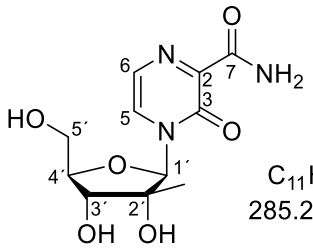

49
$C_{11}H_{15}N_3O_6$
285.2560 g/mol

The reaction was carried out according to general procedure IV with the protected nucleoside **48** (500 mg, 0.81 mmol) and 7 M NH_3 in MeOH (20 mL). Purification on RP_{18} silica gel by automated flash chromatography (H_2O/CH_3CN; 100:0 to 0:100 v/v) provided **49** (221 mg, 95%) as a colorless solid.

The analytical data was in accordance with those described.[119]

^{1}*H*-NMR (400 MHz, D_2O): δ [ppm] = 8.25 (d, $^3J_{HH}$ = 4.28 Hz, 1H, *H*-5), 7.79 (d, $^3J_{HH}$ = 4.20 Hz, 1H, *H*-6), 6.35 (s, 1H, *H*-1´), 4.17 (ddd, $^3J_{HH}$ = 9.56 Hz, $^3J_{HH}$ = 3.74 Hz, $^3J_{HH}$ = 2.34 Hz, 1H, *H*-4´), 4.11 (dd, $^2J_{HH}$ = 13.19 Hz, $^3J_{HH}$ = 2.29 Hz, 1H, *H*-5´), 3.96 (d, $^3J_{HH}$ = 9.57 Hz, 1H, *H*-3´), 3.93 (dd, $^2J_{HH}$ = 13.14 Hz, $^3J_{HH}$ = 3.79 Hz, 1H, *H*-5´), 1.07 (s, 3H, 2´-C-C*H*$_3$).

^{13}*C*-NMR (101 MHz, D_2O): δ [ppm] = 166.2 (*C*-7), 156.0 (*C*-3), 143.7 (*C*-2), 129.4 (*C*-5), 125.4 (*C*-6), 92.4 (*C*-1´), 82.5 (*C*-4´), 79.7 (*C*-2´), 72.4 (*C*-3´), 59.7 (*C*-5´), 19.3 (2´-C-*C*H$_3$).

HRMS (ESI$^+$): *m/z* = calcd: 308.0859 [M+Na]$^+$, found: 308.0834 [M+Na]$^+$.

2´-*C*-Methyl-T-1106 methyl ester 83

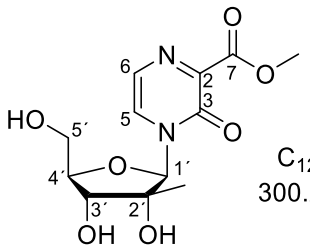

83
$C_{12}H_{16}N_2O_7$
300.2670 g/mol

The reaction was carried out according to general procedure III with the protected nucleoside **48** (2.00 g, 3.26 mmol) in MeOH (20 mL) and sodium methoxide solution (60 µL, 5.4 M in MeOH).

Purification on RP_{18} silica gel by automated flash chromatography (H_2O/CH_3CN; 100:0 to 0:100 v/v) provided **83** (925 mg, 94%) as a colorless solid.

^{1}*H*-NMR (500 MHz, D_2O): δ [ppm] = 8.29 (d, $^3J_{HH}$ = 4.32 Hz, 1H, *H*-5), 7.68 (d, $^3J_{HH}$ = 4.25 Hz, 1H, *H*-6), 6.28 (s, 1H, *H*-1´), 4.12 (ddd, $^3J_{HH}$ = 9.56 Hz, $^3J_{HH}$ = 3.80 Hz, $^3J_{HH}$ = 2.46 Hz, 1H, *H*-4´), 4.07 (dd, $^2J_{HH}$ = 13.37 Hz, $^3J_{HH}$ = 2.29 Hz, 1H, *H*-5´), 3.95 (s, 3H, -OCH_3), 3.92 (d, $^3J_{HH}$ = 9.73 Hz, 1H, *H*-3´), 3.89 (dd, $^2J_{HH}$ = 13.20 Hz, $^3J_{HH}$ = 3.80 Hz, 1H, *H*-5´), 1.09 (s, 3H, 2´-C-CH_3).

^{13}*C*-NMR (125 MHz, D_2O): δ [ppm] = 164.7 (*C*-7), 156.5 (*C*-3), 146.3 (*C*-2), 130.5 (*C*-5), 124.8 (*C*-6), 90.9 (*C*-1´), 83.7 (*C*-4´), 79.2 (*C*-2´), 72.9 (*C*-3´), 60.5 (*C*-5´), 52.4 (-O*C*H_3), 20.1 (2´-C-*C*H_3).

HRMS (ESI^+): *m/z* = calcd: 323.0850 $[M+Na]^+$, found: 323.0848 $[M+Na]^+$.

2´-*C*-Methyl-5´-*O*-*tert*-butyldimethylsilyl-T-1106 methyl ester 84

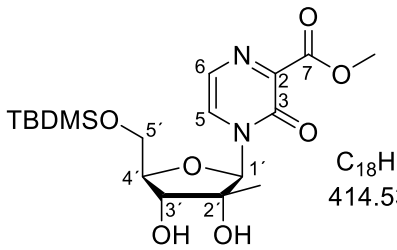

84
$C_{18}H_{30}N_2O_7Si$
414.5300 g/mol

2'-*C*-Methyl-T-1106 methyl ester **83** (500 mg, 1.66 mmol) and *tert*-butyldimethylsilyl chloride (374 mg, 2.49 mmol) were dissolved in pyridine (20 mL) and stirred overnight at room temperature. After all volatiles were removed under reduced pressure, purification on silica gel by automated flash chromatography (CH_2Cl_2/MeOH; 50:1 to 20:1 v/v) provided **84** (569 mg, 82%) as a colorless solid.

^{1}*H*-NMR (600 MHz, $CDCl_3$): *δ* [ppm] = 8.24 (d, $^3J_{HH}$ = 4.23 Hz, 1H, *H*-5), 7.54 (d, $^3J_{HH}$ = 4.21 Hz, 1H, *H*-6), 6.25 (s, 1H, *H*-1´), 4.11 – 4.08 (m, 2H, *H*-4´, *H*-5´), 3.97 (s, 3H, -OCH_3), 3.91 (dd, $^2J_{HH}$ = 11.93 Hz, $^3J_{HH}$ = 2.42 Hz, 1H, *H*-5´), 3.88 (d, $^3J_{HH}$ = 7.51 Hz, 1H, *H*-3´), 1.15 (s, 3H, 2´-C-CH_3), 0.94 (s, 9H, -SiC(CH_3)$_3$), 0.14 (s, 6H, -Si(CH_3)$_2$).

^{13}*C*-NMR (150 MHz, $CDCl_3$): *δ* [ppm] = 163.1 (*C*-7), 154.0 (*C*-3), 144.5 (*C*-2), 128.3 (*C*-5), 123.9 (*C*-6), 92.7 (*C*-1´), 84.7 (*C*-4´), 78.8 (*C*-2´), 73.1 (*C*-3´), 61.3 (*C*-5´), 53.2 (-O*C*H_3), 26.1 (-SiC(*C*H_3)$_3$), 20.5 (2´-C-*C*H_3), 18.6 (-Si*C*(CH$_3$)$_3$), 5.4, 5,3 (-Si(*C*H_3)$_2$).

HRMS (ESI^+): *m/z* = calcd: 437.1735 $[M+Na]^+$, found: 437.1734 $[M+Na]^+$.

2´,3´-Di-*O*-benzoyl-2´-*C*-methyl-5´-*O*-*tert*-butyldimethylsilyl-T-1106 methyl ester 85

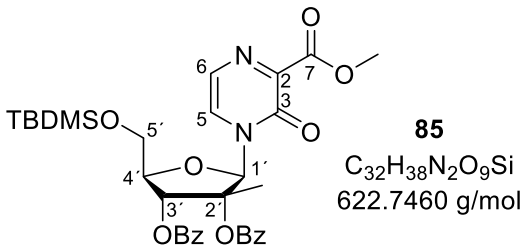

To a solution of 2'-*C*-methyl-5'-*O*-*tert*-butyldimethylsilyl-T-1106 methyl ester **84** (550 mg, 1.32 mmol) and 4-DMAP (324 mg, 2.65 mmol) in CH_2Cl_2 (20 mL) were added Et_3N (3 mL) and benzoyl chloride (459 µL, 5.59 mmol). After the reaction mixture was stirred overnight at room temperature, the reaction was quenched by the addition of sat. aq. $NaHCO_3$. Subsequently, the organic phase was washed with sat. aq. $NaHCO_3$, dried over $MgSO_4$ and all volatiles were removed under reduced pressure. Purification of the crude product on silica gel by automated flash chromatography (petroleum ether/ethyl acetate; 5:1 to 3:1 v/v) provided **85** (760 mg, 92%) as a colorless foam.

^{1}*H*-NMR (600 MHz, $CDCl_3$): δ [ppm] = 8.07 – 8.05 (m, 3H, *H*-5, *H*-Bz), 7.81 (dd, $^3J_{HH}$ = 8.18 Hz, $^4J_{HH}$ = 1.12 Hz, 2H, *H*-Bz), 7.54 (tt, $^3J_{HH}$ = 7.44 Hz, $^4J_{HH}$ = 1.35 Hz, 1H, *H*-Bz), 7.49 (d, $^3J_{HH}$ = 4.36 Hz, 1H, *H*-6), 7.46 (tt, $^3J_{HH}$ = 7.48 Hz, $^4J_{HH}$ = 1.32 Hz, 1H, *H*-Bz), 7.41 (dd, $^3J_{HH}$ = 8.18 Hz, 2H, *H*-Bz), 7.23 (dd, $^3J_{HH}$ = 8.18 Hz, 2H, *H*-Bz), 6.94 (s, 1H, *H*-1´), 5.72 (d, $^3J_{HH}$ = 5.74 Hz, 1H, *H*-3´), 4.50 (dt, $^3J_{HH}$ = 5.83 Hz, $^4J_{HH}$ = 2.00 Hz, 1H, *H*-4), 4.13 (dd, $^2J_{HH}$ = 11.83 Hz, $^3J_{HH}$ = 2.08 Hz, 1H, *H*-5´), 4.05 (dd, $^2J_{HH}$ = 11.91 Hz, $^3J_{HH}$ = 2.04 Hz, 1H, *H*-5´), 3.98 (s, 3H, -OCH_3), 1.62 (s, 3H, 2´-C-CH_3), 0.97 (s, 9H, -SiC(CH_3)$_3$), 0.18 (s, 3H, -Si(CH_3)$_2$), 0.17 (s, 3H, -Si(CH_3)$_2$).

^{13}*C*-NMR (150 MHz, $CDCl_3$): δ [ppm] = 165.4 (*C*-Bz), 165.3 (*C*-Bz), 163.1 (*C*-7), 153.0 (*C*-3), 146.3 (*C*-2), 133.6 (*C*-Bz), 133.5 (*C*-Bz), 130.1 (2C, *C*-Bz), 129.9 (*C*-5), 129.8 (2C, *C*-Bz), 128.8 (*C*-Bz), 128.6 (2C, *C*-Bz), 128.5 (2C, *C*-Bz), 128.2 (*C*-Bz), 122.5 (*C*-6), 89.2 (*C*-1´), 85.9 (*C*-2´), 84.1 (*C*-4´), 74.9 (*C*-3´), 61.9 (*C*-5´), 53.2 (-O*C*H$_3$), 26.1 (-SiC(*C*H$_3$)$_3$), 18.7 (2´-C-*C*H$_3$), 18.6 (-Si*C*(CH$_3$)$_3$), -5.3 (-Si(*C*H$_3$)$_2$).

HRMS (ESI$^+$): *m/z* = calcd: 622.2239 [M+Na]$^+$, found: 622.2239 [M+Na]$^+$.

2´,3´-Di-*O*-benzoyl-2´-*C*-methyl-T-1106 methyl ester 86

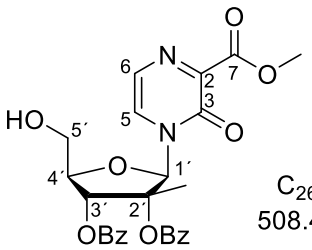

86
$C_{26}H_{24}N_2O_9$
508.4830 g/mol

To a solution of 2′,3′-Di-*O*-benzoyl-2′-*C*-methyl-5′-*O*-tert-butyldimethylsilyl-T-1106 methyl ester **85** (750 mg, 1.20 mmol) in MeOH (5 mL) acetyl chloride (13 µL, 0.18 mmol) was added. After the reaction mixture was stirred overnight at room temperature, the reaction was quenched by the addition of sat. aq. $NaHCO_3$. Subsequently, the organic phase was washed with sat. aq. $NaHCO_3$, dried over $MgSO_4$ and all volatiles were removed under reduced pressure. Purification of the crude product on silica gel by automated flash chromatography (petroleum ether/ethyl acetate; 2:1 to 1:1 v/v) provided **86** (501 mg, 82%) as a colorless foam.

^{1}*H*-NMR (400 MHz, $CDCl_3$): δ [ppm] = 8.09 (dd, $^3J_{HH}$ = 8.38 Hz, $^4J_{HH}$ = 1.36 Hz, 2H, *H*-Bz), 8.02 (d, $^3J_{HH}$ = 4.45 Hz, 1H, *H*-5), 7.91 (dd, $^3J_{HH}$ = 8.40 Hz, $^4J_{HH}$ = 1.38 Hz, 2H, *H*-Bz), 7.58 (tt, $^3J_{HH}$ = 7.65 Hz, $^4J_{HH}$ = 1.19 Hz, 1H, *H*-Bz), 7.55 – 7.50 (m, 2H, *H*-6, *H*-Bz), 7.44 (dd, $^3J_{HH}$ = 7.53 Hz, 2H, *H*-Bz), 7.31 (dd, $^3J_{HH}$ = 7.84 Hz, 2H, *H*-Bz), 6.83 (s, 1H, *H*-1´), 5.68 (d, $^3J_{HH}$ = 6.84 Hz, 1H, *H*-3´), 4.50 (dt, $^3J_{HH}$ = 6.71 Hz, $^4J_{HH}$ = 2.88 Hz, 1H, *H*-4), 4.15 (dd, $^2J_{HH}$ = 12.61 Hz, $^3J_{HH}$ = 2.38 Hz, 1H, *H*-5´), 4.01 (dd, $^2J_{HH}$ = 12.54 Hz, $^3J_{HH}$ = 2.04 Hz, 1H, *H*-5´), 3.99 (s, 3H, -OCH_3), 1.68 (s, 3H, 2´-C-CH_3).

^{13}*C*-NMR (100 MHz, $CDCl_3$): δ [ppm] = 165.9 (*C*-Bz), 165.1 (*C*-Bz), 163.6 (*C*-7), 152.9 (*C*-3), 146.7 (*C*-2), 133.8 (*C*-Bz), 133.5 (*C*-Bz), 130.0 (2C, *C*-Bz), 129.9 (2C, *C*-Bz), 129.8 (*C*-5), 128.6 (2C, *C*-Bz), 128.5 (3C, *C*-Bz), 128.5 (*C*-Bz), 122.8 (*C*-6), 89.7 (*C*-1´), 86.1 (*C*-2´), 82.9 (*C*-4´), 74.6 (*C*-3´), 61.0 (*C*-5´), 53.0 (-O*C*H_3), 18.2 (2´-C-*C*H_3).

HRMS (ESI$^+$): *m/z* = calcd: 531.1374 $[M+Na]^+$, found: 531.1374 $[M+Na]^+$.

2´-Fluoro-2´-*C*-methyl-T-1106 51

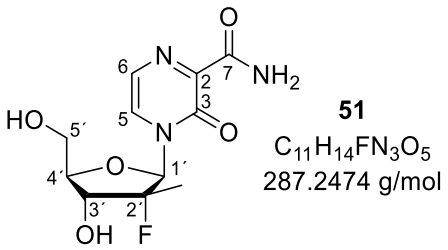

51

$C_{11}H_{14}FN_3O_5$

287.2474 g/mol

Step 1: The reaction was carried out according to general procedure II with **20** (1.77 g, 11.5 mmol), ammonium sulfate (6 mg, 0.05 mmol) and HMDS (15 mL), followed by the ribose **27** (1.50 g, 3.82 mmol) and tin tetrachloride (20.0 mL, 20.0 mmol, 1 M solution in CH_2Cl_2) in CH_3CN (30 mL) and CH_2Cl_2 (15 mL). Purification of the crude product on silica gel by automated flash chromatography (CH_2Cl_2/MeOH; 60:1 to 30:1 v/v) provided **50** (561 mg, 29%) as a colorless foam.

^{1}*H*-NMR (600 MHz, $CDCl_3$): δ [ppm] = 8.09 – 8.05 (m, 2H, *H*-Bz), 8.01 – 7.96 (m, 2H, *H*-Bz), 7.63 – 7.53 (m, 4H, *H*-Bz, *H*-5, *H*-6), 7.49 –7.43 (m, 2H, *H*-Bz), 7.41 –7.38 (m, 2H, *H*-Bz), 6.66 (d, $^3J_{HF}$ = 19.07 Hz, 1H, *H*-1‘), 5.76 (dd, $^3J_{HF}$ = 22.19 Hz, $^3J_{HH}$ = 8.81 Hz, 1H, *H*-3‘), 4.89 – 4.83 (m, 1H, *H*-4‘), 4.74 (dd, $^2J_{HH}$ = 12.45 Hz, $^3J_{HH}$ = 3.62 Hz, 1H, *H*-5‘), 4.56 (dd, $^2J_{HH}$ = 12.42 Hz, $^3J_{HH}$ = 4.47 Hz, 1H, *H*-5‘), 3.98 (s, 3H, -OC*H*$_3$), 1.65 (d, $^3J_{HF}$ = 22.45 Hz, 3H, 2´-C-C*H*$_3$).

Step 2: The reaction was carried out according to general procedure IV with the protected nucleoside **50** (561 mg, 1.10 mmol) and 30 mL of 7 M NH_3 in MeOH. Purification on RP_{18} silica gel by automated flash chromatography (H_2O/CH_3CN; 100:0 to 0:100 v/v) provided **51** (250 mg, 79%) as a colorless solid.

The analytical data was in accordance with those described.[150]

^{1}*H*-NMR (600 MHz, D_2O): *δ* [ppm] = 7.93 (dd, $^3J_{HH}$ = 4.29 Hz, $^5J_{HH}$ = 2.69 Hz, 1H, *H*-5), 7.74 (d, $^3J_{HH}$ = 4.24 Hz, 1H, *H*-6), 6.59 (d, $^3J_{HF}$ = 18.75 Hz, 1H, *H*-1‘), 4.44 – 4.40 (m, 1H, *H*-4‘), 4.26 (dd, $^3J_{HF}$ = 23.86 Hz, $^3J_{HH}$ = 9.57 Hz, 1H, *H*-3‘), 4.01 (dd, $^2J_{HH}$ = 12.94 Hz, $^3J_{HH}$ = 2.18 Hz, 1H, *H*-5‘), 3.79 (dd, $^2J_{HH}$ = 12.74 Hz, $^3J_{HH}$ = 4.56 Hz, 1H, *H*-5‘), 1.59 (d, $^3J_{HF}$ = 23.20 Hz, 3H, 2´-C-C*H*$_3$).

^{13}*C*-NMR (150 MHz, D_2O): *δ* [ppm] = 166.7 (*C*-7), 155.7 (*C*-3), 143.2 (*C*-2), 130.5 (d, $^4J_{CF}$ = 4.40 Hz, *C*-5), 124.3 (*C*-6), 99.6 (d, $^1J_{CF}$ = 190.07 Hz, *C*-2´), 87.6 (d, $^2J_{CF}$ = 14.98 Hz, *C*-1´), 82.9 (*C*-4´), 72.9 (d, $^2J_{CF}$ = 17.79 Hz, *C*-3´), 60.0 (*C*-5´), 19.9 (d, $^2J_{CF}$ = 24.97 Hz, 2´-C-*C*H$_3$).

^{19}*F*-NMR (564 MHz, $CDCl_3$): *δ* [ppm] = -165.1 (m).

Methyl 4-(5´-*O*-benzoyl-2´-*O*-acetyl-3´-deoxy-β-D-ribofuranosyl)-3-oxo-2-pyrazinecarboxylate 45

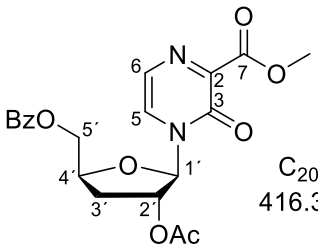

The reaction was carried out according to general procedure II with **20** (1.10 g, 6.54 mmol), ammonium sulfate (8 mg, 0.06 mmol) and HMDS (15 mL), followed by 5-*O*-benzoyl-1,2-di-*O*-acetyl-3-deoxy-D-ribofuranose **22** (702 mg, 2.17 mmol) and tin tetrachloride (6.54 mL, 6.54 mmol, 1 M solution in CH_2Cl_2) in CH_3CN (25 mL) and CH_2Cl_2 (10 mL). Purification of the crude product on silica gel (CH_2Cl_2/MeOH; 100:1 v/v) provided **45** (514 mg, 57%) as a colorless foam.

The analytical data was in accordance with those described.[119]

^{1}*H*-NMR (300 MHz, $CDCl_3$): δ [ppm] = 8.06 – 8.02 (m, 2H, *H*-Bz), 7.85 (d, $^3J_{HH}$ = 4.41 Hz, 1H, *H*-5), 7.58 (tt, $^3J_{HH}$ = 7.34 Hz, $^4J_{HH}$ = 1.47 Hz, 1H, *H*-Bz), 7.51 – 7.46 (m, 2H, *H*-Bz), 7.32 (d, $^3J_{HH}$ = 4.35 Hz, 1H, *H*-6), 6.01 (s, 1H, H-1´), 5.42 – 5.39 (m, 1H, H-4´), 4.83 – 4.75 (m, 2H, *H*-5´, *H*-2´), 4.62 (dd, $^2J_{HH}$ = 13.17 Hz, $^3J_{HH}$ = 4.80 Hz, 1H, *H*-5´), 3.96 (s, 3H, -OC*H*$_3$), 2.21 – 2.17 (m, 2H, *H*-3´) 2.15 (s, 3H, *H*-Ac).

HRMS (ESI$^+$): *m/z* = calcd: 439.1112 $[M+Na]^+$, found: 439.1113 $[M+Na]^+$.

3´-Deoxy-T-1106 40

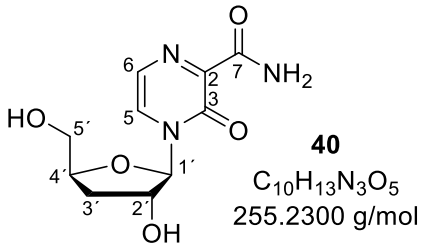

The reaction was carried out according to general procedure IV with the protected nucleoside **45** (1.12 g, 2.69 mmol) and 30 mL of 7 M NH_3 in MeOH. Purification on RP_{18} silica gel by automated flash chromatography (H_2O/CH_3CN; 100:0 to 0:100 v/v) provided **40** (681 mg, 94%) as a light-yellow solid.

The analytical data was in accordance with those described.[119]

^{1}*H*-NMR (500 MHz, D_2O): δ [ppm] = 8.29 (d, $^{3}J_{HH}$ = 4.18 Hz, 1H, *H*-5), 7.75 (s, 1H, $^{3}J_{HH}$ = 4.22 Hz, H-*6*), 6.00 (s, 1H, *H*-1´), 4.69 – 4.65 (m, 1H, *H*-4´), 4.52 (d, $^{3}J_{HH}$ = 4.5z7 Hz, 1H, *H*-2´), 4.05 (dd, $^{2}J_{HH}$ = 13.03 Hz, $^{3}J_{HH}$ = 2.80 Hz, 1H, *H*-5´), 3.84 (dd, $^{2}J_{HH}$ = 12.95 Hz, $^{3}J_{HH}$ = 4.81 Hz, 1H, *H*-5´), 2.02 (dd, $^{2}J_{HH}$ = 14.02 Hz, $^{3}J_{HH}$ = 5.43 Hz, 1H, *H*-3´), 1.90 (ddd, $^{2}J_{HH}$ = 14.09 Hz, $^{3}J_{HH}$ = 5.75 Hz, $^{3}J_{HH}$ = 5.40 Hz, 1H, *H*-3´).

^{13}*C*-NMR (125 MHz, D_2O): δ [ppm] = 166.2 (*C*-7), 156.3 (*C*-3), 143.2 (*C*-2), 129.5 (*C*-5), 124.8 (*C*-6), 91.1 (*C*-1´), 83.6 (*C*-4´) 76.2 (*C*-2´), 62.1 (*C*-5´), 32.2 (*C*-3´).

HRMS (ESI+): *m/z* = calcd: 278.0747 $[M+Na]^+$, found: 278.0747 $[M+Na]^+$.

Methyl 4-(5´-*O*-benzoyl-2´-*O*-acetyl-3´-deoxy-3´-fluoro-β-D-ribofuranosyl)-3-oxo-2-pyrazinecarboxylate 46

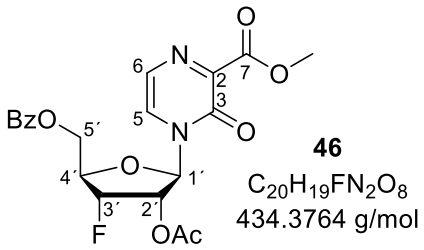

46

$C_{20}H_{19}FN_2O_8$

434.3764 g/mol

The reaction was carried out according to general procedure II with **20** (1.33 g, 8.64 mmol), ammonium sulfate (16 mg, 0.12 mmol) and HMDS (20 mL), followed by 5-*O*-benzoyl-1,2-di-*O*-acetyl-3-deoxy-3-fluoro-D-ribofuranose **23** (2.14 g, 6.17 mmol) and tin tetrachloride (7.72 mL, 7.72 mmol, 1 M solution in CH_2Cl_2) in CH_3CN (60 mL) and CH_2Cl_2 (20 mL). Purification of the crude product on silica gel (CH_2Cl_2/MeOH; 100:1 v/v) provided **46** (1.89 g, 67%) as a colorless foam.

^{1}*H*-NMR (600 MHz, $CDCl_3$): δ [ppm] = 8.03 – 8.01 (m, 2H, *H*-Bz), 7.63 – 7.60 (m, 1H, *H*-Bz), 7.49 – 7.46 (m, 3H, *H*-5, *H*-Bz), 7.31 (d, $^{3}J_{HH}$ = 4.48 Hz, 1H, *H*-6), 6.24 (d, $^{3}J_{HH}$ = 5.02 Hz, 1H, *H*-1), 5.47 – 5.43 (m, 1H, *H*-2) 5.40 (dt, $^{2}J_{HF}$ = 72.61 Hz, $^{3}J_{HH}$ = 4.72 Hz, 1H, *H*-3), 4.76 – 4.69 (m, 2H, *H*-4, *H*-5), 4.64 – 4.61 (m, 1H, *H*-5) 3.96 (s, 3H, -OC*H*$_3$), 2.17 (s, 3H, *H*-Ac).

^{13}*C*-NMR (150 MHz, $CDCl_3$): δ [ppm] = 169.8 (*C*-Ac), 166.0 (*C*-Bz), 163.3 (*C*-7), 152.9 (*C*-3), 146.7 (*C*-2), 134.0 (*C*-Bz), 129.7 (2C, *C*-Bz), 129.0 (*C*-Bz), 128.9 (2C, *C*-Bz), 127.2 (*C*-6), 123.1 (C-5), 88.7 (d, $^{3}J_{CF}$ = 1.40 Hz, *C*-1), 88.6 (d, $^{1}J_{CF}$ = 193.85 Hz, *C*-3), 81.2 (d, $^{2}J_{CF}$ = 25.49 Hz, *C*-4), 74.1 (d, $^{2}J_{CF}$ = 14.75 Hz, *C*-2), 63.1 (d, $^{3}J_{CF}$ = 6.23 Hz, *C*-5), 53.2 (-O*C*H$_3$), 20.6 (*C*-Ac).

^{19}F-NMR (564 MHz, $CDCl_3$): δ [ppm] = -201.8 (m).

HRMS (ESI^+): *m/z* = calcd: 457.1017 $[M+Na]^+$, found: 457.1016 $[M+Na]^+$.

3´-Fluoro-T-1106 41

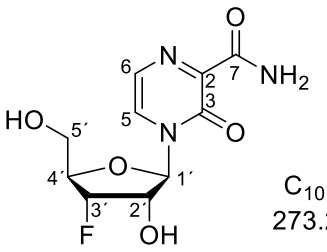

41
$C_{10}H_{12}FN_3O_5$
273.2204 g/mol

The reaction was carried out according to general procedure IV with the protected nucleoside **46** (550 mg, 1.26 mmol) and 30 mL of 7 M NH_3 in MeOH. Purification on RP_{18} silica gel by automated flash chromatography (H_2O/CH_3CN; 100:0 to 0:100 v/v) provided **41** (288 mg, 83%) as a colorless solid.

^1H-NMR (600 MHz, D_2O): δ [ppm] = 8.14 (d, $^3J_{HH}$ = 4.38 Hz, 1H, *H*-5), 7.76 (d, 1H, $^3J_{HH}$ = 4.53 Hz, *H*-6), 6.33 (d, $^3J_{HH}$ = 5.8 Hz, 1H, *H*-1´), 5.23 (ddd, $^2J_{HF}$ = 53.32 Hz, $^3J_{HH}$ = 4.80 Hz, $^3J_{HH}$ = 3.16 Hz, 1H, *H*-3´), 4.58 (ddd, $^2J_{HF}$ = 23.80 Hz, $^3J_{HH}$ = 6.74 Hz, $^3J_{HH}$ = 3.16 Hz, 1H, *H*-4´), 4.53 (ddd, $^2J_{HF}$ = 17.79 Hz, $^3J_{HH}$ = 5.77 Hz, $^3J_{HH}$ = 4.62 Hz, 1H, *H*-2´), 3.94 (dd, $^2J_{HH}$ = 13.06 Hz, $^3J_{HH}$ = 3.28 Hz, 1H, *H*-5´), 3.90 (dd, $^2J_{HH}$ = 12.87 Hz, $^3J_{HH}$ = 3.83 Hz, 1H, *H*-5´).

^{13}C-NMR (150 MHz, D_2O): δ [ppm] = 166.2 (*C*-7), 155.1 (*C*-3), 143.3 (*C*-2), 129.0 (*C*-5), 125.0 (*C*-6), 91.1 (d, $^1J_{CF}$ = 185.50 Hz, *C*-3´), 88.7 (*C*-1´) 81.2 (d, $^2J_{CF}$ = 23.10 Hz, *C*-4´), 74.1 (d, $^2J_{CF}$ = 16.6 Hz, *C*-2´), 60.2 (d, $^3J_{CF}$ = 8.23 Hz, *C*-5´).

^{19}F-NMR (564 MHz, D_2O): δ [ppm] = -203.3.

HRMS (ESI^+): *m/z* = calcd: 296.0653 $[M+Na]^+$, found: 296.0653 $[M+Na]^+$.

Methyl 4-(5´-*O*-benzoyl-2´-*O*-acetyl-3´-deoxy-3´-azido-β-D-ribofuranosyl)-3-oxo-2-pyrazinecarboxylate 47

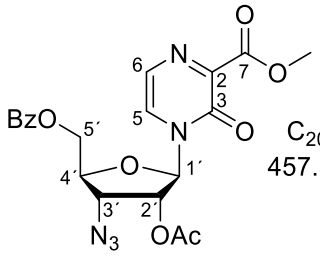

47
$C_{20}H_{19}N_5O_8$
457.3990 g/mol

The reaction was carried out according to general procedure II with **20** (777 mg, 5.04 mmol), ammonium sulfate (8 mg, 0.06 mmol) and HMDS (15 mL), followed by 3-azido-5-*O*-benzoyl-3-deoxy-1,2-*O*-diacetyl-D-ribofuranose **24** (613 mg, 1.69 mmol) and tin tetrachloride (2.48 mL, 2.48 mmol, 1 M solution in CH_2Cl_2) in CH_3CN (38 mL) and CH_2Cl_2 (16 mL). Purification of the crude product on silica gel (CH_2Cl_2/MeOH; 60:1 v/v) provided **47** (657 mg, 85%) as a colorless foam.

^{1}*H*-NMR (600 MHz, $CDCl_3$): δ [ppm] = 8.06 – 8.04 (m, 2H, *H*-Bz), 7.65 – 7.61 (m, 2H, *H*-5, *H*-Bz), 7.51 – 7.47 (m, 2H, *H*-Bz), 7.30 (d, $^3J_{HH}$ = 4.32 Hz, 1H, *H*-6), 6.24 (d, $^3J_{HH}$ = 1.89 Hz, 1H, *H*-1´), 5.63 (dd, $^3J_{HH}$ = 5.53 Hz, $^3J_{HH}$ = 2.03 Hz, 1H, *H*-2´), 4.73 (dd, $^2J_{HH}$ = 12.69 Hz, $^3J_{HH}$ = 2.56 Hz, 1H, *H*-5´), 4.58 (dd, $^2J_{HH}$ = 12.76 Hz, $^3J_{HH}$ = 3.41 Hz, 1H, *H*-5´), 4.36 (dt, $^3J_{HH}$ = 9.09 Hz, $^3J_{HH}$ = 3.41 Hz, 1H, *H*-4´), 4.31 (dd, $^2J_{HH}$ = 9.03 Hz, $^3J_{HH}$ = 5.35 Hz, 1H, *H*-3´), 3.96 (s, 3H, -OC*H*$_3$), 2.22 (s, 3H, *H*-Ac).

^{13}*C*-NMR (150 MHz, $CDCl_3$): δ [ppm] = 169.5 (*C*-Ac), 166.1 (*C*-Bz), 163.3 (*C*-7), 152.8 (*C*-3), 146.4 (*C*-2), 134.0 (*C*-Bz), 129.8 (2C, *C*-Bz), 129.2 (*C*-Bz), 128.9 (2C, *C*-Bz), 127.5 (*C*-6), 123.1 (*C*-5), 91.6 (*C*-1), 80.7 (*C*-4), 75.4 (*C*-2), 62.3 (*C*-5), 59.7 (*C*-3), 53.2 (-O*C*H$_3$), 20.6 (*C*-Ac).

3´-Azido-T-1106 42

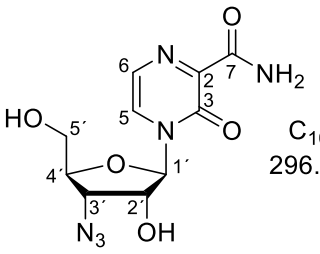

42
$C_{10}H_{12}N_6O_5$
296.2430 g/mol

The reaction was carried out according to general procedure IV with the protected nucleoside **47** (611 mg, 1.34 mmol) and 37 mL of 7 M NH_3 in MeOH. Purification on RP_{18} silica gel by automated

flash chromatography (H_2O/CH_3CN; 100:0 to 0:100 v/v) provided **42** (331 mg, 83%) as a colorless solid.

^{1}*H*-NMR (500 MHz, D_2O): δ [ppm] = 8.30 (d, $^3J_{HH}$ = 4.22 Hz, 1H, *H*-5), 7.78 (d, $^3J_{HH}$ = 4.26 Hz, 1H, *H*-6), 6.09 (d, $^3J_{HH}$ = 1.64 Hz, 1H, *H*-1´), 4.60 (dd, $^3J_{HH}$ = 5.06 Hz, $^3J_{HH}$ = 1.56 Hz, 1H, *H*-2´), 4.34 (dt, $^3J_{HH}$ = 9.01 Hz, $^3J_{HH}$ = 2.95 Hz, 1H, *H*-4´), 4.11 (dd, $^2J_{HH}$ = 13.26 Hz, $^3J_{HH}$ = 2.79 Hz, 1H, *H*-5´), 4.05 (dd, $^3J_{HH}$ = 9.12 Hz, $^3J_{HH}$ = 5.56 Hz, 1H, *H*-3´), 3.92 (dd, $^2J_{HH}$ = 13.24 Hz, $^3J_{HH}$ = 3.63 Hz, 1H, *H*-5´).

^{13}*C*-NMR (125 MHz, D_2O): δ [ppm] = 166.6 (*C*-7), 156.1 (*C*-3), 143.9 (*C*-2), 129.3 (*C*-5), 125.3 (*C*-6), 91.9 (*C*-1´), 82.9 (*C*-4´), 75.5 (*C*-2´), 60.0 (*C*-5´), 59.4 (*C*-3´).

HRMS (ESI^+): *m/z* = calcd: 319.0761 $[M+Na]^+$, found: 319.0763 $[M+Na]^+$.

6-Methyl-T-1106 131

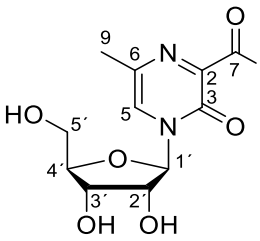

131
$C_{11}H_{15}N_3O_6$
285.2560 g/mol

Step 1: The reaction was carried out according to general procedure II with **129** (500 mg, 2.97 mmol), ammonium sulfate (6 mg, 0.06 mmol) and HMDS (10 mL), followed by tetra-*O*-acetyl-β-D-ribofuranose **52** (662 mg, 2.08 mmol) and tin tetrachloride (2.97 mL, 2.97 mmol, 1 M solution in CH_2Cl_2) in CH_3CN (25 mL) and CH_2Cl_2 (10 mL). Purification of the crude product on silica gel (CH_2Cl_2/MeOH; 60:1 v/v) provided **130** (580 mg, 65%) as a colorless foam.

Step 2: The reaction was carried out according to general procedure IV with the protected nucleoside **130** (580 mg, 1.36 mmol) and 20 mL of 7 M NH_3 in MeOH. Purification on RP_{18} silica gel by automated flash chromatography (H_2O/CH_3CN; 100:0 to 0:100 v/v) provided **131** (280 mg, 72%) as a light-yellow solid.

^{1}*H*-NMR (400 MHz, D_2O): δ [ppm] = 8.18 (s, 1H, *H*-5), 6.09 (d, $^3J_{HH}$ = 1.79 Hz, 1H, *H*-1´), 4.30 (dd, $^3J_{HH}$ = 4.88 Hz, $^3J_{HH}$ = 1.82 Hz, 1H, *H*-2´), 4.25 (dt, $^3J_{HH}$ = 8.24 Hz, $^3J_{HH}$ = 3.04 Hz, 1H, *H*-4´), 4.20 (dd, $^3J_{HH}$ = 8.03 Hz, $^3J_{HH}$ = 4.69 Hz, 1H, *H*-3´), 4.09 (dd, $^2J_{HH}$ = 12.94 Hz, $^3J_{HH}$ = 2.50 Hz, 1H, *H*-5´), 3.91 (dd, $^2J_{HH}$ = 13.17 Hz, $^3J_{HH}$ = 3.65 Hz, 1H, *H*-5´), 2.39 (s, 3H, *H*-9).

^{13}C-NMR (101 MHz, D_2O): δ [ppm] = 166.8 (*C*-7), 154.8 (*C*-3), 141.1 (*C*-2), 134.4 (*C*-6), 126.7 (*C*-5), 91.1 (*C*-1´), 83.6 (*C*-4´), 74.7 (*C*-2´), 68.0 (*C*-3´), 59.6 (*C*-5´), 18.8 (*C*-9).

HRMS (ESI^+): *m/z* = calcd: 308.0853 $[M+Na]^+$, found: 308.0855 $[M+Na]^+$.

6-Methyl-2´-C-methyl-T-1106 134

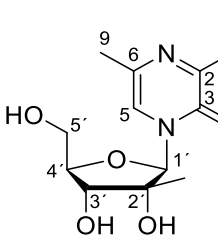

134
$C_{12}H_{17}N_3O_6$
299.2830 g/mol

Step 1: The reaction was carried out according to general procedure II with **129** (410 mg, 2.43 mmol), ammonium sulfate (6 mg, 0.06 mmol) and HMDS (10 mL), followed by tetra-*O*-benzoyl-2'-*C*-methyl-β-D-ribofuranose **26** (990 mg, 1.70 mmol) and tin tetrachloride (2.43 mL, 2.43 mmol, 1 M solution in CH_2Cl_2) in CH_3CN (25 mL) and CH_2Cl_2 (10 mL). Purification of the crude product on silica gel (CH_2Cl_2/MeOH; 60:1 v/v) provided **133** (350 mg, 33%) as a colorless foam.

Step 2: The reaction was carried out according to general procedure IV with the protected nucleoside **133** (325 mg, 0.51 mmol) and 20 mL of 7 M NH_3 in MeOH. Purification on RP_{18} silica gel by automated flash chromatography (H_2O/CH_3CN; 100:0 to 0:100 v/v) provided **134** (152 mg, 97%) as a colorless solid.

^1H-NMR (600 MHz, D_2O): *δ* [ppm] = 8.18 (s, 1H, *H*-5), 6.09 (d, $^3J_{HH}$ = 1.79 Hz, 1H, *H*-1´), 4.30 (dd, $^3J_{HH}$ = 4.88 Hz, $^3J_{HH}$ = 1.82 Hz, 1H, *H*-2´), 4.25 (dt, $^3J_{HH}$ = 8.24 Hz, $^3J_{HH}$ = 3.04 Hz, 1H, *H*-4´), 4.20 (dd, $^3J_{HH}$ = 8.03 Hz, $^3J_{HH}$ = 4.69 Hz, 1H, *H*-3´), 4.09 (dd, $^2J_{HH}$ = 12.94 Hz, $^3J_{HH}$ = 2.50 Hz, 1H, *H*-5´), 3.91 (dd, $^2J_{HH}$ = 13.17 Hz, $^3J_{HH}$ = 3.65 Hz, 1H, *H*-5´), 2.39 (s, 3H, *H*-9), 1.10 (s, 3H, 2´-C-CH_3´).

^{13}C-NMR (150 MHz, D_2O): *δ* [ppm] = 166.9 (*C*-7), 154.7 (*C*-3), 141.9 (*C*-2), 134.4 (*C*-5), 126.5 (*C*-6), 91.9 (*C*-1´), 82.1 (*C*-4´), 79.3 (*C*-2´), 71.7 (*C*-3´), 59.1 (*C*-5´), 18.8 (*C*-9), 18.7 (2´-C-*C*H_3).

HRMS (ESI^+): *m/z* = calcd: 322.1009 $[M+Na]^+$, found: 322.1010 $[M+Na]^+$.

5-Fluoro-2´-*C*-metyl-uridine 216

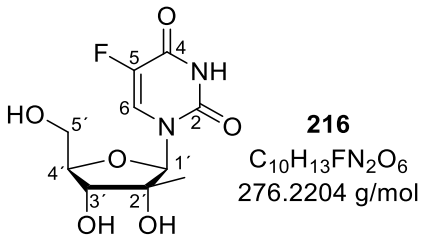

216

$C_{10}H_{13}FN_2O_6$

276.2204 g/mol

Step 1: The reaction was carried out according to general procedure II with **214** (1.34 g, 10.3 mmol), ammonium sulfate (15 mg, 0.12 mmol) and HMDS (20 mL) (note: to obtain a clear solution, the reaction mixture had to be stirred for 3 h), followed by 1,2,3,5-tetra-*O*-benzoyl-2-*C*-methyl-D-ribofuranose **26** (2.00 g, 3.44 mmol) and tin tetrachloride (4.13 mL, 4.13 mmol, 1 M solution in CH_2Cl_2) in CH_3CN (40 mL) and CH_2Cl_2 (15 mL). Purification of the crude product on silica gel (CH_2Cl_2/MeOH; 60:1 v/v) provided **215** (1.74 g, 86%) as a colorless solid.

^{1}*H*-NMR (500 MHz, $CDCl_3$): δ [ppm] = 8.98 (d, $^4J_{HF}$ = 3.31 Hz, 1H, -N*H*), 8.09 – 8.05 (m, 4H, *H*-Bz), 7.86 (d, $^3J_{HH}$ = 7.62 Hz, 2H, *H*-Bz), 7.68 (d, $^3J_{HH}$ = 6.08 Hz, 1H, *H*-6), 7.61 – 7.56 (m, 2H, *H*-Bz), 7.51 – 7.42 (m, 5H, *H*-Bz), 7.28 – 7.25 (m, 2H, *H*-Bz), 6.52 (s, 1H, *H*-1´), 5.71 (d, $^3J_{HH}$ = 4.72 Hz, 1H, *H*-3´), 4.90 – 4.83 (m, 2H, *H*-5´), 4.65 – 4.62 (m, 1H, H-4´), 1.77 (s, 3H, 2´-C-C*H*$_3$).

Step 2: The reaction was carried out according to the general procedure IV with the protected nucleoside **215** (1.70 g, 2.88 mmol) and 20 mL of 7M NH_3 in MeOH. Purification on RP_{18} silica gel with automated flash chromatography (H_2O/CH_3CN; 100:0 to 0:100 v/v) provided **216** (755 mg, 93%) as a light-yellow solid.

^{1}*H*-NMR (600 MHz, D_2O): δ [ppm] = 8.17 (d, $^3J_{HH}$ = 6.57 Hz, 1H, *H*-6), 5.99 (d, $^3J_{HH}$ = 1.57 Hz, 1H, *H*-1´), 4.06 – 4.02 (m, 2H, *H*-4´, *H*-5´), 3.93 (d, $^3J_{HH}$ = 9.57 Hz, 1H, *H*-3´), 3.87 (dd, $^2J_{HH}$ = 13.19 Hz, $^3J_{HH}$ = 3.62 Hz, 1H, *H*-5´), 1.22 (s, 3H, 2´-C-C*H*$_3$).

^{13}*C*-NMR (151 MHz, D_2O): δ [ppm] = 159.7 (d, $^2J_{CF}$ = 25.44 Hz, *C*-4), 150.4 (*C*-2), 140.7 (d, $^1J_{CF}$ = 233.57 Hz, *C*-5), 125.1 (d, $^2J_{CF}$ = 35.30 Hz, *C*-6), 91.6 (*C*-1'), 81.7 (*C*-4'), 79.1 (*C*-2'), 71.9 (*C*-3'), 59.2 (*C*-5'), 18.7 (2´-C-*C*H$_3$).

^{19}*F*-NMR (565 MHz, D_2O): δ [ppm] = -165.5 (d, $^3J_{FH}$ = 6.85 Hz).

HRMS (ESI$^+$): *m/z* = calcd: 299.0650[M+Na]$^+$, found: 299.0645 [M+Na]$^+$.

1-Cyano-2,3,5-tri-*O*-benzoyl-β-D-ribofuranose 64

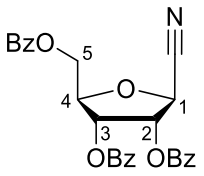

64
$C_{27}H_{21}NO_7$
471.4650 g/mol

Ribose **63** (4.00 g, 7.98 mmol) was dissolved in nitromethane (20 mL). Then, TMSCN (1.00 mL, 7.96 mmol) and $BF_3 \cdot Et_2O$ (0.25 mL, 1.97 mmol) were added, and the reaction mixture was stirred for 2 h at room temperature, followed by the addition of TMSCN (0.50 mL, 4.00 mmol). After the reaction mixture was stirred for 1 h at room temperature, the reaction was quenched by the addition of sat. aq. $NaHCO_3$ (100 mL). The mixture was extracted with ethyl acetate, the combined organic layers were washed with sat. aq. NaCl, dried over $MgSO_4$ and all volatiles were removed under reduced pressure. Purification of the crude product on silica gel (petroleum ether/ethyl acetate; 7:3 v/v) provided **64** (3.53 g, 94%) as a colorless foam.

The analytical data was in accordance with those described.[180]

^{1}*H*-NMR (300 MHz, $CDCl_3$): δ [ppm] = 8.00 – 7.94 (m, 2H, *H*-Ph), 7.84 – 7.73 (m, 4H, *H*-Ph), 7.49 – 7.35 (m, 3H, *H*-Ph), 7.34 – 7.19 (m, 6H, *H*-Ph), 5.85 (dd, $^3J_{HH}$ = 5.2, 4.3 Hz, 1H, *H*-2), 5.70 (t, $^3J_{HH}$ = 5.4 Hz, 1H, *H*-3´), 4.82 (d, $^3J_{HH}$ = 4.3 Hz, 1H, *H*-1), 4.63 – 4.52 (m, 2H, *H*-4, *H*-5), 4.51 – 4.38 (m, 1H, *H*-5).

Methyl 1-(2´,3´,5´-tri-*O*-benzoyl-β-D-ribofuranosyl)-thiazolincarboxylate 67

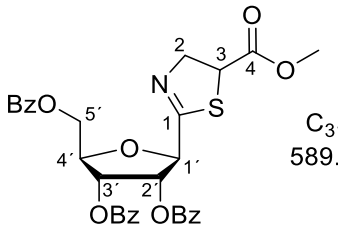

67
$C_{31}H_{27}NO_9S$
589.6150 g/mol

To a solution of **64** (268 mg, 0.56 mmol) in CH_2Cl_2 (10 mL) was added L-cysteine methyl ester hydrochloride (208 mg, 1.20 mmol) and triethylamine (156 µL, 1.11 mmol) over 6 h (4 portions, every 2 h). After the reaction mixture was stirred overnight, CH_2Cl_2 was added, and the organic layer was subsequently washed with H_2O, sat. aq. NaCl, dried over $MgSO_4$ and all volatiles were removed under reduced pressure, providing **64** as an orange oil. The product was used in the next step without further purification.

The analytical data was in accordance with those described.[183]

^{1}*H*-NMR (300 MHz, $CDCl_3$): δ [ppm] = 8.15 (s, 1H, *H*-2), 8.14 – 8.04 (m, 2H, *H*-Ph), 8.04 – 7.95 (m, 2H, *H*-Ph), 7.95 – 7.84 (m, 2H, *H*-Ph), 7.63 – 7.50 (m, 3H, *H*-Ph), 7.50 – 7.30 (m, 6H, *H*-Ph), 5.95 – 5.83 (m, 2H, *H*-2´, *H*-3´), 5.80 – 5.71 (m, 1H, *H*-1´), 4.89 (dd, $^2J_{HH}$ = 12.2 Hz, $^3J_{HH}$ = 3.1 Hz, 1H, *H*-5´a), 4.77 (q, $^3J_{HH}$ = 3.7 Hz, 1H, *H*-4´), 4.61 (dd, $^2J_{HH}$ = 12.2 Hz, $^3J_{HH}$ = 3.9 Hz, 1H, *H*-5´b), 3.92 (s, 3H, -OC*H*$_3$).

Methyl 1-(2´,3´,5´-tri-*O*-benzoyl-β-D-ribofuranosyl)-thiazolcarboxylate 68

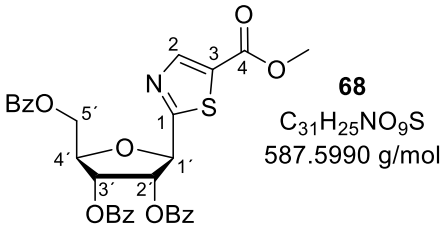

68
$C_{31}H_{25}NO_9S$
587.5990 g/mol

To a solution of **64** (378 mg, 0.56 mmol) in CH_2Cl_2 (10 mL) were added DBU (164 µL, 1.08 mmol) and $CBrCl_3$ (61 µL, 0.62 mmol) dropwise at 0 °C. After the reaction mixture was stirred for 3 h at room temperature, all volatiles were removed under reduced pressure. The residue was taken up in ethyl acetate and washed with sat. aq. NH_4Cl, dried over $MgSO_4$ and all volatiles were removed under reduced pressure. Purification of the crude product on silica gel (petroleum ether/ethyl acetate; 1:1 v/v) provided **68** (252 mg, 75% over 2 steps) as a light-yellow foam.

The analytical data was in accordance with those described.[183]

^{1}*H*-NMR (300 MHz, $CDCl_3$): δ [ppm] = 8.15 (s, 1H, *H*-2), 8.14 – 8.04 (m, 2H, *H*-Ph), 8.04 – 7.95 (m, 2H, *H*-Ph), 7.95 – 7.84 (m, 2H, *H*-Ph), 7.63 – 7.50 (m, 3H, H-Ph), 7.50 – 7.30 (m, 6H, *H*-Ph), 5.95 – 5.83 (m, 2H, *H*-2´, *H*-3´), 5.80 – 5.71 (m, 1H, H-1´), 4.89 (dd, $^2J_{HH}$ = 12.2 Hz, $^3J_{HH}$ = 3.1 Hz, 1H, *H*-5´), 4.77 (q, $^3J_{HH}$ = 3.7 Hz, 1H, *H*-4´), 4.61 (dd, $^2J_{HH}$ = 12.2 Hz, $^3J_{HH}$ = 3.9 Hz, 1H, *H*-5´), 3.92 (s, 3H, -OC*H*$_3$).

2,5-Anhydro-D-allonthioamid-3,4,6-tri-*O*-benzoyl 65

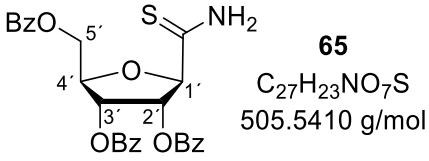

65
$C_{27}H_{23}NO_7S$
505.5410 g/mol

To a solution of **64** (309 mg, 0.65 mmol) in toluene/Et_2O (10:1.5) were added Lawesson's reagent (402 mg, 0.99 mmol) and $BF_3 \cdot Et_2O$ (1.00 mL, 8.10 mmol). The reaction mixture was stirred at 50 °C

for 3 h and then overnight at room temperature. The reaction was quenched by the addition of solid $NaHCO_3$. After all volatiles were removed under reduced pressure, the residue was taken up in CH_2Cl_2 and filtered. Subsequently, the solvent was removed under reduced pressure. Purification of the crude product on silica gel (petroleum ether/ethyl acetate; 4:1 v/v) provided **65** (182 mg, 55%) as a light-yellow foam.

The analytical data was in accordance with those described.[180]

^{1}*H*-NMR (500 MHz, DMSO-d_6): δ [ppm] = 9.32 (br, s, 1H, -NH_2), 8.52 (br, s, 1H, -NH_2), 7.17 (m, 2H, *H*-Ph), 7.14 – 7.07 (m, 2H, *H*-Ph), 7.00 (m, 2H, *H*-Ph), 6.87 – 6.76 (m, 4H, *H*-Ph), 6.72 – 6.55 (m, 6H, *H*-Ph), 5.10 (t, $^3J_{HH}$ = 5.1 Hz, 1H, *H*-2´), 4.85 (t, $^3J_{HH}$ = 5.4 Hz, 1H, *H*-3´), 4.16 (d, $^3J_{HH}$ = 4.9 Hz, 1H, *H*-1´), 3.99 – 3.90 (m, 1H, *H*-4´), 3.88 – 3.74 (m, 2H, *H*-5´).

Ethyl-2-(2´,3´,5´-tri-*O*-benzoyl-β-D-ribofuranosyl)-thiazol-4´-carboxylate 66

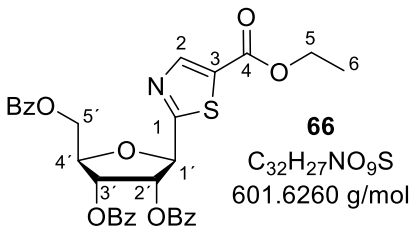

To a solution of **65** (414 mg, 0.82 mmol) in DMF (10 mL) was added $NaHCO_3$ (693 mg, 8.20 mmol) and ethyl bromopyruvate (300 µL, 2.46 mmol) at 0°C. Afterwards the reaction mixture was stirred at 0°C for 5 h. After the reaction mixture was cooled to -15°C a mixture of TFAA (450 µL, 2.46 mmol) and 2,6-lutidine (600 µL, 4.92 mmol) in DMF (2 mL) was added to quench the reaction. The mixture was stirred for 1 h at rt and filtrated to remove the precipitated solid. After all volatiles were removed under reduced pressure the residue was taken up in CH_2Cl_2 and the organic phase was washed with sat. aq. $NaHCO_3$, sat. aq. NaCl, dried over $MgSO_4$ and all volatiles were removed under reduced pressure. Purification of the crude product on silica gel (CH_2Cl_2/MeOH 100:1 v/v) provided **66** (60 mg, 12%) as an orange-yellow oil.

The analytical data was in accordance with those described.[180]

^{1}*H*-NMR (400 MHz, $CDCl_3$): δ [ppm] = 8.13 (s, 1H, *H*-2), 8.08 (m, 2H, *H*-Ph), 8.00 (m, 2H, *H*-Ph), 7.91 (m, 2H, *H*-Ph), 7.60 – 7.52 (m, 3H, *H*-Ph), 7.47 – 7.31 (m, 6H, *H*-Ph), 5.89 (m, 2H, *H*-4´, *H*-3´), 5.75 (d, $^3J_{HH}$ = 4.8 Hz, 1H, *H*-1´), 4.89 (dd, $^2J_{HH}$ = 12.1 Hz, $^3J_{HH}$ = 3.1 Hz, 1H, *H*-5´), 4.79 – 4.73 (m,

1H, *H*-2´), 4.62 (dd, $^{2}J_{HH}$ = 12.2 Hz, $^{3}J_{HH}$ = 4.0 Hz, 1H, *H*-5´), 4.43 – 4.33 (m, 2H, *H*-5), 1.37 (t, $^{3}J_{HH}$ = 7.1 Hz, 3H, *H*-6).

Tiazofurin 61

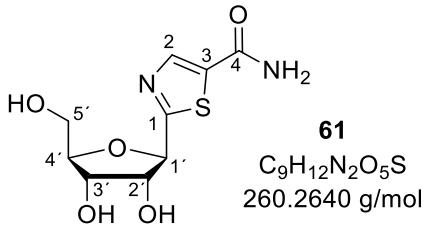

61
$C_9H_{12}N_2O_5S$
260.2640 g/mol

The reaction was carried out according to general procedure IV with the protected nucleoside **66** (252 mg, 0.42 mmol) and 10 mL of 7 M NH_3 in MeOH. Purification on RP_{18} silica gel by automated flash chromatography (H_2O/CH_3CN; 100:0 to 0:100 v/v) provided **61** (76 mg, 87%) as a colorless solid.

The analytical data was in accordance with those described.[183]

^{1}*H*-NMR (500 MHz, D_2O): δ [ppm] = 8.28 (s, 1H, H-2), 5.20 (d, $^{3}J_{HH}$ = 5.4 Hz, 1H, *H*-1´), 4.38 (dd, $^{3}J_{HH}$ = 5.4, 4.9 Hz, 1H, *H*-2´), 4.25 – 4.20 (m, 1H, *H*-3´), 4.19 (dd, $^{3}J_{HH}$ = 5.2, 3.2 Hz, 1H, *H*-4´), 3.89 (dd, $^{2}J_{HH}$ = 12.5 Hz, $^{3}J_{HH}$ = 3.2 Hz, 1H, *H*-5´), 3.79 (dd, $^{2}J_{HH}$ = 12.5 Hz, $^{3}J_{HH}$ = 5.3 Hz, 1H, *H*-5´).

^{13}*C*-NMR (125 MHz, D_2O): δ [ppm] = 170.9 (C-1), 152.1 (C-3), 139.2 (C-4), 126.6 (C-2), 85.9 (C-4´), 80.9 (C-1´), 76.3 (C-2´), 71.5 (C-3´), 63.6 (C-5´).

HRMS (ESI^-): *m/z* = calcd: 283.0359 $[M+Na]^+$, found: 283.0360 $[M+Na]^+$.

5.3.5 Synthesis of nucleoside-5´-monophosphates

T-1106-5´-monophosphate 59

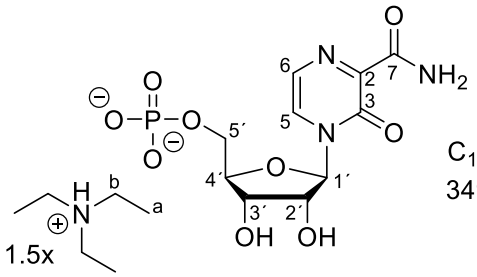

59
$C_{10}H_{12}N_3O_9P^{2-}$
349.1929 g/mol

Step 1: The reaction was carried out according to general procedure V with T-1106 methyl ester **54** (100 mg, 0.35 mmol), proton sponge (150 mg, 0.70 mmol) and $POCl_3$ (127 µL, 1.40 mmol) in

trimethyl phosphate (3 mL) for 15 min. Purification by ion-exchange chromatography using a DEAE-Sephadex® A-25 column (H_2O/1 M TEAB; 100:0 to 0:100 v/v) and RP_{18} flash column chromatography (H_2O/CH_3CN; 100:0 to 0:100 v/v) provided the triethylammonium salt of the monophosphate (148 mg, 74%). **Step 2:** The reaction was carried out according to general procedure IV with the monophosphate (100 mg, 0.18 mmol) and 7 M NH_3 in MeOH (4 mL). Purification on RP_{18} silica gel by automated flash chromatography (H_2O/CH_3CN; 100:0 to 0:100 v/v) provided **59** (91 mg, 93%) as a colorless solid.

The analytical data was in accordance with those described.[120]

^{1}*H*-NMR (600 MHz, D_2O): δ [ppm] = 8.41 (d, $^3J_{HH}$ = 4.26 Hz, 1H, *H*-5), 7.82 (d, $^3J_{HH}$ = 4.27 Hz, 1H, *H*-6), 6.13 (d, $^3J_{HH}$ = 1.65 Hz, 1H, *H*-1´), 4.40 – 4.30 (m, 4.09 – 4.06, 4H, *H*-2´, *H*-3´, *H*-4´, *H*-5´) (dd, $^2J_{HH}$ = 11.85 Hz, $^3J_{HH}$ = 4.94 Hz, 1H, *H*-5´), 3.20 (q, $^3J_{HH}$ = 7.29 Hz, 9H, *H*-b), 1.28 (t, $^3J_{HH}$ = 7.35 Hz, 15H, *H*-a).

^{13}*C*-NMR (150 MHz, D_2O): δ [ppm] = 166.0 (*C*-7), 155.6 (*C*-3), 142.2 (*C*-2), 129.4 (*C*-5), 125.2 (*C*-6), 90.8 (*C*-1´), 82.8 (d, $^3J_{HP}$ = 8.96 Hz, *C*-4´), 74.9 (*C*-2´), 68.1 (*C*-3´), 62.6 (d, $^3J_{HP}$ = 4.78 Hz, *C*-5´).

^{31}*P*-NMR (242 MHz, D_2O): δ [ppm] = 0.83 (s).

HRMS (ESI^-): *m/z* = calcd: 350.0395 $[M-H]^-$, found: 350.0402 $[M-H]^-$.

3´-Fluoro-T-1106-5´-monophosphate 198

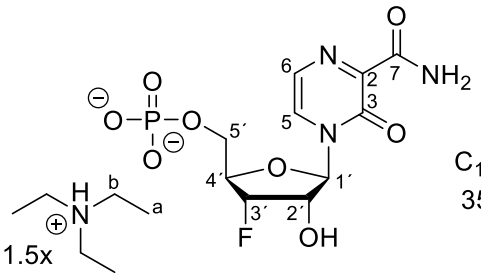

198
$C_{10}H_{11}FN_3O_8P^{2-}$
351.1843 g/mol

The reaction was carried out according to the general procedure V, using 3´-fluoro-T-1106 **41** (180 mg, 0.66 mmol), $POCl_3$ (180 µL, 1.97 mmol) and proton sponge (286 mg, 1.33 mmol) in trimethyl phosphate (6 mL) for 20 min. Purification by ion-exchange chromatography using a DEAE-Sephadex® A-25 column (H_2O/1 M TEAB; 100:0 to 0:100 v/v) and RP_{18} flash column chromatography (H_2O/CH_3CN; 100:0 to 0:100 v/v) provided the triethylammonium salt of **198** (106 mg, 31%) as a colorless solid.

^{1}*H*-NMR (600 MHz, D_2O): *δ* [ppm] = 8.26 (d, $^{3}J_{HH}$ = 4.35 Hz, 1H, *H*-5), 7.69 (d, $^{3}J_{HH}$ = 4.27 Hz, 1H, *H*-6), 6.38 (d, $^{3}J_{HH}$ = 6.60 Hz, 1H, *H*-1´), 5.09 (ddd, $^{2}J_{HF}$ = 54.11 Hz, $^{3}J_{HH}$ = 4.34 Hz, $^{3}J_{HH}$ = 1.82 Hz, 1H, *H*-3´), 4.47 (ddd, $^{2}J_{HF}$ = 24.28 Hz, $^{3}J_{HH}$ = 2.58 Hz, $^{3}J_{HH}$ = 2.13 Hz, 1H, *H*-4´), 4.42 (ddd, $^{2}J_{HF}$ = 21.24 Hz, $^{3}J_{HH}$ = 6.59 Hz, $^{3}J_{HH}$ = 4.30 Hz, 1H, *H*-2´), 4.09 – 4.06 (m, 2H, *H*-5´), 3.18 (q, $^{3}J_{HH}$ = 7.31 Hz, 9H, *H*-b), 1.19 (t, $^{3}J_{HH}$ = 7.35 Hz, 15H, *H*-a).

^{31}*P*-NMR (242 MHz, D_2O): *δ* [ppm] = 2.09 (s).

^{19}*F*-NMR (564 MHz, D_2O): δ [ppm] = -201.7 (m).

HRMS (ESI^+): *m/z* = calcd: 376.0316 $[M+Na]^+$, found: 376.0317 $[M+Na]^+$.

2-Amino-adenosine-5´-monophosphate 206

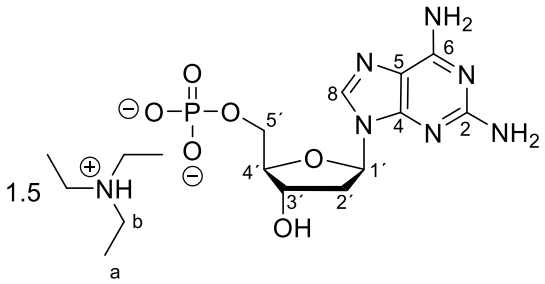

206
$C_{10}H_{13}N_6O_6P^{2-}$
344.2249 g/mol

The reaction was carried out according to the general procedure V, using 2-amino adenosine **207** (220 mg, 0.83 mmol), $POCl_3$ (301 µL, 3.31 mmol) and proton sponge (354 mg, 3.31 mmol) in trimethyl phosphate (1.5 mL) for 2 h. Purification by ion-exchange chromatography using a DEAE-Sephadex® A-25 column (H_2O/1 M TEAB; 100:0 to 0:100 v/v) and RP_{18} flash column chromatography (H_2O/CH_3CN; 100:0 to 0:100 v/v) provided the triethylammonium salt of **206** (202 mg, 49%) as a colorless solid.

^{1}*H*-NMR (300 MHz, D_2O): *δ* [ppm] = 8.08 (s, 1H, *H*-8), 6.25 (t, $^{3}J_{HH}$ = 6.69 Hz, 1H, *H*-1´), 4.70 – 4.66 (m, 1H, *H*-4´), 4.24 – 4.20 (m, 1H, *H*-3´), 4.03 – 4.00 (m, 2H, *H*-5´), 3.16 (q, $^{3}J_{HH}$ = 7.33 Hz, 9H, *H*-b), 2.72 (ddd, $^{2}J_{HH}$ = 14.14 Hz, $^{3}J_{HH}$ = 7.59 Hz, $^{3}J_{HH}$ = 6.06 Hz, 1H, *H*-1´), 2.50 (ddd, $^{2}J_{HH}$ = 14.14 Hz, $^{3}J_{HH}$ = 7.59 Hz, $^{3}J_{HH}$ = 6.06 Hz, 1H, *H*-1´), 1.25 (t, $^{3}J_{HH}$ = 7.37 Hz, 15H, *H*-a).

^{13}*C*-NMR (150 MHz, D_2O): *δ* [ppm] = 158.4 (*C*-6), 155.1(*C*-2), 150.4 (*C*-4), 137.5 (*C*-8), 112.6 (*C*-5), 85.8 (d, $^{3}J_{CP}$ = 8.61 Hz, *C*-4´), 83.2 (*C*-1´), 71.3 (*C*-3´´), 64.5 (d, $^{2}J_{CP}$ = 4.97 Hz, *C*-5´), 46.6 (*C*-b), 38.9 (*C*-2´), 8.17 (*C*-a).

^{31}*P*-NMR (242 MHz, D_2O): *δ* [ppm] = 1.18 (s).

HRMS (ESI$^-$): *m/z* = calcd: 345.0718 [M-H]$^-$, found: 345.0718 [M-H]$^-$.

Remdesivir nucleoside-5´-monophosphate (GS-441524 monophosphate) 221

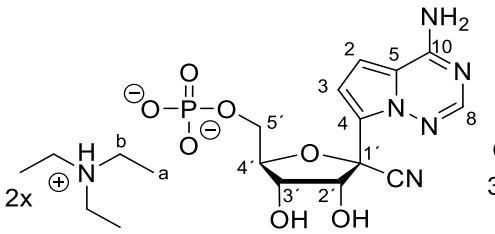

221
$C_{12}H_{12}N_5O_7P^{2-}$
369.2309 g/mol

The reaction was carried out according to the general procedure V, using GS-441524 **220** (84 mg, 0.29 mmol) and $POCl_3$ (52 µL, 0.58 mmol) in trimethyl phosphate (3 mL) for 2 h. Purification by ion-exchange chromatography using a DEAE-Sephadex® A-25 column (H_2O/1 M TEAB; 100:0 to 0:100 v/v) and RP_{18} flash column chromatography (H_2O/CH_3CN; 100:0 to 0:100 v/v) provided the triethylammonium salt of **221** (116 mg, 56%) as a colorless solid.

^{1}*H*-NMR (500 MHz, D_2O): δ [ppm] = 7.91 (s, 1H, H-8), 7.00 (d, $^3J_{HH}$ = 4.67 Hz, 1H, *H*-5), 6.90 (d, 1H, $^3J_{HH}$ = 4.87 Hz, *H*-6), 4.96 (d, $^3J_{HH}$ = 5.54 Hz, 1H, *H*-2´), 4.50 – 4.47 (m, 1H, *H*-4´), 4.43 (dd, $^3J_{HH}$ = 5.74 Hz, $^3J_{HH}$ = 3.54 Hz, 1H, *H*-3´), 3.95 (ddd, $^2J_{HH}$ = 11.95 Hz, $^3J_{HP}$ = 5.81 Hz, $^3J_{HH}$ = 3.90 Hz, 1H, *H*-5´), 3.89 (ddd, $^2J_{HH}$ = 11.66 Hz, $^3J_{HP}$ = 4.91 Hz, $^3J_{HH}$ = 4.01 Hz, 1H, *H*-5´), 3.17 (q, $^3J_{HH}$ = 7.51 Hz, 12H, *H*-b), 1.25 (t, $^3J_{HH}$ = 7.28 Hz, 12H, *H*-a).

^{13}*C*-NMR (125 MHz, D_2O): δ [ppm] = 156.1 (*C*-10), 147.7 (*C*-8), 123.5 (*C*-4), 117.8 (C-1´-*C*N), 117.0 (*C*-5), 111.4 (*C*-2), 102.7 (*C*-1), 86.0 (d, $^2J_{CP}$ = 8.89 Hz, *C*-4´), 76.9 (C-2´), 75.2 (*C*-1´), 70.8 (*C*-3´), 63.9 (d, $^2J_{CP}$ = 4.26 Hz, *C*-5´), 47.0 (*C*-b), 8.6 (*C*-a).

^{31}*P*-NMR (161 MHz, D_2O): δ [ppm] = 3.84 (s).

HRMS (ESI$^-$): *m/z* = calcd: 370.0558 [M-H]$^-$, found: 370.0558 [M-H]$^-$.

JD-004-3´-monophosphate 208

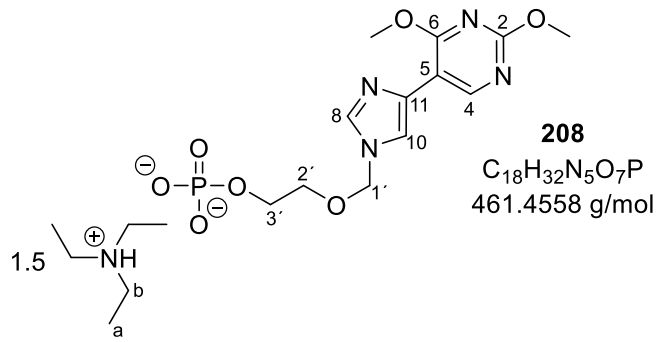

The reaction was carried out according to the general procedure V, using 2-((4-(2,4-dimethoxypyrimidin-5-yl)-1*H*-imidazol-1-yl)methoxy)ethan-1-ol **207** (42 mg, 0.15 mmol), $POCl_3$ (55 µL, 0.60 mmol) and proton sponge (64 mg, 0.30 mmol) in trimethyl phosphate (1.5 mL) for 1 h. Purification on RP_{18} silica gel with automated flash chromatography (H_2O/CH_3CN; 100:0 to 0:100 v/v) yielded the triethylammonium salt of **208** (65 mg, 81%) as a colorless solid.

^{1}*H*-NMR (600 MHz, D_2O): δ [ppm] = 8.48 (s, 1H, *H*-4), 8.18 (d, $^4J_{HH}$ = 1.05 Hz, 1H, *H*-8), 7.69 (d, $^4J_{HH}$ = 1.26 Hz, 1H, *H*-10), 5.55 (s, 2H, *H*-1´), 4.02 (s, 3H, -OC*H*$_3$), 4.01 – 4.00 (m, 2H, *H*-2´), 3.96 (s, 3H, -OC*H*$_3$), 3.78 – 3.77 (m, 2H, *H*-3´), 3.19 (q, $^3J_{HH}$ = 7.42 Hz, 9H, *H*-b), 1.27 (t, $^3J_{HH}$ = 7.39 Hz, 15H, *H*-a).

^{13}*C*-NMR (150 MHz, D_2O): δ [ppm] = 167.1 (*C*-6), 163.5 (*C*-2), 153.9 (*C*-4), 137.7 (*C*-8), 130.9 (*C*-11), 119.0 (*C*-10), 107.5 (*C*-5), 76.9 (*C*-1´), 68.5 (d, $^2J_{CP}$ = 7.76 Hz, *C*-3´), 64.1 (d, $^3J_{CP}$ = 5.09 Hz, *C*-2´), 55.1 (-O*C*H$_3$), 54.4 (-O*C*H$_3$), 46.6 (*C*-b), 8.2 (*C*-a).

^{31}*P*-NMR (242 MHz, D_2O): δ [ppm] = 0.41 (s).

HRMS (ESI$^-$): *m/z* = calcd: 360.0835 [M-H]$^-$, found: 360.0835 [M-H]$^-$.

5.3.6 Synthesis of nucleoside-5´-diphosphates

T-1106-5´-diphosphate 58

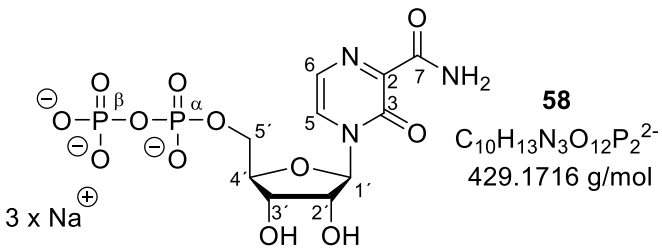

T-1106-5´monophosphate **59** (30 mg, 0.05 mmol) was suspended in CH_3CN (1 mL) before Et_3N (90 µL, 0.65 mmol) and TFAA (75 µL, 0.54 mmol) were added dropwise. After the reaction mixture was stirred for 10 min at room temperature, all volatiles were removed under reduced pressure, and the residue was dissolved again in CH_3CN (1 mL). The solution was then treated with Et_3N (75 µL, 0.54 mmol) and 1-methylimidazole (25 µL, 0.32 mmol). After the reaction mixture was stirred for another 10 min at room temperature, it was added dropwise via a syringe pump (0.2 mL/min) to a solution of monobasic tetra-*n*-butylammonium phosphate (406 µL, 0.16 mmol, 0.4 M solution in CH_3CN) in CH_3CN (1 mL). Subsequently, the reaction mixture was stirred for 30 minutes at room temperature before all volatiles were removed under reduced pressure. The residue was taken up in water and washed three times with CH_2Cl_2. The aqueous phase was then concentrated under reduced pressure, and the residue was purified by automated column chromatography, first using a DEAE-Sephadex® A-25 column (H_2O/1 M TEAB; 100:0 to 0:100 v/v) and then by RP_{18} flash column chromatography (H_2O/CH_3CN; 100:0 to 0:100 v/v), which provided the triethylammonium salt of **58**. The counter ions were exchanged to sodium by dissolving the triethylammonium salt in a minimum amount of water before adding a solution of 0.2 M $NaClO_4$ in acetone (40 mL). The suspension was centrifuged, the supernatant was discarded, and the pellet was washed with acetone twice to yield the sodium salt of **58** (18 mg, 80%) as a colorless solid.

The analytical data was in accordance with those described.[120]

^{1}*H*-NMR (400 MHz, D_2O): δ [ppm] = 8.49 (d, $^3J_{HH}$ = 4.37 Hz, 1H, *H*-5), 7.88 (d, $^3J_{HH}$ = 4.28 Hz, 1H, *H*-6), 6.08 (d, $^3J_{HH}$ = 1.76 Hz, 1H, *H*-1´), 4.46 (ddd, $^2J_{HH}$ = 12.1 Hz, $^3J_{HP}$ = 4.41 Hz, $^3J_{HH}$ = 2.01 Hz, 1H, *H*-5´), 4.42 – 4.35 (m, 3H, *H*-2´, *H*-3´, *H*-4´), 4.27 (ddd, $^2J_{HH}$ = 12.2 Hz, $^3J_{HP}$ = 5.37 Hz, $^3J_{HH}$ = 2.09 Hz, 1H, *H*-5´).

^{31}*P*-NMR (162 MHz, D_2O): δ [ppm] = -10.59 (d, $^2J_{PP}$ = 20.49 Hz, *P*-α), -11.32 (d, $^2J_{PP}$ = 20.55 Hz, *P*-β).

Remdesivir nucleoside-5´-diphosphate (GS-441524 diphosphate) 219

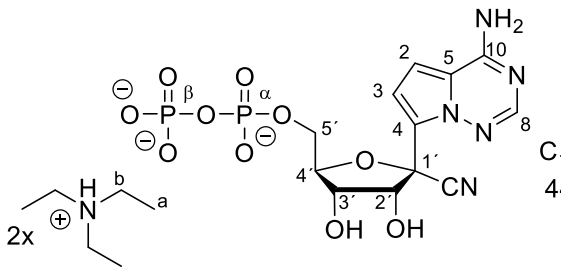

219
$C_{12}H_{12}N_5O_{10}P_2^{3-}$
448.2022 g/mol

GS-441524 monophosphate **221** (60 mg, 0.16 mmol) was suspended in CH_3CN (3 mL) before Et_3N (269 µL, 1.94 mmol) and TFAA (224 µL, 1.62 mmol) were added dropwise. After the reaction mixture was stirred for 10 min at room temperature, all volatiles were removed under reduced pressure, and the residue was dissolved again in CH_3CN (3 mL). The solution was then treated with Et_3N (224 µL, 1.62 mmol) and 1-methylimidazole (77 µL, 0.97 mmol). After the reaction mixture was stirred for another 10 min at room temperature, it was added dropwise via a syringe pump (0.2 mL/min) to a solution of monobasic tetra-*n*-butylammonium phosphate (1.21 mL, 0.97 mmol, 0.4 M solution in CH_3CN) in CH_3CN (2 mL). Subsequently, the reaction mixture was stirred for 30 min at room temperature before all volatiles were removed under reduced pressure. The residue was taken up in water and washed three times with CH_2Cl_2. The aqueous phase was then concentrated under reduced pressure, and the residue was purified by automated column chromatography, using a DEAE-Sephadex® A-25 column (H_2O/1 M TEAB; 100:0 to 0:100 v/v), and then by RP_{18} flash column chromatography (H_2O/CH_3CN; 100:0 to 0:100 v/v), which provided the triethylammonium salt of **219** (64 mg, 89%) as a colorless solid.

^{1}*H*-NMR (500 MHz, D_2O): δ [ppm] = 7.96 (s, 1H, H-8), 7.06 (d, $^3J_{HH}$ = 4.75 Hz, 1H, *H*-5), 6.95 (d, 1H, $^3J_{HH}$ = 4.80 Hz, *H*-6), 4.99 (d, $^3J_{HH}$ = 5.05 Hz, 1H, *H*-2´), 4.55 – 4.52 (m, 2H, *H*-4´, *H*-3´), 4.18 (ddd, $^2J_{HH}$ = 11.91 Hz, $^3J_{HP}$ = 6.48 Hz, $^3J_{HH}$ = 3.01 Hz, 1H, *H*-5´), 4.08 (ddd, $^2J_{HH}$ = 11.78 Hz, $^3J_{HP}$ = 5.15 Hz, $^3J_{HH}$ = 2.79 Hz, 1H, *H*-5´), 3.20 (q, $^3J_{HH}$ = 8.08 Hz, 12H, *H*-b), 1.28 (t, $^3J_{HH}$ = 7.25 Hz, 18H, *H*-a).

^{31}*P*-NMR (162 MHz, D_2O): δ [ppm] = -9.47 (d, $^2J_{PP}$ = 21.9 Hz, *P*-β), -11.3 (d, $^2J_{PP}$ = 21.0 Hz, *P*-α).

5.3.7 Synthesis of nucleoside-5´-triphosphates

T-1106-5´-triphosphate 14

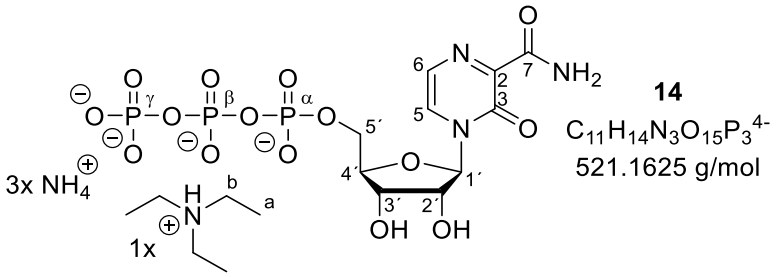

Step 1: The reaction was carried out according to general procedure VI with T-1106 methyl ester **54** (100 mg, 0.35 mmol), proton sponge (150 mg, 0.70 mmol) and $POCl_3$ (96 µL, 1.05 mmol) in trimethyl phosphate (5 mL) for 15 min, followed by the addition of tributylammonium pyrophosphate (477 mg, 0.87 mmol) and tributylamine (576 µL, 2.11 mmol) in CH_3CN (1 mL) for 2 h. Purification by ion-exchange chromatography using a DEAE-Sephadex® A-25 column (H_2O/1 M TEAB; 100:0 to 0:100 v/v) and RP_{18} flash column chromatography (H_2O/CH_3CN; 100:0 to 0:100 v/v) provided the triethylammonium salt of the triphosphate methyl ester (135 mg, 41%). **Step 2:** The reaction was carried out according to general procedure IV with the triphosphate methyl ester (135 mg, 0.14 mmol) and 7 M NH_3 in MeOH (4 mL). Purification on RP_{18} silica gel by automated flash chromatography (H_2O/CH_3CN; 100:0 to 0:100 v/v) provided **14** (122 mg, 90%) as a colorless solid.

The analytical data was in accordance with those described.[120]

^{1}*H*-NMR (600 MHz, D_2O): δ [ppm] = 8.37 (d, $^3J_{HH}$ = 4.22 Hz, 1H, *H*-5), 7.87 (d, $^3J_{HH}$ = 4.25 Hz, 1H, *H*-6), 6.15 (d, $^3J_{HH}$ = 1.97 Hz, 1H, *H*-1´), 4.49 (dd, $^2J_{HH}$ = 12.1 Hz, $^3J_{HH}$ = 1.24 Hz, 1H, *H*-5´), 4.42 – 4.37 (m, 3H, *H*-2´, *H*-3´, *H*-4´), 4.32 (dd, $^2J_{HH}$ = 12.2 Hz, $^3J_{HH}$ = 2.04 Hz, 1H, *H*-5´), 3.21 (q, $^3J_{HH}$ = 7.48 Hz, 18H, *H*-b), 1.30 (t, $^3J_{HH}$ = 7.48 Hz, 27H, *H*-a).

^{13}*C*-NMR (150 MHz, D_2O): δ [ppm] = 167.1 (*C*-7), 155.5 (*C*-3), 141.7 (*C*-2), 129.4 (*C*-5), 125.4 (*C*-6), 89.5 (*C*-1´), 82.7 (d, $^3J_{CP}$ = 9.31 Hz, *C*-4´), 74.9 (*C*-2´), 68.0 (*C*-3´), 63.8 (d, $^2J_{CP}$ = 5.70 Hz, *C*-5´), 45.8 (*C*-b), 8.21 (*C*-a).

^{31}*P*-NMR (202 MHz, D_2O): δ [ppm] = -9.69 (d, $^2J_{PP}$ = 19.6 Hz, P-γ), -10.2 (d, $^2J_{PP}$ = 20.1 Hz, P-α), -22.0 (t, $^2J_{PP}$ = 20.1 Hz, *P*-β).

2´-*C*-Methyl-T-1106-5´-triphosphate 15

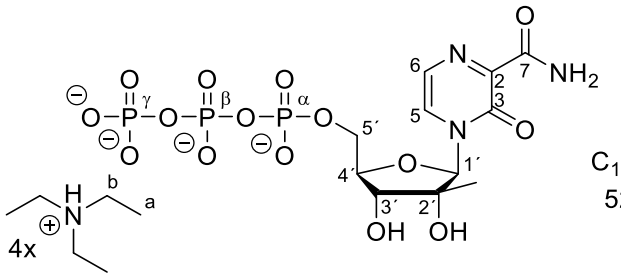

15
$C_{11}H_{14}N_3O_{15}P_3^{4-}$
521.1625 g/mol

The reaction was carried out according to the general procedure VI with 2'-*C*-methyl-T-1106 **49** (50 mg, 0.18 mmol), proton sponge (130 mg, 0.61 mmol) and $POCl_3$ (64 µL, 0.70 mmol) in trimethyl phosphate (3 mL) for 15 min, followed by the addition of tributylammonium pyrophosphate (410 mg, 0.46 mmol) and tributylamine (250 µL, 1.05 mmol) in CH_3CN (1 mL) for 2 h. Purification by ion-exchange chromatography using a DEAE-Sephadex® A-25 column (H_2O/1 M TEAB; 100:0 to 0:100 v/v) and RP_{18} flash column chromatography (H_2O/CH_3CN; 100:0 to 0:100 v/v) provided the triethylammonium salt of **16** (90 mg, 55%) as a colorless solid.

The analytical data was in accordance with those described.[119]

2´-Fluoro-2´-*C*-methyl-T-1106-5´-triphosphate 16

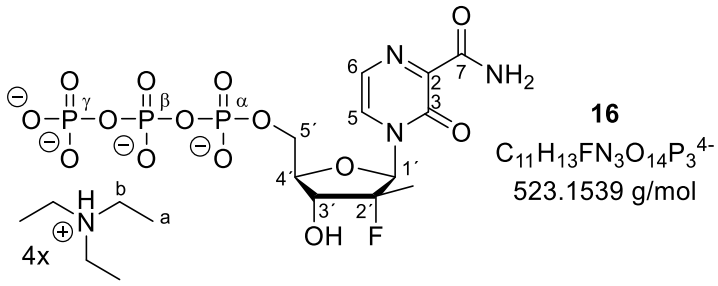

16
$C_{11}H_{13}FN_3O_{14}P_3^{4-}$
523.1539 g/mol

The reaction was carried out according to the general procedure VI with 2'-fluoro-2'-*C*-methyl-T-1106 **51** (87 mg, 0.30 mmol), proton sponge (130 mg, 0.61 mmol) and $POCl_3$ (55 µL, 0.61 mmol) in trimethyl phosphate (5 mL) for 15 min, followed by the addition of tributylammonium pyrophosphate (683 mg, 0.76 mmol) and tributylamine (432 µL, 1.82 mmol) in CH_3CN (1 mL) for 2 h. Purification by ion-exchange chromatography using a DEAE-Sephadex® A-25 column (H_2O/1 M TEAB; 100:0 to 0:100 v/v) and RP_{18} flash column chromatography (H_2O/CH_3CN; 100:0 to 0:100 v/v) provided the triethylammonium salt of **16** (119 mg, 42%) as a colorless solid.

^{1}H-NMR (600 MHz, CD_3OD): δ [ppm] = 7.84 (dd, $^{3}J_{HH}$ = 4.44 Hz, $^{5}J_{HH}$ = 2.51 Hz, 1H, *H*-5), 7.61 (d, $^{3}J_{HH}$ = 4.23 Hz, 1H, *H*-6), 6.49 (d, $^{3}J_{HF}$ = 18.5 Hz, 1H, *H*-1‘), 4.36 – 4.27 (m, 3H, *H*-3´, *H*-4‘, *H*-5´), 4.21 (dd, $^{2}J_{HH}$ = 11.7 Hz, $^{3}J_{HH}$ = 2.98 Hz, 1H, *H*-5‘), 3.11 (q, $^{3}J_{HH}$ = 7.33 Hz, 24H, *H*-b), 1.50 (d, $^{3}J_{HF}$ = 22.3 Hz, 3H, 2´-C-CH_3), 1.22 (t, $^{3}J_{HH}$ = 7.25 Hz, 36H, *H*-a).

^{13}C-NMR (150 MHz, CD_3OD): δ [ppm] = 166.1 (*C*-7), 155.0 (*C*-3), 144.8 (*C*-2), 131.4 (d, $^{4}J_{CF}$ = 4.25 Hz, *C*-5), 124.7 (*C*-6), 100.8 (d, $^{1}J_{CF}$ = 191.9 Hz, *C*-2´), 89.4 (d, $^{2}J_{CF}$ = 15.0 Hz, *C*-1´), 82.9 (d, $^{3}J_{CP}$ = 9.04 Hz, *C*-4´), 74.4 (d, $^{2}J_{CF}$ = 17.1 Hz, *C*-3´), 60.0 (d, $^{2}J_{CP}$ = 5.71 Hz, *C*-5´), 47.4 (*C*-b), 18.4 (d, $^{2}J_{CF}$ = 25.4 Hz, 2´-C-*C*H_3) 9.1 (*C*-a).

^{19}F-NMR (564 MHz, CD_3OD): δ [ppm] = -167.8 (m).

^{31}P-NMR (242 MHz, CD_3OD): δ [ppm] = -10.6 (d, $^{3}J_{PP}$ = 20.9 Hz, *P*-γ), -11.2 (d, $^{3}J_{PP}$ = 21.7 Hz, *P*-α), -23.9 (t, $^{3}J_{PP}$ = 21.6 Hz, *P*-β).

HRMS (MALDI$^-$): *m/z* = calcd: 525.9834 $[M-H]^-$, found: 525.9954 $[M-H]^-$.

3´-Deoxy-T-1106-5´-triphosphate 17

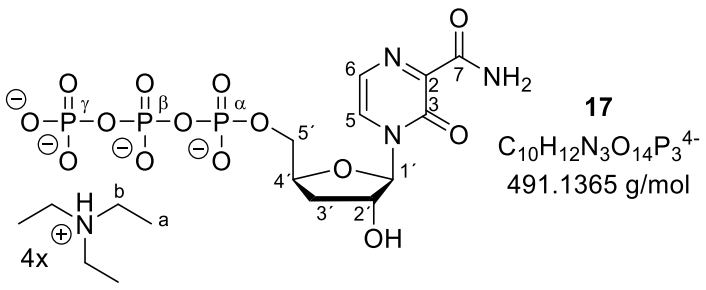

17

$C_{10}H_{12}N_3O_{14}P_3^{4-}$

491.1365 g/mol

The reaction was carried out according to the general procedure VI with 3´-deoxy-T-1106 **40** (29 mg, 0.10 mmol), proton sponge (45 mg, 0.21 mmol) and $POCl_3$ (38 µL, 0.42 mmol) in 2 mL trimethyl phosphate for 15 min. Followed by the addition of tributyl ammonium pyrophosphate (143 mg, 0.26 mmol) and tributylamine (173 µL, 0.60 mmol) in CH_3CN (1.0 mL) for 2 h. Purification by ion-exchange chromatography using a DEAE-Sephadex® A-25 column (H_2O/1 M TEAB; 100:0 to 0:100 v/v) and RP_{18} flash column chromatography (H_2O/CH_3CN; 100:0 to 0:100) provided the triethylammonium salt of **17** (45 mg, 38%) as a colorless solid.

^{1}H-NMR (500 MHz, CD_3OD-d_4): δ [ppm] = 8.55 (d, $^{3}J_{HH}$ = 4.16 Hz, 1H, *H*-5), 7.88 (d, $^{3}J_{HH}$ = 4.13 Hz, 1H, *H*-6), 5.95 (s, 1H, *H*-1‘), 4.73 – 4.64 (m, 1H, *H*-4´), 4.56 – 4.48 (m, 1H, *H*-2´), 4.42 – 4.40 (m,

1H, *H*-5´), 3.54 – 3.52 (m, 1H, *H*-5´), 3.22 (q, $^3J_{HH}$ = 7.3 Hz, 24H, *H*-b), 2.26 – 2.12 (m, 1H, *H*-3´), 2.05 – 2.95 (m, 1H, *H*-3´), 1.30 (t, $^3J_{HH}$ = 7.3 Hz, 36H, *H*-a).

^{31}*P*-NMR (162 MHz, CD_3OD-d_4): δ [ppm] = -9.97 (d, $^2J_{PP}$ = 20.5 Hz, *P*-γ), -11.0 (d, $^2J_{PP}$ = 20.5 Hz, *P*-α), -23.1 (t, $^2J_{PP}$ = 21.3 Hz, *P*-β).

3´-Fluoro-T-1106-5´-triphosphate 18

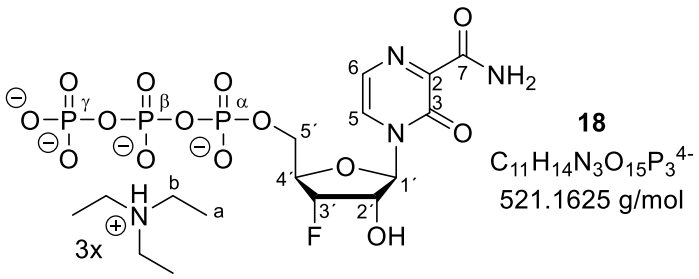

The reaction was carried out according to general procedure VI with 3'-fluoro-T-1106 **41** (92 mg, 0.34 mmol), proton sponge (144 mg, 0.67 mmol) and $POCl_3$ (61 µL, 0.67 mmol) in trimethyl phosphate (5 mL) for 15 min, followed by the addition of tributylammonium pyrophosphate (760 mg, 0.84 mmol) and tributylamine (522 µL, 2.02 mmol) in CH_3CN (1 mL) for 2 h. Purification by ion-exchange chromatography using a DEAE-Sephadex® A-25 column (H_2O/1 M TEAB; 100:0 to 0:100 v/v) and RP_{18} flash column chromatography (H_2O/CH_3CN; 100:0 to 0:100 v/v) provided the triethylammonium salt of **18** (143 mg, 52%) as a colorless solid.

^{1}*H*-NMR (600 MHz, CD_3OD): *δ* [ppm] = 8.33 (d, $^3J_{HH}$ = 4.32 Hz, 1H, *H*-5), 7.80 (d, $^3J_{HH}$ = 4.23 Hz, 1H, *H*-6), 6.49 (d, $^3J_{HH}$ = 7.36 Hz, 1H, *H*-1'), 5.33 (ddd, $^2J_{HF}$ = 54.0 Hz, $^3J_{HH}$ = 3.98 Hz, $^3J_{HH}$ = 0.66 Hz, 1H, *H*-3'), 4.59 (ddd, $^3J_{HF}$ = 23.3 Hz, $^3J_{HH}$ = 7.53 Hz, $^3J_{HH}$ = 4.17 Hz, 1H, *H*-2'), 4.57 – 4.52 (m, 1H, *H*-4'), 4.37 (ddd, $^3J_{HH}$ = 11.8 Hz, $^3J_{HH}$ = 5.95 Hz, $^3J_{HH}$ = 1.73 Hz, 1H, *H*-5'), 4.26 (ddd, $^2J_{HH}$ = 11.6 Hz, $^3J_{HH}$ = 2.40 Hz, $^3J_{HH}$ = 2.26 Hz, 1H, *H*-5'), 3.19 (q, $^3J_{HH}$ = 7.37 Hz, 18H, *H*-b), 1.31 (t, $^3J_{HH}$ = 7.28 Hz, 27H, *H*-a).

^{13}*C*-NMR (150 MHz, CD_3OD): *δ* [ppm] = 166.2 (*C*-7), 157.3 (*C*-3), 144.8 (C-2), 130.6 (C-5), 126.0 (C-6), 94.1 (d, $^1J_{CF}$ = 184.1 Hz, *C*-3´), 88.3 (*C*-1´) 81.2 (dd, $^2J_{CF}$ = 24.1 Hz, $^3J_{CP}$ = 9.23 Hz, *C*-4´), 79.9 (d, $^2J_{CF}$ = 16.3 Hz, *C*-2´), 66.3 (dd, $^3J_{CF}$ = 21.7 Hz, $^2J_{CP}$ = 5.17 Hz, *C*-5´), 46.6 (*C*-b), 8.20 (*C*-a).

^{19}*F*-NMR (154 MHz, CD_3OD): *δ* [ppm] = -201.1 (m).

^{31}P-NMR (242 MHz, CD_3OD): δ [ppm] = -9.29 (d, $^3J_{PP}$ = 21.2 Hz, P-γ), -10.5 (d, $^3J_{PP}$ = 22.2 Hz, P-α), -22.7 (t, $^3J_{PP}$ = 21.2 Hz, *P*-β).

HRMS (MALDI$^-$): *m/z* = calcd: 511.9678 $[M-H]^-$, found: 511.9865 $[M-H]^-$.

3´-Azido-T-1106-5´-triphosphate 19

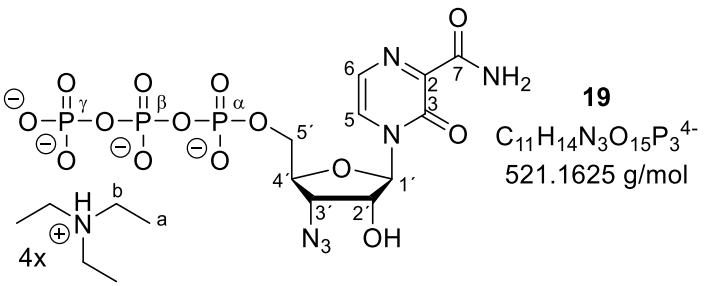

The reaction was carried out according to the general procedure VI with 3'-azido-T-1106 **42** (80 mg, 0.27 mmol), proton sponge (116 mg, 0.54 mmol) and $POCl_3$ (71 µL, 0.81 mmol) in trimethyl phosphate (2 mL) for 15 min, followed by the addition of tributylammonium pyrophosphate (609 mg, 0.68 mmol) and tributylamine (382 µL, 1.62 mmol) in CH_3CN (1 mL) for 2 h. Purification by ion-exchange chromatography using a DEAE-Sephadex® A-25 column (H_2O/1 M TEAB; 100:0 to 0:100 v/v) and RP_{18} flash column chromatography (H_2O/CH_3CN; 100:0 to 0:100 v/v) provided the triethylammonium salt of **19** (108 mg, 69%) as a colorless solid.

^1H-NMR (600 MHz, D_2O): δ [ppm] = 8.33 (d, $^3J_{HH}$ = 3.99 Hz, 1H, *H*-5), 7.85 (d, $^3J_{HH}$ = 3.87 Hz, 1H, *H*-6), 6.17 (d, $^3J_{HH}$ = 2.74 Hz, 1H, *H*-1´), 4.60 (dd, $^3J_{HH}$ = 5.25 Hz, $^3J_{HH}$ = 2.96 Hz, 1H, *H*-2´), 4.48 – 4.44 (m, 2H, *H*-4´, *H*-5´), 4.32 – 4.27 (m, *H*-3´, *H*-5´), 3.21 (q, $^3J_{HH}$ = 7.45 Hz, 24H, *H*-b), 1.28 (t, $^3J_{HH}$ = 7.25 Hz, 36H, *H*-a).

^{13}C-NMR (150 MHz, D_2O): δ [ppm] = 166.3 (*C*-7), 155.8 (*C*-3), 142.3 (*C*-2), 129.1 (*C*-5), 125.4 (*C*-6), 90.4 (*C*-1´), 81.8 (d, $^3J_{CP}$ = 9.24 Hz, *C*-2´), 75.5 (*C*-4´), 64.1 (d, $^2J_{CP}$ = 5.60 Hz, *C*-5´), 59.2 (*C*-3´), 46.6 (*C*-b), 8.20 (*C*-a).

^{31}P-NMR (242 MHz, D_2O): δ [ppm] = -11.0 (d, $^2J_{PP}$ = 19.8 Hz, *P*-γ), -11.6 (d, $^2J_{PP}$ = 19.1 Hz, *P*-α), -23.4 (t, $^2J_{PP}$ = 19.4 Hz, *P*-β).

HRMS (MALDI$^-$): *m/z* = calcd: 534.9786 $[M-H]^-$, found: 534.9955 $[M-H]^-$.

6-Methyl-T-1106-5´-triphosphate 132

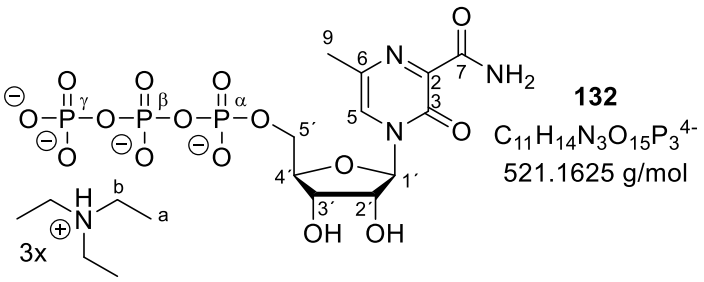

132
$C_{11}H_{14}N_3O_{15}P_3^{4-}$
521.1625 g/mol

The reaction was carried out according to the general procedure VI with 6-methyl-T-1106 **131** (29 mg, 0.10 mmol), proton sponge (45 mg, 0.21 mmol) and $POCl_3$ (38 µL, 0.42 mmol) in trimethyl phosphate (2 mL) for 15 min, followed by the addition of tributylammonium pyrophosphate (143 mg, 0.26 mmol) and tributylamine (173 µL, 0.60 mmol) in CH_3CN (1 mL) for 2 h. Purification by ion-exchange chromatography using a DEAE-Sephadex® A-25 column (H_2O/1 M TEAB; 100:0 to 0:100 v/v) and RP_{18} flash column chromatography (H_2O/CH_3CN; 100:0 to 0:100 v/v) provided the triethylammonium salt of **132** (45 mg, 38%) as a colorless solid.

^{1}*H*-NMR (600 MHz, D_2O): *δ* [ppm] = 8.20 (s, 1H, *H*-5), 6.13 (d, $^3J_{HH}$ = 2.22 Hz, 1H, *H*-1´), 4.49 – 4.30 (m, 5H, *H*-2´, *H*-3´, *H*-4´, *H*-5´), 3.21 (q, $^3J_{HH}$ = 7.40 Hz, 18H, *H*-b), 2.44 (s, 3H, *H*-9), 1.29 (t, $^3J_{HH}$ = 7.36 Hz, 27H, *H*-a).

^{13}*C*-NMR (150 MHz, D_2O): *δ* [ppm] = 166.1 (*C*-7), 154.9 (*C*-3), 141.0 (*C*-2), 134.9 (*C*-5), 127.0 (*C*-6), 90.6 (*C*-1´), 82.7 (d, $^3J_{CP}$ = 9.31 Hz, *C*-4´), 75.0 (*C*-2´), 67.9 (*C*-3´), 63.7 (d, $^2J_{PP}$ = 5.27 Hz, *C*-5´), 46.6 (*C*-b), 19.0 (*C*-9), 8.2 (*C*-a).

^{31}*P*-NMR (121 MHz, D_2O): *δ* [ppm] = -10.7 (d, $^2J_{PP}$ = 19.7 Hz, *P*-γ), -11.7 (d, $^2J_{PP}$ = 20.1 Hz, *P*-α), -23.3 (t, $^2J_{PP}$ = 20.0 Hz, *P*-β).

HRMS (MALDI$^-$): *m/z* = calcd: 523.9897 $[M-H]^-$, found: 524.0027 $[M-H]^-$.

6-Methyl-2´-*C*-methyl-T-1106-5´-triphosphate 135

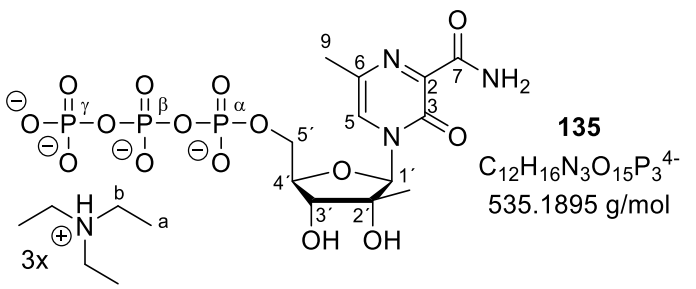

135
$C_{12}H_{16}N_3O_{15}P_3^{4-}$
535.1895 g/mol

The reaction was carried out according to the general procedure VI with 6-methyl-2′-C-methyl-T-1106 **134** (25 mg, 0.08 mmol), proton sponge (35 mg, 0.17 mmol) and $POCl_3$ (30 µL, 0.33 mmol) in trimethyl phosphate (1 mL) for 15 min, followed by the addition of tributylammonium pyrophosphate (114 mg, 0.21 mmol) and tributylamine (138 µL, 0.50 mmol) in CH_3CN (1 mL) for 2 h. Purification by ion-exchange chromatography using a DEAE-Sephadex® A-25 column (H_2O/1 M TEAB; 100:0 to 0:100 v/v) and RP_{18} flash column chromatography (H_2O/CH_3CN; 100:0 to 0:100 v/v) provided the triethylammonium salt of **135** (37 mg, 47%) as a colorless solid.

^{1}*H*-NMR (400 MHz, D_2O): δ [ppm] = 8.20 (s, 1H, *H*-5), 6.34 (s, 1H, *H*-1′), 4.45 – 4.33 (m, 2H, *H*-5′), 4.26 (bs, 2H, H-3′, H-4′), 3.21 (q, $^3J_{HH}$ = 7.40 Hz, 18H, *H*-b), 2.45 (s, 1H, *H*-9), 1.29 (t, $^3J_{HH}$ = 7.36 Hz, 27H, *H*-a) 1.14 (s, 1H, 2′-C-CH_3).

^{13}*C*-NMR (100 MHz, D_2O): δ [ppm] = 166.1 (*C*-7), 154.7 (*C*-3), 141.8 (*C*-2), 134.9 (*C*-5), 126.9 (*C*-6), 91.8 (*C*-1′), 81.1 (d, $^3J_{CP}$ = 9.40 Hz, *C*-4′), 79.7 (*C*-2′), 70.6 (*C*-3′), 58.9 (*C*-5′), 46.6 (*C*-b), 19.0 (*C*-9), 18.9 (2′-C-*C*H_3) 8.2 (*C*-a).

^{31}*P*-NMR (161 MHz, D_2O): δ [ppm] = -6.40 (d, $^2J_{PP}$ = 21.4 Hz, *P*-γ), -11.6 (d, $^2J_{PP}$ = 19.9 Hz, *P*-α), -22.5 (t, $^2J_{PP}$ = 20.6 Hz, *P*-β).

HRMS (MALDI$^-$): *m/z* = calcd: 538.0034 $[M-H]^-$, found: 538.0194 $[M-H]^-$.

Tiazofurin-5′-triphosphate 69

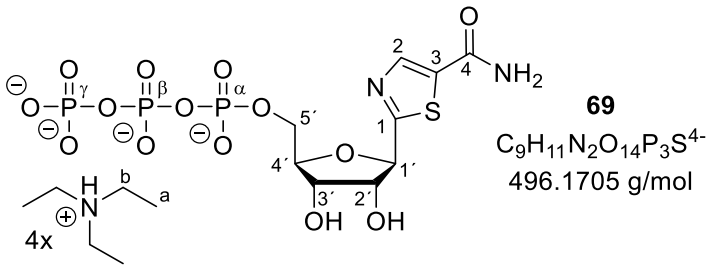

69
$C_9H_{11}N_2O_{14}P_3S^{4-}$
496.1705 g/mol

The reaction was carried out according to the general procedure VI with Tiazofurin **61** (100 mg, 0.38 mmol), proton sponge (162 mg, 0.76 mmol) and $POCl_3$ (69 µL, 0.76 mmol) in trimethyl phosphate (5 mL) for 30 min, followed by the addition of tributylammonium pyrophosphate (521 mg, 0.95 mmol) and tributylamine (620 µL, 2.28 mmol) in CH_3CN (1.9 mL) for 30 min. Purification by ion-exchange chromatography using a DEAE-Sephadex® A-25 column (H_2O/1 M TEAB; 100:0 to 0:100 v/v) and RP_{18} flash column chromatography (H_2O/CH_3CN; 100:0 to 0:100 v/v) provided the triethylammonium salt of **69** (151 mg, 53%) as a colorless solid.

^{1}H-NMR (500 MHz, MeOD-d_4): δ [ppm] = 8.17 (s, 1H, *H*-2), 5.04 (d, $^{3}J_{HH}$ = 5.73 Hz, 1H, *H*-1´), 4.35 (dd, $^{3}J_{HH}$ = 5.11, $^{3}J_{HH}$ = 3.89 Hz, 1H, *H*-3´), 4.31 – 4.27 (m, 1H, *H*-2´), 4.27 – 4.16 (m, 3H, *H*-4´, *H*-5´), 3.18 (q, $^{3}J_{HH}$ = 7.36 Hz, 24H, *H*-b), 1.30 (t, $^{3}J_{HH}$ = 7.34 Hz, 36H, *H*-a).

^{13}C-NMR (125 MHz, MeOD-d_4): δ [ppm] = 173.8 (*C*-4), 150.7 (*C*-3), 125.8 (*C*-2), 85.4 (*C*-2´), 82.9 (*C*-1´), 78.8 (*C*-3´), 72.9 (*C*-4´), 66.8 (d, $^{2}J_{CP}$ = 5.2 Hz, *C*-5´), 46.5 (*C*-b), 9.1 (*C*-a).

^{31}P-NMR (162 MHz, MeOD-d_4): δ [ppm] = -10.4 (d, $^{2}J_{PP}$ = 21.0 Hz, *P*-γ), -11.2 (d, $^{2}J_{PP}$ = 20.9 Hz, *P*-α), -23.7 (t, $^{2}J_{PP}$ = 21.3 Hz, *P*-β).

HRMS (MALDI^{-}): *m/z* = calcd: 498.9384 $[M-H]^{-}$, found: 498.9484 $[M-H]^{-}$.

Remdesivir nucleoside-5´-triphosphate (GS-441524 triphosphate) 6

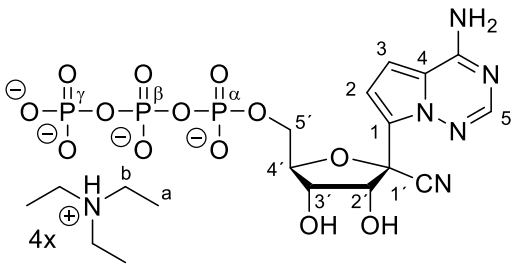

6
$C_{12}H_{12}N_5O_{13}P_3^{4-}$
527.1735 g/mol

The reaction was carried out according to the general procedure VI with GS-441524 **60** (45 mg, 0.15 mmol), proton sponge (66 mg, 0.31 mmol) and $POCl_3$ (28 µL, 0.31 mmol) in trimethyl phosphate (2 mL) for 30 min, followed by the addition of tributylammonium pyrophosphate (210 mg, 0.39 mmol) and tributylamine (220 µL, 0.92 mmol) in CH_3CN (0.8 mL) for 30 min. Purification by ion-exchange chromatography using a DEAE-Sephadex® A-25 column (H_2O/1 M TEAB; 100:0 to 0:100 v/v) and RP_{18} flash column chromatography (H_2O/CH_3CN; 100:0 to 0:100 v/v) provided the triethylammonium salt of **6** (21 mg, 22%) as a colorless solid.

The analytical data was in accordance with those described.[174]

^{1}H-NMR (600 MHz, D_2O): δ [ppm] = 7.94 (s, 1H, *H*-8), 7.07 (d, $^{3}J_{HH}$ = 4.66 Hz, 1H, *H*-5), 6.95 (d, 1H, $^{3}J_{HH}$ = 4.76 Hz, *H*-6), 5.02 (d, $^{3}J_{HH}$ = 5.57 Hz, 1H, *H*-2´), 4.57 (dd, $^{3}J_{HH}$ = 6.48 Hz, $^{3}J_{HH}$ = 3.01 Hz, 1H, *H*-3´), 4.55 – 4.52 (m, 1H, *H*-4´), 4.21 (ddd, $^{2}J_{HH}$ = 11.9 Hz, $^{3}J_{HP}$ = 6.49 Hz, $^{3}J_{HH}$ = 3.10 Hz, 1H, *H*-5´), 4.07 (ddd, $^{2}J_{HH}$ = 11.9 Hz, $^{3}J_{HP}$ = 4.82 Hz, $^{3}J_{HH}$ = 3.34 Hz, 1H, *H*-5´), 3.19 (q, $^{3}J_{HH}$ = 8.12 Hz, 24H, *H*-b), 1.27 (t, $^{3}J_{HH}$ = 7.29 Hz, 36H, *H*-a).

^{13}C-NMR (125 MHz, D_2O): δ [ppm] = 155.9 (*C*-10), 147.7 (*C*-8), 123.0 (*C*-4), 116.63 (1´-*C*N), 116.60 (*C*-5), 111.6 (*C*-2), 102.3 (*C*-1), 85.2 (d, $^2J_{CP}$ = 9.23 Hz, *C*-4´), 76.3 (*C*-2´), 74.8 (*C*-1´), 69.8 (*C*-3´), 64.6 (d, $^2J_{CP}$ = 4.63 Hz, *C*-5´), 46.6 (*C*-b), 8.6 (*C*-a).

^{31}P-NMR (162 MHz, D_2O): δ [ppm] = -10.8 (d, $^2J_{PP}$ = 19.4 Hz, *P*-α), -11.5 (d, $^2J_{PP}$ = 19.9 Hz, *P*-γ), -23.3 (t, $^2J_{PP}$ = 17.9 Hz, *P*-β).

6-Azauridine-5'-triphosphate 72

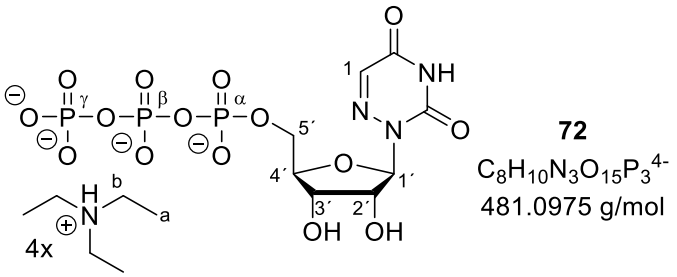

The reaction was carried out according to the general procedure VI with 6-azauridine **70** (50 mg, 0.20 mmol), proton sponge (87 mg, 0.41 mmol) and $POCl_3$ (37 µL, 0.41 mmol) in trimethyl phosphate (2.5 mL) for 15 min, followed by the addition of tributylammonium pyrophosphate (279 mg, 0.51 mmol) and tributylamine (336 µL, 1.22 mmol) in CH_3CN (0.9 mL) for 30 min. Purification by ion-exchange chromatography using a DEAE-Sephadex® A-25 column (H_2O/1 M TEAB; 100:0 to 0:100 v/v) and RP_{18} flash column chromatography (H_2O/CH_3CN; 100:0 to 0:100 v/v) provided the triethylammonium salt of **72** (45 mg, 38%) as a colorless solid.

^1H-NMR (400 MHz, D_2O): δ [ppm] = 7.56 (s, 1H, *H*-1), 6.16 (d, $^3J_{HH}$ = 4.32 Hz, 1H, *H*-1´), 4.67 (dd, $^3J_{HH}$ = 5.33, $^3J_{HH}$ = 4.37 Hz, 1H, *H*-2´), 4.52 (d, $^3J_{HH}$ = 5.31 Hz, 1H, *H*-3´), 4.27 (q, $^3J_{HH}$ = 4.79 Hz, 1H, *H*-4´), 4.21 – 4.10 (m, 2H, *H*-5´), 3.22 (q, $^3J_{HH}$ = 7.34 Hz, 24H, *H*-b), 1.30 (t, $^3J_{HH}$ = 7.26 Hz, 36H, *H*-a).

^{31}P-NMR (162 MHz, D_2O): δ [ppm] = -9.44 (d, $^2J_{PP}$ = 21.5 Hz, *P*-γ), -11.3 (d, $^2J_{PP}$ = 19.9 Hz, *P*-α), -23.1 (t, $^2J_{PP}$ = 20.0 Hz, *P*-β).

HRMS (MALDI$^-$): *m/z* = calcd: 483.9565 $[M-H]^-$, found: 483.9725 $[M-H]^-$.

Mizoribine-5'-triphosphate 73

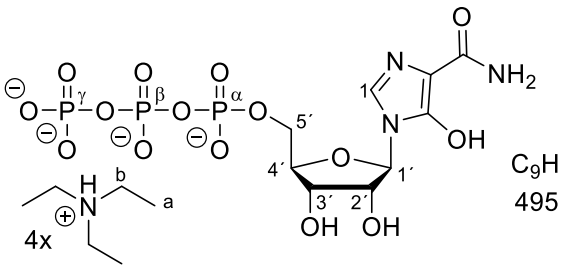

73
$C_9H_{12}N_3O_{15}P_3^{4-}$
495.1245 g/mol

The reaction was carried out according to the general procedure VI with Mizoribine **71** (50 mg, 0.19 mmol), proton sponge (83 mg, 0.39 mmol) and $POCl_3$ (35 µL, 0.39 mmol) in trimethyl phosphate (2.5 mL) for 30 min, followed by the addition of tributylammonium pyrophosphate (263 mg, 0.48 mmol) and tributylamine (275 µL, 1.16 mmol) in CH_3CN (0.9 mL) for 30 min. Purification by ion-exchange chromatography using a DEAE-Sephadex® A-25 column (H_2O/1 M TEAB; 100:0 to 0:100 v/v) and RP_{18} flash column chromatography (H_2O/CH_3CN; 100:0 to 0:100 v/v) provided the triethylammonium salt of **73** (41 mg, 36%) as a colorless solid.

^{1}*H*-NMR (400 MHz, D_2O): δ [ppm] = 7.48 (s, 1H, *H*-1), 5.55 (d, $^3J_{HH}$ = 6.21 Hz, 1H, *H*-1´), 4.48 – 4.43 (m, 1H, *H*-2´), 4.40 (dd, $^3J_{HH}$ = 5.30, $^3J_{HH}$ = 3.38 Hz, 1H, *H*-3´), 4.21 – 4.06 (m, 3H, *H*-4´, *H*-5´), 3.13 (q, $^3J_{HH}$ = 7.6 Hz, 24H, *H*-b), 1.21 (t, $^3J_{HH}$ = 7.30 Hz, 36H, *H*-a).

^{31}*P*-NMR (162 MHz, D_2O): δ [ppm] = -9.65c (d, $^2J_{PP}$ = 21.9 Hz, *P*-γ), -11.2 (d, $^2J_{PP}$ = 19.5 Hz, *P*-α), -22.8 (t, $^2J_{PP}$ = 19.1 Hz, *P*-β).

HRMS (MALDI$^-$): *m/z* = calcd: 497.9610 $[M-H]^-$, found: 497.9771 $[M-H]^-$.

***N*^{4}-Hydroxycytidine-5'-triphosphate 74**

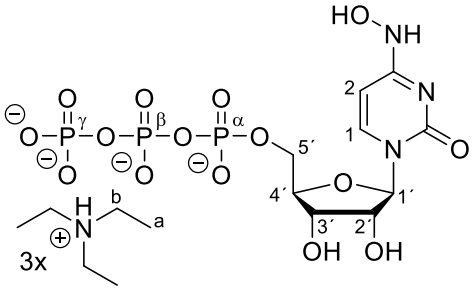

74
$C_9H_{12}N_3O_{15}P_3^{4-}$
495.1245 g/mol

A pressure tube was charged with cytidine triphosphate disodium salt **75** (137 mg, 0.26 mmol) and 2 N aqueous hydroxylamine solution (2.0 mL, 4.0 mmol). Afterwards, a few drops of 10% aqueous NaOH solution were added to adjust the solution to pH 5. The sealed tube was stirred

for 5 h at 55 °C before the reaction was quenched by the addition of 50 mM TEAB. After all volatiles were removed under reduced pressure, the residue was subjected to a DEAE-Sephadex® A-25 column (H_2O/1 M TEAB; 100:0 to 0:100 v/v) using an automated flash system. Fractions containing the desired product were concentrated under reduced pressure and subjected to RP18 silica gel using automated flash chromatography (H_2O/CH_3CN; 100:0 to 0:100 v/v), providing the triethylammonium salt of **74** (47 mg, 31%) as a colorless solid.

^{1}*H*-NMR (500 MHz, D_2O): δ [ppm] = 7.30 (d, $^3J_{HH}$ = 8.17 Hz, 1H, *H*-1), 5.98 (d, $^3J_{HH}$ = 6.20 Hz, 1H, *H*-2), 5.88 (d, $^3J_{HH}$ = 8.06 Hz, 1H, *H*-1´), 4.42 – 4.36 (m, 2H, *H*-2´, *H*-3´), 4.26 – 4.16 (m, 3H, *H*-4´, *H*-5´), 3.20 (q, $^3J_{HH}$ = 7.29 Hz, 18H, *H*-b), 1.30 (t, $^3J_{HH}$ = 7.31 Hz, 27H, *H*-a).

^{31}*P*-NMR (202 MHz, D_2O): δ [ppm] = -9.72 (d, $^2J_{PP}$ = 19.7 Hz, *P*-γ), -10.3 (d, $^2J_{PP}$ = 20.5 Hz, *P*-α), -22.1 (t, $^2J_{PP}$ = 19.4 Hz, *P*-β).

HRMS (MALDI$^-$): *m/z* = calcd: 497.9610 $[M-H]^-$, found: 497.9799 $[M-H]^-$.

5-Fluoro-2´-*C*-methyl-uridine-5´-triphosphate 218

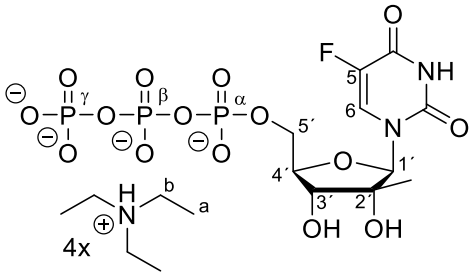

218
$C_{10}H_{12}FN_2O_{15}P_3^{4-}$
512.1269 g/mol

The monophosphate **217** (40 mg, 0.07 mmol) was suspended in CH_3CN (1.5 mL), before Et_3N (122 µL, 0.88 mmol) and TFAA (102 µL, 0.74 mmol) were added dropwise. After stirring the reaction mixture for 10 min at room temperature, all volatiles were removed under reduced pressure, and the residue was dissolved again in CH_3CN (1.5 mL). The solution was then treated with Et_3N (102 µL, 0.74 mmol) and 1-methylimidazole (35 µL, 0.44 mmol). After stirring for another 10 min at room temperature, the mixture was added dropwise via a syringe pump (0.2 mL/min) to a solution of tributylammonium pyrophosphate (120 mg, 0.22 mmol) in CH_3CN (1.5 mL). Subsequently, the reaction mixture was stirred for 30 min at room temperature, then all volatiles were removed under reduced pressure. The residue was taken up in water and washed three times with CH_2Cl_2. The aqueous phase was then concentrated under reduced pressure, and the residue was purified using automated column chromatography on a DEAE-

Sephadex® A-25 column (H_2O/1 M TEAB; 100:0 to 0:100 v/v) and RP_{18} flash chromatography (H_2O/CH_3CN; 100:0 to 0:100 v/v) providing the triethylammonium salt of **218** (55 mg, 80%) as a colorless solid.

^{1}*H*-NMR (300 MHz, D_2O): δ [ppm] = 8.00 (d, $^3J_{HF}$ = 6.39 Hz, 1H, *H*-6), 6.04 (d, $^3J_{HH}$ = 1.80 Hz, 1H, *H*-1´), 4.38 – 4.34 (m, 2H, H-3´, *H*-4´), 4.11 – 4.09 (m, 2H, *H*-5´), 3.20 (q, $^3J_{HH}$ = 7.31 Hz, 24H, *H*-b), 1.28 (t, $^3J_{HH}$ = 7.26 Hz, 36H, *H*-a), 1.19 (s, 3H, 2´-C-C*H*$_3$).

^{31}*P*-NMR (121 MHz, D_2O): δ [ppm] = -6.61 (d, $^2J_{PP}$ = 21.2 Hz, *P*-α), -11.5 (d, $^2J_{PP}$ = 20.0 Hz, *P*-γ), -22.6 (t, $^2J_{PP}$ = 20.5 Hz, *P*-β).

^{19}*F*-NMR (564 MHz, D_2O): δ [ppm] = -160.4 (m).

HRMS (MALDI$^-$): *m/z* = calcd: 514.9675 [M-H]$^-$, found: 514.9817 [M-H]$^-$.

5.3.8 Synthesis of masking units

4-(Hydroxymethyl)phenyl-pentadecanoate 189

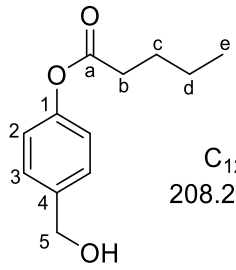

189
$C_{12}H_{16}O_3$
208.2570 g/mol

To a solution of 4-hydroxybenzyl alcohol **188** (1.10 g, 8.86 mmol) and Et_3N (1.10 mL, 7.97 mmol) in THF (15 mL), a solution of valeryl chloride (962 µL, 26.7 mmol) in THF (8 mL) was added dropwise over 15 minutes at 0°C. The reaction mixture was stirred overnight at room temperature and filtered. After all volatiles were removed under reduced pressure, purification on silica gel with automated flash chromatography (petroleum ether/ethyl acetate; 4:1 to 2:1 v/v) provided **189** (685 mg, 37%) as a colorless solid.

The analytical data was in accordance with those described.[120]

^{1}*H*-NMR (400 MHz, $CDCl_3$): *δ* [ppm] = 7.36 (d, $^3J_{HH}$ = 8.54 Hz, 2H, *H*-3), 7.06 (d, $^3J_{HH}$ = 8.48 Hz, 2H, *H*-2), 4.67 (s, 2H, *H*-5), 2.56 (t, $^3J_{HH}$ = 7.59 Hz, 2H, *H*-b), 1.74 (p, $^3J_{HH}$ = 7.75 Hz, 2H, *H*-c), 1.44 (sx, $^3J_{HH}$ = 7.63 Hz, 2H, *H*-d), 0.97 (t, $^3J_{HH}$ = 7.29 Hz, 3H, *H-J*).

4-(Hydroxymethyl)phenyl-pentadecanoate 187

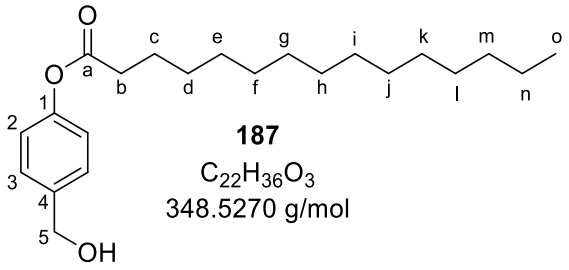

187
$C_{22}H_{36}O_3$
348.5270 g/mol

Step 1: To a solution of pentadecanoic acid **185** (2.00 g, 8.25 mmol) and DMF (1 drop) in CH_2Cl_2 (50 mL), was added oxalyl chloride (920 µL, 10.7 mmol). After stirring the reaction mixture for 2 h at room temperature, all volatiles were removed under reduced pressure. The crude product **186** was used in the next step without further purification. **Step 2:** To a solution of 4-hydroxybenzyl alcohol **188** (1.10 g, 8.86 mmol) and Et_3N (1.10 mL, 26.7 mmol) in THF (15 mL), a solution of **186** (2.08 g, 7.97 mmol) in THF (8 mL) was added dropwise over 15 minutes at 0°C. The reaction mixture was stirred overnight at room temperature and filtered. After all volatiles were removed under reduced pressure, the crude product was purified on silica gel with automated flash chromatography (petroleum ether/ethyl acetate; 4:1 to 2:1 v/v), providing **187** (862 mg, 29%) as a colorless solid.

The analytical data was in accordance with those described.[120]

^{1}*H*-NMR (400 MHz, $CDCl_3$): δ [ppm] = 7.37 (d, $^3J_{HH}$ = 8.30 Hz, 2H, *H*-3), 7.05 (d, $^3J_{HH}$ = 8.26 Hz, 2H, *H*-2), 4.68 (s, 2H, *H*-5), 2.55 (t, $^3J_{HH}$ = 7.54 Hz, 2H, *H*-b), 1.75 (q, $^3J_{HH}$ = 7.42 Hz, 2H, *H*-c), 1.41 - 1.26 (m, 22H, *H*-d, *H*-e, *H*-f, *H*-g, *H*-h, *H*-i, *H*-j, *H*-k, *H*-l, *H*-m, *H*-n), 0.89 (t, $^3J_{HH}$ = 6.75 Hz, 3H, *H*-o).

4-(Hydroxymethyl)phenyl-decanoate 195

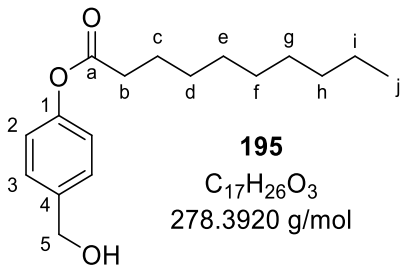

195
$C_{17}H_{26}O_3$
278.3920 g/mol

To a solution of 4-hydroxybenzyl alcohol **188** (3.98 g, 32.0 mmol) and Et_3N (3.75 mL, 26.7 mmol) in THF (30 mL), a solution of decanoyl chloride (5.42 mL, 26.7 mmol) in THF (15 mL) was added dropwise over 15 minutes at 0°C. The reaction mixture was stirred overnight at room temperature and filtered. After all volatiles were removed under reduced pressure, purification

on silica gel with automated flash chromatography (petroleum ether/ethyl acetate; 4:1 to 2:1 v/v) provided **195** (4.31 g, 48%) as a colorless solid.

The analytical data was in accordance with those described.[241]

^{1}*H*-NMR (400 MHz, $CDCl_3$): δ [ppm] = 7.35 (d, $^{3}J_{HH}$ = 8.70 Hz, 2H, *H*-3), 7.05 (d, $^{3}J_{HH}$ = 8.49 Hz, 2H, *H*-2), 4.68 (s, 2H, *H*-5), 2.55 (t, $^{3}J_{HH}$ = 7.52 Hz, 2H, *H*-b), 1.75 (q, $^{3}J_{HH}$ = 7.65 Hz, 2H, *H*-c), 1.45 – 1.28 (m, 12H, *H*-d, *H*-e, *H*-f, *H*-g, *H*-h, *H*-i), 0.89 (t, $^{3}J_{HH}$ = 6.75 Hz, 3H, *H*-j).

^{13}*C*-NMR (101 MHz, $CDCl_3$): δ [ppm] = 172.5 (*C*-a), 150.3 (*C*-1), 138.5 (*C*-4), 128.2 (2C, *C*-3), 121.8 (2C, *C*-2), 64.5 (*C*-5), 34.5 (*C*-b), 32.0 (*C*-h), 29.5 (*C*-d), 29.4 (2C, *C*-e, *C*-f) 29.2 (*C*- g), 25.1 (*C*-c), 22.8 (*C*-i), 14.2 (*C*-j).

HRMS (ESI^{+}): *m/z* = calcd: 301.1774 $[M+Na]^{+}$, found: 301.1772 $[M+Na]^{+}$.

Bis-(*N,N*-di*iso*propylamino)-4-pentanoylbenzylphosphoramidit 191

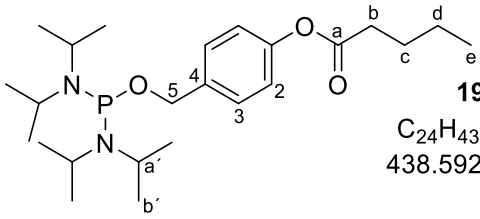

191

$C_{24}H_{43}N_2O_3P$

438.5928 g/mol

Bis(di*iso*propylamino)chlorophosphine **190** (700 mg, 2.62 mmol) was dissolved in THF (10 mL) and cooled to 0 °C. Over a period of twenty minutes, a solution of alcohol **189** (655 mg, 3.14 mmol) and Et_3N (1.09 mL, 7.87 mmol) in THF (10 mL) was added dropwise. The reaction mixture was then warmed to room temperature and stirred for 18 hours. The resulting solid was filtered, washed with ethyl acetate, and all volatiles were removed under reduced pressure. The obtained residue was purified by column chromatography on silica gel (petroleum ether/ethyl acetate; 5:1 v/v + 5% Et_3N), yielding **191** (1.26 g, 91%) as a colorless oil.

The analytical data was in accordance with those described.[120]

^{1}*H*-NMR (400 MHz, $CDCl_3$): δ [ppm] = 7.29 (d, $^{3}J_{HH}$ = 8.46 Hz, 2H, *H*-2), 6.95 (d, $^{3}J_{HH}$ = 8.49 Hz, 2H, *H*-3), 4.67 (d, $^{3}J_{HP}$ = 7.74, 2H, *H*-5), 3.50 (dh, $^{3}J_{HP}$ = 10.9 Hz, $^{3}J_{HH}$ = 6.72 Hz, 4H, *H*-a´), 2.48 (t, $^{3}J_{HH}$ = 7.48 Hz, 2H, *H*-b), 1.67 (p, $^{3}J_{HH}$ = 7.52 Hz, 2H, *H*-c), 1.37 (sx, $^{3}J_{HH}$ = 7.32 Hz, 2H, *H*-d), 1.10 (dd, $^{3}J_{HH}$ = 6.81 Hz, $^{4}J_{HH}$ = 2.65 Hz, 24H, *H*-b´), 0.90 (t, $^{3}J_{HH}$ = 7.36 Hz, 3H, *H*-e).

^{31}P-NMR (162 MHz, $CDCl_3$): δ [ppm] = 123.5 (s).

(4-Pentanoyloxybenzyl-(4-pentadecanoyloxybenzyl)-di*iso*propylphosphoramidit 192

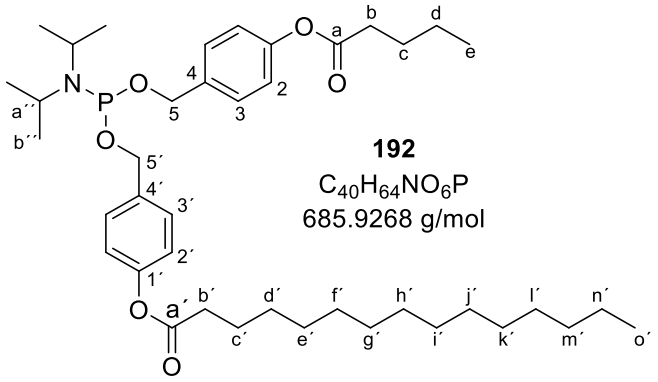

After the alcohol **187** (648 mg, 1.86 mmol) and the phosphoramidite **191** (1.22 g, 2.79 mmol) were dissolved in THF (15 mL) and cooled to 0°C, the 4,5-dicyanoimidazole activator solution (7.44 mL, 1.86 mmol, 0.25 M in CH_3CN) was added dropwise. After complete addition, the reaction mixture was stirred for an additional hour at room temperature, and then all volatiles were removed under reduced pressure. Purification of the crude product by column chromatography on silica gel (petroleum ether/ethyl acetate; 5:1 v/v + 5% Et_3N) yielded **192** (765 mg, 60%) as a colorless oil.

The analytical data was in accordance with those described.[120]

^{1}H-NMR (400 MHz, $CDCl_3$): δ [ppm] = 7.35 (d, $^{3}J_{HH}$ = 8.65 Hz, 4H, *H*-2, *H*-2´), 7.03 (d, $^{3}J_{HH}$ = 8.64 Hz, 4H, *H*-3, *H*-3´), 4.74 (dd, $^{2}J_{HH}$ = 12.8 Hz, $^{3}J_{HP}$ = 8.09, 2H, *H*-5, *H*-5´), 4.66 (dd, $^{2}J_{HH}$ = 12.4 Hz, $^{3}J_{HP}$ = 8.43 Hz, 2H, *H*-5, *H*-5´), 3.69 (dh, $^{3}J_{HP}$ = 10.3 Hz, $^{3}J_{HH}$ = 6.82 Hz, 2H, *H*-a´´), 2.57 – 2.52 (m, 4H, *H*-b, *H*-b´), 1.74 (p, $^{3}J_{HH}$ = 7.40 Hz, 4H, *H*-c, *H*-c´), 1.44 (sx, $^{3}J_{HH}$ = 7.40 Hz, 4H, *H*-d, *H*-d´), 1.33 – 1.26 (m, 20H, *H*-e´, *H*-f´, *H*-g´, *H*-h´, *H*-i´, *H*-j ´, *H*-k´, *H*-l´, *H*-m´, *H*-n´), 1.20 (d, $^{3}J_{HH}$ = 6.82 Hz, 12H, *H*-b´´), 0.97 (t, $^{3}J_{HH}$ = 7.26 Hz, 3H, *H*-e), 0.88 (t, $^{3}J_{HH}$ = 7.25 Hz, 3H, *H*-o´).

^{31}P-NMR (162 MHz, $CDCl_3$): δ [ppm] = 147.9 (s).

Bis(4-decanoyloxybenzyl)-phosphonate /(C9C9AB)-*H*-Phosphonat 197

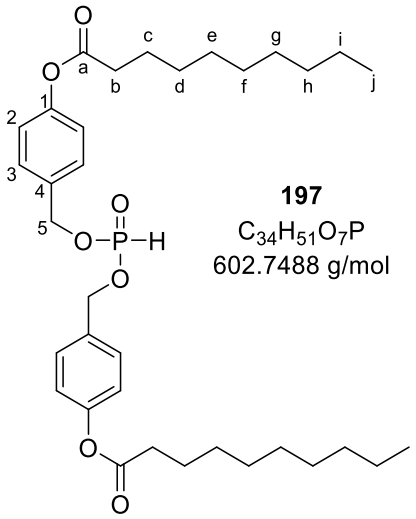

197
$C_{34}H_{51}O_7P$
602.7488 g/mol

To a solution of 4-(hydroxymethyl)phenyl decanoate **195** (3.40 g, 12.2 mmol) in pyridine (40 mL), diphenyl phosphonate **196** (1.17 mL, 5.82 mmol) was added, and the reaction was stirred overnight at 50°C. After all volatiles were removed under reduced pressure, the residue was co-evaporated with toluene twice. The crude product was purified by recrystallization from methanol, followed by automated flash chromatography (petroleum ether/ethyl acetate; 2:1 to 1:1 v/v) to provide **197** (2.27 g, 63%) as a colorless solid.

The analytical data was in accordance with those described.

^{1}*H*-NMR (400 MHz, $CDCl_3$): δ [ppm] = 7.38 – 7.34 (m, 4H, *H*-2), 7.10 – 7.06 (m, 4H, *H*-3), 6.91 (d, $^{1}J_{HP}$ = 709.5 Hz, 1H, *P*-H), 5.09 – 4.98 (m, 4H, *H*-5), 2.55 (t, $^{3}J_{HH}$ = 7.92 Hz, 4H, *H*-b), 1.75 (p, $^{3}J_{HH}$ = 7.27 Hz, 4H, *H*-c), 1.44 – 1.27 (m, 24H, *H*-alkyl), 0.88 (t, $^{3}J_{HH}$ = 7.36, 6.5 Hz, 6H, *H*-j).

^{13}*C*-NMR (101 MHz, $CDCl_3$): δ [ppm] = 172.3 (2C, *C*-a), 151.1 (2C, *C*-1), 133.1 (d, $^{3}J_{CP}$ = 6.04 Hz, 2C, *C*-4), 129.4 (4C, *C*-2), 122.1 (4C, *C*-3), 66.8 (d, $^{2}J_{CP}$ = 6.41 Hz, 2C, *C*-5), 34.5 (2C, *C*-b), 32.0 (2C, *C*-h), 29.5 (2C, *C*-d), 29.4 (4C, *C*-e, *C*-f), 29.2 (2C, *C*-g), 25.0 (2C, *C*-c), 22.8 (2C, *C*-i), 14.3 (2C, *C*-j).

^{31}*P*-NMR (162 MHz, $CDCl_3$): δ [ppm] = 7.70 (s).

HRMS (ESI^+): *m/z* = calcd: 625.3265 $[M+Na]^+$, found: 625.3260 $[M+Na]^+$.

5.3.9 Synthesis of Di- and Tri*PPP*ro compounds

β-(4-Pentadecanoyloxybenzyl)-(4-pentanoyloxybenzyl)-T-1106-5´-diphosphate 184

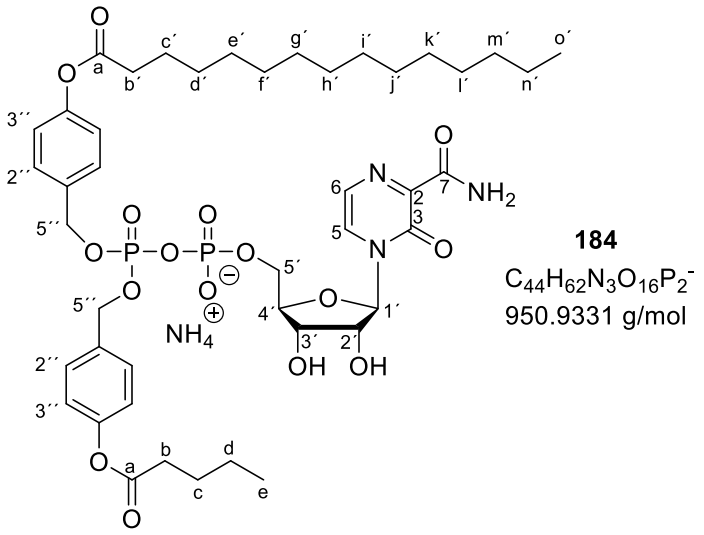

After T-1106-5´-monophopshate **59** (40 mg, 0.089 mmol) and the phosphoramidite **192** (109 mg, 0.16 mmol) were dissolved in CH_3CN (2 mL), the 4,5-dicyanoimidazole activator solution (638 µL, 0.16 mmol, 0.25 M in CH_3CN) was added dropwise. After complete addition, the reaction mixture was stirred for an additional 30 minutes at room temperature before adding *tert*-butyl hydroperoxide (741 µL, 4.07 mmol, 5.5 M in decane). Subsequently, the mixture was stirred for another 30 minutes before all volatiles were removed under reduced pressure. The residue was purified on RP_{18} silica gel with automated flash chromatography (H_2O/CH_3CN; 100:0 to 0:100 v/v), followed by ion-exchange on Dowex (H^+/NH_4^+) and a second purification on RP_{18} silica gel with automated flash chromatography (H_2O/CH_3CN; 100:0 to 0:100 v/v), and finally freeze-dried. This process yielded **184** (45 mg, 53%) as a colorless cotton.

The analytical data was in accordance with those described.[120]

^{1}*H*-NMR (400 MHz, CD_3OD): δ [ppm] = 8.32 (d, $^3J_{HH}$ = 4.13 Hz, 1H, *H*-5), 7.74 (d, $^3J_{HH}$ = 4.17 Hz, 1H, *H*-6), 7.44 – 7.41 (m, 4H, *H*-2, *H*-2´), 7.09 - 7.03 (m, 4H, *H*-3), 6.08 ($^3J_{HH}$ = 1.90 Hz, 1H, *H*-1´), 5.17 – 5.11 (m, 4H, -C*H*$_2$Ph), 4.74 (dd, $^2J_{HH}$ = 12.8 Hz, $^3J_{HP}$ = 8.09, 2H, *H*-5´´), 4.45 – 4.41 (m, 1H, *H*-5´), 4.30 – 4.25 (m, 2H, *H*-4´, *H*-5´), 4.20 – 4.15 (m, 2H, *H*-3´, *H*-5´), 2.62 – 2.57 (m, 4H, *H*-b, *H*-b´), 1.79 – 1.69 (m, 4H, *H*-c, *H*-c´), 1.47 (sx, $^3J_{HH}$ = 7.45 Hz, 4H, *H*-d, *H*-d´), 1.38 – 1.28 (m, 20H, *H*-e´, *H*-f´, *H*-g´, *H*-h´, *H*-i´, *H*-j´, *H*-k´, *H*-l´, *H*-m´, *H*-n´), 1.01 (t, $^3J_{HH}$ = 7.35 Hz, 3H, *H*-e), 0.93 (t, $^3J_{HH}$ = 7.07 Hz, 3H, *H*-o´).

^{31}P-NMR (162 MHz, D_2O): δ [ppm] = -11.9 (d, $^2J_{PP}$ = 20.3 Hz, *P*-α), -12.7 (d, $^2J_{PP}$ = 20.4 Hz, *P*-β).

γ-Bis(4-decanoyloxybenzyl)-3´-fluoro-T-1106-5´-triphosphate 202

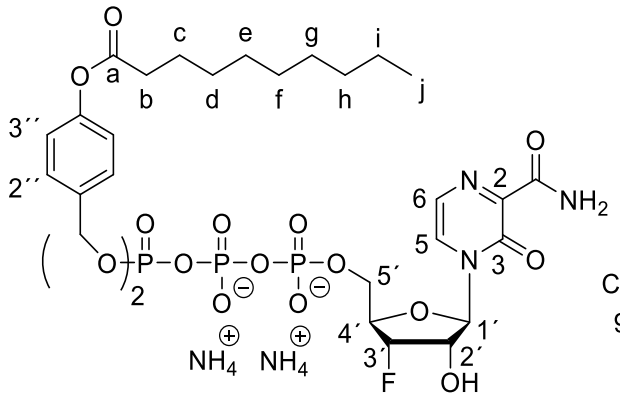

202
$C_{44}H_{61}N_3O_{15}FP_2^-$
952.9127 g/mol

The first reaction step was carried out according to general procedure VII, using bis(4-decanoyloxybenzyl)phosphonate **197** (180 mg, 0.30 mmol), *N*-chlorosuccinimide (89 mg, 0.67 mmol), tetra-*n*-butylammonium phosphate solution (2.26 mL, 0.88 mmol, 0.4 M in CH_3CN), and CH_3CN (6 mL). The resulting crude pyrophosphate **199** was used without further purification or analysis. The synthesis of the TriPPPro-NTP compound was subsequently carried out according to general procedure VII. The pyrophosphate **199** obtained in the first step was used in CH_3CN (4 mL), together with a solution of TFAA (212 µL, 1.42 mmol) and Et_3N (338 µL, 2.44 mmol) in CH_3CN (1.5 mL). For the subsequent activation, 1-methylimidazole (56 µL, 0.69 mmol) and CH_3CN (6 mL) were used. Thereafter, a solution of 3´-fluoro-T-1106-5´-monophosphate **198** (62 mg, 0.14 mmol) in DMF (3 mL) was added, and the reaction mixture was stirred for two hours at room temperature. Purification on RP_{18} silica gel by automated flash chromatography (H_2O/CH_3CN; 100:0 to 0:100 v/v), Dowex ion-exchange (NH_4^+), and RP18 silica gel by automated flash chromatography (H_2O/CH_3CN; 100:0 to 0:100 v/v), followed by freeze-drying, provided **202** (32 mg, 25%) as a colorless cotton-like solid.

^1H-NMR (600 MHz, MeOD-d_4): δ [ppm] = = 8.28 (d, $^3J_{HH}$ = 4.20 Hz, 1H, *H*-5), 7.77 (d, 1H, $^3J_{HH}$ = 4.32 Hz, *H*-6), 7.42 – 7.39 (m, 4H, *H*-3´´), 7.07 – 7.03 (m, 4H, *H*-2´´), 6.45 (d, $^3J_{HH}$ = 7.10 Hz, 1H, *H*-1´), 5.25 (ddd, $^2J_{HF}$ = 53.8 Hz, $^3J_{HH}$ = 4.37 Hz, $^3J_{HH}$ = 1.73 Hz, 1H, *H*-3´), 5.20 – 5.14 (m, 4H, -CH_2-Ph), 4.55 – 4.49 (m, 2H, *H*-2´, *H*-4´), 4.35 – 4.29 (m, 2H, *H*-5´), 2.58 (t, $^3J_{HH}$ = 7.57 Hz, 4H, *H*-b), 1.74 (p, $^3J_{HH}$ = 7.57 Hz, 4H, *H*-c), 1.45 – 1.29 (m, 24H, *H*-d, *H*-e, *H*-f, *H*-g, *H*-h, *H*-i), 0.92 (t, $^3J_{HH}$ = 7.41 Hz, 6H, *H*-j).

^{31}P-NMR (242 MHz, MeOD-d_4): δ [ppm] = -12.1 (d, $^{2}J_{PP}$ = 19.8 Hz, *P*-α), -11.5 (d, $^{2}J_{PP}$ = 17.5 Hz, *P*-γ), -23.9 (t, $^{2}J_{PP}$ = 18.1 Hz, *P*-β).

^{19}F-NMR (564 MHz, MeOD-d_4): δ [ppm] = -202.0 (m).

γ-Bis(4-decanoyloxybenzyl)-thymidine-5´-triphosphate 205

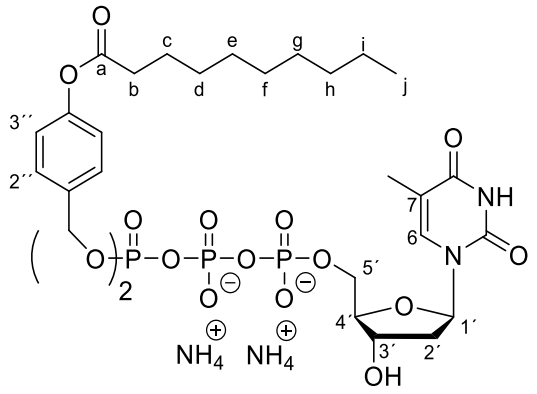

205
$C_{44}H_{63}N_2O_{18}P_3^{2-}$
1000.9064 g/mol

The first reaction step was carried out according to general procedure VII, using bis(4-decanoyloxybenzyl)phosphonate **197** (310 mg, 0.51 mmol), *N*-chlorosuccinimide (171 mg, 1.28 mmol), tetra-*n*-butylammonium phosphate solution (3.86 mL, 1.53 mmol, 0.4 M in CH_3CN), and CH_3CN (10 mL). The resulting crude pyrophosphate **199** was used without further purification or analysis (yield: 380 mg, 79%) as a light-yellow resin. The synthesis of the TriPPPro-NTP compound was subsequently carried out according to general procedure VII. The pyrophosphate **199** obtained in the first step was used in CH_3CN (4 mL), together with a solution of TFAA (404 µL, 2.56 mmol) and Et_3N (647 µL, 4.10 mmol) in CH_3CN (3 mL). For activation, 1-methylimidazole (116 µL, 1.28 mmol) and DMF (5 mL) were used. Next, a solution of the uridine-5'-monophosphate **206** (80 mg, 0.17 mmol) in DMF (2 mL) was added, and the reaction mixture was stirred for 2 h at room temperature. Purification on RP_{18} silica gel with automated flash chromatography (H_2O/CH_3CN; 100:0 to 0:100 v/v), followed by ion-exchange on Dowex (NH_4^+), a second purification on RP_{18} silica gel with automated flash chromatography (H_2O/CH_3CN; 100:0 to 0:100 v/v), and finally freeze-drying, yielded **205** (62 mg, 34%) as a colorless cotton.

^{1}H-NMR (600 MHz, MeOD-d_4): δ [ppm] = 7.80 (s, 1H, *H*-6), 7.40 (d, $^{3}J_{HH}$ = 8.49 Hz, 4H, *H*-2´´), 7.04 (d, $^{3}J_{HH}$ = 8.41 Hz, 4H, *H*-2´´), 6.32 (dd, $^{3}J_{HH}$ = 7.63 Hz, $^{3}J_{HH}$ = 6.04 Hz, 1H, *H*-1´), 5.20 – 5.14 (m, 4H, -CH_2-Ph), 4.58 (dt, $^{3}J_{HH}$ = 6.33 Hz, $^{3}J_{HH}$ = 3.00 Hz, 1H, H-3´), 4.28 – 4.20 (m, 2H, *H*-5´), 4.02 (q, $^{3}J_{HH}$ = 2.83 Hz, 1H, *H*-4´), 2.58 (t, $^{3}J_{HH}$ = 7.49 Hz, 4H, *H*-b), 2.30 – 2.23 (m, 1H, *H*-2´), 2.19 (ddd, $^{2}J_{HH}$ =

13.5 Hz, $^{3}J_{HH}$ = 6.14 Hz, $^{3}J_{HH}$ = 3.21 Hz, 1H, *H*-2´), 1.92 (d, $^{4}J_{HH}$ = 1.00 Hz, 3H, *H*-7), 1.74 (p, $^{3}J_{HH}$ = 7.56 Hz, 4H, *H*-c), 1.46 – 1.28 (m, 24H, *H*-d, *H*-e, *H*-f, *H*-g, *H*-h, *H*-i,), 0.90 (t, $^{3}J_{HH}$ = 7.08 Hz, 6H, *H*-j).

^{31}P-NMR (243 MHz, MeOD-d_4): δ [ppm] = -11.8 (d, $^{2}J_{PP}$ = 19.8 Hz, *P*-α), -13.2 (d, $^{2}J_{PP}$ = 17.2 Hz, *P*-γ), -23.8 (t, $^{2}J_{PP}$ = 18.1 Hz, *P*-β).

HRMS (ESI$^-$): *m/z* = calcd: 1001.3372 [M-H]$^-$, found: 1001.3373 [M-H]$^-$.

γ-Bis(4-decanoyloxybenzyl)-adenosine-5´-triphosphate 203

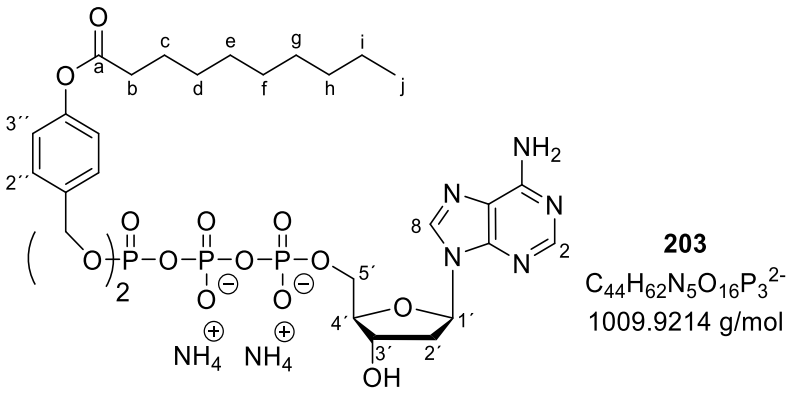

The first reaction step was carried out according to general procedure VII, using bis(4-decanoyloxybenzyl)phosphonate **197** (310 mg, 0.51 mmol), *N*-chlorosuccinimide (171 mg, 1.28 mmol), tetra-*n*-butylammonium phosphate solution (3.86 mL, 1.53 mmol, 0.4 M in CH_3CN), and CH_3CN (10 mL). The resulting crude pyrophosphate **199** was used without further purification or analysis (yield: 380 mg, 79%) as a light-yellow resin. The synthesis of the TriPPPro-NTP compound was subsequently carried out according to general procedure VII. The pyrophosphate **199** obtained in the first step was used in CH_3CN (4 mL), together with a solution of TFAA (404 µL, 2.56 mmol) and Et_3N (647 µL, 4.10 mmol) in CH_3CN (3 mL). For activation, 1-methylimidazole (116 µL, 1.28 mmol) and DMF (5 mL) were used. Next, a solution of the adenosine-5´-monophosphate **205** (93 mg, 0.17 mmol) in DMF (2 mL) was added, and the reaction mixture was stirred for 2 h at room temperature. Purification on RP18 silica gel with automated flash chromatography (H_2O/CH_3CN; 100:0 to 0:100 v/v), followed by ion-exchange on Dowex (NH_4^+), a second round of purification on RP18 silica gel with automated flash chromatography (H_2O/CH_3CN; 100:0 to 0:100 v/v), and finally freeze-drying, yielded **203** (63 mg, 35%) as a colorless cotton.

^{1}H-NMR (400 MHz, MeOD-d_4): δ [ppm] = 8.65 (s, 1H, *H*-6), 8.23 (s, 1H, *H*-8), 7.39 – 7.36 (m, 4H, *H*-3´´), 7.04 – 7.00 (m, 4H, *H*-2´´), 6.45 (t, $^{3}J_{HH}$ = 6.48 Hz, 1H, *H*-1´), 5.20 – 5.13 (m, 4H, -CH_2-Ph), 4.58 (dt, $^{3}J_{HH}$ = 6.85 Hz, $^{3}J_{HH}$ = 3.59 Hz, 1H, H-3´), 4.36 – 4.24 (m, 2H, *H*-5´), 4.19 – 4.15 (m, 1H, *H*-4´), 2.68 – 2.61 (m, 1H, *H*-2´), 2.58 (t, $^{3}J_{HH}$ = 7.49 Hz, 4H, *H*-b), 2.44 (ddd, $^{2}J_{HH}$ = 12.78 Hz, $^{3}J_{HH}$ = 6.22 Hz, 3.47 Hz, 1H, *H*-2´), 1.74 (p, $^{3}J_{HH}$ = 6.96 Hz, 4H, *H*-c), 1.46 – 1.28 (m, 24H, *H*-d, *H*-e, *H*-f, *H*-g, *H*-h, *H*-i,), 0.92 (t, $^{3}J_{HH}$ = 6.79 Hz, 6H, *H*-j).

^{31}P-NMR (161 MHz, MeOD-d_4): δ [ppm] = -11.5 (d, $^{2}J_{PP}$ = 19.4 Hz, *P*-α), -13.2 (d, $^{2}J_{PP}$ = 16.5 Hz, *P*-γ), -23.5 (t, $^{2}J_{PP}$ = 17.7 Hz, *P*-β).

HRMS (ESI$^-$): *m/z* = calcd: 1010.3488 $[M-H]^-$, found: 1010.3490 $[M-H]^-$.

γ-Bis(4-decanoyloxybenzyl)-2-amino-adenosine-5´-triphosphate 204

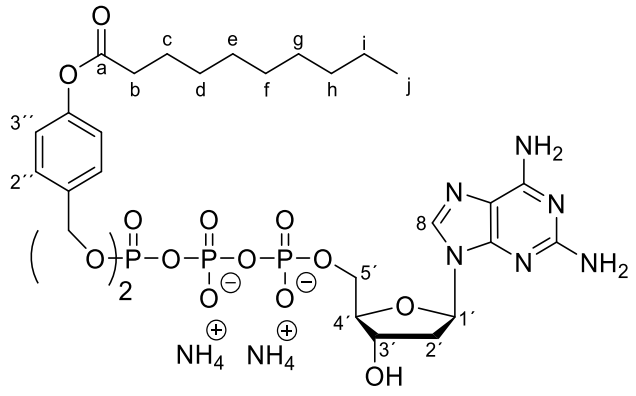

204
$C_{44}H_{63}N_6O_{16}P_3^{2-}$
1024.9364 g/mol

The first reaction step was carried out according to general procedure VII, using bis(4-decanoyloxybenzyl)phosphonate **197** (310 mg, 0.51 mmol), *N*-chlorosuccinimide (171 mg, 1.28 mmol), tetra-*n*-butylammonium phosphate solution (3.86 mL, 1.53 mmol, 0.4 M in CH_3CN), and CH_3CN (10 mL). The resulting crude pyrophosphate **199** was used without further purification or analysis (yield: 380 mg, 79%) as a light-yellow resin. The synthesis of the TriPPPro-NTP compound was subsequently carried out according to general procedure VII. The pyrophosphate **199** obtained in the first step was used in CH_3CN (4 mL), together with a solution of TFAA (404 µL, 2.56 mmol) and Et_3N (647 µL, 4.10 mmol) in CH_3CN (3 mL). For activation, 1-methylimidazole (116 µL, 1.28 mmol) and DMF (5 mL) were used. Next, a solution of the nucleoside-5'-monophosphate **206** (96 mg, 0.17 mmol) in DMF (2 mL) was added, and the reaction mixture was stirred for 2 h at room temperature. Purification on RP_{18} silica gel with automated flash chromatography (H_2O/CH_3CN; 100:0 to 0:100 v/v), followed by ion-exchange on Dowex (NH_4^+), a

second purification on RP_{18} silica gel with automated flash chromatography (H_2O/CH_3CN; 100:0 to 0:100 v/v), and finally freeze-drying, yielded **204** (40 mg, 22%) as a colorless cotton.

^{1}*H*-NMR (400 MHz, MeOD-d_4): δ [ppm] = 8.15 (s, 1H, *H*-8), 7.41 – 7.38 (m, 4H, *H*-3´´), 7.01 – 6.95 (m, 4H, *H*-2´´), 6.41 (t, $^3J_{HH}$ = 6.59 Hz, 1H, *H*-1´), 5.18 – 5.11 (m, 4H, -CH_2-Ph), 4.69 (dt, $^3J_{HH}$ = 6.33 Hz, $^3J_{HH}$ = 3.26 Hz, 1H, H-3´), 4.32 – 4.20 (m, 2H, *H*-5´), 4.17 – 4.14 (m, 1H, *H*-4´), 2.57 (t, $^3J_{HH}$ = 7.32 Hz, 4H, *H*-b), 2.45 – 2.41 (m, 1H, *H*-2´), 2.35 (ddd, $^2J_{HH}$ = 13.2 Hz, $^3J_{HH}$ = 5.98 Hz, 3.48 Hz, 1H, *H*-2´), 1.72 (p, $^3J_{HH}$ = 7.22 Hz, 4H, *H*-c), 1.43 – 1.27 (m, 24H, *H*-d, *H*-e, *H*-f, *H*-g, *H*-h, *H*-i,), 0.91 (t, $^3J_{HH}$ = 6.89 Hz, 6H, *H*-j).

^{31}*P*-NMR (161 MHz, MeOD-d_4): δ [ppm] = -11.5 (d, $^2J_{PP}$ = 19.4 Hz, *P*-α), -13.2 (d, $^2J_{PP}$ = 16.5 Hz, *P*-γ), -23.5 (t, $^2J_{PP}$ = 17.7 Hz, *P*-β).

HRMS (ESI$^-$): *m/z* = calcd: 1025.3597 [M-H]$^-$, found: 1025.3582 [M-H]$^-$.

γ-(Butyl)octadecyl-JD-004-3´-triphosphate 211

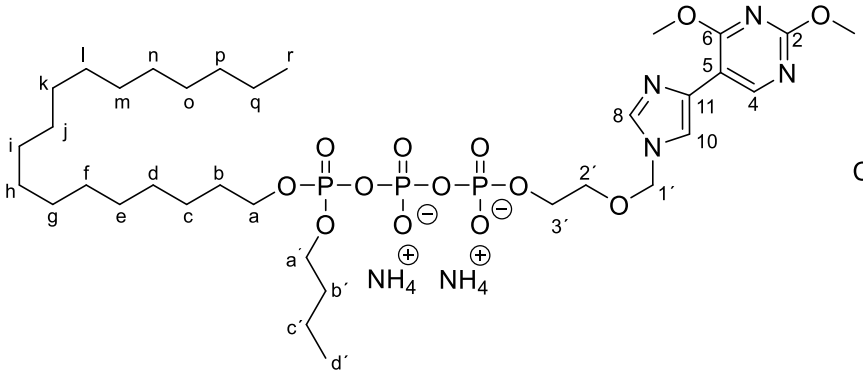

211
$C_{34}H_{61}N_4O_{13}P_3^{2-}$
826.7994 g/mol

The first reaction step was carried out according to general procedure VII, using butyloctadecylphosphonate **211** (200 mg, 0.51 mmol), *N*-chlorosuccinimide (170 mg, 1.28 mmol), tetra-*n*-butylammonium phosphate solution (3.84 mL, 1.53 mmol, 0.4 M in CH_3CN), and CH_3CN (10 mL). The resulting crude pyrophosphate **209** was used without further purification or analysis (yield: 271 mg, 78%) as a light-yellow resin. The synthesis of the TriPPPro-NTP compound was subsequently carried out according to general procedure VII. The pyrophosphate **209** obtained in the first step was used in CH_3CN (4 mL), together with a solution of TFAA (356 µL, 2.25 mmol) and Et_3N (571 µL, 4.10 mmol) in CH_3CN (3 mL). For activation, 1-methylimidazole (102 µL, 1.28 mmol) and DMF (5 mL) were used. Next, a solution of the nucleoside-5'-monophosphate **208** (79 mg, 0.15 mmol) in DMF (2 mL) was added, and the reaction mixture was stirred for 2 h at room

temperature. Purification on RP_{18} silica gel with automated flash chromatography (H_2O/CH_3CN; 100:0 to 0:100 v/v), followed by ion-exchange on Dowex (NH_4^+), a second purification on RP_{18} silica gel with automated flash chromatography (H_2O/CH_3CN; 100:0 to 0:100 v/v), and finally freeze-drying, yielded **211** (37 mg, 28%) as a colorless cotton.

^{1}*H*-NMR (600 MHz, MeOD-d_4): δ [ppm] = 9.10 (s, 1H, *H*-8), 8.78 (s, 1H, *H*-4), 7.96 (d, $^4J_{HH}$ = 1.29 Hz, 1H, *H*-10), 5.71 (s, 2H, *H*-1´), 4.20 – 4.17 (m, 4H, *H*-a, *H*-a´), 4.17 (s, 3H, -OC*H*$_3$), 4.16 – 4.13 (m, 2H, H-2´), 4.04 (s, 3H, -OC*H*$_3$), 3.78 – 3.77 (m, 2H, H-3´), 1.71 – 1.65 (m, 4H, *H*-b, *H*-b´), 1.46 – 1.35 (m, 4H, *H*-c, *H*-c´), 1.33 – 1.27 (m, 28H, *H*-d, *H*-e, *H*-f, *H*-g, *H*-h, *H*-i, *H*-j, *H*-k, *H*-l, *H*-m, *H*-n, *H*-o, *H*-p, *H*-q), 0.94 (t, $^3J_{HH}$ = 7.51 Hz, 3H, *H*-d´), 0.90 (t, $^3J_{HH}$ = 7.51 Hz, 3H, *H*-r).

^{13}*C*-NMR (151 MHz, MeOD-d_4): δ [ppm] = 168.6 (*C*-6), 166.3 (*C*-2), 157.3 (*C*-4), 138.4 (*C*-8), 129.2 (*C*-11), 120.0 (*C*-10), 105.5 (*C*-5), 79.7 (*C*-1´), 70.6 (d, $^2J_{CP}$ = 7.79 Hz, *C*-3´), 69.7 (d, $^2J_{CP}$ = 6.51 Hz, *C*-a), 69.4 (d, $^2J_{CP}$ = 6.41 Hz, *C*-a´), 66.7 (d, $^3J_{HH}$ = 5.67 Hz, *C*-2´), 55.8 (-O*C*H$_3$), 55.3 (-O*C*H$_3$), 33.4, 33.3, 33.1, 31.4, 31.3, 30.8, 30.75, 30.72, 30.70, 30.5, 30.3, 23.7, (*C*-b, *C*-b´, *C*-d, *C*-e, *C*-f, *C*-g, *C*-h, *C*-i, *C*-j, *C*-k, *C*-l, *C*-m, *C*-n, *C*-o, *C*-p, *C*-q), 26.6 (*C*-c), 19.8 (*C*-c´), 14.5 (*C*-r), 14.0 (*C*-d´).

^{31}*P*-NMR (243 MHz, MeOD-d_4): δ [ppm] = -11.7 (d, $^2J_{PP}$ = 18.9 Hz, *P*-α), -12.9 (d, $^2J_{PP}$ = 17.1 Hz, *P*-γ), -23.8 (t, $^2J_{PP}$ = 18.0 Hz, *P*-β).

HRMS (ESI$^-$): *m/z* = calcd: 827.3517 [M-H]$^-$, found: 827.3510 [M-H]$^-$.

γ-(Butyl)octadecyl-JD-004-3´-triphosphonate 212

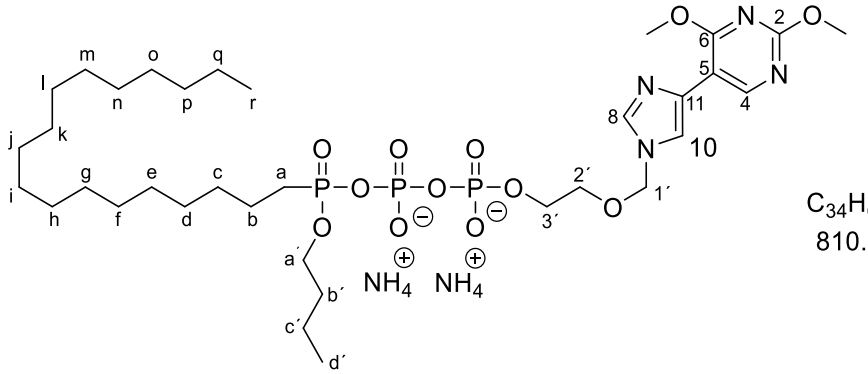

The first reaction step was carried out according to general procedure VII, using butyloctadecylphosphinate **212** (200 mg, 0.53 mmol), *N*-chlorosuccinimide (178 mg, 1.33 mmol), tetra-*n*-butylammonium phosphate solution (4.00 mL, 1.60 mmol, 0.4 M in CH_3CN), and CH_3CN (10 mL). The resulting crude pyrophosphate **210** was used without further purification or analysis

(yield: 310 mg, 80%) as a light-yellow resin. The synthesis of the TriPPPro-NTP compound was subsequently carried out according to general procedure VII. The pyrophosphate **210** obtained in the first step was used in CH_3CN (4 mL), together with a solution of TFAA (388 µL, 2.79 mmol) and Et_3N (622 µL, 4.46 mmol) in CH_3CN (3 mL). For activation, 1-methylimidazole (111 µL, 1.39 mmol) and DMF (5 mL) were used. Next, a solution of the nucleoside-5'-monophosphate **208** (86 mg, 0.15 mmol) in DMF (2 mL) was added, and the reaction mixture was stirred for 2 h at room temperature. Purification on RP_{18} silica gel with automated flash chromatography (H_2O/CH_3CN; 100:0 to 0:100 v/v), followed by ion-exchange on Dowex (NH_4^+), a second purification on RP_{18} silica gel with automated flash chromatography (H_2O/CH_3CN; 100:0 to 0:100 v/v), and finally freeze-drying, yielded **212** (22 mg, 12%) as a colorless cotton.

^{1}*H*-NMR (600 MHz, MeOD-d_4): δ [ppm] = 9.11 (s, 1H, *H*-8), 8.78 (s, 1H, *H*-4), 7.96 (d, $^4J_{HH}$ = 1.22 Hz, 1H, *H*-10), 5.72 (s, 2H, *H*-1´), 4.22 – 4.18 (m, 2H, *H*-a´), 4.17 (s, 3H, -OC*H*$_3$), 4.16 – 4.13 (m, 2H, H-2´), 4.05 (s, 3H, -OC*H*$_3$), 3.88 - 3.78 (m, 2H, *H*-3´), 2.06 – 2.00 (m, 2H, *H*-a´), 1.69 – 1.61 (m, 4H, *H*-b, *H*-b´), 1.45 – 1.38 (m, 4H, *H*-c, *H*-c´), 1.33 – 1.28 (m, 28H, *H*-d, *H*-e, *H*-f, *H*-g, *H*-h, *H*-i, *H*-j, *H*-k, *H*-l, *H*-m, *H*-n, *H*-o, *H*-p, *H*-q), 0.94 (t, $^3J_{HH}$ = 7.39 Hz, 3H, *H*-d´), 0.90 (t, $^3J_{HH}$ = 6.98 Hz, 3H, *H*-r).

^{31}*P*-NMR (243 MHz, MeOD-d_4): δ [ppm] = 24.2 (d, $^2J_{PP}$ = 23.2 Hz, *P*-α), -11.6 (d, $^2J_{PP}$ = 19.6 Hz, *P*-γ), -23.8 (t, $^2J_{PP}$ = 21.3 Hz, *P*-β).

HRMS (ESI$^-$): *m/z* = calcd: 811.3582 [M-H]$^-$, found: 811.3585 [M-H]$^-$.

5.3.10 Synthesis of nucleoside-5´-α-thio-triphosphates

Tetrafluoropyridine-4-thiol 91

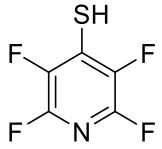

91
C_5HF_4NS
183.1236 g/mol

Sodium hydrosulfide hydrate (12.3 g, 166 mmol) was suspended in MeOH (25 mL) and stirred at room temperature for 30 min until most of the solid had dissolved. After the reaction mixture was cooled to 0 °C, pentafluoropyridine **90** (12.8 g, 75.7 mmol) was added slowly, ensuring that the internal reaction temperature did not exceed 30 °C. After the resulting suspension was stirred for 5 min, all volatiles were removed under reduced pressure. The residue was treated with 4 M HCl solution (45 mL) and extracted three times with hexane. The combined organic layers were

dried over $MgSO_4$, and all volatiles were removed under reduced pressure to yield **91** (11.7 g, 85%) as a colorless liquid that formed crystals after being stored overnight at −20 °C.

The analytical data was in accordance with those described.[207]

^{19}F-NMR (564 MHz, $CDCl_3$): δ [ppm] = -90.8, -139.7 (m).

Bis(perfluoropyridin-4-yl)-phosphorotetrathioate 92

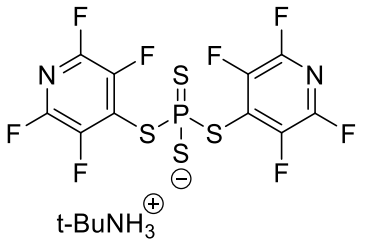

92
$C_{14}H_{12}F_8N_3PS_4$
533.4720 g/mol

Phosphorus pentasulfide (1.70 g, 3.82 mmol) and tetrafluoropyridine-4-thiol **91** (2.10 g, 11.4 mmol) were suspended in CH_2Cl_2 (13 mL) and cooled to 0 °C. Subsequently, *tert*-butylamine (1.56 mL, 1.50 mmol) was added dropwise and the reaction mixture was stirred overnight at room temperature. The reaction mixture was quenched by the addition of water (13 mL), followed by the addition of hexane (13 mL). The resulting suspension was stirred for 30 min before the solid was filtered off. The solid was washed with water (6 mL), CH_2Cl_2/hexane (1:1, 3 × 6 mL) and hexane (6 mL). Drying of the resulting solid overnight under reduced pressure provided **92** (1.21 g, 59%) as a white solid.

The analytical data was in accordance with those described.[207]

^1H-NMR (600 MHz, CD_3CN): δ [ppm] = 7.95 – 7.78 (m, 3H, -NH_3), 1.55 (s, 9H, *t*-Bu).

^{19}F-NMR (564 MHz, CD_3CN): δ [ppm] = -93.9, -133.3 (m).

^{31}P-NMR (242 MHz, CD_3CN): δ [ppm] = 92.56 (s).

HRMS (ESI^-): *m/z* = calcd: 458.8559 $[M-H]^-$, found: 458.8556 $[M-H]^-$.

Reduction of (-)-*cis*-limonene oxide 95

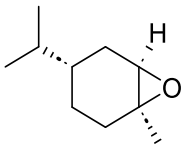

95
$C_{10}H_{18}O$
154.2530 g/mol

(-)-*cis*-limonene oxide **93** (3.00 mL, 17.9 mmol) was dissolved in MeOH (12 mL) before PtO_2 (40 mg, 0.18 mmol) was added, and the reaction mixture was stirred overnight under a H_2 atmosphere. After TLC showed complete conversion of the starting material (no staining with cold $KMnO_4$ solution), the reaction mixture was filtered through a pad of Celite and washed with CH_2Cl_2 (20 mL). After all volatiles were removed under reduced pressure (>100 mbar, 35 °C), crude compound **95** was obtained as a light-brown oil and used in the next step without further purification.

HRMS (ESI$^+$): *m/z* = calcd: 432.0296 $[M+H]^+$, found: 432.0295 $[M+H]^+$.

Reduction of (+)-*cis*-limonene oxide 96

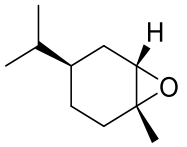

96
$C_{10}H_{18}O$
154.2530 g/mol

The (+)- epoxide **96** was prepared in same why as the (-)-epoxide **95** starting from (+)-*cis*-limonene oxide **94**.

(+)-Ψ* Reagent 97

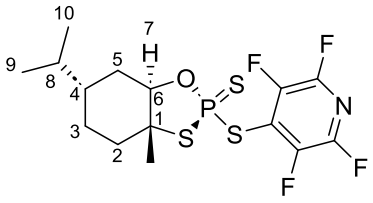

97
$C_{15}H_{18}F_4NOPS_3$
431.4624 g/mol

After a solution of compound **92** (1.00 g, 1.87 mmol) in CH_2Cl_2 (3.5 mL) was cooled to −78 °C, MeOH (350 µL), crude epoxide **95** (6 mL), and trifluoroacetic acid (433 µL, 5.62 mmol) were added consecutively. After the reaction mixture was stirred at −78 °C for 5 min, the cooling bath was removed and the mixture was stirred for 1 h at room temperature. Subsequently, the reaction mixture was diluted with hexane (7 mL) and washed consecutively with water and 10% aqueous K_2HPO_4. The organic phase was dried over $MgSO_4$ and all volatiles were removed under reduced pressure. Purification of the crude product by silica gel chromatography (petroleum ether/ethyl acetate; 10:1 to 4:1 v/v) provided **97** (430 mg, 53%) as a colorless semi-solid that crystallized after being stored at −20 °C overnight.

The analytical data was in accordance with those described.[207]

^{1}H-NMR (600 MHz, $CDCl_3$): δ [ppm] = 4.51 (ddd, $^{3}J_{HH}$ = 13.0 Hz, $^{3}J_{HH}$ = 6.13 Hz, $^{4}J_{HH}$ = 3.71 Hz, 1H, *H*-7), 2.27 – 2.25 (m, 1H, *H*-2), 2.05 – 2.00 (m, 1H, *H*-5), 1.96 – 1.93 (m, 1H, *H*-3), 1.83 – 1.77 (m, 3H, *H*-2, *H*-5, *H*-8), 1.67 (s, 3H, -CH_3), 1.66 – 1.56 (m, 2H, *H*-3, *H*-4), 1.02 (d, $^{3}J_{HH}$ = 6.13 Hz, 6.64 Hz, *H*-9 or *H*-10), 0.97 (d, $^{3}J_{HH}$ = 6.13 Hz, 6.43 Hz, *H*-9 or *H*-10).

^{19}F-NMR (564 MHz, $CDCl_3$): δ [ppm] = -88.5, -132.5 (m).

^{31}P-NMR (242 MHz, $CDCl_3$): δ [ppm] = 96.42 (s).

HRMS (ESI^+): *m/z* = calcd: 432.0296 $[M+H]^+$, found: 432.0295 $[M+H]^+$.

(-)-Ψ* Reagent 98

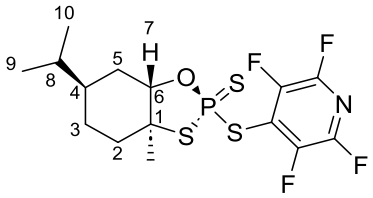

98
$C_{15}H_{18}F_4NOPS_3$
431.4624 g/mol

The (-)-Ψ* reagent **98** was prepared in same why as the (+)-Ψ* reagent **97** in a yield of 49% using epoxide **96.** All characterization data were identical.

4-(Hydroxymethyl)phenyl benzoate 101

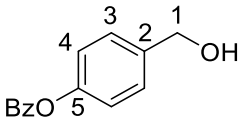

101
$C_{14}H_{12}O_3$
228.2470 g/mol

Step 1: After 4-hydroxybenzaldehyd **99** (6.12 g, 50.1 mmol) was dissolved in THF (50 mL), Et_3N (8.33 mL, 60.1 mmol) was added. Afterwards benzoyl chloride (6.10 mL, 52.6 mmol) was added dropwise at 0°C. The reaction mixture was stirred overnight at room temperature. The reaction mixture was diluted with ethyl acetate (100 mL) and filtered through a pad of Celite. The filtrate was washed with sat. aq. NH_4Cl and dried over $MgSO_4$, and all volatiles were removed under reduced pressure to yield crude 4-formylphenyl benzoate **100** (11.1 g), which was used in the next step without further purification.

Step 2: After 4-formylphenyl benzoate **100** (11.0 g, 48.6 mmol) was dissolved in THF (50 mL), the reaction mixture was cooled to 0°C before $NaBH_4$ (5.51 g, 0.14 mol) was added in three portions. Afterwards the reaction mixture was warmed to room temperature over 2 h and sat. aq. NH_4Cl was added carefully to quench the reaction. The mixture was diluted with ethyl acetate and the

aqueous phase was extracted with ethyl acetate. The combined organic layers were dried over $MgSO_4$ and reduced under reduced pressure to yield **101** (10.9 g, 98% over two steps) as a white solid.

The analytical data was in accordance with those described.[207]

^{1}*H*-NMR (600 MHz, MeOD-d_4): δ [ppm] = 8.18 – 8.16 (m, 2H, *H*-Bz), 7.68 (tt, $^3J_{HH}$ = 7.45 Hz, $^4J_{HH}$ = 1.18 Hz, 1H, *H*-Bz), 7.56 – 7.54 (m, 2H, *H*-Bz), 7.43 (dd, $^3J_{HH}$ = 8.38 Hz, $^4J_{HH}$ = 2.16 Hz, 2H, *H*-2), 7.19 (dd, $^3J_{HH}$ = 8.53 Hz, $^4J_{HH}$ = 1.96 Hz, 2H, *H*-3), 4.64 (s, 2H, *H*-1).

^{13}*C*-NMR (150 MHz, MeOD-d_4): δ [ppm] = 166.7 (*C*-Bz), 151.6 (*C*-5), 140.6 (*C*-2), 134.9 (*C*-Bz), 131.0 (2C, *C*-Bz), 130.8 (*C*-Bz), 129.8 (2C, *C*-Bz), 129.1 (2C, *C*-3), 122.7 (2C, *C*-4), 64.7 (*C*-1).

4-((Phosphonooxy)methyl)phenyl benzoate 102

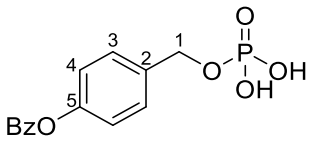

102
$C_{14}H_{13}O_6P$
308.2258 g/mol

To a solution of 4-(hydroxymethyl)phenyl benzoate **101** (2.93 g, 12.8 mmol) in THF (25 mL), pyrophosphoryl chloride (5.33 mL, 38.5 mmol) was added dropwise over 10 min at −78 °C. After the reaction mixture was stirred for 4 h at −78 °C, the reaction was quenched by the addition of water. By the addition of sat. aq. $NaHCO_3$, the pH of the resulting solution was adjusted to 8. Conc. HCl was added dropwise to the resulting suspension until a clear solution was formed. The reaction mixture was extracted with ethyl acetate, the combined organic layers were washed with water, dried over $MgSO_4$ and all volatiles were removed under reduced pressure to yield a white solid. The solid was suspended in CH_2Cl_2 and filtered. The filter cake was washed with CH_2Cl_2 and dried under reduced pressure to afford **102** (837 mg, 29%) as a white crystalline solid.

The analytical data was in accordance with those described.[207]

^{1}*H*-NMR (300 MHz, MeOD-d_4): δ [ppm] = 8.13 (d, $^3J_{HH}$ = 6.73 Hz, 2H, *H*-Bz), 7.65 (t, $^3J_{HH}$ = 6.39 Hz, 1H, *H*-Bz), 7.52 (d, $^3J_{HH}$ = 6.65 Hz, 2H, *H*-Bz), 7.45 (d, $^3J_{HH}$ = 7.54 Hz, 2H, *H*-2), 7.19 (d, $^3J_{HH}$ = 7.63 Hz, 2H, *H*-3), 4.99 (d, $^3J_{HP}$ = 6.88 Hz, 2H, *H*-1).

^{13}C-NMR (75 MHz, MeOD-d_4): δ [ppm] = 166.6 (*C*-Bz), 152.2 (*C*-5), 136.2 (d, $^{3}J_{CP}$ = 7.87 Hz, *C*-2), 135.0 (*C*-Bz), 131.0 (2C, *C*-Bz), 130.8 (*C*-Bz), 129.9 (2C, *C*-Bz), 129.8 (2C, *C*-3), 122.9 (2C, *C*-4), 68.6 (d, $^{2}J_{CP}$ = 5.28 Hz, *C*-1).

^{31}P-NMR (121 MHz, MeOD-d_4): δ [ppm] = - 0.05 (s).

HRMS (ESI$^-$): *m/z* = calcd: 307.0377 [M-H]$^-$, found: 307.0379 [M-H]$^-$.

Bis-*O*-(9*H*-fluoren-9-ylmethyl)-*N,N*-di*iso*propylaminophosphoramidite 103

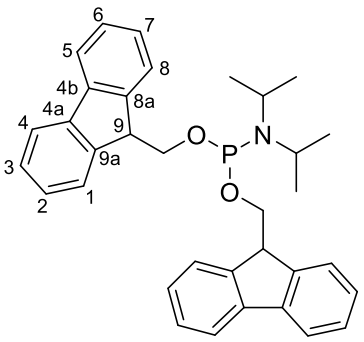

103
$C_{34}H_{36}NO_2P$
521.6408 g/mol

Dichloro-*N,N*-di*iso*propylphosphoramidite **106** (2.37 g, 11.7 mmol) was dissolved in THF (20 mL) and cooled to 0 °C. Subsequently, Et_3N (3.41 mL, 24.6 mmol) and a solution of 9-fluorenemethanol **107** (4.60 g, 23.4 mmol) in THF (15 mL) were added dropwise. After the reaction mixture was stirred overnight at room temperature, it was filtered, the filtrate was dried over $MgSO_4$ and all volatiles were removed under reduced pressure. Purification of the crude product by silica gel chromatography (petroleum ether/ethyl acetate; 96:4 v/v, 1% Et_3N) provided **103** (4.12 g, 67%) as a yellow semi-solid.

The analytical data was in accordance with those described.[207]

^{1}H-NMR (300 MHz, $CDCl_3$): δ [ppm] = 7.68 – 7.64 (m, 4H, *H*-1, *H*-8), 7.59 – 7.54 (m, 4H, *H*-4, *H*-5), 7.33 – 7.26 (m, 4H, *H*-2, *H*-7), 7.24 – 7.16 (m, 4H, *H*-3, *H*-6), 4.09 (t, $^{3}J_{HH}$ = 7.02 Hz, 2H, *H*-9), 3.92 (dt, $^{3}J_{HH}$ = 9.89 Hz, $^{4}J_{HH}$ = 6.68 Hz, 2H, -C*H*$_2$), 3.72 (dt, $^{3}J_{HH}$ = 9.85 Hz, $^{4}J_{HH}$ = 6.73 Hz, 2H, -C*H*$_2$), 3.59 (h, $^{3}J_{HH}$ = 6.69 Hz, 2H, *i*Pr-C*H*), 1.07 (d, $^{3}J_{HH}$ = 6.64 Hz, 12H, *i*Pr-C*H*$_3$).

^{13}C-NMR (75 MHz, MeOD-d_4): δ [ppm] = 145.1, 144.8 (*C*-8a, *C*-9a), 141.5, 141.4 (*C*-4a, *C*-4b), 127.53, 127.49 (*C*-2, *C*-7), 126.96, 126.93 (*C*-3, *C*-6), 125.6, 125.3 (*C*-4, *C*-5), 120.0, 119.9 (*C*-1, *C*-8), 66.0 (d, $^{2}J_{CP}$ = 17.2 Hz, -*C*H$_2$), 49.3 (d, $^{3}J_{CP}$ = 7.69 Hz, *C*-9), 43.2 (d, $^{2}J_{CP}$ = 12.4 Hz, *i*Pr-*C*H), 24.7 (d, $^{3}J_{CP}$ = 7.20 Hz, *i*Pr-*C*H$_3$).

^{31}P-NMR (121 MHz, MeOD-d_4): δ [ppm] = 144.36 (s).

HRMS (ESI$^-$): *m/z* = calcd: 743.1605 [M-H]$^-$, found: 743.1602 [M-H]$^-$.

Diphosphate donor 87

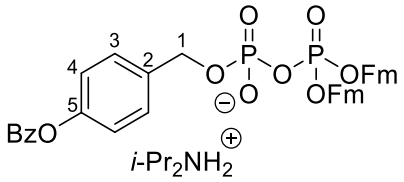

87
$C_{48}H_{49}NO_9P_2$
845.8655 g/mol

Bis-*O*-(9H-fluoren-9-ylmethyl)-*N,N*-di*iso*propylaminophosphoramidite **103** (1.27 g, 2.44 mmol) was dissolved in CH_3CN (7 mL), followed by the addition of monophosphate **102** (628 mg, 2.03 mmol) and Et_3N (282 µL, 2.03 mmol). After the reaction mixture was stirred for 2 min, 5-phenyl-1*H*-tetrazole (446 mg, 3.05 mmol) was added and the reaction mixture was stirred for 1 h before *tert*-butyl hydroperoxide (741 µL, 4.07 mmol, 5.5 M in decane) was added. The reaction mixture was then stirred for another 1 h. The reaction mixture was filtered through a pad of Celite and washed with ethyl acetate. Purification was performed by loading the filtrate onto a 20 g column packed with silica gel, eluting with 200 mL ethyl acetate to CH_2Cl_2/MeOH (15:1 v/v). Due to the fact that the crude product was still slightly contaminated with side products, a second purification step on silica gel (CH_2Cl_2/MeOH; 15:1 v/v) was performed. All product-containing fractions were combined and all volatiles were removed under reduced pressure. The resulting white solid was suspended in CH_2Cl_2 and filtered. The filtrate was concentrated under reduced pressure to provide **87** (837 mg, 46%) as a white foam.

The analytical data was in accordance with those described.[207]

^1H-NMR (300 MHz, $CDCl_3$): δ [ppm] = 8.19 – 8.15 (m, 2H, *H*-Bz), 7.71 – 7.62 (m, 5H, *H*-Bz, *H*-Fm), 7.54 – 7.46 (m, 6H, *H*-Bz, *H*-Fm), 7.41 – 7.28 (m, 6H, *H*-2, *H*-Fm), 7.21 – 7.13 (m, 4H, *H*-Fm), 7.08 – 7.05 (m, 2H, *H*-3), 5.01 – 4.99 (m, 2H, *H*-1), 4.29 – 4.19 (m, 4H, *H*-Fm), 4.12 (t, $^3J_{HH}$ = 6.76 Hz, *H*-Fm), 3.19 (h, $^3J_{HH}$ = 6.71 Hz, 2H, *i*Pr-C*H*), 1.22 (d, $^3J_{HH}$ = 6.56 Hz, 12H, *i*Pr-CH_3).

^{31}P-NMR (121 MHz, $CDCl_3$): δ [ppm] = -11.7 (d, $^2J_{PP}$ = 20.5 Hz), 13.4 (d, $^2J_{PP}$ = 20.2 Hz).

2´-*C*-Methyl-T-1106-5´-α-thio-(R_P)-triphosphate 78

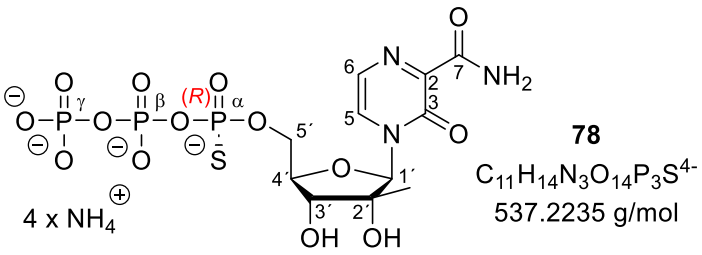

Pyrophosphate **87** (150 mg, 0.18 mmol) was dissolved in CH_3CN (2.0 mL). Then, DBU (106 µL, 0.70 mmol) was added and the reaction mixture was stirred for 10 min. Afterwards, freshly flame-dried 3 Å molecular sieves (200 mg, powder form) and (+)-Ψ* reagent **97** (99 mg, 0.23 mmol) were added, and the reaction mixture was stirred at room temperature for 15 min. Subsequently, the protected nucleoside **86** (180 mg, 0.35 mmol) and a second portion of DBU (159 µL, 1.06 mmol) were added, and the reaction mixture was stirred for 5 h at room temperature. After confirming the completion of the reaction by ^{31}P-NMR, the reaction mixture was filtered. The solid residue was washed with CH_3CN and the filtrate was concentrated to approximately 1 mL under reduced pressure. Concentrated aq. NH_3 solution (5 mL) was then added. After stirring the reaction mixture overnight at room temperature, it was diluted with water and washed with ethyl acetate. The aqueous phase was concentrated under reduced pressure to about 2 mL. The solution was then added dropwise to a solution of 0.2 M $NaClO_4$ in acetone (40 mL). The suspension was centrifuged, the supernatant was discarded and the pellet was washed with acetone twice. The crude product was purified by ion-exchange chromatography using a DEAE-Sephadex® A-25 column (H_2O/1 M NH_4HCO_3; 100:0 to 0:100 v/v) and RP18 flash column chromatography (H_2O/CH_3CN; 100:0 to 0:100 v/v). Fractions containing the product were concentrated under reduced pressure and subsequently co-evaporated with water three additional times. The solid residue was dissolved in a minimal amount of water and freeze-dried to provide the ammonium salt of **78** (26 mg, 24%) as a colorless solid.

^{1}*H*-NMR (400 MHz, D_2O): δ [ppm] = 8.41 (d, $^3J_{HH}$ = 4.18 Hz, 1H, *H*-5), 7.88 (d, $^3J_{HH}$ = 4.48 Hz, 1H, *H*-6), 6.37 (s, 1H, *H*-1´), 4.55 (ddd, $^2J_{HH}$ = 12.2 Hz, $^3J_{HH}$ = 5.62 Hz, $^3J_{HP}$ = 2.01 Hz, 1H, *H*-5´), 4.42 (ddd, $^2J_{HH}$ = 12.2 Hz, $^3J_{HH}$ = 7.26 Hz, $^3J_{HP}$ = 2.07 Hz, 1H, *H*-5´), 4.32 – 4.28 (m, 1H, *H*-4´), 4.20 (d, $^3J_{HH}$ = 9.54 Hz, 1H, *H*-3´), 1.16 (s, 3H, 2´-C-C*H*$_3$).

^{13}C-NMR (101 MHz, D_2O): δ [ppm] = 166.1 (*C*-7), 155.6 (*C*-3), 143.2 (*C*-2), 129.6 (*C*-5), 125.5 (*C*-6), 91.9 (*C*-1´), 80.8 (d, $^3J_{CP}$ = 9.55 Hz, *C*-4´), 79.6 (*C*-2´), 71.1 (*C*-3´), 63.4 (d, $^3J_{CP}$ = 6.14 Hz, *C*-5´), 18.8 (2´-C-CH_3).

^{31}P-NMR (161 MHz, D_2O): δ [ppm] = 42.9 (d, $^2J_{PP}$ = 28.2 Hz, *P*-α), -7.91 (d, $^2J_{PP}$ = 20.6 Hz, *P*-γ), -23.4 (dd, $^2J_{PP}$ = 28.0 Hz, $^2J_{PP}$ = 20.8 Hz, *P*-β).

HRMS (MALDI$^-$): *m/z* = calcd: 539.9649 $[M-H]^-$, found: 539.9952 $[M-H]^-$.

2´-C-Methyl-T-1106-5´-α-thio-(S_P)-triphosphate) 79

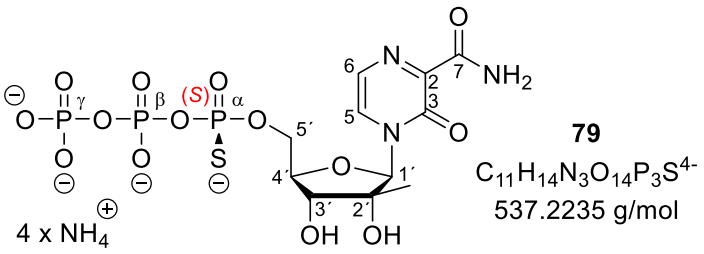

Pyrophosphate **87** (155 mg, 0.18 mmol) was dissolved in CH_3CN (2.0 mL). DBU (106 µL, 0.70 mmol) was then added and the reaction mixture was stirred for 10 min. Afterwards, freshly flame-dried 3 Å molecular sieves (200 mg, powder form) and (−)-Ψ* reagent **98** (102 mg, 0.24 mmol) were added, and the reaction mixture was stirred at room temperature for 15 min. Subsequently, the protected nucleoside **86** (186 mg, 0.37 mmol) and a second portion of DBU (164 µL, 1.10 mmol) were added, and the reaction mixture was stirred for 5 h at room temperature. All the following purification steps were performed according to the procedure for the *R*p-anomer **78**. The ammonium salt of the *S*p-anomer **79** (36 mg, 32%) was obtained as a colorless solid.

^{1}H-NMR (400 MHz, D_2O): δ [ppm] = 8.48 (d, $^3J_{HH}$ = 4.29 Hz, 1H, *H*-5), 7.88 (d, $^3J_{HH}$ = 4.27 Hz, 1H, *H*-6), 6.37 (s, 1H, *H*-1´), 4.52 (ddd, $^2J_{HH}$ = 12.4 Hz, $^3J_{HH}$ = 5.22 Hz, $^3J_{HP}$ = 2.09 Hz, 1H, *H*-5´), 4.44 (ddd, $^2J_{HH}$ = 12.4 Hz, $^3J_{HH}$ = 7.41 Hz, $^3J_{HP}$ = 2.06 Hz, 1H, *H*-5´), 4.32 – 4.28 (m, 1H, *H*-4´), 4.20 (d, $^3J_{HH}$ = 9.45 Hz, 1H, *H*-3´), 1.16 (s, 3H, 2´-C-CH_3).

^{31}P-NMR (161 MHz, D_2O): δ [ppm] = 43.1 (d, $^2J_{PP}$ = 26.8 Hz, *P*-α), -8.83 (d, $^2J_{PP}$ = 20.7 Hz, *P*-γ), -23.6 (dd, $^2J_{PP}$ = 26.8 Hz, $^2J_{PP}$ = 20.2 Hz, *P*-β).

HRMS (MALDI$^-$): *m/z* = calcd: 539.9649 $[M-H]^-$, found: 539.9912 $[M-H]^-$.

5.3.11 Synthesis of T-1106-ProTide compounds

***N*-(Chlorophenoxyphosphinothioyl)-L-alanine 1-methylethyl ester 113**

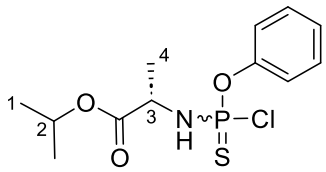

113
$C_{12}H_{17}ClNO_3PS$
321.7558 g/mol

Step 1: To a solution of phenol **111** (1.00 g, 10.6 mmol) and phosphorus thiotrichloride (1.10 mL, 10.6 mmol) in CH_2Cl_2 (20 mL), Et_3N (1.47 mL, 10.6 mmol) was added dropwise at 0 °C. The reaction mixture was allowed to slowly warm to room temperature and was then stirred overnight. Subsequently, the formed precipitate was filtered off and washed twice with Et_2O. All solvents were removed under reduced pressure to provide 1-phenol-dichlorophosphothioate **112** (2.16 g, 90%) as a light-yellow oil.

Step 2: To a solution of 1-phenol-dichlorophosphothioate **112** (1.94 g, 8.56 mmol) and L-alanine isopropyl ester hydrochloride (1.43 g, 8.56 mmol) in CH_2Cl_2 (50 mL), Et_3N (2.37 mL, 17.1 mmol) was added dropwise at 0 °C. After the reaction mixture was stirred overnight at room temperature, all volatiles were removed under reduced pressure. Purification of the crude product on silica gel with automated flash chromatography (petroleum ether/ethyl acetate; 10:1 to 1:1 v/v) provided **113** (2.45 g, 89%) as a colorless oil (approximately a 1:1 mixture of diastereomers).

^{1}*H*-NMR (400 MHz, $CDCl_3$): δ [ppm] = 7.40 – 7.35 (m, 2H, *H*-Ph), 7.33 – 7.28 (m, 2H, *H*-Ph), 7.27 – 7.22 (m, 1H, *H*-Ph), 5.15 – 5.03 (m, 1H, *H*-2), 4.64 – 4.46 (m, 1H, -N*H*), 4.35 – 4.19 (m, 1H, *H*-3), 1.53 – 1.50 (m, 3H, *H*-4), 1.31 – 1.24 (m, 6H, *H*-1).

^{31}*P*-NMR (161 MHz, $CDCl_3$): δ [ppm] = 64.8 (s), 64.7 (s).

HRMS (ESI^+): *m/z* = calcd: 344.0247 $[M+Na]^+$, found: 344.0246 $[M+Na]^+$.

_N_-[(2,3,4,5,6-Pentafluorophenoxy)phenoxyphosphinothioyl]-L-alanine 1-methylethyl ester 114

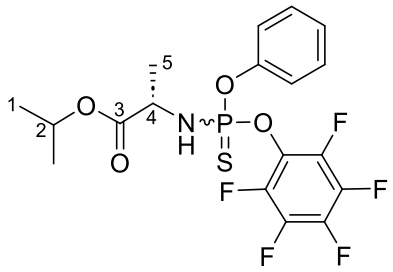

114
$C_{18}H_{17}F_5NO_4PS$
469.3628 g/mol

To a solution of *N*-(chlorophenoxyphosphinothioyl)-L-alanine isopropyl ester **113** (213 mg, 0.66 mmol) and pentafluorophenol (121 mg, 0.66 mmol) in CH_2Cl_2 (5 mL), Et_3N (184 µL, 1.32 mmol) was added dropwise at 0 °C. After the reaction mixture was stirred overnight at room temperature, all volatiles were removed under reduced pressure. Purification of the crude product on silica gel with automated flash chromatography (petroleum ether/ethyl acetate; 10:1 to 1:1 v/v) provided **114** (216 mg, 70%) as a colorless solid (approximately a 1:1 mixture of diastereomers).

^{1}*H*-NMR (400 MHz, $CDCl_3$): *δ* [ppm] = 7.39 – 7.35 (m, 2H, *H*-Ph), 7.31 – 7.28 (m, 2H, *H*-Ph), 7.25 – 7.21 (m, 1H, *H*-Ph), 5.12 – 5.04 (m, 1H, *H*-2), 4.42 – 4.22 (m, 2H, *H*-4, -N*H*), 1.53 – 1.50 (d, $^3J_{HH}$ = 6.93 Hz, 3H, *H*-4), 1.30 – 1.26 (m, 6H, *H*-1).

^{13}*C*-NMR (150 MHz, $CDCl_3$): *δ* [ppm] = 172.7 - 172.5 (m, *C*-3), 150.6 – 150.5 (m, *C*-Ph), 142.7 (2C, *C*-Ph), 140.9 (2C, *C*-Ph), 138.9 (*C*-Ph), 137.1 (*C*-Ph), 132.7 (*C*-Ph), 129.75 – 129.73 (m, 2C, *C*-Ph), 125.86, 126.85 (m, *C*-Ph), 121.16, 121.13 (m, 2C, *C*-Ph), 69.8, 67.7 (*C*-4), 51.5 (*C*-2), 21.82 – 21.77 (m, 2C, *C*-1), 21.1 – 21.0 (m, *C*-5).

^{19}*F*-NMR (565 MHz, $CDCl_3$): *δ* [ppm] = -151.82 – 151.93 (m, 2F), -159.26 – 159.35 (m, 1F), -162.34 – 162.5 (m, 2F).

^{31}*P*-NMR (161 MHz, $CDCl_3$): δ [ppm] = 65.0 (t, $^4J_{PF}$ = 2.20 Hz), 64.8 (t, $^4J_{PF}$ = 2.20 Hz).

HRMS (ESI$^+$): *m/z* = calcd: 492.0428 $[M+Na]^+$, found: 492.0428 $[M+Na]^+$.

***N*-(Chlorophenoxyphosphinothioyl)-L-alanine 2-ethylbutyl ester 116**

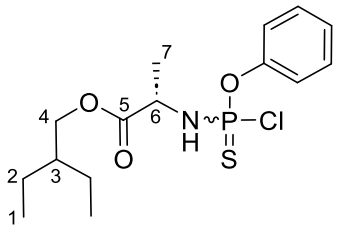

116
$C_{15}H_{23}ClNO_3PS$
363.8368 g/mol

To a solution of 1-phenol-dichlorophosphothioate **112** (2.40 g, 10.5 mmol) and L-alanine 2-ethylbutyl ester hydrochloride (2.21 g, 10.5 mmol) in CH_2Cl_2 (50 mL), Et_3N (2.93 mL, 21.1 mmol) was added dropwise at 0 °C. After the reaction mixture was stirred overnight at room temperature, all volatiles were removed under reduced pressure. Purification of the crude product on silica gel by automated flash chromatography (petroleum ether/ethyl acetate; 10:1 to 1:1 v/v) provided **116** (2.15 g, 62%) as a colorless oil (approximately a 1:1 mixture of diastereomers).

^{1}*H*-NMR (400 MHz, $CDCl_3$): δ [ppm] = 7.40 – 7.35 (m, 2H, *H*-Ph), 7.33 – 7.28 (m, 2H, *H*-Ph), 7.27 – 7.22 (m, 1H, *H*-Ph), 4.71 – 4.54 (m, 1H, -N*H*), 4.41 – 4.26 (m, 1H, *H*-6), 4.18 – 4.07 (m, 2H, *H*-4), 1.60 – 1.50 (m, 4H, *H*-7, *H*-3), 1.42 – 1.33 (m, 4H, *H*-2), 0.93 – 0.87 (m, 6H, *H*-1).

^{13}*C*-NMR (101 MHz, $CDCl_3$): δ [ppm] = 173.0 – 172.9 (m, *C*-5), 150.2 – 150.0 (m, *C*-Ph), 129.75 – 129.71 (m, 2C, *C*-Ph), 126.13 – 126.11 (m, *C*-Ph), 121.40 – 121.35 (m, 2C, *C*-Ph), 68.1, 67.9 (*C*-4), 51.9, 51.6 (d, $^2J_{CP}$ = 1.22 Hz, *C*-6), 40.4 (*C*-7), 23.33 – 23.28 (m, 2C, *C*-2), 20.8 – 20.7 (m, *C*-3), 11.09 – 11.05 (m, 2C, *C*-1).

^{31}*P*-NMR (161 MHz, $CDCl_3$): δ [ppm] = 64.7 (s), 64.7 (s).

HRMS (ESI^+): *m/z* = calcd: 386.0717 $[M+Na]^+$, found: 386.0718 $[M+Na]^+$.

***N*-(Chlorophenoxyphosphinyl)-L-alanine 1-methylethyl ester 120**

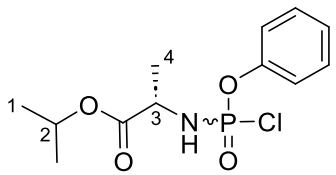

120
$C_{12}H_{17}ClNO_4P$
305.6948 g/mol

To a solution of phenyl dichlorophosphate **119** (1.00 g, 4.74 mmol) and L-alanine isopropyl ester hydrochloride (795 mg, 4.74 mmol) in CH_2Cl_2 (25 mL), Et_3N (1.31 mL, 9.48 mmol) was added

dropwise at -78 °C. After the reaction mixture was stirred overnight at room temperature, all volatiles were removed under reduced pressure. Purification of the crude product on silica gel with automated flash chromatography (petroleum ether/ethyl acetate; 10:1 to 1:1 v/v) provided **120** (1.34 g, 92%) as a colorless oil (approximately a 1:1 mixture of diastereomers).

^{1}*H*-NMR (400 MHz, $CDCl_3$): δ [ppm] = 7.45 – 7.32 (m, 2H, *H*-Ph), 7.28 – 7.15 (m, 2H, *H*-Ph), 5.02 (s, $^{3}J_{HH}$ = 6.25 Hz, 1H, *H*-2), 4.33 – 4.18 (m, 1H, -N*H*), 4.18 – 4.07 (m, 1H, *H*-3), 1.51 – 1.49 (m, 3H, *H*-4), 1.30 – 1.26 (m, 6H, *H*-1).

^{31}*P*-NMR (161 MHz, $CDCl_3$): δ [ppm] = 8.07 (s), 7.69 (s).

HRMS (ESI^+): *m/z* = calcd: 328.0476 $[M+Na]^+$, found: 328.0468 $[M+Na]^+$.

***N*-(Chlorophenoxyphosphinyl)-L-alanine 2-ethylbutyl ester 121**

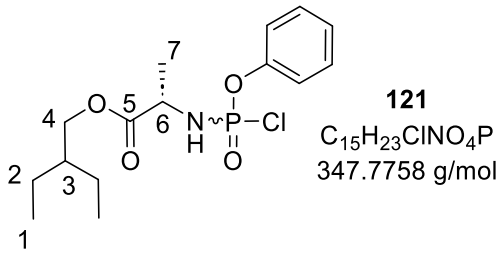

121
$C_{15}H_{23}ClNO_4P$
347.7758 g/mol

To a solution of phenyl dichlorophosphate **119** (2.40 g, 10.7 mmol) and L-alanine 2-ethylbutyl ester hydrochloride (795 mg, 4.74 mmol) in CH_2Cl_2 (25 mL), Et_3N (1.31 mL, 9.48 mmol) was added dropwise at −78 °C. After the reaction mixture was stirred overnight at room temperature, all volatiles were removed under reduced pressure. Purification of the crude product on silica gel by automated flash chromatography (petroleum ether/ethyl acetate; 10:1 to 1:1 v/v) provided **121** (1.42 g, 86%) as a colorless oil (approximately a 1:1 mixture of diastereomers).

^{1}*H*-NMR (400 MHz, $CDCl_3$): δ [ppm] = 7.40 – 7.34 (m, 2H, *H*-Ph), 7.32 – 7.21 (m, 2H, *H*-Ph), 7.19 – 7.09 (m, 1H, *H*-Ph), 4.40 – 4.18 (m, 1H, -N*H*), 4.16 – 4.09 (m, 2H, *H*-4), 4.07 – 3.93 (m, 1H, *H*-6), 1.60 – 1.48 (m, 3H, *H*-7), 1.43 – 1.28 (m, 5H, *H*-2, *H*-3), 0.92 – 0.83 (m, 6H, *H*-1).

^{31}*P*-NMR (161 MHz, $CDCl_3$): δ [ppm] = 8.03 (s), 7.70 (s).

HRMS (ESI^+): *m/z* = calcd: 370.0945 $[M+Na]^+$, found: 370.0952 $[M+Na]^+$.

5´-(Isopropyl ((*S*)-hydroxy(phenoxy)phosphoryl)-L-alaninate)-2´-C-methyl-T-1106 108

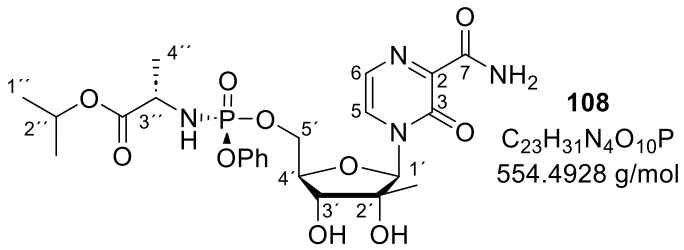

To a suspension of 2′-*C*-methyl-T-1106 **49** (51 mg, 0.18 mmol) in THF (5 mL), *tert*-butylmagnesium chloride in THF (210 µL, 0.36 mmol, 1.7 M solution in THF) was added dropwise at 0 °C. The suspension was stirred at 0 °C for an additional 30 min before a solution of (*S*)-*iso*propyl-2-(((*S*)-(perfluorophenoxy)(phenoxy)phosphoryl)amino)propanoate **107** (121 mg, 0.27 mmol) in THF (5 mL) was added dropwise. The reaction mixture was stirred for further 30 min at 0 °C before it was warmed to room temperature. After stirring overnight, the reaction mixture was quenched by the addition of sat. aq. NH_4Cl solution and extracted with CH_2Cl_2 twice. The organic layer was dried over $MgSO_4$ and all volatiles were removed under reduced pressure. Purification of the crude product on silica gel with automated flash chromatography (CH_2Cl_2/MeOH; 100:0 to 20:1 v/v) provided **108** (45 mg, 45%) as a colorless solid.

^{1}*H*-NMR (400 MHz, $CDCl_3$): δ [ppm] = 9.04 (s, 1H, -NH_2), 7.88 (d, $^3J_{HH}$ = 4.23 Hz, 1H, *H*-5), 7.72 (d, $^3J_{HH}$ = 4.12 Hz, 1H, *H*-6), 7.36 – 7.32 (m, 2H, *H*-Ph), 7.25 – 7.16 (m, 3H, *H*-Ph), 6.19 (s, 2H, *H*-1´, -NH_2), 5.02 (s, $^3J_{HH}$ = 6.34 Hz, 1H, *H*-2´´), 4.54 (ddd, $^2J_{HH}$ = 12.5 Hz, $^3J_{HH}$ = 8.23 Hz, $^3J_{PH}$ = 2.53 Hz, 1H, *H*-5´), 4.41 (ddd, $^2J_{HH}$ = 12.3 Hz, $^3J_{PH}$ = 8.73 Hz, $^3J_{HH}$ = 3.10 Hz, 1H, *H*-5´), 4.24 – 4.22 (m, 1H, *H*-4´), 4.01 – 3.93 (m, 2H, *H*-3´´, -N*H*), 3.88 (d, $^3J_{HH}$ = 6.79 Hz, 3H, *H*-3´), 1.39 (d, $^3J_{HH}$ = 6.72 Hz, 3H, *H*-4´´), 1.25 (d, $^3J_{HH}$ = 2.64 Hz, 3H, *H*-1´´), 1.23 (d, $^3J_{HH}$ = 2.66 Hz, 3H, *H*-1´´), 1.01 (s, 3H, 2´-C-CH_3).

^{31}*P*-NMR (161 MHz, $CDCl_3$): δ [ppm] = 3.38 (s).

HRMS (ESI$^+$): *m/z* = calcd: 577.1670 $[M+Na]^+$, found: 577.1666 $[M+Na]^+$.

5´-(2-Ethylbutyl ((S)-hydroxy(phenoxy)phosphoryl)-L-alaninate)-2´-*C*-methyl-T-1106 110

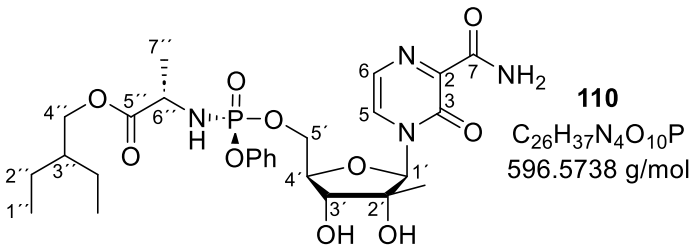

To a suspension of 2′-*C*-methyl-T-1106 **49** (57 mg, 0.20 mmol) in THF (5 mL), *tert*-butylmagnesium chloride in THF (235 µL, 0.36 mmol, 1.7 M solution in THF) was added dropwise at 0 °C. The suspension was stirred at 0 °C for an additional 30 min before a solution of 2-ethylbutyl-((*S*)-(perfluorophenoxy)(phenoxy)phosphoryl)-L-alaninate **109** (148 mg, 0.30 mmol) in THF (5 mL) was added dropwise. The reaction mixture was stirred for further 30 min at 0 °C before it was warmed to room temperature. After stirring overnight, the reaction mixture was quenched by the addition of sat. aq. NH_4Cl solution and extracted with CH_2Cl_2 twice. The organic layer was dried over $MgSO_4$ and all volatiles were removed under reduced pressure. Purification of the crude product on silica gel with automated flash chromatography (CH_2Cl_2/MeOH; 100:0 to 20:1 v/v) provided **110** (67 mg, 56%) as a colorless solid.

^{1}*H*-NMR (600 MHz, MeOD-d_4): δ [ppm] = 8.03 (s, 1H, *H*-5), 7.63 (s, 1H, *H*-6), 7.41 – 7.38 (m, 2H, *H*-Ph), 7.31 – 7.29 (m, 2H, *H*-Ph), 7.24 – 7.20 (m, 1H, *H*-Ph), 6.31 (s, 1H, *H*-1´), 4.58 (ddd, $^2J_{HH}$ = 11.9 Hz, $^3J_{HH}$ = 5.66 Hz, $^3J_{PH}$ = 1.84 Hz, 1H, *H*-5´), 4.45 (ddd, $^2J_{HH}$ = 11.9 Hz, $^3J_{HH}$ = 6.28 Hz, $^3J_{PH}$ = 3.29 Hz, 1H, *H*-5´), 4.25 – 4.22 (m, 1H, *H*-4´), 4.06 (dd, $^2J_{HP}$ = 11.0 Hz, $^3J_{HH}$ = 5.02 Hz, 1H, -N*H*), 4.03 – 3.91 (m, 3H, *H*-4´´, *H*-6´´), 3.86 (d, $^3J_{HH}$ = 9.34 Hz, 1H, *H*-3´), 1.39 (d, $^3J_{HH}$ = 7.19 Hz, 3H, *H*-7´´), 1.38 – 1.33 (m, 5H, *H*-2´´, *H*-3´´), 1.08 (s, 3H, 2´-C-C*H*$_3$), 0.89 (t, $^3J_{HH}$ = 7.44 Hz, 6H, *H*-1´´).

^{31}*P*-NMR (243 MHz, MeOD-d_4): δ [ppm] = 3.81 (s).

HRMS (ESI$^+$): *m/z* = calcd: 619.2139 $[M+Na]^+$, found: 619.2132 $[M+Na]^+$.

5´-(Isopropyl (hydroxy(phenoxy)phosphorothioyl)-L-alaninate)-2´-*C*-methyl-T-1106 115

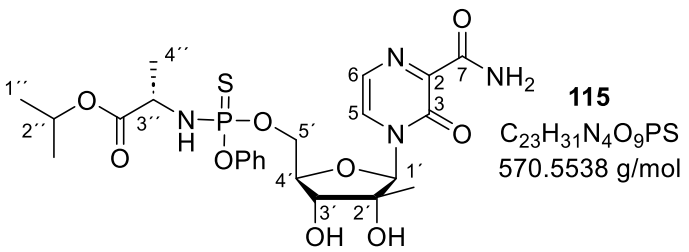

To a solution of 2'-*C*-methyl-T-1106 **49** (53 mg, 0.19 mmol) in CH_3CN (2 mL), 1-methylimidazole (91 µL, 0.36 mmol) was added. After the reaction mixture was stirred for 15 min at room temperature, a solution of *N*-(chlorophenoxyphosphinothioyl)-L-alanine 1-methylethyl ester **113** (178 mg, 0.55 mmol) in CH_3CN (1 mL) was added dropwise. Subsequently, the reaction mixture was stirred overnight at room temperature before all volatiles were removed under reduced pressure. Purification of the crude product on silica gel with automated flash chromatography (CH_2Cl_2/MeOH; 100:0 to 20:1 v/v) provided **115** (26 mg, 25%) as a light-yellow solid, which was obtained as a mixture of diastereomers.

^{1}*H*-NMR (400 MHz, MeOD-d_4): δ [ppm] = Major-Diastereomer: 8.13 (d, $^3J_{HH}$ = 3.87 Hz, 1H, *H*-5), 7.58 (d, $^3J_{HH}$ = 4.12 Hz, 1H, *H*-6), 7.40 – 7.29 (m, 3H, *H*-Ph), 7.26 – 7.18 (m, 2H, *H*-Ph), 6.32 (s, 1H, *H*-1´), 5.02 (d, $^3J_{HH}$ = 5.80 Hz, 1H, *H*-2´´), 4.64 – 4.58 (m, 1H, *H*-5´), 4.41 (ddd, $^2J_{HH}$ = 11.6 Hz, $^3J_{HH}$ = 6.35 Hz, $^3J_{PH}$ = 3.20 Hz, 1H, *H*-5´), 4.31 – 4.23 (m, 1H, *H*-4´), 4.20 – 4.03 (m, 2H, *H*-3´, *H*-3´´), 3.90 (t, $^3J_{HH}$ = 9.36 Hz, 1H, -N*H*), 1.39 (d, $^3J_{HH}$ = 7.10 Hz, 3H, *H*-4´´), 1.27 (d, $^3J_{HH}$ = 2.15 Hz, 3H, *H*-1´´), 1.25 (d, $^3J_{HH}$ = 2.23 Hz, 3H, *H*-1´´), 1.10 (s, 3H, 2´-C-C*H*$_3$).

Minor-Diastereomer: 8.24 (d, $^3J_{HH}$ = 4.06 Hz, 1H, *H*-5), 7.67 (d, $^3J_{HH}$ = 4.33 Hz, 1H, *H*-6), 7.40 – 7.29 (m, 3H, *H*-Ph), 7.26 – 7.18 (m, 2H, *H*-Ph), 6.35 (s, 1H, *H*-1´), 5.02 (d, $^3J_{HH}$ = 5.80 Hz, 1H, *H*-2´´), 4.64 – 4.58 (m, 1H, *H*-5´), 4.48 (ddd, $^2J_{HH}$ = 11.9 Hz, $^3J_{HH}$ = 6.55 Hz, $^3J_{PH}$ = 2.45 Hz, 1H, *H*-5´), 4.31 – 4.23 (m, 1H, *H*-4´), 4.20 – 4.03 (m, 2H, *H*-3´, *H*-3´´), 3.90 (t, $^2J_{HP}$ = 10.47, $^3J_{HH}$, = 9.36 Hz, 1H, -N*H*), 1.36 (d, $^3J_{HH}$ = 7.19 Hz, 3H, *H*-4´´), 1.27 (d, $^3J_{HH}$ = 2.15 Hz, 3H, *H*-1´´), 1.25 (d, $^3J_{HH}$ = 2.23 Hz, 3H, *H*-1´´), 1.10 (s, 3H, 2´-C-C*H*$_3$).

^{31}*P*-NMR (161 MHz, MeOD-d_4): δ [ppm] = 68.5 (s, major), 68.7 (s, minor).

HRMS (ESI$^+$): *m/z* = calcd: 619.2139 $[M+Na]^+$, found: 619.2132 $[M+Na]^+$.

5´-(2-Ethylbutyl (hydroxy(phenoxy)phosphorothioyl)-L-alaninate)-2´-*C*-methyl-T-1106 117

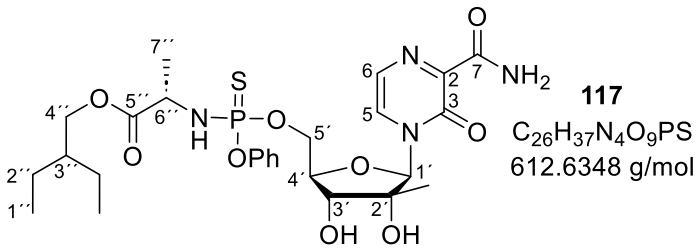

To a solution of 2'-*C*-methyl-T-1106 **49** (50 mg, 0.18 mmol) in CH_3CN (2 mL), 1-methylimidazole (86 µL, 0.88 mmol) was added. After the reaction mixture was stirred for 15 min at room temperature, a solution of *N*-(chlorophenoxyphosphinothioyl)-L-alanine 2-ethylbutyl ester **116** (168 mg, 0.53 mmol) in CH_3CN (1 mL) was added dropwise. Subsequently, the reaction mixture was stirred overnight at room temperature before all volatiles were removed under reduced pressure. Purification of the crude product on silica gel with automated flash chromatography (CH_2Cl_2/MeOH; 100:0 to 20:1 v/v) provided **117** (78 mg, 73%) as a light-yellow solid, which was obtained as a mixture of diastereomers.

^{1}*H*-NMR (600 MHz, MeOD-d_4): δ [ppm] = Major-Diastereomer: 8.10 (d, $^3J_{HH}$ = 3.36 Hz, 1H, *H*-5), 7.56 (d, $^3J_{HH}$ = 3.88 Hz, 1H, *H*-6), 7.38 – 7.34 (m, 2H, *H*-Ph), 7.32 – 7.29 (m, 2H, *H*-Ph), 7.23 – 7.15 (m, 1H, *H*-Ph), 6.30 (s, 1H, *H*-1´), 4.58 (ddd, $^2J_{HH}$ = 12.2 Hz, $^3J_{HH}$ = 6.92 Hz, $^3J_{PH}$ = 1.81 Hz, 1H, *H*-5´), 4.38 (ddd, $^2J_{HH}$ = 11.9 Hz, $^3J_{HH}$ = 6.33 Hz, $^3J_{PH}$ = 3.28 Hz, 1H, *H*-5´), 4.28 – 4.22 (m, 1H, *H*-4´), 4.21 – 4.16 (m, 1H, -N*H*), 4.09 – 4.06 (m, 2H, *H*-4´´), 4.03 – 4.02 (m, 1H, *H*-6´´), 3.86 (d, $^3J_{HH}$ = 9.47 Hz, 1H, *H*-3´), 1.40 (d, $^3J_{HH}$ = 7.00 Hz, 3H, *H*-7´´), 1.39 – 1.30 (m, 5H, *H*-2´´, *H*-3´´), 1.09 (s, 3H, 2´-C-C*H*$_3$), 0.92 – 0.89 (m, 6H, *H*-1´´).

Minor-Diastereomer: 8.22 (d, $^3J_{HH}$ = 3.52 Hz, 1H, *H*-5), 7.66 (d, $^3J_{HH}$ = 3.54 Hz, 1H, *H*-6), 7.38 – 7.34 (m, 2H, *H*-Ph), 7.32 – 7.29 (m, 2H, *H*-Ph), 7.23 – 7.15 (m, 1H, *H*-Ph), 6.33 (s, 1H, *H*-1´), 4.60 (ddd, $^2J_{HH}$ = 12.2 Hz, $^3J_{HH}$ = 5.22 Hz, $^3J_{PH}$ = 2.12 Hz, 1H, *H*-5´), 4.47 (ddd, $^2J_{HH}$ = 11.8 Hz, $^3J_{HH}$ = 6.72 Hz, $^3J_{PH}$ = 2.53 Hz, 1H, *H*-5´), 4.28 – 4.22 (m, 1H, *H*-4´), 4.21 – 4.16 (m, 1H, -N*H*), 4.09 – 4.06 (m, 2H, *H*-4´´), 4.02 – 4.00 (m, 1H, *H*-6´´), 3.89 (d, $^3J_{HH}$ = 9.30 Hz, 1H, *H*-3´), 1.40 (d, $^3J_{HH}$ = 7.00 Hz, 3H, *H*-7´´), 1.39 – 1.30 (m, 5H, *H*-2´´, *H*-3´´), 1.08 (s, 3H, 2´-C-C*H*$_3$), 0.92 – 0.89 (m, 6H, *H*-1´´).

^{31}*P*-NMR (161 MHz, MeOD-d_4): δ [ppm] = 68.44 (s, major), 68.65 (s, minor).

HRMS (ESI$^+$): *m/z* = calcd: 635.1911 $[M+Na]^+$, found: 635.1956 $[M+Na]^+$.

5´-(Isopropyl (hydroxy(phenoxy)phosphoryl)-L-alaninate)-T-1106 122

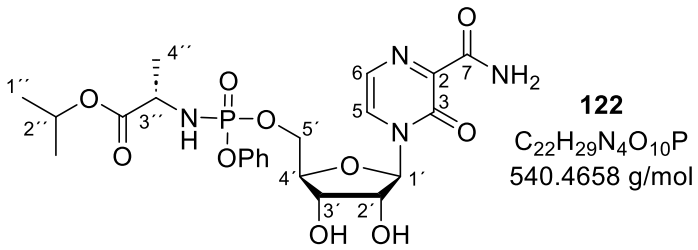

122
$C_{22}H_{29}N_4O_{10}P$
540.4658 g/mol

To a solution of T-1106 **13** (33 mg, 0.12 mmol) in CH_3CN (1.5 mL), 1-methylimidazole (60 µL, 0.61 mmol) was added. After the reaction mixture was stirred for 15 min at room temperature, a solution of *N*-(chlorophenoxyphosphinyl)-L-alanine 1-methylethyl ester **120** (111 mg, 0.37 mmol) in CH_3CN (1 mL) was added dropwise. Subsequently, the reaction mixture was stirred overnight at room temperature before all volatiles were removed under reduced pressure. Purification of the crude product on silica gel with automated flash chromatography (CH_2Cl_2/MeOH; 100:0 to 20:1 v/v) provided **122** (15 mg, 22%) as a light-yellow solid, which was obtained as a mixture of diastereomers.

^{1}*H*-NMR (600 MHz, MeOD-d_4): δ [ppm] = 8.03 (d, $^3J_{HH}$ = 4.40 Hz, 1H, *H*-5a), 8.02 (d, $^3J_{HH}$ = 4.43 Hz, 1H, H-5b), 7.67 (d, $^3J_{HH}$ = 4.35 Hz, 1H, *H*-6a), 7.62 (d, $^3J_{HH}$ = 4.32 Hz, 1H, *H*-6b), 7.61 – 7.52 (m, 2H, *H*-Ph), 7.47 – 7.40 (m, 2H, *H*-Ph), 7.37 – 7.32 (m, 1H, *H*-Ph), 6.29 – 6.22 (m, 1H, *H*-1´), 5.08 – 4.84 (m, 3H, *H*-2´´, *H*-5´), 4.70 – 4.62 (m, 1H, *H*-4´), 4.57 – 4.37 (m, 2H, *H*-3´, *H*-3´´), 3.94 – 3.90 (m, 1H, -N*H*), 1.44 – 1.38 (m, 3H, *H*-4´´), 1.36 – 1.31 (m, 6H, *H*-1´´).

^{31}*P*-NMR (161 MHz, MeOD-d_4): δ [ppm] = 2.86, 1.65.

HRMS (ESI$^+$): *m/z* = calcd: 601.2274 $[M+IsoProp+H]^+$, found: 602.1109 $[M+ IsoProp+H]^+$.

5´-(2-Ethylbutyl (hydroxy(phenoxy)phosphoryl)-L-alaninate)-T-1106 123

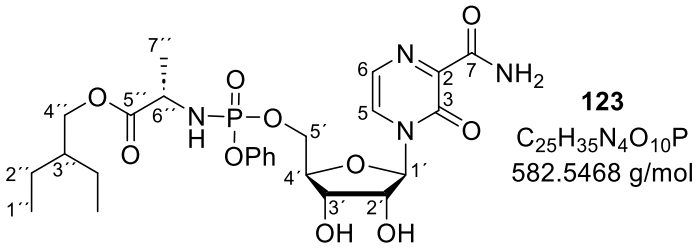

123
$C_{25}H_{35}N_4O_{10}P$
582.5468 g/mol

To a solution of T-1106 **13** (24 mg, 0.09 mmol) in CH_3CN (1 mL), 1-methylimidazole (43 µL, 0.44 mmol) was added. After the reaction mixture was stirred for 15 min at room temperature,

a solution of *N*-(chlorophenoxyphosphinothioyl)-L-alanine 2-ethylbutyl ester **121** (92 mg, 0.270 mmol) in CH_3CN (0.5 mL) was added dropwise. Subsequently, the reaction mixture was stirred overnight at room temperature before all volatiles were removed under reduced pressure. Purification of the crude product on silica gel with automated flash chromatography (CH_2Cl_2/MeOH; 100:0 to 20:1 v/v) provided **123** (21 mg, 42%) as a light-yellow solid, which was obtained as a mixture of diastereomers.

^{1}*H*-NMR (600 MHz, MeOD-d_4): δ [ppm] = 8.06 (d, $^3J_{HH}$ = 4.45 Hz, 1H, *H*-5a), 7.99 (d, $^3J_{HH}$ = 4.43 Hz, 1H, H-5b), 7.64 (d, $^3J_{HH}$ = 4.26 Hz, 1H, *H*-6a), 7.54 (d, $^3J_{HH}$ = 4.48 Hz, 1H, *H*-6b), 7.27 – 7.07 (m, 4H, *H*-Ph), 7.02 – 6.87 (m, 1H, *H*-Ph), 6.11 – 6.09 (m, 1H, *H*-1´), 4.54 – 4.31 (m, 2H, *H*-5´), 4.25 – 4.16 (m, 1H, *H*-4´), 4.13 – 4.07 (m, 1H, -N*H*), 4.00 – 3.80 (m, 3H, *H*-4´´, *H*-6´´), 3.70 – 3.60 (m, 1H, *H*-3´), 1.33 – 1.17 (m, 8H, *H*-2´´, *H*-3´´, *H*-7´´), 0.83 – 0.74 (m, 6H, *H*-1´´).

^{31}*P*-NMR (161 MHz, MeOD-d_4): δ [ppm] = 4.07, 3.85 (s).

HRMS (ESI$^+$): *m/z* = calcd: 605.1983 $[M+Na]^+$, found: 605.1984 $[M+Na]^+$.

5.3.12 Synthesis of T-1106-C-nucleosides-5´-triphosphates

4-(2´,3´,5´,Tri-*O*-benzyl-1´hydroxy-D-ribofuranosyl)-3-fluoropyridine 151

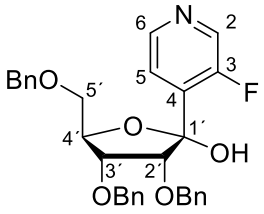

151
$C_{31}H_{30}FNO_5$
515.5814 g/mol

The reaction was carried out according to the general procedure VIII with 3-fluoropyridine **150** (2.40 g, 24.7 mmol) and LDA (24.9 mL, 24.9 mmol, 1 M solution in THF) in THF (50 mL), followed by the addition of lactone **148** (5.17 g, 12.4 mmol) in THF (10 mL). Purification of the crude product on silica gel with automated flash chromatography (petroleum ether/ethyl acetate; 10:1 to 3:1 v/v) provided **151** (4.57 g, 69%) as a colorless oil, which was obtained as a mixture of anomers.

^{1}*H*-NMR (600 MHz, $CDCl_3$): *δ* [ppm] = Major-anomer: 8.28 (d, $^3J_{HF}$ = 2.93 Hz, 1H, *H*-2), 8.26 (d, $^3J_{HH}$ = 4.85 Hz, 1H, *H*-6), 7.64 (dd, $^4J_{HF}$ = 6.75 Hz, $^3J_{HH}$ = 4.97 Hz, 1H, *H*-5), 7.29 – 7.09 (m, 15H, *H*-Bn), 4.96 (bs, 1H, -O*H*), 4.57 – 4.42 (m, 6H, *H*-Bn), 4.40 (q, $^3J_{HH}$ = 4.48 Hz, 1H, *H*-4´), 4.19 (d, $^3J_{HH}$ =

4.94 Hz, 1H, *H*-2´), 4.01 (dd, $^{3}J_{HH}$ = 5.49 Hz, $^{3}J_{HH}$ = 4.30 Hz, 1H *H*-3´), 3.55 (d, $^{3}J_{HH}$ = 4.48 Hz, 1H, *H*-5´).

Minor-anomer: 8.32 (d, $^{3}J_{HF}$ = 4.60 Hz, 1H, *H*-6), 8.31 (d, $^{3}J_{HH}$ = 2.72 Hz, 1H, *H*-2), 7.64 (dd, $^{4}J_{HF}$ = 6.33 Hz, $^{3}J_{HH}$ = 4.99 Hz, 1H, *H*-5), 7.29 – 7.09 (m, 15H, *H*-Bn), 4.96 (bs, 1H, -O*H*), 4.57 – 4.42 (m, 6H, *H*-Bn), 4.37 – 4.35 (m, 1H, H-4´), 4.26 (dd, $^{3}J_{HH}$ = 4.01 Hz, $^{3}J_{HH}$ = 2.43 Hz, 1H, *H*-3´), 4.04 (d, $^{3}J_{HH}$ = 7.21 Hz, 1H, *H*-2´), 3.69 (dd, $^{2}J_{HH}$ = 10.4 Hz, $^{3}J_{HH}$ = 2.47 Hz, 1H *H*-5´), 3.42 (dd, $^{2}J_{HH}$ = 10.6 Hz, $^{3}J_{HH}$ = 2.26 Hz, 1H, *H*-5´).

^{13}*C*-NMR (150 MHz, $CDCl_3$): δ [ppm] = Major-anomer: 156.8 (d, $^{1}J_{CF}$ = 259.5 Hz, *C*-3), 146.0 (d, $^{4}J_{HF}$ = 5.26 Hz, *C*-6), 138.9 (d, $^{2}J_{CF}$ = 25.9 Hz, *C*-2), 138.0 (*C*-Bn), 137.3 (*C*-Bn), 136.9 (*C*-Bn), 136.1 (d, $^{2}J_{CF}$ = 8.28 Hz, *C*-4), 128.8 – 127.6 (m, 14C, *C*-Bn), 127.1 (*C*-Bn), 123.5 (C-5), 100.7 (d, $^{3}J_{CF}$ = 3.06 Hz, *C*-1´), 81.0 (*C*-4´), 80.1 (d, $^{4}J_{CF}$ = 2.33 Hz, *C*-2´), 77.3 (*C*-3´), 73.6 (*C*-Bn), 73.4 (*C*-Bn), 72.9 (*C*-Bn), 69.4 (*C*-5´).

^{19}*F*-NMR (564 MHz, $CDCl_3$): δ [ppm] = Major-anomer: -127.7 (dd, $^{4}J_{HF}$ = 7.06 Hz, $^{3}J_{HF}$ = 2.64 Hz), Minor-anomer: -128.7 (d, $^{4}J_{HF}$ = 6.18 Hz).

HRMS (ESI^{+}): *m/z* = calcd: 516.2180 $[M+H]^{+}$, found: 516.2178 $[M+H]^{+}$.

4-(2´,3´,5´,Tri-*O*-benzyl-1´-*O*-acetyl-D-ribofuranosyl)-3-fluoropyridine 152

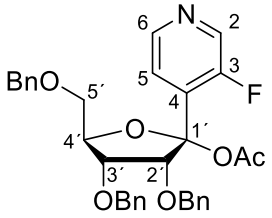

152
$C_{33}H_{32}FNO_6$
557.6184 g/mol

The reaction was carried out according to the general procedure IX with lactol **151** (1.95 g, 3.78 mmol) and LiHMDS (5.67 mL, 5.67 mmol, 1 M solution in THF) in THF (10 mL), followed by the addition of acetic anhydride (536 µL, 5.67 mmol). Purification of the crude product on silica gel with automated flash chromatography (petroleum ether/ethyl acetate; 10:1 to 3:1 v/v) provided **152** (1.77 g, 82%) as a colorless oil, which was obtained as a mixture of anomers.

^{1}*H*-NMR (600 MHz, $CDCl_3$): δ [ppm] = Major-anomer: 8.30 (d, $^{3}J_{HF}$ = 2.90 Hz, 1H, *H*-2), 8.15 (d, $^{3}J_{HH}$ = 5.01 Hz, 1H, *H*-6), 7.48 (dd, $^{4}J_{HF}$ = 6.67 Hz, $^{3}J_{HH}$ = 5.07 Hz, 1H, *H*-5), 7.34 – 7.12 (m, 15H, *H*-Bn), 4.63 – 4.48 (m, 4H, *H*-Bn), 4.47 – 4.46 (m, 1H, *H*-4´), 4.45 – 4.36 (m, 2H, *H*-Bn), 3.93 (dd, $^{3}J_{HH}$ =

5.50 Hz, $^{3}J_{HH}$ = 4.65 Hz, 1H, *H*-3´), 3.81 (d, $^{3}J_{HH}$ = 5.69 Hz, 1H, *H*-2´), 3.75 (dd, $^{2}J_{HH}$ = 10.46 Hz, $^{3}J_{HH}$ = 3.00 Hz, 1H, H-5´), 3.50 (dd, $^{2}J_{HH}$ = 10.6 Hz, $^{3}J_{HH}$ = 2.69 Hz, 1H, H-5´), 2.12 (s, 3H, *H*-Ac).

Minor-anomer: 8.37 (d, $^{3}J_{HF}$ = 4.83 Hz, 1H, *H*-6), 8.31 (d, $^{3}J_{HH}$ = 2.44 Hz, 1H, *H*-2), 7.66 (dd, $^{4}J_{HF}$ = 6.88 Hz, $^{3}J_{HH}$ = 5.09 Hz, 1H, *H*-5), 7.29 – 7.09 (m, 13H, *H*-Bn), 6.82 – 6.81 (m, 2H, *H*-Bn), 4.63 – 4.61 (m, 1H, *H*-Bn), 4.58 (d, $^{3}J_{HH}$ = 3.97 Hz, H-2´), 4.58 – 4.47 (m, 2H, *H*-Bn), 4.44 – 4.43 (m, 1H, H-4´), 4.42 – 4.36 (m, 2H, *H*-Bn), 4.30 (dd, $^{3}J_{HH}$ = 3.78 Hz, $^{3}J_{HH}$ = 1.59 Hz, 1H, *H*-3´), 4.19 (d, $^{2}J_{HH}$ = 11.7 Hz, 1H, *H*-Bn), 3.80 (dd, $^{3}J_{HH}$ = 11.2 Hz, $^{3}J_{HH}$ = 2.44 Hz, 1H, *H*-5´), 3.54 (dd, $^{3}J_{HH}$ = 11.4 Hz, $^{3}J_{HH}$ = 2.47 Hz, 1H, *H*-5´), 1.59 (s, 3H, *H*-Ac).

^{13}*C*-NMR (150 MHz, $CDCl_3$): δ [ppm] = Major-anomer: 169.3 (*C*-Ac), 155.4 (d, $^{1}J_{CF}$ = 259.1 Hz, *C*-3), 146.0 (d, $^{4}J_{HF}$ = 5.48 Hz, *C*-6), 138.8 (d, $^{2}J_{CF}$ = 25.7 Hz, *C*-2), 138.9 (2C, *C*-Bn), 137.1 (*C*-Bn), 136.1 (d, $^{2}J_{CF}$ = 8.69 Hz, *C*-4), 128.7 – 127.8 (m, 15C, *C*-Bn), 122.3 (*C*-5), 103.7 (d, $^{3}J_{CF}$ = 2.64 Hz, *C*-1´), 83.7 (*C*-2´), 83.6 (*C*-4´), 75.4 (*C*-3´), 73.7 (*C*-Bn), 73.6 (*C*-Bn), 72.7 (*C*-Bn), 69.1 (*C*-5´) 21.7 (C-Ac).

^{19}*F*-NMR (564 MHz, $CDCl_3$): δ [ppm] = Major-anomer: -130.2 (dd, $^{4}J_{HF}$ = 7.08 Hz, $^{3}J_{HF}$ = 2.48 Hz), Minor-anomer: -131.1 (d, $^{4}J_{HF}$ = 6.38 Hz).

HRMS (ESI^+): *m/z* = calcd: 558.2286 $[M+H]^+$, found: 558.2283 $[M+H]^+$.

4-(2´,3´,5´,Tri-*O*-benzyl-β-D-ribofuranosyl)-3-fluoropyridine 153

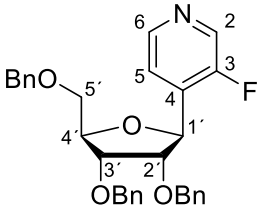

153
$C_{31}H_{30}FNO_4$
499.5824 g/mol

The acetylated lactone **152** (100 mg, 0.18 mmol) was dissolved in CH_2Cl_2 (2 mL), before Et_3SiH (687 µL, 4.30 mol) and BF_3-Et_2O (45 µL, 0.36 mmol) were added. After 1 h, TLC analysis showed no complete conversion, therefore, a second portion of $BF_3{\cdot}Et_2O$ (45 µL, 0.36 mmol) was added, and the reaction mixture was stirred for an additional hour at room temperature. The reaction was quenched by the addition of aq. $NaHCO_3$. Subsequently the mixture was extracted with CH_2Cl_2 three times and the combined organic layers were washed with sat. aq. $NaHCO_3$ and sat. aq. NaCl. The organic layer was then dried over $MgSO_4$, and all volatiles were removed under reduced pressure. Purification of the crude product on silica gel with automated flash

chromatography (petroleum ether/ethyl acetate; 10:1 to 4:1 v/v) provided the nucleoside **153** (55 mg, 58%) as a colorless solid.

^{1}*H*-NMR (600 MHz, $CDCl_3$): δ [ppm] = 8.37 (d, $^{3}J_{HF}$ = 1.71 Hz, 1H, *H*-2), 8.18 (d, $^{3}J_{HH}$ = 4.94 Hz, 1H, *H*-6), 7.62 (dd, $^{4}J_{HF}$ = 6.57 Hz, $^{3}J_{HH}$ = 5.76 Hz, 1H, *H*-5), 7.37 – 7.27 (m, 15H, *H*-Bn), 5.40 (d, $^{3}J_{HH}$ = 3.44 Hz, 1H, *H*-1´), 4.70 (d, $^{2}J_{HH}$ = 12.2 Hz, 1H, *H*-Bn), 4.62 (d, $^{2}J_{HH}$ = 8.25 Hz, 1H, *H*-Bn), 4.60 (d, $^{2}J_{HH}$ = 7.83 Hz, 1H, *H*-Bn), 4.55 (d, $^{2}J_{HH}$ = 6.93 Hz, 1H, *H*-Bn), 4.53 (d, $^{2}J_{HH}$ = 6.84 Hz, 1H, *H*-Bn), 4.41 (d, $^{2}J_{HH}$ = 12.0 Hz, 1H, *H*-Bn), 4.40 – 4.38 (m, 1H, *H*-4´), 4.02 (dd, $^{3}J_{HH}$ = 7.10 Hz, $^{3}J_{HH}$ = 4.75 Hz, 1H, *H*-3´), 3.94 (dd, $^{3}J_{HH}$ = 4.94 Hz, $^{3}J_{HH}$ = 4.12 Hz, 1H, *H*-2´), 3.87 (dd, $^{2}J_{HH}$ = 10.9 Hz, $^{3}J_{HH}$ = 2.77 Hz, 1H, *H*-5´), 3.68 (dd, $^{2}J_{HH}$ = 10.9 Hz, $^{3}J_{HH}$ = 3.22 Hz, 1H, *H*-5´).

^{13}*C*-NMR (150 MHz, $CDCl_3$): δ [ppm] = 156.7 (d, $^{1}J_{CF}$ = 255.9 Hz, *C*-3), 146.2 (d, $^{4}J_{HF}$ = 4.97 Hz, *C*-6), 138.1 (*C*-Bn), 137.7 (*C*-Bn), 137.6 (*C*-Bn), 137.5 (d, $^{2}J_{CF}$ = 23.7 Hz, *C*-2), 136.7 (d, $^{2}J_{CF}$ = 10.4 Hz, *C*-4), 128.6 (3C, *C*-Bn), 128.5 (3C, *C*-Bn), 128.1 (2C, *C*-Bn), 128.01 (*C*-Bn), 128.00 (*C*-Bn), 127.95 (2C, *C*-Bn), 127.90 (*C*-Bn), 127.8 (2C, *C*-Bn), 122.4 (C-5), 81.7 (*C*-2´), 80.9 (*C*-4´), 76.5 (2C, *C*-1´, C-3´), 73.6 (*C*-Bn), 72.3 (*C*-Bn), 71.9 (*C*-Bn), 69.3 (*C*-5´).

^{19}*F*-NMR (564 MHz, $CDCl_3$): -132.1 (d, $^{4}J_{HF}$ = 6.31 Hz).

HRMS (ESI^+): *m/z* = calcd: 500.2231 $[M+H]^+$, found: 500.2228 $[M+H]^+$.

4-(2´,3´,5´,Tri-*O*-benzyl-β-D-ribofuranosyl)-2-amide-3-fluoropyridine 156

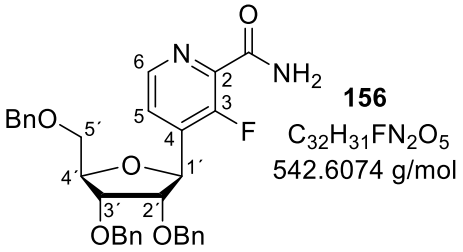

156
$C_{32}H_{31}FN_2O_5$
542.6074 g/mol

Step 1: To a solution of the nucleoside **153** (916 mg, 1.83 mmol) in CH_2Cl_2 (10 mL), *m*-CPBA (1.58 g, 9.16 mmol) was added. The reaction mixture was stirred for 2 h and then quenched by the addition of sat. aq. Na_2SO_3. Subsequently, the mixture was extracted with CH_2Cl_2 three times. The organic layer was then dried over $MgSO_4$ and all volatiles were removed under reduced pressure. Purification of the crude product on silica gel with automated flash chromatography (CH_2Cl_2/MeOH; 50:1 to 20:1 v/v) provided **154** as a colorless solid, which was dissolved in CH_3CN (10 mL). After the addition of TMSCN (574 µL, 4.59 mmol) and Et_3N (424 µL, 3.06 mmol), the

reaction mixture was refluxed for 5 h. Subsequently, the reaction was quenched by the addition of sat. aq. $NaHCO_3$ and the mixture was extracted with CH_2Cl_2 three times. The organic layer was then dried over $MgSO_4$ and all volatiles were removed under reduced pressure. Purification of the crude product on silica gel with automated flash chromatography (petroleum ether/ethyl acetate; 4:1 to 2:1 v/v) provided the nucleoside **155** (584 mg, 61%) as a colorless solid.

^{1}*H*-NMR (300 MHz, $CDCl_3$): δ [ppm] = 8.06 (d, $^3J_{HH}$ = 4.90 Hz, 1H, *H*-6), 7.62 (dd, $^4J_{HF}$ = 5.88 Hz, $^3J_{HH}$ = 5.29 Hz, 1H, *H*-5), 7.32 – 7.17 (m, 15H, *H*-Bn), 5.27 (d, $^3J_{HH}$ = 3.73 Hz, 1H, *H*-1´), 4.57 – 4.35 (m, 6H, *H*-Bn), 4.33 – 4.29 (m, 1H, *H*-4´), 3.95 (dd, $^3J_{HH}$ = 6.42 Hz, $^3J_{HH}$ = 4.61 Hz, 1H, *H*-3´), 3.94 (dd, $^3J_{HH}$ = 4.92 Hz, $^3J_{HH}$ = 4.37 Hz, 1H, *H*-2´), 3.80 (dd, $^2J_{HH}$ = 11.0 Hz, $^3J_{HH}$ = 2.68 Hz, 1H, *H*-5´), 3.59 (dd, $^2J_{HH}$ = 11.0 Hz, $^3J_{HH}$ = 2.68 Hz, 1H, *H*-5´).

Step 2: To a solution of the nucleoside **155** (450 mg, 0.85 mmol) in DMSO (12 mL), ground K_2CO_3 (474 mg, 3.43 mmol) and hydrogen peroxide (30%, 7.5 mL) were added. The reaction mixture was stirred for 1 h at room temperature and quenched with sat. aq. Na_2SO_3. Subsequently, the mixture was extracted three times with CH_2Cl_2 and the combined organic layers were washed with sat. aq. $NaHCO_3$ and sat. aq. NaCl. The organic layer was then dried over $MgSO_4$ and all volatiles were removed under reduced pressure. Purification of the crude product on silica gel with automated flash chromatography (petroleum ether/ethyl acetate; 2:1 to 1:1 v/v) provided **156** (253 mg, 54%) as a colorless solid.

^{1}*H*-NMR (600 MHz, $CDCl_3$): δ [ppm] = 7.99 (d, $^3J_{HH}$ = 4.72 Hz, 1H, *H*-6), 7.86 (dd, $^4J_{HF}$ = 5.47 Hz, $^3J_{HH}$ = 4.74 Hz, 1H, *H*-5), 7.60 (bs, 1H, -NH_2), 7.32 – 7.18 (m, 15H, *H*-Bn), 5.68 (bs, 1H, -NH_2), 5.41 (s, 1H, *H*-1´), 4.75 (d, $^2J_{HH}$ = 12.1 Hz, 1H, *H*-Bn), 4.60 (d, $^2J_{HH}$ = 12.0 Hz, 1H, *H*-Bn), 4.54 (d, $^2J_{HH}$ = 11.6 Hz, 1H, *H*-Bn), 4.49 – 4.47 (m,2H, *H*-Bn), 4.35 – 4.33 (m, 1H, *H*-4´), 4.31 (d, $^2J_{HH}$ = 11.8 Hz, 1H, *H*-Bn), 3.98 – 3.95 (m, 2H, *H*-3´, *H*-2´), 3.88 (dd, $^2J_{HH}$ = 10.8 Hz, $^3J_{HH}$ = 2.58 Hz, 1H, *H*-5´), 3.65 (dd, $^2J_{HH}$ = 10.8 Hz, $^3J_{HH}$ = 2.85 Hz, 1H, *H*-5´).

^{13}*C*-NMR (150 MHz, $CDCl_3$): δ [ppm] = 164.9 (d, $^3J_{CF}$ = 5.44 Hz, *C*-7), 156.5 (d, $^1J_{CF}$ = 272.8 Hz, *C*-3), 144.2 (d, $^4J_{CF}$ = 6.33 Hz, *C*-6), 140.2 (d, $^2J_{CF}$ = 11.7 Hz, *C*-4), 138.1 (*C*-Bn), 138.70 (*C*-Bn), 138.69 (*C*-Bn), 136.4 (d, $^2J_{CF}$ = 4.29 Hz, *C*-2), 128.56 (4C, *C*-Bn), 128.53 (4C, *C*-Bn), 128.03 (2C, *C*-Bn), 128.02 (*C*-Bn), 127.95 (*C*-Bn), 127.93 (2C, *C*-Bn), 127.88 (*C*-Bn), 126.8 (d, $^3J_{CF}$ = 1.77 Hz, *C*-5), 81.5 (*C*-2´), 80.3 (*C*-4´), 77.6 (d, $^3J_{CF}$ = 4.04 Hz, *C*-1´), 76.0 (*C*-3´), 73.6 (*C*-Bn), 72.4 (*C*-Bn), 72.1 (*C*-Bn), 68.7 (C-5´).

^{19}F-NMR (564 MHz, $CDCl_3$): -125.5 (d, $^4J_{HF}$ = 4.78 Hz).

HRMS (ESI^+): *m/z* = calcd: 543.2289 $[M+H]^+$, found: 543.2289 $[M+H]^+$.

4-(-β-D-Ribofuranosyl)-2-amide-3-fluoropyridine 157

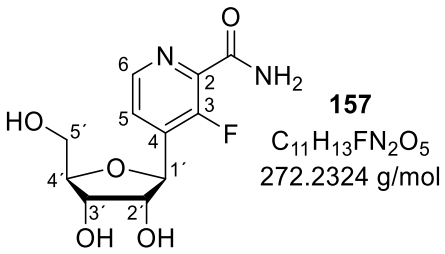

157

$C_{11}H_{13}FN_2O_5$

272.2324 g/mol

A solution of the nucleoside **156** (230 mg, 0.42 mmol) in CH_2Cl_2 (3 mL) was cooled to -78 °C before BCl_3 (1.69 mL, 1.69 mmol, 1 M solution in CH_2Cl_2) was added dropwise. After the reaction mixture was stirred for 1 h at -78 °C, the reaction was quenched by the addition of MeOH, followed by water. Subsequently, all volatiles were removed under reduced pressure. Purification of the crude product on RP18 with automated flash chromatography (H_2O/CH_3CN; 100:0 to 0:100) provided **157** (73 mg, 68%) as a colorless solid.

^1H-NMR (600 MHz, DMSO-d_6): δ [ppm] = 8.40 (d, $^3J_{HH}$ = 4.82 Hz, 1H, *H*-6), 8.02 (bs, 1H, -NH_2), 7.83 (dd, $^4J_{HF}$ = 5.58 Hz, $^3J_{HH}$ = 4.97 Hz, 1H, *H*-5), 7.67 (bs, 1H, -NH_2), 5.73 (bs, 3H, -O*H*), 5.41 (d, $^3J_{HH}$ = 5.56 Hz, 1H, *H*-1´), 3.90 – 3.84 (m, 3H, *H*-2´, *H*-3´, *H*-4´), 3.65 (dd, $^2J_{HH}$ = 11.9 Hz, $^3J_{HH}$ = 3.54 Hz, 1H, *H*-5´), 3.56 (dd, $^2J_{HH}$ = 11.9 Hz, $^3J_{HH}$ = 4.08 Hz, 1H, *H*-5´).

^{13}C-NMR (150 MHz, $CDCl_3$): δ [ppm] = 164.8 (d, $^3J_{CF}$ = 4.37 Hz, *C*-7), 155.2 (d, $^1J_{CF}$ = 267.5 Hz, *C*-3), 144.3 (d, $^4J_{CF}$ = 6.11 Hz, *C*-6), 139.7 (d, $^2J_{CF}$ = 10.6 Hz, *C*-4), 139.6 (d, $^2J_{CF}$ = 6.44 Hz, *C*-2), 125.0 (*C*-5), 84.6 (*C*-2´), 77.2 (*C*-4´), 77.0 (*C*-1´), 70.1 (*C*-3´), 61.1 (*C*-5´).

^{19}F-NMR (564 MHz, $CDCl_3$): -128.2 (d, $^4J_{HF}$ = 4.53 Hz).

HRMS (ESI^+): *m/z* = calcd: 273.0880 $[M+H]^+$, found: 273.0881 $[M+H]^+$.

4-(-β-D-Ribofuranosyl)-2-amide-3-fluoropyridine-5´-triphosphate 158

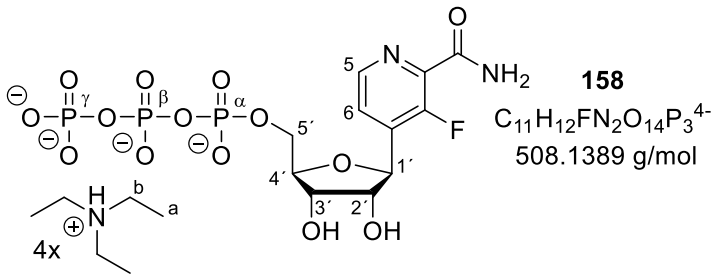

The reaction was carried out according to the general procedure VI with 4-(-β-D-ribofuranosyl)-2-amide-3-fluoropyridine **157** (20 mg, 0.09 mmol), proton sponge (31 mg, 0.15 mmol) and $POCl_3$ (27 µL, 0.29 mmol) in trimethyl phosphate (1 mL) for 15 min, followed by the addition of tributylammonium pyrophosphate (100 mg, 0.18 mmol) and tributylamine (121 µL, 0.43 mmol) in CH_3CN (1 mL) for 30 min. Purification by ion-exchange chromatography using a DEAE-Sephadex® A-25 column (H_2O/1 M TEAB; 100:0 to 0:100 v/v) and RP_{18} flash column chromatography (H_2O/CH_3CN; 100:0 to 0:100 v/v) provided the triethylammonium salt of **158** (44 mg, 65%) as a colorless solid.

^{1}*H*-NMR (300 MHz, DMSO-d_6): δ [ppm] = 8.41 (d, $^3J_{HH}$ = 4.85 Hz, 1H, *H*-6), 8.04 (bs, 1H, -NH_2), 7.89 (dd, $^4J_{HF}$ = 5.78 Hz, $^3J_{HH}$ = 5.08 Hz, 1H, *H*-5), 7.62 (bs, 1H, -NH_2),), 5.00 (d, $^3J_{HH}$ = 5.06 Hz, 1H, *H*-1´), 4.03 – 3.86 (m, 5H, *H*-2´, *H*-3´, *H*-4´, H-5´).

^{31}*P*-NMR (121 MHz, DMSO-d_6): δ [ppm] = -10.5 (d, $^2J_{PP}$ = 19.2 Hz, *P*-α), -13.2 (d, $^2J_{PP}$ = 25.7 Hz, *P*-γ), -23.3 (dd, $^2J_{PP}$ = 25.9 Hz, $^2J_{PP}$ = 19.3 Hz, *P*-β).

^{19}*F*-NMR (564 MHz, DMSO-d_6): δ [ppm] = -128.2 (d, $^4J_{HF}$ = 4.56 Hz).

HRMS (MALDI$^-$): *m/z* = calcd: 510.9725 $[M-H]^-$, found: 510.9904 $[M-H]^-$.

2,3-*O*-Isopropyliden-D-ribono-1,4-lactone 139

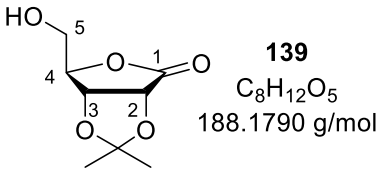

D-Ribono-1,4-lactone **138** (3.93 g, 26.5 mmol) was dissolved in acetone (80 mL), and conc. H_2SO_4 (2.4 mL) was added. After the reaction mixture was stirred overnight, it was cooled to 0 °C and Na_2CO_3 was added until pH = 6 was reached. The precipitated solid was removed by filtration and

extensively washed with acetone. After all volatiles were removed under reduced pressure, the crude product was purified on silica gel (petroleum ether/ethyl acetate; 1:1 v/v) to provide **139** (3.65 g, 73%) as a colorless oil.

^{1}*H*-NMR (400 MHz, $CDCl_3$): δ [ppm] = 4.83 (d, $^{3}J_{HH}$ = 5.58 Hz, 1H, *H*-3), 4.78 (d, $^{3}J_{HH}$ = 5.58 Hz, 1H, *H*-2), 4.63 (t, $^{3}J_{HH}$ = 1.94 Hz, 1H, *H*-4), 4.00 (dd, $^{2}J_{HH}$ = 12.3 Hz, $^{3}J_{HH}$ = 2.34 Hz, 1H, *H*-5), 3.80 (dd, $^{2}J_{HH}$ = 12.2 Hz, $^{3}J_{HH}$ = 1.66 Hz, 1H, *H*-5), 1.47 (s, 3H, O-C-(CH_3)$_2$), 1.38 (s, 3H, O-C-(CH_3)$_2$).

^{13}*C*-NMR (101 MHz, $CDCl_3$): δ [ppm] = 175.1 (*C*-1), 113.3 (*C*-$(CH_3)_2$), 82.8 (*C*-4), 78.4 (*C*-2), 75.78 (*C*-3), 62.1 (*C*-5), 26.9 (C-(*C*H_3)$_2$), 25.6 (C-(*C*H_3)$_2$).

HRMS (ESI^+): *m/z* = calcd: 188.0685 $[M+Na]^+$, found: 188.0615 $[M+Na]^+$.

5-*O*-(*tert*-Butyldiphenylsilyl)-2,3-*O*-Isopropyliden-D-ribono-1,4-lactone 140

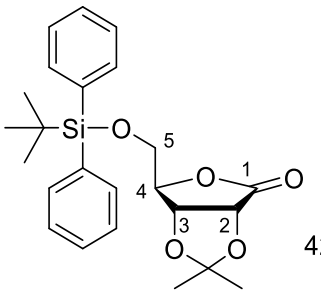

140
$C_{24}H_{30}O_5Si$
426.5840 g/mol

2,3-*O*-Isopropylidene-D-ribono-1,4-lactone **139** (3.58 g, 19.0 mmol) as well as imidazole (2.59 g, 38.0 mmol) were dissolved in CH_2Cl_2 (55 mL) and *tert*-butyldiphenylsilyl chloride (5.86 mL, 22.8 mmol) was added. After the reaction mixture was stirred overnight at room temperature, the reaction was quenched by the addition of water. The organic phase was washed with sat. aq. NaCl, dried over $MgSO_4$ and all volatiles were removed under reduced pressure. Purification of the crude product on silica gel (petroleum ether/ethyl acetate; 4:1 v/v) provided **140** (4.83 g, 60%) as a colorless oil.

The analytical data was in accordance with those described.[242]

^{1}*H*-NMR (400 MHz, $CDCl_3$): δ [ppm] = 7.73 – 7.61 (m, 4H, *H*-Aryl), 7.48 – 7.38 (m, 6H, *H*-Aryl) 4.90 (d, $^{3}J_{HH}$ = 5.79 Hz, 1H, *H*-3), 4.78 (d, $^{3}J_{HH}$ = 5.61 Hz, 1H, *H*-2), 4.63 (t, $^{3}J_{HH}$ = 1.95 Hz, 1H, *H*-4), 3.91 (dd, $^{2}J_{HH}$ = 11.6 Hz, $^{3}J_{HH}$ = 2.26 Hz, 1H, *H*-5), 3.75 (dd, $^{2}J_{HH}$ = 11.6 Hz, $^{3}J_{HH}$ = 1.54 Hz, 1H, *H*-5), 1.49 (s, 3H, O-C-(CH_3)$_2$), 1.40 (s, 3H, O-C-(CH_3)$_2$), 1.07 – 1.05 (m, 9H, *H*-*t*-Butyl).

^{13}C-NMR (150 MHz, $CDCl_3$): δ [ppm] = 174.2 (*C*-1), 135.7 (2C, *C*-Aryl), 135.6 (2C, *C*-Aryl), 134.9 (*C*-Aryl), 132.5 (*C*-Aryl), 131.6 (*C*-Aryl), 130.3 (*C*-Aryl), 129.8 (*C*-Aryl), 128.1 (2C, *C*-Aryl), 127.9 (*C*-Aryl), 113.3 (*C*-$(CH_3)_2$), 82.5 (*C*-4), 78.6 (*C*-2), 75.9 (*C*-3), 63.7 (*C*-5), 26.9 (C-(*C*$H_3)_3$), 26.8 (2C, C-(*C*$H_3)_3$, C-(*C*$H_3)_2$), 26.6 (C-(*C*$H_3)_3$), 25.7 (C-(*C*$H_3)_2$), 19.2 (*C*-$(CH_3)_3$).

HRMS (ESI^+): *m/z* = calcd: 449.1755 $[M+Na]^+$, found: 449.1755 $[M+Na]^+$.

2,3-*O*-Isopropyliden-2-*C*-methyl-D-ribono-1,4-lactone 160

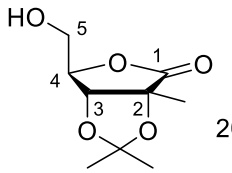

160
$C_9H_{14}O_5$
202.2060 g/mol

2-*C*-Methyl-D-ribono-1,4-lactone **159** (2.00 g, 12.3 mmol) was dissolved in acetone (40 mL) and conc. H_2SO_4 (1.2 mL) was added. After the reaction mixture was stirred overnight, it was cooled to 0 °C, and Na_2CO_3 was added until pH = 6 was reached. The precipitated solid was removed by filtration and extensively washed with acetone. After all volatiles were removed under reduced pressure, the crude product was purified on silica gel (petroleum ether/ethyl acetate; 1:1 v/v) to provide **160** (2.48 g, 99%) as a colorless oil.

The analytical data was in accordance with those described.[243]

^1H-NMR (600 MHz, $CDCl_3$): δ [ppm] = 4.54 – 4.53 (m, 2H, *H*-3, *H*-4) 3.97 (dd, $^2J_{HH}$ = 12.6 Hz, $^3J_{HH}$ = 3.05 Hz, 1H, *H*-5), 3.81 (dd, $^2J_{HH}$ = 12.6 Hz, $^3J_{HH}$ = 2.71 Hz, 1H, *H*-5), 1.64 (s, 3H, 2-C-CH_3), 1.43 (s, 3H, O-C-(C$H_3)_2$), 1.41 (s, 3H, O-C-(C$H_3)_2$).

^{13}C-NMR (150 MHz, $CDCl_3$): δ [ppm] = 176.9 (*C*-1), 112.3 (*C*-$(CH_3)_2$), 83.5 (*C*-3), 82.9 (*C*-2), 82.6 (*C*-4), 62.1 (*C*-5), 26.9 (C-(*C*$H_3)_2$), 26.3 (C-(*C*$H_3)_2$), 19.8 (2-C-*C*H_3).

HRMS (ESI^+): *m/z* = calcd: 225.0733 $[M+Na]^+$, found: 225.0738 $[M+Na]^+$.

5-*O*-(*tert*-Butyldiphenylsilyl)-2,3-*O*-*iso*propyliden-2-*C*-methyl-D-ribono-1,4-lactone 161

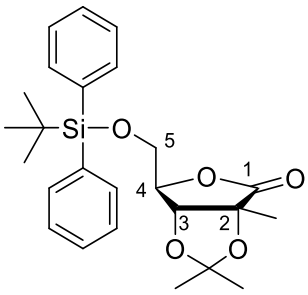

161
$C_{25}H_{32}O_5Si$
440.6110 g/mol

2,3-*O*-Isopropylidene-2-*C*-methyl-D-ribono-1,4-lactone **160** (2.75 g, 13.6 mmol) as well as imidazole (1.85 g, 27.2 mmol) were dissolved in CH_2Cl_2 (40 mL) and *tert*-butyldiphenylsilyl chloride (4.19 mL, 16.3 mmol) was added. After the reaction mixture was stirred overnight at room temperature, the reaction was quenched by the addition of water. The organic phase was washed with sat. aq. NaCl, dried over $MgSO_4$ and all volatiles were removed under reduced pressure. Purification of the crude product on silica gel (petroleum ether/ethyl acetate; 4:1 v/v) provided **161** (3.35 g, 55%) as a colorless oil.

The analytical data was in accordance with those described.[243]

^{1}*H*-NMR (400 MHz, $CDCl_3$): δ [ppm] = 7.73 – 7.63 (m, 4H, *H*-Aryl), 7.48 – 7.36 (m, 6H, *H*-Aryl) 4.53 – 4.50 (m, 2H, *H*-3, *H*-4) 3.82 (d,$^3J_{HH}$ = 3.64 Hz, 2H, *H*-5), 1.59 (s, 3H, 2-C-C*H*$_3$), 1.44 (s, 3H, O-C-(C*H*$_3$)$_2$), 1.43 (s, 3H, O-C-(C*H*$_3$)$_2$), 1.07 – 1.06 (m, 9H, *H*-*t*-Butyl).

^{13}*C*-NMR (150 MHz, $CDCl_3$): δ [ppm] = 176.3 (*C*-1), 135.7 (2C, *C*-Aryl), 135.6 (2C, *C*-Aryl), 135.0 (*C*-Aryl), 132.5 (*C*-Aryl), 132.2 (*C*-Aryl), 130.3 (*C*-Aryl), 129.8 (*C*-Aryl), 128.1 (2C, *C*-Aryl), 127.9 (*C*-Aryl), 112.5 (*C*-(CH$_3$)$_2$), 83.0 (*C*-3), 82.5 (*C*-2), 82.3 (*C*-4), 64.3 (*C*-5), 27.1 (C-(*C*H$_3$)$_2$), 27.0 (C-(*C*H$_3$)$_2$), 26.9 (3C, C-(*C*H$_3$)$_3$), 20.5 (2-C-*C*H$_3$), 19.3 (*C*-(CH$_3$)$_3$).

HRMS (ESI$^+$): *m/z* = calcd: 463.1911 [M+Na]$^+$, found: 463.1909 [M+Na]$^+$.

3,5-(1,1,3,3-Tetraisopropyldisiloxane-1,3-diyl)-2-deoxy-2-fluoro-2-*C*-methyl-D-ribono-1,4-lactone 174

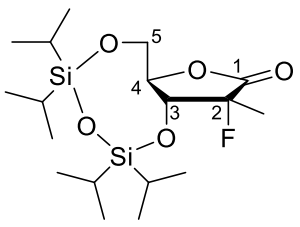

174
$C_{18}H_{35}FO_5Si_2$
406.6414 g/mol

2-Deoxy-2-fluoro-2-*C*-methyl-D-ribono-1,4-lactone **173** (3.54 g, 21.5 mmol) and 4-DMAP (1.31 g, 10.7 mmol) were dissolved in pyridine (50 mL) and 1,1,3,3-tetraisopropyl-1,3-dichlorodisiloxane (4.19 mL, 16.3 mmol) was added dropwise at 0°C. After the reaction mixture was stirred overnight at room temperature, all volatiles were removed under reduced pressure. Purification of the crude product on silica gel with automated flash chromatography (petroleum ether/ethyl acetate; 20:1 to 4:1 v/v) provided **174** (7.90 g, 90%) as a colorless syrup.

The analytical data was in accordance with those described.[244]

^{1}*H*-NMR (600 MHz, $CDCl_3$): δ [ppm] = 4.40 (dt, $^{3}J_{HH}$ = 8.54 Hz, $^{3}J_{HH}$ = 2.48 Hz, 1H, *H*-4), 4.19 (dd, $^{2}J_{HH}$ = 13.6 Hz, $^{3}J_{HH}$ = 2.20 Hz, 1H, *H*-5), 4.14 (dd, $^{3}J_{HF}$ = 25.1 Hz, $^{3}J_{HH}$ = 8.55 Hz, 1H, *H*-3), 4.08 (dd, $^{2}J_{HH}$ = 13.6 Hz, $^{3}J_{HH}$ = 2.76 Hz, 1H, *H*-5), 1.61 (d, $^{3}J_{HF}$ = 25.1 Hz, 3H, 2-C-CH_3), 1.11 – 0.98 (m, 28H, *H*-Isopropyl).

^{13}*C*-NMR (150 MHz, $CDCl_3$): δ [ppm] = 169.8 (d, $^{2}J_{CF}$ = 20.9 Hz, *C*-1), 92.6 (d, $^{1}J_{CF}$ = 184.8 Hz, *C*-2), 81.2 (*C*-4), 72.6 (d, $^{3}J_{HF}$ = 16.4 Hz, *C*-3), 59.2 (*C*-5), 17.4 – 17.0 (m), 13.9, 13.1, 12.8, 12.7 (13C, 2´-C-*C*H_3, *C*-Isopropyl).

^{19}*F*-NMR (564 MHz, $CDCl_3$): δ [ppm] = -173.5 (m).

HRMS (ESI^+): *m/z* = calcd: 407.2079 $[M+Na]^+$, found: 407.2070 $[M+Na]^+$.

4-(5´-*O*-(*tert*-Butyldiphenylsilyl)-1´-hydroxy-2´,3´-*O*-isopropyliden-D-ribofuranosyl)-2-cyano-3-fluoropyridine 142

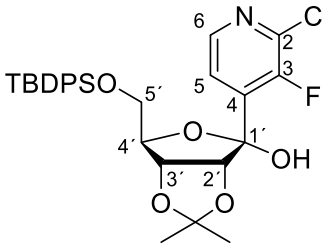

142
$C_{30}H_{33}FN_2O_5Si$
548.6864 g/mol

The reaction was carried out according to the general procedure VIII with 2-cyano-3-fluoropyridine **141** (2.90 g, 23.7 mmol) and LDA (24.0 mL, 23.9 mmol, 1 M solution in THF) in THF (75 mL), followed by the addition of lactone **140** (5.06 g, 11.8 mmol) in THF (17 mL). Purification of the crude product on silica gel with automated flash chromatography (petroleum ether/ethyl acetate; 10:1 to 3:1 v/v) provided **142** (4.69 g, 69%) as a colorless solid, which was obtained as a mixture of anomers.

^{1}H-NMR (600 MHz, $CDCl_3$): δ [ppm] = Major-anomer: 8.48 (d, $^{3}J_{HH}$ = 4.76 Hz, 1H, *H*-6), 7.85 (dd, $^{4}J_{HF}$ = 6.04 Hz, $^{3}J_{HH}$ = 5.29, 1H, *H*-5), 7.70 (dd, $^{3}J_{HH}$ = 8.31 Hz, $^{4}J_{HH}$ = 1.31 Hz, 2H, *H*-Ph), 7.64 (dd, $^{3}J_{HH}$ = 8.15 Hz, $^{4}J_{HH}$ = 1.40 Hz, 2H, *H*-Ph), 7.52 – 7.42 (m, 6H, *H*-Ph), 5.53 (bs, 1H, -O*H*), 4.94 (dd, $^{3}J_{HH}$ = 5.89 Hz, $^{3}J_{HH}$ = 2.19 Hz, 1H, *H*-3´), 4.85 (dd, $^{3}J_{HH}$ = 5.75 Hz, $^{3}J_{HH}$ = 0.84 Hz, 1H, *H*-2´), 4.45-4.42 (m, 1H, *H*-4´), 3.95 (dd, $^{2}J_{HH}$ = 11.5 Hz, $^{3}J_{HH}$ = 2.43 Hz, 1H, *H*-5´), 3.75 (dd, $^{2}J_{HH}$ = 11.5 Hz, $^{3}J_{HH}$ = 2.70 Hz, 1H, *H*-5´), 1.25 (s, 3H, C-(CH_3)$_2$), 1.18 (s, 3H, C-(CH_3)$_2$), 1.12 (s, 9H, C-(CH_3)$_3$).

Minor-anomer: 8.42 (d, $^{3}J_{HH}$ = 4.86 Hz, 1H, *H*-6), 7.61 (dd, $^{4}J_{HF}$ = 8.11 Hz, $^{3}J_{HH}$ = 5.21, 1H, *H*-5), 7.70 (dd, $^{3}J_{HH}$ = 8.22 Hz, $^{4}J_{HH}$ = 1.29 Hz, 2H, *H*-Ph), 7.59 (dd, $^{3}J_{HH}$ = 8.22 Hz, $^{4}J_{HH}$ = 1.34 Hz, 2H, *H*-Ph), 7.52 – 7.46 (m, 2H, *H*-Ph), 7.39 – 7.36 (m, 4H, *H*-Ph), 5.53 (bs, 1H, -O*H*), 4.88 – 4.87 (m, 1H, *H*-3´), 4.77 (dd, $^{3}J_{HH}$ = 7.21 Hz, $^{3}J_{HH}$ = 1.15 Hz, 1H, *H*-2´), 4.38- 4.36 (m, 1H, *H*-4´), 3.95 (dd, $^{2}J_{HH}$ = 11.5 Hz, $^{3}J_{HH}$ = 2.43 Hz, 1H, *H*-5´), 3.87 (dd, $^{2}J_{HH}$ = 11.4 Hz, $^{3}J_{HH}$ = 3.82 Hz, 1H, *H*-5´), 1.68 (s, 3H, C-(CH_3)$_2$), 1.43 (s, 3H, C-(CH_3)$_2$), 1.00 (s, 9H, C-(CH_3)$_3$).

^{13}C-NMR (150 MHz, $CDCl_3$): δ [ppm] = Major-anomer: 159.1 (d, $^{1}J_{CF}$ = 273.3 Hz, *C*-3), 146.6 (d, $^{4}J_{HF}$ = 5.45 Hz, *C*-6), 137.7 (d, $^{2}J_{CF}$ = 11.1 Hz, *C*-4), 135.9 (2C, *C*-Ph), 135.7 (2C, *C*-Ph), 131.4 (*C*-Ph), 131.2 (*C*-Ph), 130.8 (*C*-Ph), 130.6 (*C*-Ph), 128.4 (2C, *C*-Ph), 128.3 (2C, *C*-Ph), 126.6 (d, $^{3}J_{CF}$ = 2.98 Hz, *C*-5), 123.2 (d, $^{2}J_{CF}$ = 16.7 Hz, *C*-2), 113.5 (d, $^{3}J_{CF}$ = 3.98 Hz, -*C*N), 113.2 (*C*-(CH$_3$)$_2$), 105.7 (d, $^{3}J_{CF}$ = 2.39 Hz, C-1´), 93.9 (C-2´), 88.1 (C-3´), 82.0 (C-4´), 65.5 (C-5´), 27.0 (3C, C-(*C*H$_3$)$_3$), 26.2 (C-(*C*H$_3$)$_2$), 25.0 (C-(*C*H$_3$)$_2$), 19.3 (*C*-(CH$_3$)$_3$).

^{19}F-NMR (564 MHz, $CDCl_3$): δ [ppm] = Major-anomer: -115.4 (dd, $^{4}J_{HF}$ = 5.67 Hz, $^{5}J_{HF}$ = 1.79 Hz), Minor-anomer: -116.3 (d, $^{4}J_{HF}$ = 5.83 Hz).

4-(5´-O-(*tert*-Butyldiphenylsilyl)-1´-*O*-acetyl-2´,3´-*O*-isopropyliden-2´-*C*-methyl-D-ribofuranosyl)-2-cyano-3-fluoropyridine 143

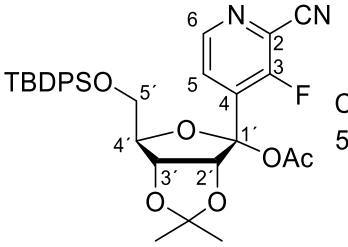

143
$C_{32}H_{35}FN_2O_6Si$
590.7234 g/mol

The reaction was carried out according to the general procedure IX with lactol **142** (4.30 g, 7.83 mmol) and LiHMDS (11.7 mL, 11.7 mmol, 1 M solution in THF) in THF (20 mL), followed by

the addition of acetic anhydride (1.11 mL, 11.7 mmol). Purification of the crude product on silica gel with automated flash chromatography (petroleum ether/ethyl acetate; 10:1 to 3:1) provided **143** (3.24 g, 71%) as a colorless solid, which was obtained as a mixture of anomers.

^{1}*H*-NMR (600 MHz, $CDCl_3$): δ [ppm] = Major-anomer: 8.37 (d, $^{3}J_{HH}$ = 4.93 Hz, 1H, *H*-6), 7.82 (dd, $^{4}J_{HF}$ = 6.01 Hz, $^{3}J_{HH}$ = 4.94, 1H, *H*-5), 7.60 (dd, $^{3}J_{HH}$ = 8.20 Hz, $^{4}J_{HH}$ = 1.37 Hz, 2H, *H*-Ph), 7.57 (dd, $^{3}J_{HH}$ = 8.14 Hz, $^{4}J_{HH}$ = 1.29 Hz, 2H, *H*-Ph), 7.49 – 7.40 (m, 6H, *H*-Ph), 4.81 (dd, $^{3}J_{HH}$ = 6.52 Hz, $^{3}J_{HH}$ = 2.23 Hz, 1H, *H*-3´), 4.60 (d, $^{3}J_{HH}$ = 6.45 Hz, 1H, *H*-2´), 4.55 (q, $^{3}J_{HH}$ = 2.40 Hz, 1H, *H*-4´), 4.06 (dd, $^{2}J_{HH}$ = 11.6 Hz, $^{3}J_{HH}$ = 2.73 Hz, 1H, *H*-5´), 3.62 (dd, $^{2}J_{HH}$ = 11.5 Hz, $^{3}J_{HH}$ = 2.40 Hz, 1H, *H*-5´), 2.13 (s, 3H, *H*-Ac), 1.71 (s, 3H, C-(CH_3)$_2$), 1.38 (s, 3H, C-(CH_3)$_2$), 0.98 (s, 9H, C-(CH_3)$_3$).

Minor-anomer: 8.50 (d, $^{3}J_{HH}$ = 5.00 Hz, 1H, *H*-6), 7.85 (dd, $^{4}J_{HF}$ = 6.01 Hz, $^{3}J_{HH}$ = 4.94, 1H, *H*-5), 7.68 – 7.65 (m, 1H, *H*-Ph), 7.49 – 7.37 (m, 9H, *H*-Ph), 5.00 (dd, $^{3}J_{HH}$ = 5.83 Hz, $^{3}J_{HH}$ = 1.96 Hz, 1H, *H*-3´), 4.92 (dd, $^{3}J_{HH}$ = 5.68 Hz, $^{3}J_{HH}$ = 1.02 Hz, 1H, *H*-2´), 4.61- 4.59 (m, 1H, *H*-4´), 3.77 (dd, $^{2}J_{HH}$ = 10.5 Hz, $^{3}J_{HH}$ = 4.84 Hz, 1H, *H*-5´), 3.68 (dd, $^{2}J_{HH}$ = 10.5 Hz, $^{3}J_{HH}$ = 8.31 Hz, 1H, *H*-5´), 2.04 (s, 3H, *H*-Ac), 1.71 (s, 3H, C-(CH_3)$_2$), 1.11 (s, 9H, C-(CH_3)$_3$), 1.08 (s, 3H, C-(CH_3)$_2$).

^{13}*C*-NMR (150 MHz, $CDCl_3$): δ [ppm] = Major-anomer: 168.8 (*C*-Ac), 157.7 (d, $^{1}J_{CF}$ = 273.1 Hz, *C*-3), 146.9 (d, $^{4}J_{CF}$ = 5.44 Hz, *C*-6), 137.8 (d, $^{2}J_{CF}$ = 9.78 Hz, *C*-4), 135.68 (*C*-Ph), 135.67 (*C*-Ph), 135.62 (2C, *C*-Ph), 132.7 (*C*-Ph), 132.6 (*C*-Ph), 130.33 (*C*-Ph), 130.32 (*C*-Ph), 128.2 (*C*-Ph), 128.1 (2C, *C*-Ph), 128.0 (*C*-Ph), 126.6 (*C*-5), 123.7 (d, $^{2}J_{CF}$ = 15.9 Hz, *C*-2), 116.0 (*C*-(CH_3)$_2$), 113.0 (d, $^{3}J_{CF}$ = 4.86 Hz, -*C*N), 102.5 (*C*-1´), 87.5 (*C*-2´), 84.6 (*C*-3´), 80.9 (*C*-4´), 63.7 (*C*-5´), 26.9 (3C, C-(*C*H_3)$_3$), 26.1 (C-(*C*H_3)$_2$), 25.6 (C-(*C*H_3)$_2$), 21.6 (*C*-Ac), 19.3 (*C*-(CH_3)$_3$).

Minor-anomer: 168.2 (*C*-Ac), 157.6 (d, $^{1}J_{CF}$ = 269.7 Hz, *C*-3), 146.6 (d, $^{4}J_{CF}$ = 5.39 Hz, *C*-6), 136.2 (d, $^{2}J_{CF}$ = 9.97 Hz, *C*-4), 135.68 (*C*-Ph), 135.67 (*C*-Ph), 135.62 (2C, *C*-Ph), 133.0 (*C*-Ph), 132.8 (*C*-Ph), 130.22 (*C*-Ph), 130.20 (*C*-Ph), 128.2 (*C*-Ph), 128.1 (2C, *C*-Ph), 128.0 (*C*-Ph), 127.7 (*C*-5), 122.8 (d, $^{2}J_{CF}$ = 16.4 Hz, *C*-2), 113.8 (*C*-(CH_3)$_2$), 113.2 (d, $^{3}J_{CF}$ = 4.50 Hz, -*C*N), 107.8 (*C*-1´), 87.6 (*C*-2´), 86.7 (*C*-3´), 82.0 (*C*-4´), 64.0 (*C*-5´), 26.9 (3C, C-(*C*H_3)$_3$), 25.9 (C-(*C*H_3)$_2$), 25.0 (C-(*C*H_3)$_2$), 21.4 (*C*-Ac), 19.4 (*C*-(CH_3)$_3$).

^{19}*F*-NMR (564 MHz, $CDCl_3$): δ [ppm] = Major-anomer: -118.4 (d, $^{4}J_{HF}$ = 5.80 Hz), Minor-anomer: -119.0 (d, $^{4}J_{HF}$ = 5.51 Hz).

HRMS (ESI$^+$): *m/z* = calcd: 591.2320 $[M+H]^+$, found: 591.2324 $[M+H]^+$.

4-(5´-*O*-(*tert*-Butyldiphenylsilyl)-2´,3´-*O*-isopropyliden-D-ribofuranosyl)-2-cyano-3-fluoropyridine 144

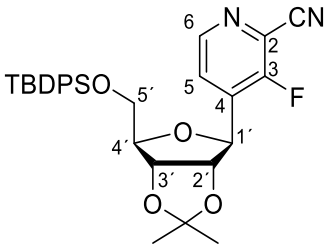

144
$C_{30}H_{33}FN_2O_4Si$
532.6874 g/mol

The acetylated lactone **143** (3.10 g, 4.13 mmol) was dissolved in CH_2Cl_2 (60 mL) before Et_3SiH (20.2 mL, 0.13 mol) and $BF_3{\cdot}Et_2O$ (1.33 mL, 10.5 mmol) were added. After 1 h, TLC analysis showed incomplete conversion. Therefore, a second portion of $BF_3{\cdot}Et_2O$ (1.33 mL, 10.5 mmol) was added and the reaction mixture was stirred for an additional hour at room temperature. The reaction was quenched by the addition of aq. $NaHCO_3$. Subsequently, the mixture was extracted three times with CH_2Cl_2, and the combined organic layers were washed with sat. aq. $NaHCO_3$ and sat. aq. NaCl. The organic layer was then dried over $MgSO_4$ and all volatiles were removed under reduced pressure. Purification of the crude product on silica gel with automated flash chromatography (petroleum ether/ethyl acetate; 10:1 to 4:1) provided **144** (2.34 g, 84%) as a colorless solid, which was obtained as a mixture of anomers.

^{1}*H*-NMR (600 MHz, $CDCl_3$): δ [ppm] = Major-anomer: 8.45 (d, $^3J_{HH}$ = 4.75 Hz, 1H, *H*-6), 7.76 (dd, $^4J_{HF}$ = 5.45 Hz, $^3J_{HH}$ = 5.02, 1H, *H*-5), 7.76 – 7.67 (m, 4H, *H*-Ph), 7.48 – 7.37 (m, 6H, *H*-Ph), 5.59 (d, $^3J_{HH}$ = 4.58 Hz, 1H, *H*-1´), 5.11 – 5.09 (m, 1H, *H*-2´), 4.94 (d, $^3J_{HH}$ = 6.34 Hz, 1H, *H*-3´), 4.35 (t, $^3J_{HH}$ = 2.68 Hz, 1H, *H*-4´), 3.94 (dd, $^2J_{HH}$ = 11.9 Hz, $^3J_{HH}$ = 3.00 Hz, 1H, *H*-5´), 3.79 (dd, $^2J_{HH}$ = 11.4 Hz, $^3J_{HH}$ = 2.95 Hz, 1H, *H*-5´), 1.27 (s, 3H, C-(CH_3)$_2$), 1.23 (s, 3H, C-(CH_3)$_2$), 1.10 (s, 9H, C-(CH_3)$_3$).

Minor-anomer: 8.34 (d, $^3J_{HH}$ = 4.81 Hz, 1H, *H*-6), 7.76 (dd, $^4J_{HF}$ = 5.84 Hz, $^3J_{HH}$ = 5.35, 1H, *H*-5), 7.76 – 7.67 (m, 4H, *H*-Ph), 7.48 – 7.37 (m, 6H, *H*-Ph), 5.18 (d, $^3J_{HH}$ = 4.92 Hz, 1H, *H*-1´), 4.76 (dd, $^3J_{HH}$ = 6.46 Hz, $^3J_{HH}$ = 3.30 Hz, 1H, *H*-3´), 4.55 (dd, $^3J_{HH}$ = 6.33, $^3J_{HH}$ = 5.52 Hz, 1H, *H*-2´), 4.29 (q, $^3J_{HH}$ = 3.66 Hz, 1H, *H*-4´), 4.00 (dd, $^2J_{HH}$ = 11.9 Hz, $^3J_{HH}$ = 3.03 Hz, 1H, *H*-5´), 3.87 (dd, $^2J_{HH}$ = 11.5 Hz, $^3J_{HH}$ = 3.40 Hz, 1H, *H*-5´), 1.63 (s, 3H, C-(CH_3)$_2$), 1.36 (s, 3H, C-(CH_3)$_2$), 1.04 (s, 9H, C-(CH_3)$_3$).

^{13}*C*-NMR (150 MHz, $CDCl_3$): δ [ppm] = Major-anomer: 158.3 (d, $^1J_{CF}$ = 269.5 Hz, *C*-3), 146.8 (d, $^4J_{CF}$ = 5.15 Hz, *C*-6), 137.1 (d, $^2J_{CF}$ = 11.3 Hz, *C*-4), 135.7 (2C, *C*-Ph), 135.6 (2C, *C*-Ph), 132.58 (*C*-Ph), 132.53 (*C*-Ph), 130.3 (*C*-Ph), 130.2 (*C*-Ph), 128.09 (2C, *C*-Ph), 128.09 (2C, *C*-Ph), 127.2 (d, $^3J_{CF}$ =

2.95 Hz, *C*-5), 121.9 (d, $^{2}J_{CF}$ = 15.0 Hz, *C*-2), 113.3 (d, $^{3}J_{CF}$ = 4.37 Hz, -*C*N), 113.0 (*C*-$(CH_3)_2$), 84.7 (*C*-4´), 83.5 (*C*-3´), 82.0 (*C*-2´), 78.3 (*C*-1´), 66.2 (*C*-5´), 27.0 (3C, C-(*C*$H_3)_3$), 26.0 (C-(*C*$H_3)_2$), 24.7 (C-(*C*$H_3)_2$), 19.2 (*C*-$(CH_3)_3$).

Minor-anomer: 159.0 (d, $^{1}J_{CF}$ = 268.1 Hz, *C*-3), 147.1 (d, $^{4}J_{CF}$ = 5.51 Hz, *C*-6), 138.6 (d, $^{2}J_{CF}$ = 11.3 Hz, *C*-4), 135.7 (2C, *C*-Ph), 135.6 (2C, *C*-Ph), 133.1 (*C*-Ph), 132.9 (*C*-Ph), 130.2 (*C*-Ph), 130.1 (*C*-Ph), 128.02 (2C, *C*-Ph), 127.97 (2C, *C*-Ph), 126.1 (d, $^{3}J_{CF}$ = 2.83 Hz, *C*-5), 122.6 (d, $^{2}J_{CF}$ = 15.83 Hz, *C*-2), 115.0 (*C*-$(CH_3)_2$), 113.3 (d, $^{3}J_{CF}$ = 4.54 Hz, -*C*N), 86.7 (*C*-2´), 86.1 (*C*-4´), 81.7 (*C*-3´), 79.9 (*C*-1´), 64.1 (*C*-5´), 27.7 (C-(*C*$H_3)_2$), 27.0 (3C, C-(*C*$H_3)_3$), 25.6 (C-(*C*$H_3)_2$), 19.4 (*C*-$(CH_3)_3$).

^{19}*F*-NMR (564 MHz, $CDCl_3$): δ [ppm] = Major-anomer: -121.5 (d, $^{4}J_{HF}$ = 5.29 Hz), Minor-anomer: -120.2 (d, $^{4}J_{HF}$ = 5.44 Hz).

HRMS (ESI$^+$): *m/z* = calcd: 533.2266 $[M+H]^+$, found: 533.2266 $[M+H]^+$.

4-(2´,3´-*O*-Isopropyliden-D-ribofuranosyl)-2-amide-3-fluoropyridine 145

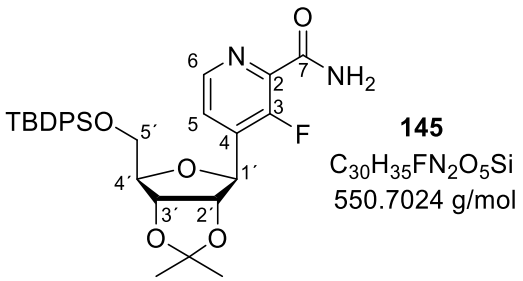

145
$C_{30}H_{35}FN_2O_5Si$
550.7024 g/mol

To a solution of the nucleoside **144** (1.38 g, 2.59 mmol) in DMSO (40 mL), ground K_2CO_3 (1.42 g, 10.3 mmol) and hydrogen peroxide (30%, 26 mL) were added. The reaction mixture was stirred for 1 h at room temperature and quenched with sat. aq. Na_2SO_3. Subsequently, the mixture was extracted three times with CH_2Cl_2 and the combined organic layers were washed with sat. aq. $NaHCO_3$ as well as sat. aq. NaCl. The organic layer was then dried over $MgSO_4$ and all volatiles were removed under reduced pressure. Purification of the crude product on silica gel with automated flash chromatography (petroleum ether/ethyl acetate; 2:1 to 1:1 v/v) provided **145** (1.05 g, 72%) as a colorless solid.

^{1}*H*-NMR (300 MHz, $CDCl_3$): δ [ppm] = α-Anomer: 8.36 (d, $^{3}J_{HH}$ = 4.81 Hz, 1H, *H*-6), 7.71 (dd, $^{4}J_{HF}$ = 5.65 Hz, $^{3}J_{HH}$ = 5.62, 2H, -NH_2, *H*-5), 7.67 – 7.62 (m, 4H, *H*-Ph), 7.47 – 7.34 (m, 6H, *H*-Ph), 5.62 (d, $^{3}J_{HH}$ = 4.51 Hz, 1H, H-1´), 5.58 (bs, 1H, -NH_2), 5.14 – 5.09 (m, 1H, *H*-2´), 4.93 (d, $^{3}J_{HH}$ = 5.67 Hz, 1H,

H-3´), 4.32 (t, $^3J_{HH}$ = 2.99 Hz, 1H, *H*-4´), 3.92 (dd, $^2J_{HH}$ =11.4 Hz, $^3J_{HH}$ = 3.24 Hz, 1H, *H*-5´), 3.76 (dd, $^2J_{HH}$ = 11.3 Hz, $^3J_{HH}$ = 3.18 Hz, 1H, *H*-5´), 1.25 (s, 6H, C-(C*H*$_3$)$_2$), 1.08 (s, 9H, C-(C*H*$_3$)$_3$).

HRMS (ESI$^+$): *m/z* = calcd: 551.2371 [M+H]$^+$, found: 551.2379 [M+H]$^+$.

4-(2´,3´-*O*-isopropyliden-D-ribofuranosyl)-2-amide-3-fluoropyridine 146

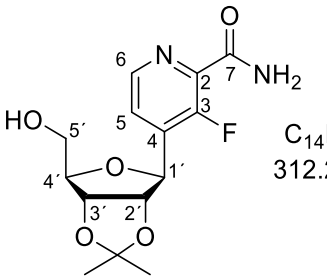

146
$C_{14}H_{17}FN_2O_5$
312.2974 g/mol

To a solution of the nucleoside **145** (189 mg, 0.35 mmol) in THF (2.5 mL) was added TBAF (368 µL, 0.36 mmol, 1 M solution in THF). After the reaction mixture was stirred for 1 h at room temperature, it was quenched with sat. aq. $NaHCO_3$. Subsequently, the mixture was extracted three times with CH_2Cl_2 and the combined organic layers were washed with sat. aq. $NaHCO_3$ as well as sat. aq. NaCl. The organic layer was then dried over $MgSO_4$ and all volatiles were removed under reduced pressure. Purification of the crude product on silica gel with automated flash chromatography (CH_2Cl_2/MeOH; 100:1 to 20:1 v/v) provided **146** (60 mg, 57%) as a colorless solid.

^{1}*H*-NMR (300 MHz, MeOD-*d*$_4$): *δ* [ppm] = α-Anomer: 8.45 (d, $^3J_{HH}$ = 4.93 Hz, 1H, *H*-6), 7.72 (dd, $^4J_{HF}$ = 5.28 Hz, $^3J_{HH}$ = 4.89, 1H, *H*-5), 5.51 (d, $^3J_{HH}$ = 4.41 Hz, 1H, *H*-1´), 5.17 – 5.13 (m, 1H, *H*-2´), 4.94 (d, $^3J_{HH}$ = 6.02 Hz, 1H, *H*-3´), 4.33 (t, $^3J_{HH}$ = 4.56 Hz, 1H, *H*-4´), 3.94 (d, $^3J_{HH}$ = 4.71 Hz, 1H, *H*-5´), 1.28 (s, 3H, C-(C*H*$_3$)$_2$), 1.24 (s, 3H, C-(C*H*$_3$)$_2$).

HRMS (ESI$^+$): *m/z* = calcd: 313.1193 [M+H]$^+$, found: 313.1200 [M+H]$^+$.

4-(α-D-Ribofuranosyl)-2-amide-3-fluoropyridine 147

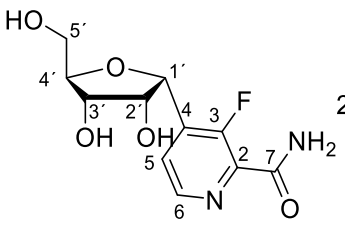

147
$C_{11}H_{13}FN_2O_5$
272.2324 g/mol

To a solution of the nucleoside **146** (50 mg, 0.16 mmol) in MeOH (2 mL) was added Dowex 50W H$^+$ form (160 mg). The reaction mixture was stirred for 1 h at 70 °C. Subsequently, the reaction

mixture was filtered and all volatiles were removed under reduced pressure. Purification of the crude product on silica gel with automated flash chromatography (H_2O/CH_3CN; 100:0 to 0:100 v/v) provided **147** (36 mg, 79%) as a colorless solid.

^{1}*H*-NMR (600 MHz, D_2O): δ [ppm] = 8.47 (d, $^3J_{HH}$ = 5.07 Hz, 1H, *H*-6), 7.81 (dd, $^4J_{HF}$ = 5.58 Hz, $^3J_{HH}$ = 5.07, 1H, *H*-5), 5.33 (d, $^3J_{HH}$ = 3.65 Hz, 1H, *H*-1´), 4.62 – 4.60 (m, 1H, *H*-4´), 4.40 (dd, $^3J_{HH}$ = 8.90 Hz, $^3J_{HH}$ = 4.49 Hz, 1H, *H*-3´), 3.97 (dd, $^2J_{HH}$ = 12.5 Hz, $^3J_{HH}$ = 2.54 Hz, 1H, *H*-5´), 3.88 (dd, $^2J_{HH}$ = 12.5 Hz, $^3J_{HH}$ = 5.15 Hz, 1H, *H*-5´), 4.06 (ddd, $^3J_{HH}$ = 8.00 Hz, $^3J_{HH}$ = 5.11 Hz, $^3J_{HH}$ = 2.50 Hz, 1H, *H*-4´).

^{13}*C*-NMR (150 MHz, D_2O): δ [ppm] = 167.6 (d, $^3J_{CF}$ = 4.36 Hz, *C*-7), 155.3 (d, $^1J_{CF}$ = 264.2 Hz, *C*-3), 144.9 (d, $^4J_{CF}$ = 5.88 Hz, *C*-6), 137.9 (d, $^2J_{CF}$ = 12.8 Hz, *C*-4), 136.9 (d, $^2J_{CF}$ = 10.4 Hz, *C*-2), 126.6 (d, $^3J_{CF}$ = 2.57 Hz, *C*-5), 81.3 (*C*-4´), 76.8 (d, $^3J_{CF}$ = 2.10 Hz, *C*-1´), 72.2 (*C*-2´), 71.8 (*C*-3´), 61.2 (*C*-5´).

^{19}*F*-NMR (564 MHz, D_2O): δ [ppm] = -127.2 (d, $^4J_{HF}$ = 4.43 Hz).

HRMS (ESI^+): *m/z* = calcd: 273.0880 $[M+H]^+$, found: 273.0883 $[M+H]^+$.

4-(5´-*O*-(*tert*-Butyldiphenylsilyl)-1´-hydroxy-2´,3´-*O*-isopropyliden-2´-methyl-*C*-D-ribofuranosyl)-2-cyano-3-fluoropyridine 162

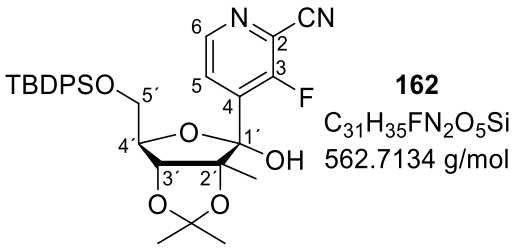

162
$C_{31}H_{35}FN_2O_5Si$
562.7134 g/mol

The reaction was carried out according to the general procedure VIII with 2-cyano-3-fluoropyridine **141** (590 mg, 4.83 mmol) and LDA (4.88 mL, 4.88 mmol, 1 M solution in THF) in THF (35 mL), followed by the addition of lactone **161** (1.06 g, 2.41 mmol) in THF (5 mL). Purification of the crude product on silica gel with automated flash chromatography (petroleum ether/ethyl acetate; 10:1 to 3:1 v/v) provided **162** (580 mg, 65%) as a colorless solid, which was obtained as a mixture of anomers.

^{1}*H*-NMR (600 MHz, $CDCl_3$): δ [ppm] = Major-anomer: 8.48 (d, $^3J_{HH}$ = 4.87 Hz, 1H, *H*-6), 7.85 (dd, $^4J_{HF}$ = 5.96 Hz, $^3J_{HH}$ = 4.89, 1H, *H*-5), 7.72 – 7.65 (m, 4H, *H*-Ph), 7.51 – 7.39 (m, 6H, *H*-Ph), 5.15 (bs, 1H, -O*H*), 4.65 (d, $^3J_{HH}$ = 1.73 Hz, 1H, *H*-3´), 4.42 – 4.40 (m, 1H, *H*-4´), 3.89 (dd, $^2J_{HH}$ = 11.6 Hz, $^3J_{HH}$

= 3.18 Hz, 1H, *H*-5´), 3.75 (dd, $^{2}J_{HH}$ = 11.5 Hz, $^{3}J_{HH}$ = 2.59 Hz, 1H, *H*-5´), 1.64 (s, 3H, 2´-C-C*H*$_3$), 1.35 (s, 3H, C-(C*H*$_3$)$_2$), 1.29 (s, 3H, C-(C*H*$_3$)$_2$), 1.12 (s, 9H, C-(C*H*$_3$)$_3$).

Minor-anomer: 8.44 (d, $^{3}J_{HH}$ = 4.75 Hz, 1H, *H*-6), 7.72 – 7.65 (m, 5H, *H*-5, *H*-Ph), 7.51 – 7.39 (m, 6H, *H*-Ph), 4.77 (bs, 1H, -O*H*), 4.59 (d, $^{3}J_{HH}$ = 3.67 Hz, 1H, *H*-3´), 4.42- 4.40 (m, 1H, *H*-4´), 4.02 (dd, $^{2}J_{HH}$ = 11.7 Hz, $^{3}J_{HH}$ = 3.37 Hz, 1H, *H*-5´), 3.95 (dd, $^{2}J_{HH}$ = 11.7 Hz, $^{3}J_{HH}$ = 3.10 Hz, 1H, *H*-5´), 1.69 (s, 3H, 2´-C-C*H*$_3$), 1.50 (s, 3H, C-(C*H*$_3$)$_2$), 1.19 (s, 3H, C-(C*H*$_3$)$_2$), 1.07 (s, 9H, C-(C*H*$_3$)$_3$).

^{13}*C*-NMR (150 MHz, $CDCl_3$): δ [ppm] = Major-anomer: 159.3 (d, $^{1}J_{CF}$ = 273.1 Hz, *C*-3), 146.3 (d, $^{4}J_{CF}$ = 5.51 Hz, *C*-6), 137.6 (d, $^{2}J_{CF}$ = 9.93 Hz, *C*-4), 135.8 (2C, *C*-Ph), 135.7 (2C, *C*-Ph), 131.5 (*C*-Ph), 131.3 (*C*-Ph), 130.6 (*C*-Ph), 130.5 (*C*-Ph), 128.31 (2C, *C*-Ph), 128.26 (2C, *C*-Ph), 127.9 (d, $^{3}J_{CF}$ = 25.5 Hz, *C*-5), 123.7 (d, $^{2}J_{CF}$ = 18.46 Hz, *C*-2), 113.8 (*C*-(CH$_3$)$_2$), 113.6 (d, $^{3}J_{CF}$ = 3.96 Hz, -*C*N), 106.7 (d, $^{3}J_{CF}$ = 3.29 Hz, *C*-1´), 93.9 (*C*-2´), 88.1 (*C*-3´), 85.8 (*C*-4´), 65.2 (*C*-5´), 28.3 (C-(*C*H$_3$)$_2$), 27.6 (C-(*C*H$_3$)$_2$), 27.0 (3C, C-(*C*H$_3$)$_3$), 20.5 (d, $^{5}J_{CF}$ = 4.65 Hz, 2´-C-*C*H$_3$), 19.3 (*C*-(CH$_3$)$_3$).

Minor-anomer: 159.3 (d, $^{1}J_{CF}$ = 273.1 Hz, *C*-3), 147.0 (d, $^{4}J_{CF}$ = 5.59 Hz, *C*-6), 138.6 (d, $^{2}J_{CF}$ = 9.60 Hz, *C*-4), 135.8 (2C, *C*-Ph), 135.7 (2C, *C*-Ph), 131.5 (*C*-Ph), 131.3 (*C*-Ph), 130.6 (*C*-Ph), 130.5 (*C*-Ph), 128.3 (2C, *C*-Ph), 128.26 (2C, *C*-Ph), 126.7 (*C*-5), 123.7 (d, $^{2}J_{CF}$ = 18.5 Hz, *C*-2), 116.7 (*C*-(CH$_3$)$_2$), 113.6 (d, $^{3}J_{CF}$ = 3.96 Hz, -*C*N), 102.3 (*C*-1´), 93.9 (*C*-2´), 86.6 (*C*-3´), 82.1 (*C*-4´), 63.2 (*C*-5´), 27.2 (C-(*C*H$_3$)$_2$), 27.0 (3C, C-(*C*H$_3$)$_3$), 26.0 (C-(*C*H$_3$)$_2$), 22.9 (2´-C-*C*H$_3$), 19.4 (*C*-(CH$_3$)$_3$).

^{19}*F*-NMR (564 MHz, $CDCl_3$): δ [ppm] = Major-anomer: -112.9 (d, $^{4}J_{HF}$ = 5.94 Hz), Minor-anomer: -116.3 (bs).

HRMS (ESI$^+$): *m/z* = calcd: 563.2371 $[M+H]^+$, found: 563.2370 $[M+H]^+$.

4-(5´-*O*-(*tert*-Butyldiphenylsilyl)-1´-*O*-acetyl-2´,3´-*O*-*iso*propyliden-2´-*C*-methyl-D-ribofuranosyl)-2-cyano-3-fluoropyridine 163

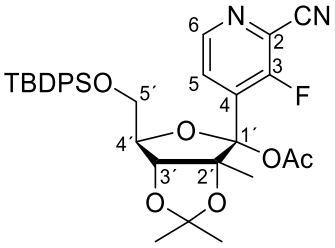

163
$C_{33}H_{37}FN_2O_6Si$
604.7504 g/mol

The reaction was carried out according to the general procedure IX with lactol **162** (800 mg, 1.42 mmol) and LiHMDS (2.13 mL, 2.13 mmol, 1 M solution in THF) in THF (5 mL), followed by the

addition of acetic anhydride (202 µL, 2.13 mmol). Purification of the crude product on silica gel with automated flash chromatography (petroleum ether/ethyl acetate; 10:1 to 3:1 v/v) provided **163** (682 mg, 79%) as a colorless solid, which was obtained as a mixture of anomers.

^{1}*H*-NMR (600 MHz, $CDCl_3$): δ [ppm] = Major-anomer: 8.48 (d, $^{3}J_{HH}$ = 4.94 Hz, 1H, *H*-6), 7.81 (bs, 1H, *H*-5), 7.72 – 7.64 (m, 4H, *H*-Ph), 7.49 – 7.40 (m, 6H, *H*-Ph), 4.54 – 4.51 (m, 2H, *H*-3´, *H*-4´), 3.79 (dd, $^{2}J_{HH}$ = 10.5 Hz, $^{3}J_{HH}$ = 5.25 Hz, 1H, *H*-5´), 3.62 (dd, $^{2}J_{HH}$ = 10.2 Hz, $^{3}J_{HH}$ = 9.48 Hz, 1H, *H*-5´), 1.80 (s, 3H, *H*-Ac), 1.56 (s, 3H, 2´-C-CH_3), 1.31 (s, 3H, C-(CH_3)$_2$), 1.10 (s, 9H, C-(CH_3)$_3$), 1.09 (s, 3H, C-(CH_3)$_2$).

Minor-anomer: 8.46 (d, $^{3}J_{HH}$ = 4.94 Hz, 1H, *H*-6), 7.72 – 7.65 (m, 5H, *H*-5, *H*-Ph), 7.49 – 7.40 (m, 6H, *H*-Ph), 4.54 – 4.51 (m, 1H, *H*-3´), 4.41 (q, $^{3}J_{HH}$ = 3.31 Hz, 1H, H-4´), 3.98 (dd, $^{2}J_{HH}$ = 11.8 Hz, $^{3}J_{HH}$ = 3.83 Hz, 1H, *H*-5´), 3.95 (dd, $^{2}J_{HH}$ = 11.7 Hz, $^{3}J_{HH}$ = 3.21 Hz, 1H, *H*-5´), 2.12 (s, 3H, *H*-Ac), 1.71 (s, 3H, 2´-C-CH_3), 1.44 (s, 3H, C-(CH_3)$_2$), 1.07 (s, 9H, C-(CH_3)$_3$), 1.01 (s, 3H, C-(CH_3)$_2$).

^{13}*C*-NMR (150 MHz, $CDCl_3$): δ [ppm] = Major-anomer: 168.0 (*C*-Ac), 157.6 (d, $^{1}J_{CF}$ = 273.1 Hz, *C*-3), 146.5 (d, $^{4}J_{CF}$ = 5.36 Hz, *C*-6), 136.5 (d, $^{2}J_{CF}$ = 9.57 Hz, *C*-4), 135.8 (3C, *C*-Ph), 135.7 (2C, *C*-Ph), 133.0 (*C*-Ph), 132.79 (*C*-Ph), 132.76 (*C*-Ph), 130.25 (2C, *C*-Ph), 130.23 (2C, *C*-Ph), 127.9 (d, $^{3}J_{CF}$ = 25.5 Hz, *C*-5), 123.7 (d, $^{2}J_{CF}$ = 18.5 Hz, *C*-2), 113.6 (*C*-(CH_3)$_2$), 113.3 (d, $^{3}J_{CF}$ = 4.06 Hz, -*C*N), 108.4 (*C*-1´), 93.8 (*C*-2´), 88.2 (*C*-3´), 85.9 (*C*-4´), 63.6 (*C*-5´), 27.0 (3C, C-(*C*H_3)$_3$), 26.7 (C-(*C*H_3)$_2$), 26.6 (C-(*C*H_3)$_2$), 26.2 (2´-C-*C*H_3), 21.3 (*C*-Ac), 19.4 (*C*-(CH_3)$_3$).

Minor-anomer: 168.8 (*C*-Ac), 157.6 (d, $^{1}J_{CF}$ = 273.1 Hz, *C*-3), 146.8 (d, $^{4}J_{CF}$ = 5.28 Hz, *C*-6), 136.5 (d, $^{2}J_{CF}$ = 9.57 Hz, *C*-4), 135.8 (3C, *C*-Ph), 135.7 (2C, *C*-Ph), 133.0 (*C*-Ph), 132.79 (*C*-Ph), 132.76 (*C*-Ph), 130.25 (2C, *C*-Ph), 130.23 (2C, *C*-Ph), 127.9 (d, $^{3}J_{CF}$ = 25.5 Hz, *C*-5), 123.7 (d, $^{2}J_{CF}$ = 18.5 Hz, *C*-2), 113.6 (*C*-(CH_3)$_2$), 113.3 (d, $^{3}J_{CF}$ = 4.06 Hz, -*C*N), 108.4 (*C*-1´), 91.3 (*C*-2´), 85.6 (*C*-3´), 83.5 (*C*-4´), 63.2 (*C*-5´), 27.0 (3C, C-(*C*H_3)$_3$), 26.3 (C-(*C*H_3)$_2$), 22.8 (C-(*C*H_3)$_2$), 21.3 (2C, *C*-Ac, 2´-C-*C*H_3), 19.4 (*C*-(CH_3)$_3$).

^{19}*F*-NMR (564 MHz, $CDCl_3$): δ [ppm] = Major-anomer: -118.6 (d, $^{4}J_{HF}$ = 5.94 Hz), Minor-anomer: -117.3 (bs).

HRMS (ESI$^+$): *m/z* = calcd: 605.2477 $[M+H]^+$, found: 605.2495 $[M+H]^+$.

4-(5´-*O*-(*tert*-Butyldiphenylsilyl)-1´-*O*-acetyl-2´,3´-*O*-*iso*propyliden-2´-*C*-methyl-D-ribofuranosyl)-2-cyano-3-fluoropyridine 165

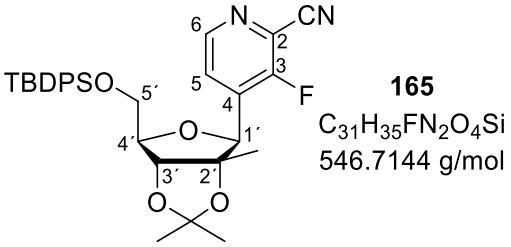

165
$C_{31}H_{35}FN_2O_4Si$
546.7144 g/mol

The acetylated lactone **163** (2.50 g, 4.13 mmol) was dissolved in CH_2Cl_2 (50 mL) before Et_3SiH (15.8 mL, 99.2 mmol) and $BF_3{\cdot}Et_2O$ (1.05 mL, 8.26 mmol) were added. After 1 h, TLC analysis showed nearly no conversion. Therefore, a second portion of $BF_3{\cdot}Et_2O$ (1.05 mL, 8.26 mmol) was added, and the reaction mixture was stirred overnight at room temperature. The reaction was quenched by the addition of aq. $NaHCO_3$. Subsequently, the mixture was extracted three times with CH_2Cl_2 and the combined organic layers were washed with sat. aq. $NaHCO_3$ as well as sat. aq. NaCl. The organic layer was then dried over $MgSO_4$ and all volatiles were removed under reduced pressure. Purification of the crude product on silica gel with automated flash chromatography (petroleum ether/ethyl acetate; 95:5 to 85:15 v/v) provided the α-anomer **164** (852 mg, 38%) and the β-anomer **165** (955 mg, 42%) as colorless solids.

^{1}*H*-NMR (600 MHz, $CDCl_3$): δ [ppm] = β-Anomer: 8.45 (d, $^3J_{HH}$ = 4.85 Hz, 1H, *H*-6), 7.72 (dd, $^3J_{HH}$ = 8.28 Hz, $^4J_{HH}$ = 1.41 Hz, 2H, *H*-Ph), 7.69 (dd, $^3J_{HH}$ = 8.26 Hz, $^4J_{HH}$ = 1.42 Hz, 2H, *H*-Ph), 7.57 (dd, $^4J_{HF}$ = 5.21 Hz, $^3J_{HH}$ = 5.05 Hz, 1H, *H*-5), 7.49 – 7.32 (m, 6H, *H*-Ph), 5.16 (s, 1H, *H*-1´), 4.46 (d, $^3J_{HH}$ = 2.52 Hz, 1H, *H*-3´), 4.27 (q, $^3J_{HH}$ = 3.87 Hz, 1H, *H*-4´), 3.92 (d, $^3J_{HH}$ = 4.07 Hz, 2H, *H*-5´), 1.64 (s, 3H, C-(C*H*$_3$)$_2$), 1.42 (s, 3H, C-(C*H*$_3$)$_2$), 1.09 (s, 9H, C-(C*H*$_3$)$_3$), 1.00 (s, 3H, 2´-C-C*H*$_3$).

α-Anomer: 8.52 (d, $^3J_{HH}$ = 4.73 Hz, 1H, *H*-6), 7.76 (dd, $^4J_{HF}$ = 5.25 Hz, $^3J_{HH}$ = 5.17 Hz, 1H, *H*-5), 7.67 – 7.65 (m, 4H, *H*-Ph), 7.47 – 7.37 (m, 6H, *H*-Ph), 5.25 (s, 1H, *H*-1´), 4.66 (d, $^3J_{HH}$ = 1.01 Hz, 1H, *H*-3´), 4.33 (dt, $^3J_{HH}$ = 4.37 Hz, $^3J_{HH}$ = 1.06 Hz, 1H, *H*-4´), 3.86 (dd, $^3J_{HH}$ = 11.6 Hz, $^3J_{HH}$ = 4.77 Hz, 1H, *H*-5´), 3.81 (dd, $^3J_{HH}$ = 11.2 Hz, $^3J_{HH}$ = 4.17 Hz, 1H, *H*-5´), 1.56 (d, $^4J_{HH}$ = 1.70 Hz, 3H, 2´-C-C*H*$_3$), 1.34 (s, 3H, C-(C*H*$_3$)$_2$), 1.30 (s, 3H, C-(C*H*$_3$)$_2$), 1.10 (s, 9H, C-(C*H*$_3$)$_3$).

^{13}*C*-NMR (150 MHz, $CDCl_3$): δ [ppm] = β-Anomer: 158.8 (d, $^1J_{CF}$ = 268.0 Hz, *C*-3), 146.6 (d, $^4J_{CF}$ = 5.41 Hz, *C*-6), 136.5 (d, $^2J_{CF}$ = 11.0 Hz, *C*-4), 135.8 (2C, *C*-Ph), 132.8 (*C*-Ph), 132.7 (*C*-Ph), 130.18 (2C, *C*-Ph), 130.16 (2C, *C*-Ph), 128.2 (d, $^3J_{CF}$ = 2.70 Hz, *C*-5), 128.04 (2C, *C*-Ph), 128.01 (2C, *C*-Ph),

122.2 (d, $^{2}J_{CF}$ = 16.0 Hz, *C*-2), 113.4 (*C*-$(CH_3)_2$), 113.3 (d, $^{3}J_{CF}$ = 4.54 Hz, -*C*N), 90.9 (*C*-2´), 89.2 (*C*-3´), 85.1 (*C*-4´), 81.5 (*C*-1´), 65.1 (*C*-5´), 27.5 (C-$(CH_3)_2$), 27.2 (C-$(CH_3)_2$), 27.0 (3C, C-$(CH_3)_3$), 22.9 (d, $^{3}J_{CF}$ = 4.02 Hz, 2´-C-*C*H_3), 19.3 (*C*-$(CH_3)_3$).

α-Anomer: 158.0 (d, $^{1}J_{CF}$ = 271.4 Hz, *C*-3), 146.9 (d, $^{4}J_{CF}$ = 5.44 Hz, *C*-6), 136.4 (d, $^{2}J_{CF}$ = 11.9 Hz, *C*-4), 135.77 (2C, *C*-Ph), 135.76 (2C, *C*-Ph), 133.2 (*C*-Ph), 133.1 (*C*-Ph), 130.15 (2C, *C*-Ph), 130.12 (2C, *C*-Ph), 128.0 (2C, *C*-Ph), 126.6 (d, $^{3}J_{CF}$ = 2.56 Hz, *C*-5), 122.2 (d, $^{2}J_{CF}$ = 16.0 Hz, *C*-2), 114.9 (*C*-$(CH_3)_2$), 113.1 (d, $^{3}J_{CF}$ = 4.35 Hz, -*C*N), 89.5 (*C*-2´), 87.1 (*C*-3´), 83.8 (*C*-4´), 81.2 (*C*-1´), 63.8 (*C*-5´), 28.3 (*C*-$(CH_3)_2$), 27.0 (3C, C-$(CH_3)_3$), 26.8 (C-$(CH_3)_2$), 20.3 (2´-C-*C*H_3), 19.4 (*C*-$(CH_3)_3$).

^{19}F-NMR (564 MHz, $CDCl_3$): δ [ppm] = β-anomer: -118.1 (d, $^{4}J_{HF}$ = 5.87 Hz), α-anomer: -120.5 (d, $^{4}J_{HF}$ = 3.79 Hz).

HRMS (ESI^+): *m/z* = calcd: 547.2422 $[M+H]^+$, found: 547.2426 $[M+H]^+$.

4-(5´-*O*-(*tert*-Butyldiphenylsilyl)-2´,3´-*O*-*iso*propyliden-2´-*C*-methyl-β-D-ribofuranosyl)-2-amide-3-fluoropyridine 167

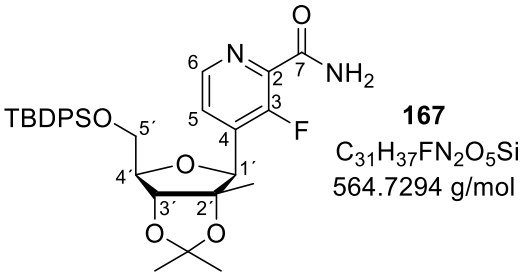

167
$C_{31}H_{37}FN_2O_5Si$
564.7294 g/mol

To a solution of the nucleoside **165** (426 mg, 0.78 mmol) in DMSO (12 mL), ground K_2CO_3 (429 mg, 3.11 mmol) and hydrogen peroxide (30%, 8 mL) were added. The reaction mixture was stirred for 1 h at room temperature and quenched with sat. aq. Na_2SO_3. Subsequently, the mixture was extracted three times with CH_2Cl_2 and the combined organic layers were washed with sat. aq. $NaHCO_3$ as well as sat. aq. NaCl. The organic layer was then dried over $MgSO_4$ and all volatiles were removed under reduced pressure. Purification of the crude product on silica gel with automated flash chromatography (petroleum ether/ethyl acetate; 2:1 to 1:1 v/v) provided **167** (258 mg, 71%) as a colorless solid.

^{1}H-NMR (600 MHz, $CDCl_3$): δ [ppm] = β-Anomer: 8.32 (d, $^{3}J_{HH}$ = 4.75 Hz, 1H, *H*-6), 7.74 (dd, $^{3}J_{HH}$ = 8.24 Hz, $^{4}J_{HH}$ = 1.34 Hz, 2H, *H*-Ph), 7.70 (dd, $^{3}J_{HH}$ = 8.13 Hz, $^{4}J_{HH}$ = 1.37 Hz, 2H, *H*-Ph), 7.67 (bs, 1H, -NH_2), 7.56 (dd, $^{4}J_{HF}$ = 5.56 Hz, $^{3}J_{HH}$ = 4.49 Hz, 1H, *H*-5), 7.48 – 7.45 (m, 2H, *H*-Ph), 7.44 – 7.40 (m,

4H, *H*-Ph), 5.76 (bs, 1H, -NH_2), 5.24 (s, 1H, *H*-1´), 4.45 (d, $^3J_{HH}$ = 2.63 Hz, 1H, *H*-3´), 4.26 (q, $^3J_{HH}$ = 3.93 Hz, 1H, *H*-4´), 3.92 (dd, $^3J_{HH}$ = 4.07 Hz, $^4J_{HH}$ = 1.42 Hz, 2H, *H*-5´), 1.63 (s, 3H, C-(CH_3)$_2$), 1.39 (s, 3H, C-(CH_3)$_2$), 1.09 (s, 9H, C-(CH_3)$_3$), 1.01 (s, 3H, 2´-C-CH_3).

^{13}*C*-NMR (150 MHz, $CDCl_3$): δ [ppm] = β-Anomer: 164.5 (d, $^3J_{CF}$ = 5.56 Hz, *C*-7), 157.1 (d, $^1J_{CF}$ = 275.0 Hz, *C*-3), 143.7 (d, $^4J_{CF}$ = 5.61 Hz, *C*-6), 137.8 (d, $^2J_{CF}$ = 12.47 Hz, *C*-4), 136.8 (d, $^2J_{CF}$ = 4.23 Hz, *C*-2), 135.8 (4C, *C*-Ph), 133.2 (*C*-Ph), 133.1 (*C*-Ph), 130.10 (2C, *C*-Ph), 130.07 (2C, *C*-Ph), 128.0 (2C, *C*-Ph), 126.3 (d, $^3J_{CF}$ = 1.78 Hz, *C*-5), 114.8 (*C*-(CH_3)$_2$), 89.6 (*C*-2´), 87.2 (*C*-3´), 83.6 (*C*-4´), 81.4 (*C*-1´), 63.9 (*C*-5´), 28.4 (C-(*C*H_3)$_2$), 27.0 (3C, C-(*C*H_3)$_3$), 26.9 (C-(*C*H_3)$_2$), 20.5 (2´-C-*C*H_3), 19.4 (*C*-(CH_3)$_3$).

^{19}*F*-NMR (564 MHz, $CDCl_3$): δ [ppm] = β-anomer: -121.5 (s).

HRMS (ESI^+): *m/z* = calcd: 565.2528 $[M+H]^+$, found: 565.2528 $[M+H]^+$.

4-(5´-O-(*tert*-Butyldiphenylsilyl)-2´,3´-*O*-isopropyliden-2´-*C*-methyl-α-D-ribofuranosyl)-2-amide-3-fluoropyridine 166

The α-anomer was synthesized in the same way as the β-anomer: Using nucleoside **164** (450 mg, 0.83 mmol) in DMSO (7 mL), together with K_2CO_3 (454 mg, 3.29 mmol) and hydrogen peroxide (30%, 7 mL), provided **166** (330 mg, 57%) as a colorless solid.

^{1}*H*-NMR (300 MHz, $CDCl_3$): δ [ppm] = α-Anomer: 8.37 (d, $^3J_{HH}$ = 4.53 Hz, 1H, *H*-6), 7.74 – 7.65 (m, 6H, *H*-5, -NH_2 *H*-Ph), 7.47 – 7.33 (m, 6H, *H*-Ph), 6.14 (bs, 1H, -NH_2), 5.53 (s, 1H, *H*-1´), 4.67 (d, $^3J_{HH}$ = 0.79 Hz, 1H, *H*-3´), 4.26 (t, $^3J_{HH}$ = 4.70 Hz, 1H, *H*-4´), 3.85 (dd, $^2J_{HH}$ =11.1 Hz, $^3J_{HH}$ = 4.62 Hz, 1H, *H*-5´), 3.79 (dd, $^2J_{HH}$ = 11.3 Hz, $^3J_{HH}$ = 4.20 Hz, 1H, *H*-5´), 1.58 (d, $^4J_{HH}$ = 1.75 Hz, 3H, 2´-C-CH_3), 1.34 (s, 6H, C-(CH_3)$_2$), 1.09 (s, 9H, C-(CH_3)$_3$).

4-(2´,3´-*O*-*Iso*propyliden-2´-*C*-methyl-β-D-ribofuranosyl)-2-amide-3-fluoropyridine 169

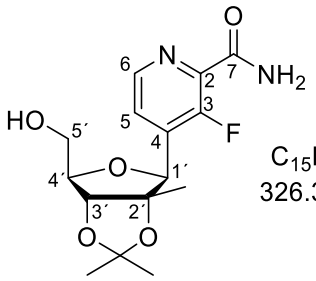

169
$C_{15}H_{19}FN_2O_5$
326.3244 g/mol

To a solution of the nucleoside **167** (750 mg, 1.32 mmol) in THF (15 mL) was added TBAF (1.46 mL, 1.46 mmol, 1 M solution in THF). After the reaction mixture was stirred for 1 h at room

temperature, it was quenched with sat. aq. $NaHCO_3$. Subsequently, the mixture was extracted three times with CH_2Cl_2 and the combined organic layers were washed with sat. aq. $NaHCO_3$ as well as sat. aq. NaCl. The organic layer was then dried over $MgSO_4$ and all volatiles were removed under reduced pressure. Purification of the crude product on silica gel with automated flash chromatography (CH_2Cl_2/MeOH; 100:1 to 20:1 v/v) provided **169** (431 mg, 99%) as a colorless solid.

^{1}*H*-NMR (600 MHz, $CDCl_3$): δ [ppm] = β-Anomer: 8.35 (d, $^3J_{HH}$ = 4.80 Hz, 1H, *H*-6), 7.66 (dd, $^4J_{HF}$ = 4.41 Hz, $^3J_{HH}$ = 4.21 Hz, 2H, -N*H*$_2$, *H*-5), 6.15 (bs, 1H, -N*H*$_2$), 5.24 (s, 1H, *H*-1´), 4.39 (d, $^3J_{HH}$ = 2.81 Hz, 1H, *H*-3´), 4.26 (q, $^3J_{HH}$ = 3.64 Hz, 1H, *H*-4´), 3.94 (dd, $^2J_{HH}$ = 12.0 Hz, $^3J_{HH}$ = 1.42 Hz, 1H, *H*-5´), 3.84 (dd, $^2J_{HH}$ = 12.0 Hz, $^3J_{HH}$ = 4.59 Hz, 1H, *H*-5´), 1.62 (s, 3H, C-(C*H*$_3$)$_2$), 1.38 (s, 3H, C-(C*H*$_3$)$_2$), 1.06 (s, 3H, 2´-C-C*H*$_3$).

^{13}*C*-NMR (150 MHz, $CDCl_3$): δ [ppm] = β-Anomer: 164.5 (d,$^3J_{CF}$ = 5.39 Hz, *C*-7), 157.0 (d, $^1J_{CF}$ = 273.1 Hz, *C*-3), 144.0 (d, $^4J_{CF}$ = 6.28 Hz, *C*-6), 137.1 (d, $^2J_{CF}$ = 12.8 Hz, *C*-4), 136.9 (d, $^2J_{CF}$ = 4.54 Hz, *C*-2), 126.4 (d, $^3J_{CF}$ = 2.13 Hz, *C*-5), 114.9 (*C*-(CH$_3$)$_2$), 89.7 (*C*-2´), 87.3 (*C*-3´), 83.7 (*C*-4´), 81.8 (*C*-1´), 62.8 (*C*-5´), 28.3 (C-(*C*H$_3$)$_2$), 26.8 (C-(*C*H$_3$)$_2$), 20.1 (2´-C-*C*H$_3$).

^{19}*F*-NMR (564 MHz, $CDCl_3$): δ [ppm] = β-anomer: -121.9 (d, $^4J_{HF}$ = 5.00 Hz).

HRMS (ESI$^+$): *m/z* = calcd: 327.1350 [M+H]$^+$, found: 327.1356 [M+H]$^+$.

4-(2´,3´-*O*-isopropyliden-2´-*C*-methyl-α-D-ribofuranosyl)-2-amide-3-fluoropyridine 168

The α-anomer was synthesized in the same way as the β-anomer: Using nucleoside **166** (300 mg, 0.53 mmol) in THF (7 mL), together with TBAF (584 µL, 0.58 mmol, 1 M solution in THF), provided **168** (172 mg, 99%) as a colorless solid.

^{1}*H*-NMR (300 MHz, $CDCl_3$): δ [ppm] = α-Anomer: 8.35 (d, $^3J_{HH}$ = 4.68 Hz, 1H, *H*-6), 7.72 (dd, $^4J_{HF}$ = 4.52 Hz, $^3J_{HH}$ = 4.72 Hz, 2H, -N*H*$_2$, *H*-5), 5.98 (bs, 1H, -N*H*$_2$), 5.30 (s, 1H, *H*-1´), 4.50 (d, $^3J_{HH}$ = 0.71 Hz, 1H, *H*-3´), 4.39 (t, $^3J_{HH}$ = 5.21 Hz, 1H, *H*-4´), 3.94 (dd, $^2J_{HH}$ = 12.0 Hz, $^3J_{HH}$ = 1.42 Hz, 1H, *H*-5´), 3.81 (d, $^3J_{HH}$ = 5.36 Hz, 2H, *H*-5´), 1.68 (d, $^4J_{HH}$ = 1.80 Hz, 3H, 2´-C-C*H*$_3$), 1.32 (s, 3H, C-(C*H*$_3$)$_2$), 1.28 (s, 3H, C-(C*H*$_3$)$_2$).

4-(2´-*C*-Methyl-β-D-ribofuranosyl)-2-amide-3-fluoropyridine 171

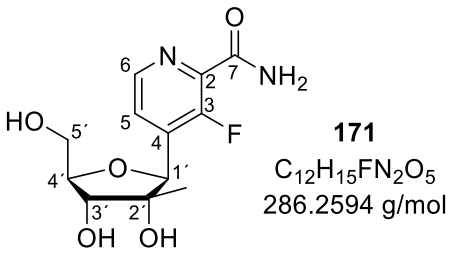

171
$C_{12}H_{15}FN_2O_5$
286.2594 g/mol

To a solution of the nucleoside **169** (380 mg, 1.16 mmol) in MeOH (10 mL) was added Dowex 50W H^+ form (2.00 g). The reaction mixture was stirred for 1 h at 70 °C. Subsequently, the reaction mixture was filtered and all volatiles were removed under reduced pressure. Purification of the crude product on silica gel with automated flash chromatography (H_2O/CH_3CN; 100:0 to 0:100 v/v) provided **170** (283 mg, 85%) as a colorless solid.

^{1}*H*-NMR (600 MHz, D_2O): δ [ppm] = β-Anomer: 8.46 (d, $^3J_{HH}$ = 4.83 Hz, 1H, *H*-6), 7.83 (dd, $^4J_{HF}$ = 5.15 Hz, $^3J_{HH}$ = 5.15 Hz, 1H, *H*-5), 5.32 (s, 1H, *H*-1´), 4.06 (ddd, $^3J_{HH}$ = 7.97 Hz, $^3J_{HH}$ = 5.17 Hz, $^3J_{HH}$ = 2.80 Hz, 1H, *H*-4´), 4.02 (dd, $^2J_{HH}$ = 12.7 Hz, $^3J_{HH}$ = 2.77 Hz, 1H, *H*-5´), 3.88 (dd, $^2J_{HH}$ = 12.6 Hz, $^3J_{HH}$ = 5.53 Hz, 1H, *H*-5´), 4.39 (d, $^3J_{HH}$ = 7.73 Hz, 1H, *H*-3´), 0.98 (s, 3H, 2´-C-CH_3).

^{13}*C*-NMR (150 MHz, D_2O): δ [ppm] = β-Anomer: 167.6 (d, $^3J_{CF}$ = 4.32 Hz, *C*-7), 155.6 (d, $^1J_{CF}$ = 265.0 Hz, *C*-3), 144.1 (d, $^4J_{CF}$ = 5.92 Hz, *C*-6), 138.0 (d, $^2J_{CF}$ = 12.1 Hz, *C*-4), 137.6 (d, $^2J_{CF}$ = 10.5 Hz, *C*-2), 126.4 (d, $^3J_{CF}$ = 2.21 Hz, *C*-5), 82.4 (*C*-4´), 81.0 (*C*-1´), 78.8 (*C*-2´), 74.5 (*C*-3´), 61.0 (*C*-5´), 20.3 (2´-C-*C*H_3).

^{19}*F*-NMR (564 MHz, D_2O): δ [ppm] = β-anomer: -126.1 (d, $^4J_{HF}$ = 5.29 Hz).

HRMS (ESI^+): *m/z* = calcd: 287.1037 $[M+H]^+$, found: 287.1035 $[M+H]^+$.

4-(2´-*C*-Methyl-α-D-ribofuranosyl)-2-amide-3-fluoropyridine 170

The α-anomer was synthesized in the same way as the β-anomer: Using nucleoside **168** (130 mg, 0.40 mmol) in MeOH (4 mL), along with Dowex 50W (1.00 g) provided **170** (92 mg, 95%) as a colorless solid.

^{1}*H*-NMR (300 MHz, D_2O): δ [ppm] = α-Anomer: 8.49 (d, $^3J_{HH}$ = 4.92 Hz, 1H, *H*-6), 7.81 (dd, $^4J_{HF}$ = 5.02 Hz, $^3J_{HH}$ = 5.02 Hz, 1H, *H*-5), 5.42 (s, 1H, *H*-1´), 4.20 (ddd, $^3J_{HH}$ = 9.09 Hz, $^3J_{HH}$ = 4.46 Hz, $^3J_{HH}$ =

2.23 Hz, 1H, *H*-4´), 4.15 (d, $^{3}J_{HH}$ = 8.86 Hz, 1H, *H*-3´), 4.02 (dd, $^{2}J_{HH}$ = 12.7 Hz, $^{3}J_{HH}$ = 2.23 Hz, 1H, *H*-5´), 3.88 (dd, $^{2}J_{HH}$ = 12.5 Hz, $^{3}J_{HH}$ = 4.48 Hz, 1H, *H*-5´), 1.38 (d, $^{3}J_{HH}$ = 2.80 Hz, 3H, 2´-C-C*H*$_3$).

4-(2´-*C*-Methyl-β-D-ribofuranosyl)-2-amide-3-fluoropyridine-5´-triphosphate 172

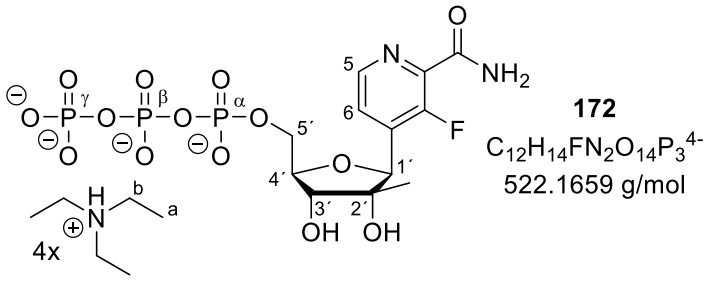

The reaction was carried out according to the general procedure VI with nucleoside **171** (25 mg, 0.09 mmol), proton sponge (38 mg, 0.17 mmol) and $POCl_3$ (32 µL, 0.35 mmol) in trimethyl phosphate (1 mL) for 15 min, followed by the addition of tributylammonium pyrophosphate (119 mg, 0.22 mmol) and tributylamine (144 µL, 0.52 mmol) in CH_3CN (1 mL) for 30 min. Purification by ion-exchange chromatography using a DEAE-Sephadex® A-25 column (H_2O/1 M TEAB; 100:0 to 0:100 v/v) and RP_{18} flash column chromatography (H_2O/CH_3CN; 100:0 to 0:100 v/v) provided the triethylammonium salt of **172** (31 mg, 42%) as a colorless solid.

^{1}*H*-NMR (600 MHz, D_2O): *δ* [ppm] = 8.52 (d, $^{3}J_{HF}$ = 4.92 Hz, 1H, *H*-6), 7.98 (dd, $^{4}J_{HF}$ = 6.01 Hz, $^{3}J_{HH}$ = 4.98 Hz, 1H, *H*-5), 5.38 (s, 1H, *H*-1´), 4.41 (ddd, $^{2}J_{HH}$ = 11.8 Hz, $^{3}J_{HH}$ = 5.31 Hz, $^{4}J_{HH}$ = 2.65 Hz, 1H, *H*-5´), 4.32 (ddd, $^{2}J_{HH}$ = 11.9 Hz, $^{3}J_{HH}$ = 6.25 Hz, $^{4}J_{HH}$ = 3.95 Hz, 1H, *H*-5´), 4.22 – 4.18 (m, 1H, *H*-4´), 4.01 (d, $^{3}J_{HH}$ = 8.17 Hz, 1H, *H*-3´), 3.20 (q, $^{3}J_{HH}$ = 7.32 Hz, 18H, *H*-b), 1.28 (t, $^{3}J_{HH}$ = 7.38 Hz, 27H, *H*-a), 1.02 (s, 3H, 2´-C-C*H*$_3$).

^{31}*P*-NMR (121 MHz, D_2O): *δ* [ppm] = -6.61 (d, $^{2}J_{PP}$ = 21.2 Hz, *P*-α), -11.5 (d, $^{2}J_{PP}$ = 20.0 Hz, *P*-γ), -22.6 (t, $^{2}J_{PP}$ = 20.5 Hz, *P*-β).

^{19}*F*-NMR (564 MHz, D_2O): *δ* [ppm] = -126.6 (m).

HRMS (MALDI$^-$): *m/z* = calcd: 525.9955 [M-H]$^-$, found: 525.0065 [M-H]$^-$.

4-(3´,5´-*O*-(1,1,3,3-Tetraisopropyldisiloxane-1,3-diyl)-2´-deoxy-2´-fluoro-1´-hydroxy-2´-*C*-methyl-D-ribofuranosyl)-2-cyano-3-fluoropyridine 175

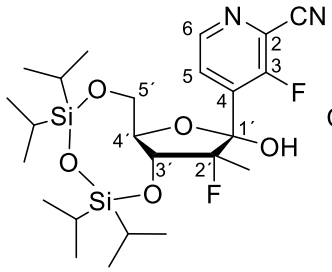

175
$C_{24}H_{38}F_2N_2O_5Si_2$
528.7438 g/mol

The reaction was carried out according to the general procedure VIII with 2-cyano-3-fluoropyridine **141** (2.10 g, 17.2 mmol) and LDA (17.4 mL, 17.4 mmol, 1 M solution in THF) in THF (50 mL), followed by the addition of lactone **174** (3.49 g, 8.60 mmol) in THF (12 mL). Purification of the crude product on silica gel with automated flash chromatography (petroleum ether/ethyl acetate; 10:1 to 4:1 v/v) provided **175** (2.10 g, 46%) as a colorless solid, which was obtained as a mixture of anomers.

^{1}*H*-NMR (600 MHz, $CDCl_3$): *δ* [ppm] = Major-anomer: 8.53 (d, $^3J_{HH}$ = 4.78 Hz, 1H, *H*-6), 7.76 (dd, $^4J_{HF}$ = 5.96 Hz, $^3J_{HH}$ = 4.99 Hz, 1H, *H*-5), 4.49 (dd, $^3J_{HF}$ = 24.9 Hz, $^3J_{HH}$ = 8.99 Hz, 1H, *H*-3´), 4.22 (ddt, $^3J_{HH}$ = 9.14 Hz, $^3J_{HH}$ = 1.96 Hz, $^4J_{HF}$ = 1.14 Hz, 1H, *H*-4´), 4.00 (dd, $^2J_{HH}$ = 13.2 Hz, $^3J_{HH}$ = 2.32 Hz, 1H, *H*-5), 3.93 (dd, $^2J_{HH}$ = 13.2 Hz, $^3J_{HH}$ = 2.65 Hz, 1H, *H*-5), 1.49 (d, $^3J_{HF}$ = 22.3 Hz, 3H, 2´-C-C*H*$_3$), 1.11 – 1.03 (m, 28H, *H*-Isopropyl).

Minor-anomer: 8.50 (d, $^3J_{HH}$ = 4.79 Hz, 1H, *H*-6), 7.76 (dd, $^4J_{HF}$ = 6.03 Hz, $^3J_{HH}$ = 4.83 Hz, 1H, *H*-5), 4.45 (dd, $^3J_{HF}$ = 24.8 Hz, $^3J_{HH}$ = 11.6 Hz, 1H, *H*-3´), 4.22 (ddt, $^3J_{HH}$ = 9.14 Hz, $^3J_{HH}$ = 1.96 Hz, $^4J_{HF}$ = 1.14 Hz, 1H, *H*-4´), 4.02 (dd, $^2J_{HH}$ = 12.5 Hz, $^3J_{HH}$ = 2.60 Hz, 1H, *H*-5), 3.93 (dd, $^2J_{HH}$ = 13.2 Hz, $^3J_{HH}$ = 2.65 Hz, 1H, *H*-5), 1.36 (d, $^3J_{HF}$ = 23.2 Hz, 3H, 2´-C-C*H*$_3$), 1.03 – 0.98 (m, 28H, *H*-Isopropyl).

^{13}*C*-NMR (150 MHz, $CDCl_3$): *δ* [ppm] = Major-anomer: 159.7 (d, $^1J_{CF}$ = 274.9 Hz, *C*-3), 146.6 (d, $^4J_{CF}$ = 6.10 Hz, *C*-6), 136.8 (d, $^2J_{CF}$ = 8.79 Hz, *C*-4), 128.2 (*C*-5), 124.1 (d, $^2J_{CF}$ = 18.3 Hz, *C*-2), 113.6 (d, $^3J_{CF}$ = 3.71 Hz, -*C*N), 103.3 (dd, $^2J_{CF}$ = 27.7 Hz, $^3J_{CF}$ = 3.34 Hz, *C*-1´), 101.5 (d, $^1J_{CF}$ = 188.5 Hz, *C*-2´), 81.2 (*C*-4´), 72.9 (d, $^2J_{CF}$ = 17.0 Hz, *C*-3´), 60.8 (*C*-5´), 17.6 – 17.0 (m), 14.0, 13.2, 12.8, 12.7 (13C, 2´-C-*C*H$_3$, *C*-Isopropyl).

^{19}*F*-NMR (564 MHz, $CDCl_3$): δ [ppm] = Major-anomer: -115.2 (d, $^4J_{HF}$ = 5.70 Hz), -173.5 (m); Minor-anomer: -112.0 (d, $^4J_{HF}$ = 5.15 Hz), -173.5 (m).

HRMS (ESI$^+$): *m/z* = calcd: 529.2359 [M+H]$^+$, found: 529.2353 [M+H]$^+$.

4-(3´,5´-*O*-(1,1,3,3-Tetraisopropyldisiloxane-1,3-diyl)-2´-deoxy-2´-fluoro-2´-*C*-methyl-1´-*O*-acetyl-D-ribofuranosyl)-2-cyano-3-fluoropyridine 176

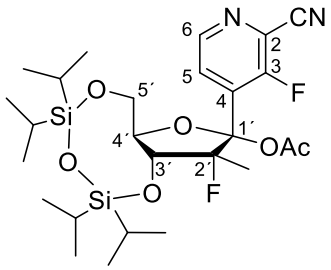

176
$C_{26}H_{40}F_2N_2O_6Si_2$
570.7808 g/mol

The reaction was carried out according to the general procedure IX with lactol **175** (1.95 g, 3.69 mmol) and LiHMDS (5.53 mL, 5.53 mmol, 1 M solution in THF), followed by the addition of acetic anhydride (523 µL, 5.53 mmol). Purification of the crude product on silica gel with automated flash chromatography (petroleum ether/ethyl acetate; 10:1 to 3:1 v/v) provided **176** (1.43 g, 68%) as a colorless solid, which was obtained as a mixture of anomers.

^{1}*H*-NMR (600 MHz, $CDCl_3$): δ [ppm] = Major-anomer: 8.50 (d, $^3J_{HH}$ = 4.86 Hz, 1H, *H*-6), 8.19 (dd, $^4J_{HF}$ = 6.30 Hz, $^3J_{HH}$ = 4.99 Hz, 1H, *H*-5), 4.38 (dd, $^3J_{HH}$ = 9.05 Hz, $^3J_{HH}$ = 1.09 Hz, 1H, *H*-4´), 4.33 (dd, $^2J_{HH}$ = 13.6 Hz, $^3J_{HH}$ = 0.74 Hz, 1H, *H*-5´), 4.04 (dd, $^2J_{HH}$ = 13.2 Hz, $^3J_{HH}$ = 2.65 Hz, 1H, *H*-5´), 3.98 (dd, $^3J_{HF}$ = 23.3 Hz, $^3J_{HH}$ = 9.09 Hz, 1H, *H*-3´), 2.17 (s, 3H, *H*-Ac), 1.29 (d, $^3J_{HF}$ = 22.4 Hz, 3H, 2´-C-CH_3), 1.13 – 0.99 (m, 28H, *H*-Isopropyl).

Minor-anomer: 8.55 (d, $^3J_{HH}$ = 4.98 Hz, 1H, *H*-6), 7.76 (dd, $^4J_{HF}$ = 7.13 Hz, $^3J_{HH}$ = 4.87 Hz, 1H, *H*-5), 4.54 (dd, $^3J_{HF}$ = 25.8 Hz, $^3J_{HH}$ = 8.65 Hz, 1H, *H*-3´), 4.38 (dd, $^3J_{HH}$ = 9.05 Hz, $^3J_{HH}$ = 1.09 Hz, 1H, *H*-4´), 4.09 (dd, $^2J_{HH}$ = 13.2 Hz, $^3J_{HH}$ = 3.19 Hz, 1H, *H*-5´), 4.04 (dd, $^2J_{HH}$ = 13.2 Hz, $^3J_{HH}$ = 2.65 Hz, 1H, *H*-5´), 1.56 (d, $^3J_{HF}$ = 22.3 Hz, 3H, 2´-C-CH_3), 1.03 – 0.98 (m, 28H, *H*-Isopropyl).

^{13}*C*-NMR (150 MHz, $CDCl_3$): δ [ppm] = Major-anomer: 168.7 (*C*-Ac), 157.1 (d, $^1J_{CF}$ = 270.4 Hz, *C*-3), 147.6 (d, $^4J_{CF}$ = 5.74 Hz, *C*-6), 137.8 (d, $^2J_{CF}$ = 9.15 Hz, *C*-4), 127.5 (*C*-5), 123.3 (d, $^2J_{CF}$ = 17.7 Hz, *C*-2), 112.8 (d, $^3J_{CF}$ = 3.85 Hz, -*C*N), 103.4 (dd, $^2J_{CF}$ = 15.7 Hz, $^3J_{CF}$ = 2.74 Hz, *C*-1´), 99.7 (d, $^1J_{CF}$ = 206.2 Hz, *C*-2´), 82.5 ($^3J_{CF}$ = 2.35 Hz, *C*-4´), 71.0 (d, $^2J_{CF}$ = 17.7 Hz, *C*-3´), 59.5 (*C*-5´), 21.1 (*C*-Ac), 17.4 – 16.8 (m), 13.6, 13.0, 12.9, 12.6 (13C, 2´-C-*C*H$_3$, *C*-Isopropyl).

^{19}F-NMR (564 MHz, $CDCl_3$): δ [ppm] = Major-anomer: -118.4 (d, $^4J_{HF}$ = 6.04 Hz); Minor-anomer: -119.0 (d, $^4J_{HF}$ = 5.38 Hz).

HRMS (ESI^+): *m/z* = calcd: 571.2465 $[M+H]^+$, found: 571.2464 $[M+H]^+$.

6. References

[1] F. Witzmann, K. M. Claeson, O. Hampe, F. Wieder, A. Hilger, I. Manke, M. Niederhagen, B. M. Rothschild, P. Asbach, Paget disease of bone in a Jurassic dinosaur, *Current Biology* **2011**, *21*, 647-648.

[2] A. Tarantola, Four Thousand Years of Concepts Relating to Rabies in Animals and Humans, Its Prevention and Its Cure, *Trop. Med. Infec. Dis.* **2017**, *2*.

[3] A. Lwoff, The Concept of Virus, *J. gen. Microbiol.* **1957**, *17*, 239–253.

[4] G. Bordenave, Louis Pasteur (1822-1895), *Microbes and infection* **2003**, *5*, 553–560.

[5] A. Lustig, A. J. Levine, One hundred years of virology, *J Virol* **1992**, *66*, 4629–4631.

[6] P. Dersch, M. Stadler(Ed.) *Current Topics in Microbiology and Immunology*, *Vol. 398*, Springer, **2016**.

[7] J. Travis, Reviving the Antibiotic Miracle? As the development of antibiotic-resistant bacteria accelerates, research on new antibiotics lags. But a few promising lines of investigation remain open, *Science* **1994**, *264*, 360–362.

[8] D. A. Henderson, The eradication of smallpox--an overview of the past, present, and future, *Vaccine* **2011**, *29*, D7-9.

[9] D. C. Hsu, R. J. O'Connell, Progress in HIV vaccine development, *Human vaccines & immunotherapeutics* **2017**, *13*, 1018–1030.

[10] B. Shanmugaraj, R. Kothalam, T. A. A. Mohamed Sheik, A brief overview on the threat of zoonotic viruses, *Microbes and Infectious Diseases* **2024**, *6*, 2034–2041.

[11] L.-F. Wang, D. E. Anderson, Viruses in bats and potential spillover to animals and humans, *Current Opinion in Virology* **2019**, *34*, 79–89.

[12] M. I. Nelson, M. Worobey, Origins of the 1918 Pandemic: Revisiting the Swine "Mixing Vessel" Hypothesis, *Am. J. Epidemiol,* **2018**, *187*, 2498–2502.

[13] A. Marí Saéz, S. Weiss, K. Nowak, V. Lapeyre, F. Zimmermann, A. Düx, H. S. Kühl, M. Kaba, S. Regnaut, K. Merkel et al., Investigating the zoonotic origin of the West African Ebola epidemic, *EMBO Mol Med* **2015**, *7*, 17–23.

[14] A. Banerjee, A. C. Doxey, K. Mossman, A. T. Irving, Unraveling the Zoonotic Origin and Transmission of SARS-CoV-2, *Trends in ecology & evolution* **2021**, *36*, 180–184.

[15] J. Cleland, World Population Growth; Past, Present and Future, *Environ Resource Econ* **2013**, *55*, 543–554.

[16] J. García-Moreno, Zoonoses in a changing world, *BioScience* **2023**, *73*, 711–720.

[17] M. R. Farzanegan, H. F. Gholipour, M. Feizi, R. Nunkoo, A. E. Andargoli, International Tourism and Outbreak of Coronavirus (COVID-19): A Cross-Country Analysis, *Journal of Travel Research* **2021**, *60*, 687–692.

[18] V. Marie, M. L. Gordon, The (Re-)Emergence and Spread of Viral Zoonotic Disease: A Perfect Storm of Human Ingenuity and Stupidity, *Viruses* **2023**, *15*.

[19] W. Leal Filho, L. Ternova, S. A. Parasnis, M. Kovaleva, G. J. Nagy, Climate Change and Zoonoses: A Review of Concepts, Definitions, and Bibliometrics, *Int. J. Environ. Res. Public Health* **2022**, *19*.

[20] Alexander E. Gorbalenya, Susan C. Baker, Ralph S. Baric, Raoul J. de Groot, Christian Drosten, Anastasia A. Gulyaeva, Bart L. Haagmans, Chris Lauber, Andrey M. Leontovich, Benjamin W. Neuman et al., The species Severe acute respiratory syndrome-related coronavirus: classifying 2019-nCoV and naming it SARS-CoV-2, *Nat Microbiol* **2020**, *5*, 536–544.

[21] N. Zhu, D. Zhang, W. Wang, X. Li, B. Yang, J. Song, X. Zhao, B. Huang, W. Shi, R. Lu et al., A Novel Coronavirus from Patients with Pneumonia in China, 2019, *N Engl J Med* **2020**, *382*, 727–733.

[22] C. Cao, Z. Cai, X. Xiao, J. Rao, J. Chen, N. Hu, M. Yang, X. Xing, Y. Wang, M. Li et al., The architecture of the SARS-CoV-2 RNA genome inside virion, *Nat Commun* **2021**, *12*, 3917.

[23] F. Nazir, A. John Kombe Kombe, Z. Khalid, S. Bibi, H. Zhang, S. Wu, T. Jin, SARS-CoV-2 replication and drug discovery, *Molecular and Cellular Probes* **2024**, *77*, 101973.

[24] P. V'kovski, A. Kratzel, S. Steiner, H. Stalder, V. Thiel, Coronavirus biology and replication: implications for SARS-CoV-2, *Nat Rev Microbiol* **2021**, *19*, 155–170.

[25] M. Hoffmann, H. Kleine-Weber, S. Pöhlmann, A Multibasic Cleavage Site in the Spike Protein of SARS-CoV-2 Is Essential for Infection of Human Lung Cells, *Molecular Cell* **2020**, *78*, 779-784.

[26] R. Wölfel, V. M. Corman, W. Guggemos, M. Seilmaier, S. Zange, M. A. Müller, D. Niemeyer, T. C. Jones, P. Vollmar, C. Rothe et al., Virological assessment of hospitalized patients with COVID-2019, *Nature* **2020**, *581*, 465–469.

[27] J. Shang, Y. Wan, C. Luo, G. Ye, Q. Geng, A. Auerbach, F. Li, Cell entry mechanisms of SARS-CoV-2, *Proc. Natl. Acad. Sci. U.S.A.* **2020**, *117*, 11727–11734.

[28] X. Xia, Domains and Functions of Spike Protein in Sars-Cov-2 in the Context of Vaccine Design, *Viruses* **2021**, *13*.

[29] S. Steiner, A. Kratzel, G. T. Barut, R. M. Lang, E. Aguiar Moreira, L. Thomann, J. N. Kelly, V. Thiel, SARS-CoV-2 biology and host interactions, *Nat Rev Microbiol* **2024**, *22*, 206–225.

[30] S. Bertram, I. Glowacka, M. A. Müller, H. Lavender, K. Gnirss, I. Nehlmeier, D. Niemeyer, Y. He, G. Simmons, C. Drosten et al., Cleavage and activation of the severe acute respiratory syndrome coronavirus spike protein by human airway trypsin-like protease, *J Virol* **2011**, *85*, 13363–13372.

[31] M. Hoffmann, H. Kleine-Weber, S. Schroeder, N. Krüger, T. Herrler, S. Erichsen, T. S. Schiergens, G. Herrler, N.-H. Wu, A. Nitsche et al., SARS-CoV-2 Cell Entry Depends on ACE2 and TMPRSS2 and Is Blocked by a Clinically Proven Protease Inhibitor, *Cell* **2020**, *181*, 271-280.

[32] Graham Simmons, Dhaval N. Gosalia, Andrew J. Rennekamp, Jacqueline D. Reeves, Scott L. Diamond, Inhibitors of cathepsin L prevent severe acute respiratory syndrome coronavirus entry, *Proc. Natl. Acad. Sci. U.S.A.* **2005**, 11876–11881.

[33] J. F.-W. Chan, X. Huang, B. Hu, Y. Chai, H. Shi, T. Zhu, T. T.-T. Yuen, Y. Liu, H. Liu, J. Shi et al., Altered host protease determinants for SARS-CoV-2 Omicron, *Sci. Adv.* **2023**, eadd3867.

[34] Y. Wu, S. Zhao, Furin cleavage sites naturally occur in coronaviruses, *Stem Cell Research* **2020**, *50*, 102115.

[35] H. Kim, Y. Kang, S. Kim, D. Park, S.-Y. Heo, J.-S. Yoo, I. Choi, M. P. A. N, J.-W. Ahn, J.-S. Yang et al., The host protease KLK5 primes and activates spike proteins to promote human betacoronavirus replication and lung inflammation, *Sci. Signal.* **2024**, *17*, eadn3785.

[36] S. Seth, J. Batra, S. Srinivasan, COVID-19: Targeting Proteases in Viral Invasion and Host Immune Response, *Front. Mol. Biosci.* **2020**, *7*, 215.

[37] F. Wu, S. Zhao, B. Yu, Y.-M. Chen, W. Wang, Z.-G. Song, Y. Hu, Z.-W. Tao, J.-H. Tian, Y.-Y. Pei et al., A new coronavirus associated with human respiratory disease in China, *Nature* **2020**, *579*, 265–269.

[38] J. Osipiuk, S.-A. Azizi, S. Dvorkin, M. Endres, R. Jedrzejczak, K. A. Jones, S. Kang, R. S. Kathayat, Y. Kim, V. G. Lisnyak et al., Structure of papain-like protease from SARS-CoV-2 and its complexes with non-covalent inhibitors, *Nat Commun* **2021**, *12*, 743.

[39] Z. Jin, X. Du, Y. Xu, Y. Deng, M. Liu, Y. Zhao, B. Zhang, X. Li, L. Zhang, C. Peng et al., Structure of Mpro from SARS-CoV-2 and discovery of its inhibitors, *Nature* **2020**, *582*, 289–293.

[40] M. Thoms, R. Buschauer, M. Ameismeier, L. Koepke, T. Denk, M. Hirschenberger, H. Kratzat, M. Hayn, T. Mackens-Kiani, J. Cheng et al., Structural basis for translational shutdown and immune evasion by the Nsp1 protein of SARS-CoV-2, *Science* **2020**, 1249–1255.

[41] E. J. Snijder, E. Decroly, J. Ziebuhr, The Nonstructural Proteins Directing Coronavirus RNA Synthesis and Processing, *Advances in Virus Research* **2016**, *96*, 59–126.

[42] G. Wolff, C. E. Melia, E. J. Snijder, M. Bárcena, Double-Membrane Vesicles as Platforms for Viral Replication, *Trends in Microbiology* **2020**, *28*, 1022–1033.

[43] M. Cortese, J.-Y. Lee, B. Cerikan, C. J. Neufeldt, V. M. J. Oorschot, S. Köhrer, J. Hennies, N. L. Schieber, P. Ronchi, G. Mizzon et al., Integrative Imaging Reveals SARS-CoV-2-Induced Reshaping of Subcellular Morphologies, *Cell Host & Microbe* **2020**, *28*, 853-866.

[44] M. Ji, M. Li, L. Sun, H. Zhao, Y. Li, L. Zhou, Z. Yang, X. Zhao, W. Qu, H. Xue et al., VMP1 and TMEM41B are essential for DMV formation during β-coronavirus infection, *J. Cell. Biol.* **2022**, *221*.

[45] Y. Gao, L. Yan, Y. Huang, F. Liu, Y. Zhao, L. Cao, T. Wang, Q. Sun, Z. Ming, L. Zhang et al., Structure of the RNA-dependent RNA polymerase from COVID-19 virus, *Science* **2020**, *368*, 779–782.

[46] H. S. Hillen, G. Kokic, L. Farnung, C. Dienemann, D. Tegunov, P. Cramer, Structure of replicating SARS-CoV-2 polymerase, *Nature* **2020**, *584*, 154–156.

[47] Q. Wang, J. Wu, H. Wang, Y. Gao, Q. Liu, an Mu, W. Ji, L. Yan, Y. Zhu, C. Zhu et al., Structural Basis for RNA Replication by the SARS-CoV-2 Polymerase, *Cell* **2020**, *182*, 417-428.e13.

[48] K. J. Mickolajczyk, P. M. M. Shelton, M. Grasso, X. Cao, S. E. Warrington, A. Aher, S. Liu, T. M. Kapoor, Force-dependent stimulation of RNA unwinding by SARS-CoV-2 nsp13 helicase, *Biophysical Journal* **2021**, *120*, 1020–1030.

[49] J. Chen, B. Malone, E. Llewellyn, M. Grasso, P. M. M. Shelton, P. D. B. Olinares, K. Maruthi, E. T. Eng, H. Vatandaslar, B. T. Chait et al., Structural Basis for Helicase-Polymerase Coupling in the SARS-CoV-2 Replication-Transcription Complex, *Cell* **2020**, *182*, 1560-1573.e13.

[50] J. Chen, Q. Wang, B. Malone, E. Llewellyn, Y. Pechersky, K. Maruthi, E. T. Eng, J. K. Perry, E. A. Campbell, D. E. Shaw et al., Ensemble cryo-EM reveals conformational states of the

nsp13 helicase in the SARS-CoV-2 helicase replication-transcription complex, *Nat Struct Mol Biol* **2022**, *29*, 250–260.

[51] B. Malone, J. Chen, Q. Wang, E. Llewellyn, Y. J. Choi, P. D. B. Olinares, X. Cao, C. Hernandez, E. T. Eng, B. T. Chait et al., Structural basis for backtracking by the SARS-CoV-2 replication-transcription complex, *Proc. Natl. Acad. Sci. U.S.A.* **2021**, *118*.

[52] A. Shannon, B. Selisko, N.-T.-T. Le, J. Huchting, F. Touret, G. Piorkowski, V. Fattorini, F. Ferron, E. Decroly, C. Meier et al., Rapid incorporation of Favipiravir by the fast and permissive viral RNA polymerase complex results in SARS-CoV-2 lethal mutagenesis, *Nat Commun* **2020**, *11*, 4682.

[53] E. C. Smith, H. Blanc, M. C. Surdel, M. Vignuzzi, M. R. Denison, Coronaviruses lacking exoribonuclease activity are susceptible to lethal mutagenesis: evidence for proofreading and potential therapeutics, *PLoS Pathog* **2013**, *9*, e1003565.

[54] S. Lin, H. Chen, Z. Chen, F. Yang, F. Ye, Y. Zheng, J. Yang, X. Lin, H. Sun, L. Wang et al., Crystal structure of SARS-CoV-2 nsp10 bound to nsp14-ExoN domain reveals an exoribonuclease with both structural and functional integrity, *Nucleic Acids Research* **2021**, *49*, 5382–5392.

[55] I. Sola, F. Almazán, S. Zúñiga, L. Enjuanes, Continuous and Discontinuous RNA Synthesis in Coronaviruses, *Annu. Rev. Virol.* **2015**, *2*, 265–288.

[56] P. J. Talbot, *Corona- and Related Viruses*. *Current Concepts in Molecular Biology and Pathogenesis*, Springer, Boston, **1995**.

[57] S. Lu, Q. Ye, D. Singh, Y. Cao, J. K. Diedrich, J. R. Yates, E. Villa, D. W. Cleveland, K. D. Corbett, The SARS-CoV-2 nucleocapsid phosphoprotein forms mutually exclusive condensates with RNA and the membrane-associated M protein, *Nat Commun* **2021**, *12*, 502.

[58] H. Yao, Y. Song, Y. Chen, N. Wu, J. Xu, C. Sun, J. Zhang, T. Weng, Z. Zhang, Z. Wu et al., Molecular Architecture of the SARS-CoV-2 Virus, *Cell* **2020**, *183*, 730-738.e13.

[59] C. A. M. de Haan, P. J. M. Rottier, Molecular interactions in the assembly of coronaviruses, *Advances in Virus Research* **2005**, *64*, 165–230.

[60] B. Boson, V. Legros, B. Zhou, E. Siret, C. Mathieu, F.-L. Cosset, D. Lavillette, S. Denolly, The SARS-CoV-2 envelope and membrane proteins modulate maturation and retention of the spike protein, allowing assembly of virus-like particles, *J. Biol. Chem.* **2021**, *296*, 100111.

[61] J. L. Nieto-Torres, C. Verdiá-Báguena, J. M. Jimenez-Guardeño, J. A. Regla-Nava, C. Castaño-Rodriguez, R. Fernandez-Delgado, J. Torres, V. M. Aguilella, L. Enjuanes, Severe acute

respiratory syndrome coronavirus E protein transports calcium ions and activates the NLRP3 inflammasome, *Virology* **2015**, *485*, 330–339.

[62] Di Chen, Q. Zheng, L. Sun, M. Ji, Y. Li, H. Deng, H. Zhang, ORF3a of SARS-CoV-2 promotes lysosomal exocytosis-mediated viral egress, *Developmental Cell* **2021**, *56*, 3250-3263.e5.

[63] S. Ghosh, T. A. Dellibovi-Ragheb, A. Kerviel, E. Pak, Q. Qiu, M. Fisher, P. M. Takvorian, C. Bleck, V. W. Hsu, A. R. Fehr et al., β-Coronaviruses Use Lysosomes for Egress Instead of the Biosynthetic Secretory Pathway, *Cell* **2020**, *183*, 1520-1535.

[64] European Medicines Agency, Bimervax, https://www.ema.europa.eu/en/medicines/human/EPAR/bimervax#product-info, **03.11.2025**.

[65] European Medicines Agency, Nuvaxovid, https://www.ema.europa.eu/en/medicines/human/EPAR/nuvaxovid, **03.11.2025**.

[66] European Medicines Agency, Comirnaty, https://www.ema.europa.eu/en/medicines/human/EPAR/comirnaty, **03.11.2025**.

[67] European Medicines Agency, Spikevax, https://www.ema.europa.eu/en/medicines/human/EPAR/spikevax, **03.11.2025**.

[68] B. Malone, N. Urakova, E. J. Snijder, E. A. Campbell, Structures and functions of coronavirus replication-transcription complexes and their relevance for SARS-CoV-2 drug design, *Nat Rev Mol Cell Biol* **2022**, *23*, 21–39.

[69] M. D. Hall, J. M. Anderson, A. Anderson, D. Baker, J. Bradner, K. R. Brimacombe, E. A. Campbell, K. S. Corbett, K. Carter, S. Cherry et al., Report of the National Institutes of Health SARS-CoV-2 Antiviral Therapeutics Summit, *The Journal of Infectious Diseases* **2021**, *224*, S1-S21.

[70] S. P. Otto, A. MacPherson, C. Colijn, Endemic does not mean constant as SARS-CoV-2 continues to evolve, *Evolution* **2024**, *78*, 1092–1108.

[71] W. Cui, Y. Duan, Y. Gao, W. Wang, H. Yang, Structural review of SARS-CoV-2 antiviral targets, *Structure* **2024**, *32*, 1301–1321.

[72] Q. Lan, Y. Yan, G. Zhang, S. Xia, J. Zhou, L. Lu, S. Jiang, Clinical development of antivirals against SARS-CoV-2 and its variants, *Current Research in Microbial Sciences* **2024**, *6*, 100208.

[73] L. Du, Y. Yang, X. Zhang, Neutralizing antibodies for the prevention and treatment of COVID-19, *Cellular & Molecular Immunology* **2021**, *18*, 2293–2306.

[74] C. O. Barnes, C. A. Jette, M. E. Abernathy, K.-M. A. Dam, S. R. Esswein, H. B. Gristick, A. G. Malyutin, N. G. Sharaf, K. E. Huey-Tubman, Y. E. Lee et al., SARS-CoV-2 neutralizing antibody structures inform therapeutic strategies, *Nature* **2020**, *588*, 682–687.

[75] C. Kim, D.-K. Ryu, J. Lee, Y.-I. Kim, J.-M. Seo, Y.-G. Kim, J.-H. Jeong, M. Kim, J.-I. Kim, P. Kim et al., A therapeutic neutralizing antibody targeting receptor binding domain of SARS-CoV-2 spike protein, *Nat Commun* **2021**, *12*, 288.

[76] R. Shi, C. Shan, X. Duan, Z. Chen, P. Liu, J. Song, T. Song, X. Bi, C. Han, L. Wu et al., A human neutralizing antibody targets the receptor-binding site of SARS-CoV-2, *Nature* **2020**, *584*, 120–124.

[77] J. Dong, S. J. Zost, A. J. Greaney, T. N. Starr, A. S. Dingens, E. C. Chen, R. E. Chen, J. B. Case, R. E. Sutton, P. Gilchuk et al., Genetic and structural basis for SARS-CoV-2 variant neutralization by a two-antibody cocktail, *Nat Microbiol* **2021**, *6*, 1233–1244.

[78] B. Ju, Q. Zhang, J. Ge, R. Wang, J. Sun, X. Ge, J. Yu, S. Shan, B. Zhou, S. Song et al., Human neutralizing antibodies elicited by SARS-CoV-2 infection, *Nature* **2020**, *584*, 115–119.

[79] R. Shi, C. Shan, X. Duan, Z. Chen, P. Liu, J. Song, T. Song, X. Bi, C. Han, L. Wu et al., A human neutralizing antibody targets the receptor-binding site of SARS-CoV-2, *Nature* **2020**, *584*, 120–124.

[80] Johanna Hansen et al., Studies in humanized mice and convalescent humans yield a SARS-CoV-2 antibody cocktail, *Science* **2020**, *369*, 1010–1014.

[81] Y. Chen, X. Zhao, H. Zhou, H. Zhu, S. Jiang, P. Wang, Broadly neutralizing antibodies to SARS-CoV-2 and other human coronaviruses, *Nat Rev Immunol* **2023**, *23*, 189–199.

[82] C. Kim, D.-K. Ryu, J. Lee, Y.-I. Kim, J.-M. Seo, Y.-G. Kim, J.-H. Jeong, M. Kim, J.-I. Kim, P. Kim et al., A therapeutic neutralizing antibody targeting receptor binding domain of SARS-CoV-2 spike protein, *Nat Commun* **2021**, *12*, 288.

[83] Bryan E. Jones et al., The neutralizing antibody, LY-CoV555, protects against SARS-CoV-2 infection in nonhuman primates, *Sci. Transl. Med.* **2021**, *13*, eabf1906.

[84] P. Wang, M. S. Nair, L. Liu, S. Iketani, Y. Luo, Y. Guo, M. Wang, J. Yu, B. Zhang, P. D. Kwong et al., Antibody resistance of SARS-CoV-2 variants B.1.351 and B.1.1.7, *Nature* **2021**, *593*, 130–135.

[85] J. Ai, X. Wang, X. He, X. Zhao, Y. Zhang, Y. Jiang, M. Li, Y. Cui, Y. Chen, R. Qiao et al., Antibody evasion of SARS-CoV-2 Omicron BA.1, BA.1.1, BA.2, and BA.3 sub-lineages, *Cell Host & Microbe* **2022**, *30*, 1077-1083.e4.

[86] D. Pinto, Y.-J. Park, M. Beltramello, A. C. Walls, M. A. Tortorici, S. Bianchi, S. Jaconi, K. Culap, F. Zatta, A. de Marco et al., Cross-neutralization of SARS-CoV-2 by a human monoclonal SARS-CoV antibody, *Nature* **2020**, *583*, 290–295.

[87] C. L. Magnus, A. Hiergeist, P. Schuster, A. Rohrhofer, J. Medenbach, A. Gessner, D. Peterhoff, B. Schmidt, Targeted escape of SARS-CoV-2 in vitro from monoclonal antibody S309, the precursor of sotrovimab, *Front. Immunol.* **2022**, *13*, 966236.

[88] K. Westendorf, S. Žentelis, L. Wang, D. Foster, P. Vaillancourt, M. Wiggin, E. Lovett, R. van der Lee, J. Hendle, A. Pustilnik et al., LY-CoV1404 (bebtelovimab) potently neutralizes SARS-CoV-2 variants, *Cell reports* **2022**, *39*, 110812.

[89] T. Zhou, L. Wang, J. Misasi, A. Pegu, Y. Zhang, D. R. Harris, A. S. Olia, C. A. Talana, E. S. Yang, M. Chen et al., Structural basis for potent antibody neutralization of SARS-CoV-2 variants including B.1.1.529, *Science* **2022**, *376*, eabn8897.

[90] Y. Cao, W. Song, L. Wang, P. Liu, C. Yue, F. Jian, Y. Yu, A. Yisimayi, P. Wang, Y. Wang et al., Characterizations of enhanced infectivity and antibody evasion of Omicron BA.2.75, *Cell Host & Microbe* **2022**, *30*, 1527-1539.e5.

[91] X. Ju, Z. Wang, P. Wang, W. Ren, Y. Yu, Y. Yu, B. Yuan, J. Song, X. Zhang, Y. Zhang et al., SARS-CoV-2 main protease cleaves MAGED2 to antagonize host antiviral defense, *mBio* **2023**, *14*, e0137323.

[92] R. Hilgenfeld, From SARS to MERS: crystallographic studies on coronaviral proteases enable antiviral drug design, *The FEBS journal* **2014**, *281*, 4085–4096.

[93] J. T. Lee, Q. Yang, A. Gribenko, B. S. Perrin, Y. Zhu, R. Cardin, P. A. Liberator, A. S. Anderson, L. Hao, Genetic Surveillance of SARS-CoV-2 Mpro Reveals High Sequence and Structural Conservation Prior to the Introduction of Protease Inhibitor Paxlovid, *mBio* **2022**, *13*, e0086922.

[94] A. Zagórska, A. Czopek, M. Fryc, J. Jończyk, Inhibitors of SARS-CoV-2 Main Protease (Mpro) as Anti-Coronavirus Agents, *Biomolecules* **2024**, *14*.

[95] The crystal structures of severe acute respiratory syndrome virus main protease and its complex with an inhibitor, *Proc. Natl. Acad. Sci. U.S.A.* **2003**, *100*, 13190–13195.

[96] M. D. Sacco, C. Ma, P. Lagarias, A. Gao, J. A. Townsend, X. Meng, P. Dube, X. Zhang, Y. Hu, N. Kitamura et al., Structure and inhibition of the SARS-CoV-2 main protease reveal strategy for developing dual inhibitors against Mpro and cathepsin L, *Sci. Adv.* **2020**, *6*, eabe0751.

[97] Y. Unoh, S. Uehara, K. Nakahara, H. Nobori, Y. Yamatsu, S. Yamamoto, Y. Maruyama, Y. Taoda, K. Kasamatsu, T. Suto et al., Discovery of S-217622, a Noncovalent Oral SARS-CoV-2 3CL Protease Inhibitor Clinical Candidate for Treating COVID-19, *J. Med. Chem.* **2022**, *65*, 6499–6512.

[98] N. Drayman, J. K. DeMarco, K. A. Jones, S.-A. Azizi, H. M. Froggatt, K. Tan, N. I. Maltseva, S. Chen, V. Nicolaescu, S. Dvorkin et al., Masitinib is a broad coronavirus 3CL inhibitor that blocks replication of SARS-CoV-2, *Science* **2021**, *373*, 931–936.

[99] A. J. W. te Velthuis, J. J. Arnold, C. E. Cameron, S. H. E. van den Worm, E. J. Snijder, The RNA polymerase activity of SARS-coronavirus nsp12 is primer dependent, *Nucleic Acids Research* **2010**, *38*, 203–214.

[100] K. C. Lehmann, A. Gulyaeva, J. C. Zevenhoven-Dobbe, G. M. C. Janssen, M. Ruben, H. S. Overkleeft, P. A. van Veelen, D. V. Samborskiy, A. A. Kravchenko, A. M. Leontovich et al., Discovery of an essential nucleotidylating activity associated with a newly delineated conserved domain in the RNA polymerase-containing protein of all nidoviruses, *Nucleic Acids Research* **2015**, *43*, 8416–8434.

[101] R. N. Kirchdoerfer, A. B. Ward, Structure of the SARS-CoV nsp12 polymerase bound to nsp7 and nsp8 co-factors, *Nat Commun* **2019**, *10*, 2342.

[102] O. B. Peersen, Picornaviral polymerase structure, function, and fidelity modulation, *Virus Research* **2017**, *234*, 4–20.

[103] H. Jia, P. Gong, A Structure-Function Diversity Survey of the RNA-Dependent RNA Polymerases From the Positive-Strand RNA Viruses, *Front. Microbiol.* **2019**, *10*, 1945.

[104] W. Yin, C. Mao, X. Luan, D.-D. Shen, Q. Shen, H. Su, X. Wang, F. Zhou, W. Zhao, M. Gao et al., Structural basis for inhibition of the RNA-dependent RNA polymerase from SARS-CoV-2 by remdesivir, *Science* **2020**, *368*, 1499–1504.

[105] K. Ben Ouirane, Y. Boulard, S. Bressanelli, The hepatitis C virus RNA-dependent RNA polymerase directs incoming nucleotides to its active site through magnesium-dependent dynamics within its F motif, *J. Biol. Chem.* **2019**, *294*, 7573–7587.

[106] P. Gong, O. B. Peersen, Structural basis for active site closure by the poliovirus RNA-dependent RNA polymerase, *Proc. Natl. Acad. Sci. U.S.A.* **2010**, *107*, 22505–22510.

[107] T. A. Steitz, A mechanism for all polymerases, *Nature* **1998**, *391*, 231–232.

[108] M. G. Santoro, E. Carafoli, Remdesivir: From Ebola to COVID-19, *Biochemical and Biophysical Research Communications* **2021**, *538*, 145–150.

[109] C. J. Gordon, E. P. Tchesnokov, E. Woolner, J. K. Perry, J. Y. Feng, D. P. Porter, M. Götte, Remdesivir is a direct-acting antiviral that inhibits RNA-dependent RNA polymerase from severe acute respiratory syndrome coronavirus 2 with high potency, *J. Biol. Chem.* **2020**, *295*, 6785–6797.

[110] U.S. Food and Drug Administration, Coronavirus (COVID-19) Update: FDA Authorizes Additional Oral Antiviral for Treatment of COVID-19 in Certain Adults, https://www.fda.gov/news-events/press-announcements/coronavirus-covid-19-update-fda-authorizes-additional-oral-antiviral-treatment-covid-19-certain, **21.08.2025**.

[111] S. Masyeni, M. Iqhrammullah, A. Frediansyah, F. Nainu, T. Tallei, T. B. Emran, Y. Ophinni, K. Dhama, H. Harapan, Molnupiravir: A lethal mutagenic drug against rapidly mutating severe acute respiratory syndrome coronavirus 2-A narrative review, *J. Med. Virol.* **2022**, *94*, 3006–3016.

[112] F. Kabinger, C. Stiller, J. Schmitzová, C. Dienemann, G. Kokic, H. S. Hillen, C. Höbartner, P. Cramer, Mechanism of molnupiravir-induced SARS-CoV-2 mutagenesis, *Nat Struct Mol Biol* **2021**, *28*, 740–746.

[113] K. Shiraki, T. Daikoku, Favipiravir, an anti-influenza drug against life-threatening RNA virus infections, *Pharmacology & Therapeutics* **2020**, *209*, 107512.

[114] S. J. Smither, L. S. Eastaugh, J. A. Steward, M. Nelson, R. P. Lenk, M. S. Lever, Post-exposure efficacy of oral T-705 (Favipiravir) against inhalational Ebola virus infection in a mouse model, *Antiviral Research* **2014**, *104*, 153–155.

[115] L. Delang, R. Abdelnabi, J. Neyts, Favipiravir as a potential countermeasure against neglected and emerging RNA viruses, *Antiviral Research* **2018**, *153*, 85–94.

[116] L. Naesens, L. W. Guddat, D. T. Keough, A. B. P. van Kuilenburg, J. Meijer, J. Vande Voorde, J. Balzarini, Role of human hypoxanthine guanine phosphoribosyltransferase in activation of the antiviral agent T-705 (favipiravir), *Molecular Pharmacology* **2013**, *84*, 615–629.

[117] Y. Furuta, T. Komeno, T. Nakamura, Favipiravir (T-705), a broad spectrum inhibitor of viral RNA polymerase, *Proc. Jpn. Acad. Ser. B* **2017**, *93*, 449–463.

[118] J. Huchting, M. Winkler, H. Nasser, C. Meier, Synthesis of T-705-Ribonucleoside and T-705-Ribonucleotide and Studies of Chemical Stability, *ChemMedChem* **2017**, *12*, 652–659.

[119] Benedikt Ganter, *Master thesis*, Universität Hamburg, Hamburg, **2020**.

[120] J. Huchting, E. Vanderlinden, M. Winkler, H. Nasser, L. Naesens, C. Meier, Prodrugs of the Phosphoribosylated Forms of Hydroxypyrazinecarboxamide Pseudobase T-705 and Its De-Fluoro Analogue T-1105 as Potent Influenza Virus Inhibitors, *J. Med. Chem.* **2018**, *61*, 6193–6210.

[121] C. Meier, Nucleoside diphosphate and triphosphate prodrugs - An unsolvable task?, *Antiviral Chemistry & Chemotherapy* **2017**, *25*, 69–82.

[122] L. P. Jordheim, D. Durantel, F. Zoulim, C. Dumontet, Advances in the development of nucleoside and nucleotide analogues for cancer and viral diseases, *Nat Rev Drug Discov* **2013**, *12*, 447–464.

[123] J. Rautio, H. Kumpulainen, T. Heimbach, R. Oliyai, D. Oh, T. Järvinen, J. Savolainen, Prodrugs: design and clinical applications, *Nat Rev Drug Discov* **2008**, *7*, 255–270.

[124] P. Ettmayer, G. L. Amidon, B. Clement, B. Testa, Lessons learned from marketed and investigational prodrugs, *J. Med. Chem.* **2004**, *47*, 2393–2404.

[125] Y. Mehellou, H. S. Rattan, J. Balzarini, The ProTide Prodrug Technology: From the Concept to the Clinic, *J. Med. Chem.* **2018**, *61*, 2211–2226.

[126] M. Slusarczyk, M. H. Lopez, J. Balzarini, M. Mason, W. G. Jiang, S. Blagden, E. Thompson, E. Ghazaly, C. McGuigan, Application of ProTide technology to gemcitabine: a successful approach to overcome the key cancer resistance mechanisms leads to a new agent (NUC-1031) in clinical development, *J. Med. Chem.* **2014**, *57*, 1531–1542.

[127] E. Murakami, T. Tolstykh, H. Bao, C. Niu, H. M. M. Steuer, D. Bao, W. Chang, C. Espiritu, S. Bansal, A. M. Lam et al., Mechanism of activation of PSI-7851 and its diastereoisomer PSI-7977, *J. Biol. Chem.* **2010**, *285*, 34337–34347.

[128] C McGuigan, PW Sutton, D Cahard, K Turner, G O'Leary, Y Wang, M Gumbleton, Synthesis, Anti-Human Immunodeficiency Virus Activity and Esterase Lability of Some Novel Carboxylic Ester-Modified Phosphoramidate Derivatives of Stavudine (d4T), *Antiviral Chemistry & Chemotherapy*, 473–479.

[129] A. Q. Siddiqui, C. McGuigan, C. Ballatore, F. Zuccotto, I. H. Gilbert, E. de Clercq, J. Balzarini, Design and synthesis of lipophilic phosphoramidate d4T-MP prodrugs expressing high potency against HIV in cell culture: structural determinants for in vitro activity and QSAR, *J. Med. Chem.* **1999**, *42*, 4122–4128.

[130] G. Birkus, R. Wang, X. Liu, N. Kutty, H. MacArthur, T. Cihlar, C. Gibbs, S. Swaminathan, W. Lee, M. McDermott, Cathepsin A is the major hydrolase catalyzing the intracellular hydrolysis of the antiretroviral nucleotide phosphonoamidate prodrugs GS-7340 and GS-9131, *Antimicrobial Agents and Chemotherapy* **2007**, *51*, 543–550.

[131] G. Birkus, N. Kutty, G.-X. He, A. Mulato, W. Lee, M. McDermott, T. Cihlar, Activation of 9-(R)-2-(S)-(S)-1-(Isopropoxycarbonyl)ethylamino phenoxyphosphinyl-methoxypropyladenine (GS-7340) and other tenofovir phosphonoamidate prodrugs by human proteases, *Molecular Pharmacology* **2008**, *74*, 92–100.

[132] William Thomson, Dave Nicholls, William J. Irwin, Julian S. Al-Mushadani, Sally Freeman, braham Karpas, Juraj Petrik, Naheed Mahmood and Alan J. Hayd, Synthesis, Bioactivation and Anti-HIV Activity of the Bis(4-acyloxybenzyl) and Mono(4-acyloxybenzyl) Esters of the 5'-Monophosphate of AZT, *J. Chem. Soc. Perkin Trans.* **1993**, 1239.

[133] H. J. Jessen, T. Schulz, J. Balzarini, C. Meier, Bioreversible protection of nucleoside diphosphates, *Angew. Chem. Int. Ed. Engl.* **2008**, *47*, 8719–8722.

[134] T. Gollnest, T. Dinis de Oliveira, A. Rath, I. Hauber, D. Schols, J. Balzarini, C. Meier, Membrane-permeable Triphosphate Prodrugs of Nucleoside Analogues, *Angew. Chem. Int. Ed. Engl.* **2016**, *55*, 5255–5258.

[135] T. Gollnest, T. D. de Oliveira, D. Schols, J. Balzarini, C. Meier, Lipophilic prodrugs of nucleoside triphosphates as biochemical probes and potential antivirals, *Nat Commun* **2015**, *6*, 8716.

[136] A. Shannon, B. Canard, Kill or corrupt: Mechanisms of action and drug-resistance of nucleotide analogues against SARS-CoV-2, *Antiviral Research* **2023**, *210*, 105501.

[137] R. J. Glyn, G. Pattison, Effects of Replacing Oxygenated Functionality with Fluorine on Lipophilicity, *J. Med. Chem.* **2021**, *64*, 10246–10259.

[138] G. Migliaccio, J. E. Tomassini, S. S. Carroll, L. Tomei, S. Altamura, B. Bhat, L. Bartholomew, M. R. Bosserman, A. Ceccacci, L. F. Colwell et al., Characterization of resistance to non-

obligate chain-terminating ribonucleoside analogs that inhibit hepatitis C virus replication in vitro, *J. Biol. Chem.* **2003**, *278*, 49164–49170.

[139] A. Fung, Z. Jin, N. Dyatkina, G. Wang, L. Beigelman, J. Deval, Efficiency of incorporation and chain termination determines the inhibition potency of 2'-modified nucleotide analogs against hepatitis C virus polymerase, *Antimicrobial Agents and Chemotherapy* **2014**, *58*, 3636–3645.

[140] C. Qu, L. Xu, Y. Yin, M. P. Peppelenbosch, Q. Pan, W. Wang, Nucleoside analogue 2'-C-methylcytidine inhibits hepatitis E virus replication but antagonizes ribavirin, *Arch Virol* **2017**, *162*, 2989–2996.

[141] E. Lawitz, I. M. Jacobson, D. R. Nelson, S. Zeuzem, M. S. Sulkowski, R. Esteban, D. Brainard, J. McNally, W. T. Symonds, J. G. McHutchison et al., Development of sofosbuvir for the treatment of hepatitis C virus infection, *Ann. N. Y. Acad. Sci.* **2015**, *1358*, 56–67.

[142] M. J. Kim, Synthesis of 2’- C -Methyl Ribonucleoside Analogues with Modified Heterocyclic Base Moieties, *Synthetic Communications* **2010**, *40*, 2988–2999.

[143] Q. Li, R. Yang, Z. Ruan, T. Hu, H. Ding, Q. Xiao, Total Synthesis of Cordycepin, *Chin. J. Org. Chem.* **2013**, *33*, 1340.

[144] S. Wang, J. Sun, Q. Zhang, X. Cao, Y. Zhao, G. Tang, B. Yu, Amipurimycin: Total Synthesis of the Proposed Structures and Diastereoisomers, *Angew. Chem. Int. Ed. Engl.* **2018**, *130*, 2934–2938.

[145] I. A. Mikhailopulo, G. G. Sivets, A Novel Route for the Synthesis of Deoxy Fluoro Sugars and Nucleosides, *HCA* **1999**, *82*, 2052–2065.

[146] J. Bouton, A. Furquim d'Almeida, L. Maes, G. Caljon, S. van Calenbergh, F. Hulpia, Synthesis and evaluation of 3'-fluorinated 7-deazapurine nucleosides as antikinetoplastid agents, *Eur. J. Med. Chem.* **2021**, *216*, 113290.

[147] W. A. Szarek, A. Zamojski, H. N. Tiwari, E. R. Ison, A new, facile method for cleavage of acetals and dithioacetals in carbohydrate derivatives, *Tetrahedron Lett.* **1986**, *27*, 3827.

[148] S. Gadthula, C. K. Chu, R. F. Schinazi, Synthesis and anti-HIV activity of beta-D-3'-azido-2',3'-unsaturated nucleosides and beta-D-3'-azido-3'-deoxyribofuranosylnucleosides, *Nucleosides, Nucleotides & Nucleic Acids* **2005**, *24*, 1707–1727.

[149] S. A. W. Gruner, V. Truffault, G. Voll, E. Locardi, M. Stöckle, H. Kessler, Design, Synthesis, and NMR Structure of Linear and Cyclic Oligomers Containing Novel Furanoid Sugar Amino Acids, *Chem. Eur. J.* **2002**, *8*, 4365–4376.

[150] M. Bassetto, C. M. Cima, M. Basso, M. Salerno, F. Schwarze, D. Friese, J. J. Bugert, A. Brancale, Novel Nucleoside Analogues as Effective Antiviral Agents for Zika Virus Infections, *Molecules* **2020**, *25*.

[151] M. Maiti, M. Maiti, J. Rozenski, S. de Jonghe, P. Herdewijn, Aspartic acid based nucleoside phosphoramidate prodrugs as potent inhibitors of hepatitis C virus replication, *Org. Biomol. Chem.* **2015**, *13*, 5158–5174.

[152] P. G. Reddy, B.-K. Chun, H.-R. Zhang, S. Rachakonda, B. S. Ross, M. J. Sofia, Stereoselective synthesis of PSI-352938: a β-D-2'-deoxy-2'-α-fluoro-2'-β-C-methyl-3',5'-cyclic phosphate nucleotide prodrug for the treatment of HCV, *J. Org. Chem.* **2011**, *76*, 3782–3790.

[153] *Vorbrüggen Glycosylation* (Eg.Z. Wang), Wiley, **2010**, 2915–2919.

[154] A. Simoncsits and J. Tomasz, Nucleoside 5'-phosphordiamidates, synthesis and some properties, *Nucl. Acids Res.* **1975**, *2*, 1223–1233.

[155] J.Tomasz, A.Simoncsits, M.Kajtar, R.M.Krug, A.J.Shatkin, Chemical synthesis of 5'-pyrophosphate and triphosphate derivatives of 3'-5' ApA, ApG, GpA and GpG. CD study of the effect of S'-phosphate groups on the conformation of 3'-5' GpG, *Nucl. Acids Res.* **1978**, *5*, 2945–2957.

[156] J. H. v. Boom, C. Crea, W. C. Luyten, A. B. VInk, 2.2,2-Trisromoethyl Phosphoromorpholinochloridate: A Convenient Reagent For (2,2,2-Tribromomethyl)phosphoromorpholinochloridate, a convenient reagent for the synthesis of ribonucleoside mono-, di-, and triphosphates, *Tetrahedron Lett.* **1975**, 2779–2782.

[157] J. G. Moffatt, H. G. Khorana, Nucleoside Polyphosphates. X.[1] The Synthesis and Some Reactions of Nucleoside-5' Phosphoromorpholidates and Related Compounds. Improved Methods for the Preparation of Nucleoside-5' Polyphosphates, *J. Am. Chem. Soc.* **1961**, *83*, 649–658.

[158] J. G. Moffatt, A General Synthesis od Nucleoside-5´-triphosphates, *Can. J. Chem.* **1964**, *42*, 599–604.

[159] Shimazu, M., Shinozuka, K., Sawai, Facile synthesis of nucleotides containing polyphosphates by manganese(II) and cadmium(II) ion-catalyzed pyrophosphate bond formation in aqueous solution, *Tetrahedron Lett.* **1990**, *31*, 235–238.

[160] Donald E. Hoard, Donald G. Ott, Conversion of Mono- and Oligodeoxyribonucleotides to 5'-Triphosphates, *J. Am. Chem. Soc.* **1965**, *87*, 1785–1788.

[161] G. S. Cremosnik, A. Hofer, H. J. Jessen, Iterative synthesis of nucleoside oligophosphates with phosphoramidites, *Angew. Chem. Int. Ed. Engl.* **2014**, *53*, 286–289.

[162] J. Ludwig, A new route to nucleoside 5'-triphosphates., *Acta Biochim Biophys Acad Sci Hung* **1981**, *16*, 131–133.

[163] J. L. RUTH, Y.-C. CHENG, Nucleoside Analogues with Clinical Potential in Antivirus Chemotherapy, *Molecular Pharmacology* **1981**, *20*, 415–422.

[164] A. R. Kore, M. Shanmugasundaram, A. Senthilvelan, B. Srinivasan, An improved protection-free one-pot chemical synthesis of 2'-deoxynucleoside-5'-triphosphates, *Nucleosides, Nucleotides & Nucleic Acids* **2012**, *31*, 423–431.

[165] I. Gillerman, B. Fischer, An improved one-pot synthesis of nucleoside 5'-triphosphate analogues, *Nucleosides, Nucleotides & Nucleic Acids* **2010**, *29*, 245–256.

[166] Janos Ludwig/Fritz Eckstein, Rapid and Efficient Synthesis of Nucleoside S'-O-tl-Thiotriphosphates), S'-Triphosphates and 2/,3/-Cyclophosphorothioates Using 2-Chloro-4ff-l,3,2-benzodioxaphosphorin-4-onecyclophosphorothioates using 2-chloro-4H-1,3,2-benzodioxaphosphorin-4-one, *J. Org. Chem.* **1989**, *54*, 631–635.

[167] M. Yoshikawa, T. Kato, T. Takenishi, A novel method for phosphorylation of nucleosides to 5´-nucleotides, *Tetrahedron Lett.* **1967**, *50*, 5065–5068.

[168] T. L. Dangerfield, N. Z. Huang, K. A. Johnson, Remdesivir Is Effective in Combating COVID-19 because It Is a Better Substrate than ATP for the Viral RNA-Dependent RNA Polymerase, *iScience* **2020**, *23*, 101849.

[169] M. Seifert, S. C. Bera, P. van Nies, R. N. Kirchdoerfer, A. Shannon, T.-T.-N. Le, X. Meng, H. Xia, J. M. Wood, L. D. Harris et al., Inhibition of SARS-CoV-2 polymerase by nucleotide analogs from a single-molecule perspective, *eLife* **2021**, *10*.

[170] C. C. Bradley, A. J. E. Gordon, C. Wang, M. B. Cooke, B. F. Kohrn, S. R. Kennedy, O. Lichtarge, S. E. Ronca, C. Herman, RNA polymerase inaccuracy underlies SARS-CoV-2 variants and vaccine heterogeneity, *Research Square* **2022**.

[171] J. Del Martínez Río, E. Frutos-Beltrán, A. Sebastián-Martín, F. Lasala, K. Yasukawa, R. Delgado, L. Menéndez-Arias, HIV-1 Reverse Transcriptase Error Rates and Transcriptional Thresholds Based on Single-strand Consensus Sequencing of Target RNA Derived From In Vitro-transcription and HIV-infected Cells, *Journal of Molecular Biology* **2024**, *436*, 168815.

[172] X. Jia, D. Schols, C. Meier, Pronucleotides of 2',3'-Dideoxy-2',3'-Didehydrothymidine as Potent Anti-HIV Compounds, *J. Med. Chem.* **2023**, *66*, 12163–12184.

[173] S. Mohamady, S. D. Taylor, General procedure for the synthesis of dinucleoside polyphosphates, *J. Org. Chem.* **2011**, *76*, 6344–6349.

[174] T. K. Warren, R. Jordan, M. K. Lo, A. S. Ray, R. L. Mackman, V. Soloveva, D. Siegel, M. Perron, R. Bannister, H. C. Hui et al., Therapeutic efficacy of the small molecule GS-5734 against Ebola virus in rhesus monkeys, *Nature* **2016**, *531*, 381–385.

[175] S. Abu-Melha, M. M. Edrees, M. A. Said, S. M. Riyadh, N. S. Al-Kaff, S. M. Gomha, Potential COVID-19 Drug Candidates Based on Diazinyl-Thiazol-Imine Moieties: Synthesis and Greener Pastures Biological Study, *Molecules* **2022**, *27*.

[176] I. P. Singh, S. Gupta, S. Kumar, Thiazole Compounds as Antiviral Agents: An Update, *Medicinal Chemistry* **2020**, *16*, 4–23.

[177] P. C. Srivastava, V. Michael, L. B. Allen, D. G. Streeter, M. T. Campbell, J. T. Witkowski, R. W. Sidwell, R. K. Robins, Synthesis and antiviral activity of certain thiazole C-nucleosides, *J. Med. Chem.* **1977**, *20*, 257.

[178] J. D. Graci, C. E. Cameron, Mechanisms of action of ribavirin against distinct viruses, *Rev. Med. Virol.* **2006**, *16*, 37–48.

[179] E. de Clercq, C-Nucleosides To Be Revisited, *J. Med. Chem.* **2016**, *59*, 2301–2311.

[180] K. S. Ramasamy, D. Averett, A Modified Synthesis of Tiazofurin, *Nucleosides and Nucleotides* **1999**, *18*, 2425–2431.

[181] Michael Nagl, Claudia Panuschka, Andrea Barta, Walther Schmid, The BF3·OEt2-Assisted Conversion of Nitriles into Thioamides with Lawesson's Reagent, *Synthesis* **2008**, *24*, 4012–4018.

[182] A. Hantzsch, J. H. Weber, Ueber Verbindungen des Thiazols (Pyridins der Thiophenreihe), *Ber. Dtsch. Chem. Ges.* **1887**, *20*, 3118–3132.

[183] Richard S. Brown, James Dowden, Christelle Moreau, Barry V. L. Potter, A concise route to tiazofurin, *Tetrahedron Lett.* **2002**, *43*, 6561–6562.

[184] K. S. Ramasamy, R. Bandaru, D. Averett, A new synthetic methodology for tiazofurin, *J. Org. Chem.* **2000**, *65*, 5849–5851.

[185] David R. Williams, Patrick D. Lowder, Yu-Gui Gu, Dawn A. Brooks, Studies of Mild Dehydrogenations in Heterocyclic Systems, *Tetrahedron Lett.* **1997**, *38*, 331–334.

[186] S. Briolant, D. Garin, N. Scaramozzino, A. Jouan, J. M. Crance, In vitro inhibition of Chikungunya and Semliki Forest viruses replication by antiviral compounds: synergistic effect of interferon-alpha and ribavirin combination, *Antiviral Research* **2004**, *61*, 111–117.

[187] E. F. Da Silva-Júnior, G. O. Leoncini, É. E. S. Rodrigues, T. M. Aquino, J. X. Araújo-Júnior, The medicinal chemistry of Chikungunya virus, *Bioorganic & Medicinal Chemistry* **2017**, *25*, 4219–4244.

[188] J.-G. Park, G. Ávila-Pérez, A. Nogales, P. Blanco-Lobo, J. C. de La Torre, L. Martínez-Sobrido, Identification and Characterization of Novel Compounds with Broad-Spectrum Antiviral Activity against Influenza A and B Viruses, *J Virol* **2020**, *94*.

[189] Y. Kosugi, Y. Saito, S. Mori, J. Watanabe, M. Baba, S. Shigeta, Antiviral Activities of Mizoribine and other Inosine Monophosphate Dehydrogenase Inhibitors against Several Ortho- and Paramyxoviruses, *Antiviral Chemistry & Chemotherapy* **1994**, *5*, 366–371.

[190] S.-F. Li, M.-J. Gong, Y.-F. Sun, J.-J. Shao, Y.-G. Zhang, H.-Y. Chang, In Vitro and in Vivo Antiviral Activity of Mizoribine Against Foot-And-Mouth Disease Virus, *Molecules* **2019**, *24*.

[191] S. Yokota, Mizoribine: mode of action and effects in clinical use, *Pediatrics International* **2002**, *44*, 196–198.

[192] Dale L Barnard, Valerie D Hubbard, Jared Burton, Donald F Smee, John D Morrey, Inhibition of Severe Acute Respiratory Syndrome-Associated Coronavirus (SARSCoV) by Calpain Inhibitors and β-D-N4-Hydroxycytidine, *Antiviral Chemistry & Chemotherapy* **2004**, *15*, 15–22.

[193] L. Tian, Z. Pang, M. Li, F. Lou, X. An, S. Zhu, L. Song, Y. Tong, H. Fan, J. Fan, Molnupiravir and Its Antiviral Activity Against COVID-19, *Front. Immunol.* **2022**, *13*, 855496.

[194] M. L. Agostini, A. J. Pruijssers, J. D. Chappell, J. Gribble, X. Lu, E. L. Andres, G. R. Bluemling, M. A. Lockwood, T. P. Sheahan, A. C. Sims et al., Small-Molecule Antiviral β-d-N4-Hydroxycytidine Inhibits a Proofreading-Intact Coronavirus with a High Genetic Barrier to Resistance, *J Virol* **2019**, *93*.

[195] S. Zhou, C. S. Hill, S. Sarkar, L. V. Tse, B. M. D. Woodburn, R. F. Schinazi, T. P. Sheahan, R. S. Baric, M. T. Heise, R. Swanstrom, β-d-N4-hydroxycytidine Inhibits SARS-CoV-2 Through Lethal Mutagenesis But Is Also Mutagenic To Mammalian Cells, *The Journal of Infectious Diseases* **2021**, *224*, 415–419.

[196] G. Painter, G. Bluemling, M. Natchus, N4-Hydroxycytidine And Derivatives and Anti-Viral Uses Related Thereto, **2019,** WO 2019/113462. Emory University.

[197] W. Hou, Characterization of codon usage pattern in SARS-CoV-2, *Virology Journal* **2020**, *17*, 138.

[198] A. Shannon, N. T.-T. Le, B. Selisko, C. Eydoux, K. Alvarez, J.-C. Guillemot, E. Decroly, O. Peersen, F. Ferron, B. Canard, Remdesivir and SARS-CoV-2: Structural requirements at both nsp12 RdRp and nsp14 Exonuclease active-sites, *Antiviral Research* **2020**, *178*, 104793.

[199] S. Khater, P. Kumar, N. Dasgupta, G. Das, S. Ray, A. Prakash, Combining SARS-CoV-2 Proofreading Exonuclease and RNA-Dependent RNA Polymerase Inhibitors as a Strategy to Combat COVID-19: A High-Throughput in silico Screening, *Front. Microbiol.* **2021**, *12*, 647693.

[200] H. T. Baddock, S. Brolih, Y. Yosaatmadja, M. Ratnaweera, M. Bielinski, L. P. Swift, A. Cruz-Migoni, H. Fan, J. R. Keown, A. P. Walker et al., Characterization of the SARS-CoV-2 ExoN (nsp14ExoN-nsp10) complex: implications for its role in viral genome stability and inhibitor identification, *Nucleic Acids Research* **2022**, *50*, 1484–1500.

[201] F. Ferron, L. Subissi, A. T. Silveira De Morais, N. T. T. Le, M. Sevajol, L. Gluais, E. Decroly, C. Vonrhein, G. Bricogne, B. Canard et al., Structural and molecular basis of mismatch correction and ribavirin excision from coronavirus RNA, *Proc. Natl. Acad. Sci. U.S.A.* **2018**, *115*, E162-E171.

[202] S. C. J. Jorgensen, R. Kebriaei, L. D. Dresser, Remdesivir: Review of Pharmacology, Pre-clinical Data, and Emerging Clinical Experience for COVID-19, *Pharmacotherapy* **2020**, *40*, 659–671.

[203] J. J. Malin, I. Suárez, V. Priesner, G. Fätkenheuer, J. Rybniker, Remdesivir against COVID-19 and Other Viral Diseases, *Clin Microbiol Rev* **2020**, *34*.

[204] A. Shannon, A. Chazot, M. Feracci, C. Falcou, V. Fattorini, B. Selisko, S. Good, A. Moussa, J.-P. Sommadossi, F. Ferron et al., An exonuclease-resistant chain-terminating nucleotide

analogue targeting the SARS-CoV-2 replicase complex, *Nucleic Acids Research* **2024**, *52*, 1325–1340.

[205] P. F. Abolfazl Arabshahin, A simplified procedure for the synthesis of nucleoside 1-thiotriphosphates: dATPαS, dGTαPs, UTPαS and dTTPαS, *Biochemical and Biophysical Research Communications* **1994**, *1*, 150–155.

[206] L. Beigelman, G. Wang, Smith, David, Bernard, Prhavc Marija, Substituted Nucleosides, Nucleotides and Analogs Thereof, **2015,** WO 2015/054465 A1. Alios Biopharma, INC.

[207] H.-J. Zhang, M. Ociepa, M. Nassir, B. Zheng, S. A. Lewicki, V. Salmaso, H. Baburi, J. Nagel, S. Mirza, B. Bueschbell et al., Stereocontrolled access to thioisosteres of nucleoside di- and triphosphates, *Nature chemistry* **2024**, *16*, 249–258.

[208] Abu T. Khan, Ejabul Monda, A Highly Efficient and Useful Synthetic Protocol for the Cleavage of tert-Butyldimethylsilyl (TBS) Ethers Using a Catalytic Amount of Acetyl Chloride in Dry Methanol, *Synlett* **2003**, 694–698.

[209] Julian Witt, *Dissertation*, Universität Hamburg, Hamburg, **2022**.

[210] Christopher McGuigan, Ranjith N. Pathirana, Naheed Mahmood, Kevin G. Devine, Alan J. Hay, Aryl phosphate derivatives of AZT retain activity against HIV1 in cell lines which are resistant to the action of AZT, *Antiviral Research* **1992**, 311–321.

[211] M. J. Sofia, D. Bao, W. Chang, J. Du, D. Nagarathnam, S. Rachakonda, P. G. Reddy, B. S. Ross, P. Wang, H.-R. Zhang et al., Discovery of a β-d-2'-deoxy-2'-α-fluoro-2'-β-C-methyluridine nucleotide prodrug (PSI-7977) for the treatment of hepatitis C virus, *J. Med. Chem.* **2010**, *53*, 7202–7218.

[212] D. Siegel, H. C. Hui, E. Doerffler, M. O. Clarke, K. Chun, L. Zhang, S. Neville, E. Carra, W. Lew, B. Ross et al., Discovery and Synthesis of a Phosphoramidate Prodrug of a Pyrrolo2,1-ftriazin-4-amino Adenine C-Nucleoside (GS-5734) for the Treatment of Ebola and Emerging Viruses, *J. Med. Chem.* **2017**, *60*, 1648–1661.

[213] H. Chapman, M. Kernan, E. Prisbe, J. Rohloff, M. Sparacino, T. Terhorst, R. Yu, Practical synthesis, separation, and stereochemical assignment of the PMPA pro-drug GS-7340, *Nucleosides, Nucleotides & Nucleic Acids* **2001**, *20*, 621–628.

[214] C. A. Roman, J. Balzarini, C. Meier, Diastereoselective synthesis of aryloxy phosphoramidate prodrugs of 3'-deoxy-2',3'-didehydrothymidine monophosphate, *J. Med. Chem.* **2010**, *53*, 7675–7681.

[215] F. Micheli, B. Bertani, K. R. Gibson, R. Di Fabio, L. Raveglia, R. Zanaletti, S. Cremonesi, A. Pozzan, T. Semeraro, L. Tarsi et al., Substituted 2-Azabicyclo[3.1.1]Heptane And 2-Azabicyclo[3.2.1]Octane Derivatives As Orexin Receptor Antagonists, **2019,** WO 2019/043407 A1. Chronos Therapeutics Limited.

[216] R. J. Geraghty, M. T. Aliota, L. F. Bonnac, Broad-Spectrum Antiviral Strategies and Nucleoside Analogues, *Viruses* **2021**, *13*.

[217] E. de Clercq, C-Nucleosides To Be Revisited, *J. Med. Chem.* **2016**, *59*, 2301–2311.

[218] J. Stambaský, M. Hocek, P. Kocovský, C-nucleosides: synthetic strategies and biological applications, *Chemical reviews* **2009**, *109*, 6729–6764.

[219] G. Wang, J. Wan, Y. Hu, X. Wu, M. Prhavc, N. Dyatkina, V. K. Rajwanshi, D. B. Smith, A. Jekle, A. Kinkade et al., Synthesis and Anti-Influenza Activity of Pyridine, Pyridazine, and Pyrimidine C-Nucleosides as Favipiravir (T-705) Analogues, *J. Med. Chem.* **2016**, *59*, 4611–4624.

[220] L. B. Jasenka Matulic-Adamic, Synthesis of 5-(β-D-Ribofuranosyl)-Pyridin-2-one: A "Deletion-Modified" Analogue of Uridine, *Tetrahedron Lett.* **1997**, *38*, 1669–16972.

[221] C. H. Larsen, B. H. Ridgway, J. T. Shaw, K. A. Woerpel, A Stereoelectronic Model To Explain the Highly Stereoselective Reactions of Nucleophiles with Five-Membered-Ring Oxocarbenium Ions, *J. Am. Chem. Soc.* **1999**, *121*, 12208–12209.

[222] C. H. Larsen, B. H. Ridgway, J. T. Shaw, D. M. Smith, K. A. Woerpel, Stereoselective C-glycosylation reactions of ribose derivatives: electronic effects of five-membered ring oxocarbenium ions, *J. Am. Chem. Soc.* **2005**, *127*, 10879–10884.

[223] M. Urban, R. Pohl, B. Klepetarova, M. Hocek, New modular and efficient approach to 6-substituted pyridin-2-yl C-nucleosides, *J. Org. Chem.* **2006**, *71*, 7322–7328.

[224] M. Stefko, L. Slavetínská, B. Klepetárová, M. Hocek, A general and efficient synthesis of pyridin-2-yl C-ribonucleosides bearing diverse alkyl, aryl, amino, and carbamoyl groups in position 6, *J. Org. Chem.* **2010**, *75*, 442–449.

[225] M. Peifer, R. Berger, V. W. Shurtleff, J. C. Conrad, D. W. C. MacMillan, A general and enantioselective approach to pentoses: a rapid synthesis of PSI-6130, the nucleoside core of sofosbuvir, *J. Am. Chem. Soc.* **2014**, *136*, 5900–5903.

[226] Takako Sakamoto, Soh-Ichi Kaneda, Sumiko Nishimura, Hiroshi Yamanaka, Site-Selectivity in the Cyanation of 3-Substituted Pyridine 1-Oxides with Trimethylsilanecarbonitrile, *Chem. Pharm. Bull.* **1985**, *33*, 565–571.

[227] W.T. Markiewicz and M. Wiewiorowski, A new type of silyl protecting groups in nudeoside chemistry, *Nucleic Acids Research* **1976**, 185–190.

[228] G. Kokic, H. S. Hillen, D. Tegunov, C. Dienemann, F. Seitz, J. Schmitzova, L. Farnung, A. Siewert, C. Höbartner, P. Cramer, Mechanism of SARS-CoV-2 polymerase stalling by remdesivir, *Nat Commun* **2021**, *12*, 279.

[229] A. Cho, O. L. Saunders, T. Butler, L. Zhang, J. Xu, J. E. Vela, J. Y. Feng, A. S. Ray, C. U. Kim, Synthesis and antiviral activity of a series of 1'-substituted 4-aza-7,9-dideazaadenosine C-nucleosides, *Bioorganic & Medicinal Chemistry Letters* **2012**, *22*, 2705–2707.

[230] T. N. Poudel, S. Panda, M. Orimoloye, P. Hegde, C. C. Aldrich, 1'-Cyano Intermediate Enables Rapid and Stereoretentive Access to 1'-Modified Remdesivir Nucleosides, *J. Org. Chem.* **2022**, *87*, 14452–14462.

[231] M. Štefko, L. Slavětínská, B. Klepetářová, M. Hocek, General and modular synthesis of isomeric 5-substituted pyridin-2-yl and 6-substituted pyridin-3-yl C-ribonucleosides bearing diverse alkyl, aryl, hetaryl, amino, carbamoyl, and hydroxy groups, *J. Org. Chem.* **2011**, *76*, 6619–6635.

[232] Rogers E. Harry-O'kuru, Jennifer M. Smith, Michael S. Wolfe, A Short, Flexible Route toward 2´-C-Branched Ribonucleosides, *J. Org. Chem.* **1997**, 1754–1759.

[233] B. Ganter, M. Zickler, J. Huchting, M. Winkler, A. Lüttjohann, C. Meier, G. Gabriel, S. Beck, T-705-Derived Prodrugs Show High Antiviral Efficacies against a Broad Range of Influenza A Viruses with Synergistic Effects When Combined with Oseltamivir, *Pharmaceutics* **2023**, *15*.

[234] S. Mohamady, D. L. Jakeman, An improved method for the synthesis of nucleoside triphosphate analogues, *J. Org. Chem.* **2005**, *70*, 10588–10591.

[235] V. Nikolova, K. Linnemannstöns, M.-E. Bendel, M. Machado, B. Ganter, P. Budimir, M. Vogts, C. Fischer, M. Ganter, C. Meier et al., Membrane-Permeable 5-Fluorodeoxyuridine Triphosphate Derivatives Inhibit the Proliferation of Plasmodium falciparum, *ACS Infect. Dis.* **2025**.

[236] X. Jia, G. A. Kullik, M. Bufano, A. Brancale, D. Schols, C. Meier, Membrane-permeable tenofovir-di- and monophosphate analogues, *Eur. J. Med. Chem.* **2024**, *264*, 116020.

[237] X. Jia, D. Schols, C. Meier, Lipophilic Nucleoside Triphosphate Prodrugs of Anti-HIV Active Nucleoside Analogs as Potential Antiviral Compounds, *Adv. Sci.* **2023**, *10*, e2306021.

[238] X. Jia, D. Schols, C. Meier, Potent Anti-HIV Activity of Alkyl-Modified DiPPro-Nucleotides, *Small Struct.* **2024**, *5*.

[239] Patricia Budimir, *Master thesis*, Universität Hamburg, Hamburg, **2024**.

[240] R. Fliegert, M. Sandmann, S. Tajdar, S. Sander, D. Carrillo, B. Ganter, M. Ocenas, S. Etzold, N. Pekarek, J. Berger et al., Targeting a viral macrodomain: Design, Structure-Based Optimization and Antiviral Evaluation of Nanomolar Inhibitors for Mac1 of SARS-CoV-2 **2025**.

[241] V. T. Sterrenberg, D. Stalling, J. I. H. Knaack, T. K. Soh, J. B. Bosse, C. Meier, A TriPPPro-Nucleotide Reporter with Optimized Cell-Permeable Dyes for Metabolic Labeling of Cellular and Viral DNA in Living Cells, *Angew. Chem. Int. Ed. Engl.* **2023**, *62*, e202308271.

[242] A. Alzérreca, New approach to l'C-modified riboside scaffold via stereoselective functionalization of D-(+)-ribonic-y-lactone, *Journal of Heterocyclic Chem* **2003**, *40*, 317–320.

[243] H. R. Lee, J. A. Kang, A. Y. Park, W. H. Kim, P. Chun, J. Kim, J. A. Kim, B. Lee, L. S. Jeong, H. R. Moon, Synthesis of Neplanocin A Analog with 2'-"up"-C-Methyl Substituent as Potential Anti-HCV Agent, *Bull. Korean Chem. Soc.* **2009**, *30*, 2043–2050.

[244] Z. Chen, D. Jochmans, T. Ku, J. Paeshuyse, J. Neyts, K. L. Seley-Radtke, Bicyclic and Tricyclic "Expanded" Nucleobase Analogues of Sofosbuvir: New Scaffolds for Hepatitis C Therapies, *ACS Infect. Dis.* **2015**, *1*, 357–366.

7. Hazardous substance register

Compounds	GHS pictogram	H-statements	P-statements
1,1‘-Carbonyl-imidazole		302-314	280-305+351+338-310
2-Cyano-3-fluoropyridine		301+311+331-315-319	501-261-264-270-271-280-337+313-305+351+338-361+364-332+313-301+310+330-302+352+312-304+340+311-403+233-405
3-Fluoropyridine		225-315-319	210-233-240-241-242-243-264-280-370+378-337+313-305+351+338-303+361+353-332+313-362-403+235-501
4-Hydroxy-benzaldehyde		315-319	264-280-302+352-337+313-362+364-332+313
4-Hydroxybenzyl-alcohol		315-319	264-280-302+352-337+313-362+364-332+313
5-Phenyl-1*H*-tetrazol		302-315-319-335	210-240-241-264-270-280-301+312-330-374-501
9-Fluorenylmethanol		302-315-319-335	261-305-351-338
Acetic acid		226-314	210-233-240-280-303+361+353-305+351+338
Acetic anhydride		226-302-331-314-335	210-260-280-303+361+353-305+351+338-312
Acetone		225-319-336	210-233-240-241-242-305+351+338

Acetonitrile		225-302+312+332-319	210-280-301+312-302+352-304+340-305+351+338
Acetyl chloride		225-302-314-335-412	210-233-240-241-242-243-260-261-264-270-271-273-280-301+330+331-303+361+353-304+340-305+351+338-310-312-321-330-363-370+378-403+233-403+235-405-501
Azobisisobutyronitrile		242-302-332-412	210-220-234-261-264-270-271-273-280-301+312-304+312-304+340-312-330-370+378-403+235-411-420-501
Ammonia solution 25%		314-335-410	261-271-273-280-303+361+353-305+351+338
7 M Ammonia in MeOH		225-301+311+331-314-370-410	210-273-280-303+361+353-304+340+310-305+351+338
Ammonium bicarbonate		302	264-301+330+331-312
Ammonium chloride		319-302	270-280-305+351+338
Ammonium sulfate		315-319-335	261-264-270-271-273-280-301+312-302+352-304+340-305+351+338-312-321-330-332+313-337+313-362-391-403+233-405-501

Boron trichloride 1 M solution in dichloromethane		314-336-351-301+331	304+340-280-301+330+331-305+351+338-310-303+361+353
Benzoyl chloride		331-302+312-314-317	261-280-303+361+353-304+340+310-305+351+338+310-403+233
Boron trifluoride diethyl etherate, approx. 48%		226-310-332-372	210-280-303+361+353-304+340-305+351+338-310
Bromotrichloro-methane		302+312+332-315-319-335	261-280-301+312-302+352-305+351+338-337+313
Cerium(III) chloride		315-318-319-335-410	261-264-271-273-280-302+352-304+340-305+351+338-310-312-321-332+313-337+313-362-391-403+233-405-501
Chloroform		302-331-315-319-351-361-336-372-412	201-273-301+312+330-302+352-304+340+311-308+313
Cyclopropyl magnesium bromide 0.5 M solution in THF		302-314-335-336-351	210-231+232-280-301+330+331-303+361+353-305+351+338-310
Decanoyl chloride		290-314	280-390-303+361+353-301+330+331-304+340+310-305+351+338+310

Dess-Martin periodane		272-315-319-335	210-220-261-264-302+352-305+351+338
Dichloromethane		315-319-335-336-351-373	261-281-305+351+338
Diazabicycloundecene		301-302-312-314-412	260-264-270-273-280-301+310-301+312-301+330+331-302+352-303+361+353-304+340-305+351+338-310-312-321-322-330-363-405-501
Diethylaminosulfur trifluoride		226-302-312-314-332	210-233-240-241-242-243-260-261-264-270-271-280-301+312-301+330+331-302+352-303+361+353-304+312-304+340-305+351+338-310-312-321-322-330-363-370+378-403+235-405-501
Diethyl ether		224-302-336	210-233-240-241-242-243-261-264-270-271-280-301+312-303+361+353-304+340-312-330-370+378-403+233-403+235-405-501

Dimethyl sulfoxide	This substance is not classified as dangerous according to directive 67/548/EWG.		
Diphenyl phosphite		302-314-360-370-372-340	260-201-280-308+311-303+361+353-304+340+310-305+351+338+310
Ethyl acetate		225-319-336	210-233-240-305+351+338-403+235
Ethyl bromopyruvate		315-319-335	302+352-305+351+338-304+340-312-280
Hydrogen		220-280	210-377-381-403
Hydrogen peroxide (30% in water)		318-412	273-280-305+351+338-501
Imidazole		302-314-360	263-270-280-301+310-305+351+338-308+313
Iodine		312-315-319-332-335-372-400	261-273-280-305-314-338-251
Lawesson's reagent		261-302-312-332	231+323-261-264-270-271-280-301+312-302+352-304+312-304+340-312-322-330-363-370-378-402+404-501

L-Alanine 2-ethylbutyl ester hydrochloride	This substance is not classified as dangerous according to directive 67/548/EWG.		
L-Alanine Methyl Ester Hydrochloride	This substance is not classified as dangerous according to directive 67/548/EWG.		
L-Cysteine methyl ester hydrochloride	This substance is not classified as dangerous according to directive 67/548/EWG.		
Lithium diisopropylamide 1 M solution in THF		225-250-304-314-335-336-351-361-372-411	210-280-301+330+331-303+361+353-304+340+310-305+351+338-370+378
Lithium bis(trimethylsilyl) amide 1 M solution in THF		225-304-314-335-336-351	210-280-301+330+331-303+361+353-305+351+338-310
Lithium tri-tert-butoxyaluminum hydride		260-314	223-231-232-260-280-303+361+353-305+351+338
2,6-Lutidine		226-302-315-319	210-260-302+352-305+351+338
Magnesium sulfate	This substance is not classified as dangerous according to directive 67/548/EWG.		

meta-Chloroperoxybenzoic acid		226-314-335	210-220-233-234-240-241-242-243-260-261-264-271-272-280-301+330+331-302+352-303+361+353-304+340-305+351+338-310-312-321-332+313-333+313-337+313-362-363-370+378-403+233-403+235-405-411-420-501
Methanol		225-301-302-305-311-331-370	210-280-233-301+310-303+361+353-304+340+311
Methylboronic acid		315-319	264-280-302+352-337+313-362+364-332+313
Methyl *tert*-butyl ether		225-315	210-233-240-241-242-303+361+353
Myristoyl Chloride		290-314	280-390-303+361+353-301+330+331-304+340+310-305+351+338+310
N-Chlorosuccinimide		290-302-314-335-410	260-273-280-301+312-303+361+353-305+351+338
N,N-Diemethyl formamide		226-312+332-319-360	201-210-302+352-305+351+338-308+313

N,*N*-Dimethylpyridin-4-amine		301-310-315-319-335	280-305+351+338-337+313
N-Methylimidazole		302-311-314	270-280-301+312-301+330+331-303+361+353-305+351+338
Nitromethane		226-302-332-351-361	210-308+313
Oxalyl chloride		260-301+331-314	223-231+232-280-303+361+353-304+340+310-305+351+338+310
Palladium(II) acetate		317-318-410	261-272-273-280-302+352-305+351+338
Pentadecylic acid		315-319-335-413	261-305+351+338
Pentafluorophenol		302+312-315-319	264-270-280-337+313-302+352+312-501
Pentafluoropyridine		226-315-319	210-264-280-370+378-337+313-303+361+353
Petroleum ether (50 – 70 °C)	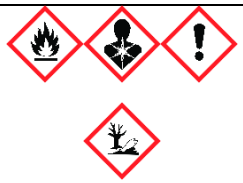	225-304-315-336-361-373-411	201-210-273-301+310-303+361+353-331
Phenyl chlorothionoformate		314	280-303+361+353-304+340+310-

			305+351+338-363-405
Phosphorus pentasulfide		228-260-302-332-400	210-223-231+232-273-370-378
Phosphorothioic trichloride		302-330-314-335	260-270-280-284-301+330+331-303+361+353-304+340+310-305+351+338-403+233-501
Phosphoryl chloride		302-330-314-372	280-301+312-303+361+353-304+340+310-305+351+338-314
Platinum(IV) oxide		272-319	220-305+351+338
Potassium carbonate		315-319-335	261-264-271-280-302+352-305+351+338
Proton sponge		315-319-335	305+351+338
Pyridine		225-302+312+332-315-319	210-280-301+312-303+361+353-304+340+312-305+351+338

Pyrophosphoryl chloride		314	260-264-280-301+330+331-302+361+354-304+340-305+354+338-316-321-363-405-501
Sodium azide		300-310-330-373-410	262-264-273-280-302+352+310-304+340+310
Sodium bicarbonate	This substance is not classified as dangerous according to directive 67/548/EWG.		
Sodium borohydride		260-301-314-360	231+232-260-280-303+361+353-304+340+310-305+351+338
Sodium carbonate		319	264-280-305+351+338-337+313
Sodium chloride	This substance is not classified as dangerous according to directive 67/548/EWG.		
Sodium hydrosulfide		251-290-301-314-400	235+410-280-301+330+331-303+361+353-305+351+338+310
Sodium hydroxide		290-314	234-260-280-303+361+353-304+340+310-305+351+338

Sodium methoxide 5.4 M solution in methanol		226-290-301-311-314-318-331-370	210-280-301+330+331-303+361+353-305+351+338-308+313-310
Sodium nitrite		272-301-319-400	210-220-264-273-301+310-305+351+338
Sodium sulfate	This substance is not classified as dangerous according to directive 67/548/EWG.		
Sulfuric acid (98%)		290-314	280-301+330+331-303+361+353-305+351+338+310
tert-Butyl hydroperoxide solution 5.5 M in decane		226-242-302-304-311-314-317-330-335-341-411	210-280-301+330+331-303+361+353-304+340+310-305+351+338-370+378
tert-Butylamine		225-302-331-314-412	210-273-280-303+361+353-304+340+310-305+351+338
tert-Butyldimethylsilyl chloride		228-314-411	210-273-280-303+361+353-305+351+338+310
tert-Butyl(chlor)diphenylsilan		314-335	261-271-280-303+361+353-304+340+310-305+351+338

tert-Butylmagnesium chloride		225-260-302-314-335-351-371-372	231+232-260-210-280-370+387-303+361+353-302+335+334-304+340+310-305+35+338+310
Tetrabutylammonium dihydrogen phosphate 0.4 M solution in acetonitrile		225-302+312+332-319	210-280-301+312-303+361+353-304+340+312-305+351+338
Tetrabutylammonium hydroxide		302-314	2800-301+330+331-303+361+353-305+351+338+310
Tetrabutylammonium fluoride 1 M solution in THF	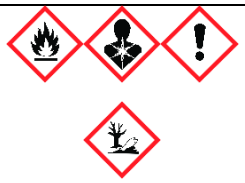	225-302-315-319-335-336-351-411	210-273-301+312-303+361+353-305+351+338-308+313
Tetrahydrofuran		225-302-319-335-336-351	201-202-210-301+312-305+351+338-308+313
1,1,3,3-Tetraisopropyl-1,3-dichlorodisiloxane		290-314	234-280-303+361+353-304+340+310-305+351+338-363
Tin(IV) chloride		314-335-412	260-280-303+361+353-304+340+310-305+351+338

Toluene		225-304-315-336-361-373-412	202-210-273-301+310-303+361+353-331
Tributylamine		302-310+330-315	260-262-280-302+352-310-304+340+310
Tributyltin hydride		301-312-315-319-360-372-410	201-273-302+352-305+351+338-308+310
Triethylamine		225-302-311+331-314-335	210-280-301+330+331-303+361+353-304+340+311-305+351+338+310
Triethylammonium bicarbonate buffer (1 M)	This substance is not classified as dangerous according to directive 67/548/EWG.		
Triethylsilane		225-410	210-303+361+353-403+233
Trifluoroacetic acid		290-331-314-412	260-273-280-303+361+353-305+351+338-312
Trifluoroacetic anhydride		314-332-412	273-280-301+310+331-303+361+353-304+340+312-305+351+338-310

Trifluoromethanesulfonic anhydride		272-302-314-335	210-220-280-301+312-303+361+353-305+351+338
Trimethylsilyl cyanide		225-300+310+330-410	210-233-273-280-303+361+353-304+340+310
Trimethylphosphate		302-315-319-340-351	201-301+312+330-302+352-305+351+338-308+313
Tris(tetrabutylammonium) hydrogen pyrophosphate		315-319-335	261-264-271-280-302+352-305+351+338
Valeroyl chloride		226-290-314-331-412	210-273-280-303+361+353-304+340+310-305+351+338
Vinylmagnesium bromide		302-314-371-372-351-335-225-260	260-231+232-210-280-370+378-303+361+353-302+335+334-304+340+310-305+351+338+310
Xantphos		315-319-335	261-264-271-280-302+352-305+351+338

8. Acknowledgements

Mein Dank gilt….

Herrn Prof. Dr. Chris Meier für die Bereitstellung des interessanten Themas sowie für das entgegenbrachte Vertrauen, diese frei bearbeiten zu dürfen. Darüber hinaus bedanke ich mich für die Unterstützung und den regen, konstruktiven Austausch.

Herrn Prof. Dr. Ralph Holl für die freundliche Übernahme des Zweitgutachtens.

Herrn Dr. Thomas Hackl, Frau Dr. Jennifer Menzel und ihren Mitarbeitern für die Anfertigung unzähliger NMR- und MS-Spektren sowie für die stetige Hilfsbereitschaft bei Problemen oder besonderen Wünschen.

Allen Mitarbeitern der übrigen Serviceeinrichtungen am Fachbereich Chemie, insbesondere Amir, Ali und Reinhart.

Besonders Herrn Dr. Bruno Canard, Herrn Prof. Bruno Coutard, Herrn Prof. Matthias Dobbelstein und deren Arbeitsgruppen für die langjährige und erfolgreiche Kooperation. Besonders möchte ich mich Frau Dr. Barbara Selisko für die Durchführung unzähliger Experimente bedanken.

Dr. Johanna Huchting für die wertvolle Unterstützung schon während meiner Masterarbeit und vor allem auch zu Beginn der Promotion.

Dr. Simon Weising für das Korrekturlesen dieser Arbeit, aber auch ganz besonders für die vielen aufbauenden Worte in den letzten Jahren.

Meinen Assistenten Dr. Vincente Sterrenberg und Matthias Winkler, von denen ich unglaublich viel lernen durften, und vor allem auch für die Unterstützung nach meinen Praktika, die mir den Start in die Promotion erheblich erleichtert hat.

Meinen Praktikanten Markus, Alja, Aleksander, Even und Julie für ihren Einsatz, der erheblich zum Gelingen dieser Arbeit beigetragen hat.

Allen aktuellen und ehemaligen Mitgliedern des AK Meiers für die tolle Arbeitsatmosphäre und die schöne gemeinsame Zeit. Insbesondere möchte ich mich bei meinem langjährigen Abzugsnachbar Dr. Xiao Jia für die unzähligen gemeinsamen Stunden im Labor bedanken, vor

allem auch dafür, dass ich nie alleine Arbeiten musste, ganz egal zu welcher Tages- oder Nachtzeit. Ein ganz besonderer Dank gilt auch meiner Lieblingslabor- und Büropartnerin Dese für tolle Zeit im Labor, auf den vielen gemeinsamen Konferenzreisen, aber auch vor allem außerhalb der Uni.

Meinen Freunden Matze, Stefan, Alex, Nils und Timo die ich während meiner Zeit am Fachbereich kennenlernen durfte.

Den vielen Nicht-Chemiker-Freunden, die mich während meiner gesamten Promotionszeit in Hamburg unterstützt haben. Besonders bedanken möchte ich mich an der Stelle bei Birgitt, Rüdiger und der gesamten Bizzarro-Gang.

Ganz besonderer Georg, der schon seit unserer gemeinsamen Schulzeit immer voll und ganz hinter mir stand und ohne den ich wahrscheinlich nie den Weg nach Hamburg gefunden hätte.

Vanni. Danke das du die letzten Jahre immer für mich da warst.

Meiner Familie, insbesondere meinen Eltern, die mich schon immer bedingungslos und uneingeschränkten unterstützt und immer an mich geglaubt haben. Ohne Euch wäre diese Arbeit niemals zu Stande gekommen.

9. Declaration on Oath

Hiermit versichere ich an Eides statt, die vorliegende Dissertationsschrift selbst verfasst und keine anderen als die angegebenen Quellen und Hilfsmittel benutzt zu haben. Sofern im Zuge der Erstellung der vorliegenden Dissertationsschrift generative Künstliche Intelligenz (gKI) basierte elektronische Hilfsmittel verwendet wurden, versichere ich, dass meine eigene Leistung im Vordergrund stand und dass eine vollständige Dokumentation aller verwendeten Hilfsmittel gemäß der Guten wissenschaftlichen Praxis vorliegt. Ich trage die Verantwortung für eventuell durch die gKI generierte fehlerhafte oder verzerrte Inhalte, fehlerhafte Referenzen, Verstöße gegen das Datenschutz- und Urheberrecht oder Plagiate.

15.12.2026 _____

Ort, Datum

_____

Unterschrift